On the Nature of Dark Matter: Phenomenological and Cosmological Probes

PhD Thesis

Miguel Escudero Abenza

IFIC - Universitat de València - CSIC
Departamento de Física Teórica
Programa de Doctorado en Física

Under the supervision of

Olga Mena Requejo
Nuria Rius Dionis

Valencia, Mayo 2018

Olga Mena Requejo, científico titular del Consejo Superior de Investigaciones Científicas, y

Nuria Rius Dionis, catedrático del Departamento de Física Teórica de la Universidad de Valencia,

Certifican:

Que la presente memoria, "On the Nature of Dark Matter: Phenomenological and Cosmological Probes" ha sido realizada bajo su dirección en el Instituto de Física Corpuscular, centro mixto de la Universidad de Valencia y del CSIC, por **Miguel Escudero Abenza**, y constituye su Tesis para optar al grado de Doctor en Ciencias Físicas.

Y para que así conste, en cumplimiento de la legislación vigente, presenta en el Departamento de Física Teórica de la Universidad de Valencia la referida Tesis Doctoral, y firman el presente certificado.

Valencia, a 7 de Mayo de 2018,

Olga Mena Requejo Nuria Rius Dionis

A mi familia y amigos,
y en especial,
a mi madre y a Andrea

Y es que no hay nada mejor que imaginar
la Física es un placer
y es que no hay nada mejor que formular
escuchar y oír a la vez

Antonio Vega, Una décima de segundo

List of Publications

This PhD thesis is based on the following publications:

- *Exploring dark matter microphysics with galaxy surveys* [1]
  M. Escudero, O. Mena, A. C. Vincent, R. J. Wilkinson and C. Boehm.
  JCAP **1509** (2015) 034, [1505.06735].

- *Cosmological searches for a noncold dark matter component* [2]
  S. Gariazzo, M. Escudero, R. Diamanti and O. Mena.
  Phys. Rev. **D96** (2017) 043501, [1704.02991].

- *Sterile neutrino portal to Dark Matter I: The $U(1)_{B-L}$ case* [3]
  M. Escudero, N. Rius and V. Sanz.
  JHEP **02** (2017) 045, [1606.01258].

- *Sterile Neutrino portal to Dark Matter II: Exact Dark symmetry* [4]
  M. Escudero, N. Rius and V. Sanz.
  Eur. Phys. J. **C77** (2017) 397, [1607.02373].

- *Toward (Finally!) Ruling Out Z and Higgs Mediated Dark Matter Models* [5]
  M. Escudero, A. Berlin, D. Hooper and M.-X. Lin.
  JCAP **1612** (2016) 029, [1609.09079].

- *Updated Collider and Direct Detection Constraints on Dark Matter Models for the Galactic Center Gamma-Ray Excess* [6]
  M. Escudero, D. Hooper and S. J. Witte.
  JCAP **1702** (2017) 038, [1612.06462].

- *Hidden Sector Dark Matter and the Galactic Center Gamma-Ray Excess: A Closer Look* [7]
  M. Escudero, S. J. Witte and D. Hooper.
  JCAP **1711** (2017) 042, [1709.07002].

Other works not included in this thesis are:

- *The present and future of the most favoured inflationary models after Planck 2015* [8]
  M. Escudero, H. Ramírez, L. Boubekeur, E. Giusarma and O. Mena.
  JCAP **1602** (2016) 020, [1509.05419].

- *A fresh look into the interacting dark matter scenario* [9]
  M. Escudero, L. Lopez-Honorez, O. Mena, S. Palomares-Ruiz and P. Villanueva-Domingo.
  1803.08427. Submitted to JCAP.

Abbreviations

ΛCDM	The standard cosmological model
ADMX	Axion Dark Matter eXperiment
AMS	The Alpha Magnetic Spectrometer
ATLAS	A Toroidal LHC ApparatuS
BAO	Baryon Acoustic Oscillations
BSM	Beyond the Standard Model
BBN	Big Bang Nucleosynthesis
BE	Bose-Einstein
CP	Charge-Parity
CDM	Cold Dark Matter
CKM	Cabibbo-Kobayashi-Maskawa
CL	Confidence Level
CMB	Cosmic Microwave Background
CMS	Compact Muon Solenoid
COBE	Cosmic Background Explorer
DESI	The Dark Energy Spectroscopic Instrument
DM	Dark Matter
DARWIN	DARk matter WImp search with liquid xenoN
DFSZ	Dine-Fischler-Srednicki-Zhitnitsky
FD	Fermi-Dirac
FERMI-LAT	The Fermi Large Area Telescope
FIRAS	The COBE Far Infrared Absolute Spectrophotometer

FLRW	Friedmann-Lemaître-Robertson-Walker
KSVZ	Kim-Shifman-Vainshtein-Zakharov
LEP	Large Electron-Positron Collider
LHC	Large Hadron Collider
LIGO	The Laser Interferometer Gravitational-Wave Observatory
LSS	Large Scale Structure
LSST	The Large Synoptic Survey Telescope
MACHO	MAssive Compact Halo Object
MATHUSALA	MAssive Timing Hodoscope for Ultra Stable neutraL pArticles
MB	Maxwell-Boltzmann
MD	Matter Dominated
MOND	MOdified Newtonian Dynamics
MW	Milky Way
NFW	Navarro, Frenk and White
NGC	New General Catalogue
PBHs	Primordial Black Holes
QED	Quantum Electrodynamics
RD	Radiation Dominated
SD	Spin-Dependent
SI	Spin-Independent
SM	Standard Model
SSB	Spontaneous Symmetry Breaking
SUSY	Supersymmetry
WIMPs	Weakly-Interacting-Massive-Particles
WMAP	Wilkinson Microwave Anisotropy Probe

Preface

In this doctoral thesis we have focused on both the phenomenological and cosmological implications of dark matter. From the cosmological perspective, we have studied the impact on the Large Scale Structure (LSS) and on the Cosmic Microwave Background (CMB) of interacting and non-cold dark matter particles. Phenomenologically, we have studied the consequences of Weakly Interacting Massive Particles (WIMPs) in the early Universe, at particle colliders, at direct detection experiments, and through their annihilation products in the Milky Way galaxy and its satellites. Special emphasis has been given to the phenomenology of models that aim to explain simultaneously both the dark matter in our Universe and the mass of the light active neutrinos.

This thesis is organized as follows: in the introductory Chapter 1 provides a brief overview of the astrophysical and gravitational evidence for dark matter, highlighting the role of dark matter in our current theoretical and observational understanding of the Universe. The standard cosmological model ΛCDM, with cold dark matter and a cosmological constant Λ is introduced. Chapter 2 is a brief summary of the Standard Model (SM) of particle physics together with possibly the most theoretically appealing mass generation mechanism for the light active neutrinos, the seesaw mechanism. Chapter 3 deals with the concepts, assumptions, and equations required to understand the hot and dense early Universe. In particular, the Boltzmann equation governing the non-equilibrium thermodynamics is presented and discussed. In Chapter 4 we review the main WIMP dark matter probes. Direct detection, indirect searches, and some of the collider constraints on weak-scale dark matter are outlined. To conclude, in Chapter 5, we summarize the main scientific results and conclusions of the research carried out for this thesis.

Finally, in Part II we present a copy of the research articles done for this study, as published in the different journals during the development of this thesis.

Por último, la Parte III consiste en un resumen detallado en español de los objetivos, motivación, metodología, resultados y conclusiones de esta tesis.

Agradecimientos

La realización de esta tesis habría sido imposible sin la ayuda y dedicación de mis directoras, Olga y Nuria. Para mi ha sido un placer trabajar con vosotras estos cuatro años. Nunca pensé que podría aprender tanto, de temas tan interesantes y pasármelo tan bien investigando. Elegir director de tesis es una lotería, pero siento que a mi me ha tocado ¡Dos veces! Mi madre siempre decía que era un tío con suerte y parece que con el doctorado no ha sido menos.

Nuria, te agradezco el tiempo que siempre me has prestado, he aprendido algo cada vez que he visitado tu despacho. Me ha gustado mucho que me dotaras de autonomía pero dándome todo lo necesario para poder desarrollar los cálculos e ideas por mi mismo. Espero que se me haya quedado algo de tu meticulosidad y tu perspectiva teórica. Te agradezco también tus consejos sobre las clases y tu interés por los cursos de doctorado.

Olga, tu guía directa, sobre todo en las etapas iniciales de la tesis, ha sido crucial para que le saque el máximo provecho al doctorado. Te agradezco mucho la pasión que transmites en todo lo que haces. Siempre disponible y dispuesta a darlo todo en nuestros proyectos. Ojalá y se me haya pegado algo de tu habilidad para generar ideas así como de tu increíble capacidad de trabajo. Muchas gracias también por presentarme a todo el mundo y por asegurarte de que estuviera bien allá donde fuéramos.

Esta tesis supone el fin de una era, pero espero que en el futuro sigamos trabajando juntos. Además, os agradezco a las dos que, aparte de en lo intelectual, os hayáis preocupado por mi en lo personal durante estos años. Para mi ha significado mucho.

I owe a great debt of gratitude to Dan Hooper for hosting me twice at Fermilab. Thank you for serving as an advisor during my periods there, for including me in every single meeting, talk or colloquium, for our very interesting shared projects, and for broadening my perspective on dark matter.

I would like to thank Ann Nelson for hosting me at the University of Washington. Thank you for being such a friendly host and for introducing me to the very interesting physics of Baryogenesis and B-mesons that I would have otherwise never explored.

In addition to those previously mentioned, during these four years I have had the pleasure to collaborate with multiple people: Aaron Vincent, Ryan Wilkinson, Céline Boehm, Héctor Ramírez, Lofti Boubekeur, Elena Giusarma, Verónica Sanz, Asher Berlin, Sam Witte, Stefano Gariazzo, Roberta Diamanti, Gordan Krnjaic, Laura López Honorez, Sergio Palomares Ruiz and Pablo Villanueva Domingo. I want to thank all of them for their expertise, advice and our fruitful collaborations. In particular, I want to thank Ryan Wilkinson for kindly helping me with CLASS and MontePython. I would like to thank Aaron Vincent for nicely hosting me at Durham and for his advice throughout these years. También quería agradecerle a Verónica Sanz su disponibilidad y todas sus enseñanzas en los que fueron mis primeros proyectos en física de partículas.

I would like to make particular mention to my closest collaborator (and good friend) Sam Witte. It has been a pleasure to carry research side by side with you at Fermilab and since. As everything in life, it is way better if shared with someone, specially someone like you. Thank you for sharing your knowledge, advice and experience with me. I am very glad that you came to Valencia! Also, I very much appreciate your help with my (sometimes broken) English.

Después de la gente que ha participado de manera directa en mi investigación, estoy especialmente agradecido con el resto de componentes del grupo de investigación SOM: Pilar Hernández, Carlos Peña y Andrea Donini. Muchas gracias por las interesantes Trobadas, por las charlas y por las discusiones de Física en general. Es un placer haber compartido grupo con gente a la que le apasiona la Física de esa manera. Además, estaré siempre en deuda con el grupo por haberme dado la oportunidad de visitar Fermilab y la Universidad de Washington. Estancias que me han encantado y que me han ayudado a ampliar mis conocimientos y mi perspectiva en la ciencia. Por supuesto, también estoy muy agradecido de haber compartido experiencias e ideas con los juniors y no tan juniors del grupo: Jordi, Marija, Héctor, Pablo, Miguel, Fer y Andrea Caputo.

Parte de mi labor durante estos años, además de investigadora, ha sido docente. Dar clase me encanta y para mi ha sido muy importante poder mejorar mis habilidades como profesor (siguiendo una ya tradición familiar). Le doy las gracias a Toni Pich por lo instructivo que ha sido compartir asignatura con él, la autonomía que me ha proporcionado y la multitud de consejos que me ha dado. También le agradezco a Javi Fuentes su aportación a los problemas, sus consejos y que me sustituyera sin problemas cuando lo necesité. Por supuesto, estoy agradecido a mis estudiantes durante estos años, los cuales espero que hayan aprendido tanto de mi como yo de ellos.

En mis cuatro años en el IFIC he tenido el placer de compartir instituto con mucha gente excelente. Estoy especialmente agradecido a Clara Murgui por su amistad y por la pasión que desprende hablando de física. También a Pablo y a Antonio por su ayuda con temas burocráticos, lectivos y de investigación. A Avelino por impulsar el journal club. A Miguel Nebot por su compañía y su toque en los partidos. Y a Juan Zúñiga por sus estupendas clases de estadística.

Para presentar una tesis en Física está claro que hay que ser Físico primero. Lo que no está garantizado es que uno se vaya a rodear de amigos increíbles estudiando la carrera. La amistad y el compañerismo del grupo me hicieron amenas las clases, el resolver cualquier problema o el enfrentarme a los exámenes. Y gracias a eso he llegado a escribir esta tesis. Solo tengo buenos recuerdos de esos años: días de biblioteca, carnavales, paellas, fiestas, conciertos, partidos, viajes y risas en general. Os agradezco mucho a todos los buenos momentos que me habéis hecho pasar. En especial a Álex, Elena, Aitor, Charlie, Miguel, David, Juanra, Alberto, José Luis, Ernesto, Samu, Clara Miralles, Héctor Masía y Marta. La alegría con la que investigo a día de hoy nació gracias a vosotros. Así que muchísimas gracias.

Me gustaría hacer mención especial a los amigos que me han acompañado desde la carrera hasta el doctorado. Quiero darle las gracias a mis míticos amigos, compañeros de piso, de carrera y de doctorado Pablo y Quique. Llevo viéndoos casi todos los días desde hace casi nueve años y no me cansaré nunca. Muchas gracias por el día a día de las comidas en el IFIC, por vuestros consejos, por vuestra ayuda, por estar siempre conmigo, por las innumerables experiencias que hemos vivido y por las que nos quedan. Por supuesto, gracias a José Ángel por su fiel amistad desde el principio de la carrera. Por hacer el esfuerzo de venirte a comer con nosotros durante estos cuatro años, por los partidos de frontón y de pádel, las carreras, los conciertos y sobre todo por las risas que nos echamos. Gracias a Héctor por compartir todas las experiencias del doctorado conmigo: las escuelas, los congresos, las clases, los cursos, Fermilab ... Gracias por las conversaciones post comida de nuestros proyectos y también por mantener a flote el equipo de fútbol (este año, después de ocho, parece que me retiro).

Aparte de a mis amigos de la carrera, quería agradecer a todos mis amigos de Orihuela por estar siempre ahí. Desde que me vine a estudiar a Valencia, me encanta volver los fines de semana para ponerme al día de lo que pasa en la city, para echar algún partidico, para reírme y en general para disfrutar con vosotros. Volver a casa estos dos últimos años no ha sido fácil, pero os agradezco que siempre hubiera algún plan sobre la mesa o alguna cervecica que tomar. Muchas gracias por ser mis amigos desde que tengo memoria.

Quería agradecer a toda mi familia por estar siempre a mi lado y apoyarme de manera incondicional. Le doy las gracias a mis abuelos, abuelas, tíos, tías, primos, primas, y padrinos. Me siento especialmente en deuda con mi tita Inma por preocuparse tanto de mi y de mis hermanos. Le agradezco a mi padre el haberme transmitido su curiosidad intelectual desde bien pequeño y apostar siempre por mi educación, a mi hermano Juanma el ser la alegría de la casa, y a mi hermano Pablo el radiar cariño y sabiduría.

Si a día de hoy soy lo que soy es gracias a mi madre: Antonia Abenza Ortiz. La admiración que siento por ti es infinita. Por tu generosidad, por tu naturaleza luchadora, por tu energía, por tu alegría, por tu arte para cocinar, para cantar, para dar clase, por tu forma de disfrutar de las cosas sencillas, por saber que las claves de la vida son la familia y los amigos. Imposible olvidar tus clases express en Bachillerato preparando la olimpiada de Física. El que siempre invitaras a mis amigos a la casa. Los detalles que has tenido con Andrea. Nuestros días de playa que tanto disfrutábamos. Los viernes por la tarde dándote el parte de la semana. Los aperitivos en la placeta. Hacer cualquier cosa a tu lado era un placer. El compartir mis experiencias contigo me han hecho disfrutarlas el doble. El trabajo y el sacrificio que has hecho por hacer mi vida perfecta es increíble. Te estaré eternamente agradecido mamá. Sé que tú serías la persona que más orgullosa estaría de esta tesis. Así que con mucho cariño te la dedico.

Por último, estoy infinitamente agradecido a la mujer de mi vida: Andrea. Por tu apoyo, amor y cariño constante. No importa lo difíciles que hayan sido las circunstancias que siempre has sabido ponerme una sonrisa en la cara y ayudarme con lo que fuera. Y claro está, que lo bueno a tu lado sabe muchísimo mejor. Imposible olvidar los thais, el cine, los viajes, las carreras, las excursiones, las pelis-manta, los paseos, nuestras conversaciones ... vamos, todo. Tu forma de ser me enamora, dura cuando toca (como cuando me ponía a divagar escribiendo esta tesis), y tierna y súper adorable el resto del tiempo. No puedo imaginar mi vida sin la mujer más guapa, inteligente, trabajadora y buena que conozco a mi lado. Gracias también por descubrirme a la familia González-Montoro. Estoy tremendamente agradecido con tus padres, tus hermanos y tu iaia Fina por cuidarme de esa manera. Andrea, eres la punta de lanza de mi felicidad. De verdad, muchas gracias por todo.

Investigar para esta tesis ha sido un placer. Doy las gracias a todos aquellos que habéis contribuido a mi felicidad durante todos estos años.
¡Va por todos vosotros!

Contents

Chapter 1

An Introduction to Dark Matter

The gravitational evidence for the existence of dark matter is overwhelming. The exquisite measurements of the Cosmic Microwave Background by the WMAP [10, 11] and Planck [12, 13] satellites have shown that 26% of the energy budget of the Universe is encoded in a form of matter that only interacts gravitationally. Furthermore, innumerable studies have shown that galaxies, clusters of galaxies and the vast majority of the virialized objects in the Universe are dominated by some matter that does not emit light, i.e. dark matter. The unambiguous evidence for dark matter strongly contrasts with the absence of signals at laboratory experiments and satellite missions targeting the non-gravitational nature of dark matter.

We devote this introductory Chapter to the astrophysical and cosmological observations that indicate the existence of dark matter and show that dark matter appears to be only gravitationally interacting. As we will examine, modified gravity theories that could account for the velocity dispersion of spiral galaxies cannot explain the observed patterns of the CMB, that can – however – easily be understood from a cold collision-less description of dark matter. In addition, the null searches for MAssive-Compact-Halo-Objects (MACHOs) point towards a fundamental particle description of dark matter. After the survey of astrophysical evidence for dark matter, the standard cosmological model ΛCDM – based on an homogeneous and isotropic Universe, preceded with an inflationary stage – currently dominated by a cosmological constant Λ and cold dark matter (CDM), will be introduced in light of its indisputable success describing the CMB and the large scale observations of our Universe. Additionally, we shall discuss some problems that the ΛCDM faces at galactic and subgalactic scales that motivate dark matter particles that may possess a primordial velocity or exhibit

some interactions with light particles; in particular, with neutrinos. Based on current laboratory and cosmological data, the main broad properties that dark matter candidates should fulfil are outlined. Finally, the most theoretically appealing dark matter candidates are discussed, in particular WIMPs and axions.

1.1 Astrophysical and Cosmological evidence for Dark Matter

The vast evidence from the gravitational interactions of dark matter comes from a diversity of sources, scales and studies. In particular, it is the combination of spiral galaxy rotation curves [14], gravitational lensing [15], and a variety of kinematical measurements [16, 17] that lead to conclude that dark matter is present in clusters of galaxies and galaxies in an amount that considerably exceeds that of normal (or baryonic) matter. Additionally, CMB observations [13] imply that 84% of the matter in the Universe is dark, and furthermore, that 26% of the energy budget of the Universe is encoded in the form of dark matter.

In 1933, Fritz Zwicky [18] discovered that the velocity dispersion of objects in the Coma cluster were too large to be solely explained by the distribution of visible matter in the cluster. He was the first to propose that some non-luminous matter should account for the rest of the matter needed to explain such high measured velocities (see [19] for a historical perspective of the dark matter problem). However, it was not until 1970 that dark matter was firmly established in the community. It was then when Rubin and Ford [20] and also Freeman [21], found that rotation velocities in the outermost regions of the Andromeda galaxy and others do not decrease but remain constant. If there were only baryonic matter, the rotation curves should fall like $v \propto 1/\sqrt{r}$ in the outermost regions of the galaxy. The fact that they flatten is attributed to invisible matter that makes up for the kinematical difference with $M(r) \propto r$ or $\rho(r) \propto r^{-2}$, so that $v = \text{cons.}$ Figure 1.1 shows the galactic rotation curve of the NGC 6503 galaxy. It is remarkable to see that the rotation curves flatten at large radii. Since these pioneers discoveries, many other spiral galactic rotation curves have been measured [14] and together with other astronomical observations [17, 22] show that generically about 95% of the matter in a galaxy is dark.

Galaxy rotation curves are not the only, but one of the many, gravitational evidences for dark matter. Einstein theory of General Relativity treats all matter at the same foot through its contribution to the total energy-momentum tensor. This means that the gravitational bending of

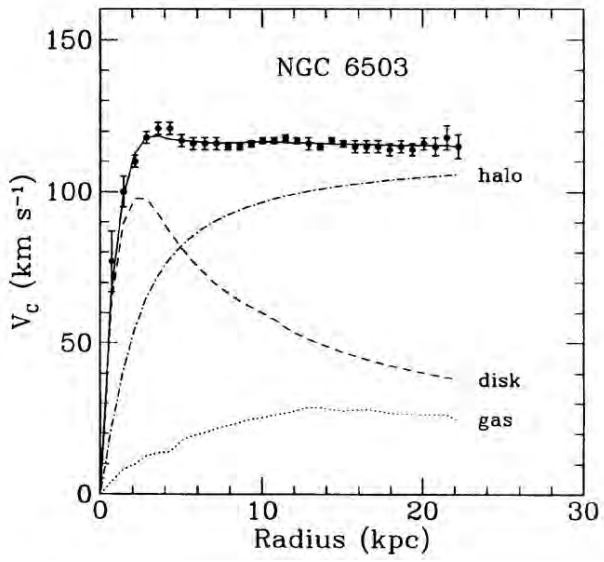

Figure 1.1: Rotation curve of the NGC 6503 spiral galaxy [23]. The curves represent the contribution from the disk, the gas and the dark matter halo. Note that the NGC 6503 galaxy has an optically visible radius of only ~ 5 kpc. The fact that the baryonic content of the galaxy cannot account for the flattening of the rotation curve at large radii requires the presence of a substantial amount of dark matter in galaxies.

light from a source through an object (lens) is only going to depend upon the mass distribution of matter within the lens; independently on the nature of this matter. Therefore, gravitational lensing [24] represents a key tool to measure matter distributions, and thus provides a very good handle on dark matter [15, 25]. In particular, gravitational lensing shows that dark matter is present at extragalactic scales. As an example, Figure 1.2 shows the lensed image of the Bullet cluster [26]. It is a cluster that has undergone a recent collision, and the fact that the mass distribution from the lensing maps reconstruction does not overlap with the X-ray emission means: *i)* that dark matter dominates the matter distribution of the cluster, and *ii)* that dark matter should not interact with itself, since the dark matter distribution was unaffected by the collision processes.

In addition to these astrophysical probes, the cosmological implications of dark matter are exceedingly indisputable. Dark matter is one of the cornerstones of the cosmological model [28, 29], and its leading role in our understanding of the Universe is as the seeder of structure formation [28, 29, 30]. Namely, dark matter perturbations are responsible for the formation of the galaxies and clusters of galaxies that we observe today. Only a Universe with $\sim$84% of the matter being non-baryonic and contributing to $\sim$26% of the energy budget of the Universe is able to reconcile the very small CMB temperature anisotropies $\delta T/T \sim 2 \times 10^{-5}$ [10, 12, 31]

Figure 1.2: Optical image of the Bullet cluster [27, 26] NASA/CXC/CfA. The red region depicts the hot gas distribution as measured in the X-ray spectrum. The blue region represents the dark matter distribution as obtained from the lensing maps. The fact that the blue and red regions do not overlap means that there should be a dominant dark matter component, and also implies that the dark matter should be weakly interacting.

with the highly non-linear Universe that we observe today. The fact that the observed properties of the local Universe ($t = 13.8 \times 10^9$ yr) match precisely those predicted by the extrapolation from the CMB epoch ($t = 3.8 \times 10^5$ yr) provides indubitable evidence for the existence of dark matter and illustrates the success of the cosmological model. Due to the leading role of dark matter in cosmology, in the following sections we present the main building blocks of the standard cosmological model, ΛCDM. In particular, the Big Bang model – based on cosmological homogeneity and isotropy – is shown to be an extraordinary framework in which for instance, the primordial light elements abundances are predicted, and in which the observed patterns of the CMB are successfully linked to the statistics of galaxies in the contemporary Universe.

For completeness, it should be noted that a modification of the Newtonian force at very small accelerations has also been proposed to explain the flattening of rotation curves in spiral galaxies [32, 33]. This framework is the so-called MOND (Modified Newtonian Dynamics) and provides very good fits to galaxy rotation curves. However, MOND has been refuted by observations [34] since this theory cannot account for the gravitational lensing observed in clusters (see e.g. Figure 1.2), or the observed patterns in

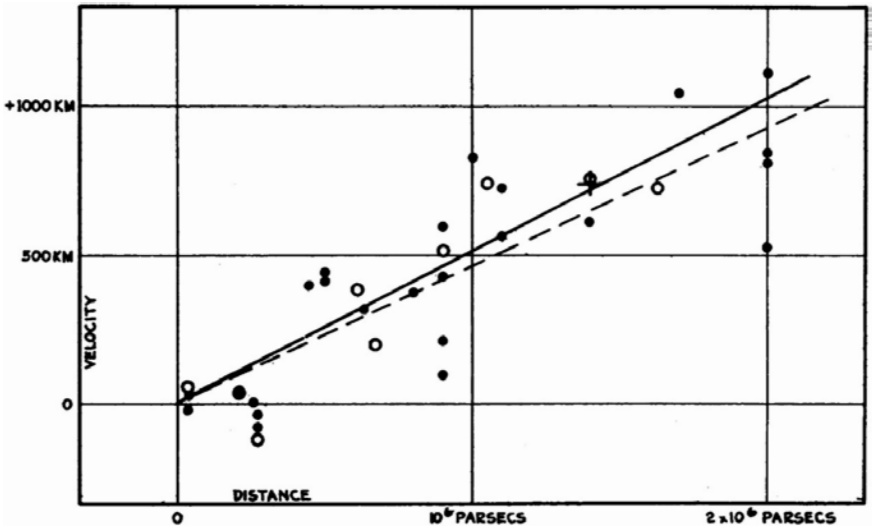

Figure 1.3: Original figure from [35] demonstrating the expansion of the Universe. On the y axis the velocity is expressed in terms of km/s and on the x axis distance is measured in pc $\equiv 3.09 \times 10^{16}$ m. The linear relation is given by Hubble's law $v = cH_0 d$. The fact that distant galaxies are receding at a velocity that scales linearly with the distance is understood as a result of the expansion of the Universe.

the Cosmic Microwave Background and the Large Scale Structure that are described in what follows.

1.2 The Expanding Universe

In 1929, Edwin Hubble [35] discovered that galaxies are receding from us at a velocity proportional to their distance through the study of Cepheid variable stars, see Figure 1.3. The fact that the Universe is expanding was a clear prediction of the Big Bang model under the assumption that the Universe is homogeneous and isotropic. This assumption is usually dubbed the *Cosmological Principle*, and as of today we are very confident that the Universe resembles highly homogeneous and isotropic [12, 13, 36, 37, 38], at least at large scales $L \gtrsim 100\,\text{Mpc}$. In addition, since Hubble's discovery, further evidence for the expansion of the Universe has been accumulated [39]. Through the study of type Ia supernovae two groups demonstrated [40, 41] that our Universe is currently undergoing a period of accelerated expansion. The driver of this accelerated expansion is the so-called dark energy, and as far as we know [13, 39], it highly resembles a cosmological constant Λ in Einstein equations.

The Big Bang theory, namely, the assumption of an homogeneous and isotropic Universe governed by the General Relativity theory, leads to a

very economical and predictive (and so far confirmed, see Sections below) backward evolution of the state of the Universe from now up to only a few milli-seconds from the beginning of the Universe. Dark matter plays an essential role in the evolution of the Universe as we understand it today. In order to comprehend such a role, the basic ingredients for describing our Universe are introduced in what follows.

The starting point of the Bing Bang theory is the assumption of an homogeneous and isotropic Universe. The space-time metric ($g_{\mu\nu}$) that respects rotation and translation invariance, is the Friedmann-Lemaître-Robertson-Walker (FLRW) metric, which in comoving coordinates reads

$$ds^2 \equiv g_{\mu\nu} dx^\mu dx^\nu = -dt^2 + a(t)^2 \left(\frac{dr^2}{1-kr^2} + r^2 d\Omega^2 \right) , \tag{1.1}$$

where $a(t)$ is the scale factor and k is $+1$, 0 or -1 for open, flat or closed space-times. From this expression one easily reads off the physical interpretation of the scale factor; assuming $k = 0$ for simplicity, a region of space of size $d = d_0$ at $t = t_0$ expands to a region of size $d_1 = d_0\, a(t_1)/a(t_0)$ at $t = t_1$. The expansion of the space-time leads to a shift in the frequencies of photons emitted and received at different times. This shift is dubbed *redshift* (z) since the Universe is expanding, and therefore photons emitted from distant galaxies are received with less energy than their emitted one. It can be expressed in terms of the scale factor as:

$$1 + z \equiv \frac{\lambda_{\rm obs}}{\lambda_{\rm emit}} = \frac{a_0}{a} , \tag{1.2}$$

where $a_0 = a(\text{today})$. Therefore Equation 1.2 provides a relationship between the scale factor, and the redshift of photons emitted at a given time.

In order to study the evolution of the scale factor, we shall employ Einstein equations that govern the dynamics of space-time

$$G_{\mu\nu} = 8\pi G\, T_{\mu\nu} , \tag{1.3}$$

where G is Newton's constant, $T_{\mu\nu}$ is the total energy-momentum tensor, and $G_{\mu\nu}$ is the Einstein tensor; that is related to the Ricci tensor and scalar as $G_{\mu\nu} = R_{\mu\nu} - \frac{1}{2} g_{\mu\nu} R$ [1].

Einstein equations connect the evolution of the metric to that of the matter via the energy-momentum tensor and vice-versa. Therefore, in order

[1] The Ricci tensor is related to the Levi-Civita connection as $R_{\mu\nu} = \partial_\alpha \Gamma^\alpha{}_{\mu\nu} - \partial_\mu \Gamma^\alpha{}_{\alpha\nu} + \Gamma^\alpha{}_{\mu\nu}\Gamma^\beta{}_{\alpha\beta} - \Gamma^\alpha{}_{\beta\nu}\Gamma^\beta{}_{\alpha\mu}$. For the Einstein-Hilbert action, the affine connection is given in terms of the metric as $\Gamma^\sigma{}_{\mu\nu} \equiv \frac{1}{2} g^{\sigma\alpha} \left(\partial_\mu g_{\nu\alpha} + \partial_\nu g_{\mu\alpha} - \partial_\alpha g_{\mu\nu} \right)$. The Ricci scalar is defined as $R \equiv R_{\mu\nu} g^{\mu\nu}$.

to study the time evolution of the scale factor, the stress energy tensor that sources the Einstein tensor should be specified. Under the assumption of homogeneity and isotropy, the stress energy-momentum tensor for matter takes the perfect fluid form[2]

$$T_\mu{}^\nu = p\, g_\mu{}^\nu + (\rho + p) U_\mu U^\nu \equiv \mathrm{diag}\,(-\rho, p, p, p)\ , \tag{1.4}$$

where U^μ is the four-velocity of the fluid, ρ represents its energy density, and p is the pressure.

The requirement of energy-momentum conservation $\nabla_\mu T^\mu{}_\nu \equiv \partial_\mu T^\mu{}_\nu + \Gamma^\mu{}_{\mu\sigma} T^\sigma{}_\nu - \Gamma^\sigma{}_{\mu\nu} T^\mu{}_\sigma = 0$ leads to the continuity equation

$$\frac{d\rho}{dt} + 3\frac{\dot{a}}{a}(\rho + p) = 0\,, \tag{1.5}$$

where $\dot{a} \equiv da/dt$. This equation, when particularized to a time independent equation of state $\omega = p/\rho$, allows one to directly integrate it. This provides the evolution of the energy density as a function of the scale factor

$$\rho(a) = \rho(a_0)\left(\frac{a}{a_0}\right)^{-3(1+\omega)}\ . \tag{1.6}$$

Cases of special interest are: non-relativistic matter with $\omega_m = 0$, $\rho_m \propto a^{-3}$, radiation with $\omega_{\mathrm{rad}} = 1/3$, $\rho_{\mathrm{rad}} \propto a^{-4}$, and vacuum energy with $\omega_\Lambda = -1$, $\rho_\Lambda = \mathrm{cons}$. This equation, for radiation, can be recast in terms of the temperature of the radiation fluid. Since for a gas of massless particles $\rho_\gamma \propto T^4$, a very simple relationship between the scale factor and the temperature of the Universe can be established

$$T = T_0\, a_0/a\,, \tag{1.7}$$

where todays temperature is obtained from the CMB intensity spectrum to be $T_0 = 2.7255 \pm 0.0006\,\mathrm{K}$ [43]. From Equation 1.7 we notice that the hotter the Universe, the smaller and the younger it was. Additionally, we notice that it is equivalent to use time, scale factor, temperature or redshift in order to identify a given epoch of the Universe.

Finally, evaluating Einstein equations for the FLRW metric[3] together with the energy-momentum tensor for a perfect fluid results in the Friedmann equations

$$\frac{\dot{a}^2}{a^2} = \frac{8\pi G}{3}\rho - \frac{k}{a^2}\,, \tag{1.8a}$$

$$\frac{\ddot{a}}{a} = -\frac{4\pi G}{3}(\rho + 3p)\ . \tag{1.8b}$$

[2]Note that an imperfect fluid with bulk viscosity will also satisfy the symmetry requirements [42].

[3]For the flat FLRW metric, the only non-vanishing components of the connection are $\Gamma^0_{ij} = \delta_{ij}\,\dot{a}a$, $\Gamma^i_{0j} = \delta^i_j\,\dot{a}/a$.

Concerning the Friedmann equations above two comments are in order: *i)* the acceleration equation for $\ddot{a}(t)$ 1.8b implies that, since our Universe today is expanding ($\dot{a}(0) > 0$), then provided that in the past the weak energy condition is not violated (that is $\rho + 3p > 0$), at some point the scale factor becomes $a \to 0$ which corresponds to the Big Bang singularity (presumably at $t = 0$). And *ii)* Equations 1.5, 1.8a, 1.8b are not independent. Only a combination of two of them is. This is a consequence of the Bianchi identities. Thus, in practice, only Equations 1.5 and 1.8a are used.

The first Friedmann equation permits the introduction of the Hubble parameter, $H \equiv \dot{a}/a$, which represents the expansion rate of the Universe. This means that the time scale of the Universe's expansion is $t \sim H^{-1}$. The Hubble constant H_0 enters precisely the velocity-distance relation found by Hubble $v = cH_0 d$. It is customary to express the Hubble constant as

$$H_0 = 100\, h\, \mathrm{km/s/Mpc}\,, \tag{1.9}$$

where h is the reduced Hubble constant and typically is $h \simeq 0.67$ [13]. Using Equation 1.8a one can define the critical density ρ_c, so that a Universe with such an energy density is flat:

$$\rho_c \equiv \frac{3H^2}{8\pi G}\,. \tag{1.10}$$

The dimensionless ratio of the energy density for a given species compared to that of the critical density Ω is given by

$$\Omega \equiv \frac{\rho}{\rho_c}\,. \tag{1.11}$$

The critical energy density today is $\rho_c/h^2 = 2 \times 10^{-29}\,\mathrm{g\,cm^{-3}}$, this means that the Universe is rather empty, recall that $\rho_{\mathrm{water}} \simeq 1\,\mathrm{g\,cm^{-3}}$.

The introduction of the energy density ratios, together with the evolution of the different species with the scale factor 1.6, leads to a very compact expression for the evolution of the Hubble parameter:

$$H^2 \equiv \left(\frac{\dot{a}}{a}\right)^2 = H_0^2 \left(\Omega_\Lambda(a_0) + \Omega_k(a_0)\, a^{-2} + \Omega_m(a_0)\, a^{-3} + \Omega_{\mathrm{rad}}(a_0)\, a^{-4}\right) \tag{1.12}$$

where the Ω_i represents the current energy density ratio of any given species. Assuming a cosmological model described by a cosmological constant and cold dark matter, ΛCDM, the latest determination of such parameters

are [13]

Cosmological Parameters Planck 2015	
Expansion	$H_0 = 67.3 \pm 0.7\,\mathrm{km/s^{-1}}$
Non-relativistic Matter	$\Omega_m = 0.316 \pm 0.009$, $\Omega_m = \Omega_{\mathrm{DM}} + \Omega_b$
Baryons	$\Omega_b = 0.0492 \pm 0.0006$
Dark Matter	$\Omega_{\mathrm{DM}} = 0.265 \pm 0.004$
Dark Energy	$\Omega_\Lambda = 0.684 \pm 0.009$
Photons	$\Omega_\gamma = (5.5 \pm 0.2) \times 10^{-5}$
Radiation	$\Omega_{\mathrm{rad}} = (9.2 \pm 0.4) \times 10^{-5}$
Curvature	$\Omega_k = -0.004 \pm 0.015$

(1.13)

Thus we notice that there is five times more dark matter than ordinary matter (nuclei). Also note that todays Universe is dominated by dark energy, which – as previously discussed – is the responsible for the accelerated expansion of the Universe [40, 41] (see [44] for a review of the observational probes for cosmic acceleration). So far, all cosmological observations imply that dark energy behaves like a cosmological constant term in Einstein equations, with a time independent equation of state $\omega_\Lambda = -1$ [13, 39]. It is worth mentioning that the accuracy of these cosmological parameters is at the percent level. Figure 1.4 depicts the evolution of the energy density ratios given the current measured cosmological parameters in ΛCDM. The time at which the energy density in matter and radiation becomes equal is pivotal for structure formation (see Section 1.2.4) and corresponds to a redshift $z_{eq} \sim 3300$ [13]. Figure 1.5 depicts the energy density encoded in various species at three key epochs of the Universe.

The Friedmann Equations 1.8 together with the continuity Equation 1.6 provide the necessary ingredients to investigate how the scale factor $a(t)$ evolves with time depending on the dominant form of matter contributing to the Universe's budget. Here we will explicit the solutions for Radiation Dominated (RD), Matter Dominated (MD) and deSitter (empty Universe) because our Universe has undergone each of these stages throughout its history. We realize that $a(t) \propto t^{2/3(1+\omega)}$, where ω is the equation of state for the dominant source of energy. This result particularized for RD, MD, and deSitter Universes reads

$$a(t) \propto t^{1/2}\,, \qquad \text{(RD)} \tag{1.14}$$

$$a(t) \propto t^{2/3}\,, \qquad \text{(MD)} \tag{1.15}$$

$$a(t) \propto e^{tH}\,. \qquad \text{(de Sitter)} \tag{1.16}$$

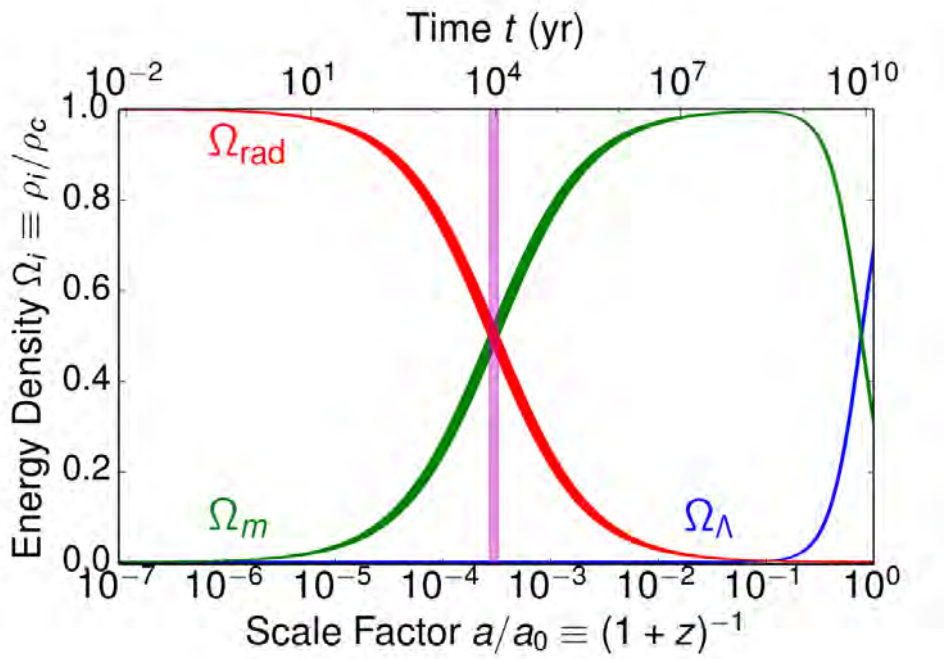

Figure 1.4: Evolution of the fractional energy densities Ω_i for ΛCDM. The thickness of the curves represents the 95% uncertainty from the cosmological parameters 1.13. The vertical magenta region depicts the matter radiation equality $z_{eq} \simeq 3300$.

Finally, it is convenient to introduce the conformal time

$$\tau \equiv \int_0^t \frac{dt'}{a(t')} = \int_0^a \frac{da'}{a'} \frac{1}{a'H(a')}\,, \tag{1.17}$$

so that $d = c\,\tau$ is the maximum distance that light could have travelled since the beginning of the Universe. Namely, τ can also be interpreted as a comoving horizon, i.e. the maximum distance between two causally connected points.

1.2.1 Big Bang Nucleosynthesis

When the Universe was only one second old, its temperature was very high $T \sim 10^{10}\,\mathrm{K} \sim$ MeV and all its components formed a hot dense plasma (as can be appreciated in Figures 1.4-1.5 the solution of the Friedmann equations 1.8 renders a hot radiation dominated early Universe). At such high temperatures, the Universe was so hot that there were no bound nuclei in the plasma (the binding energies of nuclei are $2.2\,\mathrm{MeV} < B < 8.8\,\mathrm{MeV}$). Due to the expansion, as the Universe cooled down, the photons and neutrinos present in the plasma were eventually not energetic enough to destroy

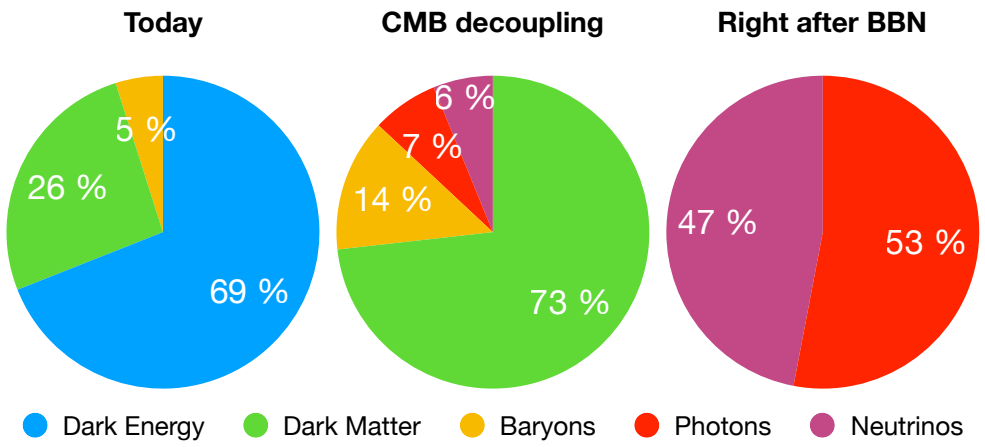

Figure 1.5: Energy density ratios at three key epochs in the expansion history of the Universe.
Left: The contemporary Universe, $t_0 = 13.8\,\text{Gyr}$ and $T_\gamma = 2.725\,\text{K} = 2.4 \times 10^{-4}\,\text{eV}$. *Middle:* The instant at which the photons decoupled from the electrons in the Universe. Namely, the CMB decoupling, $t_{\text{CMB}} \simeq 380.000\,\text{yr}$, $T_\gamma \sim 0.26\,\text{eV} \simeq 3000\,\text{K}$ and $z \sim 1100$. *Right:* The Universe right after the primordial element abundances formed $t \sim 3\,\text{min}$.

the bound nuclei and a certain amount of them remained. One of the main successes of the Big Bang model is the prediction of the primordial abundances of the light elements, namely Hydrogen (H), Deuterium (D), Helium (^{3}He, ^{4}He) and Lithium (^{7}Li) (the primordial abundances of heavier nuclei are negligible). The prediction for the light element abundances was carried out already in 1940-1950 by Gamow and collaborators [45] and later improved in [46]. The prediction of the light element abundances is solely a function of the baryon-to-photon ratio, namely $\eta = (n_B - n_{\bar{B}})/n_\gamma$, which is equivalent to a baryon density $\Omega_b h^2 \simeq 3.7 \times 10^7\,\eta$. Astrophysical measurements of the primordial abundances, in particular that of Deuterium, imply $0.021 < \Omega_b h^2 < 0.024$ at the 95% CL [47]. Figure 1.6 shows the predicted and observed element abundances as a function of the baryon-to-photon ratio. We notice the very good agreement between BBN and the CMB value for $\Omega_b h^2$, where $\eta \sim 6 \times 10^{-10}$ as inferred by CMB observations [13]. The only measured abundance that does not agree with the predictions is Lithium. This is the so-called Lithium problem[4] [48, 49].

It is worth going a step back in order to stress the importance of BBN in our understanding of the Universe. Recall that the only assumption of the Big Bang model was that of cosmological homogeneity and isotropy. When applied within the framework of General Relativity it leads to a prediction

[4]The discrepancy between the observed Lithium abundance could be a result of *i)* a stellar depletion mechanism or *ii)* new physics. However, at this point in time there is no clear resolution to the Lithium problem [48, 47]. Nevertheless, the remarkable concordance between the Deuterium abundance and the CMB expectation, is a non-trivial success.

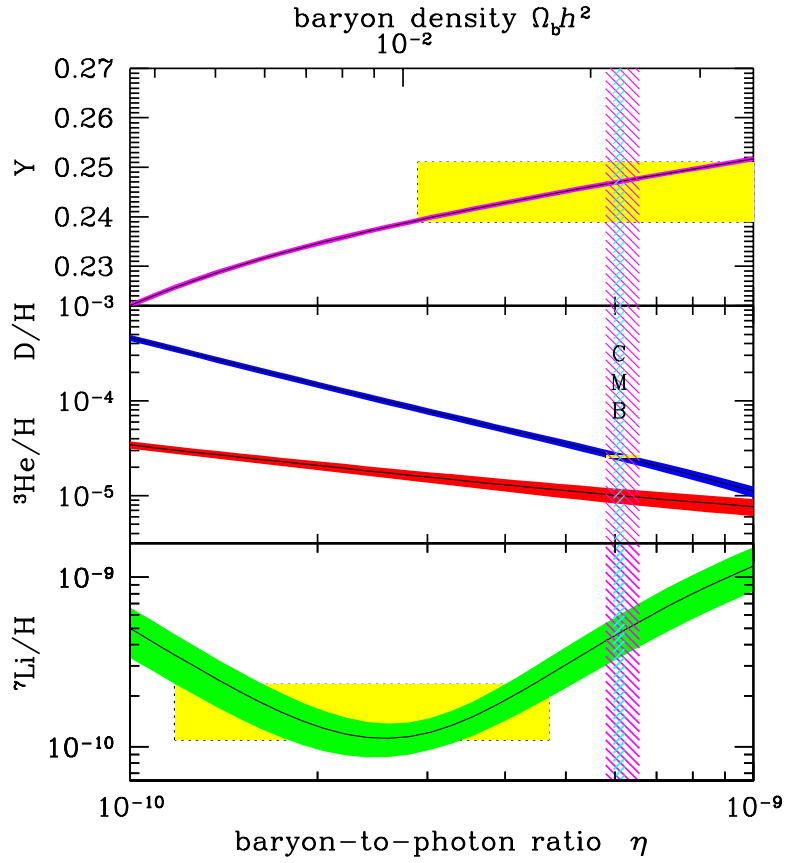

Figure 1.6: BBN predictions (bands) and measurements (boxes) of the primordial light element abundances with respect to H as a function of the baryon-to-photon ratio η and $\Omega_b h^2$ (reproduced from [47]). Y corresponds to the ^{4}He abundance. The vertical contours represent the induced values for $\Omega_b h^2$ from BBN and from CMB observations [13]. The excellent agreement between the BBN predicted abundances and those measured in stellar systems provides a very powerful check of the cosmological model. In addition, the agreement between the required $\Omega_b h^2$ at both the CMB and BBN epochs increases the confidence in the standard cosmological model.

for the light element abundances in the present Universe. The extrapolation of the Universe from $t_0 \simeq 13.8\,\mathrm{Gyr}$ to $t \sim 1\,\mathrm{s}$ is enormous, yet the predicted abundances from BBN confront very successfully the observed ones in our local Universe [47]. Therefore, BBN represents a solid validation of the assumptions and framework of the Big Bang theory.

The implications of BBN for dark matter existence are evident. Since the measured primordial abundances of the light elements imply $0.021 < \Omega_b h^2 < 0.024$ at 95% CL [47], while the total amount of matter is $\Omega_m \sim 0.3$ [17] or equivalently $\Omega_m h^2 \sim 0.14$, there should be about five times more dark matter than ordinary matter. Additionally, the success of BBN implies that dark matter should be non-baryonic.

1.2.2 Inflation

The achievement of BBN demonstrates that the Big Bang model provides successful extrapolation of the state of the Universe up to when it was only 10^{-2} s old. Yet, the Big Bang model – although proven extremely powerful – cannot address a couple of questions on its own: *i)* why is the Universe homogeneous and isotropic? This is the starting point hypothesis of the model. *ii)* Why is the Universe so flat? The CMB shows that $|\Omega_k| < 0.008$ [13] while from the Friedmann equations 1.8 we expect the curvature term to be dominant at late times. *iii)* Why is the CMB isotropic? When evaluating the comoving horizon 1.17, one notices that assuming a radiation dominated early Universe only regions of the CMB with $\theta < 1^\circ$ should have been in thermal contact, making very difficult to explain the highly isotropic CMB observations [12].

These questions are elegantly addressed if the Universe had undergone a period of accelerated expansion at very early times $t \sim 10^{-34}$ s. This accelerated expansion of the Universe is known as Inflation [50, 51, 52]. Independently of the initial conditions of the Universe; namely, even with a considerably inhomogeneous or anisotropic initial Universe, if the primeval Universe expanded exponentially e^N, with $N = 50 - 60$, then the Universe after such accelerated expansion will be extremely flat and smooth. Physically, it is easy to understand that this will be the case. If a very small region of the Universe exponentially inflates that would smooth any originally present spatial curvature or inhomogeneity on it. Clearly, the comoving horizon will be expanded by e^N and therefore the entire CMB observation will correspond to a single region of space that was originally in thermal contact, explaining its isotropy.

The inflationary stage of the Universe is usually driven by a scalar field. The Inflationary paradigm, in addition to provide an answer to the unaddressed questions of the Big Bang model, provides the seed for primordial inhomogeneities in the smooth Universe. These seeds correspond to the quantum fluctuations of the scalar field that drives the accelerated expansion period [53]. Inflation predicts an almost scale invariant primordial spectrum of cosmological perturbations. A cosmological density perturbation is defined as

$$\delta(\vec{x}) \equiv \frac{\rho(\vec{x}) - \langle\rho\rangle}{\langle\rho\rangle}\,, \tag{1.18}$$

where $\langle\rho\rangle$ is the mean density. Since the Universe is homogeneous and isotropic, it is customary to work in terms of quantities in Fourier space: $\delta(\vec{k})$ represents the Fourier transform of $\delta(\vec{x})$. The mean of a cosmological perturbation vanishes, i.e. $\langle\, \delta(\vec{k}) \,\rangle = 0$ due to isotropy and homogeneity.

But the variance is non-vanishing and given by

$$\langle\, \delta(\vec{k})\delta(\vec{k}')\,\rangle = (2\pi)^3\,\delta^3(\vec{k}-\vec{k}')\,P(k)\,, \tag{1.19}$$

where $P(k)$ is the power spectrum, which is usually parametrized as a power law $P(k) \propto k^{n_s-4}$. The inflationary prediction [53] is that $n_s \simeq 1$. This is the so-called Harrison-Zeldovich scale invariant spectrum (the delta function requires $[P] = [k]^{-3}$ and therefore if $n_s = 1$, the spectrum is scale invariant).

The ΛCDM cosmology assumes a primordial power spectrum of cosmological perturbations with $P(k) = (2\pi)^2\, A_s k^{n_s-4}$. In practice A_s and n_s are treated as unknown cosmological parameters and their latest determination is $n_s = 0.9653 \pm 0.0048$ and $A_s = (2.13 \pm 0.05) \times 10^{-9}$ [13]. The fact that n_s is slightly below 1 is also a prediction of Inflation [53] and it is understood as a feature of the end of Inflation. In addition to the previously discussed predictions, Inflation leads to a cosmological relic of gravitational waves whose effect in the CMB polarization spectra can potentially be measured by next generation of CMB experiments [54].

1.2.3 The Cosmic Microwave Background

When the Universe was 380.000 years old, and its temperature ∼3000 K, the photons became cold enough to permit the electrons in the Universe to combine with the nuclei to form atoms. This process is known as *recombination*. As soon as the electrons and present nuclei formed neutral atoms, the photons – that were more numerous than the electrons by a factor $\sim 1.7 \times 10^9$ – suddenly decoupled from the matter and were able to travel freely. Such a flash of light is the Cosmic Microwave Background. At that point in time the Universe became visible.

The CMB was discovered in 1965 by Penzias and Wilson [55], and was immediately understood as a clear consequence of the expanding Universe [56]. The CMB consists of a very isotropic background of electromagnetic radiation with a temperature $T_0 = 2.7255 \pm 0.0006\,\mathrm{K}$ [43]. The frequency spectrum of this radiation has been measured with very high precision by the FIRAS detector at the COBE satellite [57] and resembles that of a black body to an astonishing degree of accuracy (see Figure 1.7).

In addition to the frequency spectrum, the angular fluctuations of the CMB have been measured to a very high degree of accuracy by the Planck satellite [12]. Such angular anisotropies are at the level of 10^{-5} and 10^{-6} for temperature and polarization respectively. These angular fluctuations are

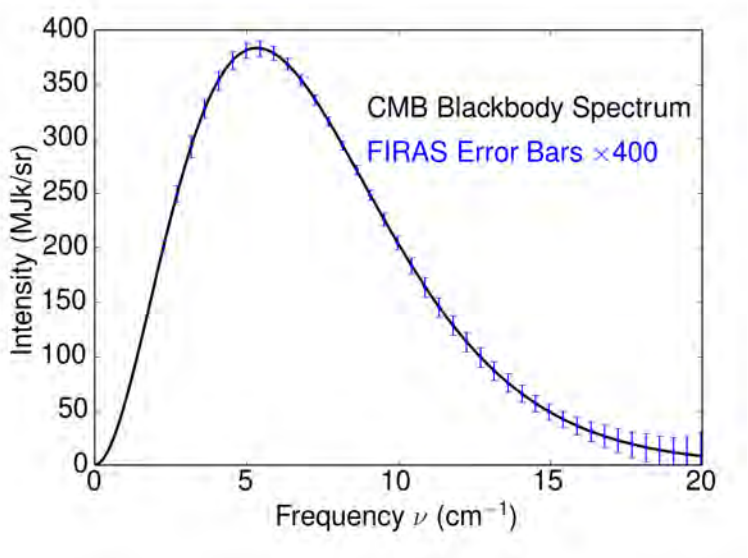

Figure 1.7: Measurements of the CMB frequency spectrum by the FIRAS detector at the COBE satellite [57] and comparison with the black body spectrum with $T_{\rm CMB} = 2.7255\,{\rm K} = 0.2349\,{\rm meV} = 11.91\,{\rm cm}^{-1}$. The agreement between the measurements and the black body spectrum is remarkable.

usually described in a spherical harmonic basis $Y_{\ell m}$:

$$T(\theta,\phi) = \sum_{\ell} \sum_{m=-\ell}^{m=\ell} a_{\ell m} Y_{\ell m}(\theta,\phi)\,. \tag{1.20}$$

The angular scales anisotropies are related to the multipole ℓ by $\theta \simeq \pi/\ell$. The monopole term ($\ell = 0$) corresponds to the measured CMB temperature, T_0. And the dipole term ($\ell = 1$) is interpreted as the Doppler boosting of the monopole term by the Solar system peculiar motion. For $\ell \geq 2$, the mean of the amplitudes vanish $\langle a_{\ell m}\rangle = 0$ (due to the homogeneity and isotropy of the Universe). Therefore, CMB observations are presented in terms of the variance (two-point correlation function) of the angular fluctuations:

$$C_\ell \equiv \frac{1}{2\ell+1} \sum_{m=-\ell}^{m=\ell} |a_{\ell m}|^2\,. \tag{1.21}$$

The anisotropies of the CMB are associated with inhomogeneities in the density perturbations of the photon fluid at the time of CMB decoupling, $4\,\delta T/T \sim \delta\rho_\gamma/\rho_\gamma$. Furthermore, the anisotropies of a given multipole are related to a density perturbation at a comoving scale of $k \sim \ell/\tau$ (where τ is the comoving horizon 1.17), so that the lowest multipoles are associated with the largest scales in the Universe. To be more precise: a temperature fluctuation in the CMB is a result of the line of sight integration of

the projection onto a 2D sphere of the photon temperature perturbations from the time of decoupling until today. Therefore, the temperature and polarization CMB spectra carry information of the Universe at the CMB decoupling and from its subsequent evolution due to this integrated effect. In particular, the CMB photons are affected by the gravitational potential and by the electron ionization fraction along the line of sight. At $z \simeq 1100$ the electrons and nuclei formed atoms, but as structures started to form at $z \lesssim 20$, the baryonic matter in them began to collapse and to form stars so that electrons became eventually free again. Observations show that by redshift $z \simeq 6$ the Universe should be fully reionized [58].

The most precise CMB observations have been obtained by the Planck satellite [12]. Figure 1.8 shows their measurements of the CMB angular temperature power spectrum. All these features have a physical interpretation. In particular, the very low multipoles are a result of the Sachs-Wolfe effect. They are due to the gravitational redshifting of photons from the primordial density fluctuations, and due to the gravitational effect of the matter distribution along the line of sight (integrated Sachs-Wolfe effect). The oscillatory peak structure is due to the harmonic nature of the coupled photon-baryon system of density fluctuations in the early Universe. Finally, the decrease of power at high multipoles is called Silk damping, and it is a result of the erase of small scale fluctuations due to Thompson scattering between the photons and electrons at the time of decoupling. The reader is referred to [59] for a careful description of the various effects and the impact of the cosmological parameters on the CMB spectra. And to the Boltzmann codes CLASS [60] and CAMB [61] for fast numerical evaluation of the CMB temperature and polarization spectra for various cosmological scenarios.

The exquisite CMB observations by the WMAP [10, 11] and Planck [12, 13] satellites have initiated the precision era in cosmology. The temperature and polarization spectra are so well measured that uncertainties on the cosmological parameters are set at the per-cent level. The CMB plays a fundamental role for the understanding of dark matter. First, with out the presence of dark matter it would be impossible to explain its features [12], thus confirming its existence. Second, it provides the most precise determination of the cosmological abundance of dark matter [13]. And third, it is extensively used to probe the non-gravitational nature of dark matter (see for instance Chapter 4, the Planck 2015 analysis [13], or the scientific publications [1, 2] presented in their full form in Part II of this thesis).

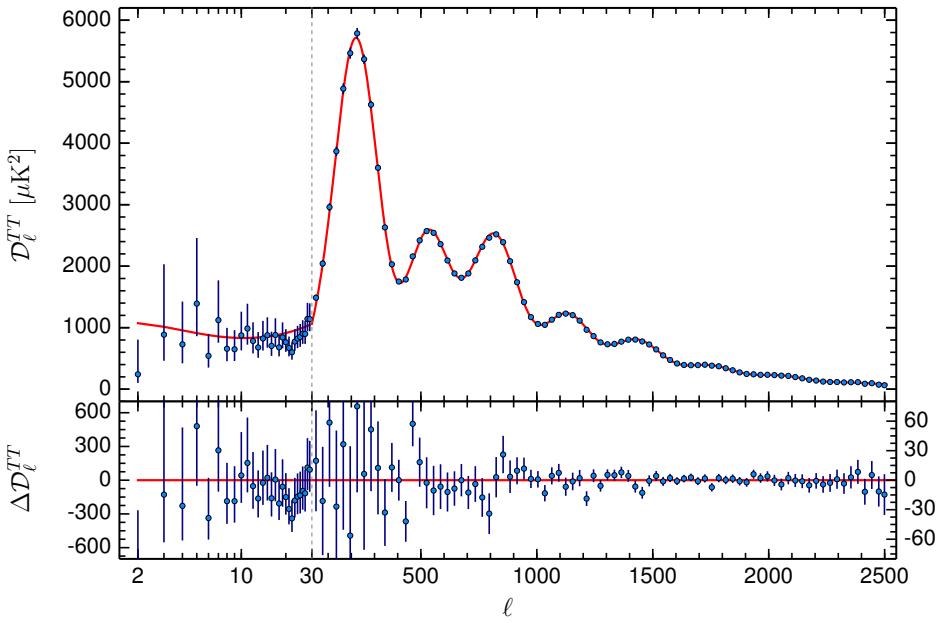

Figure 1.8: The angular CMB temperature power spectrum as measured by the Planck satellite [12, 13] (blue). The solid curve represents the best fit model. The accuracy of these measurements is unprecedented. Their interpretation provides the deepest understanding of the Universe to date.

1.2.4 Large Scale Structure

The fact that observations of the local Universe precisely match the CMB predictions makes the ΛCDM cosmological model extremely compelling. And in particular, makes the dark matter existence indisputable. Therefore, it is in order to briefly review what is the basic picture of structure formation, what are the main local cosmological probes, and what is their role in our understanding of the cosmological model.

Dark matter perturbations in the Universe are able to grow when the pressure of the Universe is small enough. This occurs after the matter-radiation equality $z_{eq} \simeq 3300$ ($t_{eq} \sim 10^4\,\mathrm{yr}$, see Figure 1.4). After matter-radiation equality matter perturbations grow linearly with the scale factor [30, 62]. However, baryonic perturbations are strongly coupled with photons until the CMB decoupling, and therefore only start growing by $z \simeq 1100$. Thus, in order to explain the very small CMB angular anisotropies [31, 10, 12] the dark matter should be the seeder of the potential wells for the galaxies and clusters of galaxies that we observe today. In particular, the CMB observations imply that $\delta\rho_{DM}/\rho_{DM} \sim 10^{-3} - 10^{-4}$ at the time of CMB decoupling. Accordingly, by redshift $z \sim 20$ the cosmological perturbations become non-linear (that is, decoupled from the universal expansion,

collapsed and reach a dynamical state near virial equilibrium [63, 64]), and hence Large Scale Structures (LSS) began to form. For excellent treatments of linear cosmological perturbations see [65, 66] and for reviews on the role of dark matter in the LSS see [28, 67].

- Baryon Acoustic Oscillations

  The electro-gravitational baryon-photon-gravity system leads to harmonic features in the photon and baryon density perturbations. These interactions lead to observational consequences in both the CMB anisotropies and in the distribution of galaxies in the local Universe. Particularly, the first peak of the CMB spectrum located at $\theta \simeq 0.8^\circ$ corresponds to an enhancement of the two-point correlation function of galaxies at $L \simeq 150\,\mathrm{Mpc}$ [62, 68]. This is the so-called BAO peak. The combination of CMB and BAO measurements provides further evidence for the ΛCDM model and reduces the uncertainties on various cosmological parameters. Currently BAOs are measured at redshifts $z \lesssim 1$ [68], see e.g. Refs. [36, 37, 38] for current data analysis and Refs. [69, 70] for future prospects.

- Weak Lensing

  The gravitational potential induced by the LSS of the Universe leads to small but observable magnifications and deformations of galaxy images [15]. The latest weak lensing measurements have been obtained by the Dark Energy Survey (DES) [71] with an accuracy on the growth of linear cosmological perturbations comparable to those reported by Planck CMB observations [12]. These two probes show an excellent agreement, therefore confirming the standard cosmological model ΛCDM and constraining several of its extensions.

- The Lyman-α forest

  The Lyman-α forest is an absorption phenomenon seen in the spectra of high redshift quasi stellar objects. The presence of the forest in the spectra is due to absorption from the ionized intergalactic medium, where most of the baryonic matter is stored. There are various astrophysical and cosmological implications of the Lyman-α forest [72]. In particular, it provides a very precise test of the dark matter substructure. CDM is expected to have plenty of substructure at small scales [73, 74]. The Lyman-α measurements [75, 76] are consistent with CDM substructure and therefore set very stringent constraints on dark matter particles that may suppress such rich substructure, as it could happen in the case of sterile neutrino dark matter [77, 78] or ultra light dark matter [79, 80].

1.3 Beyond the CDM scenario

The success of ΛCDM by describing all present astrophysical and cosmological observations at scales $L \gtrsim 1\,\mathrm{Mpc}$ is outstanding. In order to contrast cosmological measurements of the cosmic, cluster, galactic and sub-galactic observations with the predictions of the cosmological model it is necessary to rely on very powerful cosmological simulations. As soon as perturbations become non-linear, i.e. when $4\pi(k/2\pi)^3 P(k) > 1$ (see Equation 1.19) which corresponds to $k > 0.12\,\mathrm{h\,Mpc^{-1}}$ in ΛCDM, the perturbations decouple from the Universe's expansion and collapse. This non-linear process, although highly complicated, can be analytically investigated [63, 64]. However, a reliable comparison between observational data to theoretical predictions demands for high resolution cosmological simulations. The historical and current role of N-body and hydrodynamical simulations in our understanding of structure formation is impressive [28]. Particularly, N-body simulations have shown that structures form hierarchically through mergers of objects with a very wide range of mass, that the spherically averaged density profile of halos has an approximately universal form given by the NFW profile $\rho_{NFW}(r) = \rho_s/[(r/r_s)(1 + (r/r_s)^2)]$ [73, 74], and also that halo shapes are generically triaxial.

However, despite these successes, there are several discrepancies at galactic and sub-galactic scales that the cold dark matter paradigm faces [81, 82, 83]. Namely, the *missing satellites problem*. This is related to the fact that the number of observed Milky Way dwarf satellites ~ 50 [84] is well below the expected number of CDM subhalos found in numerical simulations ~ 1000 [85, 86]. Another problem is the *core v.s. cusp problem*. Namely, that the observed cores of many dark matter dominated galaxies are both less dense and less cuspy than naively predicted in ΛCDM [87, 88]. Finally, there is the *too-big-to-fail problem*, i.e. the central densities of CDM simulated dwarfs are higher than the central densities observed in the real galaxies [89] (and hence, too-big-to-fail in forming stars).

There are two possible avenues for resolving these problems. First, it may be the case that numerical CDM simulations do not account for all relevant baryonic effects (stellar cooling, supernova feedback ...) and that may be spoiling observations versus predictions [81, 82, 83, 67]. Or second, these problems may be a consequence of the non-cold nature of dark matter. From the theoretical particle physics perspective, there are various candidates that could potentially account for these discrepancies [90]. Examples are warm dark matter models with ∼keV masses [91, 92], dark matter interacting with light SM particles like photons or neutrinos [93, 94], hidden sector particles [95, 96], and dark matter particles with potential

self-interactions [97, 98, 99]. It is worth pointing out that several of these models suffer stringent constraints from the Lyman-α forest [100, 77, 78].

It is unclear whether these problems are due to the a non-cold behaviour of the dark matter particle or to baryonic effects not fully accounted for in the cosmological simulations [81]. However, from the observational perspective, future galaxy surveys – particularly LSST [101] – are expected to discover new faint, distant dwarf galaxies. The determination of their number and masses may provide the solution to the small scale crisis within the ΛCDM paradigm.

The small scale problems are of special interest for both the particle and cosmology communities since may represent the bridge between the extensions of both the Standard Model of particle physics and that of cosmology.

1.4 Dark Matter Properties

The astrophysical and cosmological evidence for dark matter is striking (as discussed in the previous sections). However, even though only the gravitational effects of dark matter have been observed, there are several constraints on the nature of the dark matter based on a multitude of observations. In what follows we detail the broad main ingredients that a dark matter candidate should posses in order to be consistent with all the current observational data.

1. Dark matter should be non-baryonic.

   The possibility of dark matter being formed by MACHOS [102] like Jupiter-like planets or stellar objects with masses below $M_\odot$ was ruled out by microlensing observations [103, 104]. Furthermore, compact objects made out of baryons should contribute to $\Omega_b h^2$ both at the BBN and CMB epochs and that is strongly ruled out by observations, since $\Omega_b h^2 = 0.02225 \pm 0.00016$ while the total matter density is $\Omega_m h^2 = 0.142 \pm 0.002$ [12].

2. CDM-like cosmological perturbations at scales $L \gtrsim 1\,\mathrm{Mpc}$.

   The outstanding success of cold dark matter in explaining the large and intermediate scale observations of the Universe places severe constraints on dark matter candidates that do not behave as cold dark matter at scales $L \gtrsim 1\,\mathrm{Mpc}$. This is a result of CMB observations [13] ($50\,\mathrm{Mpc} \lesssim L \lesssim 10^4\,\mathrm{Mpc}$), supplemented by BAO measurements [68, 36, 37, 38] ($30\,\mathrm{Mpc} \lesssim L \lesssim 200\,\mathrm{Mpc}$), and results from the Lyman-α forest [75, 76, 77, 78] ($1\,\mathrm{Mpc} \lesssim L \lesssim 20\,\mathrm{Mpc}$).

3. Dark matter should be collision-less.

   In order to explain the measurements of colliding clusters like the Bullet cluster [26] (see Figure 1.2) or the ellipsoidal form of halos required by spiral galaxy rotation measurements [105], dark matter self interactions [98] must be somewhat small $\sigma/m \lesssim 1\,\mathrm{cm}^2/\mathrm{g} \simeq 2 \times 10^{-24}\,\mathrm{cm}^2/\mathrm{GeV} = 2\,\mathrm{barn}/\mathrm{GeV}$ [105, 106, 107, 108, 109].

4. Dark matter should be weakly interacting with SM particles.

   Dark matter particles with electric charge [110] are ruled out for a variety of reasons [111]. Were the dark matter to be milli-charged ($q = \epsilon\, e$, where $\epsilon < 1$) the former constraints would be relaxed but still strong [112, 113]. Additionally, if dark matter is neutral, constraints on its electric and magnetic dipole moments still apply [114].

   Strongly interacting (with nuclei) dark matter particles [115] are ruled out since they would lead to an abnormal Earth heating rate as they would greatly exceed the measured heat flow of the Earth [116].

   The dark matter-neutrino interactions are considerably less constrained due to the elusive nature of neutrinos. Cosmological and astrophysical implications of dark matter-neutrino interactions have been studied in detail [1, 9, 117, 118, 119, 120] but these constraints are extensively less severe than for charged or strongly interacting dark matter particles.

5. The dark matter should be long lived.

   In order to account for the astrophysical observations of non-luminous matter in the Universe, the dark matter lifetime should be at least larger than the age of the Universe, $t_0 = 13.8\,\mathrm{Gyr}$ [13]. Depending on the decay channel and on its mass, its lifetime may be considerably higher [121].

To conclude, it is worth noticing that the requirement number 2 above precludes the possibility of the dark matter being composed primarily out of neutrinos. Neutrinos are hot relics and significantly reduce the dark matter substructures at rather large scales [122]. Were the dark matter to be an elementary particle, since the rest of the SM particles are either charged or short lived, the SM should be extended.

1.5 The Theory Landscape

There is a vast number of dark matter candidates in the literature. Many are theoretically well motivated candidates that satisfy the required properties listed above. The majority of these dark matter candidates are fundamental particles that are a product of, or come naturally with, a solution to one or several missing pieces of the Standard Model of particle physics: the hierarchy problem, the strong charge-parity (CP) problem, the neutrino masses, or the baryon asymmetry of the Universe. To date, the two most studied and leading dark matter candidates are WIMPs and axions. Additionally, considerable attention and interest has been given to other candidates as sterile neutrinos, asymmetric dark matter, and to primordial black holes. This list of candidates is far from being complete but certainly reflects the most popular ones. The reader is referred to [123, 124, 125] for other dark matter candidates that do not fall within these categories.

1.5.1 WIMPs

Weakly Interacting Massive Particles in the MeV-TeV mass range with interactions that are mediated by the exchange of electroweak-scale particles can be produced in the early Universe precisely in the right amount to account for the current dark matter abundance [126, 127, 128, 129]. This is the so-called WIMP miracle (see Section 3.2.1). This consideration, together with the theoretical arguments favouring the presence of new physics at the electroweak scale, has motivated the WIMP to be the leading dark matter candidate. In particular, Supersymmetry (SUSY) [130], which potentially addresses the electroweak hierarchy problem and enables gauge coupling unification, provides a natural candidate: the neutralino [131, 132, 133, 134]. However, note that WIMPs have been studied within the SUSY framework and also in other theoretical schemes. WIMPs are thermally produced in the early Universe by a freeze-out of their annihilations with light particles in the plasma. Given their production mechanism, three main WIMP detection avenues are therefore possible: *i)* direct detection; namely, the search for nuclear recoils from dark matter scatterings with nuclei at laboratory experiments, *ii)* indirect detection; i.e. the search for the WIMP annihilation products in the recent and contemporary Universe, and *iii)* collider searches; specifically via searches for particle collisions with missing energy. To date, no confirmed signal has been claimed by any experiment targeting WIMP dark matter [135, 136, 137, 13, 138, 139, 140]. These null searches are translated to non trivial constraints on very well motivated WIMP candidates (see Chapter 4 for further details). Huge experimental efforts are devoted to the search of WIMP dark matter particles, with current and near

future experimental sensitivities capable of testing a wide variety of WIMP dark matter candidates [141, 142, 143, 54, 144, 145]. These efforts will either confirm the existence of WIMP dark matter particles or substantially disfavour the WIMP hypothesis in favour of other candidates. Therefore, the following decade will be of special interest for WIMP dark matter.

1.5.2 Axions

The Peccei-Quinn mechanism is the most compelling and elegant solution to the strong CP problem of the SM [146]. The axion is the particle predicted in such mechanism [147, 148]. Yet, the axion mass is not predicted by the Peccei-Quinn mechanism itself, but depends upon the energy scale at which the mechanism is realized. It has been shown that axions with masses in the range $1 - 100\,\mu$eV could account for the dark matter of the Universe through the misalignment mechanism [149, 150, 151]. Essentially, dark matter axions will be produced in the early Universe as a result of coherent oscillations of the axion field that would result in bosonic condensates of zero momentum, and thus will behave as CDM. The couplings between dark matter axions and the rest of SM particles are model dependent but generically very small, so that, such axions go by the name of "invisible axions". The two benchmark realizations of the Peccei-Quinn mechanism at high energy scales are the KSVZ [152, 153] and DFSZ [154, 155] models. The most promising technique for detecting dark matter axions is through resonant axion production at electromagnetic cavities [156]. The ADMX collaboration [157] has been the first to test the KSVZ and DFSZ expectations ruling out axions with masses $m_a = 2.65 - 2.8\,\mu$eV. Experimental efforts for testing the axion dark matter hypothesis are under way and most of the parameter space of interest for axion dark matter is expected to be tested in the near future [157, 158]. For more details about the cosmological and particle physics implications of the axion we refer the reader to [126] and [159], and for recent developments to [160, 161].

1.5.3 Sterile Neutrinos

Neutrino masses are an obvious missing piece of the SM of particle physics. The most economical way of accounting for them is through the introduction of sterile neutrinos (see Chapter 2). Sterile neutrinos with masses of the order of the keV have been shown [162] to be a plausible dark matter candidate (see [163] for a thorough review on the subject). The sterile neutrino dark matter hypothesis is particularly appealing for a variety of reasons: *i)* such dark matter particles can naturally be produced

in the early Universe via oscillations with light active neutrinos [162], *ii)* as warm dark matter candidates, sterile neutrinos could provide a solution to the small-scale structure problems present in the CDM paradigm [91] (see Section 1.3), and *iii)* an X-ray signal at 3.5 keV as observed by Chandra [164, 165] could potentially be attributed to a sterile neutrino radiative decay. However, this scenario – although theoretically appealing [166] – to date is under strong pressure since a combination of cosmological observations together with other X-ray searches have ruled out most of the relevant parameter space region of masses and mixings attributed to sterile neutrinos as dark matter [77, 78, 167].

1.5.4 Asymmetric dark matter

The very small measured baryon-to-photon ratio in the Universe points towards a tiny asymmetry ($\sim 10^{-9}$) in the early Universe between particles and antiparticles. The motivation behind asymmetric dark matter [168] is the observation that the ordinary and dark matter abundances are comparable, $\Omega_{DM} \sim 5 \times \Omega_b$. The idea is that the mechanism that produces such asymmetry is common for both the baryons and the dark matter particles [169]. Asymmetric dark matter particles do not annihilate in the contemporary Universe, but can still be probed by a variety of searches and techniques. We refer the reader to [170] for a review of models and constraints.

1.5.5 Primordial Black Holes

Primordial black holes (PBHs) heavier than $10^{-15} M_\odot$ have lifetimes larger than the age of the Universe, and therefore serve as possible dark matter candidates [171, 172]. Since they are of primordial origin, the BBN constraints on the baryonic content of the Universe do not apply and therefore PBHs should be regarded as non-baryonic dark matter. The LIGO-Virgo collaboration has detected gravitational waves from binary black hole mergers of $\mathcal{O}(10)\, M_\odot$ [173, 174, 175, 176, 177]. The work of Ref. [178] raised the interesting possibility of whether these black holes may be of primordial origin and represent the dark matter of the Universe. A variety of constraints on PBHs as dark matter can be applied (microlensing, CMB heating, stellar disruption among others). These constraints altogether rule out PBHs being 100% of the dark matter if they have a single common mass [172]. However, extended primordial black hole mass distributions are still allowed by data [179]. Based on LIGO observations, the physics case for primordial black holes appears to be promising. On the down side,

the generation mechanism of primordial black holes of $\mathcal{O}(10)M_{\odot}$ is considerably contrived since it requires an extremely fine tuned inflationary potential [180]. LIGO has just opened the era of gravitational wave astronomy. Many more gravitational wave events are foreseen [181]. Upcoming observations, together with theoretical studies are likely to settle the case for PBHs as dark matter in the near future.

Chapter 2

The Standard Model and Neutrino Masses in a Nutshell

The Standard Model [182, 183, 184, 185, 186, 187, 188, 189, 190, 191, 192] is the gauge theory that describes the strong, and electroweak interactions of all known elementary particles. In what follows the main ingredients of the SM are briefly described. The reader is referred to [193, 194, 195] for a book and reviews on the subject.

2.1 Gauge symmetry and particle content

The symmetry group upon which the SM is based on is:

$$SU(3)_C \times SU(2)_L \times U(1)_Y \,.$$

Correspondingly, upon enforcing local gauge invariance of the Lagrangian under this symmetry, the generators of such group represent the spin-1 force carriers that mediate the strong and electroweak interactions: 8 massless gluon fields G correspond to $SU(3)_C$, and 1 massless photon γ and the massive $W^{\pm}$ and Z bosons correspond to $SU(2)_L \times U(1)_Y$. In addition to such gauge force carriers, the SM contains several fermionic particles: three families of leptons and three families of quarks, together with a scalar field ϕ. The precise quantum numbers of all these fields are summarized in table 2.1.

The covariant derivative that renders a gauge invariant Lagrangian is

$$D_\mu \equiv \partial_\mu - i g_s \frac{\lambda_a}{2} G^a_\mu - i g \, \tau_a W^a_\mu - i g' B_\mu \,, \tag{2.1}$$

	$SU(3)_C$	$SU(2)_L$	$U(1)_Y$
$L \equiv (e_L, \nu_L)^T$	**1**	**2**	$-1/2$
e_R	**1**	**1**	-1
$Q \equiv (u_L, d_L)^T$	**3**	**2**	$+1/6$
u_R	**3**	**1**	$+2/3$
d_R	**3**	**1**	$-1/3$
ϕ	**1**	**2**	$+1/2$

Table 2.1: The Standard Model particle content for one family of quarks and leptons, together with the Higgs doublet, and their associated quantum numbers.

where g_s, g, g', are the coupling constants for $SU(3)_C$, $SU(2)_L$, $U(1)_Y$ respectively; G^a_μ, W^a_μ, B_μ represent the gauge fields of each group, and λ_a are the generators of $SU(3)$ and are represented by the Gell-Mann matrices. Similarly, $\tau_a = \sigma_a/2$ are the generators of $SU(2)$ where σ_a are the Pauli matrices. In the SM, $SU(2)_L$ is called weak-isospin and its conserved charges are T_a, where $a = 1, 2, 3$. Use of the covariant derivative yields the SM kinetic terms for the fermions

$$\mathcal{L}_{\text{kin, fermions}} = i \sum_\alpha \bar{\psi}_\alpha \gamma^\mu D_\mu \psi_\alpha \,, \tag{2.2}$$

where the sum is over all the fermionic fields in Table 2.1. The kinetic gauge interactions read

$$\mathcal{L}_{\text{kin, gauge}} = -\frac{1}{4} G^a_{\mu\nu} G^{\mu\nu}_a - \frac{1}{4} W^a_{\mu\nu} W^{\mu\nu}_a - \frac{1}{4} B_{\mu\nu} B^{\mu\nu} \,, \tag{2.3}$$

where the field strength tensors are given by:

$$G^a_{\mu\nu} \equiv \partial_\mu G^a_\nu - \partial_\nu G^a_\mu + g_s f^{abc} G^b_\mu G^c_\nu \,, \tag{2.4}$$

$$W^a_{\mu\nu} \equiv \partial_\mu W^a_\nu - \partial_\nu W^a_\mu + g\, \epsilon^{abc} W^b_\mu W^c_\nu \,, \tag{2.5}$$

$$B_{\mu\nu} \equiv \partial_\mu B_\nu - \partial_\nu B_\mu \,, \tag{2.6}$$

where f^{abc} and ϵ^{abc} are the $SU(3)$ and $SU(2)$ structure constants respectively ($[\lambda_a, \lambda_b] = i f^{abc} \lambda_c$ and $[\tau_a, \tau_b] = i \epsilon^{abc} \tau_c$).

2.2 The Higgs mass generation mechanism

A direct mass term for the massive gauge bosons $W^\pm$, Z will be manifestly not gauge invariant ($W^a W_a$) and the same occurs with the fermions.

However, the Spontaneous Symmetry Breaking (SSB) of the SM gauge symmetry triggered by a scalar field accounts for all the masses in a gauge invariant manner. This is the so-called Higgs mechanism [185, 186, 187, 188, 189, 190]. In the SM, the responsible field for SSB is the Higgs doublet $\phi = (\phi^+, \phi_0)^T$ (see Table 2.1 for its corresponding quantum numbers). The most general renormalizable Lagrangian for the Higgs doublet reads

$$\mathcal{L}_{\text{Higgs}} = (D_\mu \phi)^\dagger D^\mu \phi + \mu^2 (\phi^\dagger \phi) - \lambda (\phi^\dagger \phi)^2 \,, \tag{2.7}$$

where $\mu^2 > 0$.

Imposing the vacuum condition for the potential $\partial V/\partial \phi|_{|\phi|=v/\sqrt{2}} = 0$, leads to the following relationship: $v = \sqrt{\mu^2/\lambda}$, where v is the vacuum expectation value of the scalar field ϕ. And it is measured to be $v = 246\,\text{GeV}$ [47]. As a consequence of $v \neq 0$, out of the original $SU(2)_L \times U(1)_Y$ electroweak symmetries of the Lagrangian in 2.7, only a $U(1)$ symmetry is respected by the vacuum. This allows one to write the Higgs doublet as

$$\phi = \frac{v + H(x)}{\sqrt{2}} \exp\left[i \frac{\theta^a(x)}{v} \frac{\sigma^a}{2} \right] \begin{pmatrix} 0 \\ 1 \end{pmatrix} \,, \tag{2.8}$$

where $a = 1, 2, 3$, and $\theta^a(x)$ and $H(x)$ represent the 4 degrees of freedom in the Higgs doublet. On one hand, the excitations of the H field correspond to the physical CP-even scalar Higgs boson with mass $m_H = 125\,\text{GeV}$ [196, 197, 198]. While on the other hand, $\theta^a(x)$ are the would-be Goldstone bosons. However, they can be rotated away by a suitable gauge transformation so that $\theta^a(x) = 0$ (this is the so-called Unitary gauge). With such a choice, the kinetic term of the Higgs field reads

$$(D_\mu \phi)^\dagger D^\mu \phi \to \frac{1}{2} \partial_\mu H \partial^\mu H + (v + H)^2 \left(\frac{g^2}{4} W_\mu^+ W^{\mu -} + \frac{g^2}{8 \cos^2 \theta_W} Z^\mu Z_\mu \right) \tag{2.9}$$

Where the $W^\pm$ and Z fields are related to the interaction diagonal $SU(2)_L \times U(1)_Y$ ones as

$$W^\pm \equiv \frac{1}{\sqrt{2}} \left(W_1^\mu \mp i W_2^\mu \right) \,, \tag{2.10}$$

$$\begin{pmatrix} Z^\mu \\ A^\mu \end{pmatrix} \equiv \begin{pmatrix} \cos\theta_W & -\sin\theta_W \\ \sin\theta_W & \cos\theta_W \end{pmatrix} \begin{pmatrix} W_3^\mu \\ B^\mu \end{pmatrix} \,, \tag{2.11}$$

where $\tan\theta_W = g'/g$, θ_W is the Weinberg angle, and A_μ is the photon field. Therefore, after SSB the physical gauge bosons masses are

$$m_A = 0 \,, \qquad m_Z = \frac{v\sqrt{g^2 + g'^2}}{2} \,, \qquad m_W = \frac{gv}{2} \,. \tag{2.12}$$

And thus, the photon is kept massless while the Z and $W^{\pm}$ gauge bosons get their masses from the SSB triggered by the Higgs field. The resulting symmetry breaking pattern is therefore $SU(2)_L \times U(1)_Y \to U(1)_{\rm em}$.

Finally, as a result of the mixing between the interaction and mass basis of the gauge bosons, the relationship between the electric charge Q, Hypercharge Y, and the third component of Isospin T_3 becomes

$$Q = T_3 + Y\,, \qquad e = \frac{gg'}{\sqrt{g^2+g'^2}}\,, \tag{2.13}$$

where e is the electromagnetic coupling constant.

2.3 Fermion masses and mixings

The couplings of the Higgs with the SM fermions are fixed by gauge invariance. And upon SSB the masses of all fermions (but neutrinos) are generated. The Yukawa Lagrangian reads

$$\mathcal{L}_{\rm Yukawa} = -\bar{L}Y_e e_R\phi - \bar{Q}Y_u u_R\tilde{\phi} - \bar{Q}Y_d d_R\phi + \text{h.c.}\,, \tag{2.14}$$

where $\tilde{\phi} = C\phi = i\sigma_2\phi^\star$ is the charge conjugate of ϕ, and Y_e, Y_u, Y_d are 3×3 Yukawa matrices. After SSB, the Lagrangian takes the form

$$\mathcal{L}_{\rm Yukawa} = -\left(1+\frac{H}{v}\right)\left(\bar{e}_L M_e e_R + \bar{u}_L M_u u_R + \bar{d}_L M_d d_R\right) + \text{h.c.}\,, \tag{2.15}$$

where again M_e, M_u, M_d are 3×3 mass matrices. In order to find the physical basis for the fermions, one shall diagonalize them. As an example, for the u case, one can perform a field redefinition so that $M_u = V_{u_L}^\dagger M_u^{\rm Diag} V_{u_R}$ for which the massive states are defined as $u'_L = V_{u_L}u_L$ and $u'_R = V_{u_R}u_R$. Upon diagonalization of the mass matrices, the Higgs interactions will be diagonal while the charged current interactions read

$$\mathcal{L}_{\rm CC} = \frac{g}{2\sqrt{2}}W_\mu^\dagger\left[\sum_{ij}\bar{u}'_i\gamma^\mu(1-\gamma_5)V_{ij}^{\rm CKM}d'_j + \sum_l \bar{\nu}_l\gamma^\mu(1-\gamma_5)l\right] + \text{h.c.} \tag{2.16}$$

where $V_{ij}^{\rm CKM} = V_{u_L}V_{d_L}^\dagger$ is the Cabibbo-Kobayashi-Maskawa (CKM) matrix. It is a $U(3)$ matrix, and therefore contains 3 real parameters and 6 phases. Out of them, 5 phases can be removed due to field redefinitions of the form $f \to e^{i\alpha_f}f$. Finally, the neutral current Lagrangian can be written as

$$\mathcal{L}_{\rm NC} = -eA_\mu\sum_f q_f\bar{f}\gamma^\mu f - \frac{e}{2\sin\theta_W\cos\theta_W}Z_\mu\sum_f\bar{f}\left(v_f - a_f\gamma_5\right)f\,, \tag{2.17}$$

where f represents each physical fermion, and $a_f = T_3^f$, $v_f = T_3^f(1 - 4|q_f|\sin^2\theta_W)$, and q_f is its charge and T_3 its isospin. The Standard Model Lagrangian thus reads

$$\mathcal{L}_{\text{SM}} = \mathcal{L}_{\text{kin, gauge}} + \mathcal{L}_{\text{kin, fermions}} + \mathcal{L}_{\text{Higgs}} + \mathcal{L}_{\text{Yukawa}} \,. \tag{2.18}$$

2.4 The seesaw mechanism

Neutrinos are massless in the SM. However, there is plenty of evidence that neutrinos oscillate [199] and must therefore be massive (at least two of them). A naive mass implementation is to simply include right handed components N_R into the SM. In this way, the mass generation of the neutrinos is given, as for the other fermions, by the Higgs mechanism $Y_\nu \bar{L}\phi N_R$ rendering massive Dirac neutrinos. However, since the neutrino masses are $m_\nu \lesssim 0.2\,\text{eV}$ [47] with this implementation one then faces the question of why $Y_\nu/Y_e \sim 10^{-6}$ or $Y_\nu/Y_t \sim 10^{-14}$. Such a huge difference between the mass of the neutrinos and the rest of the SM fermions seems to be pointing towards a different mass mechanism that somehow enables $m_\nu \ll m_{\ell,q}$. The fact that only the N_R are allowed by the SM gauge symmetries to have a Majorana mass term, leads to the following Yukawa Lagrangian:

$$\mathcal{L}_{N_R} = -Y_\nu \bar{L}\phi N_R - \frac{1}{2} M_R N_R^T C^{-1} N_R + \text{h.c.} \tag{2.19}$$

where M_R is the N_R Majorana mass matrix, Y_ν is the neutrino Yukawa matrix, and C is the charge conjugation matrix, so that $\psi_c = C\bar{\psi}^T$ is the charge conjugate of the ψ field. After SSB, this Lagrangian leads to the mass matrix

$$\mathcal{M}_\nu = \begin{pmatrix} 0 & m_D \\ m_D^T & M_R \end{pmatrix} \,, \tag{2.20}$$

where $m_D = Y_\nu v/\sqrt{2}$. In the limit $m_D \ll M_R$, the eigenvalues are approximately given by m_D^2/M_R and M_R, with approximately corresponding eigenvectors ν_L and N_R. This mass generation mechanism for the light active neutrinos is known as the seesaw mechanism [200, 201, 202, 203, 204]. The seesaw mechanism therefore associates the lightness of active neutrinos with the highness of the scale of the sterile neutrinos as compared with the weak scale. With $Y_\nu \sim 1$ and $m_\nu \sim 1\,\text{eV}$ the seesaw formula points to $M_R \sim 10^{15}\,\text{GeV}$ and thus very close to the Grand Unification scale. It should be noted that if $Y_\nu \ll 1$, as it is the case for the Yukawa couplings of all fermions but the top quark, the right handed neutrinos could be much lighter.

Chapter 3

Thermodynamics of the Expanding Universe

Given the current energy content of the Universe, the evolution of the Friedmann equations 1.8 leads to a radiation dominated era in the early Universe. Additionally, since the CMB temperature spectrum resembles that of a black body to an astonishing degree of accuracy (see Figure 1.7), we expect that the particles in the early Universe were kept in thermal equilibrium. Thus, it is relevant to discuss how the distribution functions of these particles f_i (or equivalently; their number, energy and pressure densities) evolve with the expansion within the assumption of thermal equilibrium.

3.1 Equilibrium Thermodynamics

The thermal distribution of a particle in a plasma at a temperature T is given by the well known Fermi-Dirac (FD) and Bose-Einstein (BE) formulae:

$$f(E) = \left[\exp\left(\frac{E-\mu}{T}\right) \pm 1\right]^{-1} , \tag{3.1}$$

where $+$ corresponds to Fermions and $-$ to Bosons. $E = \sqrt{p^2 + m^2}$ is the energy, p is the momentum, m the mass, and μ is the chemical potential (which controls the change in the number densities of particles). For a process in thermal equilibrium with $\psi_1 + \psi_2 + \psi_3 + ... \rightarrow \phi_1 + \phi_2 + \phi_3 + ...$ the following condition over the chemical potentials holds

$$\sum_i \mu_{\psi_i} = \sum_j \mu_{\phi_j} . \tag{3.2}$$

In particular, for particles and antiparticles in thermal equilibrium that can annihilate into different numbers of neutral particles leads to $\mu_\psi = -\mu_{\bar{\psi}}$. For photons, since its number is not conserved, $\mu_\gamma = 0$. Note that the presence of a non-vanishing chemical potential will point towards a conserved charge distribution in the plasma. However, the measured charge densities in the Universe are negligible [205]. Thus, in general, we shall consider $\mu_i = 0$.

From the distribution functions it is straightforward to define the number density n, the energy density ρ, and the pressure p of a given species in terms of its number of internal degrees of freedom g and its distribution function f:

$$n = \frac{g}{2\pi^2}\int_0^\infty dp\, p^2\, f(p) \qquad \equiv \frac{g}{2\pi^2}\int_m^\infty dE\, E\sqrt{E^2-m^2}\, f(E) \quad (3.3a)$$

$$\rho = \frac{g}{2\pi^2}\int_0^\infty dp\, p^2\sqrt{p^2+m^2} f(p) \equiv \frac{g}{2\pi^2}\int_m^\infty dE\, E^2\sqrt{E^2-m^2} f(E) \quad (3.3b)$$

$$p = \frac{g}{6\pi^2}\int_0^\infty dp\, \frac{p^4}{\sqrt{p^2+m^2}}\, f(p) \equiv \frac{g}{6\pi^2}\int_m^\infty dE\, (E^2-m^2)^{3/2} f(E) \quad (3.3c)$$

It is very useful to consider the limiting cases of these expressions for ultra-relativistic (i.e. $T \gg m$) and non-relativistic (that is $T \ll m$) species:

	$T \gg m$		$T \ll m$
Magnitude	Fermions	Bosons	Fermions or Bosons
n	$g\frac{3}{4}\frac{\xi(3)}{\pi^2}T^3$	$g\frac{\xi(3)}{\pi^2}T^3$	$g\left(\frac{mT}{2\pi}\right)^{3/2} e^{-(m-\mu)/T}$
ρ	$g\frac{7}{8}\frac{\pi^2}{30}T^4$	$g\frac{\pi^2}{30}T^4$	mn
p	$\rho/3$	$\rho/3$	$nT \ll \rho$
$\langle E\rangle \equiv \rho/n$	$\simeq 3.15\,T$	$\simeq 2.70\,T$	$m + \frac{3}{2}T$

(3.4)

where $\xi(3) \simeq 1.202$ and $\langle E\rangle$ is the mean energy. From these expressions we clearly notice that, within the thermal equilibrium hypothesis, the relativistic species in the plasma dominate the number density, the energy density, and the pressure. Equivalently, the number density of non-relativistic particles in the plasma is exponentially suppressed.

Assuming that all chemical potentials vanish, from Equations 3.3 we know that $T\frac{dp}{dT} = \rho + p$, using the continuity Equation 1.5 and upon use of the chain rule $\frac{d}{dt} = \frac{dT}{dt}\frac{d}{dT}$ we arrive to the entropy conservation equation:

$$\frac{d}{dt}\left(a^3\frac{\rho+p}{T}\right) \equiv \frac{d}{dt}\left(a^3\, s\right) = 0\,, \quad (3.5)$$

where s is the entropy density.

We can define the total energy density ρ, and the total entropy density s in terms of the photon temperature T, and the number of relativistic degrees of freedom contributing to each $g_\star$ and $g_{\star S}$:

$$\rho \equiv g_\star \frac{\pi^2}{30} T^4 \,, \qquad\qquad s \equiv g_{\star S} \frac{2\pi^2}{45} T^3 \,. \tag{3.6}$$

Since both the energy density and the pressure are dominated by relativistic particles; entropy conservation (3.5) leads to the very important relationship between the scale factor and the temperature

$$T_2 = T_1 \, \frac{a_1}{a_2} \left[\frac{g_{\star S}(T_1)}{g_{\star S}(T_2)} \right]^{1/3} \,. \tag{3.7}$$

Connecting the energy density with the expansion of the Universe through the Friedmann equations leads to a very convenient expression for the Hubble factor and the age of the Universe

$$H = \sqrt{\frac{8\pi}{3} \frac{\rho}{m_{Pl}}} = 1.66 \sqrt{g_\star} \frac{T^2}{m_{Pl}} \simeq 4.5 \times 10^{-25} \, \text{GeV} \sqrt{\frac{g_\star}{10.75}} \left(\frac{T}{\text{MeV}} \right)^2 \,; \tag{3.8}$$

$$t = \int_0^a \frac{da'}{H(a')a'} = \frac{1}{2H} = 0.301 g_\star^{-1/2} \frac{m_{Pl}}{T^2} \simeq 0.7 \, \text{s} \sqrt{\frac{10.75}{g_\star}} \left(\frac{\text{MeV}}{T} \right)^2 \,, \tag{3.9}$$

where $m_{Pl} = 1.22 \times 10^{19} \, \text{GeV}$ is the Planck mass, and the equations have been normalized to $g_\star = 2 + \frac{7}{8}(2+2+3+3) = 10.75$, since for temperatures $T \sim 10 \, \text{MeV}$ only photons, electrons, positrons, neutrinos and antineutrinos are present in the plasma. We therefore notice that, at a temperature of $T \sim 1 \, \text{MeV}$ the Universe was about 1 second old.

Notice that for stable particles, the thermal equilibrium assumption will eventually break down since the number density of non-relativistic particles in equilibrium exponentially decreases with temperature (see Equation 3.4); thus, the annihilation and scattering processes between these particles and the plasma will at some point become inefficient. Since the particles that fill the Universe are stable we shall study such out of equilibrium processes in depth.

3.2 Out of Equilibrium

As demonstrated in the previous Section 3.1, the fate of the number density of massive stable particles kept in thermal equilibrium is to decrease exponentially for $T \ll m$. This means that eventually, the scattering and annihilation rates with the plasma will become inefficient and the assumption of thermal equilibrium will break down. The same will be true for light and sufficiently weakly coupled species even in the relativistic regime, i.e. for $T > m$. In particular, throughout the Universe's history there have been some remarkable events that occurred out of thermal equilibrium: the neutrino decoupling $T_\nu^{\rm dec} \sim 2-3\,{\rm MeV}$, the formation of the primordial light elements $T_{\rm BBN} = 0.01 - 3\,{\rm MeV}$, and the CMB decoupling $T_{\rm CMB}^{\rm dec} \sim 3000\,{\rm K}$. In addition to those, other relevant events (yet hypothetical) as the WIMP freeze-out or Baryogenesis are described out of thermal equilibrium. Thus, due to their relevance and since one of the main focus of study in this thesis are the WIMPs, it is pertinent to study out of equilibrium processes in detail.

Prior to discussing the effects of out of equilibrium processes on the particle distribution functions involved in them; or equivalently, their number densities, it is convenient to introduce an approximate (and in most of the cases sufficiently accurate) criterion for when a given process is in thermal equilibrium with the plasma. This criterion compares the rate of a given process Γ to that of the Hubble expansion H[1]:

$$\begin{aligned} \Gamma &\gtrsim H \text{ coupled} \\ \Gamma &\lesssim H \text{ decoupled} \end{aligned} \tag{3.10}$$

We can explicitly use such criterion to estimate the temperature at which neutrinos decoupled from the plasma. From the SM neutrino interactions, we know that the scattering and annihilation rates between neutrinos with themselves and electrons is

$$\Gamma_\nu \sim G_F^2 T^5\,, \tag{3.11}$$

where $G_F = 1.166 \times 10^{-5}\,{\rm GeV}^{-2}$ is the Fermi constant [47]. By comparing this rate with the Hubble parameter 3.8 we know that neutrinos decoupled at temperatures $T_\nu^{\rm dec} \sim 2 - 3\,{\rm MeV}$ (for details see [206]). Since neutrinos decoupled well before e^+e^- annihilation, the entropy produced by e^+e^- annihilation is only released into the photon bath. This will therefore render the neutrinos with smaller temperatures than the photons in the current Universe. Imposing entropy conservation (3.5) separately for the neutrino

[1] This criterion is equivalent to compare the characteristic time scale for a given process $\tau \sim 1/\Gamma$ and the characteristic time of the Universe's expansion $t \sim 1/H$.

and electromagnetic sectors, since they are decoupled, implies that after electron positron annihilation $g_{\star S} = 3.91$, $g_\star = 3.36$, and

$$T_\gamma = \left(\frac{11}{4}\right)^{1/3} T_\nu \simeq 1.401\, T_\nu\,. \tag{3.12}$$

This relation, together with the CMB temperature $T_0 = 2.7255\,\mathrm{K}$ [43] fixes todays total entropy and number densities of photons and neutrinos as:

$$s_0 \simeq 2900\,\mathrm{cm}^{-3},\ n_{\gamma 0} \simeq 411\,\mathrm{cm}^{-3},\ n_{\nu 0} \simeq 112\,\mathrm{cm}^{-3}\,(\text{per species})\,. \tag{3.13}$$

Neutrino decoupling is an example in which the criterion $\Gamma \sim H$ (3.10) works well. However, it is worth stressing that this criterion only gives an estimate of the temperature at which a process departures from being in equilibrium with the plasma. In order to accurately model departures from thermal equilibrium, the kinetic equations for particles in the plasma should be introduced.

The kinetic equation that governs the distribution functions of interacting particles is the Liouville (or Boltzmann) equation, which in a curved space-time reads [126] (see also [207]):

$$\left(p^\sigma \frac{\partial}{\partial x^\sigma} - \Gamma^\sigma_{\mu\nu} p^\mu p^\nu \frac{\partial}{\partial p^\sigma}\right) f(\vec{x}, \vec{p}, t) = \mathcal{C}[f]\,, \tag{3.14}$$

where $\mathcal{C}[f]$ represents the collision operator. For the purpose of using Equation 3.15 for early Universe considerations, we can make use of the Levi-Civita connection for the flat FLRW metric since the early Universe should have been extremely flat. Moreover, due to cosmological homogeneity and isotropy, in the early Universe $f(\vec{x}, \vec{p}, t) = f(p, t)$ (one shall allow for small perturbations of these conditions in order to understand the formation of matter perturbations in the late time Universe [59, 65]). These simplifications lead to

$$\left(\frac{\partial}{\partial t} - Hp\frac{\partial}{\partial p}\right) f(p, t) = \mathcal{C}[f]\,, \tag{3.15}$$

where we explicitly define the collision operator $\mathcal{C}[f_a]$ for a process $a + X \leftrightarrow Y$, where $X = X_1 + X_2 + ...$ and $Y = Y_1 + Y_2 + ...$ as [206]:

$$\mathcal{C}[f_a] \equiv -\frac{1}{2E_a} \sum_{X,Y} \int \prod_i d\Pi_{X_i} \prod_j d\Pi_{Y_j} (2\pi)^4 \delta^4(p_a + p_X - p_Y) \times \tag{3.16}$$

$$\left[|\mathcal{M}|^2_{a+X\to Y} f_a \prod_i f_{X_i} \prod_j \left[1 \pm f_{Y_j}\right] - |\mathcal{M}|^2_{Y\to a+X} \prod_j f_{Y_j} \left[1 \pm f_a\right] \prod_i \left[1 \pm f_{X_i}\right] \right]\,,$$

where f_a, f_{X_i}, f_{Y_j} are the distribution functions of the particles a, X_i and Y_j respectively. The $-$ sign applies to fermions and the $+$ sign applies to bosons. $d\Pi_{X_i}$ represents the phase space of a particle X_i:

$$d\Pi_{X_i} \equiv \frac{g_{X_i}}{(2\pi)^3}\frac{d^3p}{2E}\,, \tag{3.17}$$

where g_{X_i} are the number of internal degrees of freedom. The delta function ensures energy-momentum conservation and $\mathcal{M}_{a+X\to Y}$ is the amplitude for the $a + X \to Y$ process. The physical interpretation of the two terms in Equation 3.16 is clear. The first term takes into account the decrease in the number of a-particles from the process $a + X \to Y$ and the second accounts for the inverse process $Y \to a + X$ that increases the number of a-particles in the plasma.

Algebraically, one can easily check that when the distribution functions of all the particles involved in the process are the thermal equilibrium ones (3.1), the following relation holds:

$$f_a^{eq}\prod_i f_{X_i}^{eq}\prod_j\left[1 \pm f_{Y_j}^{eq}\right] = \prod_j f_{Y_j}^{eq}\prod_i\left[1 \pm f_{X_i}^{eq}\right]\left[1 \pm f_a^{eq}\right]\,. \tag{3.18}$$

This is the so-called detailed balance relation, which means that in equilibrium, the rate of a process and of its inverse one are equal.

Integrating Equation 3.16 can be a formidable task. However, there are two simplifying assumptions that make it more tractable but still accurate. These are:

1. CP conservation[2]. This leads to $|\mathcal{M}|_{a+X\to Y} = |\mathcal{M}|_{Y\to a+X}$.
2. Maxwell-Boltzmann (MB) approximation. This allows one to neglect the quantum statistical factors in the distribution functions $f(E) \simeq e^{-(E-\mu)/T}$ and in the collision terms $1 \pm f \simeq 1$. The usefulness of this approximation is to reduce the dimensionality of the phase space integration.

Provided these two assumptions hold, upon use of Equations 3.16 and 3.18, the collision operator takes the more convenient form:

$$\mathcal{C}[f_a] = -\frac{1}{2E_a}\sum_{X,Y}\int\prod_i d\Pi_{X_i}\prod_j d\Pi_{Y_j}(2\pi)^4\delta^4(p_a + p_X - p_Y)\times \tag{3.19}$$
$$|\mathcal{M}|^2_{a+X\to Y}\left[f_a\prod_i f_{X_i} - f_a^{eq}\prod_i f_{X_i}^{eq}\right]\,.$$

[2]CP violation in the SM is very small in the quark sector, and yet to be measured in the lepton one [47]. This approximation should be disregarded in Baryogenesis.

We notice that processes with higher multiplicities are suppressed by additional powers of f[3]. This means that in the early Universe the most relevant processes are going to be $1 \leftrightarrow 2$ and $2 \leftrightarrow 2$, i.e. processes with multiplicities smaller than 2 in the initial or final states. Thus, due to their importance we will explicitly derive the relevant formulae for such processes. In addition, in order to have a feeling of what is the error that results from approximating the distributions by the MB one, an explicit example for the case of decays and inverse decays involving the full quantum statistical factors is given in Section 3.2.3.

Regarding the evolution of particles in the early Universe, it is customary to work in terms of integrated quantities as the number density, due to its simplicity. For a particle ψ, integration of Equation 3.15 (accounting for the momentum redshift $dp/dt = -Hp$[4]) gives

$$\dot{n} + 3Hn = \frac{g}{(2\pi)^3} \int d^3p \, \mathcal{C}[f_\psi] \,. \tag{3.20}$$

In the MB approximation and considering decays and annihilation processes $\psi \leftrightarrow c + d$, $\psi\psi \leftrightarrow i + j$, the above expression leads to the very familiar expression[5]

$$\dot{n} + 3Hn = -\langle \Gamma \rangle (n - n_{eq}) - \langle \sigma v \rangle \left(n^2 - n_{eq}^2 \right) \,, \tag{3.21}$$

where $\langle \Gamma \rangle$ represents the thermally averaged decay rate and $\langle \sigma v \rangle$ the thermally averaged annihilation cross section, which, upon phase space integration through the use of Equation 3.19 read as

$$\langle \Gamma \rangle = \Gamma \frac{K_1(m/T)}{K_2(m/T)} \,, \tag{3.22}$$

$$\langle \sigma_{ab\to ij} v \rangle = \frac{1}{8Tm_a^2 m_b^2 K_2(m_a/T) K_2(m_b/T)} \times \int_{(m_a+m_b)^2}^{\infty} ds \, s^{3/2} K_1\left(\frac{\sqrt{s}}{T}\right) \lambda\left[1, \frac{m_a^2}{s}, \frac{m_b^2}{s}\right] \sigma_{ab\to ij}(s) \,, \tag{3.23}$$

where Γ is the decay rate for the process $\psi \to c+d$ and $\sigma_{ab\to ij}(s)$ is the cross section for the process $a+b \to i+j$. Here K_1 and K_2 are the modified Bessel

[3]Notice that $f(E = \langle E \rangle \sim 3T) \simeq 0.05$ or $f(E = 7T) \simeq 10^{-3}$.

[4]This results from applying the geodesic equation to a particle with 4-momentum $p^\mu = \frac{dx^\mu}{d\lambda} = (E, p^i)$, since $\frac{d^2x^\mu}{d\lambda^2} + \Gamma^\mu_{\alpha\beta} \frac{dx^\alpha}{d\lambda} \frac{dx^\beta}{d\lambda} = 0$, for the i component we arrive to $\frac{dp^i}{dt} + Hp^i = 0$ using $\frac{d}{d\lambda} = \frac{dt}{d\lambda}\frac{d}{dt} = E\frac{d}{dt}$.

[5]Note that in order to arrive to Equation 3.21 we have implicitly assumed kinetic equilibrium, i.e. that the distribution function is proportional to the equilibrium one by a function that does not depend upon momentum $f = A(T) f_{eq}$ [208, 207]. If the elastic scattering rate between the ψ particle with the plasma is small enough this assumption breaks down. See [209] for a treatment of WIMP abundances including such possibility.

functions of second kind, and $\lambda(x, y, z) = x^2 + y^2 + z^2 - 2xy - 2xz - 2yz$ is the Kallen function.

Equation 3.21 can be further simplified in the case that the departures from thermal equilibrium are such that do not generate a net change in the entropy of the Universe. This is the case of non-relativistic particles. Additionally, in practice, it is usually more convenient not to work in terms of time but in terms of temperature T or equivalently $x \equiv m/T$. Since entropy is conserved (see Equation 3.5, $\dot{s} = -3Hs$) we can define the yield $Y \equiv n/s$, so that $\dot{Y} = (1/s)(\dot{n} + 3Hn)$. Assuming that the number of relativistic degrees of freedom does not change in the time-scales of interest we can use $dt/dx = 1/(Hx)$, and we can write down the evolution equation for the number density 3.21 as a function of the yield, Y:

$$\frac{dY}{dx} = -\frac{\langle\Gamma\rangle}{Hx}\left(Y - Y_{eq}\right) - \frac{s\,\langle\sigma v\rangle}{Hx}\left(Y^2 - Y_{eq}^2\right) . \tag{3.24}$$

Equation 3.24 is extensively used in order to compute the relic abundance of various particles in the early Universe. Particularly, it can be used to obtain the relic abundance of the currently most appealing dark matter candidate, the WIMP.

3.2.1 Abundance of cold relics: the WIMP freeze-out

The cosmological relic density of WIMPs was first studied by Lee and Weinberg in 1977 [127] who considered the production of heavy neutrinos in the early Universe. Since then, the production of massive stable particles in the early Universe has been thoroughly studied in [128, 129, 210] for $2 \to 2$ processes (see [209] for recent developments). It is the aim of this Section to understand, through the use of Equation 3.24, what are the desired properties of the annihilation rate for a massive stable particle in order to represent $\sim 26\%$ of the energy budget of the Universe today.

In practice, Equation 3.24 can be somewhat hard to solve numerically. Thus, we proceed as in Ref. [211] (see also [212]) in order to arrive to a more numerically tractable form. Including the possibility of changing relativistic degrees of freedom in the early Universe, Equation 3.24 for a stable particle reads

$$\frac{dY}{dx} = -Z(x)\left(Y^2 - Y_{eq}^2\right) , \tag{3.25}$$

where

$$Z(x) = \langle \sigma v \rangle \sqrt{\frac{\pi}{45}} \frac{m\, m_{Pl}}{x^2} \frac{g_\star}{\sqrt{g_{\star S}}} \left(1 + \frac{T}{3g_\star}\frac{dg_\star}{dT}\right) , \tag{3.26}$$

$$Y_{eq}(x) = \frac{45}{4\pi^4}\frac{x^2}{g_{\star S}} K_2(x) , \tag{3.27}$$

and $g_{\star S}$ and $g_\star$ are the number of relativistic degrees of freedom in entropy and energy, as defined in Equation 3.6. By defining $Y \equiv (1+\delta)Y_{eq}$, the same equation can be written for δ, leading to

$$\frac{d\delta}{dx} + (1+\delta)\frac{d\log Y_{eq}}{dx} = -Z(x)\, Y_{eq}(x)\, \delta\, (\delta + 2) . \tag{3.28}$$

This equation can be approximately solved by noticing that $\delta(x)$ grows slowly until δ becomes $\mathcal{O}(1)$. Namely, the abundance of the particle freezes out, i.e. the abundance significantly departures from its equilibrium value. This means, that in such region of δ one can safely ignore the derivative $d\delta/dx$ to find an algebraic equation for δ. Instead of solving for $\delta(x)$, we solve for the temperature at which freezes out $x_f = m/T_f$, so that

$$x_f = \log\left(\frac{\delta_f(2+\delta_f)}{1+\delta_f}\frac{Z\hat{Y}_{eq}^2}{\hat{Y}_{eq} - \frac{d\hat{Y}_{eq}}{dx}}\right)_{x_f} , \tag{3.29}$$

where $\hat{Y}_{eq} = e^{-x}Y_{eq}$. The solution to Equation 3.29 can easily be found by iteration. Finally, ignoring the inverse annihilations (i.e. the Y_{eq}^2 term in the r.h.s.) we can integrate 3.25 from x_f to ∞ to find

$$Y_0 = \frac{Y_f}{1 + Y_f A_f} , \tag{3.30}$$

where Y_0 is the yield today and

$$A_f = \int_{x_f}^{\infty} dx\, Z(x) . \tag{3.31}$$

Note that Equation 3.30 gives very accurate solutions, with a precision better than 1% if there are no thresholds at the energies of interest [211, 212]. When Equation 3.30 is particularized for s-wave annihilations (for which $\langle \sigma v \rangle$ does not depend upon the velocity), and assuming that the number of relativistic degrees of freedom does not significantly change, leads to

$$Y_0 = \sqrt{\frac{45}{\pi}}\frac{(g_\star^{1/2}/g_{\star S})x_f}{m\, m_{Pl}\, \langle \sigma v \rangle} , \tag{3.32}$$

$$\Omega h^2 = 0.12 \times \frac{x_f}{30}\frac{\sqrt{85}}{g_{\star S}/g_\star^{1/2}}\frac{2.57 \times 10^{-9}\,\mathrm{GeV}^{-2}}{\langle \sigma v \rangle} , \tag{3.33}$$

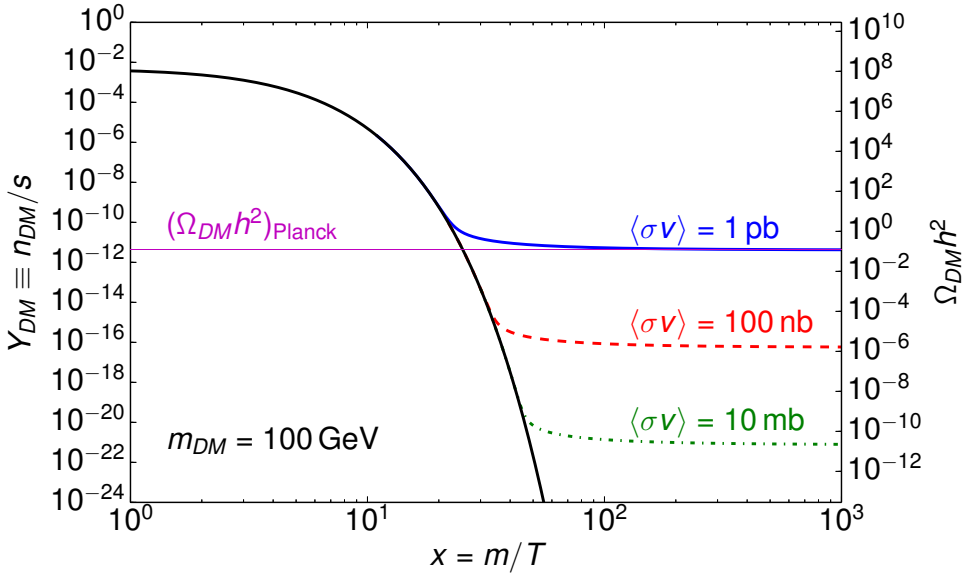

Figure 3.1: Thermal freeze-out of a $m = 100\,\text{GeV}$ particle as a function of its annihilation cross section. We also show the dark matter abundance as measured by Planck $(\Omega_{DM}h^2)_{\text{Planck}} = 0.1198 \pm 0.0015$ [13].

where for a usual WIMP $x_f \sim 15 - 30$ depending on its mass. Recall that currently $s_0 \simeq 2900\,\text{cm}^{-3}$, and $\Omega h^2 = mn_0h^2/\rho_c = mY_0s_0h^2/\rho_c$. Note that Equation 3.33 has been expressed in a very suggestive form that shows that the cold relics that have an annihilation cross section with the plasma of $\langle\sigma v\rangle \simeq (1.7 - 4.3) \times 10^{-9}\,\text{GeV}^{-2} \simeq (2 - 5) \times 10^{-26}\,\text{cm}^3/\text{s} \simeq (0.7 - 1.7)\,\text{pb}$ can provide the right abundance for dark matter today, $\Omega_{DM}h^2 = 0.1198 \pm 0.0015$ [13]. Note that the current contribution to the energy density only depends upon the annihilation cross section, and not directly on the mass as can be appreciated from Equation 3.33.

Figure 3.1 shows explicit numerical solutions to Equation 3.28. Several conclusions can be drawn from both the analytic 3.33 and numerical solutions to this equation:

1. In order to get the right dark matter abundance an annihilation cross section similar to that of weak processes is required $\langle\sigma v\rangle \simeq 1\,\text{pb} \equiv 3 \times 10^{-26}\,\text{cm}^3/\text{s}$ (note that $G_F^2 \simeq 0.05\,\text{pb}$). This number varies only within a factor of 2 for $m_\chi \in 0.1 - 10^4\,\text{GeV}$, see [211] for the precise value.

2. If the annihilation cross section were to be smaller than $\sim$ pb then the relic density of these particles will be such that they will overclose

the Universe. The fact that only $\langle\sigma v\rangle \sim$ pb provides the correct relic abundance is the so-called WIMP miracle.

3. If the annihilation cross section is similar to that of electromagnetic or strong interactions processes, the cosmological abundance of such particles is negligible. Since $\Omega_b h^2 \sim 0.022$ there should have been a very small asymmetry between baryons and antibaryons in the early Universe, $\eta = (n_B - n_{\bar{B}})/n_\gamma = (6.09 \pm 0.06) \times 10^{-10}$ [13]. This is the so-called baryon asymmetry and its generation in the early Universe is called Baryogenesis [213].

3.2.2 Abundance of hot relics

If a particle in thermal equilibrium decouples while relativistic, its current abundance is solely fixed by the ratio of its number of internal degrees of freedom to the number of relativistic degrees of freedom for the entropy density at the time of decoupling. Upon use of Equations 3.3 and 3.6 we easily find

$$Y_f = C\,\frac{45\,\xi(3)}{2\pi^4}\,\frac{g}{g_{\star S}(T_{\rm dec})} \simeq 0.28\,C\,\frac{g}{g_{\star S}(T_{\rm dec})}\,, \tag{3.34}$$

where g are the number of internal degrees of freedom of the given species, and $C = 3/4,\, 1$ for fermions and bosons respectively. We can make use of this simple calculation to know what is the current contribution from neutrinos to the total energy density budget, since they decoupled at $T \sim 2 - 3\,\text{MeV}$ and thus $g_{\star S} = 10.75$:

$$\Omega_{\bar{\nu}\nu} h^2 = \frac{s_0 Y_f m}{\rho_c} \simeq \frac{\sum m_\nu}{91.5\,\text{eV}}\,. \tag{3.35}$$

From Equation 3.35 we notice that the neutrino contribution to the current energy density is non-negligible. Requiring that the neutrinos do not overclose the Universe $\Omega_{\bar{\nu}\nu} < 1$, has been a simple argument that however has provided very strong cosmological bounds on the neutrino masses that were once more severe that those from laboratory experiments. Currently, through the effect of neutrino masses in the expansion of the Universe and from its impact on structure formation [122], cosmology provides the most stringent constraint on the sum of the neutrino masses, which to date reads $\sum m_\nu \lesssim 0.2\,\text{eV}$ at 95% CL [13, 214, 215]. The square differences in mass measured from neutrino oscillation experiments imply that $\sum m_\nu > 0.06\,\text{eV}$ [47] and therefore $\Omega_{\bar{\nu}\nu} h^2 > 0.0007$ is expected in the SM.

Very similar arguments have been invoked in order to constrain the masses of very weakly interacting particles like the gravitino or the majoron [126].

3.2.3 Decays and inverse decays: full quantum statistics

In order to test the accuracy of the Maxwell-Boltzmann approximation in the collision term 3.19 we provide in this Section an explicit integration of 3.16 including the quantum statistical factors for the case of $1 \leftrightarrow 2$ processes.

Let us consider the coupled system of Boltzmann equations for the process $a \leftrightarrow b + c$ with spins $s_a = 1$ and $s_b = s_c = 1/2$ under the assumption that a is a neutral bosonic particle and $\mathrm{Br}(a \to b+c) = \mathrm{Br}(a \to \bar{b}+\bar{c}) = 1/2$. In addition, for the sake of simplicity, we shall consider $b = \bar{b}$ and $c = \bar{c}$, and $m_b = m_c = 0$[6]. We can integrate the phase space down to a one-dimensional integral[7]:

$$\mathcal{C}[f_a] = -\frac{m_a \Gamma_a}{E_a p_a} \int_{\frac{E_a - p_a}{2}}^{\frac{E_a + p_a}{2}} dE_b F_{\mathrm{dec}}\left(E_a, E_b, E_a - E_b\right) , \tag{3.36a}$$

$$\mathcal{C}[f_b] = \frac{3}{4} \frac{m_a \Gamma_a}{E_b p_b} \int_{|(m_a^2/4p_b) - p_b|}^{\infty} \frac{dp_a p_a}{E_a} F_{\mathrm{dec}}\left(E_a, E_b, E_a - E_b\right) , \tag{3.36b}$$

$$\mathcal{C}[f_c] = \frac{3}{4} \frac{m_a \Gamma_a}{E_c p_c} \int_{|(m_a^2/4p_c) - p_c|}^{\infty} \frac{dp_a p_a}{E_a} F_{\mathrm{dec}}\left(E_a, E_c, E_a - E_c\right) , \tag{3.36c}$$

where Γ_a is the decay width. In order to get to integrals defined in terms of the energy and momenta we have used Lorentz transformations in order to go to the laboratory frame of a. The function F_{dec} is given by

$$F_{\mathrm{dec}}\left(E_a, E_b, E_c\right) = f_a \left[1 - f_b\right] \left[1 - f_c\right] - f_b f_c \left[1 + f_a\right] . \tag{3.37}$$

Explicit numerical integration of the collision term 3.36 and its comparison to that in the MB approximation 3.19 is shown in Figure 3.2. We assume thermal equilibrium and vanishing chemical potentials for all the particles. Moreover, in Figure 3.2 we only show the collision factor taking into account either production or destruction of particles, because the equilibrium condition implies they are equal and thus $C[f_a]^{eq} \equiv 0$. This is equivalent to consider $F_{\mathrm{dec}}\left(E_a, E_b, E_c\right) = f_a \left[1 - f_b\right] \left[1 - f_c\right]$ instead of Equation 3.37. The upper (middle) panel shows the collision term including the quantum statistical factors and using the MB approximation for the a-particle (b-particle). The lower panel shows the ratio between the actual rate and the one obtained in the MB approximation. It should be clear, that since in this scenario the final state particles are fermions, taking into

[6] This scenario is a slight modification of the one considered in [216]. However, note that there is a typo in that reference. The $-$ sign in their Equation 7 should be a $+$ sign.

[7] Note that the requirement of $m_{b,c} \neq 0$ still makes the collision integrals one-dimensional, $m_{b,c} \neq 0$ would only modify the integration limits due to a reduction of the phase space.

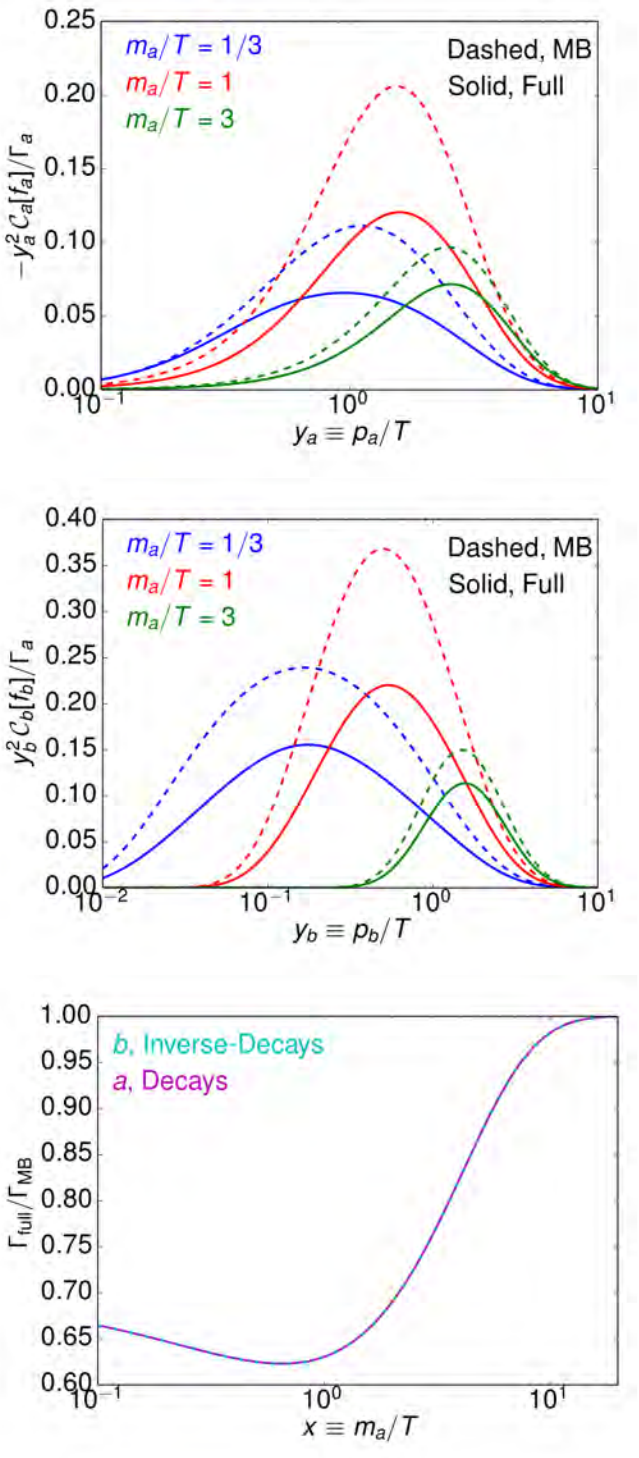

Figure 3.2: Collision terms for the $a \to b + c$ process described in the text.
Upper panel: collision operator as a function of momenta ($y_a = p_a/T$) for the decaying a-particle in the MB approximation and taking into account the quantum statistical factors (full) for various values of the mass and temperature, $m_a/T = 1/3$, 1, 3.
Middle panel: same as upper panel but for the b-particle collision operator.
Lower panel: Ratio of the rate including quantum statistical factors to that in the MB approximation.

account the statistical factors reduces the rates (this is the so-called Pauli blocking effect). From the lower panel of Figure 3.2 we realize that when the decaying particle is heavy enough, the MB approximation applies and therefore both cases agree. However, we note that for light particles the effect of quantum statistical factors becomes important. In this particular case, the rates can be modified by up to a $\sim 40\%$. Quantum statistical factors can be important in scenarios like neutrino decoupling [206]. The interested reader is referred to [217] where the phase space integration of the collision term 3.16 for the case of $2 \to 2$ annihilations is worked out in detail.

Chapter 4

Dark Matter Probes

Weakly Interacting Massive Particles can be produced in the early Universe precisely in the right abundance to be the dark matter that fills the Universe. This is the so-called WIMP miracle (see Section 3.2.1). However, the WIMP production in the early Universe only requires that the dark matter annihilates to light particles in the plasma at a rate of $\langle \sigma v \rangle |_{T \simeq m_\chi/20} \simeq 2 - 5 \times 10^{-26}\,\mathrm{cm}^3/\mathrm{s}$. And thus, the WIMP miracle on its own is too broad to pinpoint the dark matter mass neither the dark matter interactions with the SM particles. Concerning the mass, unitarity requirements on the $2 \to 2$ annihilation process, as relevant for generating the dark matter abundance, set an upper limit on the WIMP mass of $m_\chi \lesssim 100\,\mathrm{TeV}$ [218]. Additionally, the measurement of the number of relativistic species contributing to radiation at the time of the CMB sets a lower bound on the WIMP mass of $m_\chi \gtrsim 5\,\mathrm{MeV}$ [219], see Section 4.2. The range of possible WIMP masses $5\,\mathrm{MeV} \lesssim m_\chi \lesssim 100\,\mathrm{TeV}$ is large, yet even less constrained are the interactions of these dark matter candidates with the SM. Presumably, the light particles to which WIMPs annihilate in the early Universe are part of the SM[1], in which case there are three canonical strategies for searching for WIMPs [131, 132, 133]. Direct detection, indirect detection, and collider searches for dark matter represent the main WIMP dark matter probes, and their complementarity places severe constraints on the nature of the WIMP particle.

[1] Actually, regarding the abundance of such particles in our current Universe, there is no need for them to be within the SM, the only requirement is that the dark matter particles were in thermal equilibrium with a plasma with the required annihilation cross section. If the dark matter predominantly interacts with particles BSM that are very weakly coupled to the SM, they are said to belong to a dark sector [220]. See [3, 4] for dark sectors related to sterile neutrinos.

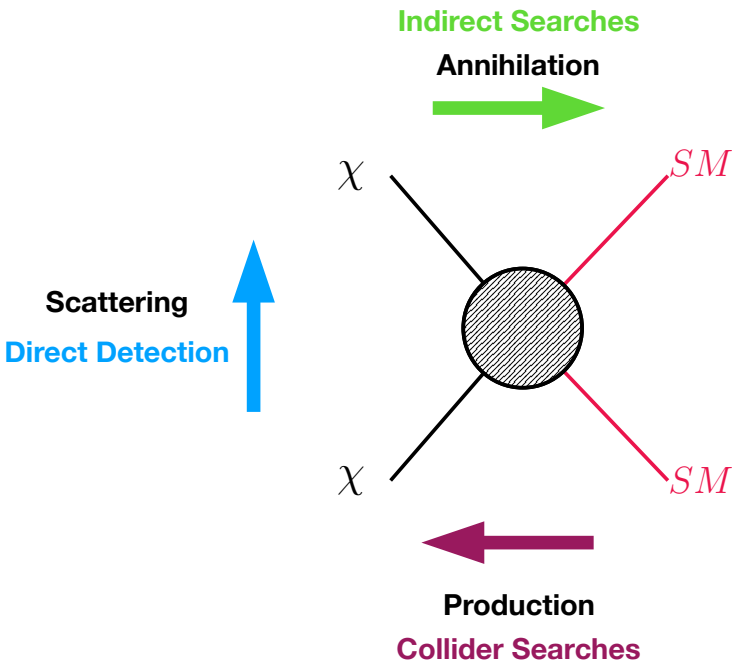

Figure 4.1: Graphical sketch of the WIMP processes that led to the main WIMP dark matter searches.

This Chapter is intended to provide an overview of the searches for WIMP dark matter particles. The physics case behind the most relevant searches, the current constrains, and their future reach is discussed in the following sections.

4.1 Direct Detection Searches

The idea behind direct detection searches is very simple, since the Milky Way is surrounded by a dark matter halo, and dark matter particles populate it, they should at some rate cross the Earth and scatter with nuclei. In practice, one expects the scattering rate to be small due to the weak interactions of WIMPs with SM particles. In addition, since dark matter velocities in the halo are similar to that of the solar system rotation $v \sim v_\odot = 220\,\mathrm{km/s}$ the amount of energy deposited after a scattering is small [221, 222]. For instance, $m_\chi = 10 - 10^3\,\mathrm{GeV}$ correspond to nuclear recoils of $E = 0.1 - 50\,\mathrm{keV}$. This energy may manifest in the detector as phonon excitations of the target material (heat), as scintillation photons from an excitation of the target nucleus, or as direct ionization of the target atoms [223]. Typical targets are noble liquids like Xenon or Argon, scintillating crystals, and detectors like Germanium. Additionally, due to the smallness of the expected rates and the very low thresholds, experiments should successfully deal with a variety of backgrounds.

Direct detection searches may be the most sensitive WIMP dark matter probe to date. Considering its relevance, following [224], we explicit the required formulae for calculating the number of events from WIMP scatterings. For a given target with mass number A, the differential rate per unit detector mass per unit time is given by the following expression

$$\frac{dR}{dE} \equiv \frac{dR}{M_{detector} dt dE} = \frac{\sigma(E)}{2\mu_{\chi A}^2} \frac{\rho_\chi}{m_\chi} \zeta(E,t)\,, \tag{4.1}$$

where $\mu_{\chi A} \equiv m_\chi m_A/(m_\chi + m_A)$ is the reduced mass of the dark matter-nucleus system, $\sigma(E)$ is the WIMP-nucleus cross section, ρ_χ is the local dark matter energy density customarily taken to be $\rho_\chi = 0.3\,\mathrm{GeV/cm^3}$ [225], and $\zeta(E,t)$ is the mean inverse speed:

$$\zeta(E,t) = \int_{u>v_{\min}} \frac{f(\mathbf{u},t)}{u}\, d^3\mathbf{u}\,, \tag{4.2}$$

where by simple kinematics, the energy of the nuclear recoil E is related to the velocity v as

$$E = \frac{\mu_{\chi A}^2}{m_A} v^2\,(1-\cos\theta) \rightarrow v_{\min} = \sqrt{\frac{m_A E}{2\mu_{\chi A}^2}}\,, \tag{4.3}$$

where $v_{\min}$ is the minimum velocity that could be attributed to a recoil of energy E. θ is the scattering angle in the center of mass frame and $f(\mathbf{u},t)$ is the distribution of dark matter velocities with respect to the detector. The form for $f(\mathbf{u},t)$ is usually taken to be a Maxwellian distribution, this choice

is the so-called Standard Halo Model. Accounting for the peculiar velocity of the Sun, neglecting the time dependence of Earth rotation around the Sun, and noting that particles with velocities $v > v_{\rm esc} = 544\,\text{km/s}$ should have escaped the Milky Way's gravitational potential, leads to an analytical expression for ζ given by:

$$\zeta(E) = \begin{cases} \frac{1}{v_0 y}, & z < y,\ x < |y-z| \\ \frac{1}{2N_{\rm esc} v_0 y}\left[\text{erf}(x+y) - \text{erf}(x-y) - \frac{4}{\sqrt{\pi}} y e^{-z^2}\right], & z > y,\ x < |y-z| \\ \frac{1}{2N_{\rm esc} v_0 y}\left[\text{erf}(z) - \text{erf}(x-y) - \frac{2}{\sqrt{\pi}}(y+z-x)e^{-z^2}\right], & |y-z| < x < y+z \\ 0, & y+z < x \end{cases} \tag{4.4}$$

where $x \equiv v_{\rm min}/v_0$, $y \equiv v_e/v_0$, $z \equiv v_{\rm esc}/v_0$ with $v_0 = 220$ km/s, $v_e = 245$ km/s and

$$N_{\rm esc} = \text{erf}(z) - 2z\exp(-z^2)/\pi^{1/2}\,. \tag{4.5}$$

Finally, we need to relate the WIMP-nucleus cross section $\sigma(E)$, with the WIMP-nucleon one. The two most common types of WIMP interactions are spin-independent (SI) and spin-dependent (SD). For them, the relation between the nucleus and nucleon cross section is given by

$$\sigma_{SI}(E) = \sigma_p \frac{\mu_{\chi A}^2}{\mu_{n\chi}^2} \frac{\left(f_p\, Z + f_n\,(A-Z)\right)^2}{f_p^2} F^2(E)\,, \tag{4.6}$$

$$\sigma_{SD}(E) = \frac{\sigma_p}{2J+1} \frac{\mu_{\chi A}^2}{\mu_{n\chi}^2} \frac{\left(a_p^2\, S_{pp}(E) + a_p\, a_n S_{pn}(E) + a_n^2 S_{nn}(E)\right)^2}{a_p^2}\,, \tag{4.7}$$

where σ_p is the WIMP-proton cross section, Z is the atomic number of the nucleus, J is the spin of the nucleus, and $\mu_{n\chi}$ is the reduced WIMP-nucleon mass. $F(E)$, $S_{pp}(E)$, $S_{pn}(E)$, $S_{nn}(E)$ are nucleon form factors that take into account the distribution of nucleons in the nucleus and therefore are nucleus dependent (see [222] for the most common ones). f_p, f_n, a_p, a_n represent the WIMP relative coupling strength between protons and neutrons. In general, one expects these couplings to be similar unless a cancellation occurs. Note for instance that, for a WIMP mediated by the SM Z, the relative strength is $f_n^Z/f_p^Z = -\frac{1/2}{1/2-2s_W^2} \simeq -22$ for $s_W^2(q \simeq 0.1\,\text{MeV}) \simeq 0.2385$ [47].

Finally, the number of expected events (N) is simply given by weighting Equation 4.1 with the detector efficiency to nuclear recoils $\epsilon(E)$:

$$N = \text{Exposure} \times \sum_i f_i R_i\,, \tag{4.8}$$

$$R = \int_{E_1}^{E_2} dE\, \epsilon(E)\, \frac{\sigma(E)}{2\mu_{\chi A}^2}\, \frac{\rho_\chi}{m_\chi}\, \zeta(E)\,, \tag{4.9}$$

where the sum is over the isotopes present in the target, E_1 and E_2 are the limits of the covered energy window in a given analysis, and the Exposure depends upon the fiducial mass and the integration time as Exposure $\equiv M_{\rm fid} \times t$.

The set of equations presented above encode the main physics and represent the standard equations describing the scattering interactions between WIMPs and nuclei. However, it is important to mention two recent relevant developments for direct detection analyses:

1. Effective Field Theory of Dark Matter Direct Detection

   In reality, the scattering of dark matter with nuclei is not necessarily SI or SD. In [226] the effective field theory of direct detection was obtained; namely, a complete map between dark matter-quark to dark matter-nucleon operators was established. The form of all possible WIMP-nucleus interactions was obtained in terms of Galilean invariant operators. In practice, one uses the machinery developed in [226] to study interactions that are not SI or SD, see also [227].

2. Halo Independent Methods

   The WIMP scattering rate depends upon various astrophysical factors [228]. In particular, it depends upon the velocity distribution of WIMPs. This velocity distribution is unknown (although it is expected to be somewhat similar to a Maxwellian distribution [229]) and assuming a particular form could spoil comparisons between experiments due to their possibly different energy windows. The work of Ref. [230] introduced an astrophysical independent method to compare direct detection experimental results. We refer the reader to [231] for the definitive statistical procedure in order to asses such halo independent analyses.

4.1.1 Experimental Situation and Prospects

The limits on the WIMP-nucleon scattering cross section from direct detection experiments have improved at an exponential rate [19] since they were first conceived [221]. Null searches from XENON1T [135], PandaX [137] and LUX [136] have set the tightest constraints to date on the WIMP-nucleon scattering cross section for SI interactions (and for SD-neutron interactions). Figure 4.2 shows the most up to date constraints on SI scatterings together with the projection for next generation of direct detection experiments. The current limits are of great relevance and generically rule out many dark matter candidates with masses $m_\chi > 10\,\text{GeV}$. The constraining power of current limits is such that they have to be taken into

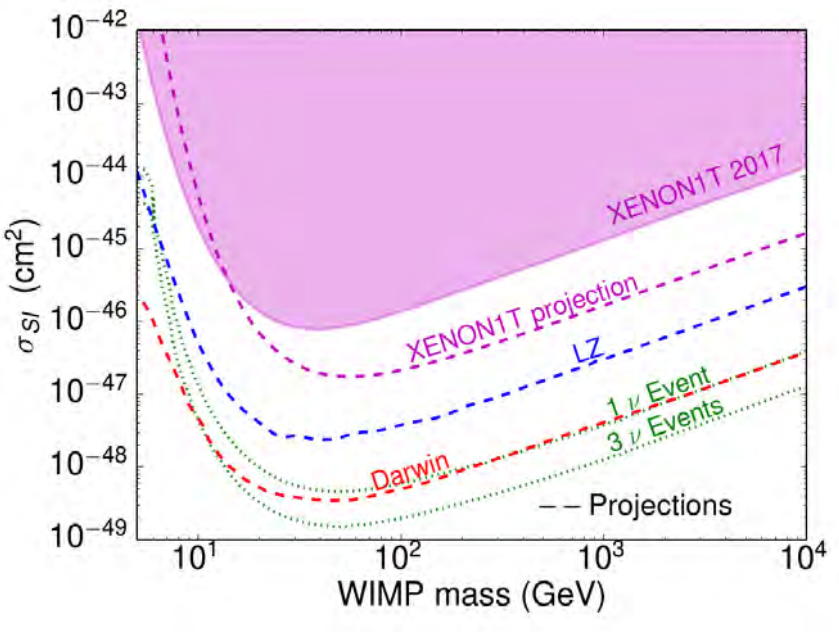

Figure 4.2: Current bounds and projections at 90% CL for various direct detection experiments for SI interactions. Bounds shown for XENON1T [135], although LUX [136] and PandaX [137] provide very similar results. We also depict the projections for the XENON1T full run [232], LZ [141] and Darwin [142]. Isocontour neutrino lines for the irreducible neutrino background [233] are shown in green, the neutrino floor.

account even for WIMP-nucleus interactions that are momentum q, velocity v, or loop-suppressed. In order to have a feeling on how such constraints probe dark matter models, Figure 4.3 shows the bounds from direct detection together with the relic abundance prediction for probably the most ubiquitous WIMPs: those that couple to the SM Z and Higgs bosons. Such models have been studied in detail by the author in [5], work presented in full form in Part II of this thesis. However, we present an updated sample here. One clearly notices that direct detection bounds represent stringent constraints on such types of models. Given that dark matter particles annihilating through their couplings with the Higgs or the Z boson are among the most natural WIMPs, this means that the WIMP paradigm is already under some pressure from the null searches from current direct detection experiments. Future planned experiments like LZ [141], DarkSide-20k [234] and Darwin [142] are expected to improve the current limits by 1-2 orders of magnitude, with projected exposures of $\sim 15\,\text{ton}\times\text{yr}$ and $\sim 200\,\text{ton}\times\text{yr}$ respectively. After such expected increase in sensitivity, the experiments will start measuring neutrinos from various sources [233]. These neutrinos will represent an irreducible background and will certainly slow further progress. This is the so-called "neutrino floor". This irreducible background

of coherent neutrino scatterings will modify the reach of future direct detection experiments to WIMP-nucleon scattering depending on the target, the exposure, the type of interactions, and the dark matter mass [235].

To conclude, direct detection represents a fundamental probe for dark matter. The current limits are of unprecedented sensitivity and rule out a variety of theoretically appealing models. However, we must note that there are very well motivated models that either have momentum, velocity or loop suppressed scatterings with nucleons and may be harder to test by this procedure. It should be clear however, that if next generation of direct detection experiments do not to find a signal, the WIMP paradigm will be under strong pressure. It should be noted that scenarios in which the dark matter scattering is suppressed, should still allow for the search of the annihilation products of dark matter particles and for their production at collider experiments. These are the subjects of study of the two next Sections.

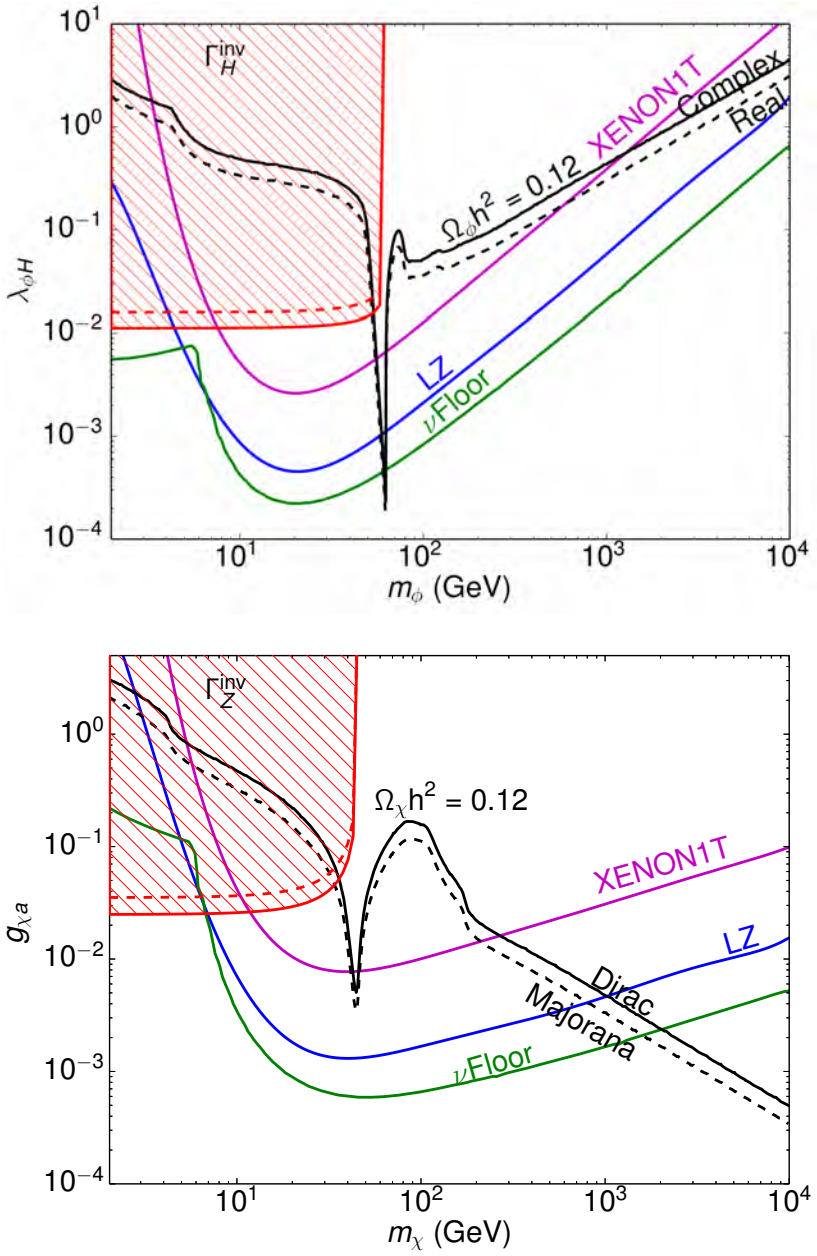

Figure 4.3: Relic abundance predictions for two benchmark dark matter models in black. The constraints from colliders are shown in red (see Section 4.3). Current bounds from direct detection are illustrated in magenta from XENON1T [135] and projections for LZ [141] are shown in blue. The *upper frame* corresponds to the Singlet Scalar model [212] and the *lower frame* corresponds to a fermionic WIMP axially coupled to the Z [236].

4.2 Indirect Detection Searches

WIMPs are thermally produced in the early Universe by a freeze-out of their annihilations with light particles in the plasma. Even though today's WIMP cosmological abundance has been considerably diluted compared to its primeval one $\bar{n}_{\rm today}/\bar{n}_{\rm early} \sim 10^{-40}$, since dark matter is present and dominates the dynamics of a variety of astrophysical environments and the Universe itself in a sizeable portion of its history $3 \lesssim z \lesssim 3000$, signals from its annihilations are expected in the current and recent Universe. From the astrophysical point of view, we expect that the WIMPs present in galaxies and clusters of galaxies annihilate, in particular in the most dense regions. From the cosmological perspective, dark matter annihilations may lead to an impact in the ionization history of the Universe, and thus, to a measurable effect on the CMB anisotropies or at experiments that target the characterization of the epoch of reionization. From a cosmic-ray perspective, the WIMP annihilation products may lead to an excess in different cosmic-rays fluxes. Particularly in gamma-rays, neutrinos, positrons and antiprotons.

The annihilation rate for selfconjugate dark matter particles, as in the early Universe, is written as

$$\Gamma = \frac{\langle \sigma v \rangle}{2} n_\chi^2 = \frac{\langle \sigma v \rangle}{2} \frac{\rho_\chi^2}{m_\chi^2} \,, \tag{4.10}$$

where $\langle \sigma v \rangle$ is the annihilation cross section, n_χ is the number density, ρ_χ is the energy density, m_χ the mass, and the factor of two avoids double counting. From this expression, it is clear that the higher the density of WIMP particles is, the larger the annihilation rate. This will be for example the case of the inner region of the Milky Way, dark matter dominated dwarf galaxies or galaxy clusters. From a cosmological point of view, we know that since $n_\chi \propto (1+z)^3$ the rate will be higher the younger and smaller the Universe was. Additionally, since CMB observations fix the energy density in dark matter $\rho_\chi = \Omega_\chi \rho_c$, the annihilation rate decreases like m_χ^{-2} provided $\langle \sigma v \rangle$ is kept constant. Thus, for heavy WIMPs, bounds from indirect or direct searches will relax simply due to the fact that there are fewer dark matter particles.

The annihilation cross section may depend upon the relative velocity of the colliding dark matter particles. The velocity dependence is directly related to the angular momentum of the collision. If the angular momentum is $L = 0$, the collision is called s-wave and does not depend upon the velocity. If the angular momentum is $L = 1$, the annihilation is called p-wave and the annihilation cross section scales as $\langle \sigma v \rangle \propto v^2$. If the annihilation is p-wave, due to the fact that in the early Universe $v^2 \sim 3T/m_\chi \sim 0.1 \times c$ the

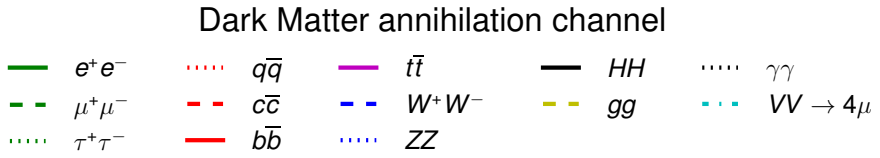

Figure 4.4: Primary annihilation spectra for a $m_\chi = 1$ TeV dark matter particle for different annihilation channels. K is the energy. Extracted from [237]. The spectra for a 2 TeV decaying particle will be the same.

WIMP freeze-out is not significantly affected [126]. However, dark matter particles with typical stellar velocities $v \sim 300\,\mathrm{km/s} \sim 10^{-3} \times c$ suffer from a $\sim 10^{-5}$ suppression in the annihilation cross section in the current Universe compared to the primeval one. This velocity dependence precludes indirect searches constraints for p-wave annihilating thermal relics.

The final annihilation products of WIMPs will be stable SM particles: photons, neutrinos, electrons and positrons, protons and antiprotons, and some stable light nuclei too. It must be noted that with respect to cosmic-ray searches, since electrons and protons are produced in a variety of astrophysical phenomena, they represent a harder target for dark matter searches. Thus, in general, cosmic-ray indirect searches of dark matter focus on photons γ, positrons e^-, antiprotons p^+, and neutrinos ν. Figure 4.4 shows the resulting spectra for various annihilation channels for a $m_\chi = 1\,\mathrm{TeV}$ WIMP.

In what follows, the physics case and status of the currently most constraining indirect dark matter searches is presented. We note that these searches only represent a subset of all the existing ones, the reader is referred to [238, 239, 240] for recent reviews on the subject.

4.2.1 Cosmological probes

The CMB and BBN periods offer unique scenarios to test a variety of BSM scenarios [13, 241, 242]. Particularly, they offer important constraints on WIMP dark matter.

4.2.1.1 Dark matter annihilations and the CMB

Observations of the Cosmic Microwave Background can constraint dark matter annihilations through their electromagnetic energy injection during the dark ages ($20 \lesssim z \lesssim 1100$). Energy injection leads to increased ionization, heating, production of Lyman-α photons and distortions of the energy spectrum of the CMB that are potentially observable. In particular, the latest Planck results [13] set a bound $f_{\mathrm{eff}} \langle \sigma v \rangle / m_\chi < 3.4 \times 10^{-28}\,\mathrm{cm^3/s/GeV}$ at 95% CL where f_{eff} is the energy injection efficiency into the medium. This efficiency depends upon the channel. Note that, for instance, a gamma-ray of $E \sim 1\,\mathrm{GeV}$ will be transparent to the intergalactic medium. The efficiency f_{eff}, is in principle a redshift dependent expression; however, it has been shown that for generic WIMP models, this time dependence can be well mimicked by a weighted constant efficiency [243]. In light of this result, Refs. [244, 245] generalized the Planck 2015 constraint and provided

a consistent treatment of the energy injection in the medium for any given WIMP model, where $f_{\rm eff} \in [0.15-0.6]$ depending on the precise annihilation channel and the mass. The main result from the Planck 2015 observations is that s-wave annihilating dark matter is ruled out for dark matter masses $m_\chi \lesssim 10\,\text{GeV}$ independently on the annihilation channel, provided it is not to neutrinos. We note that studies of the impact of p-wave annihilations in the CMB anisotropies and in reionization observables have also been carried out; however, due to the velocity suppression of p-wave annihilating dark matter, such analyses do not probe thermal dark matter candidates [246, 247].

4.2.1.2 Constraints from other energy injections at the CMB and BBN epochs

As discussed in the previous paragraph, the CMB anisotropies are very sensitive to energy depositions during the dark ages. Similarly, the production and destruction rates of light elements in the early Universe could also be severely affected by electromagnetic injections of energy. The excellent agreement between the CMB and BBN observations with the predictions assuming no additional energy injection, constraints the presence of particles in the early Universe that could inject significant electromagnetic power into the plasma. In particular, BBN excludes decaying particles with $\tau \gtrsim 1\,\text{s}$ present in thermal abundances [248], and both BBN and the CMB observations constrain other – not necessarily thermal – relics with a variety of masses, lifetimes and abundances [249, 250]. Such constraints do not directly apply to dark matter particles, but there are several models in which long-lived particles are expected to accompany the dark matter ones.

4.2.1.3 Bounds on additional relativistic species

The precise CMB observations by Planck [13] indicate that the number of neutrino-like relativistic species contributing to radiation is $N_{\rm eff} = 3.15 \pm 0.23$. The predicted value in the SM is $N_{\rm eff}^{SM} = 3.045$ [251] (the small difference from 3 is due to QED corrections, non-instantaneous neutrino decoupling and neutrino oscillations in the primeval Universe). This result implies:

1. There is a lower bound on thermal dark matter of $m_\chi \gtrsim 5\,\text{MeV}$ [219] (but for a real scalar WIMP) independently on whether the annihilation is s-wave or p-wave. Thermal dark matter particles decouple at $T \sim m_\chi/20$ and therefore, their thermal contact either with neutrinos or the electromagnetic plasma results in a net change on $N_{\rm eff}$.

2. The contribution to the relativistic energy density from additional relativistic species present at $z \gtrsim 3000$ should be small. This constraints the possibility of dark matter being accompanied by light stable particles [252]. This constraint can however be evaded provided that such light stable particles decoupled early enough, or by modifying the thermal history of the early Universe.

4.2.2 Cosmic-ray searches

4.2.2.1 Gamma-rays

The main advantage of cosmic gamma-ray searches is that photons point to their source. Yet, a variety of astrophysical phenomena, like pulsars, blazars and others generate them at the energies of interest for dark matter annihilations $E_\gamma = \text{MeV} - \text{TeV}$. So far, the most reliable source of constraints on dark matter annihilations with gamma-rays are the dwarf galaxies of the Milky Way. Dwarf galaxies are among the most dark matter dominated objects in the Universe. They are usually faint, since their number of gravitationally bounded stars is of the order of 50 and below. However, upon kinematical measurements, their gravitational potential is found to be heavily dominated by dark matter [16]. From dwarf galaxies observations [253], the Fermi-LAT [138] collaboration has been able to place very strong constraints on WIMPs annihilating to hadronic ($\bar{b}b$, $\tau^+\tau^-$) channels, ruling out dark matter masses below $\lesssim 50\,\text{GeV}$ for s-wave annihilating thermal relics. It is worth noticing that the dark matter searches in dwarf galaxies are not free of uncertainties, such as those associated with departures from spherical symmetry [254] and with issues related to stellar membership [255]. However, they are considerably less severe than other methods. In addition to dwarf galaxies, bounds on the dark matter annihilation cross section from gamma-ray searches can also be set from galaxy groups observations [256] and from the Milky Way halo emission [257].

4.2.2.2 Neutrinos

As seen in Figure 4.4, neutrinos are copiously generated by dark matter annihilations (produced either by direct decay or by charged pion decays depending on the annihilation channel). On one hand, the resulting neutrinos from the annihilation point directly to the source. But on the other hand, neutrinos have tiny cross sections and therefore are difficult to detect. Despite the elusive nature of neutrinos, limits from neutrino telescopes such as IceCube [258] and ANTARES [259] have been set by considering

dark matter annihilations from the entire Milky Way. These bounds are, however, weaker by ~ 3 orders of magnitude as compared to those from gamma-ray searches. It should also be noted that bounds from neutrino telescopes on dark matter particles exclusively annihilating to neutrinos are also three orders of magnitude above the thermal relic expectation. In addition to searches in the Milky Way, neutrino telescopes are also capable of searching for dark matter annihilations in the Sun. If the dark matter interacts with protons and it is sufficiently heavy $\gtrsim 4$ GeV, dark matter particles can be trapped in the center of the Sun and eventually annihilate (to neutrinos). By these means, the IceCube [260] and ANTARES [261] collaborations have placed competitive bounds on the proton SD cross section compared to those reported from direct detection experiments, particularly if the annihilation is to $\tau^+\tau^-$.

4.2.2.3 Positrons and antiprotons

Contrary to photons and neutrinos that point to their source, positrons and antiprotons – when generated in dark matter annihilations – are subject to diffusion in the galaxy through magnetic fields. The modelling of such diffusion processes is considerably involved and subject to many uncertainties [262]. However, from the observational perspective, the AMS-02 experiment has measured – with unprecedented accuracy – the cosmic positron [263] and antiproton [264] spectra. Despite of the modelling difficulties and the uncertainties associated with the cosmic-ray propagation in the galaxy, many groups have carried out analysis constraining dark matter annihilations using the positron and antiproton data, see for example [265] and [266, 267] respectively. The positron constraints are particularly strong for leptonic (e^+e^-, $\mu^+\mu^-$) channels, while the antiproton bounds provide a good handle on hadronic channels. The constraints and the systematic uncertainties from these studies are shown in Figure 4.5. We notice that the systematic uncertainty in these studies varies within a factor of three to ten depending on the WIMP mass, the annihilation channel, and the study.

4.2.3 Signals

4.2.3.1 The Galactic Center gamma-ray excess

In 2009 Hooper and Goodenough [269, 270] found evidence for an excess above the expected background observed in the diffuse gamma-rays coming from the Galactic Center in the Fermi-LAT data. Compared with other putative signals from dark matter annihilation, the Galactic Center

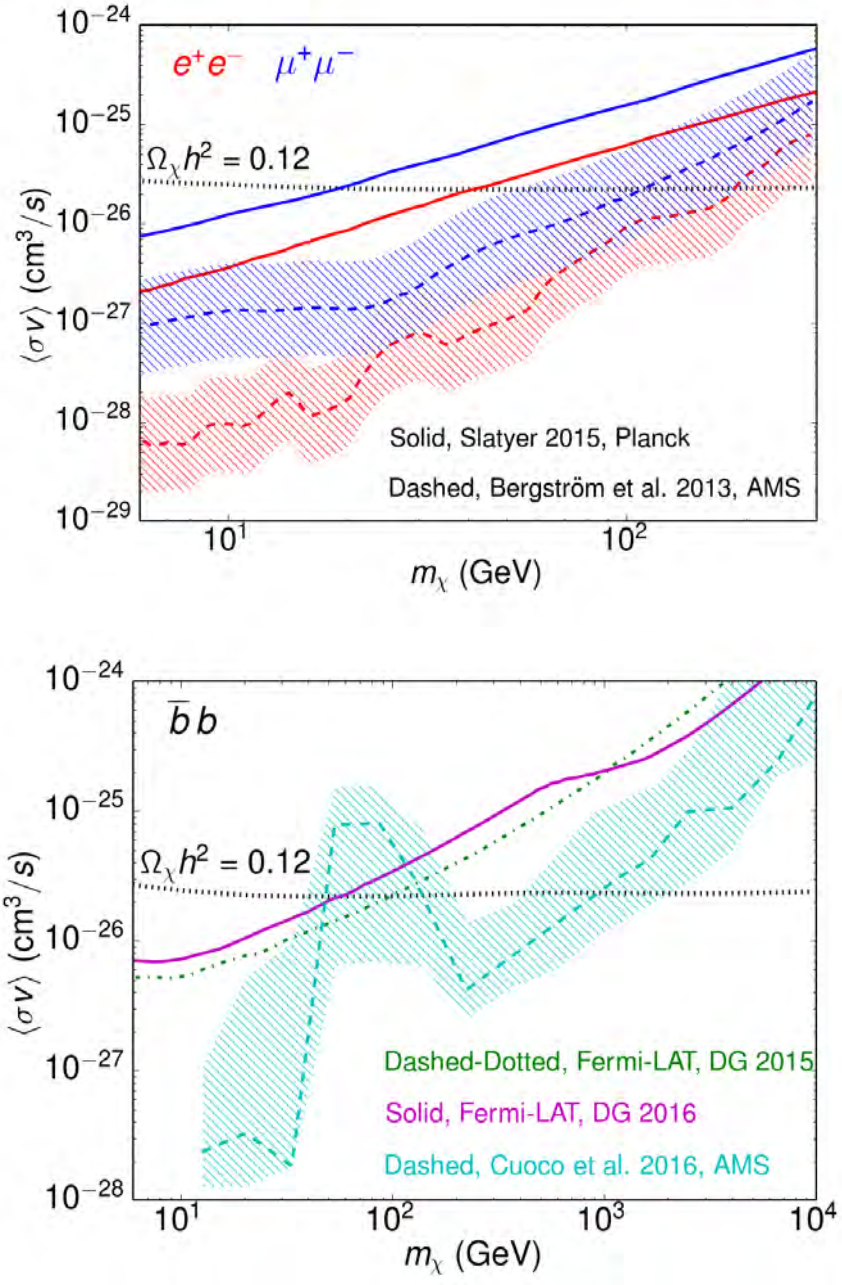

Figure 4.5: Main current constraints from indirect dark matter searches. *Upper panel:* constraints on leptonic channels. Planck 2015 [13] constraints as obtained in [244] (solid), and AMS-02 studies from [265] (dashed) where the band represents the systematic uncertainty, and in double-dotted black the thermal relic expectation from [211]. *Lower panel:* constraints on the $\bar{b}b$ channel. Constraints from the Fermi-LAT collaboration [138, 268] and from the AMS-02 antiproton spectra [266], the band represents the systematic uncertainty.

gamma-ray excess stands out. This signal has been subject of intense study over the past nine years (see Refs. [269, 270, 271, 272, 273, 274, 275] and references therein). The signal has been shown with high statistical significance to exhibit a spectrum, morphology and overall intensity that is compatible with that predicted from annihilating dark matter particles in the form of a $\sim$30-70 GeV thermal relic distributed with a profile similar to that favored by numerical simulations. In addition to the dark matter annihilation interpretation, millisecond pulsars have been proposed to explain the excess – since they have a very similar gamma-ray spectrum – and they represent the leading astrophysical interpretation [276, 277, 278]. Yet, this interpretation will require pulsar populations which are very different from those observed in the environments of globular clusters or in the field of the Milky Way. At this point in time, however, there is no clear resolution to the question of the origin of the Galactic Center excess. Radio searches for millisecond pulsars populations have been proposed [279] and continuous observations by the Fermi-LAT satellite on Milky Way dwarf galaxies may shed light (never better said) on the actual interpretation. In this thesis, we have highlighted the viability of a dark matter interpretation of the Galactic Center gamma-ray excess [6, 7].

4.2.3.2 Cosmic-ray antiprotons

A $\sim$4.5 σ antiproton excess [266, 267] has been reported from measurements of the cosmic-ray antiproton spectrum by AMS-02, peaking at energies of approximately $\sim$10-20 GeV. Furthermore, the characteristics of the antiproton and the Galactic Center gamma-ray excesses suggest that they could potentially be generated by annihilations of the same dark matter candidate. For the simple case of a dark matter candidate that annihilates directly to $b\bar{b}$, masses in the range of $\sim$50-90 GeV have been shown to be able to accommodate the spectral shape of the antiproton excess [266, 267].

4.2.4 Summary and Outlook

Indirect searches of dark matter represent a key tool to test the dark matter nature (see Figure 4.5 for a compilation of constraints). The high precision observations of the CMB by the Planck satellite have ruled out s-wave annihilating dark matter for $m_\chi \lesssim 10\,\text{GeV}$ [13] independently on the annihilation channel [244], but to neutrinos. Along these lines, future CMB Stage-IV experiments could potentially test s-wave thermal dark matter for $m_\chi \lesssim 40\,\text{GeV}$ [54]. CMB observations [13], through the measurement of the number of the effective relativistic species, constrain the thermal history of

the Universe and prohibit the existence of a number of long-lived particles that could potentially be related to the dark matter particle. Furthermore, such constraints have significant room for improvement since stage-IV CMB experiments [54] will reach unprecedented sensitivity to $N_{\rm eff}$ ($\sigma(N_{\rm eff}) \gtrsim 0.03$) and will improve our knowledge of the thermal history of the Universe. Gamma-ray searches currently constrain dark matter hadronic annihilation channels for s-wave thermal relics of masses $\lesssim 50\,\text{GeV}$. The Fermi-LAT collaboration [143] foresees that with 15 years of data, and taking into account the likely discovery of new Milky Way satellites by upcoming photometric galaxy surveys like LSST [101], the bounds on $b\bar{b}$ and $\tau^+\tau^-$ annihilations could strengthen for thermal relics to 400 GeV and 200 GeV respectively (unless excesses at dwarf galaxies appear, which would be even more interesting). The positron and antiproton cosmic-ray spectrum measurements also provide a good handle on dark matter annihilations [265, 266, 267]. At present, the resulting bounds from such analyses are subject to more uncertainties than those from CMB studies or from Milky Way dwarf galaxies gamma-ray searches. However, if these uncertainties are reduced in future studies, positron and antiproton searches will provide robust tests on annihilating dark matter.

The indirect searches possibilities are countless. In addition to those previously discussed, the upcoming 21-cm cosmological observations may prove useful for constraining annihilating dark matter [280, 281]. Gamma-ray observatories targeting the TeV dark matter region like CTA [282], or the continuous observation of extragalactic neutrinos by the IceCube telescope [283] could be relevant for heavy dark matter relics. Finally, although we have restricted ourselves to the hypothesis that dark matter is stable, indirect searches show that the dark matter lifetime, depending on the decay channel, should be orders of magnitude higher than the age of the Universe [121, 246, 284, 285, 286].

To conclude, indirect dark matter searches are crucial probes of dark matter. Via their variety of approaches, methods and perspectives a plethora of theoretical scenarios have been tested. However, the unfeasible reach of indirect searches to thermal candidates produced via p-wave annihilations in the early Universe make indirect dark matter searches mandatory to be complemented with direct detection and collider searches.

4.3 Collider Searches

Motivated by the simplicity of the WIMP miracle, it is expected for the dark matter to have some sizeable (although weak) interactions with SM particles. However, the WIMP miracle on its own does not provide enough information to pin down what are the precise non-gravitational interactions of the dark matter particle. Therefore, some theoretical input is needed in order to provide guidance to what such interactions may be. Theoretical models attempt to simultaneously explain various missing pieces in the SM, like neutrino masses, the strong CP problem or the hierarchy problem, together with the dark matter problem. It is usually the case that very well motivated theories and models that account for dark matter include other non-stable and less weakly interacting particles that are often easier to detect than the dark matter itself and can lead to very particular signatures at colliders. This is for instance the case of Supersymmetry [130, 131]. Despite the clear model dependence of the signatures to expect at lepton and hadron colliders from dark matter and their BSM accompanying particles, there are a few model independent signatures and processes that may point more directly to WIMP dark matter.

Based on the fact that *i)* dark matter should have a lifetime considerably larger than the age of the Universe $t = 13.8\,\mathrm{Gyr}$, and *ii)* WIMPs are neutral and weakly interactive; if produced at particle colliders, WIMPs would escape the detector and their presence would only be then attributed to some missing energy or momentum transfer in the collision. From this perspective, the main model-independent constraints and signatures of dark matter at colliders are summarized in the following (see Figure 4.6). For a complete status of the dark matter searches at the Large Hadron Collider (LHC) the reader is referred to the ATLAS and CMS exotic results [139, 140]. For a review of the LHC dark matter searches we refer the reader to Ref. [287], for their interpretation in the context of simplified dark matter models, see [288], and for unitarity and gauge invariance implications of simplified dark matter models see [289].

4.3.1 The Higgs

The Higgs, being the main character in the SSB of the SM, plays a pivotal role in the electroweak interactions within the SM. From this perspective, its connection with WIMPs seems very plausible and theoretically appealing. The Higgs behaviour, based on its measured properties [198], resembles so far that predicted by the SM. The precision of such measurements constrains severely some dark matter models. Particularly, dark

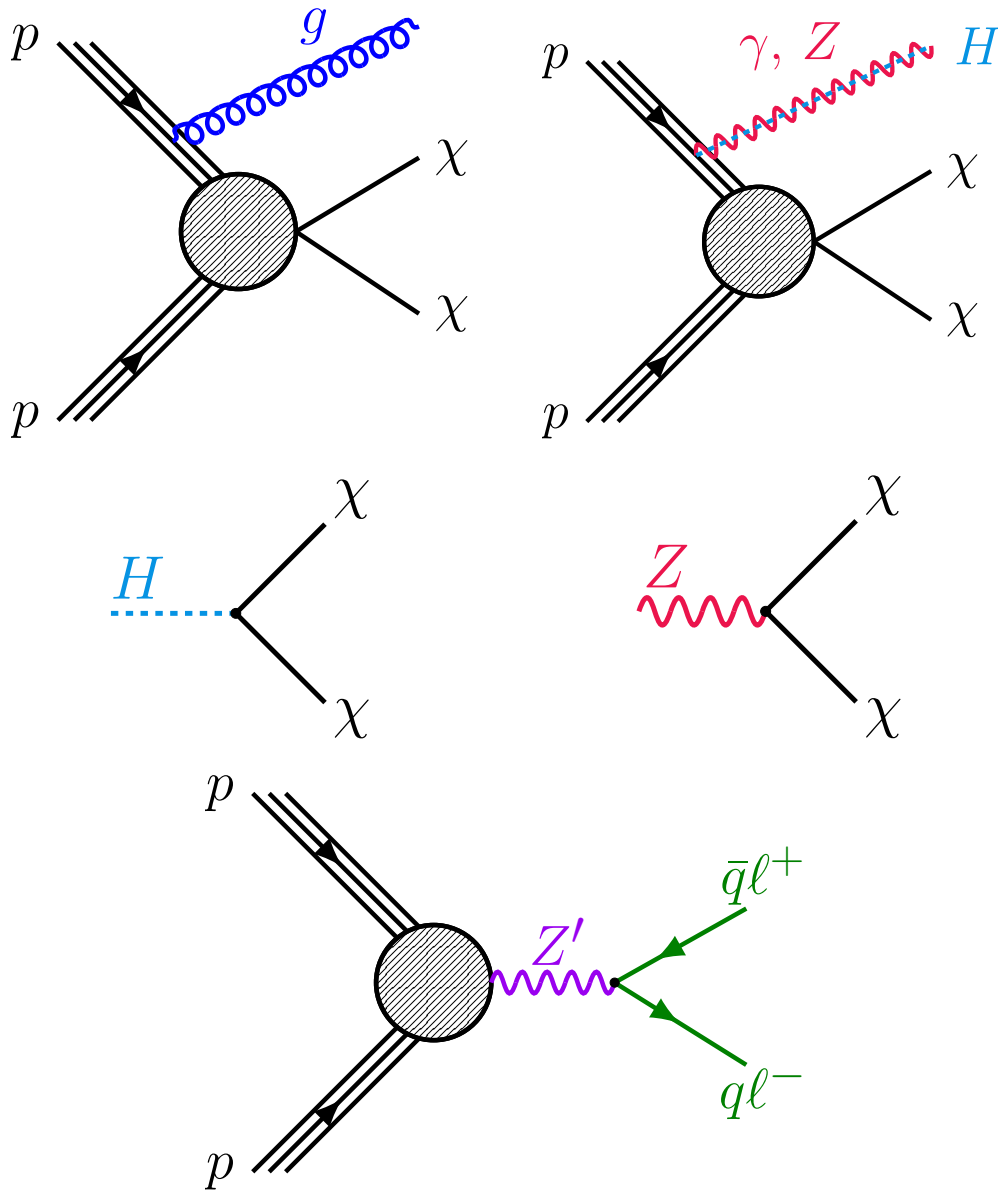

Figure 4.6: Diagrams of some of the main processes that constrain dark matter at particle colliders. *Upper panel*: monojet and mono-γ-Z-H dark matter production diagrams. *Middle panel*: Higgs and Z invisible decays. *Lower panel*: Drell-Yan dilepton or dijet production of a Z' mediator.

matter couplings with the Higgs will induce new invisible decays of such scalar, provided $m_\chi < m_H/2$. In the SM, this branching ratio is quite small $\mathrm{Br}^{\mathrm{SM}}(H \to \mathrm{inv}) = \mathrm{Br}(H \to \bar{\nu}\bar{\nu}\nu\nu) \simeq 10^{-4}$. From the LHC data, the ATLAS and CMS collaborations report a 95% CL upper limit on such invisible decay of $\mathrm{Br}(H \to \mathrm{inv}) < 0.23$ [290, 291]. This constraint usually rules out WIMPs coupled to the Higgs with masses $m_\chi \lesssim m_H/2$, see for instance Refs. [3, 4, 5] presented in full form in Part II of this thesis. In addition to possible direct couplings of the Higgs to dark matter, it is worth mentioning that to date, the only mass mechanism displayed in nature is the Higgs mechanism. Thus, it seems very plausible that dark matter masses are generated from the same mechanism but through a different scalar field. In general, these new scalar states will mix with the SM Higgs leading to small departures from its predicted rates within the SM. In this spirit, precision Higgs measurements performed at the LHC probe – although indirectly – the mass generation of dark matter particles. Thus, since the Higgs represents such a portal to dark matter, its characterization may be fundamental to probe the nature of dark matter.

4.3.2 The Z

The Z boson is, together with the photon, the responsible of the neutral current interactions within the SM. Its properties were measured at the per-mil level at LEP [292]. Similarly to what happens with the Higgs, were the dark matter to couple directly to the Z, there would be very little room for dark matter being thermally produced in the early Universe with $m_\chi \lesssim m_Z/2$ [5]. In addition to such direct constraint, the Z precision observables have accurately shaped the SSB pattern of the SM, and therefore particles accompanying the dark matter that could spoil such pattern suffer from very strong constraints.

4.3.3 Dilepton/dijet

In the case that WIMPs do not directly couple to SM bosons, but interact with leptons or quarks through a BSM mediator, very strong constraints from the LHC and other collider experiments apply. Processes involving two leptons in the final state (e or μ) are among the best characterized Drell-Yan processes in the SM. In addition, in regions of invariant dilepton mass sufficiently outside the Z resonance the backgrounds are rather small. The power of these constraints is such that they allow to rule out dark matter particles coupled to these mediators even when $m_\chi \sim m_{Z'}/2$; i.e. when the relic abundance is produced on resonance. For instance, the recent

LHCb [293] and ATLAS [294] analyses severely constrain particles decaying to muons in the mass range $0.2\,\text{GeV} \lesssim m_{Z'} \lesssim 70\,\text{GeV}$ and to electrons and muons in the mass range $150\,\text{GeV} \lesssim m_{Z'} \lesssim 3.5\,\text{TeV}$ respectively. For mediators that couple predominatly to quarks, recent dijet analysis [295] provide stringent constraints in the $200\,\text{GeV} \lesssim m_{Z'} \lesssim 3.5\,\text{TeV}$ mass range [296, 297].

4.3.4 Monojet

If dark matter is produced at hadron collider experiments, it is expected to be produced together with one or more QCD jets from initial state radiation. In a given collision, requiring one jet to be very energetic and considering only processes with large missing momentum transfer has led to strong constraints on dark matter models with leptophobic and coloured mediators by the ATLAS [298] and CMS [299] collaborations.

4.3.5 Mono-V-Higgs

In a similar fashion to monojet searches, a γ, Z or H could be emitted from initial state radiation in association with dark matter, although with a smaller cross section. However, on the bright side, photons, leptonically decaying Z's, and various Higgs decays render very clean signatures at the detector. Therefore, searches focused on such channels also provide somewhat strong constraints [298, 300, 301], particularly to dark matter mediators that couple significantly to the electroweak bosons. Note that constraints from such searches are expected to significantly improve in the future since they are mostly statistically limited.

4.3.6 Low energy probes

Electron-positron colliders at energies $E = m_\Upsilon \simeq 10\,\text{GeV}$ offer very stringent tests for light dark matter. Particularly, the BaBar collaboration has placed strong constrains on light mediators that decay to charged leptons [302] (e and μ), and also to mediators that decay invisibly [303] in the mass range $\sim 0.2 - 10$ GeV.

4.3.7 Summary and Outlook

To conclude, almost independently on the dark matter nature, provided it is somehow related to the SM, there are various ways of probing dark matter at collider experiments. The direct production of dark matter particles

via monojet or mono-γ-Z-H searches offers very model independent constraints. The invisible decays of the Higgs or the Z bosons provide strong constraints on light dark matter particles with electroweak interactions. In addition, searches for mediator particles that connect the SM to dark matter represent very stringent constraints for WIMPs that do not directly couple to SM particles. Figure 4.6 shows an schematic representation of the main ways of testing dark matter at colliders, and Figure 4.7 shows a sample of constraints for leptophobic dark matter models. From Figure 4.7 one can appreciate the complementarity of the different searches and the high sensitivity reached at the LHC experiments.

So far no conclusive evidence for BSM physics has been claimed at any particle collider. However, the very precise data acquired at colliders as LEP, LHC and BaBar have shaped our understanding of the plausible theoretical models that could account for the dark matter in the Universe. In particular, they have pushed WIMPs to energy scales above the TeV in a wide variety of channels. The future of collider probes for dark matter seems promising with the upcoming upgrades at LHC, the already ongoing installation of Belle-II [145], and the possible exploration of the long lived frontier by MATHUSALA [304]. Thus, collider searches for dark matter offer a controlled and very precise test of the WIMP hypothesis. There are however two limitations of collider searches *i)* if the dark matter is heavier than the collider maximum center of mass energy, it cannot be produced by pure kinematics, and *ii)* if a detection of a particle with the desired properties of a dark matter candidate is made at a collider experiment, further confirmation from direct or indirect searches will be required in order to identify it with the dark matter particle that constitutes the non-baryonic matter of our Universe.

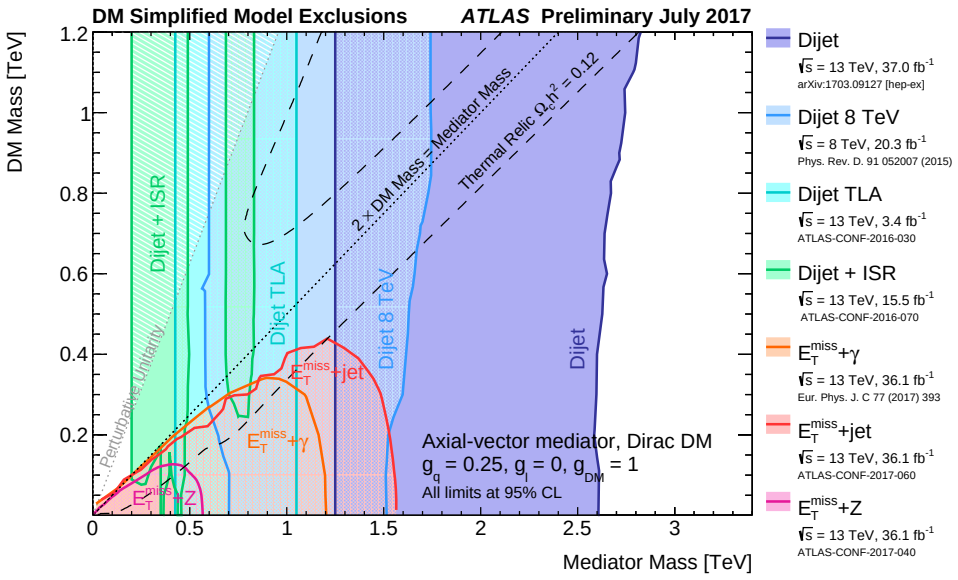

Figure 4.7: ATLAS constraints on leptophobic dark matter models. Reproduced from [139].

4.4 Finale

At present, WIMP dark matter is subject to very strong constraints from null searches at direct detection experiments [135, 137, 136] (Section 4.1), the absence of confirmed signals from indirect searches [13, 138, 241, 242, 265, 266, 267] (Section 4.2), and the lack of any sign of new physics at collider experiments [139, 140] (Section 4.3). Although at this point in time already under some experimental pressure, the WIMP paradigm still elegantly addresses the production of dark matter in the early Universe and theoretically it is successfully linked with theories and models that simultaneously confront various missing pieces in the SM. In addition, WIMPs have led to a plethora of experimental ideas that are currently probing the consequences of the existence of such dark matter particles in a fully complementary way. There are ongoing and future experimental efforts [141, 142, 143, 54, 144, 145] to test the dark matter nature, and it does not seem unlikely that in the near future a signal could be observed at any experiment targeting WIMPs. What it is certainly expected is that the experimental results in the years to come will shape our theoretical understanding of the nature of dark matter, possibly in an unforeseen way.

Chapter 5

Summary and Conclusions

As outlined in the Introduction 1, the astrophysical and cosmological evidence for the existence of dark matter is overwhelming. Dark matter dominates the dynamics of galaxies, clusters of galaxies and the vast majority of the virialized objects in the Universe. The cosmological implications are perhaps even more striking: dark matter seeds the large scale structures that we observe today. Furthermore, high precision CMB observations by the Planck satellite [13] show that $\sim 84\%$ of the matter in the Universe is non-baryonic, and that dark matter represents $\sim 26\%$ of the Universe's energy budget (when interpreted within the ΛCDM paradigm). The unambiguous evidence for dark matter, and the motivation for particle dark matter, strongly contrasts with the lack of new physics in all other experiments. In the absence of evidence for particle dark matter, in this thesis we have taken a broad phenomenological approach studying the complementarity of cosmological and particle physics probes of thermal dark matter candidates. In what follows, the motivation and main results from each of the individual studies presented in this thesis are discussed.

As outlined in Section 1.4 and reviewed in Chapter 4, the dark matter interactions with SM particles are strongly constrained. However, due to their elusive nature, neutrinos represent the exception to this rule. In order to constrain the possibility that neutrinos interact with dark matter we analized the cosmological implications of dark matter-neutrino scattering for current and future CMB and LSS observations [1]. These cosmological probes are affected by dark matter-neutrino scattering via collisional damping, suppressing the matter power spectrum at small scales. In our study we combined Planck 2013 CMB observations with the WiggleZ matter power spectrum measurements in the redshift interval $0.1 < z < 0.9$. We obtained the tightest constraints on dark matter-neutrino interactions from cosmol-

ogy within the linear regime, i.e. when the cosmological perturbations can be solved with out the need for numerical N-body simulations. Additionally, we provided forecasted sensitivity analysis for upcoming galaxy surveys, such as DESI, in the context of dark matter-neutrino interactions.

Given the complexity of the interactions and particle content in the Standard Model, one might question the often used simplifying assumption that dark matter is comprised of a single particle species. We have recently entered an era of precision cosmology that offers a quantitative test of this assumption. In [2] we considered a scenario with both cold and non-cold dark matter particles. We confronted this model with the latest CMB observations by the Planck satellite, tomographic weak lensing measurements from the KiDS survey, and the observed number of Milky Way dwarf galaxies. The combination of this measurements covers the linear, mildly non-linear and the highly non-linear regimes of cosmological perturbations. As a result of this study, we were able to constrain the abundance of non cold dark matter in a manner that is complementary to constraints derived from the Lyman-α forest.

Neutrino masses and the nature of dark matter are perhaps the two most obvious missing pieces of the SM. It is therefore theoretically appealing to link both phenomena within the same model. In [3], we linked the dark matter particle with sterile neutrinos – responsible for the light active neutrino masses via the type-I seesaw mechanism – within a spontaneously broken global $U(1)_{B-L}$ symmetry. One of the main consequences of this scenario is the appearance in the spectrum of a massless Goldstone boson, the *majoron*. The rich phenomenology of the model was explored in detail. We tested the viability of the model with collider, direct detection and indirect searches. In particular, we realized that when the CP-even scalar in the model is sufficiently heavy, the dark matter annihilates predominantly to sterile neutrinos in the contemporary Universe. We showed that due to the presence of the massless majoron, dark matter annihilations can only be probed by gamma-ray searches for dark matter masses $\gtrsim m_W$. In complementary work [4], we considered dark matter confined to a dark sector, with interactions only connected to the SM via sterile neutrinos. In this model, the sterile neutrinos – being singlets under both groups – represent the link between the dark sector and the SM. Within this framework, the dark group is global and remains unbroken; and thus, the dark matter is naturally stable by virtue of being the lightest particle of the dark sector. We detailed the phenomenology of the scenario, testing its validity with collider constraints, direct detection and indirect detection searches. Within this set up, the dark matter relic abundance is solely set by annihilations to sterile neutrinos. This leads to observable signatures at experiments sensitive to dark matter annihilations like Fermi-LAT or Planck.

As discussed in the Introduction 1, the WIMP represents the leading theoretical dark matter candidate. We detailed its early Universe production in 3.2.1 and several searching probes and methods in Chapter 4. There are many electroweak processes through which a WIMP could potentially annihilate; however, none of them are as ubiquitous across the landscape of dark matter models than those which result from couplings between the dark matter and the SM Z or Higgs bosons. In [5] we focused on the subset of models in which the dark matter annihilates through the exchange of either the Z or the Higgs bosons. We considered fermionic, scalar, and vector dark matter candidates within a model-independent context, and found that the overwhelming majority of these dark matter candidates are already ruled out by existing experiments. Furthermore, we showed that future direct detection experiments will probe nearly the entire parameter space of the models considered in this study, with the sole exception of a dark matter candidate with purely pseudoscalar couplings to the Higgs.

While there exist various putative dark matter-like signals, the Galactic Center gamma-ray excess as reported by the Fermi Gamma-Ray Space Telescope stands out. This signal has been deeply studied over the past nine years and has been shown with high statistical significance to exhibit a spectrum, morphology and overall intensity that is compatible with that predicted from annihilating WIMPs. The observation favours a dark matter mass of $\sim$30-70 GeV with a distribution comparable to what is found in numerical simulations. Millisecond pulsars have also been shown to posses a spectrum capable of accounting for the excess. At this point in time, however, there is no conclusive answer to the question of the origin of the Galactic Center excess. From the theoretical perspective, it is fundamental to know what kind of dark matter particles could account for the Galactic Center gamma-ray excess. In [6] we considered an exhaustive list of simplified models that are capable of generating the observed gamma-ray excess and confronted them with current constraints from collider and direct detection experiments. We showed that both s-wave spin-1 mediator dark matter models and dark matter annihilating via a t-channel are ruled out by a combination of LHC and PandaX/LUX constraints. We also showed that models with a pseudoscalar mediator remain viable. The very strong constraints from both collider and direct detection experiments motivate the possibility that dark matter resides in a so-called hidden sector. Hidden sectors are those in which the mediator's coupling to the dark matter particles are much larger than those of the SM. Taking such a ratio of couplings strongly reduces the production of the mediator at colliders and forces dark matter annihilation to proceed through cascade decays into the SM (this is also the case of the scenarios explored in [3, 4]). In [7], we considered various hidden dark matter sectors where the final state annihilation was to

dark Z's, dark scalars, or an admixture of the two. We identified the broad regions of parameter space in which the observed spectrum and intensity of the Galactic Center gamma-ray excess can arise from thermal dark matter and remain consistent with all current constraints (in particular from dwarf galaxies gamma-ray searches by the Fermi-LAT collaboration). In addition, we pointed out that cosmic-ray antiproton measurements could potentially discriminate some hidden sector models from more conventional dark matter scenarios.

To summarize, in this thesis we have investigated the cosmological and phenomenological implications of dark matter. Cosmologically we have broadly focused on the complementarity of early and late Universe probes, including scenarios beyond the canonical ΛCDM model. In particular, we have tested dark matter-neutrino interactions and cold plus non-cold dark matter cosmologies. These studies help in shaping our understanding of how the non-gravitational nature of dark matter may impact the observable Universe. From a phenomenological perspective, we have focused on the potential connection between dark matter and sterile neutrinos and on generic WIMP dark matter models, in particular those that could account for the Galactic Center gamma-ray excess. The former allow us to gain insight on the possible nature of dark matter should it be related with the neutrino mass generation mechanism. In our investigations of WIMP dark matter models, we have quantitatively showed the extent to which Z and Higgs dark matter mediated models are probed by current and future experiments, and we have highlighted the viability of a dark matter interpretation of the Galactic Center gamma-ray excess.

The complementary approach followed in this thesis has been shown to be very useful in constraining the nature of dark matter. At this point in time, however, we still do not know what the dark matter is. Yet, this thesis has served to constrain various possibilities and to explore the phenomenology of very well-motivated candidates. In the years to come, data from upcoming galaxy surveys, CMB stage IV experiments, direct detection experiments, colliders, and experiments searching indirectly for dark matter signatures will certainly shape our understanding of the nature of dark matter.

Bibliography

[1] M. Escudero, O. Mena, A. C. Vincent, R. J. Wilkinson and C. Boehm, *Exploring dark matter microphysics with galaxy surveys*, *JCAP* **1509** (2015) 034, [1505.06735]. Cited on page i, 16, 21, 71, and 257.

[2] S. Gariazzo, M. Escudero, R. Diamanti and O. Mena, *Cosmological searches for a noncold dark matter component*, *Phys. Rev.* **D96** (2017) 043501, [1704.02991]. Cited on page i, 16, 72, and 257.

[3] M. Escudero, N. Rius and V. Sanz, *Sterile neutrino portal to Dark Matter I: The $U(1)_{B-L}$ case*, *JHEP* **02** (2017) 045, [1606.01258]. Cited on page i, 47, 66, 72, 73, and 258.

[4] M. Escudero, N. Rius and V. Sanz, *Sterile Neutrino portal to Dark Matter II: Exact Dark symmetry*, *Eur. Phys. J.* **C77** (2017) 397, [1607.02373]. Cited on page i, 47, 66, 72, 73, and 259.

[5] M. Escudero, A. Berlin, D. Hooper and M.-X. Lin, *Toward (Finally!) Ruling Out Z and Higgs Mediated Dark Matter Models*, *JCAP* **1612** (2016) 029, [1609.09079]. Cited on page i, 52, 66, 73, and 259.

[6] M. Escudero, D. Hooper and S. J. Witte, *Updated Collider and Direct Detection Constraints on Dark Matter Models for the Galactic Center Gamma-Ray Excess*, *JCAP* **1702** (2017) 038, [1612.06462]. Cited on page i, 62, 73, and 259.

[7] M. Escudero, S. J. Witte and D. Hooper, *Hidden Sector Dark Matter and the Galactic Center Gamma-Ray Excess: A Closer Look*, *JCAP* **1711** (2017) 042, [1709.07002]. Cited on page i, 62, 73, and 260.

[8] M. Escudero, H. Ramírez, L. Boubekeur, E. Giusarma and O. Mena, *The present and future of the most favoured inflationary models after Planck 2015*, *JCAP* **1602** (2016) 020, [1509.05419]. Cited on page ii.

[9] M. Escudero, L. Lopez-Honorez, O. Mena, S. Palomares-Ruiz and P. Villanueva Domingo, *A fresh look into the interacting dark matter scenario*, 1803.08427. Cited on page ii, and 21.

[10] WMAP collaboration, C. L. Bennett et al., *Nine-Year Wilkinson Microwave Anisotropy Probe (WMAP) Observations: Final Maps and Results*, *Astrophys. J. Suppl.* **208** (2013) 20, [1212.5225]. Cited on page 1, 3, 16, and 17.

[11] WMAP collaboration, G. Hinshaw et al., *Nine-Year Wilkinson Microwave Anisotropy Probe (WMAP) Observations: Cosmological Parameter Results*, *Astrophys. J. Suppl.* **208** (2013) 19, [1212.5226]. Cited on page 1, and 16.

[12] Planck collaboration, R. Adam et al., *Planck 2015 results. I. Overview of products and scientific results*, *Astron. Astrophys.* **594** (2016) A1, [1502.01582]. Cited on page 1, 3, 5, 13, 14, 16, 17, 18, 20, and 254.

[13] Planck collaboration, P. A. R. Ade et al., *Planck 2015 results. XIII. Cosmological parameters*, *Astron. Astrophys.* **594** (2016) A13, [1502.01589]. Cited on page 1, 2, 5, 8, 9, 11, 12, 13, 14, 16, 17, 20, 21, 22, 42, 43, 57, 58, 61, 62, 69, 71, 249, 251, and 254.

[14] Y. Sofue and V. Rubin, *Rotation curves of spiral galaxies*, *Ann. Rev. Astron. Astrophys.* **39** (2001) 137–174, [astro-ph/0010594]. Cited on page 2, and 250.

[15] M. Bartelmann and P. Schneider, *Weak gravitational lensing*, *Phys. Rept.* **340** (2001) 291–472, [astro-ph/9912508]. Cited on page 2, 3, 18, and 250.

[16] M. Mateo, *Dwarf galaxies of the Local Group*, *Ann. Rev. Astron. Astrophys.* **36** (1998) 435–506, [astro-ph/9810070]. Cited on page 2, and 59.

[17] N. A. Bahcall, R. Cen, R. Dava, J. P. Ostriker and Q. Yu, *The mass-to-light function: Antibias and ω_m*, *The Astrophysical Journal* **541** (2000) 1. Cited on page 2, 12, and 250.

[18] F. Zwicky, *Die Rotverschiebung von extragalaktischen Nebeln*, *Helv. Phys. Acta* **6** (1933) 110–127. Cited on page 2.

[19] G. Bertone and D. Hooper, *A History of Dark Matter*, *Submitted to: Rev. Mod. Phys.* (2016) , [1605.04909]. Cited on page 2, and 51.

[20] V. C. Rubin and W. K. Ford, Jr., *Rotation of the Andromeda Nebula from a Spectroscopic Survey of Emission Regions*, *Astrophys. J.* **159** (1970) 379–403. Cited on page 2.

[21] K. C. Freeman, *On the disks of spiral and SO Galaxies*, *Astrophys. J.* **160** (1970) 811. Cited on page 2.

[22] M. Bartelmann, *The Dark Universe*, *Rev. Mod. Phys.* **82** (2010) 331–382, [0906.5036]. Cited on page 2.

[23] K. G. Begeman, A. H. Broeils and R. H. Sanders, *Extended rotation curves of spiral galaxies: Dark haloes and modified dynamics*, *Mon. Not. Roy. Astron. Soc.* **249** (1991) 523. Cited on page 3.

[24] P. Schneider, J. Ehlers and E. E. Falco, *Gravitational Lenses*. 1992, 10.1007/978-3-662-03758-4. Cited on page 3.

[25] Y. Mellier, *Probing the universe with weak lensing*, *Ann. Rev. Astron. Astrophys.* **37** (1999) 127–189, [astro-ph/9812172]. Cited on page 3.

[26] D. Clowe, M. Bradac, A. H. Gonzalez, M. Markevitch, S. W. Randall, C. Jones et al., *A direct empirical proof of the existence of dark matter*, *Astrophys. J.* **648** (2006) L109–L113, [astro-ph/0608407]. Cited on page 3, 4, and 21.

[27] M. Markevitch, *Chandra observation of the most interesting cluster in the universe*, astro-ph/0511345. Cited on page 4.

[28] C. S. Frenk and S. D. M. White, *Dark matter and cosmic structure*, *Annalen Phys.* **524** (2012) 507–534, [1210.0544]. Cited on page 3, 18, and 19.

[29] P. J. E. Peebles, *Growth of the nonbaryonic dark matter theory*, *Nat. Astron.* **1** (2017) 0057, [1701.05837]. Cited on page 3.

[30] T. Padmanabhan, *Structure Formation in the Universe*, *Cambridge University Press* (1993) . Cited on page 3, and 17.

[31] COBE collaboration, G. F. Smoot et al., *Structure in the COBE differential microwave radiometer first year maps*, *Astrophys. J.* **396** (1992) L1–L5. Cited on page 3, and 17.

[32] M. Milgrom, *A Modification of the Newtonian dynamics as a possible alternative to the hidden mass hypothesis*, *Astrophys. J.* **270** (1983) 365–370. Cited on page 4.

[33] M. Milgrom, *MOND: A pedagogical review*, *Acta Phys. Polon.* **B32** (2001) 3613, [astro-ph/0112069]. Cited on page 4.

[34] S. Dodelson, *The Real Problem with MOND*, *Int. J. Mod. Phys.* **D20** (2011) 2749–2753, [1112.1320]. Cited on page 4.

[35] E. Hubble, *A Relation between Distance and Radial Velocity among Extra-Galactic Nebulae*, *Proceedings of the National Academy of Science* **15** (Mar., 1929) 168–173. Cited on page 5.

[36] BOSS collaboration, L. Anderson et al., *The clustering of galaxies in the SDSS-III Baryon Oscillation Spectroscopic Survey: baryon acoustic oscillations in the Data Releases 10 and 11 Galaxy samples*, *Mon. Not. Roy. Astron. Soc.* **441** (2014) 24–62, [1312.4877]. Cited on page 5, 18, and 20.

[37] A. J. Ross, L. Samushia, C. Howlett, W. J. Percival, A. Burden and M. Manera, *The clustering of the SDSS DR7 main Galaxy sample ? I. A 4 per cent distance measure at* $z = 0.15$, *Mon. Not. Roy. Astron. Soc.* **449** (2015) 835–847, [1409.3242]. Cited on page 5, 18, and 20.

[38] F. Beutler, C. Blake, M. Colless, D. H. Jones, L. Staveley-Smith, L. Campbell et al., *The 6dF Galaxy Survey: Baryon Acoustic Oscillations and the Local Hubble Constant*, *Mon. Not. Roy. Astron. Soc.* **416** (2011) 3017–3032, [1106.3366]. Cited on page 5, 18, and 20.

[39] SDSS collaboration, M. Betoule et al., *Improved cosmological constraints from a joint analysis of the SDSS-II and SNLS supernova samples*, *Astron. Astrophys.* **568** (2014) A22, [1401.4064]. Cited on page 5, and 9.

[40] Supernova Search Team collaboration, A. G. Riess et al., *Observational evidence from supernovae for an accelerating universe and a cosmological constant*, *Astron. J.* **116** (1998) 1009–1038, [astro-ph/9805201]. Cited on page 5, 9, and 251.

[41] Supernova Cosmology Project collaboration, S. Perlmutter et al., *Measurements of Omega and Lambda from 42 high redshift supernovae*, *Astrophys. J.* **517** (1999) 565–586, [astro-ph/9812133]. Cited on page 5, 9, and 251.

[42] S. Weinberg, *Gravitation and Cosmology*, *John Wiley and Sons* (1972) . Cited on page 7.

[43] D. J. Fixsen, *The Temperature of the Cosmic Microwave Background*, *Astrophys. J.* **707** (2009) 916–920, [0911.1955]. Cited on page 7, 14, and 37.

[44] D. H. Weinberg, M. J. Mortonson, D. J. Eisenstein, C. Hirata, A. G. Riess and E. Rozo, *Observational Probes of Cosmic Acceleration*, *Phys. Rept.* **530** (2013) 87–255, [1201.2434]. Cited on page 9.

[45] R. A. Alpher, H. Bethe and G. Gamow, *The origin of chemical elements*, *Phys. Rev.* **73** (1948) 803–804. Cited on page 11.

[46] R. V. Wagoner, W. A. Fowler and F. Hoyle, *On the Synthesis of elements at very high temperatures*, *Astrophys. J.* **148** (1967) 3–49. Cited on page 11.

[47] Particle Data Group collaboration, C. Patrignani et al., *Review of Particle Physics*, *Chin. Phys.* **C40** (2016) 100001. Cited on page 11, 12, 29, 31, 36, 38, 43, and 50.

[48] B. D. Fields, *The primordial lithium problem*, *Ann. Rev. Nucl. Part. Sci.* **61** (2011) 47–68, [1203.3551]. Cited on page 11.

[49] R. H. Cyburt, B. D. Fields, K. A. Olive and T.-H. Yeh, *Big Bang Nucleosynthesis: 2015*, *Rev. Mod. Phys.* **88** (2016) 015004, [1505.01076]. Cited on page 11.

[50] A. H. Guth, *The Inflationary Universe: A Possible Solution to the Horizon and Flatness Problems*, *Phys. Rev.* **D23** (1981) 347–356. Cited on page 13.

[51] A. D. Linde, *A New Inflationary Universe Scenario: A Possible Solution of the Horizon, Flatness, Homogeneity, Isotropy and Primordial Monopole Problems*, *Phys. Lett.* **108B** (1982) 389–393. Cited on page 13.

[52] A. Albrecht and P. J. Steinhardt, *Cosmology for Grand Unified Theories with Radiatively Induced Symmetry Breaking*, *Phys. Rev. Lett.* **48** (1982) 1220–1223. Cited on page 13.

[53] V. F. Mukhanov, H. A. Feldman and R. H. Brandenberger, *Theory of cosmological perturbations. Part 1. Classical perturbations. Part 2. Quantum theory of perturbations. Part 3. Extensions*, *Phys. Rept.* **215** (1992) 203–333. Cited on page 13, and 14.

[54] CMB-S4 collaboration, K. N. Abazajian et al., *CMB-S4 Science Book, First Edition*, 1610.02743. Cited on page 14, 23, 62, 63, and 69.

[55] A. A. Penzias and R. W. Wilson, *A Measurement of excess antenna temperature at 4080-Mc/s*, *Astrophys. J.* **142** (1965) 419–421. Cited on page 14.

[56] R. H. Dicke, P. J. E. Peebles, P. G. Roll and D. T. Wilkinson, *Cosmic Black-Body Radiation*, *Astrophys. J.* **142** (1965) 414–419. Cited on page 14.

[57] D. J. Fixsen, E. S. Cheng, J. M. Gales, J. C. Mather, R. A. Shafer and E. L. Wright, *The Cosmic Microwave Background spectrum from the full COBE FIRAS data set*, *Astrophys. J.* **473** (1996) 576, [astro-ph/9605054]. Cited on page 14, and 15.

[58] X.-H. Fan et al., *Constraining the evolution of the ionizing background and the epoch of reionization with z 6 quasars. 2. a sample of 19 quasars*, *Astron. J.* **132** (2006) 117–136, [astro-ph/0512082]. Cited on page 16.

[59] S. Dodelson, *Modern Cosmology*. Academic Press, Amsterdam, 2003. Cited on page 16, and 37.

[60] D. Blas, J. Lesgourgues and T. Tram, *The Cosmic Linear Anisotropy Solving System (CLASS) II: Approximation schemes*, *JCAP* **1107** (2011) 034, [1104.2933]. Cited on page 16.

[61] A. Lewis and S. Bridle, *Cosmological parameters from CMB and other data: A Monte Carlo approach*, *Phys. Rev.* **D66** (2002) 103511, [astro-ph/0205436]. Cited on page 16.

[62] P. J. E. Peebles, *Principles of physical cosmology*. 1994. Cited on page 17, and 18.

[63] W. H. Press and P. Schechter, *Formation of galaxies and clusters of galaxies by selfsimilar gravitational condensation*, *Astrophys. J.* **187** (1974) 425–438. Cited on page 18, and 19.

[64] R. K. Sheth and G. Tormen, *An Excursion set model of hierarchical clustering : Ellipsoidal collapse and the moving barrier*, *Mon. Not. Roy. Astron. Soc.* **329** (2002) 61, [astro-ph/0105113]. Cited on page 18, and 19.

[65] C.-P. Ma and E. Bertschinger, *Cosmological perturbation theory in the synchronous and conformal Newtonian gauges*, *Astrophys. J.* **455** (1995) 7–25, [astro-ph/9506072]. Cited on page 18, and 37.

[66] H. Kodama and M. Sasaki, *Cosmological Perturbation Theory*, *Prog. Theor. Phys. Suppl.* **78** (1984) 1–166. Cited on page 18.

[67] M. Kuhlen, M. Vogelsberger and R. Angulo, *Numerical Simulations of the Dark Universe: State of the Art and the Next Decade*, *Phys. Dark Univ.* **1** (2012) 50–93, [1209.5745]. Cited on page 18, and 19.

[68] É. Aubourg et al., *Cosmological implications of baryon acoustic oscillation measurements*, *Phys. Rev.* **D92** (2015) 123516, [1411.1074]. Cited on page 18, and 20.

[69] DESI collaboration, A. Aghamousa et al., *The DESI Experiment Part I: Science,Targeting, and Survey Design*, 1611.00036. Cited on page 18.

[70] EUCLID collaboration, R. Laureijs et al., *Euclid Definition Study Report*, 1110.3193. Cited on page 18.

[71] DES collaboration, T. M. C. Abbott et al., *Dark Energy Survey Year 1 Results: Cosmological Constraints from Galaxy Clustering and Weak Lensing*, 1708.01530. Cited on page 18.

[72] M. Rauch, *The lyman alpha forest in the spectra of quasistellar objects*, *Ann. Rev. Astron. Astrophys.* **36** (1998) 267–316, [astro-ph/9806286]. Cited on page 18.

[73] J. F. Navarro, C. S. Frenk and S. D. M. White, *The Structure of cold dark matter halos*, *Astrophys. J.* **462** (1996) 563–575, [astro-ph/9508025]. Cited on page 18, and 19.

[74] J. F. Navarro, C. S. Frenk and S. D. M. White, *A Universal density profile from hierarchical clustering*, *Astrophys. J.* **490** (1997) 493–508, [astro-ph/9611107]. Cited on page 18, and 19.

[75] S. López, V. D'Odorico, S. L. Ellison, G. D. Becker, L. Christensen, G. Cupani et al., *XQ-100: A legacy survey of one hundred* $3.5 < z < 4.5$ *quasars observed with VLTX-shooter*, *Astronomy & Astrophysics* **594** (2016) , [1607.08776]. Cited on page 18, and 20.

[76] R. A. C. Croft, D. H. Weinberg, M. Bolte, S. Burles, L. Hernquist, N. Katz et al., *Towards a precise measurement of matter clustering: Lyman alpha forest data at redshifts 2-4*, *Astrophys. J.* **581** (2002) 20–52, [astro-ph/0012324]. Cited on page 18, and 20.

[77] V. Iršič et al., *New Constraints on the free-streaming of warm dark matter from intermediate and small scale Lyman-α forest data*, *Phys. Rev.* **D96** (2017) 023522, [1702.01764]. Cited on page 18, 20, and 24.

[78] J. Baur, N. Palanque-Delabrouille, C. Yeche, A. Boyarsky, O. Ruchayskiy, É. Armengaud et al., *Constraints from Ly-α forests on non-thermal dark matter including resonantly-produced sterile neutrinos*, *JCAP* **1712** (2017) 013, [1706.03118]. Cited on page 18, 20, and 24.

[79] V. Iršič, M. Viel, M. G. Haehnelt, J. S. Bolton and G. D. Becker, *First constraints on fuzzy dark matter from Lyman-α forest data and hydrodynamical simulations*, *Phys. Rev. Lett.* **119** (2017) 031302, [1703.04683]. Cited on page 18.

[80] E. Armengaud, N. Palanque-Delabrouille, C. Yèche, D. J. E. Marsh and J. Baur, *Constraining the mass of light bosonic dark matter using SDSS Lyman-α forest*, *Mon. Not. Roy. Astron. Soc.* **471** (2017) 4606–4614, [1703.09126]. Cited on page 18.

[81] J. S. Bullock and M. Boylan-Kolchin, *Small-Scale Challenges to the ΛCDM Paradigm*, *Ann. Rev. Astron. Astrophys.* **55** (2017) 343–387, [1707.04256]. Cited on page 19, and 20.

[82] D. H. Weinberg, J. S. Bullock, F. Governato, R. Kuzio de Naray and A. H. G. Peter, *Cold dark matter: controversies on small scales*, *Proc. Nat. Acad. Sci.* **112** (2015) 12249–12255, [1306.0913]. Cited on page 19.

[83] A. Del Popolo and M. Le Delliou, *Small scale problems of the ΛCDM model: a short review*, *Galaxies* **5** (2017) 17, [1606.07790]. Cited on page 19.

[84] DES Collaboration collaboration, A. Drlica-Wagner et al., *Eight Ultra-faint Galaxy Candidates Discovered in Year Two of the Dark Energy Survey*, *Astrophys. J.* **813** (2015) 109, [1508.03622]. Cited on page 19.

[85] A. A. Klypin, A. V. Kravtsov, O. Valenzuela and F. Prada, *Where are the missing Galactic satellites?*, *Astrophys. J.* **522** (1999) 82–92, [astro-ph/9901240]. Cited on page 19.

[86] B. Moore, *Evidence against dissipationless dark matter from observations of galaxy haloes*, *Nature* **370** (1994) 629. Cited on page 19.

[87] B. Moore, S. Ghigna, F. Governato, G. Lake, T. R. Quinn, J. Stadel et al., *Dark matter substructure within galactic halos*, *Astrophys. J.* **524** (1999) L19–L22, [astro-ph/9907411]. Cited on page 19.

[88] R. A. Flores and J. R. Primack, *Observational and theoretical constraints on singular dark matter halos*, *Astrophys. J.* **427** (1994) L1–4, [astro-ph/9402004]. Cited on page 19.

[89] M. Boylan-Kolchin, J. S. Bullock and M. Kaplinghat, *Too big to fail? The puzzling darkness of massive Milky Way subhaloes*, *Mon. Not. Roy. Astron. Soc.* **415** (2011) L40, [1103.0007]. Cited on page 19.

[90] M. R. Buckley and A. H. G. Peter, *Gravitational probes of dark matter physics*, 1712.06615. Cited on page 19.

[91] P. Bode, J. P. Ostriker and N. Turok, *Halo formation in warm dark matter models*, *Astrophys. J.* **556** (2001) 93–107, [astro-ph/0010389]. Cited on page 19, and 24.

[92] M. R. Lovell et al., *The properties of warm dark matter haloes*, *Mon. Not. Roy. Astron. Soc.* **439** (2014) 300–317, [1308.1399]. Cited on page 19.

[93] C. Boehm, H. Mathis, J. Devriendt and J. Silk, *Non-linear evolution of suppressed dark matter primordial power spectra*, *Mon. Not. Roy. Astron. Soc.* **360** (2005) 282–287, [astro-ph/0309652]. Cited on page 19.

[94] C. Bœhm, J. A. Schewtschenko, R. J. Wilkinson, C. M. Baugh and S. Pascoli, *Using the Milky Way satellites to study interactions between cold dark matter and radiation*, *Mon. Not. Roy. Astron. Soc.* **445** (2014) L31–L35, [1404.7012]. Cited on page 19.

[95] F.-Y. Cyr-Racine, R. de Putter, A. Raccanelli and K. Sigurdson, *Constraints on Large-Scale Dark Acoustic Oscillations from Cosmology*, *Phys. Rev.* **D89** (2014) 063517, [1310.3278]. Cited on page 19.

[96] M. Vogelsberger et al., *ETHOS an effective theory of structure formation: dark matter physics as a possible explanation of the small-scale CDM problems*, *Mon. Not. Roy. Astron. Soc.* **460** (2016) 1399–1416, [1512.05349]. Cited on page 19.

[97] A. A. de Laix, R. J. Scherrer and R. K. Schaefer, *Constraints of selfinteracting dark matter*, *Astrophys. J.* **452** (1995) 495, [astro-ph/9502087]. Cited on page 20.

[98] D. N. Spergel and P. J. Steinhardt, *Observational evidence for selfinteracting cold dark matter*, *Phys. Rev. Lett.* **84** (2000) 3760–3763, [astro-ph/9909386]. Cited on page 20, and 21.

[99] C. S. Kochanek and M. J. White, *A Quantitative study of interacting dark matter in halos*, *Astrophys. J.* **543** (2000) 514, [astro-ph/0003483]. Cited on page 20.

[100] R. Murgia, A. Merle, M. Viel, M. Totzauer and A. Schneider, *"Non-cold" dark matter at small scales: a general approach*, 1704.07838. Cited on page 20.

[101] LSST Science, LSST Project collaboration, P. A. Abell et al., *LSST Science Book, Version 2.0*, 0912.0201. Cited on page 20, and 63.

[102] B. Paczynski, *Gravitational microlensing by the galactic halo*, *Astrophys. J.* **304** (1986) 1–5. Cited on page 20.

[103] EROS-2 collaboration, P. Tisserand et al., *Limits on the Macho Content of the Galactic Halo from the EROS-2 Survey of the Magellanic Clouds*, *Astron. Astrophys.* **469** (2007) 387–404, [astro-ph/0607207]. Cited on page 20.

[104] MACHO collaboration, C. Alcock et al., *The MACHO project: Microlensing results from 5.7 years of LMC observations*, *Astrophys. J.* **542** (2000) 281–307, [astro-ph/0001272]. Cited on page 20.

[105] R. Dave, D. N. Spergel, P. J. Steinhardt and B. D. Wandelt, *Halo properties in cosmological simulations of selfinteracting cold dark matter*, *Astrophys. J.* **547** (2001) 574–589, [astro-ph/0006218]. Cited on page 21.

[106] J. L. Feng, M. Kaplinghat, H. Tu and H.-B. Yu, *Hidden Charged Dark Matter*, *JCAP* **0907** (2009) 004, [0905.3039]. Cited on page 21.

[107] P. Agrawal, F.-Y. Cyr-Racine, L. Randall and J. Scholtz, *Make Dark Matter Charged Again*, *JCAP* **1705** (2017) 022, [1610.04611]. Cited on page 21.

[108] S. W. Randall, M. Markevitch, D. Clowe, A. H. Gonzalez and M. Bradac, *Constraints on the Self-Interaction Cross-Section of Dark Matter from Numerical Simulations of the Merging Galaxy Cluster 1E 0657-56*, *Astrophys. J.* **679** (2008) 1173–1180, [0704.0261]. Cited on page 21.

[109] F. Kahlhoefer, K. Schmidt-Hoberg, M. T. Frandsen and S. Sarkar, *Colliding clusters and dark matter self-interactions*, *Mon. Not. Roy. Astron. Soc.* **437** (2014) 2865–2881, [1308.3419]. Cited on page 21.

[110] A. De Rujula, S. L. Glashow and U. Sarid, *Charged Dark Matter*, *Nucl. Phys.* **B333** (1990) 173–194. Cited on page 21.

[111] M. Taoso, G. Bertone and A. Masiero, *Dark Matter Candidates: A Ten-Point Test*, *JCAP* **0803** (2008) 022, [0711.4996]. Cited on page 21.

[112] S. D. McDermott, H.-B. Yu and K. M. Zurek, *Turning off the Lights: How Dark is Dark Matter?*, *Phys. Rev.* **D83** (2011) 063509, [1011.2907]. Cited on page 21.

[113] N. Vinyoles and H. Vogel, *Minicharged Particles from the Sun: A Cutting-Edge Bound*, *JCAP* **1603** (2016) 002, [1511.01122]. Cited on page 21.

[114] K. Sigurdson, M. Doran, A. Kurylov, R. R. Caldwell and M. Kamionkowski, *Dark-matter electric and magnetic dipole moments*, *Phys. Rev.* **D70** (2004) 083501, [astro-ph/0406355]. Cited on page 21.

[115] G. D. Starkman, A. Gould, R. Esmailzadeh and S. Dimopoulos, *Opening the Window on Strongly Interacting Dark Matter*, *Phys. Rev.* **D41** (1990) 3594. Cited on page 21.

[116] G. D. Mack, J. F. Beacom and G. Bertone, *Towards Closing the Window on Strongly Interacting Dark Matter: Far-Reaching Constraints from Earth's Heat Flow*, *Phys. Rev.* **D76** (2007) 043523, [0705.4298]. Cited on page 21.

[117] C. Boehm, P. Fayet and R. Schaeffer, *Constraining dark matter candidates from structure formation*, *Phys. Lett.* **B518** (2001) 8–14, [astro-ph/0012504]. Cited on page 21.

[118] R. J. Wilkinson, C. Boehm and J. Lesgourgues, *Constraining Dark Matter-Neutrino Interactions using the CMB and Large-Scale Structure*, *JCAP* **1405** (2014) 011, [1401.7597]. Cited on page 21.

[119] C. A. Argüelles, A. Kheirandish and A. C. Vincent, *Imaging Galactic Dark Matter with High-Energy Cosmic Neutrinos*, *Phys. Rev. Lett.* **119** (2017) 201801, [1703.00451]. Cited on page 21.

[120] A. O.-D. Campo, C. Boehm, S. Palomares-Ruiz and S. Pascoli, *Dark matter-neutrino interactions through the lens of their cosmological implications*, 1711.05283. Cited on page 21.

[121] A. Ibarra, D. Tran and C. Weniger, *Indirect Searches for Decaying Dark Matter*, *Int. J. Mod. Phys.* **A28** (2013) 1330040, [1307.6434]. Cited on page 21, and 63.

[122] J. Lesgourgues and S. Pastor, *Massive neutrinos and cosmology*, *Phys. Rept.* **429** (2006) 307–379, [astro-ph/0603494]. Cited on page 21, and 43.

[123] H. Baer, K.-Y. Choi, J. E. Kim and L. Roszkowski, *Dark matter production in the early Universe: beyond the thermal WIMP paradigm*, *Phys. Rept.* **555** (2015) 1–60, [1407.0017]. Cited on page 22.

[124] N. Bernal, M. Heikinheimo, T. Tenkanen, K. Tuominen and V. Vaskonen, *The Dawn of FIMP Dark Matter: A Review of Models and Constraints*, *Int. J. Mod. Phys.* **A32** (2017) 1730023, [1706.07442]. Cited on page 22.

[125] L. Hui, J. P. Ostriker, S. Tremaine and E. Witten, *Ultralight scalars as cosmological dark matter*, *Phys. Rev.* **D95** (2017) 043541, [1610.08297]. Cited on page 22.

[126] E. W. Kolb and M. S. Turner, *The Early Universe*, *Front. Phys.* **69** (1990) 1–547. Cited on page 22, 23, 37, 43, and 57.

[127] B. W. Lee and S. Weinberg, *Cosmological Lower Bound on Heavy Neutrino Masses*, *Phys. Rev. Lett.* **39** (1977) 165–168. Cited on page 22, and 40.

[128] P. Gondolo and G. Gelmini, *Cosmic abundances of stable particles: Improved analysis*, *Nucl. Phys.* **B360** (1991) 145–179. Cited on page 22, and 40.

[129] K. Griest and D. Seckel, *Three exceptions in the calculation of relic abundances*, *Phys. Rev.* **D43** (1991) 3191–3203. Cited on page 22, and 40.

[130] S. P. Martin, *A Supersymmetry primer*, hep-ph/9709356. Cited on page 22, and 64.

[131] G. Jungman, M. Kamionkowski and K. Griest, *Supersymmetric dark matter*, *Phys. Rept.* **267** (1996) 195–373, [hep-ph/9506380]. Cited on page 22, 47, and 64.

[132] G. Bertone, D. Hooper and J. Silk, *Particle dark matter: Evidence, candidates and constraints*, *Phys. Rept.* **405** (2005) 279–390, [hep-ph/0404175]. Cited on page 22, and 47.

[133] L. Bergstrom, *Dark Matter Evidence, Particle Physics Candidates and Detection Methods*, *Annalen Phys.* **524** (2012) 479–496, [1205.4882]. Cited on page 22, and 47.

[134] L. Roszkowski, E. M. Sessolo and S. Trojanowski, *WIMP dark matter candidates and searches - current issues and future prospects*, 1707.06277. Cited on page 22.

[135] XENON collaboration, E. Aprile et al., *First Dark Matter Search Results from the XENON1T Experiment*, *Phys. Rev. Lett.* **119** (2017) 181301, [1705.06655]. Cited on page 22, 51, 52, 54, 69, and 254.

[136] LUX collaboration, D. S. Akerib et al., *Results from a search for dark matter in the complete LUX exposure*, *Phys. Rev. Lett.* **118** (2017) 021303, [1608.07648]. Cited on page 22, 51, 52, 69, and 254.

[137] PandaX-II collaboration, X. Cui et al., *Dark Matter Results From 54-Ton-Day Exposure of PandaX-II Experiment*, *Phys. Rev. Lett.* **119** (2017) 181302, [1708.06917]. Cited on page 22, 51, 52, 69, and 254.

[138] DES, Fermi-LAT collaboration, A. Albert et al., *Searching for Dark Matter Annihilation in Recently Discovered Milky Way Satellites with Fermi-LAT*, *Astrophys. J.* **834** (2017) 110, [1611.03184]. Cited on page 22, 59, 61, 69, and 254.

[139] ATLAS collaboration, *Exotic Results*, . Cited on page 22, 64, 69, and 255.

[140] CMS collaboration, *Exotic Results*, . Cited on page 22, 64, 69, and 255.

[141] B. J. Mount et al., *LUX-ZEPLIN (LZ) Technical Design Report*, 1703.09144. Cited on page 23, 52, 54, and 69.

[142] DARWIN collaboration, J. Aalbers et al., *DARWIN: towards the ultimate dark matter detector*, *JCAP* **1611** (2016) 017, [1606.07001]. Cited on page 23, 52, and 69.

[143] Fermi-LAT collaboration, E. Charles et al., *Sensitivity Projections for Dark Matter Searches with the Fermi Large Area Telescope*, *Phys. Rept.* **636** (2016) 1–46, [1605.02016]. Cited on page 23, 63, and 69.

[144] G. Apollinari, O. Brüning, T. Nakamoto and L. Rossi, *High Luminosity Large Hadron Collider HL-LHC*, *CERN Yellow Report* (2015) 1–19, [1705.08830]. Cited on page 23, and 69.

[145] Belle-II collaboration, T. Abe et al., *Belle II Technical Design Report*, 1011.0352. Cited on page 23, 68, and 69.

[146] R. D. Peccei and H. R. Quinn, *CP Conservation in the Presence of Instantons*, *Phys. Rev. Lett.* **38** (1977) 1440–1443. Cited on page 23.

[147] S. Weinberg, *A New Light Boson?*, *Phys. Rev. Lett.* **40** (1978) 223–226. Cited on page 23.

[148] F. Wilczek, *Problem of Strong p and t Invariance in the Presence of Instantons*, *Phys. Rev. Lett.* **40** (1978) 279–282. Cited on page 23.

[149] L. F. Abbott and P. Sikivie, *A Cosmological Bound on the Invisible Axion*, *Phys. Lett.* **B120** (1983) 133–136. Cited on page 23.

[150] J. Preskill, M. B. Wise and F. Wilczek, *Cosmology of the Invisible Axion*, *Phys. Lett.* **B120** (1983) 127–132. Cited on page 23.

[151] J. Ipser and P. Sikivie, *Are Galactic Halos Made of Axions?*, *Phys. Rev. Lett.* **50** (1983) 925. Cited on page 23.

[152] J. E. Kim, *Weak Interaction Singlet and Strong CP Invariance*, *Phys. Rev. Lett.* **43** (1979) 103. Cited on page 23.

[153] M. A. Shifman, A. I. Vainshtein and V. I. Zakharov, *Can Confinement Ensure Natural CP Invariance of Strong Interactions?*, *Nucl. Phys.* **B166** (1980) 493–506. Cited on page 23.

[154] M. Dine, W. Fischler and M. Srednicki, *A Simple Solution to the Strong CP Problem with a Harmless Axion*, *Phys. Lett.* **104B** (1981) 199–202. Cited on page 23.

[155] A. R. Zhitnitsky, *On Possible Suppression of the Axion Hadron Interactions. (In Russian)*, *Sov. J. Nucl. Phys.* **31** (1980) 260. Cited on page 23.

[156] P. Sikivie, *Experimental Tests of the Invisible Axion*, *Phys. Rev. Lett.* **51** (1983) 1415–1417. Cited on page 23.

[157] ADMX collaboration, N. Du et al., *Search for Invisible Axion Dark Matter with the Axion Dark Matter Experiment*, *Phys. Rev. Lett.* **120** (2018) 151301, [1804.05750]. Cited on page 23.

[158] P. W. Graham, I. G. Irastorza, S. K. Lamoreaux, A. Lindner and K. A. van Bibber, *Experimental Searches for the Axion and Axion-Like Particles*, *Ann. Rev. Nucl. Part. Sci.* **65** (2015) 485–514, [1602.00039]. Cited on page 23.

[159] J. E. Kim and G. Carosi, *Axions and the Strong CP Problem*, *Rev. Mod. Phys.* **82** (2010) 557–602, [0807.3125]. Cited on page 23.

[160] O. Wantz and E. P. S. Shellard, *Axion Cosmology Revisited*, *Phys. Rev.* **D82** (2010) 123508, [0910.1066]. Cited on page 23.

[161] S. Borsanyi et al., *Calculation of the axion mass based on high-temperature lattice quantum chromodynamics*, *Nature* **539** (2016) 69–71, [1606.07494]. Cited on page 23.

[162] S. Dodelson and L. M. Widrow, *Sterile-neutrinos as dark matter*, *Phys. Rev. Lett.* **72** (1994) 17–20, [hep-ph/9303287]. Cited on page 23, and 24.

[163] M. Drewes et al., *A White Paper on keV Sterile Neutrino Dark Matter*, *JCAP* **1701** (2017) 025, [1602.04816]. Cited on page 23.

[164] E. Bulbul, M. Markevitch, A. Foster, R. K. Smith, M. Loewenstein and S. W. Randall, *Detection of An Unidentified Emission Line in the Stacked X-ray spectrum of Galaxy Clusters*, *Astrophys. J.* **789** (2014) 13, [1402.2301]. Cited on page 24.

[165] A. Boyarsky, O. Ruchayskiy, D. Iakubovskyi and J. Franse, *Unidentified Line in X-Ray Spectra of the Andromeda Galaxy and Perseus Galaxy Cluster*, *Phys. Rev. Lett.* **113** (2014) 251301, [1402.4119]. Cited on page 24.

[166] T. Asaka and M. Shaposhnikov, *The nuMSM, dark matter and baryon asymmetry of the universe*, *Phys. Lett.* **B620** (2005) 17–26, [hep-ph/0505013]. Cited on page 24.

[167] K. Perez, K. C. Y. Ng, J. F. Beacom, C. Hersh, S. Horiuchi and R. Krivonos, *Almost closing the νMSM sterile neutrino dark matter window with NuSTAR*, *Phys. Rev.* **D95** (2017) 123002, [1609.00667]. Cited on page 24.

[168] D. E. Kaplan, M. A. Luty and K. M. Zurek, *Asymmetric Dark Matter*, *Phys. Rev.* **D79** (2009) 115016, [0901.4117]. Cited on page 24.

[169] D. B. Kaplan, *A Single explanation for both the baryon and dark matter densities*, *Phys. Rev. Lett.* **68** (1992) 741–743. Cited on page 24.

[170] K. M. Zurek, *Asymmetric Dark Matter: Theories, Signatures, and Constraints*, *Phys. Rept.* **537** (2014) 91–121, [1308.0338]. Cited on page 24.

[171] G. F. Chapline, *Cosmological effects of primordial black holes*, *Nature* **253** (Jan., 1975) 251. Cited on page 24.

[172] B. Carr, F. Kuhnel and M. Sandstad, *Primordial Black Holes as Dark Matter*, *Phys. Rev.* **D94** (2016) 083504, [1607.06077]. Cited on page 24.

[173] Virgo, LIGO Scientific collaboration, B. P. Abbott et al., *Observation of Gravitational Waves from a Binary Black Hole Merger*, *Phys. Rev. Lett.* **116** (2016) 061102, [1602.03837]. Cited on page 24.

[174] Virgo, LIGO Scientific collaboration, B. P. Abbott et al., *GW151226: Observation of Gravitational Waves from a 22-Solar-Mass Binary Black Hole Coalescence*, *Phys. Rev. Lett.* **116** (2016) 241103, [1606.04855]. Cited on page 24.

[175] VIRGO, LIGO Scientific collaboration, B. P. Abbott et al., *GW170104: Observation of a 50-Solar-Mass Binary Black Hole Coalescence at Redshift 0.2*, *Phys. Rev. Lett.* **118** (2017) 221101, [1706.01812]. Cited on page 24.

[176] Virgo, LIGO Scientific collaboration, B. P. Abbott et al., *GW170814: A Three-Detector Observation of Gravitational Waves from a Binary Black Hole Coalescence*, *Phys. Rev. Lett.* **119** (2017) 141101, [1709.09660]. Cited on page 24.

[177] Virgo, LIGO Scientific collaboration, B. P. Abbott et al., *GW170608: Observation of a 19-solar-mass Binary Black Hole Coalescence*, *Astrophys. J.* **851** (2017) L35, [1711.05578]. Cited on page 24.

[178] S. Bird, I. Cholis, J. B. Muñoz, Y. Ali-Haïmoud, M. Kamionkowski, E. D. Kovetz et al., *Did LIGO detect dark matter?*, *Phys. Rev. Lett.* **116** (2016) 201301, [1603.00464]. Cited on page 24.

[179] S. Clesse and J. García-Bellido, *Seven Hints for Primordial Black Hole Dark Matter*, 1711.10458. Cited on page 24.

[180] P. Ivanov, P. Naselsky and I. Novikov, *Inflation and primordial black holes as dark matter*, *Phys. Rev.* **D50** (1994) 7173–7178. Cited on page 25.

[181] LIGO Scientific collaboration, G. M. Harry, *Advanced LIGO: The next generation of gravitational wave detectors*, *Class. Quant. Grav.* **27** (2010) 084006. Cited on page 25.

[182] S. L. Glashow, *Partial Symmetries of Weak Interactions*, *Nucl. Phys.* **22** (1961) 579–588. Cited on page 27.

[183] S. Weinberg, *A Model of Leptons*, *Phys. Rev. Lett.* **19** (1967) 1264–1266. Cited on page 27.

[184] A. Salam, *Weak and Electromagnetic Interactions*, *Conf. Proc.* **C680519** (1968) 367–377. Cited on page 27.

[185] F. Englert and R. Brout, *Broken Symmetry and the Mass of Gauge Vector Mesons*, *Phys. Rev. Lett.* **13** (1964) 321–323. Cited on page 27, and 29.

[186] P. W. Higgs, *Spontaneous Symmetry Breakdown without Massless Bosons*, *Phys. Rev.* **145** (1966) 1156–1163. Cited on page 27, and 29.

[187] P. W. Higgs, *Broken Symmetries and the Masses of Gauge Bosons*, *Phys. Rev. Lett.* **13** (1964) 508–509. Cited on page 27, and 29.

[188] G. S. Guralnik, C. R. Hagen and T. W. B. Kibble, *Global Conservation Laws and Massless Particles*, *Phys. Rev. Lett.* **13** (1964) 585–587. Cited on page 27, and 29.

[189] T. W. B. Kibble, *Symmetry breaking in nonAbelian gauge theories*, *Phys. Rev.* **155** (1967) 1554–1561. Cited on page 27, and 29.

[190] S. L. Glashow, J. Iliopoulos and L. Maiani, *Weak Interactions with Lepton-Hadron Symmetry*, *Phys. Rev.* **D2** (1970) 1285–1292. Cited on page 27, and 29.

[191] H. Fritzsch, M. Gell-Mann and H. Leutwyler, *Advantages of the Color Octet Gluon Picture*, *Phys. Lett.* **47B** (1973) 365–368. Cited on page 27.

[192] M. Y. Han and Y. Nambu, *Three Triplet Model with Double SU(3) Symmetry*, *Phys. Rev.* **139** (1965) B1006–B1010. Cited on page 27.

[193] C. Quigg, *Gauge Theories of the Strong, Weak and Electromagnetic interactions*, *Front. Phys.* **56** (1983) 1–334. Cited on page 27.

[194] A. Pich, *The Standard Model of Electroweak Interactions*, pp. 1–50, 2012. 1201.0537. Cited on page 27.

[195] A. Pich, *Aspects of quantum chromodynamics*, pp. 53–102, 1999. hep-ph/0001118. Cited on page 27.

[196] CMS collaboration, S. Chatrchyan et al., *Observation of a new boson at a mass of 125 GeV with the CMS experiment at the LHC*, *Phys. Lett.* **B716** (2012) 30–61, [1207.7235]. Cited on page 29.

[197] ATLAS collaboration, G. Aad et al., *Observation of a new particle in the search for the Standard Model Higgs boson with the ATLAS detector at the LHC*, *Phys. Lett.* **B716** (2012) 1–29, [1207.7214]. Cited on page 29.

[198] ATLAS, CMS collaboration, G. Aad et al., *Measurements of the Higgs boson production and decay rates and constraints on its couplings from a combined ATLAS and CMS analysis of the LHC pp collision data at $\sqrt{s} = 7$ and 8 TeV*, *JHEP* **08** (2016) 045, [1606.02266]. Cited on page 29, and 64.

[199] I. Esteban, M. C. Gonzalez-Garcia, M. Maltoni, I. Martinez-Soler and T. Schwetz, *Updated fit to three neutrino mixing: exploring the accelerator-reactor complementarity*, *JHEP* **01** (2017) 087, [1611.01514]. Cited on page 31.

[200] P. Minkowski, *$\mu \to e\gamma$ at a Rate of One Out of 10^9 Muon Decays?*, *Phys. Lett.* **67B** (1977) 421–428. Cited on page 31.

[201] T. Yanagida, *Horizontal Symmetry and Masses of Neutrinos*, *Conf. Proc.* **C7902131** (1979) 95–99. Cited on page 31.

[202] M. Gell-Mann, P. Ramond and R. Slansky, *Complex Spinors and Unified Theories*, *Conf. Proc.* **C790927** (1979) 315–321, [1306.4669]. Cited on page 31.

[203] S. L. Glashow, *The Future of Elementary Particle Physics*, *NATO Sci. Ser. B* **61** (1980) 687. Cited on page 31.

[204] R. N. Mohapatra and G. Senjanovic, *Neutrino Mass and Spontaneous Parity Violation*, *Phys. Rev. Lett.* **44** (1980) 912. Cited on page 31.

[205] R. A. Lyttleton and H. Bondi, *On the physical consequences of a general excess of charge*, *Proc. Roy. Soc. Lond.* **A252** (1959) 313–333. Cited on page 34.

[206] A. D. Dolgov, *Neutrinos in cosmology*, *Phys. Rept.* **370** (2002) 333–535, [hep-ph/0202122]. Cited on page 36, 37, and 46.

[207] J. Bernstein, *Kinetic Theory in the Expanding Universe* . Cambridge University Press, Cambridge, U.K., 1988, 10.1017/CBO9780511564185. Cited on page 37, and 39.

[208] J. Bernstein, L. S. Brown and G. Feinberg, *The Cosmological Heavy Neutrino Problem Revisited*, *Phys. Rev.* **D32** (1985) 3261. Cited on page 39.

[209] T. Binder, T. Bringmann, M. Gustafsson and A. Hryczuk, *Dark Matter Relic Density Revisited: The Case For Early Kinetic Decoupling*, 2018. 1805.00526. Cited on page 39, and 40.

[210] J. Edsjo and P. Gondolo, *Neutralino relic density including coannihilations*, *Phys. Rev.* **D56** (1997) 1879–1894, [hep-ph/9704361]. Cited on page 40.

[211] G. Steigman, B. Dasgupta and J. F. Beacom, *Precise Relic WIMP Abundance and its Impact on Searches for Dark Matter Annihilation*, *Phys. Rev.* **D86** (2012) 023506, [1204.3622]. Cited on page 40, 41, 42, and 61.

[212] J. M. Cline, K. Kainulainen, P. Scott and C. Weniger, *Update on scalar singlet dark matter*, *Phys. Rev.* **D88** (2013) 055025, [1306.4710]. Cited on page 40, 41, and 54.

[213] A. D. Sakharov, *Violation of CP Invariance, C asymmetry, and baryon asymmetry of the universe*, *Pisma Zh. Eksp. Teor. Fiz.* **5** (1967) 32–35. Cited on page 43.

[214] S. Vagnozzi, E. Giusarma, O. Mena, K. Freese, M. Gerbino, S. Ho et al., *Unveiling ν secrets with cosmological data: neutrino masses and mass hierarchy*, *Phys. Rev.* **D96** (2017) 123503, [1701.08172]. Cited on page 43.

[215] M. Lattanzi and M. Gerbino, *Status of neutrino properties and future prospects - Cosmological and astrophysical constraints*, *Front.in Phys.* **5** (2018) 70, [1712.07109]. Cited on page 43.

[216] A. D. Dolgov, S. H. Hansen, S. Pastor and D. V. Semikoz, *Unstable massive tau neutrinos and primordial nucleosynthesis*, *Nucl. Phys.* **B548** (1999) 385–407, [hep-ph/9809598]. Cited on page 44.

[217] S. Hannestad and J. Madsen, *Neutrino decoupling in the early universe*, *Phys. Rev.* **D52** (1995) 1764–1769, [astro-ph/9506015]. Cited on page 46.

[218] K. Griest and M. Kamionkowski, *Unitarity Limits on the Mass and Radius of Dark Matter Particles*, *Phys. Rev. Lett.* **64** (1990) 615. Cited on page 47.

[219] C. Boehm, M. J. Dolan and C. McCabe, *A Lower Bound on the Mass of Cold Thermal Dark Matter from Planck*, *JCAP* **1308** (2013) 041, [1303.6270]. Cited on page 47, and 58.

[220] M. Pospelov, A. Ritz and M. B. Voloshin, *Secluded WIMP Dark Matter*, *Phys. Lett.* **B662** (2008) 53–61, [0711.4866]. Cited on page 47.

[221] M. W. Goodman and E. Witten, *Detectability of Certain Dark Matter Candidates*, *Phys. Rev.* **D31** (1985) 3059. Cited on page 49, and 51.

[222] J. D. Lewin and P. F. Smith, *Review of mathematics, numerical factors, and corrections for dark matter experiments based on elastic nuclear recoil*, *Astropart. Phys.* **6** (1996) 87–112. Cited on page 49, and 50.

[223] T. Marrodán Undagoitia and L. Rauch, *Dark matter direct-detection experiments*, *J. Phys.* **G43** (2016) 013001, [1509.08767]. Cited on page 49.

[224] C. Savage, G. Gelmini, P. Gondolo and K. Freese, *Compatibility of DAMA/LIBRA dark matter detection with other searches*, *JCAP* **0904** (2009) 010, [0808.3607]. Cited on page 49.

[225] J. I. Read, *The Local Dark Matter Density*, *J. Phys.* **G41** (2014) 063101, [1404.1938]. Cited on page 49.

[226] A. L. Fitzpatrick, W. Haxton, E. Katz, N. Lubbers and Y. Xu, *The Effective Field Theory of Dark Matter Direct Detection*, *JCAP* **1302** (2013) 004, [1203.3542]. Cited on page 51.

[227] M. Cirelli, E. Del Nobile and P. Panci, *Tools for model-independent bounds in direct dark matter searches*, *JCAP* **1310** (2013) 019, [1307.5955]. Cited on page 51.

[228] A. M. Green, *Astrophysical uncertainties on direct detection experiments*, *Mod. Phys. Lett.* **A27** (2012) 1230004, [1112.0524]. Cited on page 51.

[229] N. Bozorgnia and G. Bertone, *Implications of hydrodynamical simulations for the interpretation of direct dark matter searches*, *Int. J. Mod. Phys.* **A32** (2017) , [1705.05853]. Cited on page 51.

[230] P. J. Fox, J. Liu and N. Weiner, *Integrating Out Astrophysical Uncertainties*, *Phys. Rev.* **D83** (2011) 103514, [1011.1915]. Cited on page 51.

[231] G. B. Gelmini, J.-H. Huh and S. J. Witte, *Unified Halo-Independent Formalism From Convex Hulls for Direct Dark Matter Searches*, *JCAP* **1712** (2017) 039, [1707.07019]. Cited on page 51.

[232] XENON collaboration, E. Aprile et al., *Physics reach of the XENON1T dark matter experiment*, *JCAP* **1604** (2016) 027, [1512.07501]. Cited on page 52.

[233] J. Billard, L. Strigari and E. Figueroa-Feliciano, *Implication of neutrino backgrounds on the reach of next generation dark matter direct detection experiments*, *Phys. Rev.* **D89** (2014) 023524, [1307.5458]. Cited on page 52.

[234] C. E. Aalseth et al., *DarkSide-20k: A 20 tonne two-phase LAr TPC for direct dark matter detection at LNGS*, *Eur. Phys. J. Plus* **133** (2018) 131, [1707.08145]. Cited on page 52.

[235] G. B. Gelmini, V. Takhistov and S. J. Witte, *Casting a Wide Signal Net with Future Direct Dark Matter Detection Experiments*, 1804.01638. Cited on page 53.

[236] J. Kearney, N. Orlofsky and A. Pierce, *Z boson mediated dark matter beyond the effective theory*, *Phys. Rev.* **D95** (2017) 035020, [1611.05048]. Cited on page 54.

[237] M. Cirelli, G. Corcella, A. Hektor, G. Hutsi, M. Kadastik, P. Panci et al., *PPPC 4 DM ID: A Poor Particle Physicist Cookbook for Dark Matter Indirect Detection*, *JCAP* **1103** (2011) 051, [1012.4515]. Cited on page 56.

[238] J. M. Gaskins, *A review of indirect searches for particle dark matter*, *Contemp. Phys.* **57** (2016) 496–525, [1604.00014]. Cited on page 57.

[239] M. Cirelli, *Indirect Searches for Dark Matter: a status review*, *Pramana* **79** (2012) 1021–1043, [1202.1454]. Cited on page 57.

[240] T. R. Slatyer, *TASI 2016 Lectures on Indirect Detection of Dark Matter*, in *Boulder, CO, USA, June 6-July 1, 2016*, 2017. 1710.05137. Cited on page 57.

[241] S. Sarkar, *Big bang nucleosynthesis and physics beyond the standard model*, *Rept. Prog. Phys.* **59** (1996) 1493–1610, [hep-ph/9602260]. Cited on page 57, and 69.

[242] M. Pospelov and J. Pradler, *Big Bang Nucleosynthesis as a Probe of New Physics*, *Ann. Rev. Nucl. Part. Sci.* **60** (2010) 539–568, [1011.1054]. Cited on page 57, and 69.

[243] D. P. Finkbeiner, S. Galli, T. Lin and T. R. Slatyer, *Searching for Dark Matter in the CMB: A Compact Parameterization of Energy Injection from New Physics*, *Phys. Rev.* **D85** (2012) 043522, [1109.6322]. Cited on page 57.

[244] T. R. Slatyer, *Indirect dark matter signatures in the cosmic dark ages. I. Generalizing the bound on s-wave dark matter annihilation from Planck results*, *Phys. Rev.* **D93** (2016) 023527, [1506.03811]. Cited on page 57, 61, and 62.

[245] T. R. Slatyer, *Indirect Dark Matter Signatures in the Cosmic Dark Ages II. Ionization, Heating and Photon Production from Arbitrary Energy Injections*, *Phys. Rev.* **D93** (2016) 023521, [1506.03812]. Cited on page 57.

[246] R. Diamanti, L. Lopez-Honorez, O. Mena, S. Palomares-Ruiz and A. C. Vincent, *Constraining Dark Matter Late-Time Energy Injection: Decays and P-Wave Annihilations*, *JCAP* **1402** (2014) 017, [1308.2578]. Cited on page 58, and 63.

[247] H. Liu, T. R. Slatyer and J. Zavala, *Contributions to cosmic reionization from dark matter annihilation and decay*, *Phys. Rev.* **D94** (2016) 063507, [1604.02457]. Cited on page 58.

[248] A. Fradette and M. Pospelov, *BBN for the LHC: constraints on lifetimes of the Higgs portal scalars*, *Phys. Rev.* **D96** (2017) 075033, [1706.01920]. Cited on page 58.

[249] M. Kawasaki, K. Kohri, T. Moroi and Y. Takaesu, *Revisiting Big-Bang Nucleosynthesis Constraints on Long-Lived Decaying Particles*, 1709.01211. Cited on page 58.

[250] A. Fradette, M. Pospelov, J. Pradler and A. Ritz, *Cosmological Constraints on Very Dark Photons*, *Phys. Rev.* **D90** (2014) 035022, [1407.0993]. Cited on page 58.

[251] P. F. de Salas and S. Pastor, *Relic neutrino decoupling with flavour oscillations revisited*, *JCAP* **1607** (2016) 051, [1606.06986]. Cited on page 58.

[252] S. Weinberg, *Goldstone Bosons as Fractional Cosmic Neutrinos*, *Phys. Rev. Lett.* **110** (2013) 241301, [1305.1971]. Cited on page 59.

[253] L. E. Strigari, *Dark matter in dwarf spheroidal galaxies and indirect detection: a review*, *Rept. Prog. Phys.* **81** (2018) 056901. Cited on page 59.

[254] N. Klop, F. Zandanel, K. Hayashi and S. Ando, *Impact of axisymmetric mass models for dwarf spheroidal galaxies on indirect dark matter searches*, *Phys. Rev.* **D95** (2017) 123012, [1609.03509]. Cited on page 59.

[255] N. W. Evans, J. L. Sanders and A. Geringer-Sameth, *Simple J-Factors and D-Factors for Indirect Dark Matter Detection*, *Phys. Rev.* **D93** (2016) 103512, [1604.05599]. Cited on page 59.

[256] M. Lisanti, S. Mishra-Sharma, N. L. Rodd and B. R. Safdi, *Search for Dark Matter Annihilation in Galaxy Groups*, *Phys. Rev. Lett.* **120** (2018) 101101, [1708.09385]. Cited on page 59.

[257] L. J. Chang, M. Lisanti and S. Mishra-Sharma, *A Search for Dark Matter Annihilation in the Milky Way Halo*, 1804.04132. Cited on page 59.

[258] IceCube collaboration, M. G. Aartsen et al., *Search for Neutrinos from Dark Matter Self-Annihilations in the center of the Milky Way with 3 years of IceCube/DeepCore*, *Eur. Phys. J.* **C77** (2017) 627, [1705.08103]. Cited on page 59.

[259] A. Albert et al., *Results from the search for dark matter in the Milky Way with 9 years of data of the ANTARES neutrino telescope*, *Phys. Lett.* **B769** (2017) 249–254, [1612.04595]. Cited on page 59.

[260] IceCube collaboration, M. G. Aartsen et al., *Search for annihilating dark matter in the Sun with 3 years of IceCube data*, *Eur. Phys. J.* **C77** (2017) 146, [1612.05949]. Cited on page 60.

[261] ANTARES collaboration, S. Adrian-Martinez et al., *Limits on Dark Matter Annihilation in the Sun using the ANTARES Neutrino Telescope*, *Phys. Lett.* **B759** (2016) 69–74, [1603.02228]. Cited on page 60.

[262] I. V. Moskalenko, A. W. Strong, J. F. Ormes and M. S. Potgieter, *Secondary anti-protons and propagation of cosmic rays in the galaxy and heliosphere*, *Astrophys. J.* **565** (2002) 280–296, [astro-ph/0106567]. Cited on page 60.

[263] AMS collaboration, M. Aguilar et al., *Electron and Positron Fluxes in Primary Cosmic Rays Measured with the Alpha Magnetic*

Spectrometer on the International Space Station, *Phys. Rev. Lett.* **113** (2014) 121102. Cited on page 60.

[264] AMS collaboration, M. Aguilar et al., *Precision Measurement of the Proton Flux in Primary Cosmic Rays from Rigidity 1 GV to 1.8 TV with the Alpha Magnetic Spectrometer on the International Space Station*, *Phys. Rev. Lett.* **114** (2015) 171103. Cited on page 60.

[265] L. Bergstrom, T. Bringmann, I. Cholis, D. Hooper and C. Weniger, *New limits on dark matter annihilation from AMS cosmic ray positron data*, *Phys. Rev. Lett.* **111** (2013) 171101, [1306.3983]. Cited on page 60, 61, 63, and 69.

[266] A. Cuoco, M. Krämer and M. Korsmeier, *Novel Dark Matter Constraints from Antiprotons in Light of AMS-02*, *Phys. Rev. Lett.* **118** (2017) 191102, [1610.03071]. Cited on page 60, 61, 62, 63, and 69.

[267] M.-Y. Cui, Q. Yuan, Y.-L. S. Tsai and Y.-Z. Fan, *Possible dark matter annihilation signal in the AMS-02 antiproton data*, *Phys. Rev. Lett.* **118** (2017) 191101, [1610.03840]. Cited on page 60, 62, 63, and 69.

[268] Fermi-LAT collaboration, M. Ackermann et al., *Searching for Dark Matter Annihilation from Milky Way Dwarf Spheroidal Galaxies with Six Years of Fermi Large Area Telescope Data*, *Phys. Rev. Lett.* **115** (2015) 231301, [1503.02641]. Cited on page 61.

[269] L. Goodenough and D. Hooper, *Possible Evidence For Dark Matter Annihilation In The Inner Milky Way From The Fermi Gamma Ray Space Telescope*, 0910.2998. Cited on page 60, and 62.

[270] D. Hooper and L. Goodenough, *Dark Matter Annihilation in The Galactic Center As Seen by the Fermi Gamma Ray Space Telescope*, *Phys.Lett.* **B697** (2011) 412–428, [1010.2752]. Cited on page 60, and 62.

[271] Fermi-LAT collaboration, M. Ackermann et al., *The Fermi Galactic Center GeV Excess and Implications for Dark Matter*, *Astrophys. J.* **840** (2017) 43, [1704.03910]. Cited on page 62.

[272] T. Daylan, D. P. Finkbeiner, D. Hooper, T. Linden, S. K. N. Portillo, N. L. Rodd et al., *The characterization of the gamma-ray signal from the central Milky Way: A case for annihilating dark matter*, *Phys. Dark Univ.* **12** (2016) 1–23, [1402.6703]. Cited on page 62.

[273] F. Calore, I. Cholis and C. Weniger, *Background model systematics for the Fermi GeV excess*, *JCAP* **1503** (2015) 038, [1409.0042]. Cited on page 62.

[274] C. Gordon and O. Macias, *Dark Matter and Pulsar Model Constraints from Galactic Center Fermi-LAT Gamma Ray Observations*, *Phys. Rev.* **D88** (2013) 083521, [1306.5725]. Cited on page 62.

[275] K. N. Abazajian and M. Kaplinghat, *Detection of a Gamma-Ray Source in the Galactic Center Consistent with Extended Emission from Dark Matter Annihilation and Concentrated Astrophysical Emission*, *Phys. Rev.* **D86** (2012) 083511, [1207.6047]. Cited on page 62.

[276] I. Cholis, D. Hooper and T. Linden, *Challenges in Explaining the Galactic Center Gamma-Ray Excess with Millisecond Pulsars*, *JCAP* **1506** (2015) 043, [1407.5625]. Cited on page 62.

[277] J. Petrovic, P. D. Serpico and G. Zaharijas, *Millisecond pulsars and the Galactic Center gamma-ray excess: the importance of luminosity function and secondary emission*, *JCAP* **1502** (2015) 023, [1411.2980]. Cited on page 62.

[278] D. Hooper, I. Cholis, T. Linden, J. Siegal-Gaskins and T. Slatyer, *Pulsars Cannot Account for the Inner Galaxy's GeV Excess*, *Phys. Rev.* **D88** (2013) 083009, [1305.0830]. Cited on page 62.

[279] F. Calore, M. Di Mauro, F. Donato, J. W. T. Hessels and C. Weniger, *Radio detection prospects for a bulge population of millisecond pulsars as suggested by Fermi LAT observations of the inner Galaxy*, *Astrophys. J.* **827** (2016) 143, [1512.06825]. Cited on page 62.

[280] L. Lopez-Honorez, O. Mena, Á. Moliné, S. Palomares-Ruiz and A. C. Vincent, *The 21 cm signal and the interplay between dark matter annihilations and astrophysical processes*, *JCAP* **1608** (2016) 004, [1603.06795]. Cited on page 63.

[281] H. Liu and T. R. Slatyer, *Too Hot, Too Cold or Just Right? Implications of a 21-cm Signal for Dark Matter Annihilation and Decay*, 1803.09739. Cited on page 63.

[282] CTA Consortium collaboration, M. Actis et al., *Design concepts for the Cherenkov Telescope Array CTA: An advanced facility for ground-based high-energy gamma-ray astronomy*, *Exper. Astron.* **32** (2011) 193–316, [1008.3703]. Cited on page 63.

[283] IceCube collaboration, M. G. Aartsen et al., *Evidence for High-Energy Extraterrestrial Neutrinos at the IceCube Detector*, *Science* **342** (2013) 1242856, [1311.5238]. Cited on page 63.

[284] G. Bertone, W. Buchmuller, L. Covi and A. Ibarra, *Gamma-Rays from Decaying Dark Matter*, *JCAP* **0711** (2007) 003, [0709.2299]. Cited on page 63.

[285] T. Cohen, K. Murase, N. L. Rodd, B. R. Safdi and Y. Soreq, *? -ray Constraints on Decaying Dark Matter and Implications for IceCube*, *Phys. Rev. Lett.* **119** (2017) 021102, [1612.05638]. Cited on page 63.

[286] T. R. Slatyer and C.-L. Wu, *General Constraints on Dark Matter Decay from the Cosmic Microwave Background*, *Phys. Rev.* **D95** (2017) 023010, [1610.06933]. Cited on page 63.

[287] F. Kahlhoefer, *Review of LHC Dark Matter Searches*, *Int. J. Mod. Phys.* **A32** (2017) 1730006, [1702.02430]. Cited on page 64.

[288] J. Abdallah et al., *Simplified Models for Dark Matter Searches at the LHC*, *Phys. Dark Univ.* **9-10** (2015) 8–23, [1506.03116]. Cited on page 64.

[289] F. Kahlhoefer, K. Schmidt-Hoberg, T. Schwetz and S. Vogl, *Implications of unitarity and gauge invariance for simplified dark matter models*, *JHEP* **02** (2016) 016, [1510.02110]. Cited on page 64.

[290] CMS collaboration, V. Khachatryan et al., *Searches for invisible decays of the Higgs boson in pp collisions at $\sqrt{s}$ = 7, 8, and 13 TeV*, *JHEP* **02** (2017) 135, [1610.09218]. Cited on page 66.

[291] ATLAS collaboration, G. Aad et al., *Constraints on new phenomena via Higgs boson couplings and invisible decays with the ATLAS detector*, *JHEP* **11** (2015) 206, [1509.00672]. Cited on page 66.

[292] SLD Electroweak Group, DELPHI, ALEPH, SLD, SLD Heavy Flavour Group, OPAL, LEP Electroweak Working Group, L3 collaboration, S. Schael et al., *Precision electroweak measurements on the Z resonance*, *Phys. Rept.* **427** (2006) 257–454, [hep-ex/0509008]. Cited on page 66.

[293] LHCb collaboration, R. Aaij et al., *Search for Dark Photons Produced in 13 TeV pp Collisions*, *Phys. Rev. Lett.* **120** (2018) 061801, [1710.02867]. Cited on page 67.

[294] ATLAS collaboration, M. Aaboud et al., *Search for new high-mass phenomena in the dilepton final state using* 36 fb^{-1} *of proton-proton collision data at* $\sqrt{s} = 13$ *TeV with the ATLAS detector*, *JHEP* **10** (2017) 182, [1707.02424]. Cited on page 67.

[295] R. M. Harris and K. Kousouris, *Searches for Dijet Resonances at Hadron Colliders*, *Int. J. Mod. Phys.* **A26** (2011) 5005–5055, [1110.5302]. Cited on page 67.

[296] ATLAS collaboration, M. Aaboud et al., *Search for new phenomena in dijet events using 37 fb^{-1} of pp collision data collected at* $\sqrt{s}$ *=13 TeV with the ATLAS detector*, *Phys. Rev.* **D96** (2017) 052004, [1703.09127]. Cited on page 67.

[297] CMS collaboration, A. M. Sirunyan et al., *Search for dijet resonances in proton-proton collisions at* $\sqrt{s}$ *= 13 TeV and constraints on dark matter and other models*, *Phys. Lett.* **B769** (2017) 520–542, [1611.03568]. Cited on page 67.

[298] ATLAS collaboration, M. Aaboud et al., *Search for dark matter at* $\sqrt{s} = 13$ *TeV in final states containing an energetic photon and large missing transverse momentum with the ATLAS detector*, *Eur. Phys. J.* **C77** (2017) 393, [1704.03848]. Cited on page 67.

[299] CMS collaboration, C. Collaboration, *Search for dark matter in final states with an energetic jet, or a hadronically decaying W or Z boson using* 12.9 fb^{-1} *of data at* $\sqrt{s} = 13$ TeV, . Cited on page 67.

[300] ATLAS collaboration, M. Aaboud et al., *Search for dark matter in association with a Higgs boson decaying to b-quarks in pp collisions at* $\sqrt{s} = 13$ *TeV with the ATLAS detector*, *Phys. Lett.* **B765** (2017) 11–31, [1609.04572]. Cited on page 67.

[301] ATLAS collaboration, M. Aaboud et al., *Search for dark matter produced in association with a hadronically decaying vector boson in pp collisions at* $\sqrt{s}$ *= 13 TeV with the ATLAS detector*, *Phys. Lett.* **B763** (2016) 251–268, [1608.02372]. Cited on page 67.

[302] BaBar collaboration, J. P. Lees et al., *Search for a Dark Photon in* e^+e^- *Collisions at BaBar*, *Phys. Rev. Lett.* **113** (2014) 201801, [1406.2980]. Cited on page 67.

[303] BaBar collaboration, J. P. Lees et al., *Search for Invisible Decays of a Dark Photon Produced in* e^+e^- *Collisions at BaBar*, *Phys. Rev. Lett.* **119** (2017) 131804, [1702.03327]. Cited on page 67.

[304] J. P. Chou, D. Curtin and H. J. Lubatti, *New Detectors to Explore the Lifetime Frontier*, *Phys. Lett.* **B767** (2017) 29–36, [1606.06298]. Cited on page 68.

[305] S. Weinberg, *The First Three Minutes. A Modern View of the Origin of the Universe*. 1977. Cited on page 252.

[306] G. B. Gelmini, *El boson de Higgs*, 1407.1741. Cited on page 252.

Part II

Scientific Research

Journal of Cosmology and Astroparticle Physics
An IOP and SISSA journal

Exploring dark matter microphysics with galaxy surveys

Miguel Escudero,[a] **Olga Mena,**[a] **Aaron C. Vincent,**[b] **Ryan J. Wilkinson**[b] **and Céline Bœhm**[b]

[a]Instituto de Física Corpuscular (IFIC), CSIC-Universitat de València, Apartado de Correos 22085, E-46071 Valencia, Spain
[b]Institute for Particle Physics Phenomenology (IPPP), Durham University, South Road, Durham DH1 3LE, U.K.

E-mail: miguel.Escudero@uv.es, omena@ific.uv.es, aaron.vincent@durham.ac.uk, ryan.wilkinson@durham.ac.uk, c.m.boehm@durham.ac.uk

Received June 17, 2015
Accepted August 13, 2015
Published September 10, 2015

Abstract. We use present cosmological observations and forecasts of future experiments to illustrate the power of large-scale structure (LSS) surveys in probing dark matter (DM) microphysics and unveiling potential deviations from the standard ΛCDM scenario. To quantify this statement, we focus on an extension of ΛCDM with DM-neutrino scattering, which leaves a distinctive imprint on the angular and matter power spectra. After finding that future CMB experiments (such as COrE+) will not significantly improve the constraints set by the *Planck* satellite, we show that the next generation of galaxy clustering surveys (such as DESI) could play a leading role in constraining alternative cosmologies and even have the potential to make a discovery. Typically we find that DESI would be an order of magnitude more sensitive to DM interactions than *Planck*, thus probing effects that until now have only been accessible via N-body simulations.

Keywords: dark matter theory, galaxy surveys, cosmological parameters from CMBR

ArXiv ePrint: 1505.06735

doi:10.1088/1475-7516/2015/09/034

JCAP09(2015)034

Contents

JCAP09(2015)034

1 Introduction

Dark matter (DM) is required to explain the galactic rotation curves, lensing and virial motions of galaxy clusters, observed matter power spectrum and cosmic microwave background (CMB) acoustic peaks. The current paradigm is that DM can be well-approximated by a collisionless fluid, consisting of weakly-interacting massive particles (WIMPs) and leading to a characteristic matter power spectrum ($\mathrm{P}(k) \propto k^{-3}$). However, direct evidence for WIMPs remains elusive and it is now legitimate to question the validity of the standard picture.

The ΛCDM framework provides an excellent fit to the currently-available data [1, 2]. Any future rejection or modification of this model must therefore come in the form of comparison with a (better) alternative hypothesis, or through the discovery of new data in direct conflict with ΛCDM predictions. Possible modifications to the Standard Model either assume new relativistic species such as sterile neutrinos [3, 4], or different DM characteristics such as interactions with particles in the visible or dark sector. Either way, these "Beyond the Standard Model" scenarios predict a modification of the ΛCDM matter power spectrum at small scales.

There is in fact a plethora of DM models in the literature that exhibit such deviations (e.g. refs. [5–27]), many of which predict additional damping and/or oscillations in the $\mathrm{P}(k)$. While CMB experiments such as *Planck* allow one to constrain the cosmological parameters with unprecedented precision [1, 2], extracting the $\mathrm{P}(k)$ from *Planck* or the next-generation of CMB probes (such as COrE+ [28] or PIXIE [29]) will be limited by the large uncertainties involved in foreground modelling, which hinder any angular power spectrum analysis at large ℓ.[1] Therefore, to unravel the nature of DM, a direct probe of the $\mathrm{P}(k)$ is needed. Here we show that the next generation of large-scale structure (LSS) surveys could provide us with key information on the particle properties of DM, due to their extremely high precision.

Galaxy clustering surveys [30–36] have already observed the imprint of Baryon Acoustic Oscillations (BAOs), a standard ruler to measure the Hubble expansion rate, $H(z)$, and the angular diameter distance, $D_{\mathrm{A}}(z)$. Recently, the Baryon Oscillation Spectroscopic Survey (BOSS) collaboration [37] reported a separate extraction of $H(z)$ and $D_{\mathrm{A}}(z)$ to a precision

[1] An additional difficulty is that the C_ℓ are the result of the convolution of the $\mathrm{P}(k)$ with a window (Bessel) function that accounts for the angular scale, thus preventing one from detecting small features in the $\mathrm{P}(k)$.

of 1% [30]. Here we show that by exploiting all of the information contained in the shape of the full P(k) (rather than solely the BAO geometrical signature [38–40]), one can test the validity of the ΛCDM model at scales below a Mpc.

For concreteness, we focus on one specific scenario, in which DM scatters elastically with the active neutrinos (hereafter, νCDM) [5–18]. Such a DM candidate erases small-scale perturbations through collisional damping [5, 7] and suppresses neutrino free-streaming in the early universe. This leaves a unique signature in the angular and matter power spectra and provides us with a framework to quantify the potential of future LSS surveys to constrain DM microphysics. We exploit both the current publicly available galaxy power spectrum data (in particular, from the *WiggleZ* survey [36]) and the expected full-shape power spectrum measurements from the forthcoming Dark Energy Spectroscopic Instrument (DESI) [41].

The structure of the paper is as follows. In section 2, we describe the νCDM scenario. In section 3, we compute up-to-date constraints using both CMB data from *Planck* and full-shape LSS data from the *WiggleZ* survey. In section 4, we perform a forecast of the sensitivity of planned experiments such as COrE+ and DESI to the νCDM framework (and any model that generates small deviations from ΛCDM). Finally, we draw our main conclusions in section 5.

2 Dark matter-neutrino interactions

In the νCDM scenario, DM remains in kinetic contact with the neutrino sector long after the chemical freeze-out (see refs. [5–18] for previous related work). Small-scale DM perturbations are then erased as a result of ongoing elastic scattering through "collisional damping" [5, 7], rather than slowly clustering under gravity. At the same time, neutrinos cannot free-stream as efficiently as in ΛCDM and behave more like a relativistic perfect fluid. The main consequences are: (i) an enhancement of the CMB acoustic peaks and (ii) a reduction of small-scale power in the matter power spectrum [9–11].

DM-neutrino interactions do not affect the background equations but they do modify the evolution of the DM and neutrino fluctuations. They can be implemented by a modification of the Euler equations. In the conformal Newtonian gauge,[2]

$$\begin{aligned}
\dot{\theta}_{\rm DM} &= k^2\psi - \mathcal{H}\theta_{\rm DM} - S^{-1}\dot{\mu}(\theta_{\rm DM} - \theta_\nu) \\
\dot{\theta}_\nu &= k^2\psi + k^2\left(\frac{1}{4}\delta_\nu - \sigma_\nu\right) - \dot{\mu}(\theta_\nu - \theta_{\rm DM}) \\
\dot{\sigma}_\nu &= \frac{4}{15}\theta_\nu - \frac{3}{10}kF_{\nu 3} - \frac{9}{10}\dot{\mu}\sigma_\nu \\
\dot{F}_{\nu\ell} &= \frac{k}{2\ell+1}\left[\ell F_{\nu(\ell-1)} - (\ell+1)F_{\nu(\ell+1)}\right] - \dot{\mu}F_{\nu\ell}, \ell \geq 3
\end{aligned} \tag{2.1}$$

where δ, θ and σ are the density, velocity and shear perturbations respectively, $F_{\nu\ell}$ refer to higher ($\ell > 2$) neutrino moments, ψ is the gravitational potential, $\mathcal{H}$ is the conformal Hubble parameter and $S \equiv (3/4)\,\rho_{\rm DM}/\rho_\nu$.

The key quantity in eq. (2.1) is $\dot{\mu} \equiv a\,\sigma_{{\rm DM}-\nu}\,n_{\rm DM}$, which can be written in terms of the dimensionless quantity u defined as

$$u \equiv \left[\frac{\sigma_{{\rm DM}-\nu}}{\sigma_{\rm Th}}\right]\left[\frac{m_{\rm DM}}{100\ {\rm GeV}}\right]^{-1} . \tag{2.2}$$

[2] In analogy to the perturbation equations governing baryon-photon interactions, see e.g. ref. [42].

JCAP09(2015)034

This variable u describes the ratio of the DM-neutrino elastic scattering cross section, $\sigma_{\rm DM-\nu}$, to the DM mass, $m_{\rm DM}$, normalised to the Thomson cross section, $\sigma_{\rm Th}$ (see ref. [6]). In our analyses, we will consider both s-wave ($\sigma_{\rm DM-\nu,0}$ = constant) and p-wave ($\sigma_{\rm DM-\nu,2} \propto T^2$) cross sections. For p-wave cross sections, we can write $u(a) = u\, a^{-2}$, where u is the present-day value and a is the cosmological scale factor, normalised to unity today. The larger the value of u, the greater the suppression in the linear matter power spectrum with respect to ΛCDM, for a given wavenumber k, as shown in figure 1 (and can also be seen in refs. [9–11]).

DM interactions leave a further imprint in the galaxy power spectrum through damped acoustic oscillations, which, in general, show up at smaller scales than those illustrated in figure 1. They were first pointed out in the context of DM-photon interactions (in the weak-coupling regime) in ref. [6] and were later observed in interactions with baryons [22], neutrinos [9, 10] and dark radiation [25, 26]. They arise because the DM fluid acquires a non-zero pressure as a result of interactions with the thermal bath and are therefore similar to the photon-baryon fluid before recombination. Although they cannot be observed using current data, they provide a characteristic signature for future experiments.

However, in addition to the models mentioned above, damped oscillations in the P(k) are also expected for certain types of self-interacting DM [43], late-forming DM [44] and atomic DM [45]. Taking all these possibilities into account, it would be difficult to determine the specific nature of the DM coupling from this feature alone. Furthermore, since the oscillations are not as prominent as in the case of DM-photon interactions [6] or atomic DM in the sDAO (strong dark acoustic oscillation) scenario [46], they may not be resolved. In this case, there could be a degeneracy with both warm DM [47] and axion DM [48] models, which predict a sharp cut-off in the matter power spectrum at small scales.

3 Current constraints

To assess how powerful the constraints from future LSS surveys can be, we first derive the limits set by current CMB and galaxy clustering surveys. These will then serve as a benchmark for our forecasts in section 4.

To perform this analysis, the modifications shown in eq. (2.1) are implemented in the Boltzmann code CLASS [49] (see also ref. [11]) and the posterior likelihoods are obtained using the Markov Chain Monte Carlo (MCMC) code MONTE PYTHON [50]. The prior ranges for these parameters are listed in table 1. Since u can vary by many orders of magnitude, we select a logarithmic prior distribution for this parameter, in contrast to the linear priors used in refs. [9–11].

For simplicity, we assume massless neutrinos[3] and fix the effective number of neutrino species, $N_{\rm eff}$, to the standard value of 3.046 [51]. We have verified that allowing $N_{\rm eff}$ to vary has an impact on the value of the Hubble parameter, H_0, but does not change the sensitivity to the u parameter.

The current CMB constraints (using *Planck* 2013 + WMAP polarisation data [1]) are shown in table 2. The corresponding upper limits on the DM-neutrino scattering cross section (at 95% CL) are

$$\sigma^{\rm (Planck)}_{\rm DM-\nu,0} \lesssim 6 \times 10^{-31}\, (m_{\rm DM}/{\rm GeV})\ \ {\rm cm}^2\,, \tag{3.1}$$

[3]This is in contrast to *Planck*, whose analysis assumes two massless and one massive neutrino with $m_\nu = 0.06\,$eV [1]. Such a small neutrino mass only affects the CMB through a slight shift in the angular diameter distance, which can be exactly compensated by a decrease in $100\,h$ of ~ 0.6 [1].

JCAP09(2015)034

Parameter	Prior
$\Omega_{\rm b}h^2$	$0.005 \to 0.1$
$\Omega_{\rm DM}h^2$	$0.01 \to 0.99$
$100\,h$	$50 \to 100$
$10^9 A_{\rm s}$	$1 \to 4$
$n_{\rm s}$	$0.5 \to 1.5$
$\tau_{\rm reio}$	$0.01 \to 0.1$
$\log(u)$ (s-wave)	$-6 \to 0$
$\log(u)$ (p-wave)	$-18 \to -11$

Table 1. Flat priors for the cosmological parameters considered here. $\Omega_{\rm b}h^2$ is the baryon density, $\Omega_{\rm DM}h^2$ is the DM density, h is the reduced Hubble parameter, $A_{\rm s}$ is the primordial spectrum amplitude, $n_{\rm s}$ is the scalar spectral index, $\tau_{\rm reio}$ is the optical depth and u is defined in eq. (2.2).

	s-wave ($u = $ const.)		p-wave ($u \propto T^2$)	
Parameter	*Planck* 2013	COrE+	*Planck* 2013	COrE+
$\Omega_{\rm b}h^2$	0.0221 ± 0.0003	0.02223 ± 0.00004	0.0221 ± 0.0003	0.02222 ± 0.00004
$\Omega_{\rm DM}h^2$	0.120 ± 0.003	0.1199 ± 0.0005	0.119 ± 0.003	0.1197 ± 0.0005
$100\,h$	70.0 ± 1.2	67.3 ± 0.2	68.0 ± 1.2	67.3 ± 0.2
$10^9 A_{\rm s}$	2.20 ± 0.06	2.207 ± 0.010	2.19 ± 0.06	2.207 ± 0.010
$n_{\rm s}$	0.961 ± 0.008	0.9656 ± 0.0017	0.961 ± 0.008	0.9639 ± 0.0019
$\tau_{\rm reio}$	0.090 ± 0.015	0.0792 ± 0.0002	0.090 ± 0.013	0.0790 ± 0.0002
$\log_{10}(u)$	< -4.04 (95% CL)	-4.33 (95% CL)	< -13.6 (95% CL)	< -14.6 (95% CL)

Table 2. Marginalised posteriors for s-wave (left) and p-wave (right) DM-neutrino scattering cross sections set by the *Planck* 2013 data (+ WMAP polarisation) (see section 3) and the COrE+ forecast (see section 4). Unless otherwise indicated, the errors represent the 68% CL.

if s-wave and

$$\sigma^{(\rm Planck)}_{{\rm DM}-\nu,2} \lesssim 2 \times 10^{-40}\,(m_{\rm DM}/{\rm GeV})\ \ {\rm cm}^2\,, \tag{3.2}$$

if p-wave. These results are consistent with those quoted by the authors of refs. [9, 10], with the caveat that they did not perform a full MCMC analysis.

We now repeat the previous analysis adding LSS data on the full shape of the matter power spectrum. Concretely, we use the galaxy clustering information from the *WiggleZ* Dark Energy Survey [36]. The *WiggleZ* sample consists of $\sim 238,000$ galaxies and covers a region of 1 Gpc^3 in redshift space. Our calculations have shown that comparable results can be obtained from the BOSS DR11 measurements [30]. Following a similar analysis to ref. [52], we construct the likelihood function as follows:

$$-\,2\,\log[L(\vartheta_\alpha)] = \chi^2(\vartheta_\alpha) = \sum_{ij} \Delta_i C^{-1}_{ij} \Delta_j\,, \tag{3.3}$$

where the covariance matrix reads

$$C_{ij} = \langle \hat{P}_{\rm halo}(k_i)\hat{P}_{\rm halo}(k_j)\rangle - \langle \hat{P}_{\rm halo}(k_i)\rangle\langle \hat{P}_{\rm halo}(k_j)\rangle\,, \tag{3.4}$$

and

$$\Delta_i \equiv \left[\hat{P}_{\rm halo}(k_i) - P_{{\rm halo},w}(k_i,\vartheta_\alpha)\right]\,. \tag{3.5}$$

JCAP09(2015)034

	s-wave ($u = \text{const.}$)		p-wave ($u \propto T^2$)	
Parameter	$k_{\rm max} = 0.12\ h\ {\rm Mpc}^{-1}$	$k_{\rm max} = 0.2\ h\ {\rm Mpc}^{-1}$	$k_{\rm max} = 0.12\ h\ {\rm Mpc}^{-1}$	$k_{\rm max} = 0.2\ h\ {\rm Mpc}^{-1}$
$\Omega_{\rm b}h^2$	0.0220 ± 0.0003	0.0219 ± 0.0003	0.0219 ± 0.0003	0.0218 ± 0.0003
$\Omega_{\rm DM}h^2$	0.122 ± 0.002	0.123 ± 0.003	0.122 ± 0.002	0.123 ± 0.002
$100\,h$	70.0 ± 1.1	66.6 ± 1.0	66.9 ± 1.1	66.7 ± 1.0
$10^9 A_{\rm s}$	2.19 ± 0.05	2.19 ± 0.05	2.19 ± 0.05	2.19 ± 0.05
$n_{\rm s}$	0.956 ± 0.007	0.956 ± 0.006	0.956 ± 0.007	0.955 ± 0.007
$\tau_{\rm reio}$	0.086 ± 0.013	0.086 ± 0.013	0.085 ± 0.013	0.085 ± 0.013
$\log_{10}(u)$	< -4.18 (95% CL)	-4.57 (95% CL)	< -13.7 (95% CL)	< -13.9 (95% CL)

Table 3. Marginalised posteriors for s-wave (left) and p-wave (right) DM-neutrino scattering cross sections set by the combination of *WiggleZ* full-shape galaxy power spectrum measurements and *Planck* 2013 (+ WMAP polarisation) data. Unless otherwise indicated, the errors represent the 68% CL.

In eq. (3.5), $\hat{P}_{\rm halo}(k_i)$ is the measured galaxy power spectrum and $P_{{\rm halo},w}(k_i, \vartheta_\alpha)$ is the theoretical expectation for the set of model parameters ϑ_α, listed in table 1. In turn, $P_{{\rm halo},w}(k_i, \vartheta_\alpha)$ is a convolution of the computed galaxy power spectrum with the survey window functions, $W(k_i, k_n)$, and is given by

$$P_{{\rm halo},w}(k_i, \vartheta_\alpha) = \sum_n \frac{W(k_i, k_n) P_{\rm halo}(k_n/a_{\rm scl}, \vartheta_\alpha)}{a_{\rm scl}^3} \,. \tag{3.6}$$

In this equation, $a_{\rm scl}$ represents the scaling, which takes into account that the observed galaxy redshift has to be translated into a distance using a fiducial model. In this case, we use the same values as in ref. [53]: $\Omega_{\rm b} = 0.049$, $\Omega_{\rm m} = 0.297$, $h = 0.7$, $n_{\rm s} = 1$ and $\sigma_8 = 0.8$. The scaling factor is given by refs. [52, 54]:

$$a_{\rm scl}^3 = \frac{D_A(z)^2 H(z)}{D_{A,{\rm fid}}(z)^2 H_{\rm fid}(z)} \,. \tag{3.7}$$

The theoretical galaxy power spectrum $P_{\rm halo}(k, \vartheta_\alpha)$ is related to the matter power spectrum $P^m(k, \vartheta_\alpha)$ through the relation

$$P_{\rm halo}(k, \vartheta_\alpha) = b^2\ P^m(k, \vartheta_\alpha)\,, \tag{3.8}$$

where b is the bias, which is assumed to be constant. We analytically marginalise over b as in ref. [55]:

$$b^2 = \frac{\sum_{ij} P_{{\rm halo},w}(k_i, \vartheta_\alpha) C_{ij}^{-1} \hat{P}_{\rm halo}(k_j)}{\sum_{ij} P_{{\rm halo},w}(k_i, \vartheta_\alpha) C_{ij}^{-1} P_{{\rm halo},w}(k_j, \vartheta_\alpha)} \,. \tag{3.9}$$

In figure 1, we show the measured galaxy power spectrum, $\hat{P}_{\rm halo}(k)$, from *WiggleZ* in the four redshift bins ($0.1 < z < 0.3$, $0.3 < z < 0.5$, $0.5 < z < 0.7$ and $0.7 < z < 0.9$) exploited in our analyses [36]. We also depict the convolved power spectrum, $P_{{\rm halo},w}(k_i, \vartheta_\alpha)$, as defined in eq. (3.6), for the ΛCDM fiducial model of ref. [53] and for two values of the u parameter ($u = 10^{-4}$ and $u = 10^{-5}$, both in the s-wave scenario). The characteristic damping of the P(k) due to the interacting DM-neutrino fluid is clearly visible and allows us to tighten the constraints with respect to the previous CMB-only analysis.

In table 3, we present the posteriors obtained using the combination of *WiggleZ* and CMB data. We perform two separate analyses, including data for which: (i) $k < k_{\rm max} = 0.12\ h\ {\rm Mpc}^{-1}$ (purely linear regime) and (ii) $k < k_{\rm max} = 0.2\ h\ {\rm Mpc}^{-1}$ (weakly non-linear regime).

JCAP09(2015)034

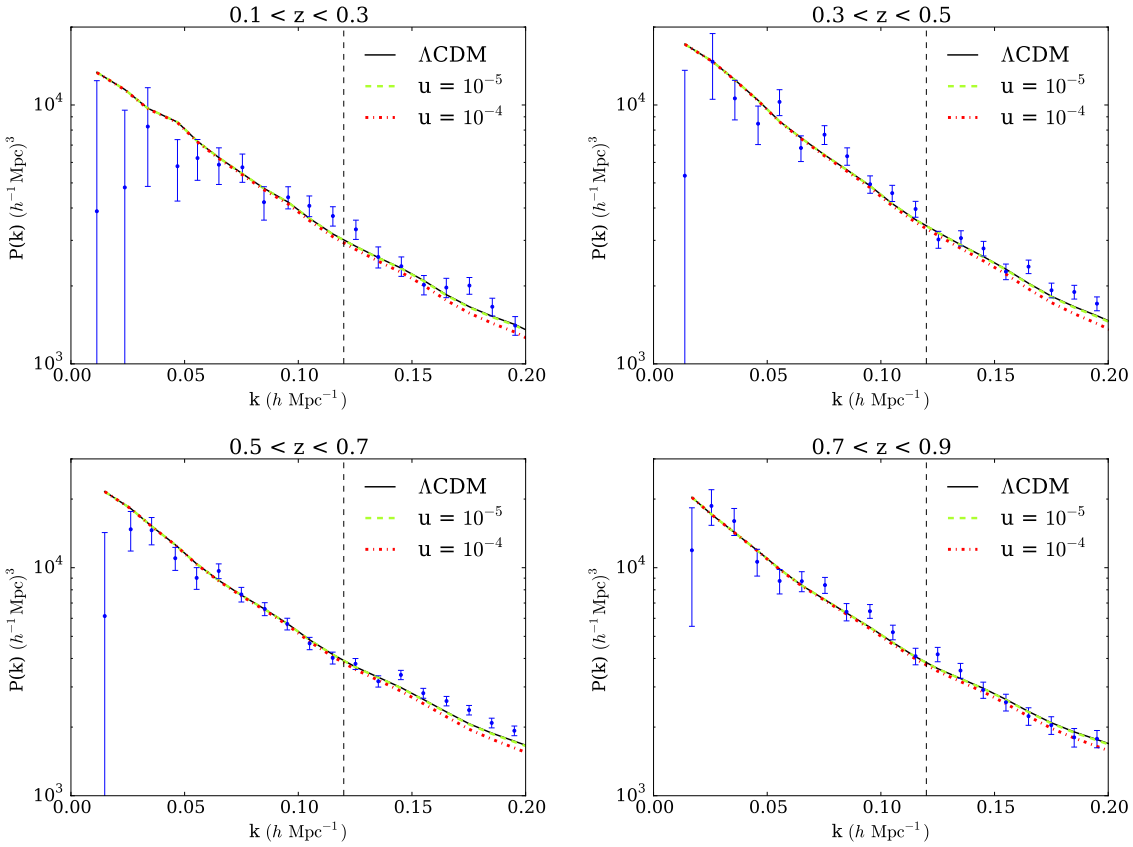

Figure 1. The data points show the galaxy power spectrum, $\hat{P}_{\rm halo}(k)$, in the four redshift bins ($0.1 < z < 0.3$, $0.3 < z < 0.5$, $0.5 < z < 0.7$ and $0.7 < z < 0.9$) measured by the *WiggleZ* survey [36]. We also depict the convolved power spectrum, $P_{{\rm halo},w}(k_i, \vartheta_\alpha)$, as defined in eq. (3.6), for the ΛCDM fiducial model of ref. [53] (solid black) and for two values of the u parameter: $u = 10^{-4}$ (dotted red) and $u = 10^{-5}$ (dashed green) in the s-wave scenario. The vertical dashed line denotes the separation between the linear ($k \lesssim 0.12\ h\ {\rm Mpc}^{-1}$) and non-linear ($k \gtrsim 0.12\ h\ {\rm Mpc}^{-1}$) regimes.

In terms of the DM-neutrino scattering cross section (at 95% CL) with $k_{\rm max} = 0.12\ h\ {\rm Mpc}^{-1}$ ($k_{\rm max} = 0.2\ h\ {\rm Mpc}^{-1}$), we obtain

$$\sigma^{\rm (WiggleZ)}_{{\rm DM}-\nu,0} \lesssim 4 \times 10^{-31}\,(m_{\rm DM}/{\rm GeV})\ {\rm cm}^2\,; \quad (\lesssim 2 \times 10^{-31}\,(m_{\rm DM}/{\rm GeV})\ {\rm cm}^2)\,, \tag{3.10}$$

for the s-wave cross section. As we shall see in the next section, these bounds are competitive with those resulting from our forecasts for the future CMB mission COrE+.

Meanwhile, for the p-wave cross section, we obtain

$$\sigma^{\rm (WiggleZ)}_{{\rm DM}-\nu,2} \lesssim 1 \times 10^{-40}\,(m_{\rm DM}/{\rm GeV})\ {\rm cm}^2\,; \quad (\lesssim 8 \times 10^{-41}\,(m_{\rm DM}/{\rm GeV})\ {\rm cm}^2)\,. \tag{3.11}$$

Therefore, including data in the weakly non-linear regime ($k < 0.2\ h\ {\rm Mpc}^{-1}$) only strengthens the constraints by a factor of 2 (s-wave) and 1.25 (p-wave) with respect to those in the purely linear regime ($k < 0.12\ h\ {\rm Mpc}^{-1}$). We note that, in the s-wave scenario, the bounds are as

JCAP09(2015)034

much as ~ 3.5 times tighter than those using only CMB measurements, showing the benefits of utilising the full shape of the P(k). The improvement is not as significant for the p-wave case because the suppression appears at larger scales (see e.g. ref. [26]).

4 Forecasts for future experiments

The CMB and LSS analyses in section 3 allowed us to obtain current constraints on the DM-neutrino elastic scattering cross section. We will now assess the power of future experiments in (i) *constraining* DM microphysics and (ii) *detecting* small deviations from the ΛCDM matter power spectrum in the weakly non-linear regime. These two analyses require slightly different methodologies. In the first case, we construct a mock catalogue based on the ΛCDM cosmology and compute the strongest possible upper limit on the u parameter using the expected sensitivity of future experiments. In the second case, the mock data assumes small but non-negligible DM-neutrino interactions in order to assess our ability to detect them and more generally, reconstruct possible deviations from ΛCDM. In both cases, we use projected sensitivities.

As in the previous section, we first consider CMB observables only and then include data from LSS surveys. We focus on two planned experiments: (i) COrE+ [28], a CMB space mission currently proposed for the 2015-2025 ESA call, and (ii) DESI [41], a multiplexed fibre-fed spectrograph to detect galaxies and quasars up to redshift $z \sim 2$, that is expected to run in the 2018-2022 timeframe.

4.1 COrE+

We first produce full mock CMB data sets (temperature and E-polarisation, plus lensing). We then compute the fiducial angular power spectra, C_ℓ, using the best-fit cosmology reported by the *Planck* 2015 final mission, including the TT, TE and EE spectra [2]. To these C_ℓ, we add a noise component N_ℓ consistent with each COrE+ channel specification and given by

$$N_\ell^{IJ} = \delta_{IJ}\,\sigma^I\sigma^J \exp\left[\ell\,(\ell+1)\,\frac{\theta^2}{8\ln 2}\right], \tag{4.1}$$

where $\sigma^{I,J}$ correspond to the temperature or polarisation errors (i.e. $I, J \in \{\mathrm{T,E}\}$). The expected temperature and polarisation sensitivities are given in table 4.

Following ref. [56], the effective χ^2 is given by

$$\chi^2_{\rm eff}(\vartheta_\alpha) = \sum_\ell (2\ell+1) f_{\rm sky}\left(\frac{D}{|\bar{C}|} + \ln\frac{|\bar{C}|}{|\hat{C}|} - 3\right), \tag{4.2}$$

where D is a certain function of the noised power spectra (see eq. (3.4) in ref. [56]) and $|\bar{C}|$ and $|\hat{C}|$ represent the determinants of the theoretical and observed covariance matrices respectively. Finally, $f_{\rm sky}$ represents the observed fraction of the sky (in practice, it weights the correlations between multipoles when the map does not cover the full sky). For this analysis, we use $f_{\rm sky} = 0.7$ [28].

The third step in our analysis is to compute a Gaussian likelihood around our fiducial spectra, using CLASS, tuned to obtain a 0.01% precision on the C_ℓ (as in ref. [56], according to eq. (4.2) and with a noise given by eq. (4.1)). Then, assuming a 4-year sensitivity and using MONTE PYTHON to sample the parameter space with the priors given in table 1, we can predict the sensitivity of COrE+ to the ΛCDM parameters. Note that we only consider

JCAP09(2015)034

Channel (GHz)	θ (arcmin)	ΔT (μK·arcmin)	ΔP (μK·arcmin)
105	10.0	2.68	4.63
135	7.8	2.63	4.55
165	6.4	2.67	4.61
195	5.4	2.63	4.54

Table 4. COrE+ 4-year sensitivity. θ is the Full Width at Half Maximum (FWHM) of the beam, ΔT and ΔP are the temperature and polarisation sensitivities respectively [28].

the TT, TE and EE observables. For simplicity, we neglect tensor modes (i.e. BT, BE and BB) as they have currently not been observed [57].

The results are presented in table 2. We infer that the future sensitivity of COrE+ to a DM-neutrino coupling would be (at 95% CL)

$$\sigma_{\mathrm{DM}-\nu,0}^{(\mathrm{COrE+})} \lesssim 3 \times 10^{-31} \, (m_{\mathrm{DM}}/\mathrm{GeV}) \ \mathrm{cm}^2 \,, \tag{4.3}$$

if s-wave and

$$\sigma_{\mathrm{DM}-\nu,2}^{(\mathrm{COrE+})} \lesssim 2 \times 10^{-41} \, (m_{\mathrm{DM}}/\mathrm{GeV}) \ \mathrm{cm}^2 \,, \tag{4.4}$$

if p-wave.

While we find that the standard cosmological parameters will be measured to much higher precision than with *Planck*, there is only a modest gain in sensitivity to the DM-neutrino cross section. Furthermore, these limits are slightly worse than those obtained after combining *Planck* with current LSS data in the weakly non-linear regime. From these results, we expect detection with COrE+ to be possible for $u \simeq 10^{-4}$.

To assess the power of COrE+ to detect and reconstruct the νCDM cosmology or similar deviations to ΛCDM, we also produce mock data sets with $u = 10^{-4}$ and $u = 10^{-5}$ as fiducial models (for s-wave interactions). We then attempt to reconstruct these models by means of the usual MCMC method. The $u = 10^{-5}$ case is presented in figure 2 (and similarly for p-wave with $u = 10^{-14}$). With COrE+–like CMB data, one may reconstruct a universe with $u = 10^{-4}$ with a 40% 1σ error. However, the $u = 10^{-5}$ case would provide us with CMB information entirely consistent with $u = 0$, in agreement with eq. (4.3). Therefore, $u \gtrsim 5 \times 10^{-5}$ is the best sensitivity that one could achieve with CMB experiments in the near future.

4.2 DESI

The DESI survey [41] is expected to provide a wealth of information on the matter distribution (i.e. the P(k)) in the Universe at relatively small scales and up to redshift $z \sim 2$. To forecast the ability of DESI to discover new physics, we first compute the expected errors from the DESI instrument, following a Fisher matrix approach, which is the usual method used to forecast galaxy survey experiments.[4,5]

The Fisher matrix is defined as the expectation value of the second derivative of the likelihood surface around its maximum. As long as the posterior distribution for the parameters

[4] http://desi.lbl.gov/.
[5] http://sci.esa.int/euclid/.

JCAP09(2015)034

is well approximated by a multivariate Gaussian function, its elements are given by [58–60]

$$F_{\alpha\beta} = \frac{1}{2}\mathrm{Tr}\left[C^{-1}\frac{\partial C}{\partial\vartheta_\alpha}C^{-1}\frac{\partial C}{\partial\vartheta_\beta}\right], \tag{4.5}$$

where $C = S + N$ is the total covariance, which consists of signal S and noise N terms. Once more, we take a fiducial cosmology defined by the parameters that best fit the *Planck* 2015 TT, TE, EE + lowP data [61] in the presence of DM-neutrino interactions with $u = 10^{-5}$ in the s-wave scenario and $u = 10^{-14}$ in the p-wave scenario.[6]

Assuming a Gaussian likelihood for the DESI band powers, the Fisher matrix can be written as:

$$\begin{aligned} F^{\mathrm{LSS}}_{\alpha\beta} &= \int_{\vec{k}_{\mathrm{min}}}^{\vec{k}_{\mathrm{max}}} \frac{\partial \ln P_{\mathrm{gg}}(\vec{k})}{\partial\vartheta_\alpha}\frac{\partial \ln P_{\mathrm{gg}}(\vec{k})}{\partial\vartheta_\beta}V_{\mathrm{eff}}(\vec{k})\frac{d\vec{k}}{2(2\pi)^3} \\ &= \int_{-1}^{1}\int_{k_{\mathrm{min}}}^{k_{\mathrm{max}}} \frac{\partial \ln P_{\mathrm{gg}}(k,\mu)}{\partial\vartheta_\alpha}\frac{\partial \ln P_{\mathrm{gg}}(k,\mu)}{\partial\vartheta_\beta}V_{\mathrm{eff}}(k,\mu) \\ &\quad \frac{2\pi k^2 dk d\mu}{2(2\pi)^3}, \end{aligned} \tag{4.6}$$

where V_{eff} is the effective volume of the survey and given by

$$V_{\mathrm{eff}}(k,\mu) = \left[\frac{nP(k,\mu)}{nP(k,\mu)+1}\right]^2 V_{\mathrm{survey}}, \tag{4.7}$$

where μ is the cosine of the angle between the vector mode ($\vec{k}$) and the vector along the line of sight, and n is the galaxy number density (which is assumed to be constant throughout each of the redshift bins).

To perform the analysis, we divide the data in redshift bins of width $\Delta z = 0.1$ and cut the small-scale data at $k = 0.25\ h\ \mathrm{Mpc}^{-1}$ to avoid the highly non-linear regime. The lowest wavenumber (i.e. the largest scale), k_{min}, is chosen to be greater than $2\pi/\Delta V^{1/3}$, where ΔV represents the volume of the redshift shell. We note that using data in the non-linear regime would require numerical simulations of this model. This has been performed for specific cases in refs. [14, 17]. As we will discuss later, constraints using this method are competitive with our DESI forecast.

The real-space linear DM power spectrum, P_{DM}, is related to the linear redshift-space galaxy power spectrum, P_{gg}, by

$$P_{\mathrm{gg}}(k) = P_{\mathrm{DM}}(k)\ (b\ +\ \beta\ \mu^2)^2, \tag{4.8}$$

where b is the bias relating galaxy to DM overdensities in real space (as in eq. (3.8)) and β is the linear growth factor.

DESI is expected to cover 14,000 deg^2 of the sky in the redshift range $0.15 < z < 1.85$. We use the values of the bias given in ref. [63] for the three types of DESI tracers, namely $b_{\mathrm{ELG}}(z)D(z) = 0.84$ for the Emission Line Galaxies (ELGs), $b_{\mathrm{LRG}}(z)D(z) = 1.7$ for the Luminous Red Galaxies (LRGs) and $b_{\mathrm{QSO}}(z)D(z) = 1.2$ for the high redshift quasars (QSOs). Here, $D(z)$ is the normalised growth factor and both the bias and the growth factor are assumed to vary in each redshift bin accordingly to these expressions. To combine the Fisher matrices from the three DESI tracers, we use the multi-tracer technique of ref. [64].

[6] See ref. [62] for more details on the Fisher matrix formalism for galaxy redshift surveys such as DESI.

JCAP09(2015)034

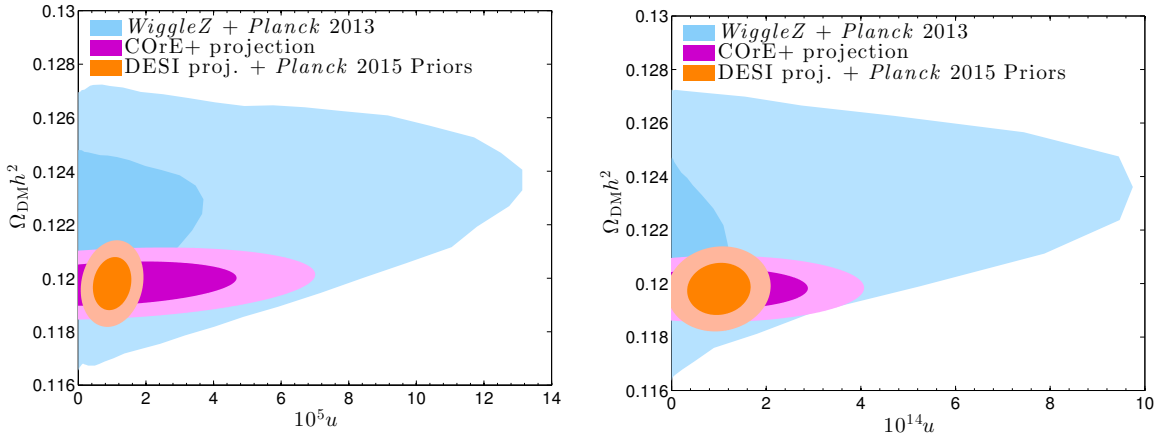

Figure 2. The 68% and 95% CL allowed regions in the ($\Omega_{\rm DM}h^2$,u) plane for the s-wave (left) and p-wave (right) scenarios. Blue: current constraints from the combination of *WiggleZ* and *Planck* 2013 data, with $k_{\rm max} = 0.12\ h\ {\rm Mpc}^{-1}$; magenta: projected sensitivity of the upcoming COrE+ CMB experiment, assuming $u = 10^{-5}$ (or $u = 10^{-14}$ if p-wave); orange: projected sensitivity of the DESI galaxy survey, again assuming $u = 10^{-5}$ (or $u = 10^{-14}$ if p-wave), with $k_{\rm max} = 0.25\ h\ {\rm Mpc}^{-1}$.

For the s-wave scenario, we obtain a 1σ error on the u parameter of

$$\delta u^{\rm (DESI)} \simeq 3.7 \times 10^{-6}\,, \tag{4.9}$$

for the fiducial value of $u = 10^{-5}$. For p-wave, we obtain:

$$\delta u^{\rm (DESI)} \simeq 4.4 \times 10^{-15}\,, \tag{4.10}$$

for the fiducial value of $u = 10^{-14}$. Crucially, DESI will ensure a $\sim 2.5\sigma$ detection of DM-neutrino interactions if the strength of such a coupling is $u \simeq 10^{-5}$ (or a $\sim 2\sigma$ detection for $u \simeq 10^{-14}$ if p-wave).

Our results are summarised in figure 2, where the DESI 68% and 95% CL allowed regions in the ($\Omega_{\rm DM}h^2$,u) plane are shown (assuming the *Planck* 2015 fiducial cosmology plus an interaction strength of $u = 10^{-5}$ if s-wave and $u = 10^{-14}$ if p-wave), along with the current constraints and the COrE+ reconstruction. One can clearly see the improvement in the extraction of a DM-neutrino coupling that will be provided by the next-generation LSS surveys. This analysis indicates that planned galaxy clustering surveys will provide an extremely powerful tool (competitive or even better than future CMB experiments) to test the fundamental properties of DM.

Since the main impact of νCDM is the damping of structure on small scales, one of the largest effects will be a reduction in the number of satellites around galaxies such as the Milky Way. Until now, the only way to study interactions at these scales has been via N-body simulations, which show that for DM-radiation couplings greater than $u \simeq 10^{-5}$, the number of satellites in the Milky Way would be much smaller than observed [14, 17]. Therefore, with the sensitivity of $u \simeq 3.7 \times 10^{-6}$ expected from DESI, we would have a handle on alternative scenarios to ΛCDM that modify our cosmic neighbourhood, independently of the assumptions that go into N-body simulations.[7]

[7]With improvements in numerical algorithms and computing power, N-body simulations are becoming increasingly more affordable and will continue to provide a complementary method to test structure formation in models beyond ΛCDM. However, they will remain computationally expensive, especially if one wishes to simulate structures on both large and small scales or test a wide range of modifications to the P(k).

JCAP09(2015)034

5 Conclusion

Cosmology provides a promising tool to measure the particle properties of dark matter (DM). A DM coupling to visible or dark radiation (including neutrinos, axions, dark photons or any other light uncharged particle) can lead to strong departures from the standard ΛCDM cosmology and produce visible signatures for CMB experiments and LSS surveys. In the specific case of DM-neutrino scattering, one expects an enhancement of the CMB acoustic peaks due to the fact that DM is strongly coupled to neutrinos and vice versa, which delays the neutrino free-streaming epoch and alters DM clustering with respect to the standard ΛCDM picture. However, the largest impact is imprinted as a damping in the matter power spectrum, surveyed by large-scale structure (LSS) galaxy surveys.

In this study, we have looked for the optimal method to measure such small departures from the ΛCDM scenario. As cosmological measurements may constitute the only tool available to detect such effects, it is crucial to study the potential sensitivity of future experiments. We have shown that i) with current CMB measurements, one can probe s-wave and p-wave DM-neutrino cross sections of $\sigma_{\mathrm{DM}-\nu,0} \lesssim 6 \times 10^{-31}\,(m_{\mathrm{DM}}/\mathrm{GeV})\ \mathrm{cm}^2$ and $\sigma_{\mathrm{DM}-\nu,2} \lesssim 2 \times 10^{-40}\,(m_{\mathrm{DM}}/\mathrm{GeV})\ \mathrm{cm}^2$, respectively (at 95% CL) and ii) by simulating a next-generation CMB experiment (i.e. a COrE+-like mission) by means of a Markov Chain Monte Carlo analysis, one can only weakly improve on the current sensitivity.

The prospects for both constraints and detection are far better for future galaxy surveys, such as the DESI or Euclid experiments. Already, current LSS data, combined with *Planck* CMB measurements, provide competitive constraints to those forecasted for a future CMB experiment such as COrE+. Future data from the DESI experiment alone could improve the current sensitivity limit by an order of magnitude, and provide an accurate (percent-level) measurement of the scattering cross section for values above that limit. Therefore, we have shown that galaxy clustering surveys are an excellent probe to detect new physics beyond ΛCDM. Remarkably, future LSS experiments will be sensitive to effects that until now have only been accessible via N-body simulations.

Acknowledgments

The authors would like to thank Andreu Ariño for useful discussions and Will Percival for precious BOSS DR11 measurements. The authors acknowledge the use of the publicly available numerical codes CLASS and MONTE PYTHON, and the data from the *Planck* Legacy Archive and *WiggleZ* survey. ME is supported by Spanish grant FPU13/03111 of the MECD. RJW is supported by the STFC grant ST/K501979/1. This work was supported by the European Union FP7 ITN INVISIBLES (Marie Curie Actions, PITN-GA-2011-289442). We would like to thank the Universitad Autónoma de Madrid and IFT for hospitality while this work was completed.

References

[1] PLANCK collaboration, P.A.R. Ade et al., *Planck 2013 results. XVI. Cosmological parameters*, *Astron. Astrophys.* **571** (2014) A16 [arXiv:1303.5076] [INSPIRE].

[2] PLANCK collaboration, R. Adam et al., *Planck 2015 results. I. Overview of products and scientific results*, arXiv:1502.01582 [INSPIRE].

[3] S. Dodelson and L.M. Widrow, *Sterile-neutrinos as dark matter*, *Phys. Rev. Lett.* **72** (1994) 17 [hep-ph/9303287] [INSPIRE].

JCAP09(2015)034

[4] J. Lesgourgues and S. Pastor, *Massive neutrinos and cosmology*, *Phys. Rept.* **429** (2006) 307 [astro-ph/0603494] [INSPIRE].

[5] C. Boehm, P. Fayet and R. Schaeffer, *Constraining dark matter candidates from structure formation*, *Phys. Lett.* **B 518** (2001) 8 [astro-ph/0012504] [INSPIRE].

[6] C. Boehm, A. Riazuelo, S.H. Hansen and R. Schaeffer, *Interacting dark matter disguised as warm dark matter*, *Phys. Rev.* **D 66** (2002) 083505 [astro-ph/0112522] [INSPIRE].

[7] C. Boehm and R. Schaeffer, *Constraints on dark matter interactions from structure formation: Damping lengths*, *Astron. Astrophys.* **438** (2005) 419 [astro-ph/0410591] [INSPIRE].

[8] E. Bertschinger, *The Effects of Cold Dark Matter Decoupling and Pair Annihilation on Cosmological Perturbations*, *Phys. Rev.* **D 74** (2006) 063509 [astro-ph/0607319] [INSPIRE].

[9] G. Mangano, A. Melchiorri, P. Serra, A. Cooray and M. Kamionkowski, *Cosmological bounds on dark matter-neutrino interactions*, *Phys. Rev.* **D 74** (2006) 043517 [astro-ph/0606190] [INSPIRE].

[10] P. Serra, F. Zalamea, A. Cooray, G. Mangano and A. Melchiorri, *Constraints on neutrino-dark matter interactions from cosmic microwave background and large scale structure data*, *Phys. Rev.* **D 81** (2010) 043507 [arXiv:0911.4411] [INSPIRE].

[11] R.J. Wilkinson, C. Boehm and J. Lesgourgues, *Constraining Dark Matter-Neutrino Interactions using the CMB and Large-Scale Structure*, *JCAP* **05** (2014) 011 [arXiv:1401.7597] [INSPIRE].

[12] L.G. van den Aarssen, T. Bringmann and C. Pfrommer, *Is dark matter with long-range interactions a solution to all small-scale problems of ΛCDM cosmology?*, *Phys. Rev. Lett.* **109** (2012) 231301 [arXiv:1205.5809] [INSPIRE].

[13] Y. Farzan and S. Palomares-Ruiz, *Dips in the Diffuse Supernova Neutrino Background*, *JCAP* **06** (2014) 014 [arXiv:1401.7019] [INSPIRE].

[14] C. Boehm, J.A. Schewtschenko, R.J. Wilkinson, C.M. Baugh and S. Pascoli, *Using the Milky Way satellites to study interactions between cold dark matter and radiation*, *Mon. Not. Roy. Astron. Soc.* **445** (2014) L31 [arXiv:1404.7012] [INSPIRE].

[15] J.F. Cherry, A. Friedland and I.M. Shoemaker, *Neutrino Portal Dark Matter: From Dwarf Galaxies to IceCube*, arXiv:1411.1071 [INSPIRE].

[16] B. Bertoni, S. Ipek, D. McKeen and A.E. Nelson, *Constraints and consequences of reducing small scale structure via large dark matter-neutrino interactions*, *JHEP* **04** (2015) 170 [arXiv:1412.3113] [INSPIRE].

[17] J.A. Schewtschenko, R.J. Wilkinson, C.M. Baugh, C. Bœhm and S. Pascoli, *Dark matter-radiation interactions: the impact on dark matter haloes*, *Mon. Not. Roy. Astron. Soc.* **449** (2015) 3587 [arXiv:1412.4905] [INSPIRE].

[18] J.H. Davis and J. Silk, *Spectral and Spatial Distortions of PeV Neutrinos from Scattering with Dark Matter*, arXiv:1505.01843 [INSPIRE].

[19] K. Sigurdson, M. Doran, A. Kurylov, R.R. Caldwell and M. Kamionkowski, *Dark-matter electric and magnetic dipole moments*, *Phys. Rev.* **D 70** (2004) 083501 [*Erratum ibid.* **D 73** (2006) 089903] [astro-ph/0406355] [INSPIRE].

[20] R.J. Wilkinson, J. Lesgourgues and C. Boehm, *Using the CMB angular power spectrum to study Dark Matter-photon interactions*, *JCAP* **04** (2014) 026 [arXiv:1309.7588] [INSPIRE].

[21] A.D. Dolgov, S.L. Dubovsky, G.I. Rubtsov and I.I. Tkachev, *Constraints on millicharged particles from Planck data*, *Phys. Rev.* **D 88** (2013) 117701 [arXiv:1310.2376] [INSPIRE].

[22] X.-l. Chen, S. Hannestad and R.J. Scherrer, *Cosmic microwave background and large scale structure limits on the interaction between dark matter and baryons*, *Phys. Rev.* **D 65** (2002) 123515 [astro-ph/0202496] [INSPIRE].

JCAP09(2015)034

[23] C. Dvorkin, K. Blum and M. Kamionkowski, *Constraining Dark Matter-Baryon Scattering with Linear Cosmology*, *Phys. Rev.* **D 89** (2014) 023519 [arXiv:1311.2937] [INSPIRE].

[24] C.-G. Park, J.-c. Hwang and H. Noh, *Axion as a cold dark matter candidate: low-mass case*, *Phys. Rev.* **D 86** (2012) 083535 [arXiv:1207.3124] [INSPIRE].

[25] R. Diamanti, E. Giusarma, O. Mena, M. Archidiacono and A. Melchiorri, *Dark Radiation and interacting scenarios*, *Phys. Rev.* **D 87** (2013) 063509 [arXiv:1212.6007] [INSPIRE].

[26] M. Blennow, E. Fernandez-Martinez, O. Mena, J. Redondo and P. Serra, *Asymmetric Dark Matter and Dark Radiation*, *JCAP* **07** (2012) 022 [arXiv:1203.5803] [INSPIRE].

[27] F.-Y. Cyr-Racine, R. de Putter, A. Raccanelli and K. Sigurdson, *Constraints on Large-Scale Dark Acoustic Oscillations from Cosmology*, *Phys. Rev.* **D 89** (2014) 063517 [arXiv:1310.3278] [INSPIRE].

[28] COrE collaboration, F.R. Bouchet et al., *COrE (Cosmic Origins Explorer) A White Paper*, arXiv:1102.2181 [INSPIRE].

[29] A. Kogut et al., *The Primordial Inflation Explorer (PIXIE): A Nulling Polarimeter for Cosmic Microwave Background Observations*, *JCAP* **07** (2011) 025 [arXiv:1105.2044] [INSPIRE].

[30] BOSS collaboration, L. Anderson et al., *The clustering of galaxies in the SDSS-III Baryon Oscillation Spectroscopic Survey: baryon acoustic oscillations in the Data Releases 10 and 11 Galaxy samples*, *Mon. Not. Roy. Astron. Soc.* **441** (2014) 24 [arXiv:1312.4877] [INSPIRE].

[31] L. Anderson et al., *The clustering of galaxies in the SDSS-III Baryon Oscillation Spectroscopic Survey: measuring D_A and H at $z = 0.57$ from the baryon acoustic peak in the Data Release 9 spectroscopic Galaxy sample*, *Mon. Not. Roy. Astron. Soc.* **439** (2014) 83 [arXiv:1303.4666] [INSPIRE].

[32] F. Beutler et al., *The 6dF Galaxy Survey: Baryon Acoustic Oscillations and the Local Hubble Constant*, *Mon. Not. Roy. Astron. Soc.* **416** (2011) 3017 [arXiv:1106.3366] [INSPIRE].

[33] C. Blake et al., *The WiggleZ Dark Energy Survey: mapping the distance-redshift relation with baryon acoustic oscillations*, *Mon. Not. Roy. Astron. Soc.* **418** (2011) 1707 [arXiv:1108.2635] [INSPIRE].

[34] N. Padmanabhan et al., *A 2 per cent distance to $z = 0.35$ by reconstructing baryon acoustic oscillations — I. Methods and application to the Sloan Digital Sky Survey*, *Mon. Not. Roy. Astron. Soc.* **427** (2012) 2132 [arXiv:1202.0090] [INSPIRE].

[35] SDSS collaboration, W.J. Percival et al., *Baryon Acoustic Oscillations in the Sloan Digital Sky Survey Data Release 7 Galaxy Sample*, *Mon. Not. Roy. Astron. Soc.* **401** (2010) 2148 [arXiv:0907.1660] [INSPIRE].

[36] D. Parkinson et al., *The WiggleZ Dark Energy Survey: Final data release and cosmological results*, *Phys. Rev.* **D 86** (2012) 103518 [arXiv:1210.2130] [INSPIRE].

[37] BOSS collaboration, K.S. Dawson et al., *The Baryon Oscillation Spectroscopic Survey of SDSS-III*, *Astron. J.* **145** (2013) 10 [arXiv:1208.0022] [INSPIRE].

[38] J. Hamann, S. Hannestad, J. Lesgourgues, C. Rampf and Y.Y.Y. Wong, *Cosmological parameters from large scale structure — geometric versus shape information*, *JCAP* **07** (2010) 022 [arXiv:1003.3999] [INSPIRE].

[39] E. Giusarma, R. De Putter and O. Mena, *Testing standard and nonstandard neutrino physics with cosmological data*, *Phys. Rev.* **D 87** (2013) 043515 [arXiv:1211.2154] [INSPIRE].

[40] E. Giusarma, R. de Putter, S. Ho and O. Mena, *Constraints on neutrino masses from Planck and Galaxy Clustering data*, *Phys. Rev.* **D 88** (2013) 063515 [arXiv:1306.5544] [INSPIRE].

[41] DESI collaboration, M. Levi et al., *The DESI Experiment, a whitepaper for Snowmass 2013*, arXiv:1308.0847 [INSPIRE].

JCAP09(2015)034

[42] C.-P. Ma and E. Bertschinger, *Cosmological perturbation theory in the synchronous and conformal Newtonian gauges*, *Astrophys. J.* **455** (1995) 7 [astro-ph/9506072] [INSPIRE].

[43] F. Atrio-Barandela and S. Davidson, *Interacting hot dark matter*, *Phys. Rev.* **D 55** (1997) 5886 [astro-ph/9702236] [INSPIRE].

[44] S. Das and N. Weiner, *Late Forming Dark Matter in Theories of Neutrino Dark Energy*, *Phys. Rev.* **D 84** (2011) 123511 [astro-ph/0611353] [INSPIRE].

[45] F.-Y. Cyr-Racine and K. Sigurdson, *Cosmology of atomic dark matter*, *Phys. Rev.* **D 87** (2013) 103515 [arXiv:1209.5752] [INSPIRE].

[46] M.R. Buckley, J. Zavala, F.-Y. Cyr-Racine, K. Sigurdson and M. Vogelsberger, *Scattering, Damping and Acoustic Oscillations: Simulating the Structure of Dark Matter Halos with Relativistic Force Carriers*, *Phys. Rev.* **D 90** (2014) 043524 [arXiv:1405.2075] [INSPIRE].

[47] M. Viel, J. Lesgourgues, M.G. Haehnelt, S. Matarrese and A. Riotto, *Constraining warm dark matter candidates including sterile neutrinos and light gravitinos with WMAP and the Lyman-alpha forest*, *Phys. Rev.* **D 71** (2005) 063534 [astro-ph/0501562] [INSPIRE].

[48] R. Hlozek, D. Grin, D.J. Marsh and P.G. Ferreira, *A search for ultralight axions using precision cosmological data*, *Phys. Rev.* **D 91** (2015) 103512 [arXiv:1410.2896] [INSPIRE].

[49] J. Lesgourgues, *The Cosmic Linear Anisotropy Solving System (CLASS) I: Overview*, arXiv:1104.2932 [INSPIRE].

[50] B. Audren, J. Lesgourgues, K. Benabed and S. Prunet, *Conservative Constraints on Early Cosmology: an illustration of the Monte Python cosmological parameter inference code*, *JCAP* **02** (2013) 001 [arXiv:1210.7183] [INSPIRE].

[51] G. Mangano, G. Miele, S. Pastor, T. Pinto, O. Pisanti and P.D. Serpico, *Relic neutrino decoupling including flavor oscillations*, *Nucl. Phys.* **B 729** (2005) 221 [hep-ph/0506164] [INSPIRE].

[52] B.A. Reid et al., *Cosmological Constraints from the Clustering of the Sloan Digital Sky Survey DR7 Luminous Red Galaxies*, *Mon. Not. Roy. Astron. Soc.* **404** (2010) 60 [arXiv:0907.1659] [INSPIRE].

[53] S. Riemer-Sorensen et al., *The WiggleZ Dark Energy Survey: Cosmological neutrino mass constraint from blue high-redshift galaxies*, *Phys. Rev.* **D 85** (2012) 081101 [arXiv:1112.4940] [INSPIRE].

[54] SDSS collaboration, M. Tegmark et al., *Cosmological Constraints from the SDSS Luminous Red Galaxies*, *Phys. Rev.* **D 74** (2006) 123507 [astro-ph/0608632] [INSPIRE].

[55] A. Lewis and S. Bridle, *Cosmological parameters from CMB and other data: A Monte Carlo approach*, *Phys. Rev.* **D 66** (2002) 103511 [astro-ph/0205436] [INSPIRE].

[56] L. Perotto, J. Lesgourgues, S. Hannestad, H. Tu and Y.Y.Y. Wong, *Probing cosmological parameters with the CMB: Forecasts from full Monte Carlo simulations*, *JCAP* **10** (2006) 013 [astro-ph/0606227] [INSPIRE].

[57] PLANCK collaboration, P.A.R. Ade et al., *Planck 2015 results. XX. Constraints on inflation*, arXiv:1502.02114 [INSPIRE].

[58] M. Tegmark, A. Taylor and A. Heavens, *Karhunen-Loeve eigenvalue problems in cosmology: How should we tackle large data sets?*, *Astrophys. J.* **480** (1997) 22 [astro-ph/9603021] [INSPIRE].

[59] G. Jungman, M. Kamionkowski, A. Kosowsky and D.N. Spergel, *Cosmological parameter determination with microwave background maps*, *Phys. Rev.* **D 54** (1996) 1332 [astro-ph/9512139] [INSPIRE].

[60] R.A. Fisher, *The Logic of Inductive Inference*, *J. Roy. Stat. Soc.* **98** (1935) 39.

JCAP09(2015)034

[61] Planck collaboration, P.A.R. Ade et al., *Planck 2015 results. XIII. Cosmological parameters*, arXiv:1502.01589 [INSPIRE].

[62] H.-J. Seo and D.J. Eisenstein, *Probing dark energy with baryonic acoustic oscillations from future large galaxy redshift surveys*, *Astrophys. J.* **598** (2003) 720 [astro-ph/0307460] [INSPIRE].

[63] A. Font-Ribera, P. McDonald, N. Mostek, B.A. Reid, H.-J. Seo and A. Slosar, *DESI and other dark energy experiments in the era of neutrino mass measurements*, *JCAP* **05** (2014) 023 [arXiv:1308.4164] [INSPIRE].

[64] L.R. Abramo and K.E. Leonard, *Why multi-tracer surveys beat cosmic variance*, *Mon. Not. Roy. Astron. Soc.* **432** (2013) 318 [arXiv:1302.5444] [INSPIRE].

JCAP09(2015)034

PHYSICAL REVIEW D **96,** 043501 (2017)

Cosmological searches for a noncold dark matter component

Stefano Gariazzo,[1] Miguel Escudero,[1] Roberta Diamanti,[2] and Olga Mena[1]
[1]*Instituto de Física Corpuscular (IFIC), CSIC-Universitat de Valencia, Apartado de Correos 22085, E-46071, Spain*
[2]*GRAPPA Institute of Physics, University of Amsterdam, Science Park 904, 1098 GL Amsterdam, Netherlands*
(Received 21 April 2017; published 4 August 2017)

We explore an extended cosmological scenario where the dark matter is an admixture of cold and additional noncold species. The mass and temperature of the noncold dark matter particles are extracted from a number of cosmological measurements. Among others, we consider tomographic weak lensing data and Milky Way dwarf satellite galaxy counts. We also study the potential of these scenarios in alleviating the existing tensions between local measurements and cosmic microwave background (CMB) estimates of the S_8 parameter, with $S_8 = \sigma_8\sqrt{\Omega_m}$, and of the Hubble constant H_0. In principle, a subdominant, noncold dark matter particle with a mass $m_X \sim$ keV, could achieve the goals above. However, the preferred ranges for its temperature and its mass are different when extracted from weak lensing observations and from Milky Way dwarf satellite galaxy counts, since these two measurements require suppressions of the matter power spectrum at different scales. Therefore, solving simultaneously the CMB-weak lensing tensions and the small scale crisis in the standard cold dark matter picture via only one noncold dark matter component seems to be challenging.

DOI: 10.1103/PhysRevD.96.043501

I. INTRODUCTION

Within the current canonical cosmological model, dubbed the ΛCDM model, the dark matter is assumed to be made of a totally cold gas of weakly interacting particles, accounting for ∼26% of the current Universe mass-energy density. This standard picture has been extremely successful in explaining both the large scale structure observations of our Universe and the pattern of the temperature and polarization fluctuations in the cosmic microwave background (CMB) [1]. Nevertheless, the mechanism explaining the origin and the physics of this cold dark matter component remains obscure [2–4], with possible candidates ranging from the GeV–TeV energy scale to very light (μeV) dark matter axions. Together with this hitherto theoretically unknown cold dark matter nature, there are a number of observations which further motivate the searches for other possible dark matter candidates.

On the one hand, there is the *small scale crisis* of the ΛCDM model. This problem is closely related to several galactic and subgalactic phenomena, as the *Milky Way satellites problem* [5,6] and the so-called *too big to fail problem* [7], which refer to the fact that the predictions from the ΛCDM picture fail in reproducing the number of low-mass subhalos expected within a Milky Way-sized halo and the measured kinematics of the Milky Way satellites, respectively. A large effort in the literature has been devoted to alleviate these problems [8–19].

On the other hand, recent measurements of tomographic weak gravitational lensing, as those from the Kilo Degree-450 deg^2 Survey (KiDS-450) [20,21], show substantial discordances with CMB measurements from Planck [1,22] in the matter perturbations at small scales. These discordances are quantified in terms of the extracted values of the amplitude of the small-scale density fluctuations, quantified by the parameter σ_8, at a given matter density, Ω_m. In particular, the quantity $S_8 = \sigma_8\sqrt{\Omega_m}$ as measured by KiDS is in tension with the Planck estimate at the level of 2.3σ [20]. Similar results had already appeared in the past from the analyses of CFHTLenS data [23,24]. A number of recent dedicated studies in the literature have shown that the CFHTLenS and the KiDS discrepancies are independent of the small-angle approximations commonly exploited in weak lensing data analyses [25–27].

Here, instead of refining cosmic shear analyses, we follow a different avenue to ameliorate these problems. In the spirit of Ref. [21], we consider a modified version of the most economical pure cold dark matter model, allowing for a mixed dark matter cosmology with an additional, nontotally cold, dark matter relic. These models with an admixture of cold and noncold dark matter particles have been dubbed mixed dark matter (MDM) models; see e.g. Refs. [28–33]. The motivation to consider these models is twofold: in addition to their potential in alleviating the tension between cosmic-shear and CMB measurements, they could also provide a solution to the aforementioned ΛCDM small-scale crisis, while leaving unchanged the predictions from the ΛCDM model at large scales. The reason is simple: the particle associated to the second, nontotally cold dark matter component will have a significant free-streaming length, that affects the matter power spectrum on the smallest scales, therefore improving the compatibility with the observations of the local Universe [34] through a reduction of the S_8 quantity.

In this study we scrutinize these mixed dark matter scenarios, using the most recent tomographic weak lensing measurements from the KiDS-450 survey, in combination with Planck CMB data. By means of these data sets we shall derive constraints on the current temperature and mass-energy density of the noncold dark matter component, searching for the most favored cosmological dark matter scenario. Furthermore, we also consider current estimates from the observed number of Milky Way satellite galaxies, comparing these results to those preferred by weak lensing data.

The structure of the paper is as follows. In Sec. II we present the methodology followed here, describing the mixed dark matter model, the included data sets and the technical details of our numerical analyses. Our results are shown in Sec. III. We draw our main conclusions in Sec. IV.

II. METHODOLOGY

A. Mixed dark matter modeling

In this paper we explore a scenario where the dark matter fluid is made of two components: one which corresponds to the standard cold dark matter (CDM) plus a second one with a nonzero temperature T_X, which is a warm dark matter (WDM) component.[1] In the following we shall refer to this model as the mixed dark matter (MDM) model. While the CDM component is simply parametrized via its energy density $\omega_c \equiv \Omega_c h^2$, the second dark matter component is parametrized through its temperature T_X and its energy density fraction f_X relative to the total dark matter component $\omega_{DM} = \omega_X + \omega_c$, defined as

$$f_X = \frac{\omega_X}{\omega_{DM}}, \tag{1}$$

where $\omega_i \equiv \Omega_i h^2$ refers to the present mass-energy density. Notice that the mass of the second, noncold dark matter particle can be computed from its energy density and its temperature using the relation

$$\omega_X = \left(\frac{T_X}{T_\nu}\right)^3 \left(\frac{m_X}{94\ \text{eV}}\right). \tag{2}$$

In our analyses we shall consider $0 \leq f_X \leq 1$ for the WDM energy density and $-1.5 \leq \log_{10}(T_X/T_\nu) \leq 0$ for its temperature. The upper temperature prior, $T_X = T_\nu$, is fixed to be the one corresponding to the pure *hot* dark matter regime, i.e. to the standard neutrino temperature, while the lower prior is chosen in order to preserve the validity of the numerical calculations for the MDM model used here, as we explain in what follows.

A crucial point when dealing with the MDM modeling is related to the power spectrum of the density perturbations, which is modified when a second nontotally cold dark matter component is also considered in the cosmological evolution. The deviations of the matter power spectrum in the MDM model from its standard shape within the CDM model may be highly nontrivial and must be treated cautiously, since we are dealing with weak lensing probes, which require a good knowledge of the perturbation behavior in the nonlinear regime.[2] We recall that the nonlinear approximations that are commonly used for the numerical computations are calibrated on N-body simulations. These calibrations, however, must be considered carefully, since the extrapolation for unusual models may spoil the correctness of the adopted formulas.

In this regard, we show in Fig. 1 the relative difference between the nonlinear matter power spectrum of some of the MDM models explored here with respect to the corresponding CDM only case. We use $\omega_{DM} = 0.12$ for all the plots, with $f_X = 0$ for the CDM-only model and $f_X = 0.5$ for the other cases, and we vary the noncold dark matter particle temperature. The panels refer to four possible nonlinear prescriptions: the standard [36–39] (upper left panel) and the accurate [40] (upper right panel) versions of the halo model, the standard `halofit` code [41] (lower left panel) and the fitting formula presented in Ref. [42] (lower right panel), that we shall adopt here (see below). Notice that the `halofit` prescription badly fails in reproducing the expected behavior of the nonlinear power spectrum when the temperature T_X of the nontotally cold dark matter particle deviates significantly from the neutrino temperature, T_ν. In the limit $T_X \to 0$, the MDM case should approach the CDM one, eventually overlapping with it, and this behavior is clearly not reproduced. The accurate halo model[3] also presents some problems at the smallest scales. Following these results, the best model to describe the nonlinear perturbation growth in the MDM case seems to be the standard halo model. However, even in this case there exists an unphysical bump at scales $k \sim 1\ h/\text{Mpc}$ which makes its predictions unreliable.

The clear failure of these three widely used nonlinear models for a significant range of temperatures T_X has motivated us to search for an alternative description of the nonlinearities in the power spectrum in the presence of an additional noncold dark matter component. We have therefore adopted the prescriptions presented in Ref. [42], that we briefly summarize here.

Starting from the standard nonlinear matter power spectrum for a CDM universe $P_{\rm CDM}$ computed with {[41,43], the

[1] We consider relics with a Fermi-Dirac distribution. A change in the distribution will not change dramatically the results, see e.g. [33].

[2] This is a delicate issue, as we are dealing with a second dark matter component different from the standard three neutrino active contribution. For the implementation of massive neutrinos in nonlinear matter power spectrum simulations, see Ref. [35].

[3] The term "accurate" is related to the fact that this improved version of the original halo model [36–39] takes into account several corrections (that include, among others, the baryonic feedback), i.e. factors that are not included in the standard halo model, see Ref. [40] for details.

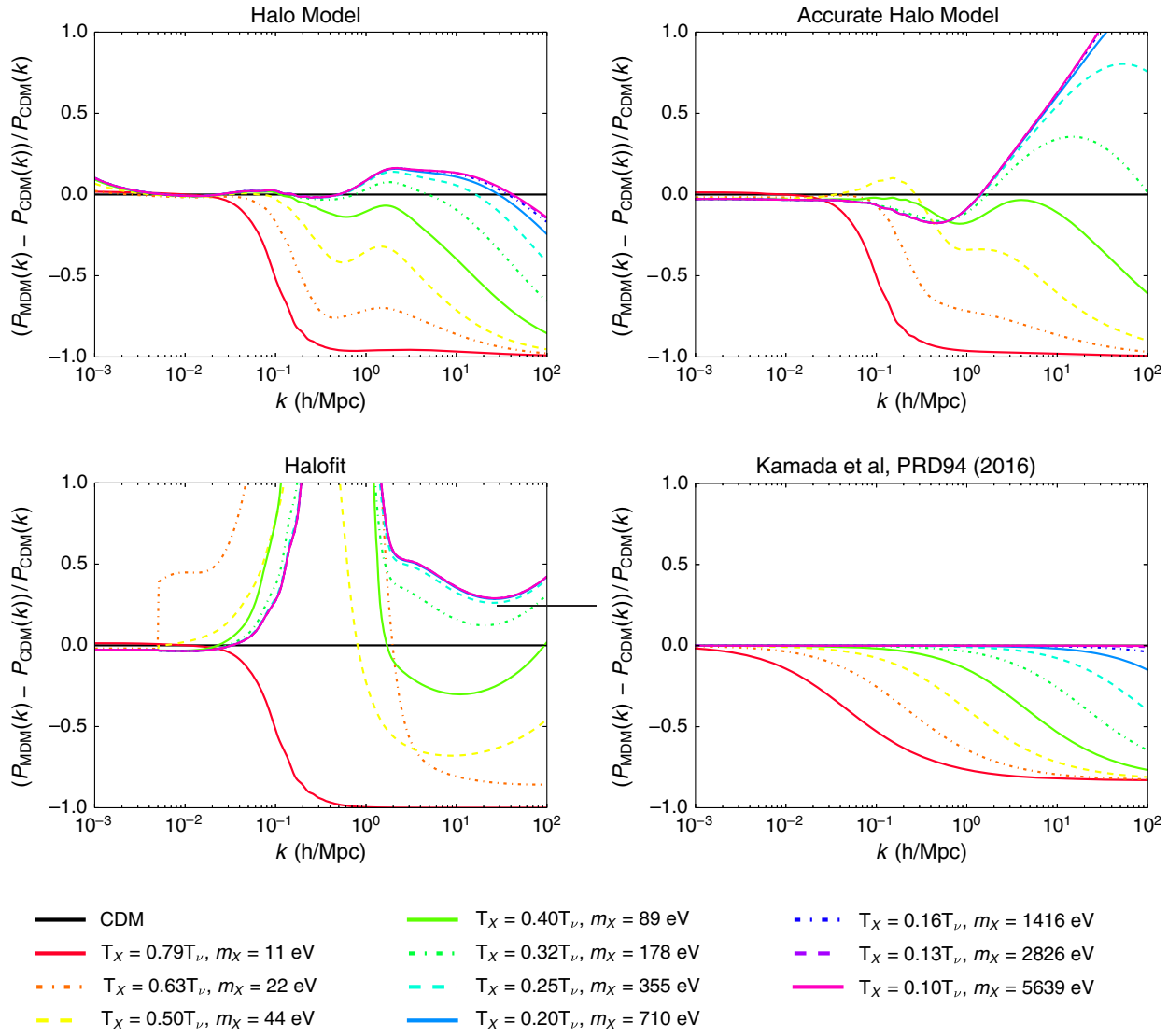

FIG. 1. Relative difference of the MDM nonlinear matter power spectrum at $z = 0$ (for $f_X = 0.5$) with different temperatures T_X, with respect to the pure CDM case (for which $f_X = 0$), for four different nonlinear approaches, as described in the text. For all of them we fix $\omega_{DM} = 0.12$. The nonlinear prescription adopted in this work, given by Ref. [42], is the one corresponding to the *lower right* panel.

authors of Ref. [42] find that the fitting function that best matches the results of N-body simulations in the presence of a noncold dark matter component is given by

$$\frac{P_{\rm MDM}(k)}{P_{\rm CDM}(k)} = T^2(k; r_X, k'_d) = (1 - r_X) + \frac{r_X}{(1 + k/k'_d)^{0.7441}}, \quad (3)$$

where the two quantities that appear in the right-hand side read as

$$r_X(f_X) = 1 - \exp\left(-a\frac{f_X^b}{1 - f_X^c}\right), \quad (4)$$

$$k'_d(k_d, f_X) = k_d \cdot f_X^{-5/6}. \quad (5)$$

In the latter equation, k_d is the damping scale given in Ref. [44] as a function of the linear growth rate $D(z)$,

$$k_d(m_X, z) = \left(\frac{m_X}{\rm keV}\right)^{2.207} D(z)^{1.583} 388.8\, h\,{\rm Mpc}^{-1}. \quad (6)$$

Finally, parameters a, b, c in Eq. (4) are obtained by fitting the parametrization above to the N-body simulation results [42],

$$a = 1.551, \qquad b = 0.5761, \qquad c = 1.263. \quad (7)$$

In all the relevant parts of our computation, therefore, we substituted the nonlinear matter power spectrum with the one given by Eq. (3). This means that we need

to compute the nonlinear matter power spectrum $P_{\rm CDM}$ in the CDM-only model using the standard HALOFIT prescription.

B. Data sets

1. Cosmic microwave background (CMB)

We consider the CMB measurements of the most recent Planck data release [1,22], using the full temperature power spectrum at all multipoles ($2 \leq \ell \leq 2500$, `Planck TT`), the polarization power spectra only in the low multipoles range ($2 \leq \ell \leq 29$, `lowP`) and the `lensing` likelihood computed from the 4-point correlation function. Since there could be still some level of residual systematics contamination [1], we neglect the polarization measurements at high multipoles (`highP`), following therefore a very conservative approach which will ensure very robust limits. We refer to the `Planck TT + lowP + lensing` combination of data as the "CMB" data set.

2. KiDS data

An essential point of this study is the addition of the measurements of the Kilo Degree Survey (KiDS) [20,21] using the methodology explained in [20].

The KiDS data can be used to reconstruct the 2-point shear correlation functions $\xi_{\pm}^{ij}(\theta)$ for the i, j tomographic bin combination at the angle θ. The data set that we use here is from KiDS-450 [20,45,46] and covers an effective area of 360 deg^2. The median redshift is $z_m = 0.53$, while the effective number density is $n_{\rm eff} = 8.5$ galaxies arcmin^{-2}. The experiment covers 7 angular bins in the range 0.5 to 72 arcmins for $\xi_{+}^{ij}(\theta)$ and 6 angular bins between 4.2 and 300 arcmins for $\xi_{-}^{ij}(\theta)$.

The calibration of the photometric redshift distributions is made through the "weighted direct calibration" (DIR) method presented in Ref. [20]. This uses the data of external, overlapping spectroscopic surveys and creates series of 1000 bootstrap realizations to obtain the uncertainties and the correlations between the tomographic bins. Each bootstrap sample is used for a fixed number of iterations of the MCMC scan performed here. This bootstrap procedure ensures that the analysis is statistically unaffected by the photometric redshift bias corrections [21], which can instead significantly change the results of the analysis of e.g. CFHTLenS data and may alleviate the tension with the value of σ_8 determined by Planck [47].

Furthermore, the KiDS data are analyzed taking into account the intrinsic galaxy alignments, for which the correlations of intrinsic ellipticities of galaxies with each other and with the shear of background sources must be considered. This is done varying two nuisance parameters: the amplitude $A_{\rm IA}$ and the redshift dependence $\eta_{\rm IA}$ (see Ref. [48]). As we have checked that our results do not change significantly if we turn on these "extended systematics" settings [21], we will only show the results obtained within the standard prescription, i.e. $\eta_{\rm IA} = 0$ and $-6 \leq A_{\rm IA} \leq 6$.

To perform the analyses as presented by the KiDS Collaboration [20,21], we should include the calculation of baryonic effects in the nonlinear matter power spectrum, that are computed using HMCODE [40]. As we discussed in Sec. II A, this code gives biased results when applied to the (unusual) MDM cosmology when the noncold dark matter temperature is much smaller than the standard neutrino one. Since we are using Eq. (3) for computing the nonlinear matter power spectrum, we shall not use HMCODE and the related prescriptions on the baryonic feedback.

3. Satellite galaxies

As we have already introduced, one of the problems of the ΛCDM model at galactic and subgalactic scales is the one of the missing satellite galaxies. Here we explain how we compute the constraints from the observations of dwarf satellite galaxies in the Milky Way (MW).

Dwarf galaxies are usually faint and small objects that must be observed and correctly identified as satellites of the MW. In the following we briefly comment on the current observational status [49,50]. The number of known standard satellites of our Galaxy is eleven. The SDSS experiment, with a sky coverage of $f_{\rm sky} \simeq 0.28$, observed other fifteen satellites [51], with a corresponding Poissonian error of ∼4. Recently, the Dark Energy Survey (DES) has reported the discovery of eight new Milky Way companions, which could potentially be ultrafaint satellite galaxies [52,53]. In the absence of a robust confirmation of the fact that these new eight DES candidates are truly all of them Milky-Way satellite galaxies, we adopt here the conservative approach of Ref. [49] and restrict ourselves to the classical satellites plus the extrapolated number of the SDSS measurements, see the discussion that follows.

We assume here that the number within the SDSS footprint is binomially distributed with probability $f_{\rm sky} \simeq 0.28$, following an isotropic distribution. Then, a SDSS-like experiment would have observed 54 MW satellite galaxies over the entire sky, with an associated (binomial distribution) error of 11. Therefore, together with the eleven classical MW satellites, this would imply a total number of $N_{\rm sat} = 65 \pm 11$. Following Ref. [49], we assume a halo-to-halo scatter [54] by reducing our estimated number of MW satellite galaxies, quoted above, by 10%. Nevertheless, we are aware that this number is probably an underestimate of the true number of dwarf satellites, as a consequence of the technical challenges of the observation. Notice however that, due to the incompleteness of the SDSS sample, it could be possible that, when accounting for corrections in e.g. the observed luminosity function, the number of satellite galaxies around the MW could be much larger than these estimates, see e.g. Ref. [55]. For this reason, we present the results obtained combining the satellites likelihood with other data sets following two different approaches. In the most conservative scenario,

labeled "SAT(low)" in the following, we apply the observed number of MW dwarf satellite galaxies $N_{\rm sat}^{\rm obs} = 58 \pm 11$ as a lower limit only, by means of a half-Gaussian likelihood, following e.g. Ref. [33]. In this conservative approach we apply the dwarf galaxy bounds only when the number of satellite galaxies predicted within a given model is below the mean number of satellite galaxies that are observed. In this way we envisage the putative situation in which not all dwarf spheroidal galaxies have been detected, being the current estimates subject to increase by ongoing and/or future searches. We also follow a more aggressive scenario in which we apply the current measurement $N_{\rm sat}^{\rm obs} = 58 \pm 11$ via a standard Gaussian likelihood. This latter case will be referred to as "SAT".

Another problem related to dwarf satellites is that it is also difficult to infer the mass of these objects, since they are dominated by dark matter, and the only possibility to measure the properties of the DM halo is through stellar kinematics inside the object. Studies that use different profiles for the halo suggest that all the known dwarfs have a mass larger than $M_{\rm min} = 10^8 h^{-1}\ M_\odot$ [56], a number that we shall use in the calculations explained below.

For the theoretical computation of the number of satellites we follow the procedure described in Refs. [33,49,57], based on a conditional mass function that is normalized taking into account the results of the N-body simulations. The function which gives the expected number of dwarf satellite galaxies with a given mass M_s reads as [49,57]

$$\frac{dN_{\rm sat}}{d\ln M_s} = \frac{1}{C_n}\frac{1}{6\pi^2}\left(\frac{M_h}{M_s}\right)\frac{P(1/R_s)}{R_s^3\sqrt{2\pi(S_s - S_h)}}. \tag{8}$$

Here $P(1/R_s = k)$ is the linear matter power spectrum for the given cosmological model, h stands for "host halo", i.e. the MW galaxy, and the subscript s stands for "satellite" or "subhalo". The coefficient $C_n = 45$ is chosen to mimic the results of N-body simulations [17]. In our calculations we assume $M_h = 1.77 \times 10^{12} h^{-1}\ M_\odot$ for the MW. This may be not the exact mass of our Galaxy, but it is chosen because it lies in the estimated range for the MW mass [58], and it matches the mass of the Aquarius-D2 simulation [59], from which the calibration on the N-body simulations results is computed [17]. The estimated number of satellites $N_{\rm sat}^{\rm th}$ is obtained integrating the above Eq. (8) between the minimum mass of satellites $M_{\rm min}$, previously described, and the mass of the host halo M_h,

$$N_{\rm sat}^{\rm th} = \int_{M_{\rm min}}^{M_h} \frac{dN_{\rm sat}}{d\ln M_s} dM_s. \tag{9}$$

The parameters describing the subhalo (or the host halo) are the radius R_s (R_h), the mass M_s (M_h) and the corresponding variance S_s (S_h). They are related by

$$S_i(M) = \frac{1}{2\pi^2}\int_0^\infty k^2 P(k) W^2(k|M) dk, \tag{10}$$

$$M_i = \frac{4\pi}{3}\Omega_m \rho_c (cR_i)^3, \tag{11}$$

where $i = s, h$. The parameter $c = 2.5$ is used to calibrate the calculation on N-body simulation results.

To evaluate the variance, we use a procedure based on a rederivation of the Press and Schechter [60] mass function, for which we use a *k-sharp filter* approach [18] to cut all the scales k below the cutoff scale $k_s = 1/R_s$, and R_s depends on the subhalo mass as in Eq. (11). This filter is written in terms of a window function

$$W(k|M) = \begin{cases} 1, & \text{if } k \le k_s(M); \\ 0, & \text{if } k > k_s(M). \end{cases} \tag{12}$$

C. Numerical analyses

We base our analyses on the standard ΛCDM model, with the addition of a second noncold dark matter component. The parameters that we vary in our analyses are then the energy density of baryons, $\omega_b \equiv \Omega_b h^2$; the total energy density of the dark matter components ω_{DM}, the fraction of the total dark matter mass-energy density in the form of noncold dark matter (f_X) and its temperature through the logarithm $\log_{10}(T_X/T_\nu)$ (see also Sec. II A); the optical depth to reionization, τ; the ratio of the sound horizon to the angular diameter distance at decoupling Θ; and the amplitude and the tilt of the primordial power spectrum of curvature perturbations, $\ln(10^{10}A_s)$ and n_s.

Other cosmological parameters are fixed to their standard values as follows. The sum of the three active neutrino masses is fixed to zero. Despite neutrino oscillation measurements tell us that at least two of the neutrinos must have a mass, with a minimum total mass of $\sum m_\nu \simeq 0.06$ eV for the normal ordering, the error that we make when fixing $\sum m_\nu \simeq 0$ is small. For the three massless neutrinos, we fix the standard value $N_{\rm eff}^\nu = 3.046$, corresponding to the three active neutrino contribution obtained in the limit of noninstantaneous neutrino decoupling [61,62].

For the Planck CMB and satellite galaxy number counts we use the Markov chain Monte Carlo (MCMC) tool Monte Python [63], interfaced with the Boltzmann solver CLASS [64]. We use then the obtained covariance matrices to run MCMC with KiDS data, by means of the Boltzmann solver `CAMB` [65] together with its MCMC companion `CosmoMC` [66].[4]

[4]For the latter one, we use the July 2015 version with the required modifications to perform the analyses of the KiDS data [21], publicly available at http://github.com/sjoudaki/kids450.

Together with the cosmological parameters, we vary all the required nuisance parameters involved in the Planck and the KiDS likelihoods.

III. RESULTS

Figure 2, left panel, depicts the 68% and 95% C.L. allowed contours in the (Ω_m, σ_8) plane resulting from a number of possible data combinations and comparing different underlying cosmological models. In the simplest ΛCDM picture, the allowed regions for the KiDS and Planck data sets do not basically overlap, showing a clear tension, as pointed out before by Refs. [20,21]. Such a tension is clearly alleviated when one considers the possible MDM extension to the minimal ΛCDM picture: notice that the contours for KiDS and Planck overlap for a larger region in the MDM case. This very same improvement can be noticed from the one-dimensional posterior probability distribution of the $S_8 = \sigma_8\sqrt{\Omega_m}$ quantity in the right panel of Fig. 2.

A possible way of quantifying the tension in the measurements of S_8 arising from the Planck and KiDS data sets in possible extensions of the ΛCDM framework has been presented and used in Ref. [21]. The tension is defined by

$$T(S_8) \equiv |\bar{S}_8^{D_1} - \bar{S}_8^{D_2}|/\sqrt{\sigma^2(S_8^{D_1}) + \sigma^2(S_8^{D_2})}, \quad (13)$$

where D_1 and D_2 refer to the Planck and KiDS data sets, $\bar{S}_8$ is the mean value over the posterior distribution and σ refers to the 68% C.L. error on S_8. If we compute the value of $T(S_8)$ from the constraints obtained within the MDM scenario explored here, we get a displacement of $T^{\rm MDM}(S_8) \simeq 1\sigma$, which indicates that the 2.3σ–2.8σ[5] obtained between Planck and KiDS S_8 values within the canonical ΛCDM scenario is considerably reduced. The level of the improvement is very similar to that reached when other possible extensions to the minimal scenario are considered, as, for instance, in the presence of a dark energy equation of state or within modified gravity models [21]. The fact that assuming a MDM scenario the tension between the Planck and KiDS constraints is strongly alleviated fully justifies the combination of these two data sets, already depicted in both panels of Fig. 2.

Figure 3 shows the two-dimensional 68% and 95% C.L. allowed contours in the (S_8, T_X/T_ν) and (S_8, f_X) planes. We illustrate the results from KiDS, CMB and their combination. We can notice from the contours shown in the left panel of Fig. 3 that there exists a degeneracy between the S_8 quantity and T_X/T_ν. The reason for that is because the larger T_X is, the closer the noncold dark matter component behaves as a hot dark matter fluid, and therefore a larger matter component (and, consequently, a larger value of S_8) would be required to compensate for the suppression of perturbations at small scales. As expected, there are no bounds on the noncold dark matter fraction f_X, as one can see in the right panel of Fig. 3. Indeed, for a very small value of T_X the noncold dark matter is observationally indistinguishable from a pure cold component, and therefore its relative abundance is perfectly compatible with $f_X = 1$.

As previously stated, the motivation for MDM scenarios is twofold. We have already shown above that a noncold dark matter component provides a possible way of alleviating the tension between Planck CMB measurements and tomographic weak lensing data from KiDS. As mentioned in our introductory section, there is another very important motivation to look for additional extensions of the minimal cold dark matter picture, namely, the so-called small scale crisis of the ΛCDM, and, in particular, the *Milky Way satellite problem* [5,6]. We have therefore also considered in our analyses the constraints from the MW dwarf satellite galaxies, that we are going to discuss in what follows.

The first panel of Fig. 4 shows the one-dimensional probability distribution of the noncold dark matter temperature relative to that of the neutrino bath T_X/T_ν. Planck CMB data measurements provide the 95% C.L. upper bound of $T_X/T_\nu < 0.4$, which could be naively translated into a contribution to $\Delta N_{\rm eff} = (T_X/T_\nu)^4 \simeq 0.02$ during the periods in the Universe expansion history in which these noncold dark matter particles are relativistic. Notice that this value is much smaller than the limit obtained from Planck CMB measurements on the contribution from (massless) dark radiation or light sterile neutrinos. However, the limits are not directly comparable as the energy density of the noncold dark matter component explored here is that of a nonrelativistic fluid for a large region of the parameter space. KiDS measurements show a preference for higher temperatures, indeed the 95% C.L. upper limit is set by the upper prior in the T_X/T_ν ($T_X/T_\nu < 1$) parameter. When analyzing KiDS data taking into account the Planck CMB constraints on all the cosmological parameters, we obtain $T_X/T_\nu < 0.6$ at 95% C.L. We also show in Fig. 4 the results obtained combining the MW satellites counts with CMB measurements. The blue curve depicts the one-dimensional probability distribution of the noncold dark matter temperature when the current estimates of MW satellite galaxies are treated as regular Gaussian priors and are combined with Planck CMB measurements. This data combination constrains the temperature to lie within a narrow region, favoring scenarios with values of T_X/T_ν in the range $0.15 < T_X/T_\nu < 0.17$, therefore smaller than those quoted

[5]The authors of [20] quote a 2.3σ tension among the obtained S_8 values from Planck (CMB temperature and low-ℓ polarization) and KiDS. Our analysis of the KiDS results with the prescriptions published together with Ref. [21] leads to a value of $T(S_8) \simeq 2.8$, with small variations when we consider our results from Planck CMB data or the Planck chains publicly available at https://wiki.cosmos.esa.int/planckpla. When the full CMB data set we explore here is considered, which includes the Planck lensing likelihood, the tension shifts to $T(S_8) \simeq 2.5$.

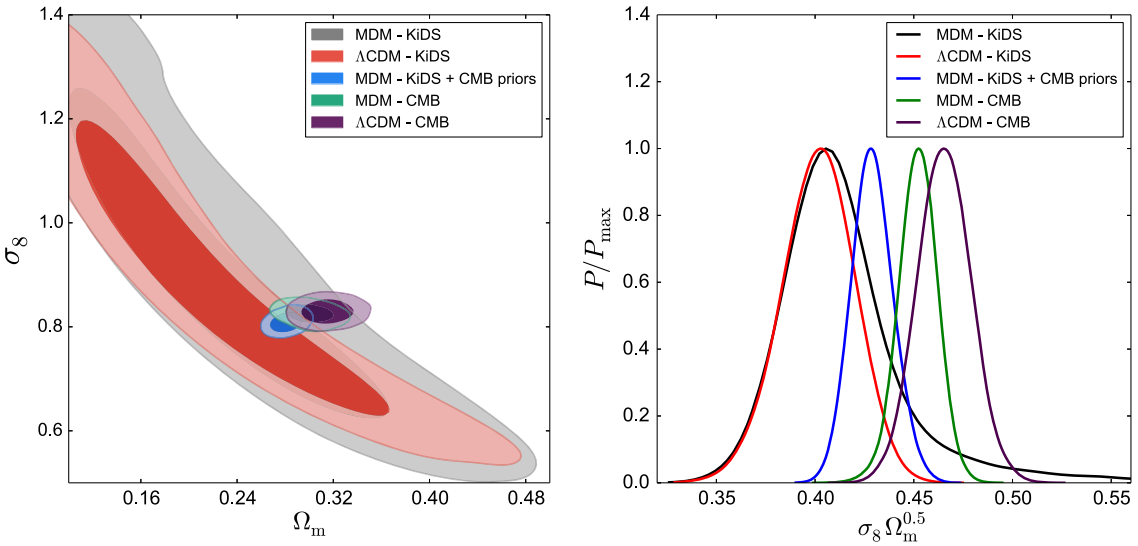

FIG. 2. Left panel: 68% and 95% C.L. allowed contours in the (Ω_m, σ_8) plane, see text for details. Right panel: one-dimensional posterior probability distribution of the S_8 quantity for the same data combinations and models shown in the left panel.

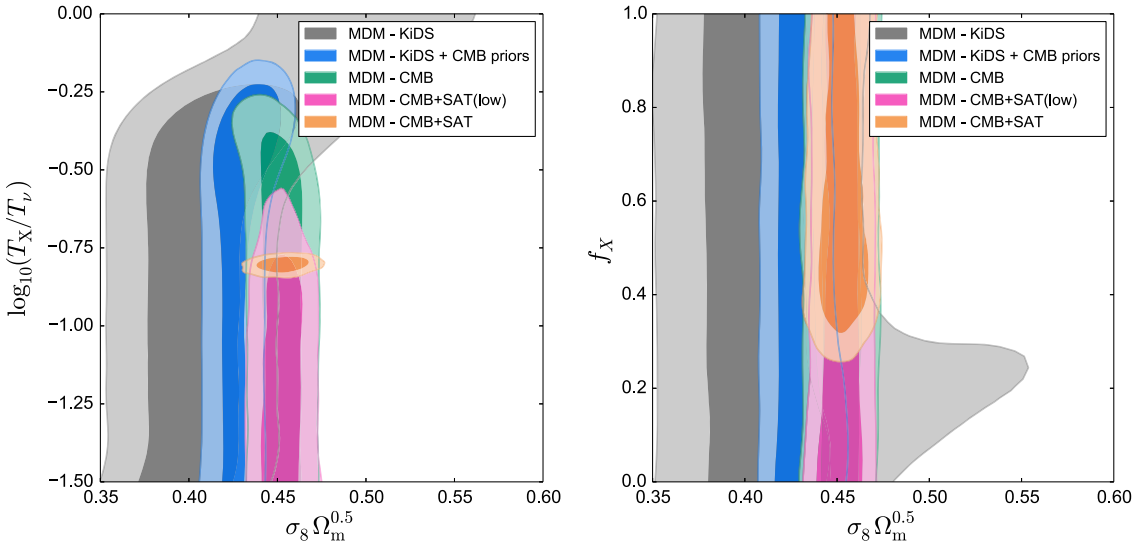

FIG. 3. 68% and 95% C.L. allowed contours in the (S_8, T_X/T_ν) and (S_8, f_X) planes resulting from different data sets: KiDS alone, CMB alone, the combination of KiDS and CMB data, and the combination of CMB measurements with MW satellite number counts, see text for details.

previously for the KiDS plus Planck MDM case. This difference can be explained in terms of the preferred value of m_X, which turns out to be larger for Planck plus MW satellites than for Planck plus KiDS data. If we instead consider the MW likelihood in the form of a conservative half-Gaussian likelihood, imposing the current observed number of galaxies only as a lower limit, there is no lower bound on the noncold dark matter temperature, as the half-Gaussian likelihood turns out to be perfectly compatible with a pure ΛCDM universe, for which the number of satellite galaxies is around 160. The upper limit on T_X/T_ν is very close to the one quoted above for our more aggressive MW likelihood scenario ($T_X/T_\nu < 0.19$ at 95% C.L.), and smaller also than the constraint obtained from Planck plus KiDS data.

The second panel of Fig. 4 shows the one-dimensional probability distribution of the noncold dark matter mass m_X.[6] Notice that there exist a 95% C.L. lower limit from Planck data on the mass of the MDM component $m_X > 32$ eV. This bound on the mass is related to the fact that, below that region, the noncold dark matter fluid

[6]We recall that m_X is a derived parameter in our analyses.

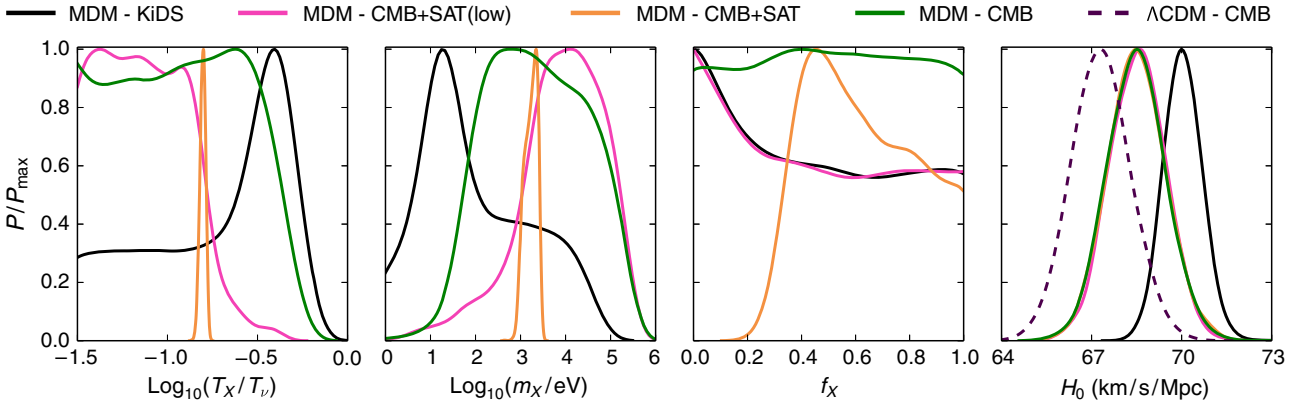

FIG. 4. One-dimensional posterior probability distribution for the T_X/T_ν ratio, for the noncold dark matter mass m_X, its relative fraction f_X and for the Hubble constant H_0 for different data combinations in the MDM scenario, see the text for details. For comparison purposes, in the case of the Hubble constant, we also depict the resulting one-dimensional distribution from a fit to Planck CMB data in the context of a ΛCDM cosmology.

behaves as a *hot* dark matter component (even if its temperature is lower than the neutrino one), and CMB observations do not allow for such large contribution from hot dark matter relics. On the other hand, KiDS measurements show a mild preference for a dark matter mass in the sub-keV region, that can provide the suppression of the small-scale perturbations required to reduce the value of the S_8 quantity for KiDS. The combination of Planck CMB plus KiDS weak lensing data does not significantly change these findings.

When considering the MW dwarf satellite constraints in their less conservative form, we observe that there is a preferred narrow region for the noncold dark matter mass, which, as we shall further illustrate in short, turns out to be very close to the warm dark matter region[7] The mass of the particle lies in the range $0.95\ \text{keV} < m_X < 2.9\ \text{keV}$ (95% C.L.). Additional and independent constraints from power spectrum measurements from the Lyman alpha forest flux and from the universe reionization history can be applied in this case, see Refs. [72–76] for the most recent analyses.

When adopting the more conservative, half-Gaussian approach for the MW likelihood, the lower bound we get for the noncold dark component is very close to the region quoted above, $m_X > 0.09$ keV at 95% C.L., as lower values of the noncold dark matter mass will lead to a very large suppression of the matter power spectrum at galactic and subgalactic scales, in which case the number of MW satellite galaxies gets strongly reduced. However, for this case, there is no upper limit on m_X, as a model with only the cold dark matter component is perfectly allowed once the upper bound in the observed number of MW galaxies is no longer considered, largely relaxing the allowed mass range.

Notice that the preferred region for the mass m_X obtained considering the MW satellites observations is larger than the one suggested by KiDS weak lensing measurements. This is due to the fact that the suppression in the growth of structure required to satisfy MW satellite galaxy observations is associated to a smaller scale (large wave number k) than the one required to explain KiDS weak lensing data. The differences in the preferred values of m_X from weak lensing and from KiDS lead to differences in the allowed values of T_X/T_ν. As previously stated, the bound on m_X directly depends on the constraint in the abundance of the particle. Consequently, the larger (smaller) the allowed mass is, the smaller (larger) the temperature should be to satisfy CMB constraints, see Eq. (2).

The bounds on the noncold dark matter fraction are shown in the third panel of Fig. 4. Planck measurements result in an almost completely flat distribution for f_X, as particles with small temperatures and large masses will produce CMB photon temperature and lensing patterns that are identical to those obtained in the pure cold dark matter case. KiDS and its combination with CMB measurements lead also to flat distributions for f_X, with limits coinciding with the assumed priors on f_X. When dealing with the MW satellites likelihood in the less conservative approach, its combination with Planck CMB sets a robust preference for $f_X > 0$, i.e. $f_X > 0.34$ at 95% C.L., while in the more conservative approach the f_X distribution is flat. Therefore, the results that we obtain when considering the MW dwarf satellites in the less conservative approach followed here strongly suggest the need for a nonzero noncold dark matter component. The explanation is simple: while we observe a number around 60 satellite galaxies, the corresponding number for a CDM-only case would be ∼160. A suppression of the matter perturbations at small scales (as, for instance, that associated to a noncold dark matter component) is required, in order to match the predicted number and the observed one.

[7]For pioneer work on WDM cosmologies see Refs. [67–71].

We can also note from the two panels of Fig. 3 that the allowed contours in the (S_8, T_X/T_ν) and (S_8, f_X) planes after considering the MW dwarf satellite galaxies likelihood do not deviate significantly from the CMB constraints. This shows that the second dark matter component required to fully explain the satellites counts at galactic scale does not help in solving the tension in the S_8 parameter that exists between Planck CMB and KiDS weak lensing data. On the other hand, there exists also the possibility that the current measures of the number of MW dwarf galaxies are only underestimations of the true number, and future observations will increase the present statistics. Figure 3 illustrates also such a possibility, when combining MW satellite number counts with CMB data. In this more conservative approach to the MW satellites problem, we can notice that the satellites limits on f_X overlap with those from the CMB, adding no extra information on the noncold dark matter abundance.

Finally, the fourth panel of Fig. 4 shows the one-dimensional posterior distribution of the Hubble constant H_0. Notice that, as in the case of Ref. [21] for other possible extensions of the ΛCDM scheme, the Hubble parameter values show a better agreement with direct estimates of H_0 [77,78] in the MDM scheme than in the pure cold dark matter scenario. The Planck constraint on the Hubble constant in the MDM scenario explored here ($H_0 = 68.5 \pm 0.9$ km s^{-1} Mpc^{-1}) is higher than in the pure ΛCDM case ($H_0 = 67.3 \pm 1$ km s^{-1} Mpc^{-1}), i.e. the mean value of H_0 is shifted by approximately 1.5σ. The reason for the larger preferred value of H_0 in the context of MDM scenarios can be understood as follows. From Fig. 2 it is straightforward to infer that the value of Ω_m in these scenarios is generically lower than in the pure ΛCDM case. This fact is reinforced when combining Planck and KiDS data. As the CMB peaks structure does not leave much freedom on the value of the physical (total) matter energy density $\Omega_m h^2$, a smaller value of Ω_m requires the mean value of H_0 to be larger, in order to leave the product $\Omega_m h^2$ unchanged. When combining Planck CMB and KiDS data sets we obtain $H_0 = 70.0 \pm 0.6$ km s^{-1} Mpc^{-1}, showing a much better matching to the Hubble parameter value extracted from local observations. This value, for instance, is consistent (within 1σ) with that of Ref. [77], $H_0 = 72.5 \pm 2.5$ km s^{-1} Mpc^{-1}, and the 3.4σ tension within the ΛCDM paradigm between CMB and the Hubble constant estimates of Ref. [78], $H_0 = 73.24 \pm 1.74$ km s^{-1} Mpc^{-1}, is reduced to the 2σ level. Finally, the combination of MW satellites and Planck data leaves unchanged the value of H_0 from CMB alone in MDM scenarios, as expected, since MW satellites observations do not require a change on the dark matter abundance but on its nature, and therefore no shift is required in H_0.

IV. CONCLUSIONS

Observations at galactic and subgalactic scales compromise the viability of the canonical ΛCDM paradigm, which otherwise provides an excellent fit to large scale structure and cosmic microwave background (CMB) observations. The number of satellite galaxies in Milky-Way (MW) sized halos and the measured kinematics of the MW satellites pose the question of whether a universe made out of a pure cold dark matter component and a dark energy fluid can successfully explain all cosmological observations. Furthermore, there are a number of additional inconsistencies among small scale predictions from the ΛCDM model and observations from recent data releases from tomographic weak gravitational lensing surveys, as those from the Kilo Degree-450 deg^2 Survey (KiDS-450) [20,21]. More concretely, there are discrepancies in the value of the amplitude of the density fluctuations at a given matter density Ω_m, commonly quantified in terms of $S_8 = \sigma_8 \sqrt{\Omega_m}$.

Models with an admixture of cold and noncold dark matter particles (MDM models) may potentially alleviate the ΛCDM observational problems outlined above, as the free streaming nature associated to a nontotally cold dark matter component will suppress the matter power spectrum on the smallest scales, leading to a better agreement among large and galactic and subgalactic scales measurements. Here we have analyzed these MDM scenarios using the most recent tomographic weak lensing measurements from the KiDS-450 survey, combining them with Planck CMB data. We have also studied the constraints derived using the current estimates for the observed number of MW satellite galaxies.

In a similar way to other extended cosmological models [21], the tension in the measurements from Planck and KiDS of the S_8 quantity is reduced from $2.3 - 2.8\sigma$ to 1σ in MDM scenarios. Furthermore, the value of the Hubble parameter H_0 is perfectly consistent with that measured by late universe observations [77]. We find $H_0 = 70.0 \pm 0.6$ km s^{-1} Mpc^{-1} after combining Planck CMB and KiDS tomographic weak lensing data, value which is in a good agreement with the Hubble parameter value extracted from local observations, see e.g. Ref. [77], which quotes a value of $H_0 = 72.5 \pm 2.5$ km s^{-1} Mpc^{-1}.

We have also searched for the allowed ranges on the noncold dark matter properties, as its temperature and its mass. We find a 95% C.L. upper limit $T_X/T_\nu < 0.6$ after combining Planck CMB and KiDS data. Current estimates of the number of satellite galaxies, $N_{\rm sat}^{\rm obs} = 58 \pm 11$, when translated into a standard Gaussian likelihood and combined with CMB measurements, prefer smaller values of the temperatures ratio ($0.15 < T_X/T_\nu < 0.17$ at 95% C.L.), as they would require larger values of m_X to suppress the growth of structure at the scales involved in MW halo observations. However, if current MW satellite observations are conservatively interpreted as a half-Gaussian likelihood, imposing the current measured number only as a lower limit, the lower bound on the noncold dark matter temperature disappears, and we obtain $T_X/T_\nu < 0.19$ at 95% C.L. Concerning the noncold dark matter mass

and its abundance, after combining Planck CMB and KiDS measurements, we find a (mild) preference for a sub-keV noncold dark matter particle mass, with no particular evidence for a nonzero abundance of such a component. However, satellite counts data, in their more aggressive interpretation and combined with CMB measurements, isolate the preferred regions $0.95\ \text{keV} < m_X < 2.9\ \text{keV}$ and $f_X > 0.34$ at 95% C.L., robustly establishing the need for the existence of such a keV warm dark matter particle. In the most conservative approach there is not such a preference for $f_X \neq 0$ and only a lower bound on the noncold dark matter mass exists, $m_X > 0.08$ keV at 95% C.L.

Therefore, a subdominant, noncold dark matter component with $m_X \sim$ keV could in principle alleviate some existing tensions between CMB and low redshift observations. However, the masses and temperatures required to explain weak lensing and MW observations are rather different. While the scale of the power spectrum suppression required by KiDS data needs a sub-keV noncold dark matter mass and a temperature $T_X \sim T_\nu/2$, the ones required by Milky Way satellites observations are associated to larger masses and smaller temperatures. Future weak lensing and MW satellites observations will further sharpen the preferred regions, either enlarging or diminishing the existing differences among the current weak lensing and MW preferred constraints for the noncold dark matter temperature and mass. Future work with simulated data will be devoted elsewhere to further corner MDM scenarios.

ACKNOWLEDGMENTS

The authors would like to thank Francisco Villaescusa-Navarro and Alexander Mead for useful discussions on the nonlinear power spectrum parametrization and Shahab Joudaki for details on the KiDS analysis. The work of S. G. was supported by the Spanish Grants No. FPA2014-58183-P, No. Multidark CSD2009-00064 and No. SEV-2014-0398 (MINECO), and No. PROMETEOII/2014/084 (Generalitat Valenciana). O. M. is supported by PROMETEOII/2014/050, by the Spanish Grant No. FPA2014–57816-P of the MINECO, by the MINECO Intramural OEP2010, by the MINECO Grant No. SEV-2014-0398 and by the European Union's Horizon 2020 research and innovation programme under the Marie Skłodowska-Curie Grants No. 690575 and No. 674896. The work of R. D. was supported by NWO through two Vidi grants and partly by University of Amsterdam. M. E. is supported by Spanish Grant No. FPU13/03111 of 6MECD.

[1] P. A. R. Ade *et al.* (Planck Collaboration), Astron. Astrophys. **594**, A13 (2016).
[2] G. Bertone, D. Hooper, and J. Silk, Phys. Rep. **405**, 279 (2005).
[3] L. Bergstrom, Ann. Phys. (Amsterdam) **524**, 479 (2012).
[4] A. Kusenko and L. J. Rosenberg, arXiv:1310.8642.
[5] A. A. Klypin, A. V. Kravtsov, O. Valenzuela, and F. Prada, Astrophys. J. **522**, 82 (1999).
[6] B. Moore, S. Ghigna, F. Governato, G. Lake, T. R. Quinn, J. Stadel, and P. Tozzi, Astrophys. J. **524**, L19 (1999).
[7] M. Boylan-Kolchin, J. S. Bullock, and M. Kaplinghat, Mon. Not. R. Astron. Soc. **422**, 1203 (2012).
[8] L. Wang, V. Gonzalez-Perez, L. Xie, A. P. Cooper, C. S. Frenk, L. Gao, W. A. Hellwing, J. Helly, M. R. Lovell, and L. Jiang, Mon. Not. R. Astron. Soc. **468**, 4579 (2017).
[9] M. R. Lovell, V. Gonzalez-Perez, S. Bose, A. Boyarsky, S. Cole, C. S. Frenk, and O. Ruchayskiy, Mon. Not. R. Astron. Soc. **468**, 2836 (2017).
[10] T. Sawala, C. S. Frenk, R. A. Crain, A. Jenkins, J. Schaye, T. Theuns, and J. Zavala, Mon. Not. R. Astron. Soc. **431**, 1366 (2013).
[11] T. Sawala *et al.*, Mon. Not. R. Astron. Soc. **457**, 1931 (2016).
[12] A. Fattahi, J. F. Navarro, T. Sawala, C. S. Frenk, L. V. Sales, K. Oman, M. Schaller, and J. Wang, arXiv:1607.06479.
[13] E. Polisensky and M. Ricotti, Mon. Not. R. Astron. Soc. **437**, 2922 (2014).
[14] M. Vogelsberger, J. Zavala, and A. Loeb, Mon. Not. R. Astron. Soc. **423**, 3740 (2012).
[15] J. A. Schewtschenko, C. M. Baugh, R. J. Wilkinson, C. Boehm, S. Pascoli, and T. Sawala, Mon. Not. R. Astron. Soc. **461**, 2282 (2016).
[16] M. R. Lovell, V. Eke, C. S. Frenk, L. Gao, A. Jenkins, T. Theuns, J. Wang, D. M. White, A. Boyarsky, and O. Ruchayskiy, Mon. Not. R. Astron. Soc. **420**, 2318 (2012).
[17] M. R. Lovell, C. S. Frenk, V. R. Eke, A. Jenkins, L. Gao, and T. Theuns, Mon. Not. R. Astron. Soc. **439**, 300 (2014).
[18] M. R. Lovell, S. Bose, A. Boyarsky, S. Cole, C. S. Frenk, V. Gonzalez-Perez, R. Kennedy, O. Ruchayskiy, and A. Smith, Mon. Not. R. Astron. Soc. **461**, 60 (2016).
[19] T. Nakama, J. Chluba, and M. Kamionkowski, Phys. Rev. D **95**, 121302 (2017).
[20] H. Hildebrandt *et al.*, Mon. Not. R. Astron. Soc. **465**, 1454 (2017).
[21] S. Joudaki *et al.*, arXiv:1610.04606 [Mon. Not. R. Astron. Soc. (to be published)].
[22] N. Aghanim *et al.* (Planck Collaboration), Astron. Astrophys. **594**, A11 (2016).
[23] M. Kilbinger *et al.*, Mon. Not. R. Astron. Soc. **430**, 2200 (2013).

[24] C. Heymans *et al.*, Mon. Not. R. Astron. Soc. **432**, 2433 (2013).
[25] P. Lemos, A. Challinor, and G. Efstathiou, J. Cosmol. Astropart. Phys. 05 (2017) 014.
[26] M. Kilbinger *et al.*, arXiv:1702.05301.
[27] T. D. Kitching, J. Alsing, A. F. Heavens, R. Jimenez, J. D. McEwen, and L. Verde, Mon. Not. R. Astron. Soc. **469**, 2737 (2017).
[28] A. Palazzo, D. Cumberbatch, A. Slosar, and J. Silk, Phys. Rev. D **76**, 103511 (2007).
[29] A. Boyarsky, J. Lesgourgues, O. Ruchayskiy, and M. Viel, J. Cosmol. Astropart. Phys. 05 (2009) 012.
[30] A. V. Maccio, O. Ruchayskiy, A. Boyarsky, and J. C. Munoz-Cuartas, Mon. Not. R. Astron. Soc. **428**, 882 (2013).
[31] D. Anderhalden, J. Diemand, G. Bertone, A. V. Maccio, and A. Schneider, J. Cosmol. Astropart. Phys. 10 (2012) 047.
[32] D. Anderhalden, A. Schneider, A. V. Maccio, J. Diemand, and G. Bertone, J. Cosmol. Astropart. Phys. 03 (2013) 014.
[33] R. Diamanti, S. Ando, S. Gariazzo, O. Mena, and C. Weniger, J. Cosmol. Astropart. Phys. 06 (2017) 008.
[34] D. H. Weinberg, J. S. Bullock, F. Governato, R. Kuzio de Naray, and A. H. G. Peter, Proc. Natl. Acad. Sci. U.S.A. **112**, 12249 (2015).
[35] Y. Ali-Haimoud and S. Bird, Mon. Not. R. Astron. Soc. **428**, 3375 (2013).
[36] U. Seljak, Mon. Not. R. Astron. Soc. **318**, 203 (2000).
[37] J. A. Peacock and R. E. Smith, Mon. Not. R. Astron. Soc. **318**, 1144 (2000).
[38] C.-P. Ma and J. N. Fry, Astrophys. J. **543**, 503 (2000).
[39] A. Cooray and R. K. Sheth, Phys. Rep. **372**, 1 (2002).
[40] A. Mead, J. Peacock, C. Heymans, S. Joudaki, and A. Heavens, Mon. Not. R. Astron. Soc. **454**, 1958 (2015).
[41] R. Takahashi, M. Sato, T. Nishimichi, A. Taruya, and M. Oguri, Astrophys. J. **761**, 152 (2012).
[42] A. Kamada, K. T. Inoue, and T. Takahashi, Phys. Rev. D **94**, 023522 (2016).
[43] R. Takahashi and K. T. Inoue, Mon. Not. R. Astron. Soc. **440**, 870 (2014).
[44] K. T. Inoue, R. Takahashi, T. Takahashi, and T. Ishiyama, Mon. Not. R. Astron. Soc. **448**, 2704 (2015).
[45] K. Kuijken *et al.*, Mon. Not. R. Astron. Soc. **454**, 3500 (2015).
[46] I. F. Conti, R. Herbonnet, H. Hoekstra, J. Merten, L. Miller, and M. Viola, Mon. Not. R. Astron. Soc. **467**, 1627 (2017).
[47] T. D. Kitching, L. Verde, A. F. Heavens, and R. Jimenez, Mon. Not. R. Astron. Soc. **459**, 971 (2016).
[48] S. Joudaki *et al.*, Mon. Not. R. Astron. Soc. **465**, 2033 (2017).
[49] A. Schneider, J. Cosmol. Astropart. Phys. 04 (2016) 059.
[50] E. Polisensky and M. Ricotti, Phys. Rev. D **83**, 043506 (2011).
[51] J. Wolf, G. D. Martinez, J. S. Bullock, M. Kaplinghat, M. Geha, R. R. Muñoz, J. D. Simon, and F. F. Avedo, Mon. Not. R. Astron. Soc., **406**, 1220 (2010).
[52] K. Bechtol *et al.* (DES Collaboration), Astrophys. J. **807**, 50 (2015).
[53] A. Drlica-Wagner *et al.* (DES Collaboration), Astrophys. J. **813**, 109 (2015).
[54] M. Boylan-Kolchin, V. Springel, S. D. M. White, and A. Jenkins, Mon. Not. R. Astron. Soc. **406**, 896 (2010).
[55] E. J. Tollerud, J. S. Bullock, L. E. Strigari, and B. Willman, Astrophys. J. **688**, 277 (2008).
[56] A. M. Brooks and A. Zolotov, Astrophys. J. **786**, 87 (2014).
[57] A. Schneider, Mon. Not. R. Astron. Soc. **451**, 3117 (2015).
[58] Q. Guo, S. White, C. Li, and M. Boylan-Kolchin, Mon. Not. R. Astron. Soc. **404**, 1111 (2010).
[59] V. Springel, J. Wang, M. Vogelsberger, A. Ludlow, A. Jenkins, A. Helmi, J. F. Navarro, C. S. Frenk, and S. D. M. White, Mon. Not. R. Astron. Soc. **391**, 1685 (2008).
[60] W. H. Press and P. Schechter, Astrophys. J. **187**, 425 (1974).
[61] G. Mangano, G. Miele, S. Pastor, T. Pinto, O. Pisanti, and P. D. Serpico, Nucl. Phys. **B729**, 221 (2005).
[62] P. F. de Salas and S. Pastor, J. Cosmol. Astropart. Phys. 07 (2016) 051.
[63] B. Audren, J. Lesgourgues, K. Benabed, and S. Prunet, J. Cosmol. Astropart. Phys. 02 (2013) 001.
[64] J. Lesgourgues, arXiv:1104.2932.
[65] A. Lewis, A. Challinor, and A. Lasenby, Astrophys. J. **538**, 473 (2000).
[66] A. Lewis and S. Bridle, Phys. Rev. D **66**, 103511 (2002).
[67] B. Moore, T. R. Quinn, F. Governato, J. Stadel, and G. Lake, Mon. Not. R. Astron. Soc. **310**, 1147 (1999).
[68] P. Bode, J. P. Ostriker, and N. Turok, Astrophys. J. **556**, 93 (2001).
[69] V. Avila-Reese, P. Colin, O. Valenzuela, E. D'Onghia, and C. Firmani, Astrophys. J. **559**, 516 (2001),.
[70] V. K. Narayanan, D. N. Spergel, R. Dave, and C.-P. Ma, Astrophys. J. **543**, L103 (2000).
[71] M. Viel, J. Lesgourgues, M. G. Haehnelt, S. Matarrese, and A. Riotto, Phys. Rev. D **71**, 063534 (2005).
[72] M. Viel, G. D. Becker, J. S. Bolton, and M. G. Haehnelt, Phys. Rev. D **88**, 043502 (2013).
[73] J. Baur, N. Palanque-Delabrouille, C. Yeche, C. Magneville, and M. Viel, J. Cosmol. Astropart. Phys. 08 (2016) 012.
[74] V. Irsic *et al.*, Phys. Rev. Lett. **96**, 023522 (2017).
[75] C. Yeche, N. Palanque-Delabrouille, J. Baur, and H. d. M. d. BourBoux, J. Cosmol. Astropart. Phys. 06 (2017) 047.
[76] L. Lopez-Honorez, O. Mena, S. Palomares-Ruiz, and P. V. Domingo, arXiv:1703.02302.
[77] G. Efstathiou, Mon. Not. R. Astron. Soc. **440**, 1138 (2014).
[78] A. G. Riess *et al.*, Astrophys. J. **826**, 56 (2016).

JHEP

Published for SISSA by Springer

Received: June 27, 2016
Revised: January 12, 2017
Accepted: January 31, 2017
Published: February 8, 2017

Sterile neutrino portal to Dark Matter I: the $U(1)_{B-L}$ case

Miguel Escudero,[a] **Nuria Rius**[a] **and Verónica Sanz**[b]

[a] *Departamento de Física Teórica and IFIC, Universidad de Valencia-CSIC, C/ Catedrático José Beltrán, 2, E-46980 Paterna, Spain*

[b] *Department of Physics and Astronomy, University of Sussex, Falmer Campus, Brighton BN1 9QH, U.K.*

E-mail: miguel.escudero@ific.uv.es, nuria.rius@ific.uv.es, v.sanz@sussex.ac.uk

Abstract: In this paper we explore the possibility that the sterile neutrino and Dark Matter sectors in the Universe have a common origin. We study the consequences of this assumption in the simple case of coupling the dark sector to the Standard Model via a global $U(1)_{B-L}$, broken down spontaneously by a dark scalar. This dark scalar provides masses to the dark fermions and communicates with the Higgs via a Higgs portal coupling. We find an interesting interplay between Dark Matter annihilation to dark scalars — the CP-even that mixes with the Higgs and the CP-odd which becomes a Goldstone boson, the Majoron — and heavy neutrinos, as well as collider probes via the coupling to the Higgs. Moreover, Dark Matter annihilation into sterile neutrinos and its subsequent decay to gauge bosons and quarks, charged leptons or neutrinos lead to indirect detection signatures which are close to current bounds on the gamma ray flux from the galactic center and dwarf galaxies.

Keywords: Beyond Standard Model, Neutrino Physics

ArXiv ePrint: 1606.01258

doi:10.1007/JHEP02(2017)045

JHEP02(2017)045

Contents

1 Introduction

The study of the dark Universe is one of the best handles to understand what lies beyond the Standard Model (SM), particularly possible connections between Dark Matter and other sectors. The SM neutrino sector is especially interesting, as the observation of neutrino masses already points to new physics beyond the SM, possibly in the form of massive right-handed neutrinos. This raises the question whether these two new forms of massive particles, Dark Matter and right-handed neutrinos, are somewhat linked.

A very minimal possibility would be that of right-handed neutrinos constituting the Dark Matter of the Universe [1]. Yet, this option is tightly constrained in a region of small mixing with active neutrinos and mass around the keV, which will be explored in upcoming experiments and potentially excluded, see [2] for a recent review on the subject.

In this paper we propose a different scenario, where sterile neutrinos and a fermionic Dark Matter particle would have a common origin within a dark sector. These dark fermions would exhibit couplings to a dark scalar, which would bring a source of Majorana masses. The right-handed neutrinos would mix with active neutrinos, providing a link to the SM, which Dark Matter would inherit via exchanges of the dark scalar. Additionally, the dark scalar could couple to the SM via a Higgs portal, providing Dark Matter yet another mechanism to communicate with the SM. In this paper we choose the rather natural option of charging the dark sector under U(1)$_{B-L}$, but another minimal choice would be to assume an exact symmetry of the dark sector which stabilizes the lightest dark

JHEP02(2017)045

particle and allows to communicate with the SM via the right-handed neutrinos, singlets under both the SM and the dark group, see [3, 4] and [5].

The paper is organized as follows. After presenting the set-up of our model in section 2, and the consequences of the breaking of $\mathrm{U}(1)_{B-L}$ in the scalar sector in section 3, we move onto the phenomenology of the model in section 4. The study of Higgs decays and direct detection in sections 4.1 and 4.2, does lead to strong contraints on the mixing between the dark scalar and the Higgs. How Dark Matter can satisfy the observed relic abundance is explored in section 4.3, and the correlation with indirect detection in section 4.4. We discuss the implications of a strongly self-interacting Dark Matter in this model in section 4.5, just before moving onto summarizing our findings in section 5. We conclude in section 6 by providing a summary of the results and outlook of possible new directions of investigation.

2 A dark sector with $\mathrm{U}(1)_{B-L}$

We consider the following set-up: we extend the SM with a complex scalar field, ϕ and n chiral (RH) fermion fields, Ψ_R. All these new fields are SM singlets, and charged under a global U(1) symmetry which can be identified with $\mathrm{U}(1)_{B-L}$, so that $L_\phi = 2$ and $L_{\Psi_R} = 1$.[1]

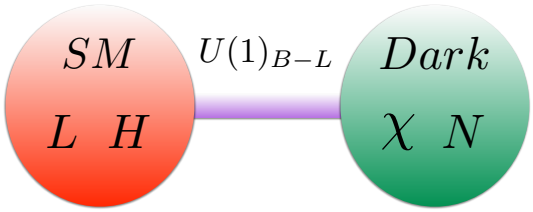

Moreover, we assume that (for the reasons explained below) some of the dark fermions have vanishing or suppressed coupling to the SM singlet operator $\overline{L}_L H$, so they could be stable (or cosmologically stable); we will denote such stable fermion(s) by χ_R, as opposed to the rest of the dark fermions, which we will call N_R.

Communication between the Standard Model fields and the new singlet sector (ϕ, Ψ_R) is determined by the $\mathrm{U}(1)_{B-L}$ charges and the requirement of renormalizability of the interactions. The relevant part of the Lagrangian reads:

$$\begin{aligned}\mathcal{L} \supset\ & \mu_H^2 H^\dagger H - \lambda_H (H^\dagger H)^2 + \mu_\phi^2 \phi^\dagger \phi - \lambda_\phi (\phi^\dagger \phi)^2 - \lambda_{H\phi} (H^\dagger H)\,(\phi^\dagger \phi) \\ & - \left(\frac{\lambda_{\chi ab}}{\sqrt{2}} \phi\, \overline{\chi}_{Ra} \chi^c_{Rb} + h.c. \right) - \left(\frac{\lambda_{Nab}}{\sqrt{2}} \phi\, \overline{N}_{Ra} N^c_{Rb} + h.c. \right) - (Y_{\alpha a} \overline{L}^\alpha_L H N_{Ra} + h.c.)\end{aligned} \tag{2.1}$$

[1] Note that $\mathrm{U}(1)_{B-L}$ is the only anomaly-free global symmetry in the SM. Therefore, extensions of the SM including a *gauged* $\mathrm{U}(1)_{B-L}$ have been considered in various contexts, and in particular in scenarios where the breaking appears at low-scale (e.g. [6–9]).

JHEP02(2017)045

where $\alpha = e, \mu, \tau$ denotes lepton flavour, a, b refers to the different dark fermion species and the Yukawa coupling matrices λ_χ, λ_N are symmetric.

The coupling between the Higgs and the complex scalar ϕ, $\lambda_{H\phi}$, is a generalized *Higgs portal* coupling, whereas the direct coupling between the right-handed fermions N_R and the SM via the mixing term $Y_{\alpha a}$ leads to masses for the active neutrinos. The Yukawa coupling between the dark scalar and dark fermions λ_χ, λ_N generates a Majorana mass for the χ fields and sterile neutrinos provided ϕ develops a vev. Details on neutrino mass generation in this set-up can be found in section 3.1.

So far, we have described a new sector linked to the origin of neutrino masses. We now consider whether this sector could also describe Dark Matter. In our set-up there are two possible candidates *1.)* the right-handed fermions χ_{Ra}, and/or *2.)* a component of the complex scalar field ϕ. We discuss in turn each possibility.

Fermionic Dark Matter: possible mechanisms to ensure stability of the dark fermions χ_R could be:

1. Z_2 *symmetry:* the simplest possibility is that the fermions χ_R are odd under an exact Z_2 symmetry, while all the SM particles, the singlet scalar ϕ and the remaining fermions N_R are even. Then, the Yukawa coupling of χ_R to SM leptons will be forbidden, resulting on a stable sterile neutrino Dark Matter.

2. *Compositeness:* the dark sector is a low-energy description of a new strongly coupled sector (charged under the global $\mathrm{U}(1)_{B-L}$), with the dark particles bound states of the strong dynamics. Mixing between the SM operator $\overline{L}^\alpha_L H$ and fermionic bound states $\mathcal{O}^a$ with lepton number are allowed, but the strength of this mixing is determined by the anomalous dimension of $\mathcal{O}^a$. One could also describe this set-up in terms of a holographic dual, where operators from a strongly coupled sector like $\mathcal{O}^a$ are represented by states living in more than 4D, $\mathcal{O}^a(x) \to \chi_R(x, z)$, with z is the extra dimensional coordinate. In this holographic picture, the SM particles (lepton doublets, Higgs) are localized at some distance from where the fields χ_R have their main support. The values of $Y_{\chi\alpha a}$ are obtained via dimensional reduction from 5D to 4D, namely computing overlaps of the wavefunctions of the Higgs, lepton doublets and dark fermions [10, 11]

$$Y_{\chi\alpha a} \propto \int dz f_H(z) f_{L^\alpha}(z) f_{\chi_{Ra}}(z)\,. \tag{2.2}$$

   In warped geometries, $\mathcal{O}(1)$ differences in localization parameters can lead to exponential hierarchies among the different entries in $Y_{\chi\alpha a}$ [12] and hence (meta)stability of some dark fermions.

3. *Exotic lepton number:* if there are at least two Weyl fermions in the dark sector, they could have lepton number different from ± 1, so that the Yukawa interaction $\overline{L}^\alpha_L H \chi_{Ra,b}$ is forbidden but the coupling $\phi\, \overline{\chi}_{Ra} \chi^c_{Rb}$ is allowed provided $L_a + L_b = -2$. This scenario leads to Dirac Dark Matter particle, and has been explored in [13] in the context of the Zee-Babu model for neutrino masses.

JHEP02(2017)045

4. *Different dark sector representations:* the dark sector could have further symmetry structure (more complex than the simple Z_2 symmetry described above), so that some of the chiral fermions are singlets under the dark symmetry group and thus can couple to $\overline{L}_L^{\alpha} H$, while χ_{Ra} may transform non trivially under the dark group. Then, $\phi\, \overline{\chi}_{Ra} \chi^c_{Ra}$ is invariant and thus allowed, but the Yukawa coupling with the SM fermions is forbidden by the dark symmetry.

In this paper we assume that either mechanism 1 or 3 are at work, and we discuss the phenomenology of these two minimal realizations. In the case of an additional dark sector symmetry, if it is global the only difference will be an extra factor in the annihilation cross sections of section 4.3, related to the dimension of the representation to which χ_R belongs, so our results can be easily re-scaled; however, if the dark symmetry is gauged, Dark Matter self-interactions could modify some of our findings.

Scalar Dark Matter: the imaginary part of the complex field (the so-called Majoron, η) could be a Dark Matter candidate [6, 14] provided it acquires a mass, e.g. via non-perturbative gravitational effects which break the global symmetry [15, 16]. For a recent review on the subject see [17].

A massive Majoron decays at tree level to a pair of light neutrinos with a rate that scales as [16]:

$$\Gamma(\eta \to \nu\nu) = \frac{m_\eta}{8\pi} \left(\frac{m_\nu}{v_\phi}\right)^2 , \tag{2.3}$$

where m_ν is the mass scale of ordinary neutrinos and v_ϕ the scale of $\mathrm{U}(1)_{B-L}$ spontaneous breaking. Therefore, for instance if $m_\eta \lesssim 10\,\mathrm{keV}$ and $v_\phi \gtrsim 10^8\,\mathrm{GeV}$, the lifetime of the Majoron can be large enough for it to be stable on cosmological scales, while for v_ϕ in the TeV range the Majoron decays very fast.

Moreover, the massive Majoron might also decay into two photons at the loop level, although this mode is model-dependent. While it does not occur in the minimal singlet Majoron scenario that we are considering, it is induced at one loop in the more general see-saw model which includes also a triplet scalar field coupled to the SM lepton doublets [18], and it could also be present if the dark sector contains other chiral fermion representations charged under the SM gauge group with masses of order $\Lambda \gg v_\phi$, which would make the global symmetry $\mathrm{U}(1)_{B-L}$ anomalous. Current experimental bounds on pseudo-Goldstone bosons with $\mathrm{BR}(\eta \to \gamma\gamma) \sim 1$ imply that it can have a lifetime longer than $\sim 10^{20}$ years if its mass is $m_\eta \lesssim 100\,\mathrm{keV}$, while for heavier masses, $m_\eta \gtrsim 10\,\mathrm{MeV}$, the lifetime has to be shorter than one minute [19].

Both Dark Matter candidates, a keV scale sterile neutrino and a massive Majoron have received much attention in the literature, so we do not explore such possibilities any further in this paper. Instead, we focus on the fermionic Dark Matter scenario extending the study to larger masses, in the typical WIMP range, which to our knowledge has not been considered up to now. It has been studied in the framework of gauged $\mathrm{U}(1)_{B-L}$, however then there is also a new Z' gauge boson and constraints from direct searches set a lower bound on the scale of $\mathrm{U}(1)_{B-L}$ symmetry breaking of order few TeV [20]. As

JHEP02(2017)045

a consequence, the correct Dark Matter relic abundance can only be obtained near the resonance regions, when twice the Dark Matter mass is approximately equal to the mass of any of the mediators [21].

Notice that our scenario differs from one without spontaneous symmetry breaking in several ways. In the absence of the $U(1)_{B-L}$ global symmetry, masses for the Dark Matter and sterile neutrinos, which explicitly break lepton number, should be added by hand instead of being a consequence of the breaking of $U(1)_{B-L}$. Therefore in that case they would be independent of their corresponding couplings to the dark scalar ϕ, while in our case they are related by the vev of ϕ (see section 3). Moreover, there would not be a Goldstone boson, and one would expect the real and the imaginary components of the scalar ϕ to have masses of the same order.

3 Parametrization of the physical states

Both the SM Higgs and the complex scalar ϕ can develop vevs, which would break the symmetry group $SU(2)_L \times U(1)_Y \times U(1)_{B-L} \to U(1)_{em} \times Z_2$. We parametrize the scalar sector as:

$$H = \begin{pmatrix} G^+ \\ \frac{v_H + \tilde{h} + iG^0}{\sqrt{2}} \end{pmatrix}, \qquad \phi = \frac{v_\phi + \tilde{\rho} + i\eta}{\sqrt{2}}, \tag{3.1}$$

where $v_H = 245\,\text{GeV}$. The minimization of the scalar potential in eq. (2.1), leads to the following tree-level relations between the Lagrangian parameters and the vacuum expectation values of the fields H, ϕ:

$$\mu_H^2 = \lambda_H v_H^2 + \frac{1}{2}\lambda_{H\phi} v_\phi^2, \qquad \mu_\phi^2 = \lambda_\phi v_\phi^2 + \frac{1}{2}\lambda_{H\phi} v_H^2. \tag{3.2}$$

The scalar sector then contains two CP even massive real scalars, $\tilde{h}$ and $\tilde{\rho}$ which mix and upon diagonalization of the mass matrix lead to the mass eigenstates h and ρ, with masses m_h and m_ρ, respectively. The state h is identified with the scalar boson of $m_h = 125$ Gev discovered at the LHC.

The masses of the physical states are:

$$m_h^2 = 2\lambda_H v_H^2 \cos^2\theta + 2\lambda_\phi v_\phi^2 \sin^2\theta - \lambda_{H\phi} v_H v_\phi \sin 2\theta \tag{3.3}$$

$$m_\rho^2 = 2\lambda_H v_H^2 \sin^2\theta + 2\lambda_\phi v_\phi^2 \cos^2\theta + \lambda_{H\phi} v_H v_\phi \sin 2\theta \tag{3.4}$$

and the mixing angle

$$\tan 2\theta = \frac{\lambda_{H\phi} v_H v_\phi}{\lambda_\phi v_\phi^2 - \lambda_H v_H^2} \tag{3.5}$$

There is also a CP odd massless real scalar η, which is the Goldstone boson of the spontaneous breaking of the global $U(1)_{B-L}$ symmetry, the Majoron [6]. We assume that, even if quantum gravity effects break the global $U(1)_{B-L}$ and provide a mass to the Majoron, it is much lighter than the other dark particles, i.e., $m_\eta \ll \mathcal{O}(\text{GeV})$ and we neglect it in our analysis.

JHEP02(2017)045

The quartic couplings in the Lagrangian can be written in terms of the physical masses and the mixing angle in the CP even scalar sector as follows:

$$\begin{aligned} \lambda_H &= \frac{m_h^2 \cos^2\theta + m_\rho^2 2v_H^2}{2v_H^2} \\ \lambda_\phi &= \frac{m_h^2 \sin^2\theta + m_\rho^2 \cos^2\theta}{2v_\phi^2} \\ \lambda_{H\phi} &= \frac{(m_\rho^2 - m_h^2)\sin 2\theta}{2v_H v_\phi} \end{aligned} \tag{3.6}$$

Regarding the (neutral) lepton sector of the model, let us denote χ the fermion without Yukawa coupling to the SM lepton doublets, i.e., the Dark Matter candidate, and N_a the fermions with couplings $Y_{\alpha a}$, i.e., the right-handed neutrinos. In terms of the Majorana fields

$$\chi = \chi_R + (\chi_R)^c\,, \qquad N = N_R + (N_R)^c\,, \tag{3.7}$$

the fermionic part of the Lagrangian (2.1) can be written as

$$\mathcal{L} = -\frac{\lambda_\chi}{\sqrt{2}}\left(\phi\,\overline{\chi}P_L\chi + \phi^*\,\overline{\chi}P_R\chi\right) - \frac{\lambda_N}{\sqrt{2}}\left(\phi\,\overline{N}P_L N + \phi^*\,\overline{N}P_R N\right) - \left(Y\overline{L}HP_R N + h.c.\right) \tag{3.8}$$

After the $\mathrm{U}(1)_{B-L}$ symmetry breaking, the chiral fermions acquire Majorana masses, $m_\chi = \lambda_\chi v_\phi$, $m_N = \lambda_N v_\phi$, and $\mathcal{L}$ becomes

$$\begin{aligned} \mathcal{L} = &-\frac{m_\chi}{2}\overline{\chi}\chi - \frac{\lambda_\chi}{2}\left[(-h\,\sin\theta + \rho\cos\theta)\overline{\chi}\chi - i\eta\overline{\chi}\gamma_5\chi\right] \\ &-\frac{m_N}{2}\overline{N}N - \frac{\lambda_N}{2}\left[(-h\,\sin\theta + \rho\cos\theta)\overline{N}N - i\eta\overline{N}\gamma_5 N\right] - \left(Y\overline{L}HP_R N + h.c.\right) \end{aligned} \tag{3.9}$$

Note that so far we have considered N and χ as Majorana fields, yet degeneracies in the fermion mass matrix could lead to Dirac states. Indeed, one could find UV models where the structure of λ_{ab} leads to two nearby states χ_1 and χ_2 which then would form a Dirac Dark Matter candidate [22]. An example of this idea has been discussed in the previous section 2 under exotic lepton number. See [23] for an alternative realization of the global $\mathrm{U}(1)_{B-L}$ symmetry in which the dark fermions can naturally be pseudo-Dirac, in the context of an extended seesaw scenario for neutrino masses.

3.1 Neutrino masses

In this section we briefly review the generation of (light) neutrino masses, namely TeV scale seesaw mechanism of type I. We denote ν_α the active neutrinos and N_s' the sterile ones. After electroweak symmetry breaking, the neutrino mass matrix in the basis (ν_α, N_s') is given by

$$\mathcal{M}_\nu = \begin{pmatrix} 0 & m_D \\ m_D^T & m_N \end{pmatrix}, \tag{3.10}$$

where $m_D = Y v_H/\sqrt{2}$ and $Y_{\alpha s}$ are the Yukawa couplings. Without loss of generality we can take the sterile neutrino Majorana mass matrix m_N real and diagonal in the N' basis.

JHEP02(2017)045

The matrix $\mathcal{M}_\nu$ can be diagonalized by a unitary matrix U, so that

$$\mathcal{M}_\nu = U^* \, Diag(m_\nu, M) \, U^\dagger \,, \tag{3.11}$$

where m_ν is the diagonal matrix with the three lightest eigenvalues of $\mathcal{M}_\nu$, of order m_D^2/m_N, and M contains the heavier ones, of order m_N.

The physical neutrinos $\mathbf{n} = (\nu_i, N_h)$ are related to the active and sterile ones, (ν_α, N'_s) by

$$\begin{pmatrix} \nu_\alpha \\ N'_s \end{pmatrix}_L = U^* \begin{pmatrix} \nu_i \\ N_h \end{pmatrix}_L . \tag{3.12}$$

The unitary matrix U can be written as

$$U = \begin{pmatrix} U_{\alpha i} & U_{\alpha h} \\ U_{si} & U_{sh} \end{pmatrix} , \tag{3.13}$$

where, at leading order in the seesaw expansion parameter, $\mathcal{O}(m_D/m_N)$:

$$\begin{aligned} U_{\alpha i} &= [U_{PMNS}]_{\alpha i} \qquad U_{sh} = I \\ U_{\alpha h} &= [m_D m_N^{-1}]^*_{\alpha h} \\ U_{si} &= -[m_N^{-1} m_D^T \, U_{PMNS}]_{si} \,. \end{aligned} \tag{3.14}$$

Notice that at this order the states N and N' coincide, so we identify them in the rest of this paper.

Neglecting the mixing between the CP-even scalars, the Yukawa coupling of the SM-like Higgs field h to the neutrinos can be written as [24]:

$$\mathcal{L}_Y = -\frac{h}{2v_H} \bar{\mathbf{n}}_i [(m_i + m_j) Re(C_{ij}) + i\gamma_5 (m_j - m_i) Im(C_{ij})] \mathbf{n}_j \,, \tag{3.15}$$

where the indices i, j refer to the light neutrinos ν_i for $i, j = 1, 2, 3$ and to N_h for $i, j = 4, 5, 6$, and the matrix C can be written in terms of the mixing matrix U as:

$$C_{ij} = \sum_{\alpha=1}^{3} U_{\alpha i} U^*_{\alpha j} \,. \tag{3.16}$$

4 Phenomenology

In this section we study the phenomenology of the proposed scenario. The main features of the model are determined by the interactions within the dark sector, i.e. Dark Matter, right-handed neutrinos, the scalar mediator ρ and the Majoron η, and communication of the dark sector with the Higgs and leptons. This table summarizes the source of constraints on the parameters of our model which we will explore in this section:

Parameter	Constraint
Mixing h and ρ	$\mathrm{BR}_{\mathrm{inv}}$ and DD
Mixing N and ν	$h \to$ exotic
Dark χ, N and ρ	Ω_{DM}, DD and ID
Majoron η	N_{eff} and SIDM

JHEP02(2017)045

Figure 1. (Left) Decay of the Higgs to two Majorons η via the mixing of the Higgs with ρ. (Right) Exotic decay of the Higgs into a light neutrino and a dark fermion via their mixing.

The mixing of the two scalars, the Higgs h and ρ, is tightly constrained by *1.)* limits on the Higgs invisible width $\mathrm{BR}_{\mathrm{inv}}$ and global fits on Higgs properties as discussed on section 4.1 and *2.)* limits on direct detection (DD) from LUX [25, 26], and XENON1T [27] in the near future, see section 4.2.

The mixing of the dark fermions N and the left-handed SM neutrinos via their coupling to the Higgs produces a spectrum of massive neutrinos (see section 3.1), but also leads to exotic decays of the Higgs to a dark fermion and a light neutrino. These are discussed in section 4.1.

The interactions and masses of the dark fermions, Dark Matter χ and heavy neutrinos N, and the dark scalar ρ can be probed in several ways. In section 4.3 we explain constraints from relic abundance $\Omega_{\mathrm{DM}}h^2$ from Planck [28, 29], which provide information on the interplay among the competing annihilation processes, mainly the balance between the right-handed neutrino channel $\chi\chi \to NN$ and the annihilation to dark scalars, $\chi\chi \to \eta\rho$ and $\to \eta\eta$. Direct detection (DD) would provide complementary information, but it relies on the mixing of the dark scalar to the Higgs as mentioned above. Finally, annihilation of Dark Matter today could lead indirect detection (ID) signatures, namely features in the gamma-ray spectrum and signals in neutrino telescopes. These are discussed in section 4.4.

Finally, properties of the Majoron dark scalar η can be probed by imprints in the CMB, such as N_{eff} (see section 4.4) as well as by constraints on self-interacting Dark Matter (SIDM) which come from lensing and numerical simulations.

To deduce the constraints, we perform a simple Monte Carlo scan over the parameters in logarithmic scale, restricting the values of the couplings to the perturbative range, $\lambda_{\chi,N,\phi} \lesssim \mathcal{O}(1)$ and the masses in the region of interest, m_χ & m_N from 1 GeV to 2 TeV, m_ρ from 0.1 GeV to 10 TeV and $|\theta|$ from 10^{-4} to π. For the numerical implementation we made use of `LanHep` [30] and `micrOMEGAs` [31] in order to obtain the correct relic abundance, Higgs decays and today's annihilation cross section. We calculate 10^6 points that match the *Planck* constraint on the Dark Matter abundance at 3σ [29], namely $\Omega h^2 = 0.1198 \pm 0.0045$.

4.1 Constraints from Higgs decays

In the two scenarios that we consider, the enlarged fermion and scalar sectors lead to new decays of the Higgs boson, h as shown in figure 1. ATLAS and CMS constrain the invisible

JHEP02(2017)045

Higgs decay branching fraction as [32, 33]

$$\mathrm{BR}_{\mathrm{inv}} = \frac{\Gamma_{\mathrm{inv}}}{\Gamma_{\mathrm{inv}} + \Gamma_{\mathrm{SM}}} < 0.23 \qquad (95\%\mathrm{CL})\,, \tag{4.1}$$

where the SM Higgs width is $\Gamma_{\mathrm{SM}} \approx 4\,\mathrm{MeV}$.

The mixing of the two CP-even real scalars induce the following decay channels:

$$\Gamma(h \to \eta\eta) = \frac{m_h^3}{32\pi v_\phi^2} \sin^2\theta \tag{4.2}$$

$$\Gamma(h \to \rho\rho) = \frac{(m_h^2 + 2m_\rho^2)^2}{128\pi m_h^2 v_H^2 v_\phi^2} \sqrt{m_h^2 - 4m_\rho^2} (v_H \cos\theta - v_\phi \sin\theta)^2 \sin^2 2\theta \tag{4.3}$$

$$\Gamma(h \to \chi\chi) = \frac{\lambda_\chi^2}{16\pi} \left(1 - \frac{4m_\chi^2}{m_h^2}\right)^{3/2} m_h \sin^2\theta \tag{4.4}$$

$$\Gamma(h \to NN) = \frac{\lambda_N^2}{16\pi} \left(1 - \frac{4m_N^2}{m_h^2}\right)^{3/2} m_h \sin^2\theta, \tag{4.5}$$

where we have neglected contributions to $h \to NN$ from the mixing among sterile and active neutrinos. This is justified by the smallness of the mixing, $\mathcal{O}(\sqrt{m_\nu/m_N})$. The decay to SM particles is modified as

$$\Gamma(h \to \mathrm{SM\,particles}) = \cos^2\theta\, \Gamma_{\mathrm{SM}}\,. \tag{4.6}$$

These global modifications of the Higgs couplings are equivalent to the well-studied case of mixing of the Higgs with a singlet and are well constrained [32, 33]. In the low m_ρ region, the constraints one obtains from the invisible width is of the same order as this overall shift, hence below we use $\mathrm{BR}_{\mathrm{inv}}$ as experimental input. Note that the corresponding expressions for ρ decays widths are obtained by exchanging $\sin\theta \to \cos\theta$ and $m_h \to m_\rho$.

From the equation of the h decay rate into two Majorons, $\Gamma(h \to \eta\eta)$, the experimental upper limit on the invisible decay width of the Higgs boson leads to the following upper bound on the mixing angle θ [34]:

$$|\tan\theta| \lesssim \sqrt{\frac{32\pi v_\phi^2 \Gamma_{\mathrm{Higgs}}^{\mathrm{SM}} \mathrm{BR}_{\mathrm{inv}}}{m_h^3(1 - \mathrm{BR}_{\mathrm{inv}})}} \sim 2.2 \times 10^{-3} \left(\frac{v_\phi}{10\,\mathrm{GeV}}\right) \tag{4.7}$$

Including the other decay processes, when kinematically allowed, would reduce further the upper limit.

The Yukawa interaction term $Y\overline{L}HP_RN$ also leads to novel Higgs decay channels into neutrinos, even in the absence of mixing between de CP-even scalars. The corresponding decay width reads (for $\theta = 0$):

$$\Gamma(h \to \mathrm{n}_i\mathrm{n}_j) = \frac{\omega}{8\pi m_h} \lambda^{1/2}(m_h^2, m_i^2, m_j^2) \left[S\left(1 - \frac{(m_i + m_j)^2}{m_h^2}\right) + P\left(1 - \frac{(m_i - m_j)^2}{m_h^2}\right)\right], \tag{4.8}$$

JHEP02(2017)045

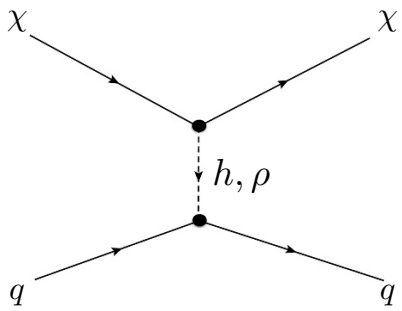

Figure 2. Dark matter interaction relevant to direct detection constraints.

where $\lambda(a,b,c)$ is the standard kinematic function, $w = 1/n!$ for n identical final particles and the scalar and pseudoscalar couplings are:

$$S = \frac{1}{v_H^2}[(m_i + m_j)Re(C_{ij})]^2\,, \qquad P = \frac{1}{v_H^2}[(m_j - m_i)Im(C_{ij})]^2\,, \tag{4.9}$$

with C_{ij} defined in eq. (3.16). The largest branching ratio is for the decay into one light and one heavy neutrino [35]:

$$\Gamma(h \to \nu N) = \frac{m_N^2}{8\pi v_H^2}\left(1 - \frac{m_N^2}{m_h^2}\right)^2 m_h |C_{\nu N}|^2\,. \tag{4.10}$$

The attainable values for the above branching fractions have been analyzed in [35], for the case of two heavy neutrinos, parameterizing the Yukawa couplings in terms of the observed light neutrino masses and mixing angles, and a complex orthogonal matrix. After imposing the relevant constraints from neutrinoless double beta decay, lepton flavour violating processes and direct searches of heavy neutrinos, they find that branching ratios of $h \to \nu N$ larger than 10^{-2} are generally ruled out for heavy neutrino masses $m_N \leq 100\,\text{GeV}$, and typically they are much smaller, due to the tiny Yukawa couplings required to fit light neutrino masses with sterile neutrinos at the electroweak scale. Therefore, the contribution of such decay modes to the Higgs decay width is negligible, and they do not alter the bounds discussed above.

4.2 Direct detection

In this scenario, Dark Matter scattering on nuclei relevant for direct Dark Matter detection is mediated via t-channel exchange by the CP even mass eigenstates, h, ρ and it is spin-independent, see figure 2.

The elastic scattering cross section of χ off a proton is given by [19]:

$$\sigma_{\chi p} = C^2\,\frac{(\lambda_\chi \sin 2\theta)^2}{4\pi v_H^2}\,\frac{m_p^4 m_\chi^2}{(m_p + m_\chi)^2}\left(\frac{1}{m_h^2} - \frac{1}{m_\rho^2}\right)^2\,, \tag{4.11}$$

where m_p stands for the proton mass and $C \simeq 0.27$ is a constant that depends on the nuclear matrix element [31].

JHEP02(2017)045

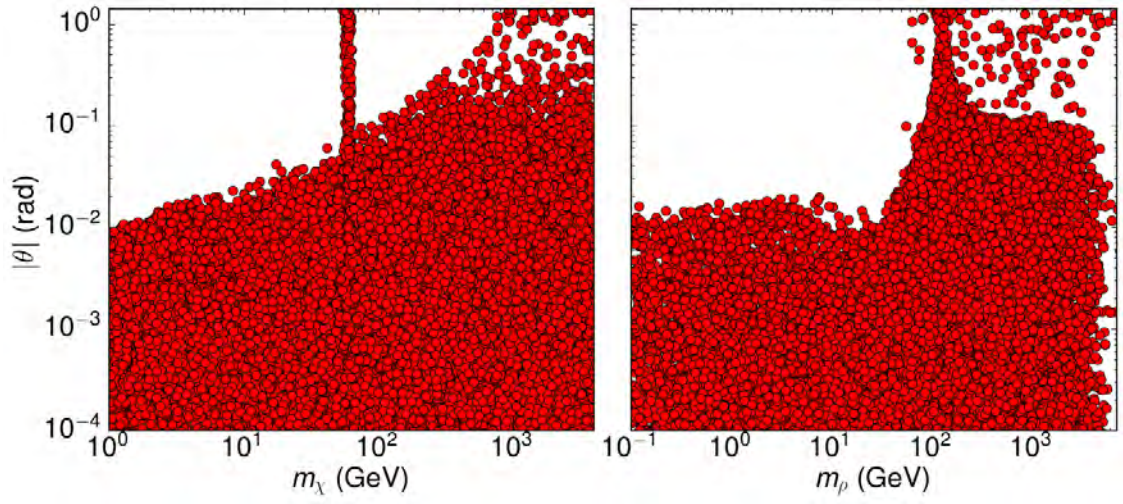

Figure 3. Allowed values of the mixing between the Higgs and the dark sector as a function of the Dark Matter mass (left) and the scalar mediator ρ (right) after imposing the constraints from LUX and the Higgs invisible decay width. Large values of the mixing are possible only in the somewhat tuned regions $m_\chi \simeq m_h/2$ and $m_\rho \simeq m_h$.

The constraints on the combination $\lambda_\chi |\sin 2\theta|$ both from the invisible Higgs decay width and from the LUX experiment [36] have been thoroughly analyzed in [19], in a model where the Dark Matter is a chiral fermion charged under a global U(1) symmetry spontaneously broken by a SM singlet scalar, ϕ. Although such scenario does not include the further interaction among ϕ and the sterile neutrinos which can be present when the global U(1) is identified with $\mathrm{U}(1)_{B-L}$, the limits from direct Dark Matter searches apply exactly the same, and the bounds from the Higgs invisible width will be even stronger in our case, since there are new non-standard decays contributing to it, namely $\Gamma(h \to NN)$.

We have analyzed the constraints on the mixing in our model, and found that for low values of m_χ and m_ρ the stronger limit comes from the invisible Higgs decay width, while for higher masses the bound is determined by direct detection experiments. When applying both constraints altogether they exclude $\theta \gtrsim 0.1$ for all parameter space but the region $m_\rho \simeq m_h$, where a cancellation in the direct detection cross section occurs, see eq. (4.11), and the regions $m_\chi \simeq m_h/2$, $m_\chi \simeq m_\rho/2$, where a resonance in the Dark Matter annihilation cross section mediated by the Higgs or the ρ occurs. These results are shown in figure 3, where the allowed values of the mixing as a function of the Dark Matter mass and mediator ρ are shown back-to-back, to illustrate the correlation between the points of $\theta \gtrsim 0.1$ and the regions where $m_\chi \simeq m_h/2$ (left) or $m_\rho \simeq m_h$ (right).

4.3 Dark Matter relic abundance

The Dark Matter annihilations into SM particles are strongly suppressed due to the bounds on θ discussed in the previous section, except when $m_\rho \simeq m_h$ and in the resonance regions $m_\chi \sim m_h/2$ or $m_\chi \sim m_\rho/2$. Moreover such annihilations channels are p-wave suppressed. Keeping in mind that these somehow fine-tuned possibilities are always open, we focus on

JHEP02(2017)045

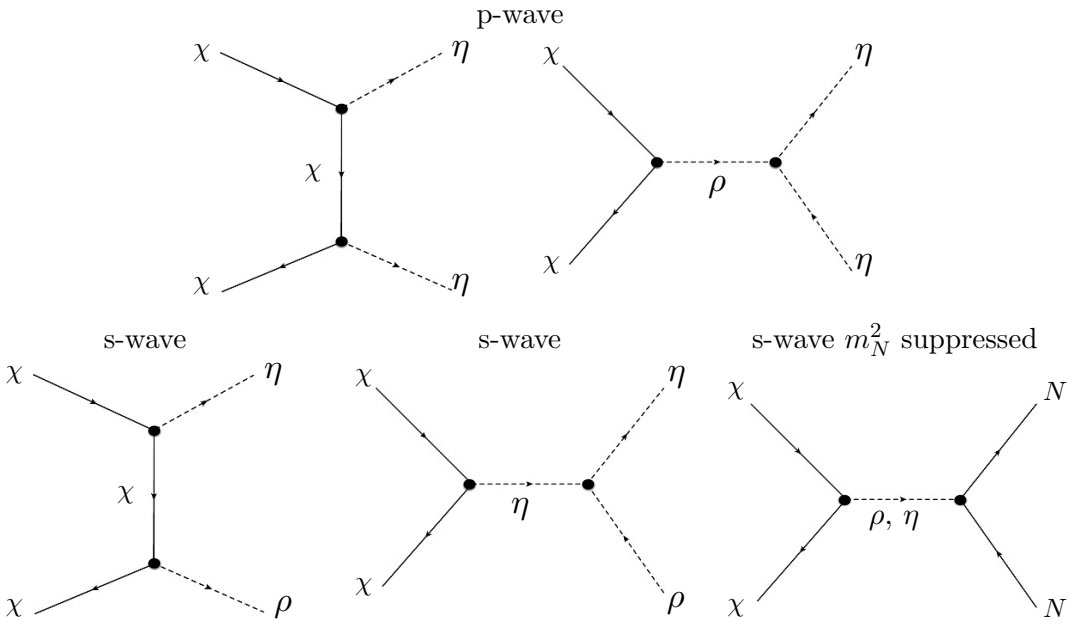

Figure 4. Diagrams relevant to the relic abundance computation.

the dominant annihilation channels, involving the new scalars ρ, η as well as the sterile neutrinos N, see figure 4. For simplicity, in the following we will only consider one generation of right-handed neutrinos, but extending the discussion to more generations will be straightforward. Therefore, in order to reduce the large number of free parameters in this analysis we set the mixing angle $\theta = 0$, and we scan over the remaining independent variables, chosen to be m_χ, m_N, m_ρ and λ_χ.

There are two channels with s-wave annihilation cross-section, the production of two right-handed neutrinos and the final state $\eta\rho$,

$$\begin{aligned}\sigma_{\chi\chi\to\rho\eta} v_{\rm rel} &= \frac{m_\chi^2}{1024\pi v_\phi^4}\left(4 - r_\rho^2\right)^3 + \mathcal{O}(v_{\rm rel}^2)\,,\\ \sigma_{\chi\chi\to NN} v_{\rm rel} &= \frac{m_N^2}{64\pi v_\phi^4}\sqrt{1 - r_N^2} + \mathcal{O}(v_{\rm rel}^2)\,.\end{aligned} \tag{4.12}$$

Other possible channels are p-wave suppressed,

$$\begin{aligned}\sigma_{\chi\chi\to\eta\eta} v_{\rm rel} &= \frac{m_\chi^2}{192\pi v_\phi^4}\frac{8 + r_\rho^4}{\left(r_\rho^2 - 4\right)^2} v_{\rm rel}^2\,,\\ \sigma_{\chi\chi\to\rho\rho} v_{\rm rel} &= \frac{m_\chi^2}{384\pi v_\phi^4}\frac{\sqrt{1 - r_\rho^2}}{\left(r_\rho^2 - 4\right)^2}\left(144 - 32 r_\rho^2\right) v_{\rm rel}^2 + \mathcal{O}(r_\rho^4).\end{aligned} \tag{4.13}$$

Here $v_{\rm rel} = 2\sqrt{1 - 4m_\chi^2/s}$ is the relative velocity of the Dark Matter in the center of mass frame and the ratios are given by $r_\rho = m_\rho/m_\chi$ and $r_N = m_N/m_\chi$.

As the annihilation channel into sterile neutrinos is not velocity suppressed, it can be comparable to the scalar channels, $\chi\chi \to \eta\eta, \rho\rho, \eta\rho$, which alike the NN channel, are not

JHEP02(2017)045

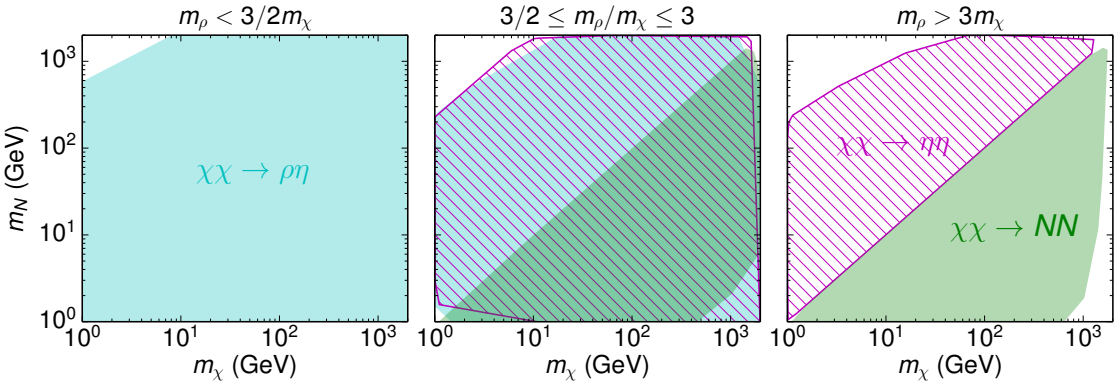

Figure 5. Allowed values of dark fermion masses, m_χ and m_N. The different colours correspond to regions in parameter space in which the annihilation channel constitutes more than 60% of the total cross section for $v = 10^{-3}c$, as relevant for indirect detection.

vanishing even in the case of zero $h - \rho$ mixing. We find that there is a significant fraction of the parameter space of the model in which the annihilation channel into NN is relevant, and even dominant. This is shown in figure 5, where allowed values of dark fermion masses, m_χ and m_N are depicted, with different colours corresponding to regions with dominance of one channel in the annihilation cross section for $v = 10^{-3}c$, as relevant for the calculation of direct detection constraints. The three panels of figure 5 correspond to different ranges of the dark scalar mass, m_ρ. In particular, in the middle panel we have singled out the region $3/2 \leq m_\rho/m_\chi \leq 3$, where the annihilation into $\eta\eta$ is resonantly enhanced.

On the other hand, the annihilation channel $\eta\rho$ tends to dominate when kinematically accessible (i.e., in the region $m_\rho < 2m_\chi$, since we are neglecting the mass of the Majoron, m_η), as it is parametrically enhanced respect to the other s-wave channel into right-handed neutrinos by $(m_\chi/m_N)^2$. Finally, in the range $m_\rho > 2m_\chi$, the two channels NN and $\eta\eta$ compete: the former dominates when $m_N \lesssim m_\chi$ and $m_\rho > 3m_\chi$, while in the resonance region $3/2 \leq m_\rho/m_\chi \leq 3$ we find that any of the two annihilation channels may dominate, as well as the $\eta\rho$ if open (central panel).

Interestingly, the $\eta\eta$ channel could have dominated the dynamics at freeze out, with the NN channel playing an spectator role, but for the usual velocities that the Dark Matter particles have in the galactic halo $v \simeq 10^{-3}c$, the NN channel could dominate the Dark Matter annihilation at later times. However, even if dominant, the cross section may be too small to lead to any indirect detection signature (see figure 8).

Notice that due to the $\mathrm{U}(1)_{B-L}$ symmetry, there is a non trivial relation between the mass of the sterile neutrinos and the Dark Matter annihilation cross section into them, since both are proportional to the coupling λ_N. As a consequence, when the sterile neutrinos are very light, and the phase space is more favourable, the coupling is too small and the annihilation into sterile neutrinos is suppressed. On the other hand, if the coupling λ_N is large, the sterile neutrinos are too heavy, and this annihilation channel is phase space suppressed or even forbidden. Due to this relation between sterile neutrino masses and coupling to the scalar ϕ, the Dark Matter annihilation cross section into NN, although

JHEP02(2017)045

s-wave, does not always dominate over the p-wave suppressed $\eta\eta$ channel, which can be enhanced near the resonance, $m_\chi \sim m_\rho/2$.

4.4 Constraints from indirect searches and CMB

Dark Matter is also searched for indirectly, through the detection of SM products (photons, neutrinos and antiparticles) from its annihilation (or decay) in dense regions of the Universe, such as the center of the Milky Way. In particular, detection of gamma rays and neutrinos are useful because the signal can be traced back to the source.

Our scenario predicts that Dark Matter particles could be annihilating in the center of the galaxy through the s-wave processes $\chi\chi \to \eta\rho, NN$, if kinematically allowed. When the first annihilation channel dominates there are not photons in the final state since ρ also decays invisibly to $\eta\eta$. Although quantum gravity effects could explicitly break the global $\mathrm{U}(1)_{B-L}$ symmetry providing a mass to the Majoron, it would decay into light neutrinos [17], for which indirect detection constraints are quite weak, as we shall discuss below. Therefore, we do not expect gamma ray signals from Majoron decays, and we are left with the constraints from the NN channel.

Thus, in order to analyze the possible indirect detection signals we next discuss the relevant decay modes of the heavy neutrinos. In this section we also neglect the CP-even scalar mixing angle, θ, which is tightly constrained by the invisible Higgs decay width and direct Dark Matter searches, so it will not affect our results below.

The decay channel $N \to \nu\eta$ is always open (provided the Majoron mass is $m_\eta < m_N$), and neglecting the masses of the decay products its partial width is given by [37]:

$$\Gamma(N \to \nu_j \eta) = \frac{m_N^3}{128\pi v_\phi^2} \sum_j |R_{Nj}|^2 \,, \tag{4.14}$$

where in the seesaw limit $R_{Nj} = 2U_{Nj} = -2(m_N^{-1} m_D^T U_{PMNS})_{Nj}$ (we have summed over all the light neutrinos in the final state) and induces typical decay widths of the order

$$\Gamma(N \to \nu\eta) \simeq \frac{1}{32\pi} \left(\frac{m_N}{v_\phi}\right)^2 m_\nu \,, \tag{4.15}$$

so that they safely decay before Big-Bang nucleosynthesis.

Regarding the decays to SM particles, they depend on the mass of the heavy lepton, m_N. In the following we discuss two cases, depending on whether the neutrino is heavier or lighter than massive vector bosons.

Light right-handed neutrino, $m_N < m_W$: if the right-handed neutrino is lighter than the W boson, N will decay through off-shell h, Z, W bosons to three fermions. Since the decay via a virtual h is further suppressed by the small Yukawa couplings of the SM fermions, it is a very good approximation to consider only the processes mediated by virtual

JHEP02(2017)045

W, Z, whose partial widths read [37]:

$$\Gamma(N \to \nu q\bar{q}) = 3\, AC_{NN}[2(a_u^2 + b_u^2) + 3(a_d^2 + b_d^2)]f(z) \tag{4.16}$$

$$\Gamma(N \to 3\nu) = AC_{NN}\left[\frac{3}{4}f(z) + \frac{1}{4}g(z,z)\right] \tag{4.17}$$

$$\Gamma(N \to \ell q\bar{q}) = 6\, AC_{NN} f(w,0) \tag{4.18}$$

$$\Gamma(N \to \nu\ell\bar{\ell}) = AC_{NN}[3(a_e^2 + b_e^2)f(z) + 3f(w) - 2a_e g(z,w)] \tag{4.19}$$

where C_{NN} is defined in eq. (3.16),

$$A \equiv \frac{G_F^2 m_N^5}{192\,\pi^3}\,, \tag{4.20}$$

a_f, b_f are the left and right neutral current couplings of the fermions ($f = q, \ell$), the variables z, w are given by

$$z = (m_N/m_Z)^2\,, \qquad w = (m_N/m_W)^2\,, \tag{4.21}$$

and the functions $f(z), f(w,0)$ and $g(z,w)$ can be found in [38].

Assuming no strong cancellations in the mixing matrix U, we expect $C_{NN} \sim m_\nu/m_N$, so from the equations above we can estimate the ratio between the total decay width to three SM particles and the invisible decay width to $\nu\eta$, given by eqs. (4.14):

$$\frac{\Gamma(N \to 3\,\mathrm{SM})}{\Gamma(N \to \nu\eta)} \sim \frac{1}{\pi^2}\left(\frac{m_N}{v_H}\right)^2\left(\frac{v_\phi}{v_H}\right)^2 \lesssim 10^{-2}\left(\frac{v_\phi}{v_H}\right)^2\,, \tag{4.22}$$

where in the last term we have used that $m_N < 80\,\mathrm{GeV}$. Therefore the three-body decays to SM particles are suppressed when $m_N < m_W$ and the right-handed neutrino decays invisibly to $\nu\eta$, unless $v_\phi \gtrsim 10\, v_H$. On the other hand, the coupling between the sterile neutrinos and the Majoron η is $\lambda_N = m_N/v_\phi \lesssim 0.05$ for $v_\phi \gtrsim 1.6\,\mathrm{TeV}$, probably too small to have a significant DM annihilation cross section into NN in the first place.

Moreover, in the NN annihilation channel also light neutrinos are copiously produced, which could lead to observable signals at IceCUBE. These will depend on the neutrino energy, and therefore a detailed study of the final state spectrum is required to set constraints. Very roughly, for heavy Dark Matter we expect very energetic neutrinos, so that this scenario could be tested with current IceCUBE data, provided $E_\nu \gtrsim 100\,\mathrm{GeV}$. If the Dark Matter is lighter, or the neutrino energy spectrum softer, DeepCore will be needed to further constrain the parameter space, since it is expected to lower the IceCUBE neutrino energy threshold to about 10 GeV.

Heavy right-handed neutrino, $m_N > m_W$: for larger values of m_N, two body decays to SM particles are open, and the corresponding widths read [24]:

$$\Gamma(N \to W^\pm \ell_\alpha^\mp) = \frac{g^2}{64\pi}|U_{\alpha N}|^2 \frac{m_N^3}{m_W^2}\left(1 - \frac{m_W^2}{m_N^2}\right)^2\left(1 + \frac{2m_W^2}{m_N^2}\right) \tag{4.23}$$

$$\Gamma(N \to Z\,\nu_\alpha) = \frac{g^2}{64\pi c_W^2}|C_{\alpha N}|^2 \frac{m_N^3}{m_Z^2}\left(1 - \frac{m_Z^2}{m_N^2}\right)^2\left(1 + \frac{2m_Z^2}{m_N^2}\right) \tag{4.24}$$

$$\Gamma(N \to h\,\nu_\alpha) = \frac{g^2}{64\pi}|C_{\alpha N}|^2 \frac{m_N^3}{m_W^2}\left(1 - \frac{m_h^2}{m_N^2}\right)^2 \tag{4.25}$$

JHEP02(2017)045

In the above expressions, we have assumed that N is a Majorana fermion. From eqs. (4.14) and (4.23), we se that in this mass range the ratio between Majoron and SM particles decay widths is approximately given by

$$\frac{\Gamma(N \to \text{SM})}{\Gamma(N \to \nu\eta)} \sim \left(\frac{v_\phi}{v_H}\right)^2 . \tag{4.26}$$

Thus in this mass range we expect a significant flux of gamma rays from the galactic center produced by SM annihilation products, and bounds can be set from the Fermi-LAT Space Telescope gamma ray data. A detailed study of the indirect detection signatures of our scenario is beyond the scope of this work, since Dark Matter does not decay directly to SM particles, as it is usually assumed in most analysis, but to two right-handed neutrinos that subsequently decay to them. Therefore we just estimate here the expected constraints using current analysis. See section 5 for a discussion on how these limits affect the allowed region in the parameter space of our model.

Dark matter particles in the galactic halo can scatter elastically with a nucleus and become trapped in the gravitational well of an astronomical object, such as the Sun. They will undergo subsequent scatterings, and eventually thermalize and concentrate at the core of the object. The Dark Matter accumulated in this way may annihilate into SM particles, in particular neutrinos that can be detected by neutrino experiments like IceCUBE or SuperKamiokande. However we do not discuss this type of indirect detection constraints here, since in our scenario the limits from direct searches are tighter and moreover they can always be avoided with a small enough mixing angle between the CP-even scalars, which suppresses the DM-nucleon elastic cross-section still getting the correct Dark Matter relic abundance through annihilation into NN or $\eta\rho$, which is our case.

Measurements of the cosmic microwave background (CMB) anisotropies are also sensitive to Dark Matter annihilation during the cosmic dark ages, because the injection of ionizing particles will increase the residual ionization fraction, broadening the last scattering surface and modifying the anisotropies. Under the assumption that the power deposited to the gas is directly proportional to that injected at the same redshift, with some efficiency factor f_{eff}, constraints can be placed on the combination $f_{\text{eff}}\langle\sigma v\rangle/m_{\text{DM}}$, for different SM annihilation channels in s wave. Again, the available calculations of f_{eff} assume that Dark Matter annihilates directly to a pair of SM particles, and thus they are not directly applicable to our model, but we can roughly estimate the expected impact of such limits in the allowed parameter space assuming as before that the constraints will be similar for cascade decays. In [39], f_{eff} has been calculated as a function of the Dark Matter mass for a range of SM final states, and using the most recent results from the Planck satellite she found that for any linear combination of SM final states which does not contain a significant branching ratio of Dark Matter annihilation directly into neutrinos one must have $\langle\sigma v\rangle \lesssim 3\times10^{-27}(m_{\text{DM}}/1\,\text{GeV})\,\text{cm}^3/\text{s}$. However in our scenario when the Dark Matter (and thus the sterile neutrino) is lighter than m_W, the final states are ν, η and therefore the above limit does not apply.

Only for higher Dark Matter masses the final annihilation products can be charged leptons and gauge bosons, but in this range the CMB limits are above the thermal relic cross section, so they do not constrain our scenario.

JHEP02(2017)045

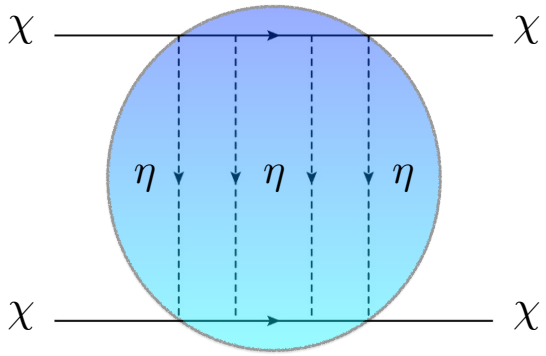

Figure 6. Diagram of self-interacting Dark Matter, via the exchange of a light pseudo-scalar.

The CMB also constrains the properties of the (massless) Majoron η, which constitutes a form of dark radiation and contribute to $N_{\rm eff}$ [34]. In ref. [19], it was shown that typically the limit on $N_{\rm eff}$ is already saturated by constraints from direct detection. In particular, for $m_\chi > 100\,\text{GeV}$, a non negligible contribution to dark radiation could only happen in a small range of m_ρ from 0.5 to 1 GeV.

4.5 Self-interacting Dark Matter

The dark sector contains a light particle, the Majoron η, coupled to Dark Matter. This opens the interesting possibility of a self-interacting Dark Matter candidate due to exchanges of the light particle via diagrams such as shown in figure 6.

Self-interacting Dark Matter could explain some of the issues encountered in simulations for small-scale structure formation which assume collisionless-DM [40], and typically predict too cuspy Dark Matter profiles. Self-interacting Dark Matter could explain the lack of satellites (although introducing baryons on the simulation seems to reduce inconsistencies [41, 42]) and more importantly the *too-big-to-fail* problem [43, 44] for $\sigma_{SI}/m_\chi \sim 0.1\text{-}10$ cm^2/g.

Direct limits on self-interactions of Dark Matter are provided by lensing. From the renowned bullet cluster limit [45] to observations of other astrophysical objects, Dark Matter self interactions have been bounded in the range of $\sigma_{SI}/m_\chi < 1$ cm^2/g. Interestingly, there has been a recent claim of a measurement of self-interactions in the system Abell 3827 [46] which lies above previous upper bounds. Note that this claim has been questioned by ref. [47], which propose modifications of the former analysis leading to limits similar to the bullet cluster's.

The effect of multiple exchanges of the light particle induces an Dark Matter effective potential between two dark particles χ of spin $\mathbf{s}$ at distance r

$$V_{\rm eff}(r) = -\frac{\lambda_\chi^2}{4r^3 m_\chi^2}\left(3(\mathbf{s}_1.\hat{r})(\mathbf{s}_2.\hat{r}) - \mathbf{s}_1.\mathbf{s}_2\right)\,, \tag{4.27}$$

where we neglected terms proportional to the (possible) Majoron mass. This potential is very singular at $r \to 0$ and requires regularization. The treatment for this case is quite

JHEP02(2017)045

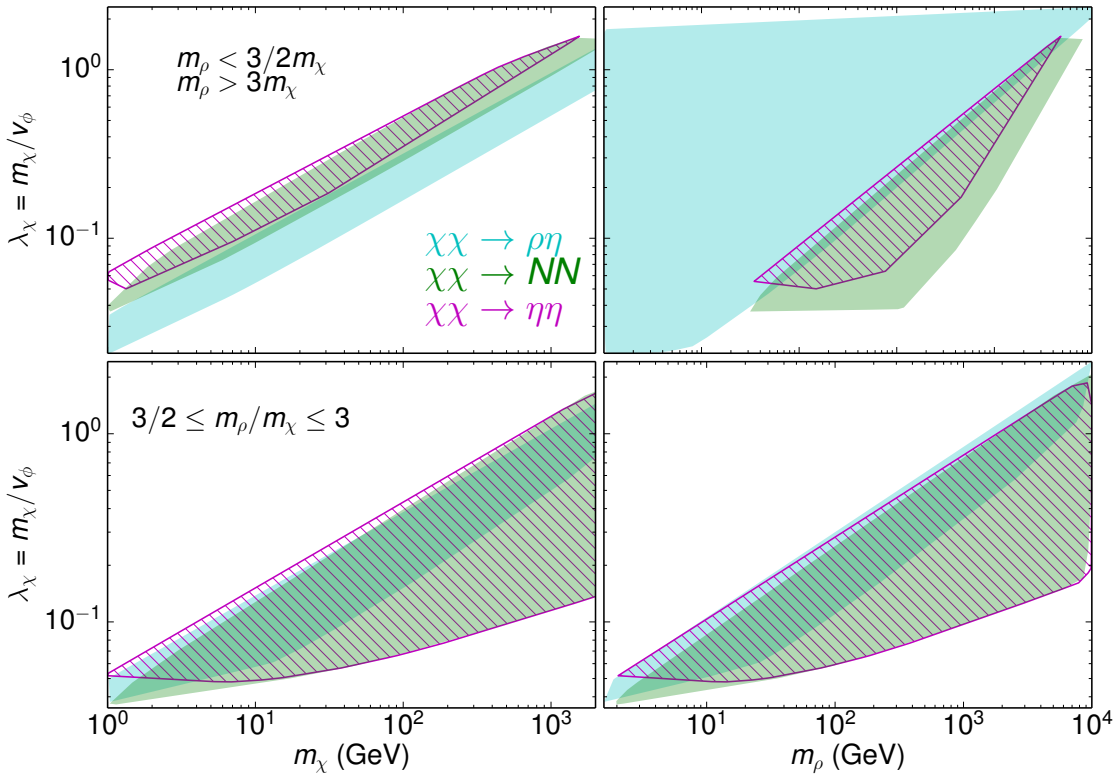

Figure 7. Coupling between the dark scalars and Dark Matter λ_χ as a function of the Dark Matter mass m_χ (left) and heavy scalar mass m_ρ (right). Outside the resonance (up) and on the resonance (down). The colors correspond to regions in parameter space in which the annihilation channel constitutes more than 60% of the total cross section for $v = 10^{-3}c$, as relevant for indirect detection.

involved, similar to a non-relativistic calculation of nucleon-nucleon interaction via the exchange of a light pion.

In the presence of these self-interactions, the annihilation cross section of a self-interacting Dark Matter would be modified respect to our discussion in section 4.3. Additional channels like $\chi\chi \to \chi\chi$ should be considered as they would be Sommerfeld-enhanced,

$$\sigma(\chi\chi \to \chi\chi) v_{\rm rel} = S \frac{3\lambda_\chi^4}{64\pi m_\chi^2}\,, \tag{4.28}$$

where S is the numerical factor due to Sommerfeld enhancement. In ref. [48], numerical calculations of S at short distances were studied for this type of potential, finding that the enhancement could reach $S \sim 10^6$ for $v_{\rm rel} = 10^{-3}$. To estimate what values of λ_χ would lead to dominance of the self-interaction dynamics via a pseudo-scalar exchange, we follow ref. [49] where the following bound is found

$$\lambda_\chi \gtrsim 0.6 \left(\frac{m_\chi}{\rm GeV}\right)^{9/4}\,. \tag{4.29}$$

Note that in our model the mass of the Dark Matter particle and λ_χ are related via the dark scalar vev v_ϕ. We explored the range of these parameters leading to the correct relic

JHEP02(2017)045

abundance and the result is shown in figure 7. The estimate in 4.29 corresponds to the upper-left corner in the left panel of this figure, away from the allowed region from the relic abundance constraint.

Moreover, there are regions of the allowed parameter space where the scalar ρ is light, and there will be exchanges of the ρ similar to those in figure 6 with ρ as a mediator. As ρ is a massive scalar mediator, the type of effective potential one would generate is Yukawa-type, with a less divergent behaviour than the pseudo-scalar. This case has been studied elsewhere, see e.g. refs. [50–54], and here we just quote the parametric dependence of the enhancement with the coupling,

$$S \sim \lambda_\chi^2 / v_{\rm rel}\,, \tag{4.30}$$

for attractive potentials and $m_\rho < m_\chi$. In the right panel of figure 7 we show values of the coupling versus the mass of the mediator, finding in the region where the Sommerfeld enhancement could dominate, the self-interaction would compete with the s-wave annihilation into $\eta\rho$. Note that a similar enhancement could happen in the channels of annihilation to right-handed neutrinos. Indeed, one could exchange light η or ρ mediators as in figure 6, but now between the Dark Matter particle and N.

We conclude that the effects of self-interactions via the exchange of a pseudo-scalar mediator do not affect our model based on a naive estimate, but the effect of scalar exchanges and impact on the annihilation of Dark Matter into right-handed neutrinos deserve further study.

5 Results

In this section we show how the constraints discussed in the previous sections affect the parameter space of our model, described by m_χ, m_N, m_ρ and the Yukawa coupling λ_χ, which fixes $v_\phi = m_\chi/\lambda_\chi$.

As discussed in section 4.4 the annihilation product of the Dark Matter particle may lead to sizeable imprints on FermiLAT or HESS or the CMB due to the emission of photons and the re-ionization power of the products of the annihilation respectively. The annihilation channels that can lead a significant signature are to right-handed neutrinos $\chi\chi \to NN$ with $NN \to W^+W^-$+leptons, whenever $m_\chi > m_W$. A precise analysis of these decay channels would require a simulation of the photon spectrum from these cascade decays, such as performed in ref. [55]. Instead, we naively show the actual bounds for a 2 to 2 process in figure 8.

Apart from signatures from gamma-rays, in our model neutrinos are typically produced in Dark Matter annihilation, leading to a flux from dense regions of Dark Matter or energy injection into the CMB. Indeed, when the right-handed neutrino channel dominates, numerous neutrinos will be produced in the annihilations. IceCUBE can constrain the cross section to neutrinos measuring the flux from nearby Galaxies and Clusters (NG) [58], the Galactic Halo (GH) [59] and the Galactic Center (GC) [60] and the CMB [39] can constrain the annihilation cross section to neutrinos from the impact on re-ionization due

JHEP02(2017)045

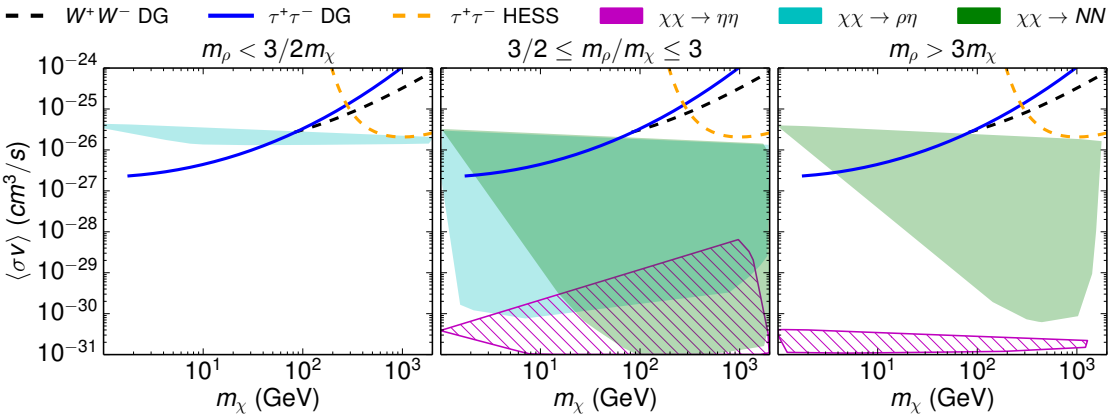

Figure 8. Annihilation cross section at $v = 10^{-3}c$ as a function of the Dark Matter mass as relevant for indirect detection. The color bands account for regions of parameter space in which the indicated annihilation channel provides more than 60% of the total cross section. Also shown in this plot exclusion curves from FermiLAT dwarf galaxies (DG) [56] and HESS galactic center (GC) [57].

to electroweak corrections. However, currently these probes lie three orders of magnitude above the model prediction, and thus cannot place a constrain on the model.

It has been noted that for Dark Matter masses above 200 GeV annihilating into a pair of light neutrinos, Fermi-LAT data on gamma-rays sets the most stringent constraints on the annihilation cross-section [61]. In principle, there would be similar limits in our scenario, but such a heavy Dark Matter will also produce W bosons and leptons, which lead to stronger bounds discussed above.

In figure 8 we summarize these results in the plane of annihilation cross section into a particular final state versus the Dark Matter mass for the three kinematical regions of interest. The colored contours correspond to regions with dominance of one channel in the relic abundance, either to dark scalars or right-handed neutrinos. As argued in section 4.4 the annihilation products from the channels $\chi\chi \to \rho\eta$ and $\chi\chi \to \eta\eta$ cannot be constrained since the ρ decays to two η's, which are invisible.

Therefore the only limits that apply are those related to annihilation into right-handed neutrinos, which is suppressed by m_N^2/m_χ^2. Promising signatures of these decays can be obtained when right-handed neutrinos undergo two-body decays in W and charged leptons or neutrinos in association with a Higgs or a Z boson, see eq. (4.23), and hence restricted to $m_\chi > m_W$. On the other hand, for low Dark Matter mass only sterile neutrinos with $m_N < m_W$ can be produced and the dominant decay $N \to \nu\eta$ is unobservable, see section 4.4. Finally, note that the diagonal feature on the green region in the right panel is due to the fact that in the scan we have considered a minimum of 1 GeV for m_N.

From these results one can conclude that the model is currently unconstrained from indirect detection once other limits are taken into account, although the prospects for future experiments deserve a detailed study.

Notice that in the absence of the global $\mathrm{U}(1)_{B-L}$ symmetry the conclusions could be quite different. First, the sterile neutrino mass would be independent of its coupling, λ_N,

JHEP02(2017)045

and there would not be any suppression of the annihilation cross section when $m_N \ll m_\chi$. Moreover, since in our case the Majoron is a Goldstone boson, it is expected to be lighter than the other scalars in the theory, and one can neglect its mass and assume that all possible annihilation and decay channels into Majorons are always kinematically allowed. However if the lepton number symmetry were explicitly broken, generically the real and imaginary components of ϕ would have similar masses, leading to cases where the channel into pseudo-scalars could be kinematically closed.

In summary, on the one hand the scenario we have considered with spontaneously broken $\mathrm{U}(1)_{B-L}$ is more constrained than the one with explicit breaking, due to relation between sterile neutrino masses and couplings to ϕ. On the other hand, if there was no symmetry, we generically would expect a heavier pseudo-scalar, which could lead to the closing of some invisible channels into Majorons. In this case, constraints from the invisible Higgs decay width would be absent, Dark Matter would only annihilate into sterile neutrinos, and the decay $N \to \nu\eta$ would not occur. Therefore limits from indirect searches, in particular the curve from Fermi-LAT dwarf galaxies on $\tau\tau$ shown in figure 8, would apply to low Dark Matter mass $\lesssim m_W$.

6 Conclusions and outlook

In this paper we have studied a simple case connecting Dark Matter and the origin of neutrino masses, where the link to the Standard Model is dictated by a global $\mathrm{U}(1)_{B-L}$ symmetry. In our model, the dark sector contains fermions, Dark Matter and right-handed neutrinos, and a complex scalar which plays the dual role of generating Majorana masses for the dark fermions and communicating with the Higgs via a Higgs portal coupling. The stability of the Dark Matter fermion can be due to an additional dark sector symmetry, compositness or exotic lepton number.

After spontaneous electroweak and $\mathrm{U}(1)_{B-L}$ symmetry breaking, the Higgs and dark scalar mix. This mixing is very constrained by bounds on the invisible width of the Higgs from the LHC and by LUX via the induced coupling of Dark Matter to the Higgs.

We then focused on other aspects of the phenomenology of this model, assuming that the stable dark fermion constitutes the main component of Dark Matter in the Universe. Due to the presence of right-handed fermions and a complex scalar in the dark sector, there is an interplay between Dark Matter annihilation to both types of particles. Dark Matter annihilation to right-handed neutrinos could dominate at freeze-out provided the scalar is heavy. And, even when Dark Matter annihilation to Majorons dominated the dynamics at freeze-out, we found that the annihilation to heavy neutrinos could control today's indirect detection signatures.

Moreover, we found a very interesting phenomenology reaching from possible signatures at colliders via exotic Higgs decays, to effects on gamma-rays from right-handed neutrino production and decays to charged particles. In this paper, we did not try to accommodate a possible excess in the gamma-ray spectrum, instead used bounds from 2-to-2 scattering, adapted to our case in a relatively naive fashion. A proper study of the spectrum of

JHEP02(2017)045

gamma-rays in our model is beyond the scope of this paper, but certainly deserves further investigation since the estimated bounds are close to the WIMP thermal cross section.

Additionally, we noted that the presence of neutrinos in decay channels could be probed in the future via neutrino telescopes and more precise studies of the CMB, but that at the moment the limits are much weaker than any other annihilations involving charged particles.

Finally, we briefly discussed the possibility of strong self-interactions of Dark Matter due to the exchange of the dark scalar. We found that Majoron exchange cannot dominate the Dark Matter dynamics, but the effect of exchanges of the dark scalar component deserves further study.

Acknowledgments

We thank Pilar Hernández, Laura Lopez-Honorez, Olga Mena, Sergio Palomares Ruiz, Roberto Ruiz de Austri, Jordi Salvadó and Sam Witte for illuminating discussions. ME specially thanks Antonia Abenza for inspiring and encouraging conversations. This work has been partially supported by the European Union's Horizon 2020 research and innovation programme under the Marie Sklodowska-Curie grant agreements No 674896 and 690575, by the Spanish MINECO under grants FPA2014-57816-P and SEV-2014-0398, and by Generalitat Valenciana grant PROMETEO/2014/050. ME is supported by Spanish Grant FPU13/03111 of MECD. NR thanks the Department of Physics and Astronomy in the University of Sussex for the warm hospitality. The work of VS is supported by the Science Technology and Facilities Council (STFC) under grant number ST/J000477/1.

References

[1] S. Dodelson and L.M. Widrow, *Sterile-neutrinos as dark matter*, *Phys. Rev. Lett.* **72** (1994) 17 [hep-ph/9303287] [INSPIRE].

[2] R. Adhikari et al., *A white paper on keV sterile neutrino dark matter*, arXiv:1602.04816 [INSPIRE].

[3] V. Gonzalez Macias and J. Wudka, *Effective theories for dark matter interactions and the neutrino portal paradigm*, *JHEP* **07** (2015) 161 [arXiv:1506.03825] [INSPIRE].

[4] V. González-Macías, J.I. Illana and J. Wudka, *A realistic model for dark matter interactions in the neutrino portal paradigm*, *JHEP* **05** (2016) 171 [arXiv:1601.05051] [INSPIRE].

[5] M. Escudero, N. Rius and V. Sanz, *Sterile neutrino portal to dark matter II: exact dark symmetry*, arXiv:1607.02373 [INSPIRE].

[6] Y. Chikashige, R.N. Mohapatra and R.D. Peccei, *Are there real Goldstone bosons associated with broken lepton number?*, *Phys. Lett.* **B 98** (1981) 265 [INSPIRE].

JHEP02(2017)045

[7] S. Khalil, *Low scale B-L extension of the Standard Model at the LHC*, *J. Phys.* **G 35** (2008) 055001 [hep-ph/0611205] [INSPIRE].

[8] S. Iso, N. Okada and Y. Orikasa, *Classically conformal B-L extended Standard Model*, *Phys. Lett.* **B 676** (2009) 81 [arXiv:0902.4050] [INSPIRE].

[9] S. Kanemura, T. Matsui and H. Sugiyama, *Neutrino mass and dark matter from gauged* $\mathrm{U}(1)_{B-L}$ *breaking*, *Phys. Rev.* **D 90** (2014) 013001 [arXiv:1405.1935] [INSPIRE].

[10] N. Arkani-Hamed, S. Dimopoulos, G.R. Dvali and J. March-Russell, *Neutrino masses from large extra dimensions*, *Phys. Rev.* **D 65** (2001) 024032 [hep-ph/9811448] [INSPIRE].

[11] N. Arkani-Hamed and M. Schmaltz, *Hierarchies without symmetries from extra dimensions*, *Phys. Rev.* **D 61** (2000) 033005 [hep-ph/9903417] [INSPIRE].

[12] Y. Grossman and M. Neubert, *Neutrino masses and mixings in nonfactorizable geometry*, *Phys. Lett.* **B 474** (2000) 361 [hep-ph/9912408] [INSPIRE].

[13] M. Lindner, D. Schmidt and T. Schwetz, *Dark matter and neutrino masses from global* $\mathrm{U}(1)_{B-L}$ *symmetry breaking*, *Phys. Lett.* **B 705** (2011) 324 [arXiv:1105.4626] [INSPIRE].

[14] J. Schechter and J.W.F. Valle, *Neutrino decay and spontaneous violation of lepton number*, *Phys. Rev.* **D 25** (1982) 774 [INSPIRE].

[15] S.R. Coleman, *Why there is nothing rather than something: a theory of the cosmological constant*, *Nucl. Phys.* **B 310** (1988) 643 [INSPIRE].

[16] E.K. Akhmedov, Z.G. Berezhiani, R.N. Mohapatra and G. Senjanović, *Planck scale effects on the majoron*, *Phys. Lett.* **B 299** (1993) 90 [hep-ph/9209285] [INSPIRE].

[17] M. Lattanzi, R.A. Lineros and M. Taoso, *Connecting neutrino physics with dark matter*, *New J. Phys.* **16** (2014) 125012 [arXiv:1406.0004] [INSPIRE].

[18] F. Bazzocchi, M. Lattanzi, S. Riemer-Sørensen and J.W.F. Valle, *X-ray photons from late-decaying majoron dark matter*, *JCAP* **08** (2008) 013 [arXiv:0805.2372] [INSPIRE].

[19] C. Garcia-Cely, A. Ibarra and E. Molinaro, *Cosmological and astrophysical signatures of dark matter annihilations into pseudo-Goldstone bosons*, *JCAP* **02** (2014) 032 [arXiv:1312.3578] [INSPIRE].

[20] M. Carena, A. Daleo, B.A. Dobrescu and T.M.P. Tait, Z' *gauge bosons at the Tevatron*, *Phys. Rev.* **D 70** (2004) 093009 [hep-ph/0408098] [INSPIRE].

[21] N. Okada and O. Seto, *Higgs portal dark matter in the minimal gauged* $\mathrm{U}(1)_{B-L}$ *model*, *Phys. Rev.* **D 82** (2010) 023507 [arXiv:1002.2525] [INSPIRE].

[22] A. De Simone, V. Sanz and H.P. Sato, *Pseudo-Dirac dark matter leaves a trace*, *Phys. Rev. Lett.* **105** (2010) 121802 [arXiv:1004.1567] [INSPIRE].

[23] J. Racker and N. Rius, *Helicitogenesis: WIMPy baryogenesis with sterile neutrinos and other realizations*, *JHEP* **11** (2014) 163 [arXiv:1406.6105] [INSPIRE].

[24] A. Pilaftsis, *Radiatively induced neutrino masses and large Higgs neutrino couplings in the Standard Model with Majorana fields*, *Z. Phys.* **C 55** (1992) 275 [hep-ph/9901206] [INSPIRE].

[25] LUX collaboration, D.S. Akerib et al., *The Large Underground Xenon (LUX) experiment*, *Nucl. Instrum. Meth.* **A 704** (2013) 111 [arXiv:1211.3788] [INSPIRE].

JHEP02(2017)045

[26] LUX collaboration, D.S. Akerib et al., *Improved limits on scattering of weakly interacting massive particles from reanalysis of* 2013 *LUX data*, *Phys. Rev. Lett.* **116** (2016) 161301 [arXiv:1512.03506] [INSPIRE].

[27] XENON collaboration, E. Aprile et al., *Physics reach of the XENON*1*T dark matter experiment*, *JCAP* **04** (2016) 027 [arXiv:1512.07501] [INSPIRE].

[28] PLANCK collaboration, J. Tauber et al., *The scientific programme of Planck*, astro-ph/0604069 [INSPIRE].

[29] PLANCK collaboration, P.A.R. Ade et al., *Planck* 2015 *results. XIII. Cosmological parameters*, *Astron. Astrophys.* **594** (2016) A13 [arXiv:1502.01589] [INSPIRE].

[30] A. Semenov, *LanHEP: a package for the automatic generation of Feynman rules in field theory. Version* 3.0, *Comput. Phys. Commun.* **180** (2009) 431 [arXiv:0805.0555] [INSPIRE].

[31] G. Bélanger, F. Boudjema, A. Pukhov and A. Semenov, *MicrOMEGAs*3*: a program for calculating dark matter observables*, *Comput. Phys. Commun.* **185** (2014) 960 [arXiv:1305.0237] [INSPIRE].

[32] ATLAS and CMS collaborations, *Measurements of the Higgs boson production and decay rates and constraints on its couplings from a combined ATLAS and CMS analysis of the LHC pp collision data at* $\sqrt{s} = 7$ *and* 8 *TeV*, ATLAS-CONF-2015-044, CERN, Geneva Switzerland, (2015) [INSPIRE].

[33] CMS and ATLAS collaborations, *Measurements of the Higgs boson production and decay rates and constraints on its couplings from a combined ATLAS and CMS analysis of the LHC pp collision data at* $\sqrt{s} = 7$ *and* 8 *TeV*, CMS-PAS-HIG-15-002, CERN, Geneva Switzerland, (2015) [INSPIRE].

[34] S. Weinberg, *Goldstone bosons as fractional cosmic neutrinos*, *Phys. Rev. Lett.* **110** (2013) 241301 [arXiv:1305.1971] [INSPIRE].

[35] A.M. Gago, P. Hernández, J. Jones-Pérez, M. Losada and A. Moreno Briceño, *Probing the type I seesaw mechanism with displaced vertices at the LHC*, *Eur. Phys. J.* **C 75** (2015) 470 [arXiv:1505.05880] [INSPIRE].

[36] LUX collaboration, D.S. Akerib et al., *First results from the LUX dark matter experiment at the Sanford Underground Research Facility*, *Phys. Rev. Lett.* **112** (2014) 091303 [arXiv:1310.8214] [INSPIRE].

[37] M.C. Gonzalez-Garcia, A. Santamaria and J.W.F. Valle, *Isosinglet neutral heavy lepton production in Z decays and neutrino mass*, *Nucl. Phys.* **B 342** (1990) 108 [INSPIRE].

[38] M. Dittmar, A. Santamaria, M.C. Gonzalez-Garcia and J.W.F. Valle, *Production mechanisms and signatures of isosinglet neutral heavy leptons in* Z^0 *decays*, *Nucl. Phys.* **B 332** (1990) 1 [INSPIRE].

[39] T.R. Slatyer, *Indirect dark matter signatures in the cosmic dark ages. I. Generalizing the bound on s-wave dark matter annihilation from Planck results*, *Phys. Rev.* **D 93** (2016) 023527 [arXiv:1506.03811] [INSPIRE].

[40] S.-H. Oh, W.J.G. de Blok, E. Brinks, F. Walter and R.C. Kennicutt, Jr, *Dark and luminous matter in THINGS dwarf galaxies*, *Astron. J.* **141** (2011) 193 [arXiv:1011.0899] [INSPIRE].

[41] G.R. Blumenthal, S.M. Faber, R. Flores and J.R. Primack, *Contraction of dark matter galactic halos due to baryonic infall*, *Astrophys. J.* **301** (1986) 27 [INSPIRE].

JHEP02(2017)045

[42] O.Y. Gnedin, A.V. Kravtsov, A.A. Klypin and D. Nagai, *Response of dark matter halos to condensation of baryons: cosmological simulations and improved adiabatic contraction model*, *Astrophys. J.* **616** (2004) 16 [astro-ph/0406247] [INSPIRE].

[43] T. Sawala, Q. Guo, C. Scannapieco, A. Jenkins and S.D.M. White, *What is the (dark) matter with dwarf galaxies?*, *Mon. Not. Roy. Astron. Soc.* **413** (2011) 659 [arXiv:1003.0671] [INSPIRE].

[44] M. Boylan-Kolchin, J.S. Bullock and M. Kaplinghat, *Too big to fail? The puzzling darkness of massive Milky Way subhaloes*, *Mon. Not. Roy. Astron. Soc.* **415** (2011) L40 [arXiv:1103.0007] [INSPIRE].

[45] M. Markevitch et al., *Direct constraints on the dark matter self-interaction cross-section from the merging galaxy cluster* 1E0657-56, *Astrophys. J.* **606** (2004) 819 [astro-ph/0309303] [INSPIRE].

[46] R. Massey et al., *The behaviour of dark matter associated with four bright cluster galaxies in the* 10 *kpc core of Abell* 3827, *Mon. Not. Roy. Astron. Soc.* **449** (2015) 3393 [arXiv:1504.03388] [INSPIRE].

[47] F. Kahlhoefer, K. Schmidt-Hoberg, J. Kummer and S. Sarkar, *On the interpretation of dark matter self-interactions in Abell* 3827, *Mon. Not. Roy. Astron. Soc.* **452** (2015) L54 [arXiv:1504.06576] [INSPIRE].

[48] B. Bellazzini, M. Cliche and P. Tanedo, *Effective theory of self-interacting dark matter*, *Phys. Rev.* **D 88** (2013) 083506 [arXiv:1307.1129] [INSPIRE].

[49] M. Archidiacono, S. Hannestad, R.S. Hansen and T. Tram, *Cosmology with self-interacting sterile neutrinos and dark matter — a pseudoscalar model*, *Phys. Rev.* **D 91** (2015) 065021 [arXiv:1404.5915] [INSPIRE].

[50] R. Iengo, *Sommerfeld enhancement: general results from field theory diagrams*, *JHEP* **05** (2009) 024 [arXiv:0902.0688] [INSPIRE].

[51] S. Cassel, *Sommerfeld factor for arbitrary partial wave processes*, *J. Phys.* **G 37** (2010) 105009 [arXiv:0903.5307] [INSPIRE].

[52] M. Cirelli, A. Strumia and M. Tamburini, *Cosmology and astrophysics of minimal dark matter*, *Nucl. Phys.* **B 787** (2007) 152 [arXiv:0706.4071] [INSPIRE].

[53] L. Lopez-Honorez, T. Schwetz and J. Zupan, *Higgs portal, fermionic dark matter and a Standard Model like Higgs at* 125 *GeV*, *Phys. Lett.* **B 716** (2012) 179 [arXiv:1203.2064] [INSPIRE].

[54] M. Lisanti, *Lectures on dark matter physics*, in *Theoretical Advanced Study Institute in Elementary Particle Physics: New Frontiers in Fields and Strings (TASI* 2015*)*, Boulder U.S.A., 1–26 June 2015 [arXiv:1603.03797] [INSPIRE].

[55] C. Garcia-Cely and J. Heeck, *Indirect searches of dark matter via polynomial spectral features*, *JCAP* **08** (2016) 023 [arXiv:1605.08049] [INSPIRE].

[56] Fermi-LAT collaboration, M. Ackermann et al., *Searching for dark matter annihilation from Milky Way dwarf spheroidal galaxies with six years of Fermi Large Area Telescope data*, *Phys. Rev. Lett.* **115** (2015) 231301 [arXiv:1503.02641] [INSPIRE].

[57] HESS collaboration, H. Abdallah et al., *Search for dark matter annihilations towards the inner galactic halo from* 10 *years of observations with H.E.S.S.*, *Phys. Rev. Lett.* **117** (2016) 111301 [arXiv:1607.08142] [INSPIRE].

JHEP02(2017)045

[58] IceCube collaboration, M.G. Aartsen et al., *IceCube search for dark matter annihilation in nearby galaxies and galaxy clusters*, *Phys. Rev.* **D 88** (2013) 122001 [arXiv:1307.3473] [INSPIRE].

[59] IceCube collaboration, M.G. Aartsen et al., *Multipole analysis of IceCube data to search for dark matter accumulated in the galactic halo*, *Eur. Phys. J.* **C 75** (2015) 20 [arXiv:1406.6868] [INSPIRE].

[60] IceCube collaboration, M.G. Aartsen et al., *Search for dark matter annihilation in the galactic center with IceCube-79*, *Eur. Phys. J.* **C 75** (2015) 492 [arXiv:1505.07259] [INSPIRE].

[61] F.S. Queiroz, C.E. Yaguna and C. Weniger, *Gamma-ray limits on neutrino lines*, *JCAP* **05** (2016) 050 [arXiv:1602.05966] [INSPIRE].

JHEP02(2017)045

Eur. Phys. J. C (2017) 77:397
DOI 10.1140/epjc/s10052-017-4963-x

THE EUROPEAN PHYSICAL JOURNAL C

Regular Article - Theoretical Physics

Sterile neutrino portal to Dark Matter II: exact dark symmetry

Miguel Escudero[1,a], **Nuria Rius**[1,b], **Verónica Sanz**[2,c]

[1] Departamento de Física Teórica and IFIC, Universidad de Valencia-CSIC, C/Catedrático José Beltrán, 2, 46980 Paterna, Spain
[2] Department of Physics and Astronomy, University of Sussex, Brighton BN1 9QH, UK

Received: 20 January 2017 / Accepted: 31 May 2017 / Published online: 14 June 2017

Abstract We analyze a simple extension of the standard model (SM) with a dark sector composed of a scalar and a fermion, both singlets under the SM gauge group but charged under a dark sector symmetry group. Sterile neutrinos, which are singlets under both groups, mediate the interactions between the dark sector and the SM particles, and generate masses for the active neutrinos via the seesaw mechanism. We explore the parameter space region where the observed Dark Matter relic abundance is determined by the annihilation into sterile neutrinos, both for fermion and scalar Dark Matter particles. The scalar Dark Matter case provides an interesting alternative to the usual Higgs portal scenario. We also study the constraints from direct Dark Matter searches and the prospects for indirect detection via sterile neutrino decays to leptons, which may be able to rule out Dark Matter masses below and around 100 GeV.

1 Introduction

Dark Matter and neutrino masses provide experimental evidence for physics beyond the standard model (SM), and finding a scenario where both phenomena are linked is an exciting possibility. Another hint to a connection between these two sectors comes from the standard mechanisms to generate the Dark Matter relic abundance and neutrino masses, as both seem to require new massive degrees of freedom, with a thermal relic and right-handed neutrinos, respectively.

An obvious possibility would be for right-handed neutrinos to constitute the Dark Matter of the Universe [1]. This option is constrained to a specific region at the keV and small mixing with active neutrinos in the minimal see saw model, but in extended scenarios a larger parameter space is allowed, for instance in the context of a gauged $B-L$ symmetry [2,3]. Upcoming experiments may be able to exclude or establish whether keV neutrinos are the origin of Dark Matter, see e.g. [4].

In this paper we take a different approach, focusing on the fact that heavy neutrinos can mediate between Dark Matter and the SM. We propose a simple extension of the SM with a new scalar and fermion, singlets under the SM gauge group but charged under a dark sector symmetry group. Sterile neutrinos, which are singlets under both groups, are able to mediate the interactions between the dark sector and the SM particles, as well as generate masses for the active neutrinos via the seesaw mechanism. Therefore, the same coupling that generates neutrino masses after electroweak symmetry breaking, determines the Dark Matter phenomenology. Indeed, Dark Matter annihilation to right-handed neutrinos and subsequent decays to SM particles characterize the computation of the relic abundance as well as indirect detection probes, respectively.

This minimal set-up has been studied in [5,6] for the case of fermion Dark Matter, under the assumption that the sterile neutrinos are pseudo-Dirac and heavier than the dark sector particles. Our analysis differs from this previous work in that: (1) we explore the region of parameter space where sterile neutrinos are lighter than the dark sector, and therefore the Dark Matter can annihilate into sterile neutrinos and (2) we extend the analysis to the scalar Dark Matter case, which was not considered before.

In a companion paper [7], we have explored an alternative scenario with the dark sector charged under $U(1)_{B-L}$, and both papers provide two distinct possibilities for a sterile neutrino portal to Dark Matter.

The paper is organized as follows. After presenting the set-up of our model in Sect. 2, we move onto the constraints from Higgs decays and direct Dark Matter searches in Sect. 3. We describe the calculation of the annihilation cross section in Sect. 4 where we impose constraints from the relic abundance of Dark Matter. These results are then linked to indirect detection probes via sterile neutrinos decays to leptons

[a] e-mail: miguel.escudero@ific.uv.es
[b] e-mail: nuria.rius@ific.uv.es
[c] e-mail: v.sanz@sussex.ac.uk

in Sect. 5. We conclude in Sect. 6 by summarizing our main findings.

2 Exact dark symmetry

This portal is based upon the assumption that the dark sector contains at least a scalar field ϕ and a fermion Ψ, which are both singlets of the SM gauge group but charged under a dark sector symmetry group, $G_{\rm dark}$, so that the combination $\overline{\Psi}\phi$ is a singlet of this hidden symmetry. Independently of the nature of the dark group, if all SM particles as well as the sterile neutrinos are singlets of $G_{\rm dark}$, the lighter of the two dark particles turns out to be stable, and therefore it may account for the Dark Matter density of the Universe.

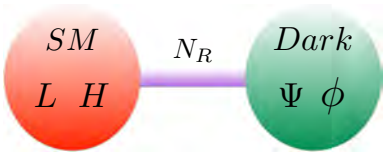

If this were the case then nothing would prevent a term like

$$\mathcal{L}_{\rm int} = -(\phi\overline{\Psi}(\lambda_s + \gamma_5\lambda_p)N + \phi^\dagger\overline{N}(\lambda_s - \gamma_5\lambda_p)\Psi) \quad (1)$$

to appear, besides the standard Higgs portal term $\lambda_{H\phi}(H^\dagger H)(\phi^\dagger\phi)$ included in the scalar potential,

$$\mathcal{L}_{\rm scalar} = \mu_H^2 H^\dagger H - \lambda_H (H^\dagger H)^2 - \mu_\phi^2\phi^\dagger\phi - \lambda_\phi(\phi^\dagger\phi)^2 - \lambda_{H\phi}(H^\dagger H)\,(\phi^\dagger\phi), \quad (2)$$

and the term responsible for the generation of neutrino masses

$$\mathcal{L}_{\nu N} = -(Y_{\alpha a}\overline{L}_L^\alpha H N_{Ra} + h.c.), \quad (3)$$

where $\alpha = e, \mu, \tau$ denotes lepton flavour and $a = 1 \ldots n$, being n the number of sterile neutrinos.

For simplicity we do not consider the possibility that the scalar ϕ gets a vev, and we restrict the discussion to the minimal matter content, although there could be more than one set of dark fermions and scalars.

Another simplifying assumption made in this paper is that the dark symmetry $G_{\rm dark}$ is a global symmetry at low energies. We are therefore neglecting the possible phenomenology of $G_{\rm dark}$ vector mediators, e.g., if the dark symmetry were local there could also be kinetic mixing among the dark gauge bosons and the SM ones, leading to further SM-dark particle interactions [8,9]. The following discussion will apply as well to this scenario, provided the kinetic mixing is negligible. Nevertheless, the UV structure and stability of Dark Matter depends on whether $G_{\rm dark}$ is a true global symmetry or a gauge symmetry. Global symmetries are sensitive to higher-dimensional operators mediated by quantum gravity effects [10], e.g. $c_\Psi\bar{\Psi}\tilde{H}^\dagger\gamma^\mu D_\mu L/M_{Pl}$ or $c_\Phi\Phi F_{\mu\nu}F^{\mu\nu}/M_{Pl}$, and could lead to disastrous decay of Dark Matter unless $c_{\Psi,\Phi} \ll 1$ [11–13].

Regarding the neutrino sector, light neutrino masses are generated via TeV scale type I seesaw mechanism, which we briefly review in the following. We denote ν_α the active neutrinos and N_s the sterile ones. After electroweak symmetry breaking, the neutrino mass matrix in the basis (ν_α, N_s) is given by

$$\mathcal{M}_\nu = \begin{pmatrix} 0 & m_D \\ m_D^T & m_N \end{pmatrix}, \quad (4)$$

where $m_D = Y v_H/\sqrt{2}$ and $Y_{\alpha s}$ are the Yukawa couplings.

The matrix $\mathcal{M}_\nu$ can be diagonalized by a unitary matrix U, so that

$$\mathcal{M}_\nu = U^*\,{\rm Diag}(m_\nu, M)\,U^\dagger, \quad (5)$$

where m_ν is the diagonal matrix with the three lightest eigenvalues of $\mathcal{M}_\nu$, of order m_D^2/m_N, and M contains the heavier ones, of order m_N.

The mass eigenstates $\mathbf{n} = (\nu_i, N_h)$ are related to the active and sterile neutrinos, (ν_α, N_s), by

$$\begin{pmatrix} \nu_\alpha \\ N_s \end{pmatrix}_L = U^* \begin{pmatrix} \nu_i \\ N_h \end{pmatrix}_L. \quad (6)$$

The unitary matrix U can be written as

$$U = \begin{pmatrix} U_{\alpha i} & U_{\alpha h} \\ U_{si} & U_{sh} \end{pmatrix}, \quad (7)$$

where, at leading order in the seesaw expansion parameter, $\mathcal{O}(m_D/m_N)$:

$$\begin{aligned} U_{\alpha i} &= [U_{\rm PMNS}]_{\alpha i} \qquad U_{sh} = I, \\ U_{\alpha h} &= [m_D m_N^{-1}]^*_{\alpha h}, \\ U_{si} &= -[m_N^{-1} m_D^T\, U_{\rm PMNS}]_{si}. \end{aligned} \quad (8)$$

Notice that at this order the states N_h and N_s coincide, so we identify them in the rest of this paper.

Neglecting the mixing between the CP-even scalars, the Yukawa coupling of the SM-like Higgs field h to the neutrinos can be written as [14]:

$$\mathcal{L}_Y = -\frac{h}{2v_H}\bar{\mathbf{n}}_i[(m_i + m_j)Re(C_{ij}) + i\gamma_5(m_j - m_i)Im(C_{ij})]\mathbf{n}_j, \quad (9)$$

where the indices i, j refer to the light neutrinos ν_i for $i, j = 1, 2, 3$ and to N_h for $i, j = 4, 5, 6$, and the matrix C can be written in terms of the mixing matrix U:

$$C_{ij} = \sum_{\alpha=1}^{3} U_{\alpha i} U^*_{\alpha j}. \quad (10)$$

A variation of this scenario has been analyzed in [5,6], where the sterile neutrinos are assumed to be pseudo-Dirac and

Table 1 Explored parameter space in the models

Case	m_Ψ (GeV)	m_ϕ (GeV)	m_N (GeV)	λ_s	$\lambda_{H\phi}$
Fermion DM	$1–2\times10^3$	$1–10^4$	$1–2\times10^3$	$10^{-4}–4\pi$	$10^{-4}–4\pi$
Scalar DM	$1–10^4$	$1–2\times10^3$	$1–2\times10^3$	$10^{-4}–4\pi$	$10^{-4}–4\pi$

heavier than the dark sector particles, ϕ, Ψ. Thus, they can be integrated out and generate at tree level the effective dimension five operator

$$\mathcal{O}^{(5)} = (\overline{\Psi}\phi)(\widetilde{H}^\dagger \ell), \tag{11}$$

which after the SM Higgs doublet acquires a vev leads to the interaction $\mathcal{O}^{(5)} = (\overline{\Psi}\phi)\nu_L v_H/\sqrt{2}$, involving a SM left-handed neutrino. This limit is in fact a (light) neutrino portal to Dark Matter. Assuming that the fermion Ψ is the Dark Matter, the model can accommodate current experimental and observational constraints if M_ψ is below ~35 GeV, or it is in a resonant region of the Higgs or Z boson, or the dark scalar and dark fermion are almost degenerate.

Our analysis is complementary, since we focus on a different region of the model parameter space: we assume that the sterile neutrinos are *lighter* than the Dark Matter and therefore the annihilation channel to NN is open. Furthermore, we study both fermion and scalar Dark Matter. Although the scalar Dark Matter case falls among the class of Higgs portal models that have been extensively studied [15–34], it is worth to explore whether the new annihilation channel into NN allows one to obtain the observed relic density in regions that are excluded in the standard Higgs portal framework.

In the following sections we describe the current constraints on the above scenario and the results of our numerical analysis, based on a Monte Carlo scan over the free parameters (m_Ψ, m_ϕ, m_N, λ_s, $\lambda_{H\phi}$) in logarithmic scale, restricting the values of the couplings and masses to the ranges displayed in Table 1. We present the analytic results for arbitrary Dark Matter—sterile neutrino couplings λ_s, λ_p, but for the numerical implementation we have chosen $\lambda_p = 0$, since as explained in Sect. 4, in this case strong constraints can be set from indirect Dark Matter searches. We made use of `LanHep` [35] and `micrOMEGAs` [36] in order to obtain the correct relic abundance, Higgs decays and today's annihilation cross section. We calculate 10^6 points that match the *Planck* constraint on the Dark Matter abundance at 3σ [37], namely $\Omega h^2 = 0.1198 \pm 0.0045$.

3 Constraints from Higgs decays and direct Dark Matter searches

The enlarged fermion and scalar sectors lead to new decays of the Higgs boson, h, which can be constrained using the ATLAS and CMS limits on the invisible Higgs decay branching fraction:

$$\mathrm{BR}_{\mathrm{inv}} = \frac{\Gamma_{\mathrm{inv}}}{\Gamma_{\mathrm{inv}} + \Gamma_{\mathrm{SM}}} < 0.23 \qquad (95\%\,\mathrm{CL}), \tag{12}$$

being the SM Higgs width $\Gamma_{\mathrm{SM}} \approx 4$ MeV.

At tree level, there are two new Higgs decay channels: when $m_\phi < m_h/2$, the standard decay of the Higgs portal scenarios, $h \to \phi\phi$ is kinematically allowed, contributing to the invisible Higgs decay width by

$$\Gamma(h \to \phi\phi) = \frac{\lambda_{H\phi}^2 v_H^2}{8\pi m_h}\sqrt{1 - \frac{4m_\phi^2}{m_h^2}} \tag{13}$$

We show in Fig. 3 the upper limit on the Higgs portal coupling $\lambda_{H\phi}$ derived from the experimental limit on the invisible Higgs decay width in Eq. (12), as a function of the singlet scalar mass, m_ϕ.

Moreover, the Yukawa interaction term $Y\overline{L}HP_RN$ also leads to novel Higgs decay channels into neutrinos. The corresponding decay width reads [14]:

$$\Gamma(h \to n_i n_j) = \frac{\omega}{8\pi m_h}\lambda^{1/2}(m_h^2, m_i^2, m_j^2) \times \left[S\left(1 - \frac{(m_i + m_j)^2}{m_h^2}\right) + P\left(1 - \frac{(m_i - m_j)^2}{m_h^2}\right)\right], \tag{14}$$

where $\lambda(a, b, c)$ is the standard kinematic function, $w = 1/n!$ for n identical final particles and the scalar and pseudoscalar couplings are:

$$S = \frac{1}{v_H^2}[(m_i + m_j)Re(C_{ij})]^2,$$
$$P = \frac{1}{v_H^2}[(m_j - m_i)Im(C_{ij})]^2, \tag{15}$$

with C_{ij} defined in Eq. (10).

The largest branching ratio is for the decay into one light and one heavy neutrino [38]:

$$\Gamma(h \to \nu N) = \frac{m_N^2}{8\pi v_H^2}\left(1 - \frac{m_N^2}{m_h^2}\right)^2 m_h |C_{\nu N}|^2. \tag{16}$$

The attainable values for the above branching fractions have been analyzed in [38], for the case of two heavy neutrinos, parameterizing the Yukawa couplings in terms of the observed light neutrino masses and mixing angles, and a

complex orthogonal matrix. After imposing the relevant constraints from neutrinoless double beta decay, lepton flavour violating processes and direct searches of heavy neutrinos, they find that branching ratios of $h \to \nu_i N_a$ larger than 10^{-2} are generally ruled out for heavy neutrino masses $M_N \leq 100$ GeV, and typically they are much smaller, due to the tiny Yukawa couplings required to fit light neutrino masses with sterile neutrinos at the electroweak scale. Therefore, the contribution of such decay modes to the Higgs decay width is negligible, and they do not alter the bounds discussed above.

At one loop, the $d = 5$ Higgs portal operator $\overline{\Psi}\Psi(H^\dagger H)$ is generated (unless the coupling of the Dark Matter to the dark scalar and sterile neutrinos is chiral, i.e., $\lambda_s = \lambda_p$ in Eq. (1)) with a coefficient given by [6]:

$$\lambda_{H\Psi}^{\text{eff}} = \lambda_{H\phi} \frac{(\lambda_s^2 - \lambda_p^2)}{16\pi^2} \frac{m_N}{(m_\phi^2 - m_N^2)^2} \times \left(m_\phi^2 - m_N^2 + m_N^2 \log \frac{m_N^2}{m_\phi^2} \right). \quad (17)$$

Thus, when $m_\Psi < m_h/2$ the invisible decay $h \to \Psi\Psi$ is also allowed with partial decay width

$$\Gamma(h \to \Psi\Psi) = \frac{(\lambda_{H\Psi}^{\text{eff}})^2}{8\pi} \left(1 - \frac{4m_\Psi^2}{m_h^2}\right)^{3/2} m_h, \quad (18)$$

and the current limit on the invisible Higgs decay branching ratio only leads to an $\mathcal{O}(1)$ constrain on $\lambda_{H\phi}$, depending on the values of the remaining free parameters, namely $\lambda_s, \lambda_p, m_N$ and m_ϕ. Notice, however, that if $m_\phi < m_h/2$, the strong constraints from the invisible Higgs decay $h \to \phi\phi$ shown in Fig. 3 will apply as well.

Concerning the bounds from direct DM searches, they also depend on which of the dark particles is lighter, and therefore stable. In order to implement such bounds we shall assume that the DM relic density is as determined by CMB measurements, since this requirement is always fulfilled in our scenario for both scalar and fermion DM, as we will see in the next section.

If DM is the dark fermion, Ψ, it only interacts with the SM quarks at one-loop level (see Fig. 1), via the induced Higgs portal operator $\overline{\Psi}\Psi(H^\dagger H)$ just discussed, and therefore the bounds from direct detection are quite weak. However, since the interaction to quarks is mediated through the Higgs, the scattering will always be spin independent. We refer the reader for the actual matrix elements to [39]. In Fig. 2 we show the excluded region by the invisible Higgs decay and current LUX [40,41] results (dark blue points), as well as the expected excluded region by XENON1T [42] (light blue) and LZ [43,44]+SuperCDMS [45] (purple). Similar constraints can be set with the current results from the PANDAX experiment [46].

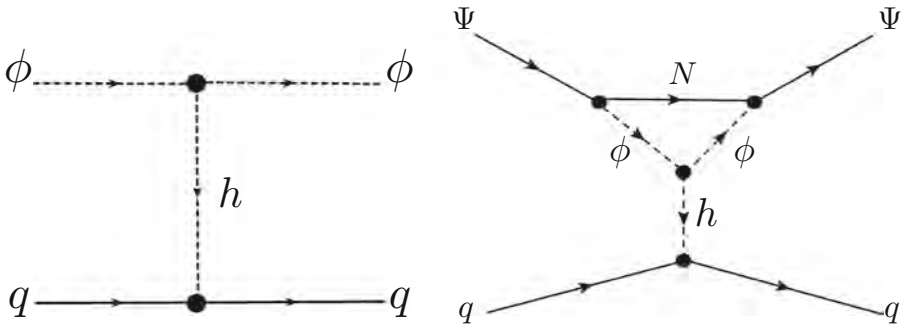

Fig. 1 *Left*, *right* elastic cross section diagrams for the scalar and fermion Dark Matter cases, respectively

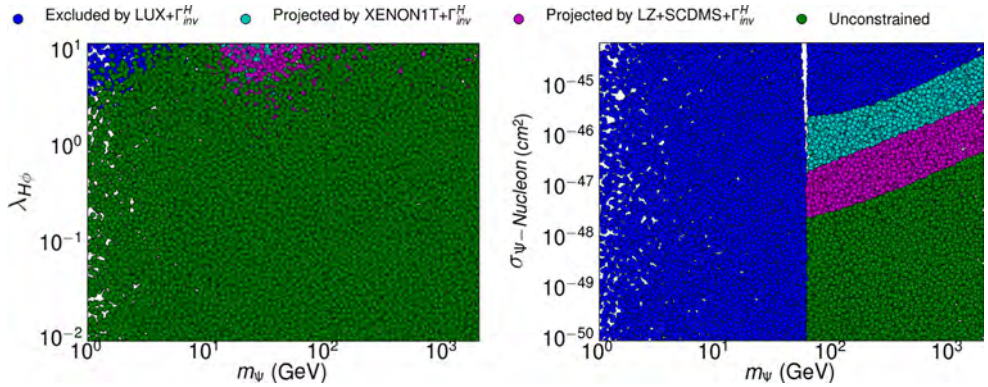

Fig. 2 Constraints on the Higgs portal coupling for fermion DM

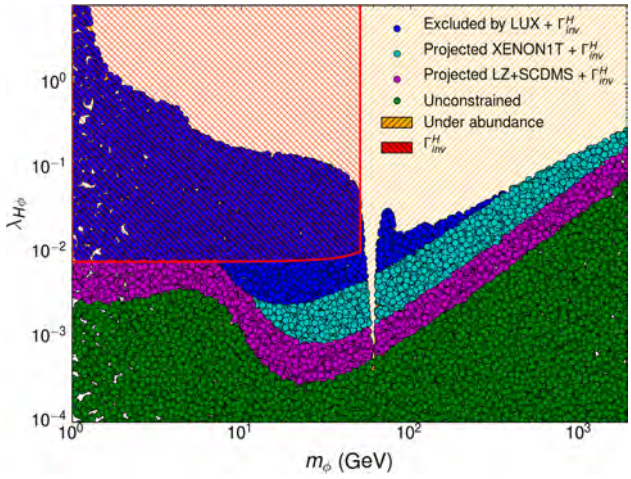

Fig. 3 Constraints on the Higgs portal coupling for scalar DM

However, if DM is the dark scalar ϕ, it interacts with the SM quarks at tree level via the Higgs portal coupling, $\lambda_{H\phi}$, and the null results from direct searches set strong limits on this parameter. This is illustrated in Fig. 3, where we show the allowed values of the Higgs portal coupling $\lambda_{H\phi}$ as a function of the DM mass, m_ϕ, derived from the invisible Higgs decay width plus LUX bounds, as well as the prospects from XENON1T and LZ+SuperCDMS. The dark blue points in the usual Higgs portal scenario would be ruled out, except for the upper limit, since the $\lambda_{H\phi}$ being too small leads to a DM relic density larger than the one determined by CMB measurements. In our scenario the alternative annihilation channel into NN provides the correct relic density, but the current constraints from LUX and Higgs invisible decay width excludes them. We notice that for $m_\phi \gtrsim 300$ GeV the usual Higgs portal model still provides the correct relic abundance. However, we find that XENON1T can be sensitive to such scenario for $m_\phi < 2$ TeV.

4 Dark Matter relic abundance

4.1 Thermal history

In order to discuss the thermal production of Dark Matter in the early Universe we will first describe the thermal history for both the scalar and fermion Dark Matter scenarios.

1. Fermion Dark Matter Ψ: At very early times ϕ, Ψ and N are in thermal equilibrium with the standard model via the Higgs portal coupling. The heavy dark particle companion will decay at $T \lesssim m_\phi$ and the dark sector may still be coupled to the standard model bath if the Yukawa couplings of the sterile neutrinos are large enough. If they are small, then the Ψ and N bath will decouple and remain in thermal equilibrium but with a different temperature.[1] Then when the temperature of such a bath is $T_D \sim m_\Psi/20$ the Dark Matter will be produced and the sterile neutrinos will decay at $T_D \lesssim m_N$. In order to check whether the decoupling of the dark sector will modify the production rate it is worth revisiting the production mechanism, see [47] for a recent discussion of decoupled dark sectors. Since the entropy is separately conserved in both the visible and the dark sectors, the standard relic abundance solution is modified approximately by a factor $\sqrt{g_\star^{\rm eff}/g_\star}$ where $g_\star$ measures the total number of relativistic degrees of freedom in the SM bath and $g_\star^{\rm eff} = g_\star + g_D(T_D/T)^4$ represents the effective number of relativistic species. Given that the number of degrees of freedom in the dark sector, g_D is much smaller than $g_\star$ and $T_D/T \sim 1$ then $\sqrt{g_\star^{\rm eff}/g_\star}$ must be close to one. Thus, a sizeable change in the couplings compared to the case in which both sectors remain in thermal equilibrium is not expected since furthermore $\Omega_\chi h^2 \propto 1/\lambda_{s,p}^4$. The only caveat to this argument occurs when $m_\chi \gtrsim m_N$, because in that case the sterile neutrinos may have a larger number density than the equilibrium one and in order to generate the same amount of Dark Matter higher couplings between χ and N will be needed. This scenario has been recently studied by [48] for the precise model proposed in this work. They found that in such region one will need couplings a factor between 1 and 4 higher depending on the Yukawa of the sterile neutrinos. Since this change is mild, for our computations we will assume that all species are equilibrium with the standard model.
2. Scalar Dark Matter ϕ: At very early times ϕ, Ψ and N are in thermal equilibrium with the standard model via the Higgs portal coupling. The heavy dark particle companion will decay at $T \lesssim m_\Psi$ and the dark sector will decouple from the standard model when the Dark Matter freezes out at $T \sim m_\Psi/20$ and the sterile neutrinos will decouple and decay at $T \lesssim m_N$.

4.2 Relic abundance

In our scenario, the annihilation cross section into two sterile neutrinos depends on the nature of the DM particle (scalar, Dirac or Majorana fermion) and the type of coupling (scalar, pseudoscalar). The relevant Feynman diagrams are shown in Fig. 4. For example, let us assume right-handed neutrinos are Majorana, and consider the two options of fermion and scalar Dark Matter:

[1] Yet, the actual value of the Yukawa couplings are not known. The naive seesaw expectation is $Y \sim \sqrt{m_\nu m_N}/v_H \sim 4 \times 10^{-8}\sqrt{m_N/(1\,\text{GeV})}$ for $m_\nu \sim 0.1$ eV, but larger couplings are consistent with neutrino masses, for instance in the context of inverse seesaw scenarios.

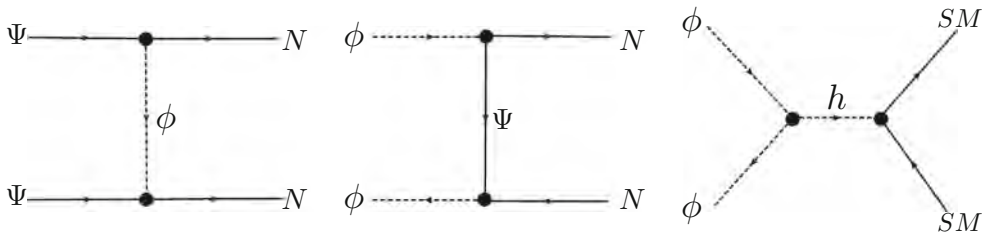

Fig. 4 Relevant annihilation channels

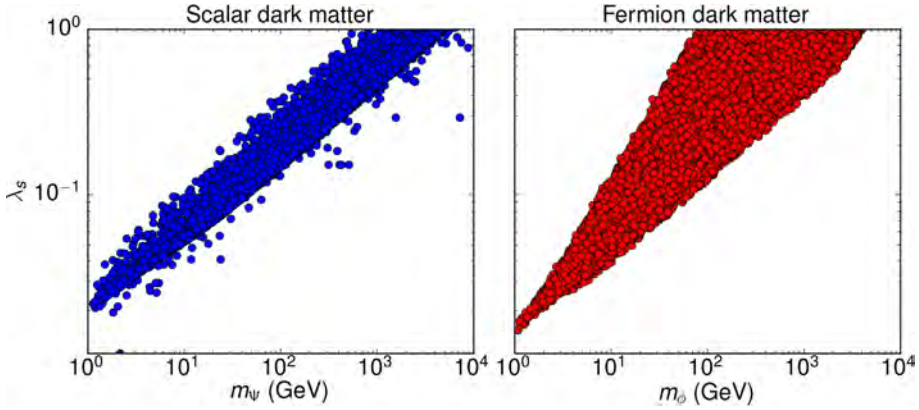

Fig. 5 Allowed parameter space of the mediator mass and coupling in the scalar (*left*) and fermion Dark Matter (*right*) cases

1. Fermion Dark Matter Ψ: The cross section for fermionic Majorana Dark Matter and complex mediator ϕ reads

$$\sigma v_{\Psi\Psi\to NN} = \frac{(\alpha+\beta\, r_{N\Psi})^2}{4\pi m_\Psi^2}\,\frac{\sqrt{1-r_{N\Psi}^2}}{(1+r_\phi^2-r_{N\Psi}^2)^2} + \mathcal{O}(v^2) \tag{19}$$

where $\alpha = \lambda_s^2 - \lambda_p^2$ and $\beta = \lambda_s^2 + \lambda_p^2$, $r_\phi = m_\phi/m_\Psi$, and $r_{N\Psi} = m_N/m_\Psi$.
One can obtain the case of a Dirac DM particle by in Eq. (19) perform the exchange $\alpha \leftrightarrow \beta$. Similarly, the case of a real scalar can be obtained by setting $\lambda_p = 0$ in Eq. (19), which leads to $\alpha = \beta = \lambda_s^2$ in this expression.
2. Scalar Dark Matter ϕ: In the case of a real scalar Dark Matter and Dirac mediator Ψ the cross section is as follows:

$$\sigma v_{\phi\phi\to NN} = \frac{(\alpha+\beta\, r_{N\Psi})^2}{2\pi m_\phi^2}\,\frac{(1-r_{N\phi}^2)^{3/2}}{(1+r_\Psi^2-r_{N\phi}^2)^2} + \mathcal{O}(v^2), \tag{20}$$

where $r_\Psi = m_\Psi/m_\phi$ and $r_{N\phi} = m_N/m_\phi$.
To obtain the expression for a complex scalar, one can multiply this equation by a factor 1/4. Similarly, to consider a Majorana mediator one would multiply the expression by a factor 4 and set λ_p to zero, $\alpha = \beta$.[2]

[2] Note that our results agree with the expressions obtained in Ref. [49], where both fermions were set to be Dirac particles.

An important observation is that there are situations where the annihilation cross section at leading order in the relative Dark Matter velocity, v, is proportional to the right-handed neutrino mass. For example, the case of a Majorana Dark Matter with chiral couplings, $|\lambda_s| = |\lambda_p|$ ($\alpha = 0$). In this case when $m_N \ll m_\phi, m_\Psi$ the cross section is effectively p-wave, which reduces the sensitivity of indirect detection probes to these scenarios.

In the following we discuss two representative cases where strong constraints can be set on the parameter space of the sterile neutrino portal, namely cases where the cross section is s-wave even for $m_N = 0$. We choose two benchmark scenarios, namely Majorana DM and real scalar DM with scalar couplings $\alpha = \beta = \lambda_s^2$. In Fig. 5 we show the allowed parameter space in the mass of the mediator versus coupling, λ_s. Besides the perturbativity limits, the coupling λ_s is constrained by the width of the mediator. In our approach, the mediator particle is treated as a narrow resonance, i.e. $\Gamma/m \ll 1$, which implies $\lambda_s \lesssim \sqrt{8\pi}$. Taking into account this limit, these plots show that the mass of the mediator must be below $m \lesssim 1$ TeV to satisfy $\Gamma \lesssim 0.1m$.

In the scalar Dark Matter case, annihilation into right-handed neutrinos (Eq. (20)) is complemented via the Higgs portal coupling $\lambda_{H\phi}$ into SM particles. Namely $b\bar{b}$ for low mass DM, and gauge bosons and Higgses for heavier DM particles. These channels could, in principle, compete with the annihilation into right-handed neutrinos, yet in Fig. 3 we showed how couplings to SM are strongly constrained by direct detection experiments (LUX) and LHC bounds on the

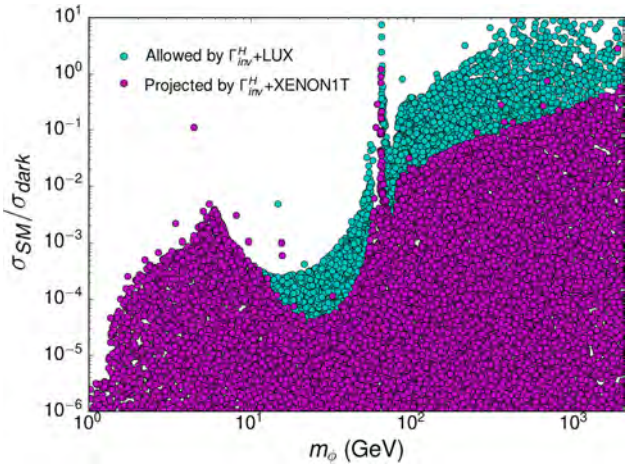

Fig. 6 Ratio between the cross section with standard model particles in the final state and sterile neutrinos in the final state at $v = 10^{-3}\,c$, as relevant for indirect detection searches. Currently, on the resonance $m_\phi \simeq m_h/2$ and for $m_\phi > 150$ GeV both cross sections are comparable. However, XENON1T could set the annihilation cross section to right-handed neutrinos to be dominant in the entire parameter space but for the resonance

invisible width of the Higgs. We find that for $m_\phi \lesssim 100$ GeV the production cannot proceed via SM particles. As a result of these bounds on the scalar portal, the relic abundance cannot be satisfied in the standard scalar Dark Matter, which leads to the conclusion that Higgs portal Dark Matter is not a viable scenario for low dark matter masses. This is not the case here, as our scalar has additional annihilation channels, via the coupling to dark fermions. One can then find viable scenarios, shown in Fig. 5, which satisfy the relic abundance and evade direct detection constraints in all the Dark Matter mass range from 1 GeV to 2 TeV.

Moreover, in the low Dark Matter mass region, annihilations to right-handed neutrinos are dominant. This is shown in Fig. 6, where we plot the ratio of annihilation cross sections via the Higgs portal and to the right-handed neutrino channel today, for relative Dark Matter velocity $v = 10^{-3}\,c$. This ratio is very small, of the order or below 0.1% for low mass, and up to 100% for $m_\phi \gtrsim 300$ GeV. When the dark matter mass is low, the regions with larger ratios are correlated with degeneracies in the dark sector, namely regions where the dark fermion mediator and the scalar are close in mass. This fact has implications in the ability of detecting Dark Matter today, which we discuss in detail in the next section. Notice that the ∼100% contributions to the Dark Matter abundance currently allowed through SM interactions for $m_\phi \gtrsim 300$ GeV, could be restricted by XENON1T to ∼10% for most parameter space.[3]

[3] The features in the low mass region of the plots are due to the fact that the contributions to the SM are mediated by the Higgs and there are several suppressions. When different channels become kinematically unaccessible, $m_\phi < m_b,\ m_\tau,\ m_c$ one finds a suppression factor of $(m_b/m_\tau)^2 \sim 4$, $(m_\tau/m_c)^2 \sim 2$, $(m_c/m_s)^2 \sim 100$ respectively.

Finally, in the fermion Dark Matter case, since the coupling to the Higgs is generated at 1-Loop, the contributions to the annihilation cross section from the SM particles is only non-negligible in the resonant region $m_\Psi \simeq m_h/2$.

5 Constraints from indirect searches and CMB

In this scenario the annihilation of Dark Matter (with $m_{\rm DM} \lesssim 100$ GeV) into right-handed neutrinos is dominant, with the heavy neutrinos decaying into SM particles via their mixing with active neutrinos. Those decays can lead to significant fluxes of gamma rays and neutrinos which can be probed by experiments. In this section we consider the impact on the model by limits from Fermi-LAT and H.E.S.S. on the gamma-ray flux from dwarf spheroidal galaxies [50] and the galactic center [51] respectively, as well as from studies of the CMB [52] and IceCUBE analysis of neutrino fluxes [53–55].

To study the indirect detection signals in this model we first need to understand how the heavy neutrino decays. If the neutrino is light, $m_N < m_W$, N will mostly decay through off-shell Z and W. These three-body partial widths can be read from Refs. [56,57] and are listed in the appendix; here we just quote the typical form it adopts:

$$\Gamma(N \to 3\,f) \approx \frac{G_F^2}{192\,\pi^3}\,|U_{\alpha N}|^2\,m_N^5, \tag{21}$$

where $U_{\alpha N}$ is the mixing matrix between the heavy and active neutrinos. For heavier N, the two-body decays into massive vector bosons or Higgs and fermions are open. In this case the partial width scales as [14]:

$$\Gamma(N \to V f) \approx \frac{g^2}{64\,\pi\,m_{W,Z,h}^2}\,|U_{\alpha N}|^2\,m_N^3. \tag{22}$$

See also the appendix for the detailed formulae.

The relative weight of the different lepton flavours to the total width depends on the model for neutrino mass generation. The large angle θ_{23} in the active neutrino mixing matrix $U_{\rm PMNS}$ suggests a similar decay rate of N into μ and τ, while the one into e is largely unconstrained. In fact, the measured mixing pattern (see for instance [58]) is close to Tri-Bimaximal, which leads to an exact $\mu - \tau$ symmetry [59]. In our case, if we assume that the largest active neutrino mass is generated by only one of the sterile neutrinos, $m_3 \approx \sum_\alpha (Y_{\alpha N} v_H)^2/m_N$ and the mixing angles are given by $U_{\alpha N} \sim Y_{\alpha N} v_H/m_N$. Then $\tan\theta_{23} \sim Y_{\mu N}/Y_{\tau N} \sim 1$ and $\tan\theta_{13} = Y_{eN}/\sqrt{Y_{\mu N}^2 + Y_{\tau N}^2} \sim 0.15$ imply that $U_{eN} \ll U_{\mu N} \approx U_{\tau N}$ [60].

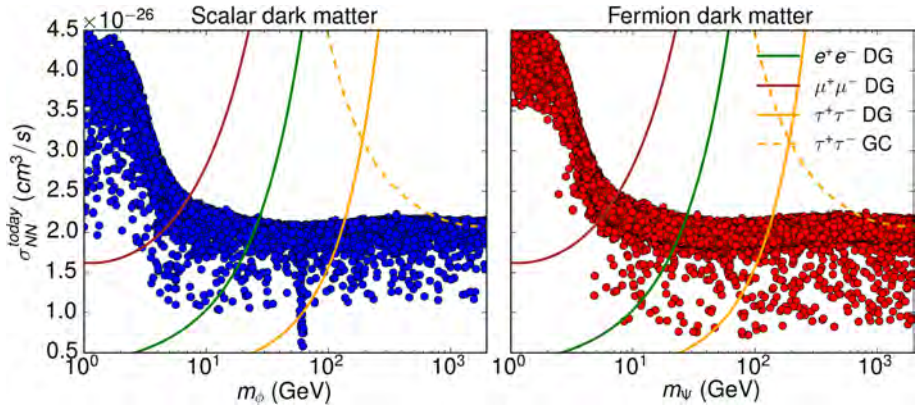

Fig. 7 Annihilation cross section today and lines of exclusion of decays to leptons from Fermi-LAT from dwarf galaxies and H.E.S.S. from the galactic center, for the cases of scalar (*left*) and fermionic (*right*) Dark Matter

A detailed study of the indirect detection signatures of our scenario is beyond the scope of this work, since DM does not decay directly to SM particles, as is usually assumed in most analyses. Therefore we just estimate here the expected constraints using current analysis, taking into account that in general the cascade decays lead to a softer energy spectrum of the final SM particles than in the standard two-body decay. In Fig. 7 we present the results of such an estimate exercise in the case of decays to leptons, where limits from Refs. [50,51] have been naively re-scaled as $m_{\rm DM} \to m_{\rm DM}/2$. We find that decays of the right-handed neutrinos resulting in tau-leptons, e.g. from $N \to \tau q q'$ or $N \to \nu \tau^+ \tau^-$, are potentially the most sensitive modes. Indeed, if these decays were dominant one could obtain a limit from indirect detection on the Dark Matter mass of $\mathcal{O}(100)$ GeV for both fermion and scalar Dark Matter. One could also use the production of quarks from off-shell W and Z to set bounds on the model.

Note that indirect detection signals in this case (i.e., $m_N < m_W$) have been studied in [61], showing that it could be possible to explain the galactic center gamma-ray excess revealed by various studies of the Fermi-LAT data in 1–4 GeV gamma rays. Indeed, assuming that DM particles annihilate into two sterile neutrinos lighter than the W boson, they find that m_N in the range 10–60 GeV can explain the observed spectrum, while the fitted annihilation cross section $\langle \sigma v \rangle$ is (0.5–5) $\times 10^{-26} {\rm cm}^3/{\rm s}$, roughly compatible with the WIMP annihilation cross section $\langle \sigma v \rangle_{\rm decouple} \sim (2-3) \times 10^{-26} {\rm cm}^3/{\rm s}$, when the Dark Matter particles decouple. More precisely, the best fit points are around $m_N \sim 30$ GeV and $m_{\rm DM} \sim 45$ GeV, which are within the ranges we have found compatible with all current experimental constraints in our model.

Finally, let us mention other sources of indirect constraints for this model. Measurements of the cosmic microwave background (CMB) anisotropies are also sensitive to Dark Matter annihilation during the cosmic dark ages, because the injection of ionizing particles will increase the residual ionization fraction, broadening the last scattering surface and modifying the anisotropies. Under the assumption that the power deposited to the gas is directly proportional to that injected at the same redshift, with some efficiency factor $f_{\rm eff}$, constraints can be placed on the combination $f_{\rm eff} \langle \sigma v \rangle / m_{\rm DM}$, for different SM annihilation channels in s wave. Again, the available calculations of $f_{\rm eff}$ assume that DM annihilates directly to a pair of SM particles [52], and thus they are not directly applicable to our model, but we can roughly estimate the expected impact of such limits in the allowed parameter space assuming as before that the constraints will be similar for cascade decays, appropriately re-scaled for $m_{\rm DM}/2$. Under these circumstances, we find these limits are weaker than the ones from Fermi-LAT discussed above.

Besides signatures from gamma rays, in the NN annihilation channel also light neutrinos are copiously produced, which could generate an observable flux from dense regions of Dark Matter. IceCUBE has set constraints on the Dark Matter annihilation cross section to neutrinos by measuring the flux from nearby Galaxies and Clusters [53], the Galactic Halo [54] and the Galactic Center [55]. However, currently these probes lie three orders of magnitude above the model prediction, and thus cannot place a constrain on our model. Dark Matter particles in the galactic halo can also scatter elastically with a nucleus and become trapped in the gravitational well of astronomical objects like the Sun, eventually thermalize and concentrate at the core of the object. Then they may annihilate into SM particles, in particular neutrinos that can be detected by neutrino experiments such as IceCUBE or SuperKamiokande. In our scenario the limits from direct searches are tighter than such indirect probes, since the interaction of Dark Matter to quarks is spin independent.

6 Conclusions and outlook

In this paper we have analyzed in detail a simple scenario of a dark sector composed of a scalar and a fermion, both singlets under the SM gauge group but charged under a dark symmetry group. This sector is linked to the origin of neutrino masses via couplings to the sterile neutrinos, which are able to mediate between the dark sector and the SM.

This scenario has been studied in Refs. [5,6], considering just the case of fermionic Dark Matter and for sterile neutrinos heavier than the dark sector, with the result that current experimental and observational constraints (electroweak precision limits, Dark Matter relic abundance, direct and indirect detection constraints), can be accommodated only for $m_{\rm DM} \lesssim 35$ GeV, or in the resonances, $m_{\rm DM} \simeq m_h, m_Z$, unless the dark scalar or dark fermion are almost degenerate.

We have extended these previous studies in two ways: we explore the phenomenology of this type of models when the sterile neutrinos are lighter than the dark sector, so that the Dark Matter annihilation channel into NN is kinematically allowed, and we consider both, fermionic and scalar Dark Matter in this context. We have performed for the first time an exhaustive numerical analysis of this alternative region of the model parameter space, and after imposing all the relevant constraints from direct detection and collider probes, we find that it is possible to obtain the observed Dark Matter relic abundance in the whole mass range explored, $m_{\rm DM} \in$ [1 GeV, 2 TeV], both for scalar and fermion Dark Matter.

We find that the scalar case is an interesting extension of the Higgs portal. Indeed, in the usual portal the constraints on the Higgs invisible decay and Dark Matter nucleon cross section rule out the possibility of the scalar as the main component of Dark Matter for $m_\phi \lesssim 100$ GeV. But in our scenario, annihilation can occur via the neutrino portal which is dominant, i.e. more than 90%, in most of the parameter space. On the other hand, in the case of a fermion Dark Matter, the contribution to the quark–Dark Matter scattering and Higgs invisible width decay is at one loop and the Higgs portal coupling is only mildly constrained.

Finally we explore the indirect detection characteristics of this model, determined by the decays of the right-handed neutrinos into SM bosons and leptons. We consider constraints from Fermi-LAT and find that those could be sensitive to Dark Matter up to the electroweak scale, $m_{\rm DM} \lesssim 100$ GeV independently of whether the Dark Matter particle is a scalar of a fermion. However, a more detailed analysis of these constraints need to be done, as we performed a naive scaling on constraints of Dark Matter decays to two SM particles. In our scenario, the more complex decays of right-handed neutrinos would lead to less energetic SM probes. Finally, we also comment on the possibility of this channel to be responsible of the gamma-ray galactic excess at few GeV.

Acknowledgements We thank Olga Mena, Sergio Palomares Ruiz, Roberto Ruiz de Austri, Jordi Salvadó, A. Vincent and J. Wudka for illuminating discussions, and Concha González-García for comments on the manuscript. ME thanks Antonia Abenza for inspiring and encouraging conversations. This work has been partially supported by the European Unions Horizon 2020 research and innovation programme under the Marie Sklodowska-Curie Grant Agreements Nos. 674896 and 690575, by the Spanish MINECO under Grants FPA2014-57816-P and SEV-2014-0398, and by Generalitat Valenciana Grant PROMETEO/2014/050. ME is supported by Spanish Grant FPU13/03111 of MECD. NR acknowledges the support from the Munich Institute for Astro- and Particle Physics (MIAPP) of the DFG cluster of excellence "Origin and Structure of the Universe". The work of VS is supported by the Science Technology and Facilities Council (STFC) under Grant Number ST/J000477/1.

Appendix: Sterile neutrino decay widths

Here we summarize the sterile neutrino decay modes, relevant for indirect Dark Matter searches.

If the sterile neutrino is lighter than the W boson, it will decay through off-shell h, Z, W bosons to three fermions. Since the decay via a virtual h is further suppressed by the small Yukawa couplings of the SM fermions, it is a very good approximation to consider only the processes mediated by virtual W, Z, whose partial widths read [56]:

$$\Gamma(N \to \nu q\bar{q}) = 3\, A C_{NN} [2(a_u^2 + b_u^2) + 3(a_d^2 + b_d^2)] f(z) \tag{A.1}$$

$$\Gamma(N \to 3\nu) = A C_{NN} \left[\frac{3}{4} f(z) + \frac{1}{4} g(z,z)\right] \tag{A.2}$$

$$\Gamma(N \to \ell q\bar{q}) = 6\, A C_{NN} f(w,0) \tag{A.3}$$

$$\Gamma(N \to \nu \ell\bar{\ell}) = A C_{NN} [3(a_e^2 + b_e^2) f(z) + 3 f(w) - 2 a_e g(z,w)] \tag{A.4}$$

where C_{NN} is defined in Eq. (10),

$$A \equiv \frac{G_F^2 m_N^5}{192\,\pi^3}, \tag{A.5}$$

a_f, b_f are the left and right neutral current couplings of the fermions ($f = q, \ell$), the variables z, w are given by

$$z = (m_N/m_Z)^2, \qquad w = (m_N/m_W)^2, \tag{A.6}$$

and the functions $f(z)$, $f(w,0)$ and $g(z,w)$ can be found in [57].

For larger values of m_N, two-body decays to SM particles are open, and the corresponding widths read [14]:

$$\Gamma(N \to W^\pm \ell_\alpha^\mp) = \frac{g^2}{64\pi} |U_{\alpha N}|^2 \frac{m_N^3}{m_W^2} \left(1 - \frac{m_W^2}{m_N^2}\right)^2 \left(1 + \frac{2m_W^2}{m_N^2}\right) \tag{A.7}$$

$$\Gamma(N \to Z\, \nu_\alpha) = \frac{g^2}{64\pi c_W^2} |C_{\alpha N}|^2 \frac{m_N^3}{m_Z^2} \left(1 - \frac{m_Z^2}{m_N^2}\right)^2 \left(1 + \frac{2m_Z^2}{m_N^2}\right) \tag{A.8}$$

$$\Gamma(N \to h\,\nu_\alpha) = \frac{g^2}{64\pi}|C_{\alpha N}|^2 \frac{m_N^3}{m_W^2}\left(1 - \frac{m_h^2}{m_N^2}\right)^2 \tag{A.9}$$

In the above expressions, we have assumed that N is a Majorana fermion. If it is Dirac, then the decay channel $N \to W^-\ell^+$ is forbidden and the decay widths into Z/h, ν are $\Gamma_D(N \to Z/h\,\nu_\ell) = \Gamma_M(N \to Z/h\,\nu_\ell)/2$.

References

1. S. Dodelson, L.M. Widrow, Sterile-neutrinos as dark matter. Phys. Rev. Lett. **72**, 17–20 (1994). arXiv:hep-ph/9303287
2. T. Basak, T. Mondal, Constraining minimal $U(1)_{B-L}$ model from dark matter observations. Phys. Rev. D **89**, 063527 (2014). arXiv:1308.0023
3. K. Kaneta, Z. Kang, H.-S. Lee, Right-handed neutrino dark matter under the B–L gauge interaction. arXiv:1606.09317
4. R. Adhikari et al., A white paper on keV sterile neutrino dark matter. Submitted to: White paper (2016). arXiv:1602.04816
5. V. Gonzalez Macias, J. Wudka, Effective theories for Dark Matter interactions and the neutrino portal paradigm. JHEP **07**, 161 (2015). arXiv:1506.03825
6. V. Gonzalez-Macias, J.I. Illana, J. Wudka, A realistic model for Dark Matter interactions in the neutrino portal paradigm. JHEP **05**, 171 (2016). arXiv:1601.05051
7. M. Escudero, N. Rius, V. Sanz, Sterile neutrino portal to Dark Matter I: the $U(1)_{B-L}$ case. arXiv:1606.01258
8. J. Heeck, H. Zhang, Exotic charges, multicomponent dark matter and light sterile neutrinos. JHEP **05**, 164 (2013). arXiv:1211.0538
9. A. de Gouvea, D. Hernández, New chiral fermions, a new gauge interaction, Dirac neutrinos, and dark matter. JHEP **10**, 046 (2015). arXiv:1507.00916
10. R. Kallosh, A.D. Linde, D.A. Linde, L. Susskind, Gravity and global symmetries. Phys. Rev. D **52**, 912–935 (1995). arXiv:hep-th/9502069
11. O. Cata, A. Ibarra, Dark matter stability without new symmetries. Phys. Rev. D **90**, 063509 (2014). arXiv:1404.0432
12. Y. Mambrini, S. Profumo, F.S. Queiroz, Dark matter and global symmetries. Phys. Lett. B **760**, 807–815 (2016). arXiv:1508.06635
13. O. Cata, A. Ibarra, S. Ingenhntt, Dark matter decays from non-minimal coupling to gravity. Phys. Rev. Lett. **117**, 021302 (2016). arXiv:1603.03696
14. A. Pilaftsis, Radiatively induced neutrino masses and large Higgs neutrino couplings in the standard model with Majorana fields. Z. Phys. C **55**, 275–282 (1992). arXiv:hep-ph/9901206
15. B. Patt, F. Wilczek, Higgs-field portal into hidden sectors. arXiv:hep-ph/0605188
16. Y.G. Kim, K.Y. Lee, The minimal model of fermionic dark matter. Phys. Rev. D **75**, 115012 (2007). arXiv:hep-ph/0611069
17. J. March-Russell, S.M. West, D. Cumberbatch, D. Hooper, Heavy dark matter through the Higgs portal. JHEP **07**, 058 (2008). arXiv:0801.3440
18. Y.G. Kim, K.Y. Lee, S. Shin, Singlet fermionic dark matter. JHEP **05**, 100 (2008). arXiv:0803.2932
19. M. Ahlers, J. Jaeckel, J. Redondo, A. Ringwald, Probing hidden sector photons through the Higgs window. Phys. Rev. D **78**, 075005 (2008). arXiv:0807.4143
20. J.L. Feng, H. Tu, H.-B. Yu, Thermal relics in hidden sectors. JCAP **0810**, 043 (2008). arXiv:0808.2318
21. S. Andreas, T. Hambye, M.H.G. Tytgat, WIMP dark matter, Higgs exchange and DAMA. JCAP **0810**, 034 (2008). arXiv:0808.0255
22. V. Barger, P. Langacker, M. McCaskey, M. Ramsey-Musolf, G. Shaughnessy, Complex singlet extension of the standard model. Phys. Rev. D **79**, 015018 (2009). arXiv:0811.0393
23. M. Kadastik, K. Kannike, A. Racioppi, M. Raidal, EWSB from the soft portal into Dark Matter and prediction for direct detection. Phys. Rev. Lett. **104**, 201301 (2010). arXiv:0912.2729
24. S. Kanemura, S. Matsumoto, T. Nabeshima, N. Okada, Can WIMP dark matter overcome the nightmare scenario? Phys. Rev. D **82**, 055026 (2010). arXiv:1005.5651
25. F. Piazza, M. Pospelov, Sub-eV scalar dark matter through the super-renormalizable Higgs portal. Phys. Rev. D **82**, 043533 (2010). arXiv:1003.2313
26. C. Arina, F.-X. Josse-Michaux, N. Sahu, A tight connection between direct and indirect detection of dark matter through Higgs portal couplings to a hidden sector. Phys. Rev. D **82**, 015005 (2010). arXiv:1004.3953
27. I. Low, P. Schwaller, G. Shaughnessy, C.E.M. Wagner, The dark side of the Higgs boson. Phys. Rev. D **85**, 015009 (2012). arXiv:1110.4405
28. A. Djouadi, O. Lebedev, Y. Mambrini, J. Quevillon, Implications of LHC searches for Higgs-portal dark matter. Phys. Lett. B **709**, 65–69 (2012). arXiv:1112.3299
29. C. Englert, T. Plehn, D. Zerwas, P.M. Zerwas, Exploring the Higgs portal. Phys. Lett. B **703**, 298–305 (2011). arXiv:1106.3097
30. J.F. Kamenik, C. Smith, Could a light Higgs boson illuminate the dark sector? Phys. Rev. D **85**, 093017 (2012). arXiv:1201.4814
31. M. Gonderinger, H. Lim, M.J. Ramsey-Musolf, Complex scalar singlet dark matter: vacuum stability and phenomenology. Phys. Rev. D **86**, 043511 (2012). arXiv:1202.1316
32. O. Lebedev, On stability of the electroweak vacuum and the Higgs portal. Eur. Phys. J. C **72**, 2058 (2012). arXiv:1203.0156
33. N. Craig, H.K. Lou, M. McCullough, A. Thalapillil, The Higgs portal above threshold. JHEP **02**, 127 (2016). arXiv:1412.0258
34. F.S. Queiroz, K. Sinha, The poker face of the Majoron dark matter model: LUX to keV line. Phys. Lett. B **735**, 69–74 (2014). arXiv:1404.1400
35. A. Semenov, LanHEP: a package for the automatic generation of Feynman rules in field theory. Version 3.0. Comput. Phys. Commun. **180**, 431–454 (2009). arXiv:0805.0555
36. G. Belanger, F. Boudjema, A. Pukhov, A. Semenov, micrOMEGAs3: a program for calculating dark matter observables. Comput. Phys. Commun. **185**, 960–985 (2014). arXiv:1305.0237
37. Planck collaboration, P.A.R. Ade et al., Planck 2015 results. XIII. Cosmological parameters. arXiv:1502.01589
38. A.M. Gago, P. Hernandez, J. Jones-Perez, M. Losada, A. Moreno Briceño, Probing the Type I Seesaw mechanism with displaced vertices at the LHC. Eur. Phys. J. C **75**, 470 (2015). arXiv:1505.05880
39. J. Kumar, D. Marfatia, Matrix element analyses of dark matter scattering and annihilation. Phys. Rev. D **88**, 014035 (2013). arXiv:1305.1611
40. LUX collaboration, D.S. Akerib et al., The large underground xenon (LUX) experiment. Nucl. Instrum. Methods A **704**, 111–126 (2013). arXiv:1211.3788
41. A. Manalaysay et al., Identification of Dark Matter 2016. https://idm2016.shef.ac.uk/indico/event/0/contribution/50/material/slides/0.pdf
42. XENON collaboration, E. Aprile et al., Physics reach of the XENON1T dark matter experiment. JCAP **1604**, 027 (2016). arXiv:1512.07501
43. LZ collaboration, D.S. Akerib et al., LUX-ZEPLIN (LZ) conceptual design report. arXiv:1509.02910
44. LZ collaboration, D.N. McKinsey, The LZ dark matter experiment. J. Phys. Conf. Ser. **718**, 042039 (2016)

45. SuperCDMS collaboration, R. Agnese et al., Improved WIMP-search reach of the CDMS II germanium data. Phys. Rev. D **92**, 072003 (2015). arXiv:1504.05871
46. PandaX-II collaboration, A. Tan et al., Dark matter results from first 98.7-day data of PandaX-II experiment. Phys. Rev. Lett. **117**, 121303 (2016). arXiv:1607.07400
47. A. Berlin, D. Hooper, G. Krnjaic, Thermal dark matter from a highly decoupled sector. Phys. Rev. D **94**, 095019 (2016). arXiv:1609.02555
48. Y.-L. Tang, S.-H. Zhu, Dark matter relic abundance and light sterile neutrinos. arXiv:1609.07841
49. A. Berlin, D. Hooper, S.D. McDermott, Simplified dark matter models for the Galactic Center gamma-ray excess. Phys. Rev. D **89**, 115022 (2014). arXiv:1404.0022
50. Fermi-LAT collaboration, M. Ackermann et al., Searching for dark matter annihilation from Milky Way dwarf spheroidal galaxies with six years of Fermi large area telescope data. Phys. Rev. Lett. **115**, 231301 (2015). arXiv:1503.02641
51. HESS collaboration, H. Abdallah et al., Search for dark matter annihilations towards the inner Galactic halo from 10 years of observations with H.E.S.S. Phys. Rev. Lett. **117**, 111301 (2016). arXiv:1607.08142
52. T.R. Slatyer, Indirect dark matter signatures in the cosmic dark ages. I. Generalizing the bound on s-wave dark matter annihilation from Planck results. Phys. Rev. D **93**, 023527 (2016). arXiv:1506.03811
53. IceCube collaboration, M.G. Aartsen et al., IceCube search for dark matter annihilation in nearby galaxies and galaxy clusters. Phys. Rev. D **88**, 122001 (2013). arXiv:1307.3473
54. IceCube collaboration, M.G. Aartsen et al., Multipole analysis of IceCube data to search for dark matter accumulated in the Galactic halo. Eur. Phys. J. C **75**, 20 (2015). arXiv:1406.6868
55. IceCube collaboration, M.G. Aartsen et al., Search for dark matter annihilation in the Galactic Center with IceCube-79. Eur. Phys. J. C **75**, 492 (2015). arXiv:1505.07259
56. M.C. Gonzalez-Garcia, A. Santamaria, J.W.F. Valle, Isosinglet neutral heavy lepton production in Z decays and neutrino mass. Nucl. Phys. B **342**, 108–126 (1990)
57. M. Dittmar, A. Santamaria, M.C. Gonzalez-Garcia, J.W.F. Valle, Production mechanisms and signatures of isosinglet neutral heavy leptons in Z^0 decays. Nucl. Phys. B **332**, 1–19 (1990)
58. M.C. Gonzalez-Garcia, M. Maltoni, T. Schwetz, Updated fit to three neutrino mixing: status of leptonic CP violation. JHEP **11**, 052 (2014). arXiv:1409.5439
59. G. Altarelli, F. Feruglio, L. Merlo, Tri-bimaximal neutrino mixing and discrete flavour symmetries. Fortsch. Phys. **61**, 507–534 (2013). arXiv:1205.5133
60. S.F. King, Large mixing angle MSW and atmospheric neutrinos from single right-handed neutrino dominance and U(1) family symmetry. Nucl. Phys. B **576**, 85–105 (2000). arXiv:hep-ph/9912492
61. Y.-L. Tang, S.-H. Zhu, Dark matter annihilation into right-handed neutrinos and the Galactic Center gamma-ray excess. arXiv:1512.02899

Journal of Cosmology and Astroparticle Physics
An IOP and SISSA journal

Toward (finally!) ruling out Z and Higgs mediated dark matter models

Miguel Escudero,[a,b,1] **Asher Berlin,**[c,2] **Dan Hooper**[b,d,e,3] **and Meng-Xiang Lin**[d,4]

[a]Instituto de Física Corpuscular (IFIC), CSIC-Universitat de València, Apartado de Correos 22085, E-46071 Valencia, Spain
[b]Fermi National Accelerator Laboratory, Center for Particle Astrophysics, Batavia, IL 60510, U.S.A.
[c]Department of Physics, University of Chicago, Chicago, IL 60637, U.S.A.
[d]Department of Astronomy and Astrophysics, University of Chicago, Chicago, IL 60637, U.S.A.
[e]Kavli Institute for Cosmological Physics, University of Chicago, Chicago, IL 60637, U.S.A.

E-mail: miguel.escudero@ific.uv.es, berlin@uchicago.edu, dhooper@fnal.gov, mxlin@uchicago.edu

Received October 9, 2016
Accepted December 6, 2016
Published December 15, 2016

Abstract. In recent years, direct detection, indirect detection, and collider experiments have placed increasingly stringent constraints on particle dark matter, exploring much of the parameter space associated with the WIMP paradigm. In this paper, we focus on the subset of WIMP models in which the dark matter annihilates in the early universe through couplings to either the Standard Model Z or the Standard Model Higgs boson. Considering fermionic, scalar, and vector dark matter candidates within a model-independent context, we find that the overwhelming majority of these dark matter candidates are already ruled out by existing experiments. In the case of Z mediated dark matter, the only scenarios that are not currently excluded are those in which the dark matter is a fermion with an axial coupling and with a mass either within a few GeV of the Z resonance ($m_{\rm DM} \simeq m_Z/2$) or greater than 200 GeV, or with a vector coupling and with $m_{\rm DM} > 6$ TeV. Several Higgs mediated scenarios are currently viable if the mass of the dark matter is near the Higgs pole ($m_{\rm DM} \simeq m_H/2$). Otherwise, the only scenarios that are not excluded are those in which

[1]ORCID: http://orcid.org/0000-0002-4487-8742.
[2]ORCID: http://orcid.org/0000-0002-1156-1482.
[3]ORCID: http://orcid.org/0000-0001-8837-4127.
[4]ORCID: http://orcid.org/0000-0003-2908-4597.

doi:10.1088/1475-7516/2016/12/029

JCAP12(2016)029

the dark matter is a scalar (vector) heavier than 400 GeV (1160 GeV) with a Higgs portal coupling, or a fermion with a pseudoscalar (CP violating) coupling to the Standard Model Higgs boson. With the exception of dark matter with a purely pseudoscalar coupling to the Higgs, it is anticipated that planned direct detection experiments will probe nearly the entire range of models considered in this study.

Keywords: dark matter theory, dark matter experiments

ArXiv ePrint: 1609.09079

JCAP12(2016)029

Contents

JCAP12(2016)029

1 Introduction

Over the past few decades, the WIMP paradigm has dominated the theoretical and experimental landscape of dark matter. Interest in dark matter in the form of weakly interacting massive particles (WIMPs) has been motivated in large part by the realization that a generic stable particle with an electroweak scale mass and interactions will freeze-out in the early universe with a thermal relic abundance that is comparable to the measured cosmological dark matter density. And although there are many electroweak processes through which a WIMP could potentially annihilate, none are as ubiquitous across the landscape of dark matter models than those which result from couplings between the dark matter and the Standard Model (SM) Z or Higgs bosons.

As direct detection, indirect detection, and collider searches for dark matter have progressed, the WIMP paradigm has become increasingly well explored and constrained. And although there remain many viable WIMP models, important experimental benchmarks have been reached, providing us with valuable information pertaining to the identity of our universe's dark matter. In this paper, we focus on the subset of models in which the dark matter annihilates through the exchange of the Z or the Higgs boson. In scenarios outside of this subset of models, WIMPs must annihilate through the exchange of particles beyond the SM if they are to avoid being overproduced in the early universe.

The remainder of this article is structured as follows. In section 2, we consider dark matter that is mediated by Z exchange, discussing fermionic, scalar and vector dark matter candidates. We find that a very significant part of this parameter space is ruled out by a combination of constraints from direct detection experiments (LUX, PandaX-II) and measurements from LEP of the invisible width of the Z. The only scenarios which remain viable at this time are those with a fermionic dark matter candidate with a nearly pure axial coupling to the Z and with a mass that lies within either a few GeV of the Z pole ($m_{\rm DM} \simeq 40$–$48\,\text{GeV}$) or that is heavier than 200 GeV, or a fermion with a vector coupling to the Z and that is heavier than 6 TeV. Much of this parameter space is expected to be

tested in the near future with direct detection experiments such as XENON1T. In section 3, we consider fermionic, scalar and vector dark matter candidates that are coupled to the SM Higgs boson. Across this class of models, we again find that the overwhelming majority of the parameter space is experimentally excluded, with the exception of scenarios in which the dark matter lies near the Higgs pole ($m_{\rm DM} \simeq m_H/2$), the dark matter is a scalar (vector) heavier than 400 GeV (1160 GeV) with a Higgs portal coupling, or the dark matter is a fermion with largely pseudoscalar couplings to the SM Higgs boson. In section 4 we discuss some caveats to our conclusions, including scenarios with a non-standard cosmological history, or models in which the dark matter coannihilates with another particle species in the early universe. We summarize our results and conclusions in section 5.

2 Z mediated dark matter

2.1 Fermionic dark matter

We begin by considering a dark matter candidate, χ, which is either a Dirac or a Majorana fermion with the following interactions with the SM Z:

$$\mathcal{L} \supset \left[a\bar{\chi}\gamma^{\mu}(g_{\chi v} + g_{\chi a}\gamma^5)\chi\right] Z_{\mu}, \tag{2.1}$$

where $a = 1\,(1/2)$ in the Dirac (Majorana) case, and $g_{\chi v}$ and $g_{\chi a}$ are the vector and axial couplings of the dark matter, respectively. Note that $g_{\chi v}$ is necessarily equal to zero in the Majorana case. These couplings allow the dark matter to annihilate through the s-channel exchange of the Z, into pairs of SM fermions or, if the dark matter is heavy enough, into ZZ, W^+W^- or Zh final states. In figure 1 we plot the fraction of annihilations which proceed to each final state, as evaluated in the early universe (at the temperature of thermal freeze-out) and for $v = 10^{-3}\,c$ (as is typically relevant for indirect detection). Throughout this paper, unless otherwise stated, we use version 4.2.5 of the publicly available code MicrOMEGAS [1] to calculate all annihilation cross sections, thermal relic abundances, and elastic scattering cross sections.

In figure 2, we explore and summarize the parameter space within this class of models. In each frame, the solid black line represents the value of the dark matter's coupling to the Z ($g_{\chi v}$ or $g_{\chi a}$) for which the calculated thermal relic abundance is equal to the measured cosmological dark matter density, $\Omega_{\chi}h^2 = 0.1198 \pm 0.0015$ [2]. If $m_{\chi} < m_Z/2$, we can further restrict the couplings of the dark matter using the measurement of the invisible Z width. The predicted contribution from Z decays to dark matter is in this case is given by:

$$\Gamma(Z \to \chi\bar{\chi}) = \frac{a\,m_Z}{12\pi}\left(1 - \frac{4m_{\chi}^2}{m_Z^2}\right)^{1/2}\left[g_{\chi a}^2\left(1 - \frac{4m_{\chi}^2}{m_Z^2}\right) + g_{\chi v}^2\left(1 + \frac{2m_{\chi}^2}{m_Z^2}\right)\right], \tag{2.2}$$

where again $a = 1(1/2)$ for dark matter that is a Dirac (Majorana) fermion. In the shaded regions appearing in the upper left corner of each frame of figure 2, the predicted invisible width of the Z exceeds the value measured at LEP by more the 2σ, corresponding to a contribution of $\Gamma_Z^{\rm inv} > 1.5\,{\rm MeV}$ [3]. Combined with relic abundance considerations, this constraint translates to $m_{\chi} > 25\,{\rm GeV}$ (32 GeV) for the case of a purely vector (axial) coupling to the Z.

Direct detection experiments provide a powerful test of dark matter candidates with non-negligible couplings to the Z. After integrating out the Z, the effective interaction relevant for dark matter scattering with nuclei is given by:

$$\mathcal{L} = \frac{1}{m_Z^2}\left[\bar{\chi}\gamma^{\mu}(g_{\chi v} + g_{\chi a}\gamma^5)\chi\right]\left[\bar{q}\gamma^{\mu}(g_{qv} + g_{qa}\gamma^5)q\right], \tag{2.3}$$

JCAP12(2016)029

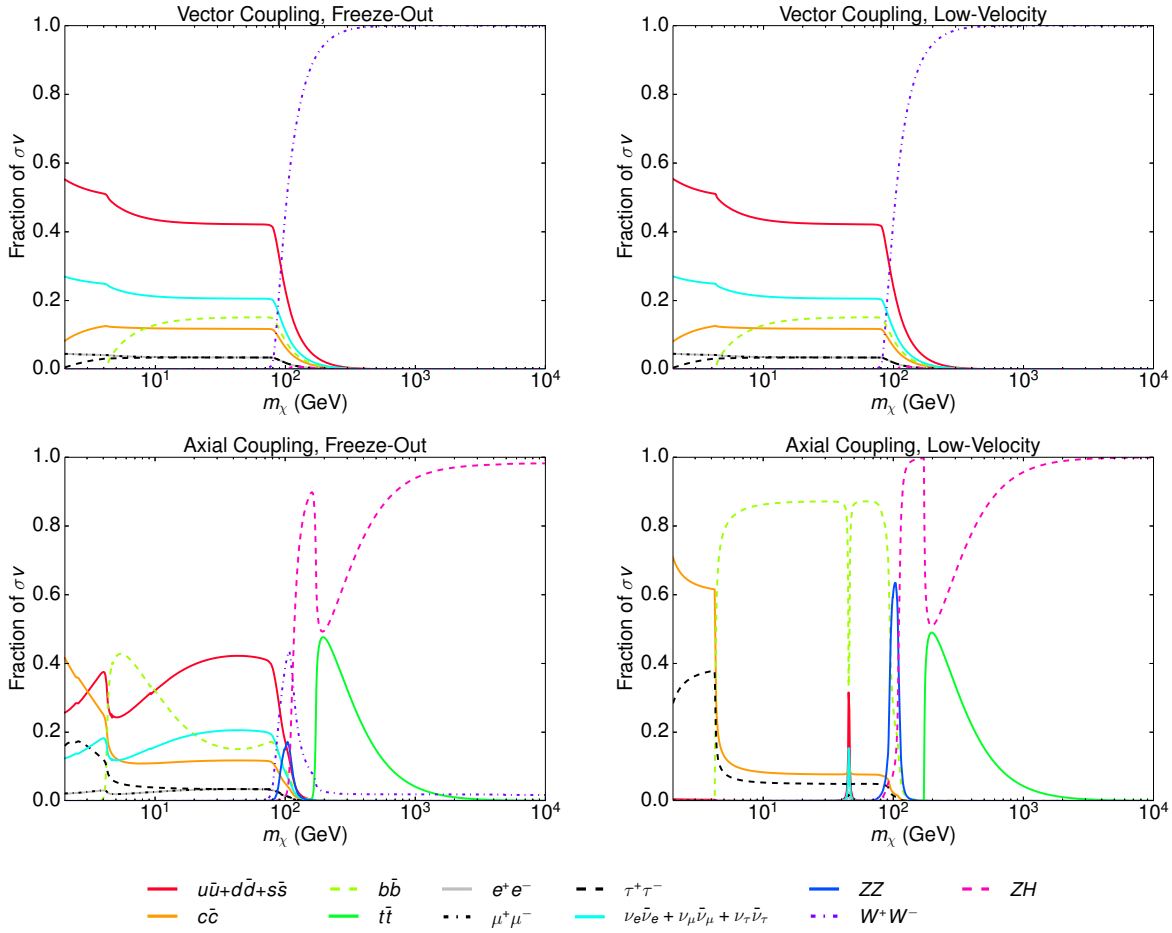

Figure 1. The fraction of dark matter annihilations that proceed to each final state, as evaluated at the temperature of thermal freeze-out (left) and at $v = 10^{-3}\,c$, as is typically relevant for indirect detection (right). The upper and lower frames correspond to dark matter in the form of a fermion with purely vector or purely axial couplings to the Z, respectively.

where $g_{uv} = g_2\left(\frac{1}{4c_W} - \frac{2s_W^2}{3c_W}\right)$, $g_{dv} = g_2\left(-\frac{1}{4c_W} + \frac{s_W^2}{3c_W}\right)$, $g_{ua} = -g_2/4c_W$, $g_{da} = g_2/4c_W$, etc. are the couplings of the Z to Standard Model quarks.

At low energies, $\bar{\Psi}\gamma^i\Psi \to 0$ and $\bar{\Psi}\gamma^0\gamma^5\Psi \to 0$, and thus only vector-vector and axial-axial interactions are not suppressed by powers of velocity or momentum transfer. These interactions lead to spin-independent and spin-dependent scattering cross sections, respectively. The solid blue curves shown in figure 2 represent the current limits on the dark matter's coupling to the Z, as derived from the results of the direct detection experiment LUX [4] (the PandaX-II experiment has placed a constraint that is only slightly weaker [5]).[1]

[1]Although the spin-independent constraints from direct detection experiments are generally presented for the case of equal couplings to protons and neutrons, we have translated these results to apply to the models at hand. It is interesting to note that a cancellation in the vector couplings of the Z to up and down quarks leads to a suppression in the effective coupling to protons. In particular, Z exchange leads to the following ratio of cross sections with neutrons and protons: $\sigma_n/\sigma_p \approx (2g_{dv} + g_{uv})^2/(2g_{uv} + g_{dv})^2 \approx 180$. We also note that since xenon contains isotopes with an odd number of neutrons (^{129}Xe and ^{131}Xe with abundances of 29.5% and 23.7%, respectively), this target is quite sensitive to spin-dependent WIMP-neutron scattering. To constrain spin-dependent scattering, we converted the results of the most recent spin-independent analysis presented by the LUX collaboration [4].

JCAP12(2016)029

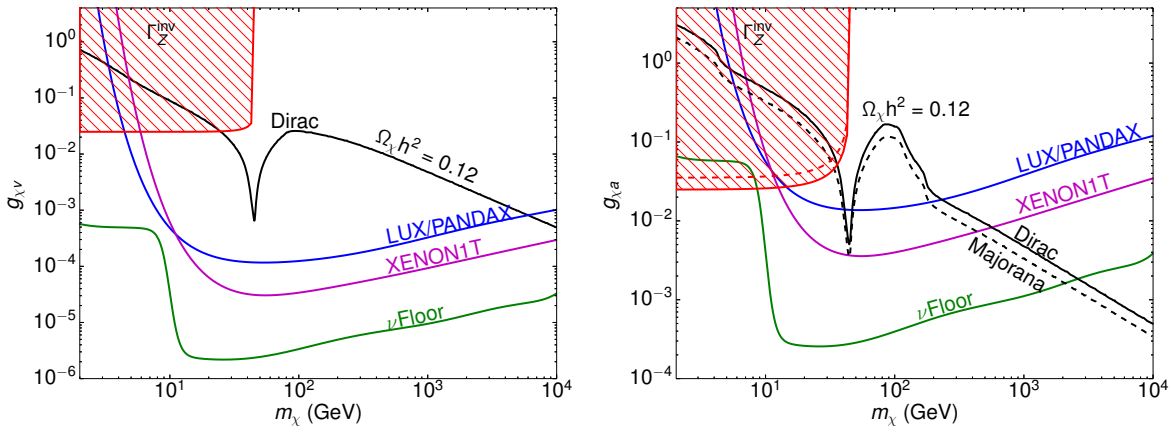

Figure 2. Constraints on the mass and couplings of a fermionic dark matter candidate that annihilates through the Z. The solid black contours indicate the value of the coupling for which the thermal relic abundance matches the measured cosmological dark matter density, $\Omega_\chi h^2 = 0.12$. The shaded regions are excluded by the measurement of the invisible Z width. The left and right frames depict the cases of a purely vector or axial coupling between the dark matter and the Z, respectively. The vast majority of this parameter space is excluded by the current constraints from LUX and PandaX-II [4, 5], and much of the currently viable parameter space is expected to be probed in the near future by XENON1T [6].

Together, these constraints rule out the majority of the parameter space for fermionic dark matter candidates that annihilate through Z exchange. After accounting for these constraints, we find that an acceptable thermal relic abundance can be obtained only in the near-resonance case [7–9] ($m_\chi = m_Z/2$) or for $m_\chi \gtrsim 200\,\text{GeV}$ with $g_{\chi a} \gg g_{\chi v}$, or for $m_\chi \gtrsim 6\,\text{TeV}$. Furthermore, with the exception of $m_\chi \gtrsim 500\,\text{GeV}$ with $g_{\chi a} \gg g_{\chi v}$, we expect that the remaining parameter space will be probed in the near future by direct detection experiments such as XENON1T [6]. We point out that for fermionic dark matter heavier than several TeV, perturbative unitarity is lost, and higher dimension operators such as those ones considered in ref. [10] may become relevant for the phenomenology. It is interesting to note that within the context of the MSSM, a bino-like neutralino (with a subdominant higgsino fraction) can possess the characteristics found within this scenario [11].

In the narrow region of viable parameter space found near the Z pole, the dark matter in this class of models annihilates with a cross section that is chirality suppressed in the low-velocity limit, $\sigma v \propto (m_f/m_\chi)^2$, leading such annihilations to proceed mostly to $b\bar{b}$ final states. In this mass range, the low-velocity cross section is sensitive to the value of the dark matter's mass, but consistently below the reach of planned indirect detection experiments (for analytic expressions of this cross section, see the appendix of ref. [17]). In figure 3, we plot the effective low-velocity annihilation cross section (as relevant for indirect detection) for fermionic dark matter with an axial coupling to the Z.[2] These cross sections are well below the constraints derived from Fermi and other existing indirect detection experiments [12–16].

2.2 Scalar dark matter

A complex scalar dark matter candidate, ϕ, can couple to the Z through the following interaction:

$$\mathcal{L} \supset i\, g_\phi \phi^\dagger \overleftrightarrow{\partial_\mu} \phi Z^\mu + g_\phi^2 \phi^2 Z^\mu Z_\mu. \tag{2.4}$$

[2]By "effective" annihilation cross section we denote the value for the case of identical annihilating particles (Majorana fermions). For a Dirac fermion (or a complex boson), the actual particle-antiparticle annihilation cross section is equal to twice this value.

JCAP12(2016)029

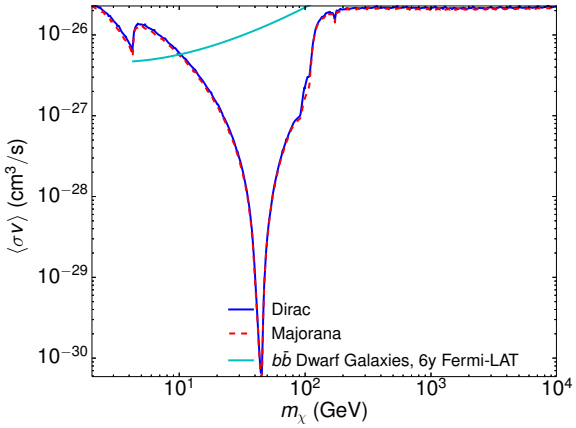

Figure 3. The effective low-velocity annihilation cross section (relevant for indirect detection) for Dirac or Majorana dark matter with an axial coupling to the Z. We note that for the masses in the range not yet excluded by LUX or PandaX-II, this cross section is well below the constraints derived from Fermi and other existing indirect detection experiments [12–16]. We also show the current constraint from Fermi's observation of dwarf spheroidal galaxies [13].

The annihilation cross section to fermion pairs in this case is suppressed by two powers of velocity, and values of g_ϕ that lead to an acceptable thermal relic abundance are shown as a black solid line in the left frame of figure 4. We also show in this figure the region of parameter space that is excluded by the measurement of the invisible width of the Z, which receives the following contribution in this case:

$$\Gamma(Z \to \phi\phi^\dagger) = \frac{g_\phi^2 m_Z}{48\pi}\left(1 - \frac{4m_\phi^2}{m_Z^2}\right)^{3/2}. \tag{2.5}$$

In this model, there is an unsuppressed cross section for spin-independent elastic scattering with nuclei, leading to very stringent constraints from LUX and PandaX-II. In the left frame of figure 4, we see that the entire parameter space in this scenario is strongly ruled out by a combination of constraints from LUX/PandaX-II and the invisible width of the Z.

2.3 Vector dark matter

An interaction between the Z and a spin-one dark matter candidate, X, can arise at tree-level only through a kinetic term. In this case, gauge invariance requires the interaction to take the following form:

$$\mathcal{L} \supset i\, g_X \left(Z^\mu\, X^{\nu\,\dagger} \partial_{[\mu} X_{\nu]} + X^\dagger_\mu X_\nu\, \partial^\mu Z^\nu\right) + \text{h.c.} \tag{2.6}$$

In the right frame of figure 4, we summarize the parameter space in this model. In particular, we apply constraints from the invisible width of the Z, which receives the following contribution in this case:

$$\Gamma(Z \to XX^\dagger) = \frac{g_X^2 m_Z \left(1 - 8r_{XZ}^2 + 28r_{XZ}^4 - 48r_{XZ}^6\right)\left(1 - 4r_{XZ}^2\right)^{1/2}}{192\pi r_{XZ}^4}, \tag{2.7}$$

where $r_{XZ} \equiv m_X/m_Z$.

JCAP12(2016)029

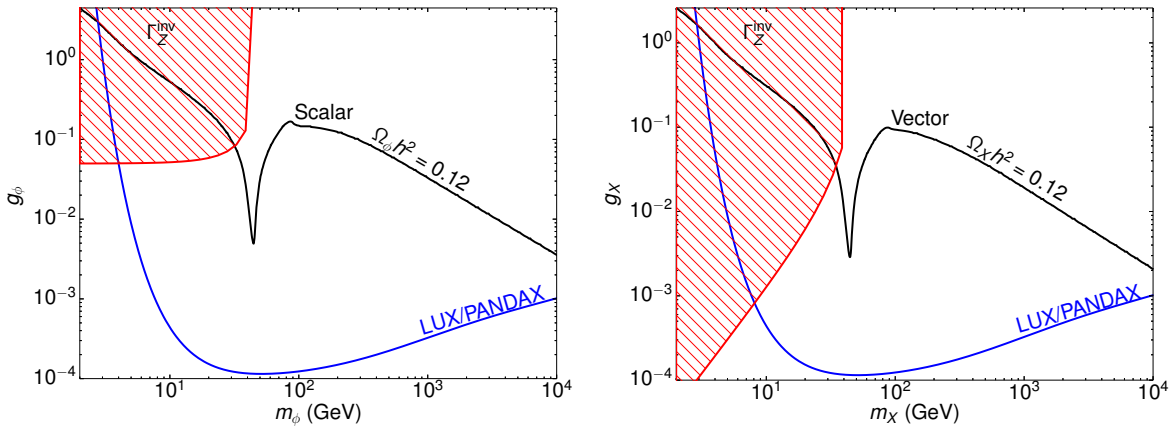

Figure 4. Constraints on mass and couplings of a complex scalar (left frame) or complex vector (right frame) dark matter candidate which annihilates through the Z. The solid black contours indicate the value of the coupling for which the thermal relic abundance matches the measured cosmological dark matter density, $\Omega_\chi h^2 = 0.12$. The shaded regions are excluded by measurements of the invisible Z width, and the regions above the solid blue line are excluded by the current constraints from LUX and PandaX-II [4, 5]. The entire parameter space in each of these scenarios is strongly ruled out.

After integrating our the Z, this model yields the following effective interaction for elastic scattering with nuclei (retaining only unsuppressed terms):

$$\mathcal{L}_{\rm eff} \supset \frac{i g_\chi g_{qv}}{m_Z^2} \left(X_\nu \partial_\mu X^{\nu\dagger} \bar{q} \gamma^\mu q + \text{h.c.} \right). \tag{2.8}$$

In the non-relativistic limit, this yields the following WIMP-nucleus cross section:

$$\begin{aligned} \sigma_{\chi N} &= \frac{g_\chi^2 \mu_{\chi N}^2}{\pi m_Z^4} \Big[Z(2g_{uv} + g_{dv}) + (A - Z)(g_{uv} + 2g_{dv}) \Big]^2 \\ &\approx \frac{g_\chi^2 (g_1^2 + g_2^2) \mu_{\chi N}^2}{16 \pi m_Z^4} (A - Z)^2, \end{aligned} \tag{2.9}$$

where Z and A are the atomic number and atomic mass of the target nucleus, and $\mu_{\chi N}$ is the reduced mass of the dark matter-nucleus system.

In the right frame of figure 4, we see that this combination of constraints from direct detection experiments and the invisible width of the Z strongly rules out the entire parameter space of this model.

3 Higgs mediated dark matter

3.1 Fermionic dark matter

In this subsection, we consider a dark matter candidate that is either a Dirac or Majorana fermion, with the following interactions with the SM Higgs boson:

$$\mathcal{L} \supset \left[a \bar{\chi} (\lambda_{\chi s} + \lambda_{\chi p} i \gamma^5) \chi \right] H, \tag{3.1}$$

where once again $a = 1(1/2)$ in the Dirac (Majorana) case. The quantities $\lambda_{\chi s}$ and $\lambda_{\chi p}$ denote the scalar and pseudoscalar couplings between the dark matter and the SM Higgs, respectively.

JCAP12(2016)029

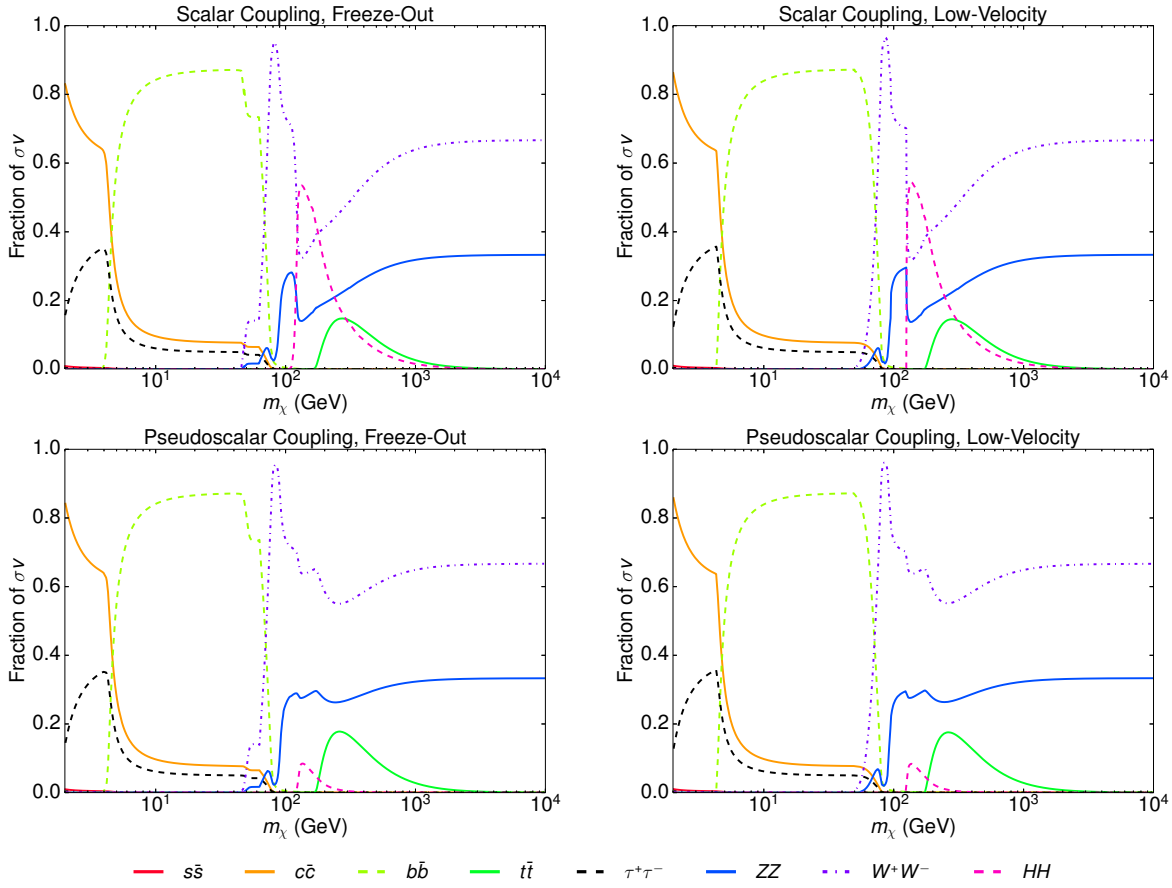

Figure 5. The fraction of dark matter annihilations that proceed to each final state, as evaluated at the temperature of thermal freeze-out (left) and at $v = 10^{-3}\,c$, as is typically relevant for indirect detection (right). The upper and lower frames correspond to dark matter in the form of a fermion with purely scalar or purely pseudoscalar couplings to the Standard Model Higgs boson, respectively.

Dark matter annihilations in this model depend strongly on the choice of scalar or pseudoscalar couplings. In particular, scalar couplings lead to an annihilation cross section that is suppressed by two powers of velocity, whereas pseudoscalar couplings generate an s-wave amplitude with no such suppression. In both cases, annihilations proceed dominantly to heavy final states (see figure 5), due to the couplings of the Higgs to the particle content of the SM.

The contribution to the invisible Higgs width in this case is given by:

$$\Gamma(H \to \chi\bar{\chi}) = \frac{a\, m_H}{8\pi}\left[\lambda_{\chi p}^2 + \lambda_{\chi s}^2\left(1 - \frac{4m_\chi^2}{m_H^2}\right)\right]\sqrt{1 - \frac{4m_\chi^2}{m_H^2}}. \tag{3.2}$$

The current experimental constraint on the invisible branching fraction of the Higgs is $\Gamma_{\rm inv}/(\Gamma_{\rm inv} + \Gamma_{\rm SM}) < 0.24$,[3] which for $\Gamma_{\rm SM}^H \approx 4.07\,\text{MeV}$ corresponds to the following:

$$\Gamma(H \to \chi\bar{\chi}) < \Gamma_{\rm SM}^H \frac{\text{BR}(H \to \text{inv})}{1 - \text{BR}(H \to \text{inv})} \approx 1.29\,\text{MeV}. \tag{3.3}$$

[3]This is derived from a combination of Run I and 2015 LHC data. See, for example, page 25 of the talk "Search for invisible decays of the 125 GeV Higgs boson using the CMS detector", by Nicholas Wardle, http://indico.cern.ch/event/432527/contributions/1071583/attachments/1320936/1980904/nckw_ICHEP_2016_hinv_cms.pdf.

JCAP12(2016)029

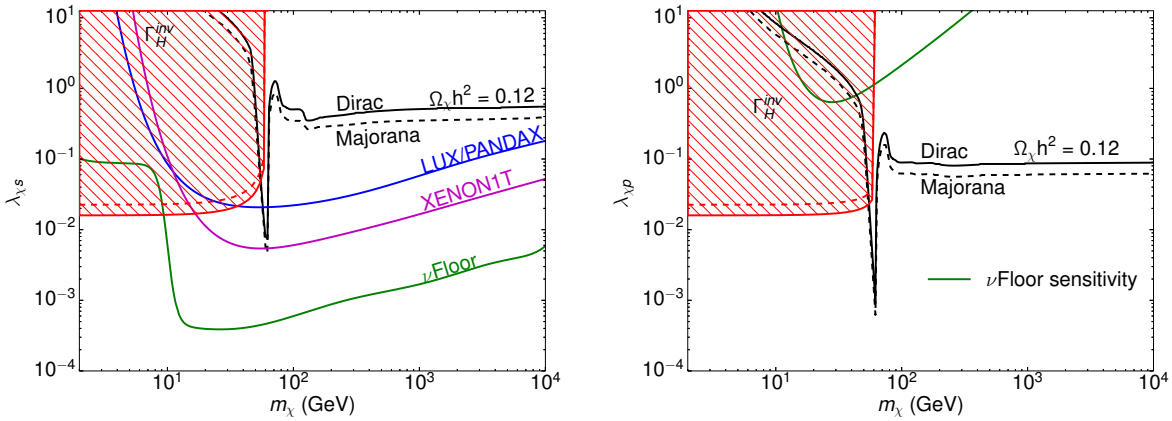

Figure 6. Constraints on mass and couplings of a fermionic dark matter candidate which annihilates through the Standard Model Higgs boson. The solid black contours indicate the value of the coupling for which the thermal relic abundance matches the measured cosmological dark matter density, $\Omega_\chi h^2 = 0.12$. The shaded regions are excluded by measurements of the invisible Higgs width. The left and right frames depict the cases of a purely scalar or pseudoscalar coupling between the dark matter and the Higgs, respectively. In the scalar case, the vast majority of this parameter space is excluded by the current constraints from LUX and PandaX-II [4, 5]. The only currently viable region ($m_\chi = 56$–$62\,\mathrm{GeV}$ is expected to be probed in the near future by XENON1T [6]. Due to the momentum suppression of the elastic scattering cross section, the case of dark matter with a pseudoscalar coupling to the Higgs is much less strongly constrained.

Elastic scattering between dark matter and nuclei is entirely spin-independent in this case, with a cross section given as follows:

$$\sigma_{\chi N} \approx \frac{\mu_{\chi N}^2}{\pi m_H^4} \left[Z f_p + (A - Z) f_n\right]^2 \left[\lambda_{\chi s}^2 + \lambda_{\chi p}^2 \frac{q^2}{4 m_\chi^2}\right], \tag{3.4}$$

where q is the momentum exchanged in the collision.

In figure 6, we summarize the constraints on this scenario. In the case of a purely scalar coupling ($\lambda_{\chi p} = 0$, shown in the left frame), the combination of the invisible Higgs width measurement and the results of direct detection experiments rule out nearly all of the parameter space. The exception is the mass range within a few GeV of the Higgs pole, $m_\chi = 56$–$62\,\mathrm{GeV}$. In this case, future experiments such as XENON1T are expected to test the remaining region of parameter space.

In the case of a purely pseudoscalar coupling ($\lambda_{\chi s} = 0$, shown in the right frame of figure 6), the momentum suppression of the elastic scattering cross section strongly reduces the prospects for direct detection experiments, earning this scenario the moniker of "coy dark matter" [18–20]. Naively, we expect the sensitivity of direct detection experiments to the coupling, $\lambda_{\chi p}$, to be suppressed relative to $\lambda_{\chi s}$ by a factor of $q/2m_\chi$, which for typical scattering events is on the order of 10^{-3}. Simply rescaling the results shown in the left frame of figure 6 by this factor leads us to conclude that current (LUX, PandaX-II) and near future (XENON1T) experiments will not be sensitive to dark matter in this scenario. It is less clear, however, whether a larger experiment, with a sensitivity to cross sections near the neutrino floor, might be sensitive to this scenario. With this in mind, we have calculated the sensitivity of such an experiment to a dark matter candidate with a momentum suppressed elastic scattering cross section with nuclei.

JCAP12(2016)029

Dark matter with velocity or momentum suppressed scattering has been considered previously in the literature (see, for example, refs. [21–30]). To compute the number of events in a large volume xenon experiment, we follow the procedure outlined in ref. [30], adopting a standard Maxwellian velocity distribution ($v_0 = 220\,\mathrm{km/s}$, $v_{\rm esc} = 544\,\mathrm{km/s}$, $\bar{v}_{\rm Earth} = 245\,\mathrm{km/s}$), a local density of $0.3\,\mathrm{GeV/cm^3}$, and a Helm form factor [31]. Regarding the detector specifications, we assume an optimistic scenario with an energy independent efficiency of 25% and perfect energy resolution. We consider events with nuclear recoil energies between 6 and 30 keV, where this lower limits was imposed in order to reduce the rate of neutrino-induced background events [32, 33]. From the calculated event rate, we apply Poisson statistics to place a 90% confidence level constraint on the dark matter coupling, assuming that zero events are observed. In the right frame of figure 6, we plot the projected constraint from such an experiment after collecting an exposure of 30 ton-years, which is approximately the exposure that we estimate will accumulate between ∼1–3 neutrino-induced background events. From this, we conclude that even with such an idealized detector, it will not be possible to test a dark matter candidate with a purely pseudoscalar coupling to the Higgs.

In the case of dark matter with a scalar coupling and near the Higgs pole, the low-velocity annihilation cross section is suppressed by two powers of velocity, making such a scenario well beyond the reach of any planned or proposed indirect detection experiment (see the left frame of figure 7). In the case of dark matter with a pseudoscalar coupling to the Higgs, however, the low-velocity annihilation rate is unsuppressed, leading to more promising prospects for indirect detection (for analytic expressions of these cross section, see the appendix of ref. [17]). In the right frame of figure 7, we plot the low-velocity annihilation cross section (as relevant for indirect detection) for fermionic (Dirac or Majorana) dark matter with a pseudoscalar coupling to the SM Higgs boson. In this case, constraints from Fermi's observations of dwarf spheroidal galaxies [13] may be relevant, depending on the precise value of the dark matter mass. We also note that uncertainties associated with the distribution of dark matter in these systems could plausibly weaken these constraints to some degree [34–37]. It may also be possible in this scenario [18, 38–41] to generate the gamma-ray excess observed from the region surrounding the Galactic Center [42–48].

3.2 Scalar dark matter

In the case of scalar dark matter with a coupling to the SM Higgs boson, we consider a Higgs Portal interaction, described by the following Lagrangian:

$$\mathcal{L} \supset a\,\lambda_{\phi H}\left[v H \phi^2 + \frac{1}{2} H^2 \phi^2\right], \tag{3.5}$$

where $a = 1\,(1/2)$ in the case of a complex (real) scalar, and v is the vacuum expectation value of the SM Higgs boson.

In this class of models, the dark matter annihilates without velocity suppression, and preferentially to heavy final states (see figure 8). The contribution to the invisible Higgs width in this case is given by:

$$\Gamma(H \to \phi\phi^\dagger) = \frac{a\,v^2\lambda_{\phi H}^2}{16\,\pi m_H}\sqrt{1 - \frac{4m_\phi^2}{m_H^2}}. \tag{3.6}$$

In figure 9, we plot a summary of the constraints in this class of models. In this case, we find that complex (real) scalar dark matter with a mass greater than 840 GeV (400 GeV) is

JCAP12(2016)029

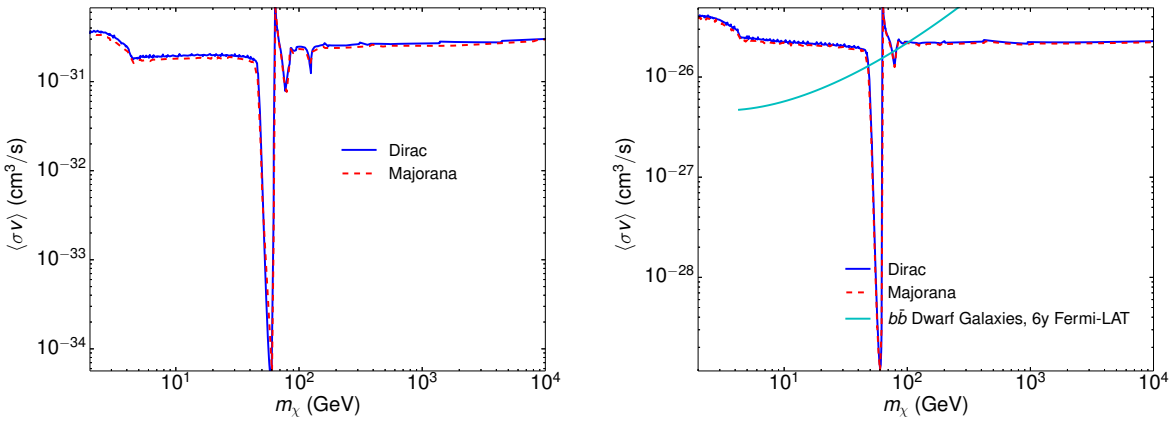

Figure 7. The effective low-velocity annihilation cross section (relevant for indirect detection) for Dirac or Majorana dark matter with a scalar (left) or pseudoscalar (right) coupling to the SM Higgs boson. For the case of scalar couplings, the cross section is always well below the sensitivity of Fermi and other existing indirect detection experiments. In the pseudoscalar case, the prospects for indirect detection are much more encouraging. In the right frame, we also show the current constraint from Fermi's observation of dwarf spheroidal galaxies [13].

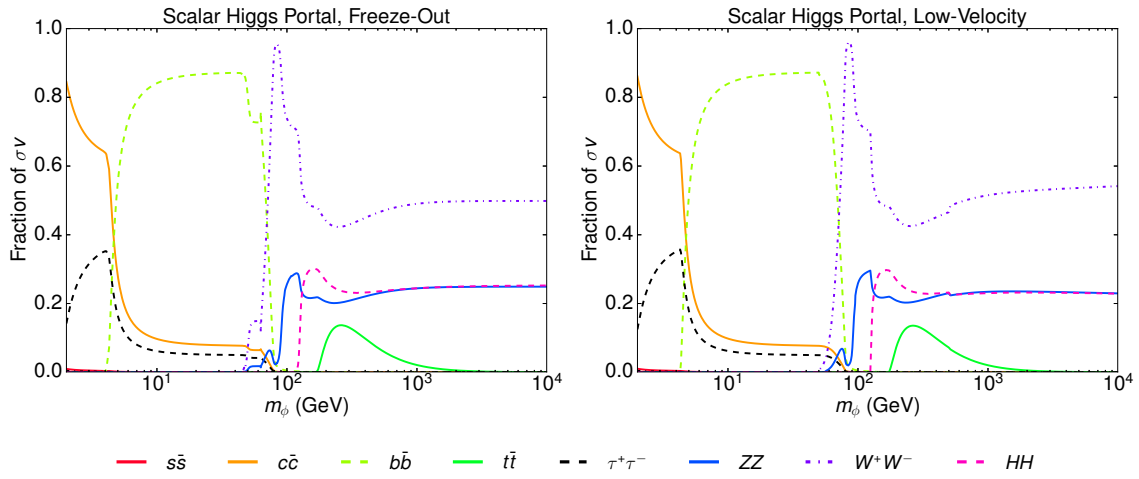

Figure 8. The fraction of dark matter annihilations that proceed to each final state, as evaluated at the temperature of thermal freeze-out (left) and at $v = 10^{-3}\,c$, as is typically relevant for indirect detection (right), for the case of scalar dark matter coupled to the Standard Model Higgs boson.

not currently constrained, along with the region near the Higgs pole. XENON1T is expected to probe the remaining high mass window up to 10 TeV (5 TeV). Similar constraints can be found in the recent analysis of [49].

In figure 10, we plot the low-velocity annihilation cross section (as relevant for indirect detection) for scalar dark matter with a Higgs portal coupling. In the currently allowed mass range near the Higgs pole, this class of models predicts a very small low-velocity annihilation cross section, which is likely unable to generate the measured intensity of the Galactic Center gamma-ray excess [42–48] (see also, refs. [50, 51]).

JCAP12(2016)029

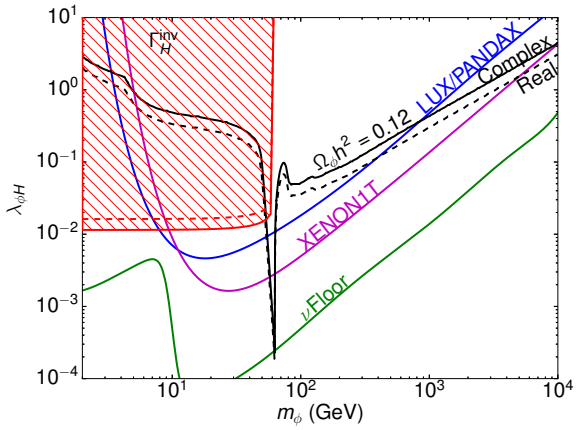

Figure 9. Constraints on mass and couplings of a complex scalar dark matter candidate which annihilates through a Higgs portal coupling. The solid black contour indicates the value of the coupling for which the thermal relic abundance matches the measured cosmological dark matter density, $\Omega_\chi h^2 = 0.12$. The shaded region is excluded by measurements of the invisible Higgs width, and the region above the solid blue line is excluded by the current constraints from LUX and PandaX-II [4, 5]. This scenario is currently viable only if the mass of the dark matter candidate is near the Higgs pole ($m \simeq m_H/2$) or if $m_\phi \gtrsim 400\,\text{GeV}$.

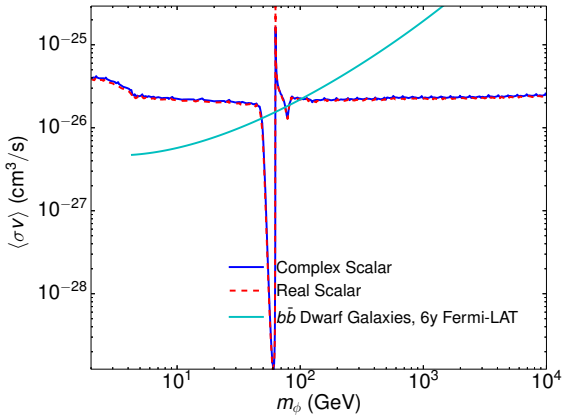

Figure 10. The effective low-velocity annihilation cross section (relevant for indirect detection) for complex or real scalar dark matter with a Higgs portal coupling. We also show the current constraint from Fermi's observation of dwarf spheroidal galaxies [13].

3.3 Vector dark matter

In the case of vector dark matter, we again consider a Higgs Portal interaction, which is described in this case by the following Lagrangian:

$$\mathcal{L} \supset a\lambda_{XH}\left[vHX^\mu X_\mu^\dagger + \frac{1}{2}H^2 X^\mu X_\mu^\dagger\right], \tag{3.7}$$

where $a = 1\,(1/2)$ in the case of a complex (real) vector. As in the cases considered in the previous subsection, dark matter annihilates without velocity suppression in this class of models, and preferentially to heavy final states (see figure 11).

JCAP12(2016)029

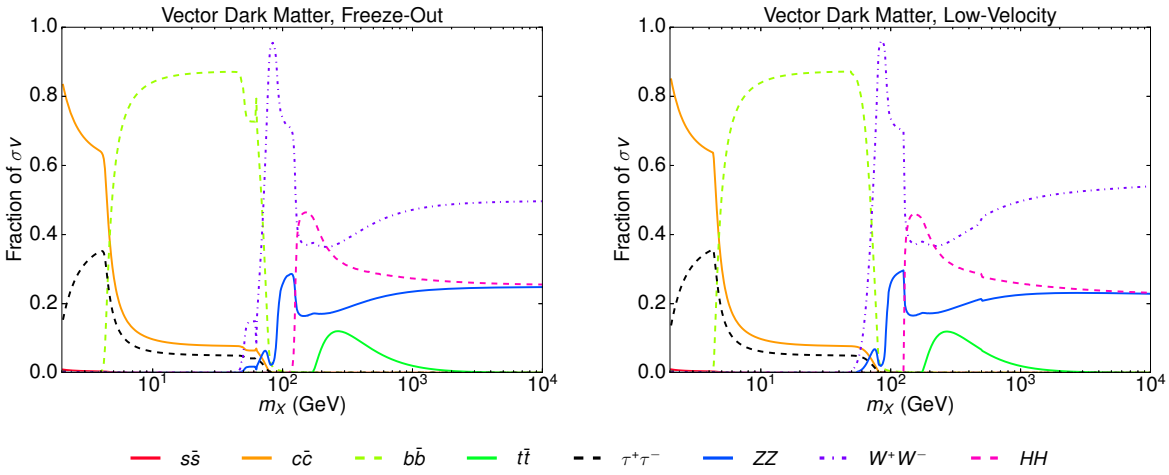

Figure 11. The fraction of dark matter annihilations that proceed to each final state, as evaluated at the temperature of thermal freeze-out (left) and at $v = 10^{-3}\,c$, as is typically relevant for indirect detection (right), for the case of dark matter in the form of a vector which annihilates through its coupling to the Standard Model Higgs boson.

The contribution to the invisible Higgs width is given in this model by:

$$\Gamma(H \to XX^\dagger) = \frac{a\,\lambda_{XH}^2 v^2 m_H^3}{64\pi m_X^4}\left(1 - 4\frac{m_X^2}{m_H^2} + 12\frac{m_X^4}{m_H^4}\right)\sqrt{1 - \frac{4m_X^2}{m_H^2}}. \tag{3.8}$$

The constraints on this scenario are summarized in figure 12. The combination of constraints from LUX/PandaX-II and on the invisible Higgs width rule out all of the parameter space in this class of models, with the exception of the mass range near the Higgs pole, $m_X \simeq m_H/2$ or for $m_X \gtrsim 1160\,\text{GeV}$. XENON1T is expected in the near future to probe most of this remaining high mass window, covering nearly the entire range of perturbative values for the coupling, $\lambda_{XH} \lesssim 4\pi$.

We plot in figure 13 the low-velocity annihilation cross section (as relevant for indirect detection) in this class of models, along with the constraints from Fermi's observations of dwarf spheroidal galaxies [13]. In the currently allowed mass range near the Higgs pole, this class of models predicts a very small low-velocity annihilation cross section, which is likely unable to generate the measured intensity of the Galactic Center gamma-ray excess [42–48].

4 Caveats

The conclusions presented here rely on a number of assumptions that we have implicitly made throughout this study. In particular, we have assumed that the thermal history of the early universe is well described by the standard radiation-dominated picture. Departures from this simple thermal history could potentially reduce the couplings of the dark matter that are required to generate an acceptable thermal relic abundance, thereby relaxing the constraints from direct detection experiments and from measurements of the invisible Z and Higgs widths. Examples of such scenarios include those in which the abundance of dark matter is depleted as a result of an out-of-equilibrium decay [52–58] or a period of late-time inflation [59–63].

JCAP12(2016)029

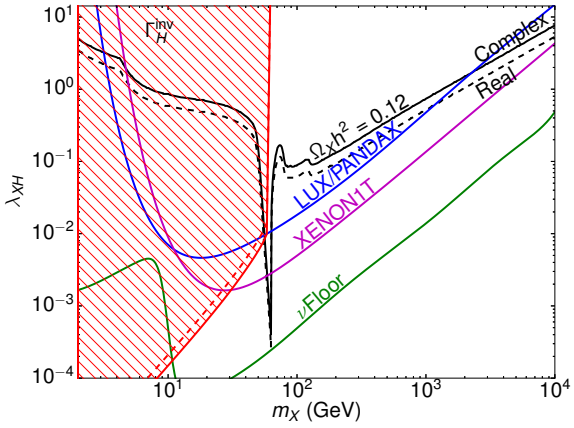

Figure 12. Constraints on mass and couplings of a complex vector dark matter candidate which annihilates through the Standard Model Higgs boson. The solid black contour indicates the value of the coupling for which the thermal relic abundance matches the measured cosmological dark matter density, $\Omega_\chi h^2 = 0.12$. The shaded region is excluded by measurements of the invisible Higgs width, and the region above the solid blue line is excluded by the current constraints from LUX and PandaX-II [4, 5]. This scenario is currently viable only if the mass of the dark matter candidate is near the Higgs pole ($m \simeq m_H/2$) or if $m_X \gtrsim 1160\,\text{GeV}$.

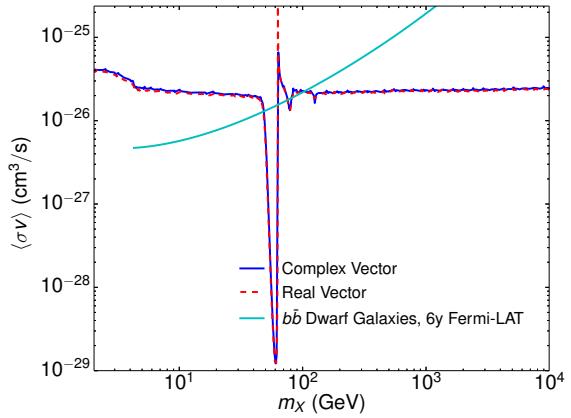

Figure 13. The effective low-velocity annihilation cross section (relevant for indirect detection) for complex or real vector dark matter with a coupling to the Standard Model Higgs boson. We also show the current constraint from Fermi's observation of dwarf spheroidal galaxies [13].

We have also limited our analysis in this paper to couplings between pairs of dark matter particles and one or more Z or Higgs bosons. We could instead have considered couplings between one dark matter particle, the Z or Higgs, and an additional state. If the additional state is not much heavier than the dark matter itself, such a coupling could allow the dark matter to be depleted in the early universe through coannihilations [64, 65], without necessarily inducing a large elastic scattering cross section with nuclei. Generally speaking, if such coannihilations are to be efficient, such states must have a mass that is within roughly $\sim$10% of the mass of the dark matter particle itself.

Phenomenology of this kind can be easily realized if we consider a Dirac fermion that is split into a pair of nearly degenerate Majorana fermions by a small Majorana mass term.

JCAP12(2016)029

Following refs. [66, 67], the Lagrangian in this scenario takes the following form:

$$\mathcal{L} \supset \frac{1}{2}\bar{\Psi}_1 i\gamma^\mu \partial_\mu \Psi_1 - \frac{1}{2}(M - m_+)\bar{\Psi}_1\Psi_1 + \frac{1}{2}\bar{\Psi}_2 i\gamma^\mu \partial_\mu \Psi_2 - \frac{1}{2}(M + m_+)\bar{\Psi}_2\Psi_2 \\ + i\,g\,Q\,Z_\mu\,\bar{\Psi}_2\gamma_\mu\Psi_1 + \frac{1}{2}\,g\,Q\,Z_\mu\,\frac{m_-}{M}\,\left(\bar{\Psi}_2\gamma^\mu\gamma^5\Psi_2 - \bar{\Psi}_1\gamma^\mu\gamma^5\Psi_1\right) + \mathcal{O}\left(\frac{m^2}{M^2}\right), \tag{4.1}$$

where Ψ_1 and Ψ_2 are the two quasi-degenerate Majorana fermions, $m_\pm = (m_L \pm m_R)/2$, and $M \gg m_{L,R}$. Setting $m_R = 0$, this reduces to

$$\mathcal{L} \supset \frac{1}{2}\bar{\Psi}_1 i\gamma^\mu \partial_\mu \Psi_1 - \frac{1}{2}M_1\bar{\Psi}_1\Psi_1 + \frac{1}{2}\bar{\Psi}_2 i\gamma^\mu \partial_\mu \Psi_2 - \frac{1}{2}M_2\bar{\Psi}_2\Psi_2 \\ + i\,g_{cv}\,Z_\mu\,\bar{\Psi}_2\gamma_\mu\Psi_1 + \frac{1}{2}g_{cv}\,Z_\mu\,\frac{M_1 - M_2}{M_1 + M_2}\,\left(\bar{\Psi}_2\gamma^\mu\gamma^5\Psi_2 - \bar{\Psi}_1\gamma^\mu\gamma^5\Psi_1\right) + \mathcal{O}\left(\frac{M_1 - M_2}{M_1 + M_2}\right)^2,$$

where the $M_1 = M - m_+$ and $M_2 = M + m_+$ are the masses of the lighter and heavier Majorana fermions, respectively. As a result of this mass splitting, all couplings between two of the same Majorana fermion and the Z are suppressed by a factor of $|M_1 - M_2|/(M_1 + M_2) = m_+/M$, strongly limiting the rates of both self-annihilation and elastic scattering with nuclei. In contrast, interactions between the two different Majorana states, $\Psi_1\,\Psi_2$, and the Z are not suppressed, potentially allowing for coannihilations to efficiently deplete their abundances in the early universe.

Throughout this study, we have assumed that there is only one relevant particle in the dark sector. In some UV complete scenarios, however, there may be exist other light particles [68–70] which relax the constraints from direct detection experiments and from measurements of the invisible Z and Higgs widths.

5 Summary and conclusions

In this study, we have systematically considered dark matter models which annihilate through couplings to the Standard Model Z or Higgs boson. Overall, we find that the vast majority of the parameter space associated with these models is ruled out by a combination of direct detection experiments (LUX, PandaX-II, etc.) and measurements at colliders of the invisible Z and Higgs widths. If no detection is made, we expect experiments such as XENON1T to entirely rule out all remaining Z mediated models in the near future, with the exception of fermionic dark matter heavier than $\sim$500 GeV and with primarily axial couplings. Such experiments are also expected to test all remaining Higgs mediated models, with the exception of scalar or vector dark matter with masses very near the Higgs annihilation resonance ($m_{\rm DM} \simeq m_H/2$) or fermionic dark matter with a pseudoscalar (CP violating) coupling to the Standard Model Higgs boson. Very heavy dark matter with a large Higgs portal coupling ($\lambda_{\phi H}, \lambda_{XH} \gg 1$) may also be beyond the reach of XENON1T, although LUX-ZEPLIN and other planned experiments will be able to probe such models.

In table 1, we summarize the various classes of dark matter models that we have considered in this study, listing in each case the range of masses (if any) that is not currently excluded experimentally. For those cases that are not already excluded, we list whether XENON1T is expected to have the sensitivity required to test each class of model. We also present the range of low-velocity annihilation cross sections that can be found within the currently acceptable mass range. For those models with roughly $\sigma v \gtrsim 3 \times 10^{-27}$ cm^3/s (corresponding to $\sigma v \gtrsim 0.3$ in the units used in the table), the Galactic Center gamma-ray excess could plausibly be generated though dark matter annihilations.

JCAP12(2016)029

Dark Matter	Z, Higgs Coupling	Direct Detection	Allowed Region	Constrained by XENON1T	Indirect Detection (10^{-26} cm^3/s)
Majorana Fermion	$\bar{\chi}\gamma^\mu\gamma^5\chi Z_\mu$	SD	$m_\chi \sim m_Z/2$ or $m_\chi \gtrsim 190\,\text{GeV}$	Yes Up to 440 GeV	$\sigma v \simeq$ small $\sigma v \simeq 2.1$–2.3
Dirac Fermion	$\bar{\chi}\gamma^\mu\chi Z_\mu$	SI	$m_\chi \gtrsim 6\,\text{TeV}$	Yes	$\sigma v \simeq 2.1$–2.3
Dirac Fermion	$\bar{\chi}\gamma^\mu\gamma^5\chi Z_\mu$	SD	$m_\chi \sim m_Z/2$ or $m_\chi \gtrsim 240\,\text{GeV}$	Yes Up to 570 GeV	$\sigma v \simeq$ small $\sigma v \simeq 2.1$–2.3
Complex Scalar	$\phi^\dagger \overleftrightarrow{\partial_\mu} \phi Z^\mu$, $\phi^2 Z^\mu Z_\mu$	SI	Excluded	–	–
Complex Vector	$(X_\nu^\dagger \partial_\mu X^\nu + \text{h.c.})\text{Z}^\mu$	SI	Excluded	–	–
Majorana Fermion	$\bar{\chi}\chi H$	SI	$m_\chi \sim m_H/2$	Yes	$\sigma v \simeq$ small
Majorana Fermion	$\bar{\chi}\gamma^5\chi H$	SI $\propto q^2$	$m_\chi \gtrsim 54\,\text{GeV}$	No	$\sigma v \simeq 0.0011$–3.4
Dirac Fermion	$\bar{\chi}\chi H$	SI	$m_\chi \sim m_H/2$	Yes	$\sigma v \simeq$small
Dirac Fermion	$\bar{\chi}\gamma^5\chi H$	SI $\propto q^2$	$m_\chi \gtrsim 56\,\text{GeV}$	No	$\sigma v \simeq 0.0012$–1.7
Real Scalar	$\phi^2 H^2$	SI	$m_\chi \sim m_H/2$ or $m_\chi \gtrsim 400\,\text{GeV}$	Maybe Up to 5 TeV	$\sigma v \simeq 0.0012$–0.019 $\sigma v \simeq 2.1$–2.3
Complex Scalar	$\phi^2 H^2$	SI	$m_\chi \sim m_H/2$ or $m_\chi \gtrsim 840\,\text{GeV}$	Maybe Up to 10 TeV	$\sigma v \simeq 0.0019$–0.017 $\sigma v \simeq 2.1$–2.3
Real Vector	$X_\mu X^\mu H^2$	SI	$m_\chi \sim m_H/2$ or $m_\chi \gtrsim 1160\,\text{GeV}$	Maybe Up to 15 TeV	$\sigma v \simeq 0.0018$–0.022 $\sigma v \simeq 2.1$–2.3
Complex Vector	$X_\mu^\dagger X^\mu H^2$	SI	$m_\chi \sim m_H/2$ or $m_\chi \gtrsim 2200\,\text{GeV}$	Maybe Yes	$\sigma v \simeq 0.0012$–0.0064 $\sigma v \simeq 2.1$–2.3

Table 1. A summary of the various classes of dark matter models that we have considered in this study. For each case, we list the range of masses (if any) that is not currently excluded experimentally. For those cases which are not already excluded, we state whether XENON1T is anticipated to be sensitive to that model. We also present the range of low-velocity annihilation cross sections that can be found in each case for masses within the currently acceptable range.

Acknowledgments

We would like to thank John Kearney for helpful conversations, and in particular for bringing to our attention an error that appeared in the first version of this paper. ME is supported by the Spanish FPU13/03111 grant of MECD and also by the European projects H2020-MSCA-RISE-2015 and H2020-MSCA-ITN-2015/674896-ELUSIVES. AB is supported by the Kavli Institute for cosmological physics at the University of Chicago through grant NSF PHY-1125897. DH is supported by the US Department of Energy under contract DE-FG02-13ER41958. Fermilab is operated by Fermi Research Alliance, LLC, under Contract No. DE-AC02-07CH11359 with the US Department of Energy. This work was carried out in part at the Aspen Center for Physics, which is supported by National Science Foundation grant PHY-1066293.

References

[1] G. Bélanger, F. Boudjema, A. Pukhov and A. Semenov, *MicrOMEGAs4.1: two dark matter candidates*, *Comput. Phys. Commun.* **192** (2015) 322 [arXiv:1407.6129] [INSPIRE].

JCAP12(2016)029

[2] Planck collaboration, P.A.R. Ade et al., *Planck 2015 results. XIII. Cosmological parameters*, *Astron. Astrophys.* **594** (2016) A13 [arXiv:1502.01589] [INSPIRE].

[3] Particle Data Group collaboration, K.A. Olive et al., *Review of Particle Physics*, *Chin. Phys.* **C 38** (2014) 090001 [INSPIRE].

[4] D.S. Akerib et al., *Results from a search for dark matter in the complete LUX exposure*, arXiv:1608.07648 [INSPIRE].

[5] PandaX-II collaboration, A. Tan et al., *Dark Matter Results from First 98.7 Days of Data from the PandaX-II Experiment*, *Phys. Rev. Lett.* **117** (2016) 121303 [arXiv:1607.07400] [INSPIRE].

[6] XENON collaboration, E. Aprile et al., *Physics reach of the XENON1T dark matter experiment*, *JCAP* **04** (2016) 027 [arXiv:1512.07501] [INSPIRE].

[7] S. Matsumoto, S. Mukhopadhyay and Y.-L.S. Tsai, *Effective Theory of WIMP Dark Matter supplemented by Simplified Models: Singlet-like Majorana fermion case*, *Phys. Rev.* **D 94** (2016) 065034 [arXiv:1604.02230] [INSPIRE].

[8] S. Matsumoto, S. Mukhopadhyay and Y.-L.S. Tsai, *Singlet Majorana fermion dark matter: a comprehensive analysis in effective field theory*, *JHEP* **10** (2014) 155 [arXiv:1407.1859] [INSPIRE].

[9] G. Arcadi, Y. Mambrini and F. Richard, *Z-portal dark matter*, *JCAP* **03** (2015) 018 [arXiv:1411.2985] [INSPIRE].

[10] A. De Simone, G.F. Giudice and A. Strumia, *Benchmarks for Dark Matter Searches at the LHC*, *JHEP* **06** (2014) 081 [arXiv:1402.6287] [INSPIRE].

[11] D. Hooper, C. Kelso, P. Sandick and W. Xue, *Closing Supersymmetric Resonance Regions With Direct Detection Experiments*, *Phys. Rev.* **D 88** (2013) 015010 [arXiv:1304.2417] [INSPIRE].

[12] D. Hooper, C. Kelso and F.S. Queiroz, *Stringent and Robust Constraints on the Dark Matter Annihilation Cross section From the Region of the Galactic Center*, *Astropart. Phys.* **46** (2013) 55 [arXiv:1209.3015] [INSPIRE].

[13] Fermi-LAT collaboration, M. Ackermann et al., *Searching for Dark Matter Annihilation from Milky Way Dwarf Spheroidal Galaxies with Six Years of Fermi Large Area Telescope Data*, *Phys. Rev. Lett.* **115** (2015) 231301 [arXiv:1503.02641] [INSPIRE].

[14] L. Bergstrom, T. Bringmann, I. Cholis, D. Hooper and C. Weniger, *New limits on dark matter annihilation from AMS cosmic ray positron data*, *Phys. Rev. Lett.* **111** (2013) 171101 [arXiv:1306.3983] [INSPIRE].

[15] G. Giesen et al., *AMS-02 antiprotons, at last! Secondary astrophysical component and immediate implications for Dark Matter*, *JCAP* **09** (2015) 023 [arXiv:1504.04276] [INSPIRE].

[16] M. Cirelli and G. Giesen, *Antiprotons from Dark Matter: Current constraints and future sensitivities*, *JCAP* **04** (2013) 015 [arXiv:1301.7079] [INSPIRE].

[17] A. Berlin, D. Hooper and S.D. McDermott, *Simplified Dark Matter Models for the Galactic Center Gamma-Ray Excess*, *Phys. Rev.* **D 89** (2014) 115022 [arXiv:1404.0022] [INSPIRE].

[18] C. Boehm, M.J. Dolan, C. McCabe, M. Spannowsky and C.J. Wallace, *Extended gamma-ray emission from Coy Dark Matter*, *JCAP* **05** (2014) 009 [arXiv:1401.6458] [INSPIRE].

[19] A. Hektor and L. Marzola, *Coy Dark Matter and the anomalous magnetic moment*, *Phys. Rev.* **D 90** (2014) 053007 [arXiv:1403.3401] [INSPIRE].

[20] J. Kozaczuk and T.A.W. Martin, *Extending LHC Coverage to Light Pseudoscalar Mediators and Coy Dark Sectors*, *JHEP* **04** (2015) 046 [arXiv:1501.07275] [INSPIRE].

[21] S. Chang, A. Pierce and N. Weiner, *Momentum Dependent Dark Matter Scattering*, *JCAP* **01** (2010) 006 [arXiv:0908.3192] [INSPIRE].

JCAP12(2016)029

[22] B. Feldstein, A.L. Fitzpatrick and E. Katz, *Form Factor Dark Matter*, *JCAP* **01** (2010) 020 [arXiv:0908.2991] [INSPIRE].

[23] S. Chang, A. Pierce and N. Weiner, *Using the Energy Spectrum at DAMA/LIBRA to Probe Light Dark Matter*, *Phys. Rev.* **D 79** (2009) 115011 [arXiv:0808.0196] [INSPIRE].

[24] K.R. Dienes, J. Kumar, B. Thomas and D. Yaylali, *Overcoming Velocity Suppression in Dark-Matter Direct-Detection Experiments*, *Phys. Rev.* **D 90** (2014) 015012 [arXiv:1312.7772] [INSPIRE].

[25] J. Fan, M. Reece and L.-T. Wang, *Non-relativistic effective theory of dark matter direct detection*, *JCAP* **11** (2010) 042 [arXiv:1008.1591] [INSPIRE].

[26] J.B. Dent, B. Dutta, J.L. Newstead and L.E. Strigari, *Effective field theory treatment of the neutrino background in direct dark matter detection experiments*, *Phys. Rev.* **D 93** (2016) 075018 [arXiv:1602.05300] [INSPIRE].

[27] A. Beniwal et al., *Combined analysis of effective Higgs portal dark matter models*, *Phys. Rev.* **D 93** (2016) 115016 [arXiv:1512.06458] [INSPIRE].

[28] V. Gluscevic, M.I. Gresham, S.D. McDermott, A.H.G. Peter and K.M. Zurek, *Identifying the Theory of Dark Matter with Direct Detection*, *JCAP* **12** (2015) 057 [arXiv:1506.04454] [INSPIRE].

[29] J. Kumar and D. Marfatia, *Matrix element analyses of dark matter scattering and annihilation*, *Phys. Rev.* **D 88** (2013) 014035 [arXiv:1305.1611] [INSPIRE].

[30] C. Savage, G. Gelmini, P. Gondolo and K. Freese, *Compatibility of DAMA/LIBRA dark matter detection with other searches*, *JCAP* **04** (2009) 010 [arXiv:0808.3607] [INSPIRE].

[31] J.D. Lewin and P.F. Smith, *Review of mathematics, numerical factors and corrections for dark matter experiments based on elastic nuclear recoil*, *Astropart. Phys.* **6** (1996) 87 [INSPIRE].

[32] J. Billard, L. Strigari and E. Figueroa-Feliciano, *Implication of neutrino backgrounds on the reach of next generation dark matter direct detection experiments*, *Phys. Rev.* **D 89** (2014) 023524 [arXiv:1307.5458] [INSPIRE].

[33] LZ collaboration, D.S. Akerib et al., *LUX-ZEPLIN (LZ) Conceptual Design Report*, arXiv:1509.02910 [INSPIRE].

[34] V. Bonnivard, C. Combet, D. Maurin and M.G. Walker, *Spherical Jeans analysis for dark matter indirect detection in dwarf spheroidal galaxies - Impact of physical parameters and triaxiality*, *Mon. Not. Roy. Astron. Soc.* **446** (2015) 3002 [arXiv:1407.7822] [INSPIRE].

[35] V. Bonnivard, D. Maurin and M.G. Walker, *Contamination of stellar-kinematic samples and uncertainty about dark matter annihilation profiles in ultrafaint dwarf galaxies: the example of Segue I*, *Mon. Not. Roy. Astron. Soc.* **462** (2016) 223 [arXiv:1506.08209] [INSPIRE].

[36] K. Ichikawa, M.N. Ishigaki, S. Matsumoto, M. Ibe, H. Sugai and K. Hayashi, *Foreground effect on the J-factor estimation of classical dwarf spheroidal galaxies*, arXiv:1608.01749 [INSPIRE].

[37] N. Klop, F. Zandanel, K. Hayashi and S. Ando, *Impact of axisymmetric mass models for dwarf spheroidal galaxies on indirect dark matter searches*, arXiv:1609.03509 [INSPIRE].

[38] A. Berlin, S. Gori, T. Lin and L.-T. Wang, *Pseudoscalar Portal Dark Matter*, *Phys. Rev.* **D 92** (2015) 015005 [arXiv:1502.06000] [INSPIRE].

[39] S. Ipek, D. McKeen and A.E. Nelson, *A Renormalizable Model for the Galactic Center Gamma Ray Excess from Dark Matter Annihilation*, *Phys. Rev.* **D 90** (2014) 055021 [arXiv:1404.3716] [INSPIRE].

[40] J. Fan, S.M. Koushiappas and G. Landsberg, *Pseudoscalar Portal Dark Matter and New Signatures of Vector-like Fermions*, *JHEP* **01** (2016) 111 [arXiv:1507.06993] [INSPIRE].

JCAP12(2016)029

[41] Y.G. Kim, K.Y. Lee, C.B. Park and S. Shin, *Secluded singlet fermionic dark matter driven by the Fermi gamma-ray excess*, *Phys. Rev.* **D 93** (2016) 075023 [arXiv:1601.05089] [INSPIRE].

[42] T. Daylan et al., *The characterization of the gamma-ray signal from the central Milky Way: A case for annihilating dark matter*, *Phys. Dark Univ.* **12** (2016) 1 [arXiv:1402.6703] [INSPIRE].

[43] D. Hooper and L. Goodenough, *Dark Matter Annihilation in The Galactic Center As Seen by the Fermi Gamma Ray Space Telescope*, *Phys. Lett.* **B 697** (2011) 412 [arXiv:1010.2752] [INSPIRE].

[44] D. Hooper and T. Linden, *On The Origin Of The Gamma Rays From The Galactic Center*, *Phys. Rev.* **D 84** (2011) 123005 [arXiv:1110.0006] [INSPIRE].

[45] L. Goodenough and D. Hooper, *Possible Evidence For Dark Matter Annihilation In The Inner Milky Way From The Fermi Gamma Ray Space Telescope*, arXiv:0910.2998 [INSPIRE].

[46] K.N. Abazajian and M. Kaplinghat, *Detection of a Gamma-Ray Source in the Galactic Center Consistent with Extended Emission from Dark Matter Annihilation and Concentrated Astrophysical Emission*, *Phys. Rev.* **D 86** (2012) 083511 [*Erratum ibid.* **D 87** (2013) 129902] [arXiv:1207.6047] [INSPIRE].

[47] C. Gordon and O. Macias, *Dark Matter and Pulsar Model Constraints from Galactic Center Fermi-LAT Gamma Ray Observations*, *Phys. Rev.* **D 88** (2013) 083521 [arXiv:1306.5725] [INSPIRE].

[48] FERMI-LAT collaboration, M. Ajello et al., *Fermi-LAT Observations of High-Energy γ-Ray Emission Toward the Galactic Center*, *Astrophys. J.* **819** (2016) 44 [arXiv:1511.02938] [INSPIRE].

[49] X.-G. He and J. Tandean, *New LUX and PandaX-II Results Illuminating the Simplest Higgs-Portal Dark Matter Models*, arXiv:1609.03551 [INSPIRE].

[50] A. Cuoco, B. Eiteneuer, J. Heisig and M. Krämer, *A global fit of the γ-ray galactic center excess within the scalar singlet Higgs portal model*, *JCAP* **06** (2016) 050 [arXiv:1603.08228] [INSPIRE].

[51] F.S. Sage and R. Dick, *Gamma ray signals of the annihilation of Higgs-portal singlet dark matter*, arXiv:1604.04589 [INSPIRE].

[52] A. Berlin, D. Hooper and G. Krnjaic, *Thermal Dark Matter From A Highly Decoupled Sector*, *Phys. Rev.* **D 94** (2016) 095019 [arXiv:1609.02555] [INSPIRE].

[53] A. Berlin, D. Hooper and G. Krnjaic, *PeV-Scale Dark Matter as a Thermal Relic of a Decoupled Sector*, *Phys. Lett.* **B 760** (2016) 106 [arXiv:1602.08490] [INSPIRE].

[54] D. Hooper, *Is the CMB Telling Us that Dark Matter is Weaker than Weakly Interacting?*, *Phys. Rev.* **D 88** (2013) 083519 [arXiv:1307.0826] [INSPIRE].

[55] N. Fornengo, A. Riotto and S. Scopel, *Supersymmetric dark matter and the reheating temperature of the universe*, *Phys. Rev.* **D 67** (2003) 023514 [hep-ph/0208072] [INSPIRE].

[56] G. Gelmini, P. Gondolo, A. Soldatenko and C.E. Yaguna, *The effect of a late decaying scalar on the neutralino relic density*, *Phys. Rev.* **D 74** (2006) 083514 [hep-ph/0605016] [INSPIRE].

[57] G. Kane, K. Sinha and S. Watson, *Cosmological Moduli and the Post-Inflationary Universe: A Critical Review*, *Int. J. Mod. Phys.* **D 24** (2015) 1530022 [arXiv:1502.07746] [INSPIRE].

[58] A.V. Patwardhan, G.M. Fuller, C.T. Kishimoto and A. Kusenko, *Diluted equilibrium sterile neutrino dark matter*, *Phys. Rev.* **D 92** (2015) 103509 [arXiv:1507.01977] [INSPIRE].

[59] H. Davoudiasl, D. Hooper and S.D. McDermott, *Inflatable Dark Matter*, *Phys. Rev. Lett.* **116** (2016) 031303 [arXiv:1507.08660] [INSPIRE].

[60] D.H. Lyth and E.D. Stewart, *Thermal inflation and the moduli problem*, *Phys. Rev.* **D 53** (1996) 1784 [hep-ph/9510204] [INSPIRE].

JCAP12(2016)029

[61] T. Cohen, D.E. Morrissey and A. Pierce, *Changes in Dark Matter Properties After Freeze-Out*, *Phys. Rev.* **D 78** (2008) 111701 [arXiv:0808.3994] [INSPIRE].

[62] T. Boeckel and J. Schaffner-Bielich, *A little inflation at the cosmological QCD phase transition*, *Phys. Rev.* **D 85** (2012) 103506 [arXiv:1105.0832] [INSPIRE].

[63] T. Boeckel and J. Schaffner-Bielich, *A little inflation in the early universe at the QCD phase transition*, *Phys. Rev. Lett.* **105** (2010) 041301 [*Erratum ibid.* **106** (2011) 069901] [arXiv:0906.4520] [INSPIRE].

[64] K. Griest and D. Seckel, *Three exceptions in the calculation of relic abundances*, *Phys. Rev.* **D 43** (1991) 3191 [INSPIRE].

[65] J. Edsjo and P. Gondolo, *Neutralino relic density including coannihilations*, *Phys. Rev.* **D 56** (1997) 1879 [hep-ph/9704361] [INSPIRE].

[66] D. Tucker-Smith and N. Weiner, *Inelastic dark matter*, *Phys. Rev.* **D 64** (2001) 043502 [hep-ph/0101138] [INSPIRE].

[67] Y. Cui, D.E. Morrissey, D. Poland and L. Randall, *Candidates for Inelastic Dark Matter*, *JHEP* **05** (2009) 076 [arXiv:0901.0557] [INSPIRE].

[68] A. Freitas, S. Westhoff and J. Zupan, *Integrating in the Higgs Portal to Fermion Dark Matter*, *JHEP* **09** (2015) 015 [arXiv:1506.04149] [INSPIRE].

[69] S. Baek, P. Ko, W.-I. Park and E. Senaha, *Higgs Portal Vector Dark Matter: Revisited*, *JHEP* **05** (2013) 036 [arXiv:1212.2131] [INSPIRE].

[70] S. Bhattacharya, S. Jana and S. Nandi, *Neutrino Masses and Scalar Singlet Dark Matter*, arXiv:1609.03274 [INSPIRE].

JCAP12(2016)029

Journal of Cosmology and Astroparticle Physics
An IOP and SISSA journal

Updated collider and direct detection constraints on Dark Matter models for the Galactic Center gamma-ray excess

Miguel Escudero,[a,b,1] **Dan Hooper**[b,c,d,2] **and Samuel J. Witte**[b,e,3]

[a]Instituto de Física Corpuscular (IFIC), CSIC-Universitat de València, Apartado de Correos 22085, E-46071 Valencia, Spain
[b]Fermi National Accelerator Laboratory, Center for Particle Astrophysics, Batavia, IL 60510, U.S.A.
[c]University of Chicago, Department of Astronomy and Astrophysics, Chicago, IL 60637, U.S.A.
[d]University of Chicago, Kavli Institute for Cosmological Physics, Chicago, IL 60637, U.S.A.
[e]University of California, Los Angeles, Department of Physics and Astronomy, Los Angeles, CA 90095, U.S.A.

E-mail: miguel.escudero@ific.uv.es, dhooper@fnal.gov, switte@physics.ucla.edu

Received December 28, 2016
Accepted February 10, 2017
Published February 20, 2017

Abstract. Utilizing an exhaustive set of simplified models, we revisit dark matter scenarios potentially capable of generating the observed Galactic Center gamma-ray excess, updating constraints from the LUX and PandaX-II experiments, as well as from the LHC and other colliders. We identify a variety of pseudoscalar mediated models that remain consistent with all constraints. In contrast, dark matter candidates which annihilate through a spin-1 mediator are ruled out by direct detection constraints unless the mass of the mediator is near an annihilation resonance, or the mediator has a purely vector coupling to the dark matter and a purely axial coupling to Standard Model fermions. All scenarios in which the dark matter annihilates through t-channel processes are now ruled out by a combination of the constraints from LUX/PandaX-II and the LHC.

Keywords: dark matter experiments, dark matter theory

ArXiv ePrint: 1612.06462

[1]ORCID: http://orcid.org/0000-0002-4487-8742.
[2]ORCID: http://orcid.org/0000-0001-8837-4127.
[3]ORCID: http://orcid.org/0000-0003-4649-3085.

doi:10.1088/1475-7516/2017/02/038

JCAP02(2017)038

Contents

1 Introduction

Over the past decade or so, a number of observations have been interpreted as possible signals of annihilating or decaying dark matter particles. Examples of such observations include the 511 keV emission from the Galactic Bulge [1], an excess of synchrotron emission known as the WMAP Haze [2, 3], an excess of high energy positrons in the cosmic ray spectrum [4, 5], a mono-energetic line of 130 GeV gamma rays from the Galactic Halo [6], and a 3.5 keV X-ray line from Perseus and other galaxy clusters [7, 8]. Each of these anomalies, however, has either failed to be confirmed by subsequent measurements [9, 10], or has been shown to be quite plausibly explained by astrophysical phenomena [11–14].

In comparison to these other anomalous signals, the gamma-ray excess observed from the Galactic Center by the Fermi Gamma-Ray Space Telescope stands out. This signal has been studied in detail over the past seven years [15–25] and has been shown with high statistical significance to exhibit a spectrum, morphology and overall intensity that is compatible with that predicted from annihilating dark matter particles in the form of a $\sim$30-70 GeV thermal relic distributed with a profile similar to that favored by numerical simulations. Although astrophysical interpretations of this signal have been proposed (consisting of either a large population of millisecond pulsars [26–33], or a series of recent leptonic cosmic-ray outbursts [34–36]), these explanations require either a significant degree of tuning in their parameters [34], or pulsar populations which are very different from those observed in the environments of globular clusters or in the field of the Milky Way [26, 31, 32]. In addition, some modest support for a dark matter interpretation of this signal has recently appeared in the form of excesses in the cosmic-ray antiproton spectrum [37–39], in the gamma-ray emission from the dwarf spheroidal galaxies Reticulum II and Tucana III [40–44], and from the observation of spatially extended gamma-ray emission from two dark matter subhalo candidates [45–48]. At this point in time, however, there is no clear resolution to the question of the origin of the Galactic Center excess.

JCAP02(2017)038

Dark Matter	*Mediator*	*Interactions*	Direct Detection
Dirac Fermion, χ	Spin-0	$\bar{\chi}\gamma^5\chi$, $\bar{f}f$	$\sigma_{\rm SI} \propto (q/2m_\chi)^2$
Majorana Fermion, χ	Spin-0	$\bar{\chi}\gamma^5\chi$, $\bar{f}f$	$\sigma_{\rm SI} \propto (q/2m_\chi)^2$
Dirac Fermion, χ	Spin-0	$\bar{\chi}\gamma^5\chi$, $\bar{f}\gamma^5 f$	$\sigma_{\rm SD} \propto (q^2/4m_n m_\chi)^2$
Majorana Fermion, χ	Spin-0	$\bar{\chi}\gamma^5\chi$, $\bar{f}\gamma^5 f$	$\sigma_{\rm SD} \propto (q^2/4m_n m_\chi)^2$
Complex Scalar, ϕ	Spin-0	$\phi^\dagger\phi$, $\bar{f}\gamma^5 f$	$\sigma_{\rm SD} \propto (q/2m_n)^2$
Real Scalar, ϕ	Spin-0	ϕ^2, $\bar{f}\gamma^5 f$	$\sigma_{\rm SD} \propto (q/2m_n)^2$
Complex Vector, X	Spin-0	$X^\dagger_\mu X^\mu$, $\bar{f}\gamma^5 f$	$\sigma_{\rm SD} \propto (q/2m_n)^2$
Real Vector, X	Spin-0	$X_\mu X^\mu$, $\bar{f}\gamma^5 f$	$\sigma_{\rm SD} \propto (q/2m_n)^2$
Dirac Fermion, χ	Spin-1	$\bar{\chi}\gamma^\mu\chi$, $\bar{b}\gamma_\mu b$	$\sigma_{\rm SI} \sim$ loop (vector)
Dirac Fermion, χ	Spin-1	$\bar{\chi}\gamma^\mu\chi$, $\bar{f}\gamma_\mu\gamma^5 f$	$\sigma_{\rm SD} \propto (q/2m_n)^2$ or $(q/2m_\chi)^2$
Dirac Fermion, χ	Spin-1	$\bar{\chi}\gamma^\mu\gamma^5\chi$, $\bar{f}\gamma_\mu\gamma^5 f$	$\sigma_{\rm SD} \sim 1$
Majorana Fermion, χ	Spin-1	$\bar{\chi}\gamma^\mu\gamma^5\chi$, $\bar{f}\gamma_\mu\gamma^5 f$	$\sigma_{\rm SD} \sim 1$
Dirac Fermion, χ	Spin-0 (t-ch.)	$\bar{\chi}(1\pm\gamma^5)b$	$\sigma_{\rm SI} \propto$ loop (vector)
Dirac Fermion, χ	Spin-1 (t-ch.)	$\bar{\chi}\gamma^\mu(1\pm\gamma^5)b$	$\sigma_{\rm SI} \propto$ loop (vector)
Complex Vector, X	Spin-1/2 (t-ch.)	$X^\dagger_\mu\gamma^\mu(1\pm\gamma^5)b$	$\sigma_{\rm SI} \propto$ loop (vector)
Real Vector, X	Spin-1/2 (t-ch.)	$X_\mu\gamma^\mu(1\pm\gamma^5)b$	$\sigma_{\rm SI} \propto$ loop (vector)

Table 1. A summary of the simplified models identified in ref. [49] as being potentially capable of generating the observed characteristics of the Galactic Center gamma-ray excess without violating collider or direct detection constraints (as of June 2014). For each model, we list the nature of the dark matter candidate and the mediator, as well as the form of the mediator's interactions. In the final column, we list whether the leading elastic scattering cross section with nuclei is spin-independent (SI) or spin-dependent (SD) and whether it is suppressed by powers of momentum, q, or by loops.

Many groups have studied dark matter models that are capable of generating the observed features of the Galactic Center excess (for an incomplete list, see refs. [49–67]). In this study, we follow an approach similar to that taken in ref. [49], and consider an exhaustive list of simplified models that are capable of generating the observed gamma-ray excess while remaining consistent with all constraints from collider and direct detection experiments. Also following ref. [49], we choose to not consider hidden sector models in this study, in which the dark matter annihilates to unstable particles which reside in the hidden sector, without sizable couplings to the Standard Model (SM) [59, 62, 63]. While such scenarios certainly remain viable, we consider them to be beyond the scope of this work.

The models found in ref. [49] to be compatible with existing constraints from direct detection and collider experiments are listed in table 1, and can be divided into three categories. First, there are models in which the dark matter annihilates into SM quarks through the s-channel exchange of a spin-zero mediator with pseudoscalar couplings. These models allow for an unsuppressed (s-wave) low-velocity annihilation cross section while generating a cross section for elastic scattering with nuclei that is suppressed by either two or four powers of momentum, thus evading direct detection constraints. In the second class of models, the dark matter annihilates through the s-channel exchange of a vector boson. In this case, it was found that direct detection constraints could be evaded if the mediator couples axially with

JCAP02(2017)038

quarks or couples only to the third generation. Lastly, there are models in which the dark matter annihilates to b-quarks through the t-channel exchange of a colored and electrically charged mediator.

In this paper, we revisit this collection of dark matter models, applying updated constraints from the Large Hadron Collider (LHC) and other collider experiments, in addition to recent constraints from the direct detection experiments LUX [68] and PandaX-II [69]. We find that many of the models previously considered within the context of the Galactic Center excess are now excluded by a combination of these constraints.

2 Constraints

In this section, we summarize the constraints that we apply in this study. In particular, we consider constraints from the LHC and other accelerators, as derived from searches for mono-X events with missing energy (where X denotes a jet, photon, or Z), di-jet resonances, di-lepton resonances, exotic Higgs decays, sbottom searches, and exotic upsilon decays [70–80]. We also summarize the current status of direct searches for dark matter, including the recent constraints presented by the LUX [68] and PandaX-II [69] Collaborations.

2.1 LHC

Searches at CMS and ATLAS provide some of the most stringent constraints on dark matter, as well as on the particles that mediate the interactions of dark matter. In this study, we consider the bounds from the LHC as applied to a wide range of simplified models, the most stringent of which arise from CMS searches for mono-jet+MET, di-jet resonances, di-lepton resonances, di-tau resonances, and sbottom searches. Although we also considered constraints from the ATLAS Collaboration, they were slightly less restrictive than those from CMS.

LHC limits are typically published in one of two ways: (1) assuming a particular model and choice of couplings, a limit is presented on the parameter space in the dark matter mass-mediator mass plane, or (2) a limit is presented on the product of the production cross section and the branching fraction for a particular process. In this study, we will present our results in terms of the mediator mass and the product of the dark matter-mediator and SM-mediator couplings. Thus applying limits from the LHC generally requires translating these bounds into the parameter space under consideration. To calculate the relevant production cross sections and branching ratios, models are built using FeynRules [81] and subsequently imported into MadGraph5_aMC@NLO [82, 83]. When necessary, we implement PYTHIA 8 [84] to hadronize the final state particles and DELPHES [85] to simulate the detector response. As appropriate, we apply the published cuts on MET, final state momentum, and final state rapidity in our calculations. Throughout this study, we calculate and present all LHC constraints at the 95% confidence level.

In scenarios with heavy mediators, it is not uncommon for the width of the mediator to be unacceptably large (i.e. as large or larger than its mass). Such widths are clearly not physical and may indicate the presence of additional particles or interactions [86–90]. Imposing unitarity and gauge invariance often restricts the mass of such additional particles to be of the same order of magnitude as the other dark sector particles, making it difficult to define the properties of these new particles such that they are beyond the reach of the LHC. Although the construction of more complicated dark sectors is beyond the scope of the work, we emphasize that it is likely that constraints derived on such models would be more restrictive than those derived here. Throughout this study, in order to maintain the

JCAP02(2017)038

validity of the theory in this region of parameter space, we apply LHC constraints assuming $\Gamma/m = 0.1$ whenever the width of the mediator would otherwise exceed this value.

2.2 LEP-II

Constraints from LEP-II on Higgs bosons in the mass range between 10 GeV and 100 GeV are extremely constraining for a wide range of beyond the SM physics scenarios. In this study we consider such limits as derived from searches for a light Higgs decaying to $b\bar{b}$ [79]. Although powerful, these constraints are rather model dependent, and generally rely on the scalar mediator's coupling to the SM gauge bosons. LEP-II constraints are presented at the 95% confidence level throughout this work, and assume a coupling to the Z-boson identical to that of the SM Higgs.

2.3 BaBar

We also consider in this study constraints derived from BaBar on upsilon decays to light scalar or pseudoscalar particles, in particular focusing on channels where the mediator subsequently decays to hadrons, muons, taus or charm quarks [91–94]. We consider relativistic and QCD corrections for the decay of a vector meson as described in ref. [80]. We note that the $\mu^+\mu^-$ channel provides the strongest constraints, but the precise values of the branching ratios of such light scalars are not well known (see e.g. refs. [80, 95]). Here, we conservatively assume a 100% branching ratio to hadrons in the mass range of $1\,\text{GeV} \lesssim m_A \lesssim 2m_\tau$. This is conservative in the sense that introducing a small branching ratio to muons strengthens the resulting bound. For $2m_\tau \lesssim m_A < 9\,\text{GeV}$, we use the branching ratios as recently computed in ref. [96] which incorporate QCD corrections. We find similar constraints as those previously obtained in the recent analysis of refs. [80] and [95] for pseudoscalar and scalar mediators, respectively. All BaBar constraints are presented at the 90% confidence level in this study.

2.4 Direct detection

The constraints utilized in this study on the dark matter's elastic scattering cross section with nuclei have been derived from the latest results of the LUX Collaboration [68], which are only slightly more stringent than those recently presented by the PANDA-X experiment [69].

For all tree-level cross sections, we use the expressions as presented in appendices B and C of ref. [49]. One-loop cross sections for the scalar mediated t-channel interaction and the s-channel vector mediated loop-suppressed interaction are provided in refs. [54] and [97], respectively. The remaining t-channel models, which are also loop suppressed, suffer from the problem that they are not generically gauge invariant. Consequently, scattering cross sections for these models are calculated by introducing a factor that suppresses the cross section by the same factor that would appear if the interaction were mediated by a massive photon, i.e. $\left(g^2 \log(m_b^2/m_{\rm med}^2)/(64\pi^2 m_{\rm med}^2)\right)^2$.

For each model, we calculate the expected number of events in a xenon target following the procedure outlined in ref. [98], adopting a standard Maxwellian velocity distribution ($v_0 = 220$ km/s, $v_{\rm esc} = 544$ km/s, $\bar{v}_{\rm Earth} = 245$ km/s), a local density of $0.3\,\text{GeV/cm}^3$ and an exposure of 3.35×10^4 kg-day. Form factors and nuclear responses are calculated following the procedures outlined in refs. [99, 100]. We take the efficiency for nuclear recoils as a function of energy from figure 2 of ref. [68], and derive bounds at the 90% confidence level, assuming 4.2 expected background events and applying Poisson statistics.

JCAP02(2017)038

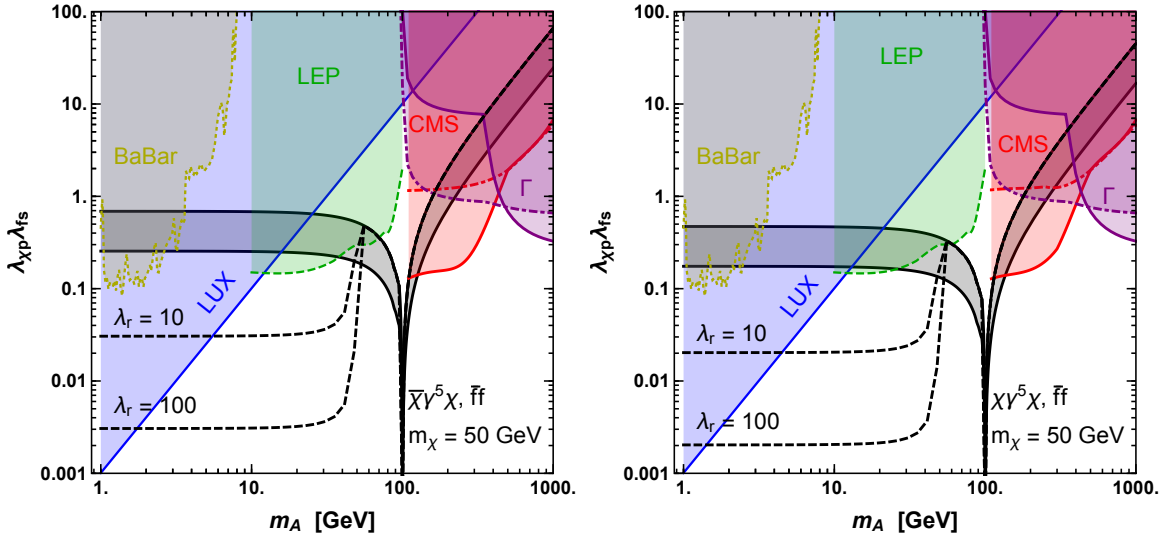

Figure 1. Constraints on a 50 GeV Dirac (left) and Majorana (right) dark matter candidate which annihilates through a spin-0 mediator with a pseudoscalar coupling to the dark matter and a (universal) scalar coupling to SM fermions. The black dashed (solid) lines include (neglect) annihilations to mediator pairs for several values of $\lambda_r \equiv \lambda_\chi/\lambda_b$. The upper boundary of the shaded black region is where the correct thermal relic abundance is obtained, whereas along the lower boundary the low-velocity annihilation cross section is at its minimum value required to potentially generate the observed gamma-ray excess. The constraints from CMS assume $\lambda_r = 1/3$ (solid) and $\lambda_r = 3$ (dash-dot), and are compared with the bounds enforcing $\Gamma_A/m_A = 0.1$ (purple) for the same coupling ratios. LEP and BaBar constraints are presented for $\lambda_r = 10$ and 1, respectively.

3 Pseudoscalar mediated dark matter

In this section, we will consider models in which the dark matter annihilates through the s-channel exchange of a spin-0 mediator, A. We begin by considering a fermionic dark matter candidate, χ, with interactions as described by the following Lagrangian:

$$\mathscr{L} \supset \left[a\bar{\chi}\lambda_{\chi p} i\gamma^5 \chi + \sum_f y_f \bar{f}\left(\lambda_{fs} + \lambda_{fp} i\gamma^5\right) f \right] A\,, \tag{3.1}$$

where $a = 1(1/2)$ for a Dirac (Majorana) dark matter candidate. Although we describe the interactions of the SM fermions in terms of their yukawas, $y_f \equiv \sqrt{2}m_f/v$, the quantities λ_{fs} and λ_{fp} allow for arbitrary values of each coupling. Here, v is the SM Higgs vacuum expectation value, i.e. $v \simeq 246\,\text{GeV}$. Assuming that λ_{bs} or λ_{bp} is not much smaller than that of the other SM fermions, dark matter will annihilate largely to $b\bar{b}$ in this model. For this dominant annihilation channel, a dark matter mass of approximately 50 GeV is required to generate the observed spectral shape of the Galactic Center excess [17, 101], and we adopt this value throughout this section.

In the left (right) frame of figure 1, we plot the constraints on the parameter space of a simplified model with dark matter in the form of a Dirac (Majorana) fermion and a mediator with a pseudoscalar coupling to the dark matter ($\bar{\chi}\gamma^5\chi$) and scalar couplings to SM fermions ($\bar{f}f$), assuming a common scalar coupling to all SM fermions (as motivated

JCAP02(2017)038

by minimal flavor violation), λ_{fs}.[1] In each frame, the upper boundary of the shaded black region represents the the value of the product of the couplings that is required to generate an acceptable thermal relic abundance, assuming standard cosmology. The lower boundary of this region corresponds to a more relaxed assumption, requiring only that the low-velocity annihilation cross section is large enough to potentially generate the observed gamma-ray excess, $\langle \sigma_{\chi\chi} v \rangle > 3 \times 10^{-27}$ cm^3/s (or twice this value in the case of a Dirac particle). If $m_A < m_\chi$, dark matter can annihilate directly to mediator pairs via t-channel χ exchange. In these figures, we plot as dashed black lines the parameter space which generates the observed thermal relic abundance for several values of $\lambda_r \equiv \lambda_\chi / \lambda_b$. One should keep in mind that if the dark matter annihilates significantly to mediator pairs in the low-velocity limit, a higher value for the dark matter mass is generally required in order for the resulting gamma-ray spectrum to be consistent with the observed features of the Galactic Center excess [53, 62, 63]. We compare these curves to the constraints derived from LUX (blue), CMS/LHC (red), LEP (green), and BaBar (yellow).

In the case of CMS, the most stringent constraint in this class of models derives from searches for events with a single jet and missing transverse energy (MET). As the sensitivity of collider searches depends not only on the product of the couplings, but also on their ratio, we present constraints for multiple values of λ_r. In figure 1, the solid (dot-dashed) lines correspond to CMS constraints for $\lambda_r = 1/3$ (3), while LEP and BaBar constraints are derived assuming $\lambda_r = 10$ and $\lambda_r = 1$, respectively. The regions bounded by a purple solid (dot-dashed) line represent those in which the calculated width of the mediator exceeds one tenth of its mass, for $\lambda_r = 1/3$ (3). As described in section 2.1, we set $\Gamma_A = 0.1\, m_A$ throughout this region of parameter space, and take this to be indicative of additional particles and/or interactions that are not described by our simplified model.

The constraints from LEP rely on an effective coupling of the SM Z to ZA, and are thus highly model dependent. While this constraint does apply, for example, to the case in which the couplings of the A to SM fermions are the result of mixing with the SM Higgs, there are many other scenarios in which a spin-0 mediator can couple to the SM fermions while having a suppressed coupling to the Z.

Several of the constraints shown in figure 1 depend on the ratios of the various couplings of the mediator. In particular, since the LHC constraints are dominated by diagrams in which a scalar mediator is produced through a top quark loop, such constraints may be much weaker if the top quark coupling is suppressed. To illustrate this, we plot in figure 2 the derived constraints assuming $\tan\beta = 10$, where $\tan\beta$ is defined as the ratio of the mediator's couplings to down-type and up-type fermions, $\tan\beta \equiv \lambda_d / \lambda_u$. While bounds from LEP, LUX and BaBar are not significantly affected by the value of $\tan\beta$, mono-jet+MET bounds can be noticeably reduced, in particular in the case of $\lambda_r \ll 1$. Increasing $\tan\beta$ also reduces the width of the mediator for $m_A > 2m_t$, potentially opening up additional parameter space.

We repeat this exercise in figure 3 for the case of a mediator with pseudoscalar couplings to both the dark matter and to SM fermions. In this case, the dark matter's elastic scattering cross section with nuclei is both spin-dependent and heavily momentum suppressed ($\sigma_{SD} \propto q^4$), making direct detection experiments largely insensitive to these models. The bounds derived from colliders, however, are relatively insensitive to whether SM fermions couple via a scalar or pseudoscalar interaction. We emphasize that, as in the previous case, a large

[1] Note that the product of couplings in these models be quite large, occasionally appearing to violate perturbativity. This need not be the case, however, as we have not included the yukawa contribution to the SM coupling, which may significantly suppress this product.

JCAP02(2017)038

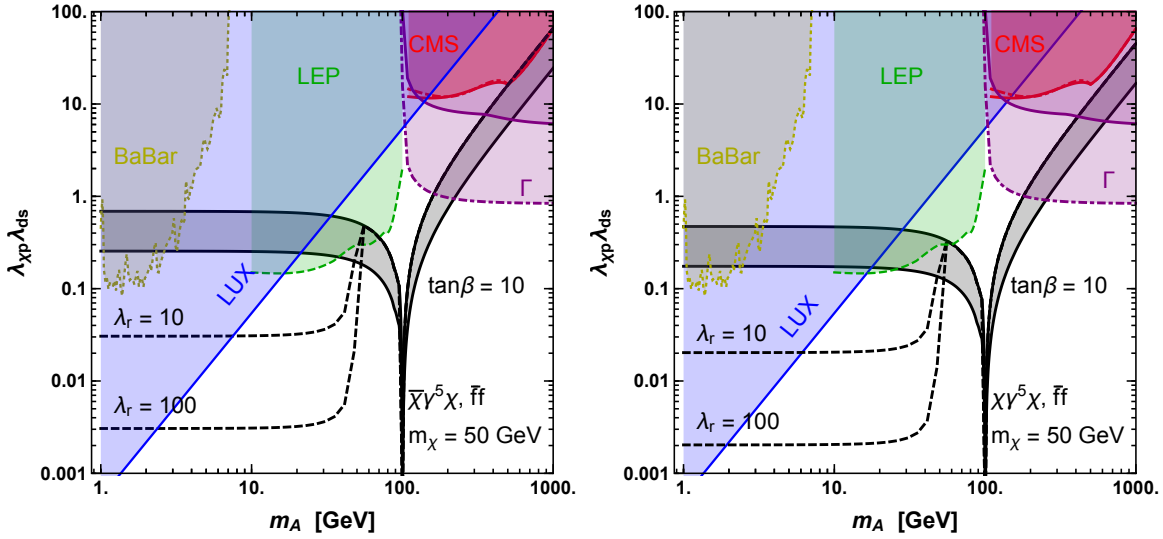

Figure 2. As in figure 1 but for $\tan\beta = 10$, where $\tan\beta$ is defined as the ratio of the mediator's couplings to down-type and up-type fermions.

portion of parameter space remains viable for this model, especially should the top-mediator coupling be suppressed.

Next, we consider dark matter in the form of a scalar ϕ, with a Lagrangian given by:

$$\mathscr{L} \supset \left[a\mu_\phi |\phi|^2 + \sum_f y_f \bar{f} \lambda_{fp} i\gamma^5 f \right] A\,, \tag{3.2}$$

where $a = 1(1/2)$ for a complex (real) dark matter particle.

The phenomenology of this model is summarized in figure 4, for the cases of a complex (left frame) or real (right frame) scalar. LHC signatures for this model are rather different from in the case of fermionic dark matter as the decay of the spin-0 mediator to dark matter is heavily suppressed. Instead, the dominant constraint from the LHC results from searches for a Higgs-like particle decaying to $\tau^+\tau^-$. At very large mediators masses, however, ($m_A \gtrsim 600\,\text{GeV}$), the branching ratio to $\tau^+\tau^-$ is reduced and di-jet resonances become slightly more constraining (this accounts for the dip-like feature appearing in the CMS bound). As in the previous scenarios, LEP bounds on scalar decays to $b\bar{b}$ are very constraining in the region $10\,\text{GeV} < \text{m}_\text{A} < 100\,\text{GeV}$, but only apply in models in which the mediator couples either directly or indirectly to the Z.

In the lower frames of figure 4 , we show how these bounds change if the mediator does not couple to leptons and has an asymmetric coupling to up-like and down-like quarks with $\tan\beta = 2$. This choice can open a window of parameter space for $100\,\text{GeV} \lesssim m_A \lesssim 2m_t$, depending on the precise values of $\tan\beta$ and λ_r.

Next, we consider the case of vector dark matter X^μ:

$$\mathscr{L} \supset \left[a\mu_X X^\mu X^\dagger_\mu + \sum_f y_f \bar{f} \lambda_{fp} i\gamma^5 f \right] A\,, \tag{3.3}$$

where $a = 1(1/2)$ for a complex (real) dark matter particle.

JCAP02(2017)038

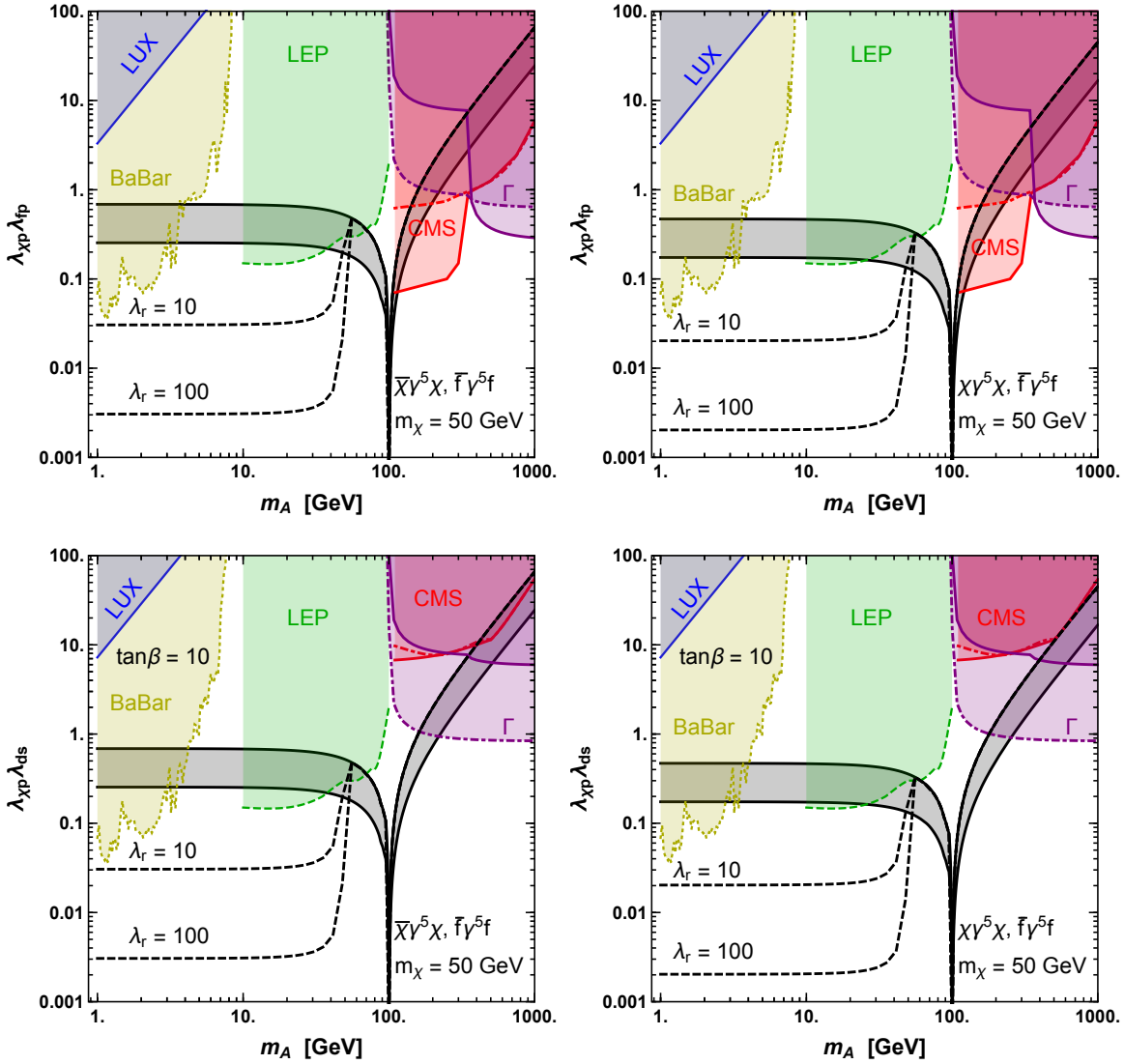

Figure 3. As in figure 1 but for a mediator with purely pseudoscalar couplings. The upper (lower) frames correspond to $\tan\beta = 1$ (10).

Constraints on this model are shown in figure 5. The dominant decay mode of the mediator in this model, and thus the most constraining LHC search, depends on the mass of the mediator. For $m_A \simeq 100\,\text{GeV}$ the dominant decay is to dark matter, and thus the most constraining search is that based on mono-jet+MET events. This picture is very different for larger mediator masses, however, for which constraints based on searches for Higgs bosons decaying to $\tau^+\tau^-$ become more stringent. Both of these search channels significantly exclude mediator masses above 100 GeV in this class of models, for both $\lambda_r = 3$ and $\lambda_r = 1/3$. Similar to in the scalar dark matter case, however, we can relax some of these constraints by suppressing the mediator's couplings to leptons and/or by increasing $\tan\beta$ (as shown in the lower frames of figure 5).

JCAP02(2017)038

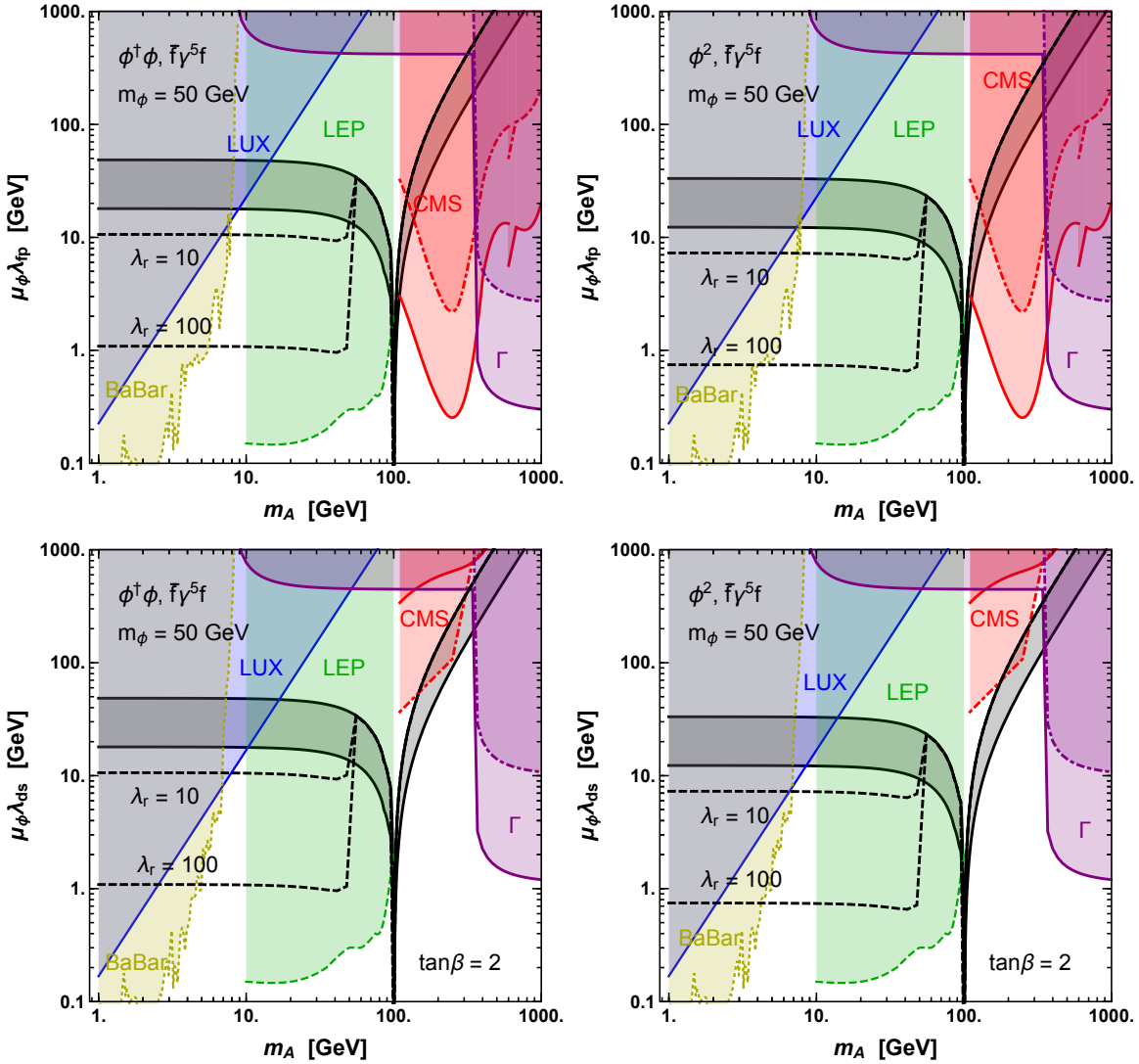

Figure 4. As in the previous figures, but for a 50 GeV complex (left) or real (right) scalar dark matter candidate, which annihilates through a spin-0 mediator with a pseudoscalar coupling to SM fermions. In the upper frames, we take the mediator's couplings to be equal for all SM fermions, whereas in the lower frames the mediator does not couple to leptons and $\tan\beta = 2$.

4 Vector mediated dark matter

In this section we consider fermonic dark matter annihilating through the s-channel exchange of a spin-1 mediator, V_μ, with Lagrangians of the form [49, 52]:

$$\mathscr{L} \supset \left[a\bar{\chi}\gamma^\mu\left(g_{\chi v} + g_{\chi a}\gamma^5\right)\chi + \sum_f \bar{f}\gamma^\mu\left(g_{fv} + g_{fa}\gamma^5\right) f \right] V_\mu \,, \tag{4.1}$$

where $a = 1(1/2)$ for a Dirac (Majorana) dark matter candidate. For the case of comparable couplings to various SM fermions this class of models require a $\simeq 35$ GeV dark matter candidate to generate a signal consistent with the Galactic Center excess. Unless stated otherwise, we will adopt this value for the dark matter mass throughout this section.

JCAP02(2017)038

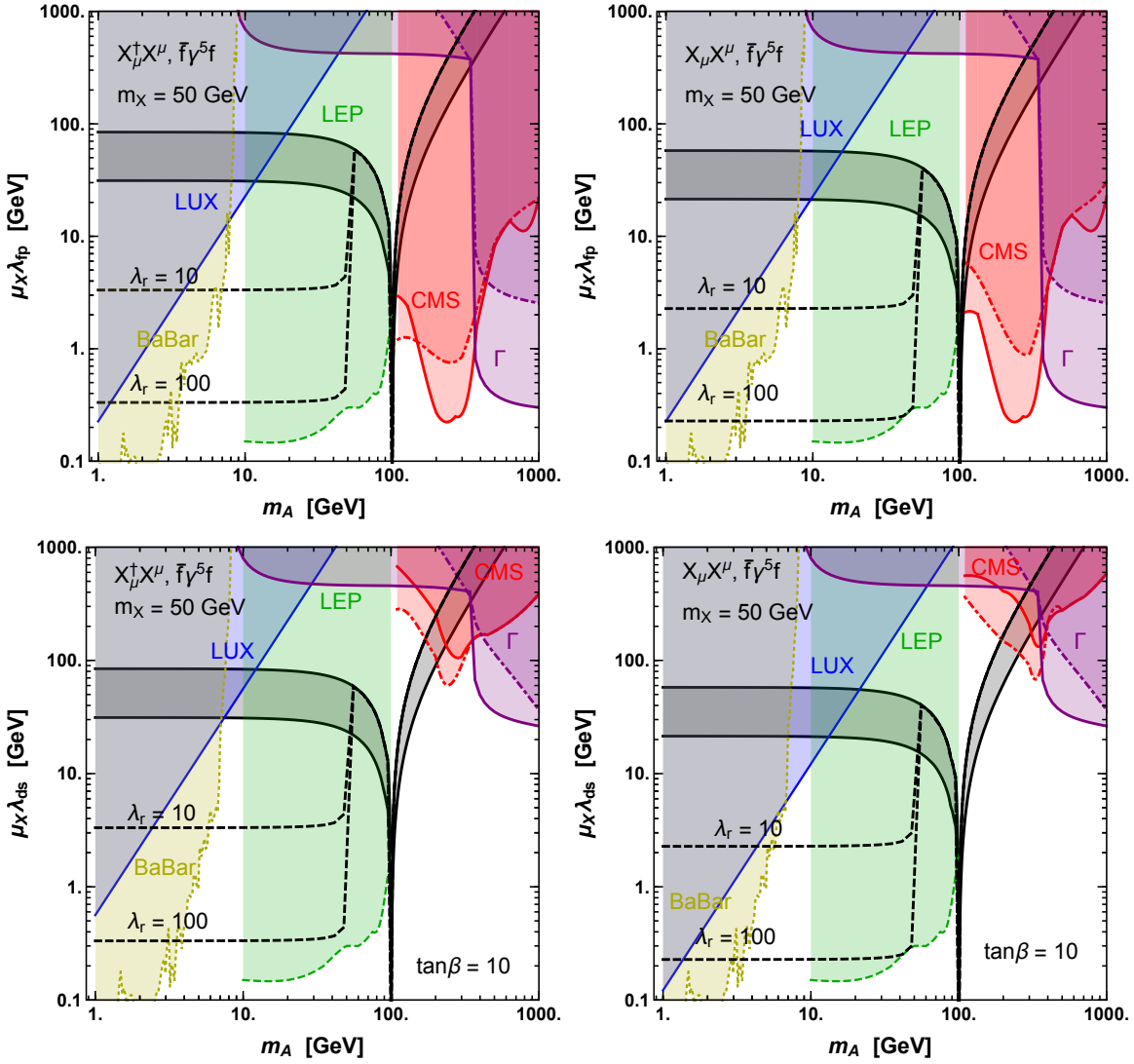

Figure 5. As in previous figures, but for a 50 GeV complex (left) and real (right) vector dark matter candidate which annihilates through a spin-0 mediator with a pseudoscalar coupling to SM fermions. In the upper frames, we take the mediator's couplings to be equal for all SM fermions, whereas in the lower frames the mediator does not couple to leptons and $\tan\beta = 10$.

We begin in figure 6 by considering the constraints on a Dirac (left) and Majorana (right) dark matter candidate that annihilates through a mediator with purely axial couplings. As spin-dependent elastic scattering with nuclei is unsuppressed in this class of models, current LUX constraints force such models to either live on resonance ($m_\chi \simeq m_V/2$), or have a mediator mass $m_V < m_\chi$ and with $\lambda_r \gg 1$. LHC constraints on this model from searches for di-lepton resonances ($m_V > 400\,\text{GeV}$) and mono-jet+MET searches ($100\,\text{GeV} < m_V < 400\,\text{GeV}$) limit mediator masses in this model to be below $\simeq 100\,\text{GeV}$. LHC bounds are shown in this figure for $\lambda_r = 1/3$ (solid) and $g_{\chi v} = 1$ (i.e. $\lambda_r \gg 1$) (dotted). Collider constraints for this model are difficult to evade as they do not rely exclusively on couplings to leptons or to specific species of quarks. Such bounds could be evaded, however, if the mediator were to couple exclusively to third generation quarks. An example of such a model

JCAP02(2017)038

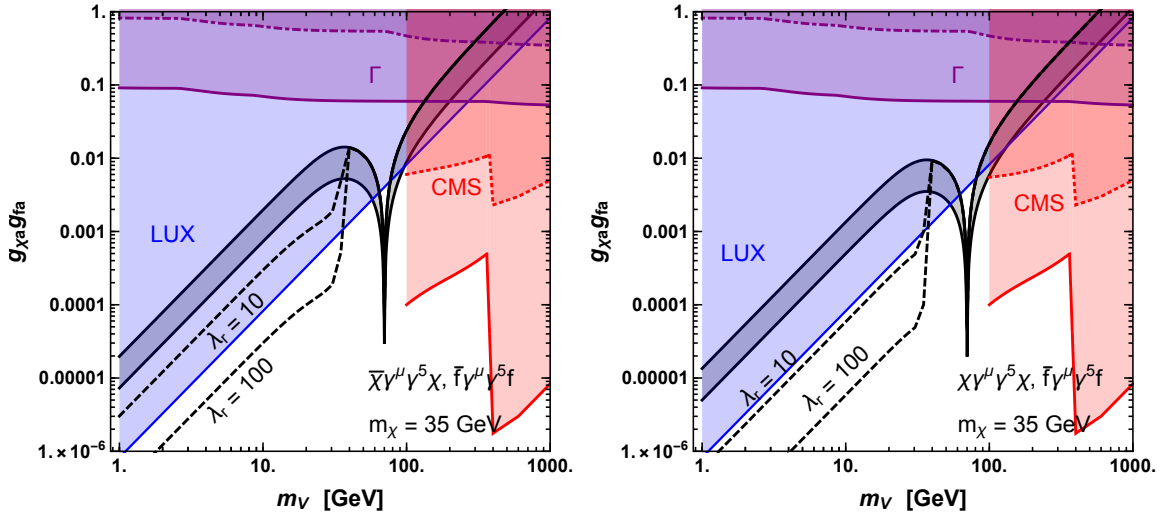

Figure 6. As in previous figures, but for a 35 GeV Dirac (left) and Majorana (right) dark matter candidate which annihilates through a spin-1 mediator with axial couplings to both dark matter and (universally) to SM fermions. In this figure, the dotted red (CMS) line corresponds to the case of $g_{\chi v} = 1$ (i.e. $\lambda_r \gg 1$).

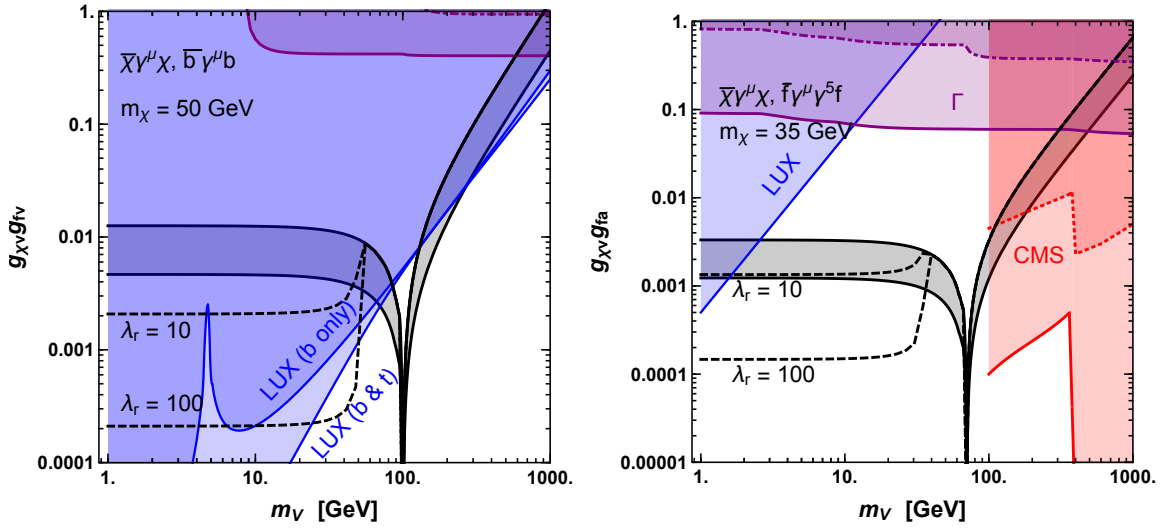

Figure 7. As in previous figures, but for a 50 GeV Dirac dark matter candidate with vector couplings to both dark matter and to b-quarks (left), and for a 35 GeV Dirac dark matter candidate with vector and axial couplings to dark matter and (universally) to SM fermions, respectively (right). LHC bounds are shown for $\lambda_r = 1/3$ (solid) and $g_{\chi v} = 1$ (i.e. $\lambda_r \gg 1$) (dotted).

is shown in the left frame of figure 7, where we consider a 50 GeV Dirac dark matter candidate that annihilates through a spin-1 mediator with vector couplings to both dark matter and b-quarks (and possibly also t-quarks). While the leading order elastic scattering diagram arises at loop level in this case, the vector coupling leads to stringent constraints from direct detection experiments. The dominant constraints from the LHC on vector mediated models typically arise from searches for mono-jet+MET events and di-lepton resonances. Since the production of the vector mediator is in most cases dominated by valence quarks, however,

JCAP02(2017)038

the sensitivity of collider searches is heavily suppressed and thus do not probe significant parameter space in this model. We do not show any LHC constraints in this figure.

In the right panel of figure 7, we consider the phenomenology of models where the mediator couples to Dirac dark matter and fermions with a vector and an axial coupling, respectively. The elastic scattering cross section in this case is both spin-dependent and momentum suppressed, and thus such experiments have only recently begun probing this model. LHC constraints from di-lepton resonances ($m_V > 400\,\mathrm{GeV}$) and mono-jet+MET searches ($100\,\mathrm{GeV} < \mathrm{m_V} < 400\,\mathrm{GeV}$) are, as before, extremely constraining. That being said, di-lepton constraints can be easily avoided if the mediator couples only to quarks, and mono-jet constraints can be significantly relaxed if the mediator couples, for example, only to the third generation. LHC bounds are shown for $\lambda_r = 1/3$ (solid) and $g_{\chi v} = 1$ (i.e. $\lambda_r \gg 1$) (dotted).

5 Dark matter annihilating through *t*-channel mediators

Finally, we consider four scenarios in which the dark matter annihilates through the t-channel exchange of a colored and electrically charged mediator to $b\bar{b}$ [54, 102, 103]. These cases consist of a Dirac dark matter candidate, χ, and spin-0 mediator, A:

$$\mathscr{L} \supset \lambda_\chi \bar{\chi}\left(1+\gamma^5\right) f A + \lambda_\chi \bar{f}\left(1-\gamma^5\right) \chi A^\dagger \,, \tag{5.1}$$

a Dirac dark matter candidate, χ, and a spin-1 mediator, V_μ:

$$\mathscr{L} \supset g_\chi \bar{\chi}\gamma^\mu\left(1+\gamma^5\right) f V_\mu + g_\chi \bar{f}\gamma^\mu\left(1-\gamma^5\right) \chi V_\mu^\dagger \tag{5.2}$$

and a real or complex vector dark matter candidate, X_μ, with a fermionic mediator, ψ:

$$\mathscr{L} \supset g_X \bar{\psi}\gamma^\mu\left(1+\gamma^5\right) f X_\mu^\dagger + g_X \bar{f}\gamma^\mu\left(1-\gamma^5\right) \psi X_\mu \,. \tag{5.3}$$

Note that we consider these specific combinations of scalar and pseudoscalar or vector and axial couplings as they are the only examples for which the scalar contact interaction with nuclei is supressed. Instead, elastic scattering occurs in each of these models through a loop-suppressed vector coupling [49, 54, 104].

In figure 8, we summarize the phenomenology of this class of models. In the upper left frame we consider the case of a Dirac dark matter particle and spin-0 mediator. In the remaining frames of this figure, we summarize the phenomenology of models with a Dirac dark matter candidate and a vector mediator (upper right), a complex vector dark matter candidate with a fermonic mediator (lower left), or a a real vector dark matter candidate with a fermonic mediator (lower right). In each case, we find that the combination of constraints from the CMS sbottom search and LUX exclude the entire parameter space of this class of models. We also note that the scenarios with a vector dark matter candidate are rather unphysical over much of the parameter space shown due to the very large width of the mediator.

6 Summary and conclusions

In this study, we have revisited the range of dark matter scenarios that could potentially generate the observed characteristics of the Galactic Center gamma-ray excess, without conflicting with any constraints from colliders or direct detection experiments. We have taken

JCAP02(2017)038

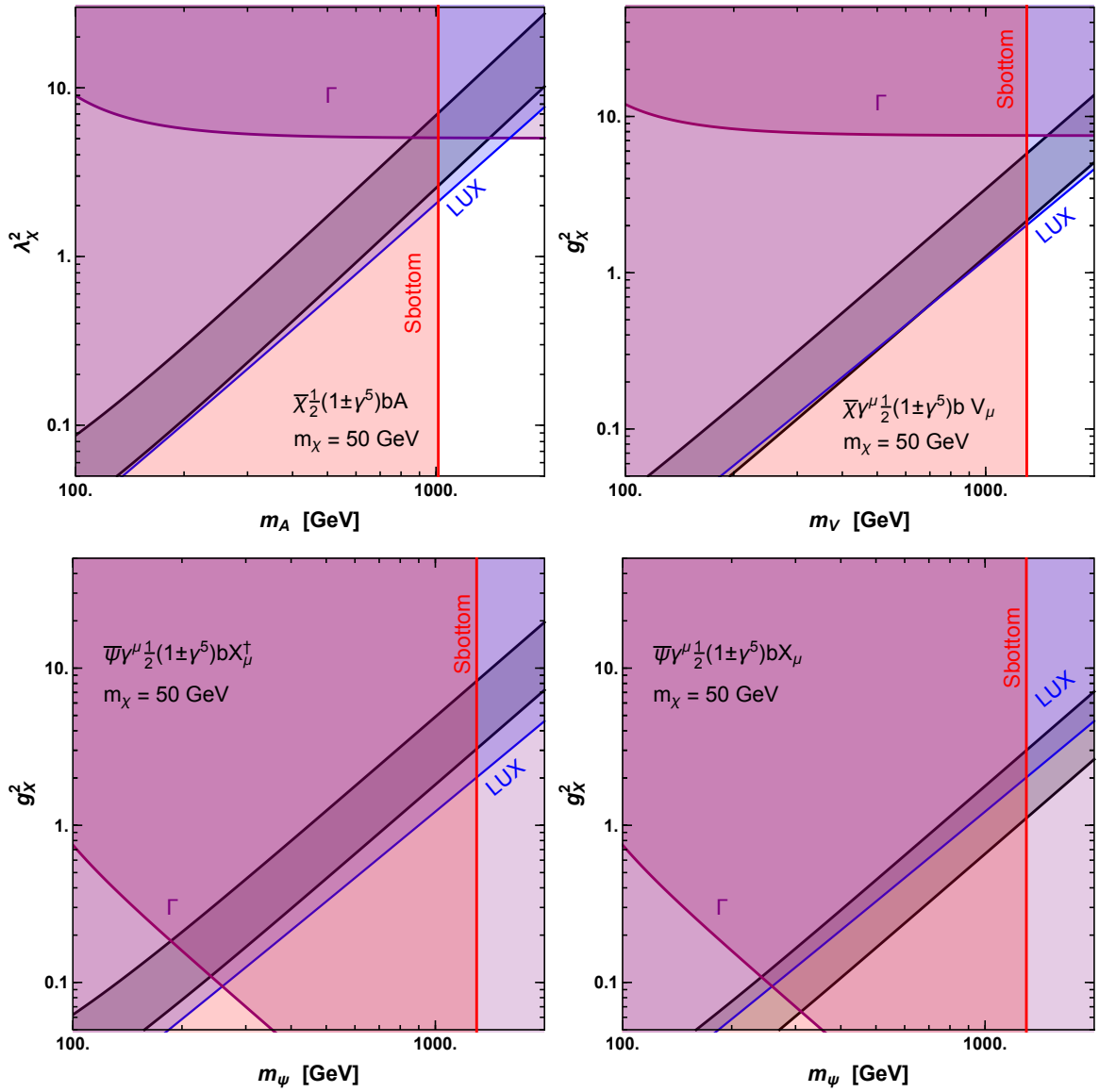

Figure 8. As in previous figures, but for a 50 GeV dark matter candidate which annihilates through a t-channel diagram to $b\bar{b}$. In the upper left (right) frame, we consider the case of a Dirac dark matter candidate with a scalar (vector) mediator. In the lower left (right) frame, the dark matter is a real (complex) vector, mediated by a Dirac fermion. The entire parameter space of these models is ruled out by the combined results of LUX and sbottom searches at the LHC.

a simplified models approach, considering the 16 scenarios that were previously found to be viable in ref. [49] (and listed in table 1). Each of these models features a low-velocity dark matter annihilation cross section that is unsuppressed (i.e. s-wave), and was found to be consistent with all constraints as of 2014. Note that we have not considered any hidden sector models (i.e. models in which the dark matter annihilates into unstable particles without sizable couplings to the Standard Model) which, although potentially viable [59, 62, 63], are beyond the scope of this work.

JCAP02(2017)038

The main results of this study can be summarized as follows:

- Scalar, fermonic, or vector dark matter that annihilates through a mediator with pseudoscalar couplings can in many cases evade all current constraints, for mediator masses between ∼10 GeV and several hundred GeV.
- Dark matter that annihilates through a spin-1 mediator is ruled out by the results of LUX/PandaX-II unless the mass of the mediator is approximately equal to twice the mass of the dark matter (near an annihilation resonance). An exception to this conclusion is found in the case of a mediator with a purely vector coupling to the dark matter and a purely axial coupling to Standard Model fermions, which is potentially viable for mediator masses between roughly ∼ 1 GeV and 200 GeV.
- All scenarios in which the dark matter annihilates through a t-channel process are now ruled out by a combination of constraints from LUX/PandaX-II and the LHC.
- Constraints from LEP-II and BaBar restrict many of the pseudoscalar mediated scenarios considered in this study. In particular, mediators with a mass in the ∼10-100 GeV range are often ruled out by LEP if they couple significantly to the Standard Model Z (such as in scenarios in which the mediator obtains its couplings to Standard Model fermions through mixing with the Higgs).

Dark matter scenarios that are capable of generating the Galactic Center excess are now significantly more constrained than they were even a few years ago. As the sensitivity of XENON1T, LZ and other direct detection experiments, as well as the LHC, continues to improve, either a discovery will be made, or the vast majority of the currently viable parameter space identified in this study will be excluded. If such searches do advance without the appearance of new signals, hidden sector scenarios will become increasingly attractive, in particular within the context of the Galactic Center.

Acknowledgments

We would like to thank Paddy Fox, Roni Harnik, Veronica Sanz, Nuria Rius, and Asher Berlin for helpful discussions. ME is supported by the Spanish FPU13/03111 grant of MECD and also by the European projects H2020-MSCA-RISE-2015 and H2020-MSCA-ITN-2015/674896-ELUSIVES. DH is supported by the US Department of Energy under contract DE-FG02-13ER41958. SW is supported under the University Research Association (URA) Visiting Scholars Award Program, and by a UCLA Dissertation Year Fellowship. Fermilab is operated by Fermi Research Alliance, LLC, under Contract No. DE-AC02-07CH11359 with the US Department of Energy.

References

[1] C. Boehm, D. Hooper, J. Silk, M. Casse and J. Paul, *MeV dark matter: has it been detected?*, *Phys. Rev. Lett.* **92** (2004) 101301 [astro-ph/0309686] [INSPIRE].

[2] D.P. Finkbeiner, *WMAP microwave emission interpreted as dark matter annihilation in the inner galaxy*, astro-ph/0409027 [INSPIRE].

[3] D. Hooper, D.P. Finkbeiner and G. Dobler, *Possible evidence for dark matter annihilations from the excess microwave emission around the center of the Galaxy seen by the Wilkinson Microwave Anisotropy Probe*, *Phys. Rev.* **D 76** (2007) 083012 [arXiv:0705.3655] [INSPIRE].

JCAP02(2017)038

[4] PAMELA collaboration, O. Adriani et al., *An anomalous positron abundance in cosmic rays with energies 1.5–100 GeV*, *Nature* **458** (2009) 607 [arXiv:0810.4995] [INSPIRE].

[5] AMS collaboration, M. Aguilar et al., *First Result from the Alpha Magnetic Spectrometer on the International Space Station: Precision Measurement of the Positron Fraction in Primary Cosmic Rays of 0.5–350 GeV*, *Phys. Rev. Lett.* **110** (2013) 141102 [INSPIRE].

[6] C. Weniger, *A Tentative Gamma-Ray Line from Dark Matter Annihilation at the Fermi Large Area Telescope*, *JCAP* **08** (2012) 007 [arXiv:1204.2797] [INSPIRE].

[7] E. Bulbul, M. Markevitch, A. Foster, R.K. Smith, M. Loewenstein and S.W. Randall, *Detection of An Unidentified Emission Line in the Stacked X-ray spectrum of Galaxy Clusters*, *Astrophys. J.* **789** (2014) 13 [arXiv:1402.2301] [INSPIRE].

[8] A. Boyarsky, O. Ruchayskiy, D. Iakubovskyi and J. Franse, *Unidentified Line in X-Ray Spectra of the Andromeda Galaxy and Perseus Galaxy Cluster*, *Phys. Rev. Lett.* **113** (2014) 251301 [arXiv:1402.4119] [INSPIRE].

[9] FERMI-LAT collaboration, M. Ackermann et al., *Search for gamma-ray spectral lines with the Fermi large area telescope and dark matter implications*, *Phys. Rev.* **D 88** (2013) 082002 [arXiv:1305.5597] [INSPIRE].

[10] HITOMI collaboration, F.A. Aharonian et al., *Hitomi constraints on the 3.5 keV line in the Perseus galaxy cluster*, arXiv:1607.07420 [INSPIRE].

[11] D. Hooper, P. Blasi and P.D. Serpico, *Pulsars as the Sources of High Energy Cosmic Ray Positrons*, *JCAP* **01** (2009) 025 [arXiv:0810.1527] [INSPIRE].

[12] I. Cholis and D. Hooper, *Dark Matter and Pulsar Origins of the Rising Cosmic Ray Positron Fraction in Light of New Data From AMS*, *Phys. Rev.* **D 88** (2013) 023013 [arXiv:1304.1840] [INSPIRE].

[13] R.M. Crocker et al., *Sub-luminous '1991bg-Like' Thermonuclear Supernovae Account for Most Diffuse Antimatter in the Milky Way*, arXiv:1607.03495 [INSPIRE].

[14] M. Su, T.R. Slatyer and D.P. Finkbeiner, *Giant Gamma-ray Bubbles from Fermi-LAT: AGN Activity or Bipolar Galactic Wind?*, *Astrophys. J.* **724** (2010) 1044 [arXiv:1005.5480] [INSPIRE].

[15] FERMI-LAT collaboration, M. Ajello et al., *Fermi-LAT Observations of High-Energy γ-Ray Emission Toward the Galactic Center*, *Astrophys. J.* **819** (2016) 44 [arXiv:1511.02938] [INSPIRE].

[16] T. Daylan, D.P. Finkbeiner, D. Hooper, T. Linden, S.K.N. Portillo, N.L. Rodd et al., *The characterization of the gamma-ray signal from the central Milky Way: A case for annihilating dark matter*, *Phys. Dark Univ.* **12** (2016) 1 [arXiv:1402.6703] [INSPIRE].

[17] F. Calore, I. Cholis and C. Weniger, *Background Model Systematics for the Fermi GeV Excess*, *JCAP* **03** (2015) 038 [arXiv:1409.0042] [INSPIRE].

[18] D. Hooper and T.R. Slatyer, *Two Emission Mechanisms in the Fermi Bubbles: A Possible Signal of Annihilating Dark Matter*, *Phys. Dark Univ.* **2** (2013) 118 [arXiv:1302.6589] [INSPIRE].

[19] C. Gordon and O. Macias, *Dark Matter and Pulsar Model Constraints from Galactic Center Fermi-LAT Gamma Ray Observations*, *Phys. Rev.* **D 88** (2013) 083521 [arXiv:1306.5725] [INSPIRE].

[20] K.N. Abazajian and M. Kaplinghat, *Detection of a Gamma-Ray Source in the Galactic Center Consistent with Extended Emission from Dark Matter Annihilation and Concentrated Astrophysical Emission*, *Phys. Rev.* **D 86** (2012) 083511 [*Erratum ibid.* **D 87** (2013) 129902] [arXiv:1207.6047] [INSPIRE].

JCAP02(2017)038

[21] D. Hooper and T. Linden, *On The Origin Of The Gamma Rays From The Galactic Center*, *Phys. Rev.* **D 84** (2011) 123005 [arXiv:1110.0006] [INSPIRE].

[22] D. Hooper and L. Goodenough, *Dark Matter Annihilation in The Galactic Center As Seen by the Fermi Gamma Ray Space Telescope*, *Phys. Lett.* **B 697** (2011) 412 [arXiv:1010.2752] [INSPIRE].

[23] L. Goodenough and D. Hooper, *Possible Evidence For Dark Matter Annihilation In The Inner Milky Way From The Fermi Gamma Ray Space Telescope*, arXiv:0910.2998 [INSPIRE].

[24] B. Zhou, Y.-F. Liang, X. Huang, X. Li, Y.-Z. Fan, L. Feng et al., *GeV excess in the Milky Way: the role of diffuse galactic gamma-ray emission templates*, *Phys. Rev.* **D 91** (2015) 123010 [arXiv:1406.6948] [INSPIRE].

[25] X. Huang, T. Enßlin and M. Selig, *Galactic dark matter search via phenomenological astrophysics modeling*, *JCAP* **04** (2016) 030 [arXiv:1511.02621] [INSPIRE].

[26] I. Cholis, D. Hooper and T. Linden, *Challenges in Explaining the Galactic Center Gamma-Ray Excess with Millisecond Pulsars*, *JCAP* **06** (2015) 043 [arXiv:1407.5625] [INSPIRE].

[27] S.K. Lee, M. Lisanti, B.R. Safdi, T.R. Slatyer and W. Xue, *Evidence for Unresolved γ-Ray Point Sources in the Inner Galaxy*, *Phys. Rev. Lett.* **116** (2016) 051103 [arXiv:1506.05124] [INSPIRE].

[28] R. Bartels, S. Krishnamurthy and C. Weniger, *Strong support for the millisecond pulsar origin of the Galactic center GeV excess*, *Phys. Rev. Lett.* **116** (2016) 051102 [arXiv:1506.05104] [INSPIRE].

[29] J. Petrović, P.D. Serpico and G. Zaharijas, *Millisecond pulsars and the Galactic Center gamma-ray excess: the importance of luminosity function and secondary emission*, *JCAP* **02** (2015) 023 [arXiv:1411.2980] [INSPIRE].

[30] D. Hooper, I. Cholis, T. Linden, J. Siegal-Gaskins and T. Slatyer, *Pulsars Cannot Account for the Inner Galaxy's GeV Excess*, *Phys. Rev.* **D 88** (2013) 083009 [arXiv:1305.0830] [INSPIRE].

[31] D. Hooper and G. Mohlabeng, *The Gamma-Ray Luminosity Function of Millisecond Pulsars and Implications for the GeV Excess*, *JCAP* **03** (2016) 049 [arXiv:1512.04966] [INSPIRE].

[32] D. Hooper and T. Linden, *The Gamma-Ray Pulsar Population of Globular Clusters: Implications for the GeV Excess*, *JCAP* **08** (2016) 018 [arXiv:1606.09250] [INSPIRE].

[33] T.D. Brandt and B. Kocsis, *Disrupted Globular Clusters Can Explain the Galactic Center Gamma Ray Excess*, *Astrophys. J.* **812** (2015) 15 [arXiv:1507.05616] [INSPIRE].

[34] I. Cholis, C. Evoli, F. Calore, T. Linden, C. Weniger and D. Hooper, *The Galactic Center GeV Excess from a Series of Leptonic Cosmic-Ray Outbursts*, *JCAP* **12** (2015) 005 [arXiv:1506.05119] [INSPIRE].

[35] J. Petrović, P.D. Serpico and G. Zaharijaš, *Galactic Center gamma-ray "excess" from an active past of the Galactic Centre?*, *JCAP* **10** (2014) 052 [arXiv:1405.7928] [INSPIRE].

[36] E. Carlson and S. Profumo, *Cosmic Ray Protons in the Inner Galaxy and the Galactic Center Gamma-Ray Excess*, *Phys. Rev.* **D 90** (2014) 023015 [arXiv:1405.7685] [INSPIRE].

[37] A. Cuoco, M. Krämer and M. Korsmeier, *Novel dark matter constraints from antiprotons in the light of AMS-02*, arXiv:1610.03071 [INSPIRE].

[38] M.-Y. Cui, Q. Yuan, Y.-L.S. Tsai and Y.-Z. Fan, *A possible dark matter annihilation signal in the AMS-02 antiproton data*, arXiv:1610.03840 [INSPIRE].

[39] D. Hooper, T. Linden and P. Mertsch, *What Does The PAMELA Antiproton Spectrum Tell Us About Dark Matter?*, *JCAP* **03** (2015) 021 [arXiv:1410.1527] [INSPIRE].

JCAP02(2017)038

[40] A. Geringer-Sameth, M.G. Walker, S.M. Koushiappas, S.E. Koposov, V. Belokurov, G. Torrealba et al., *Indication of Gamma-ray Emission from the Newly Discovered Dwarf Galaxy Reticulum II*, *Phys. Rev. Lett.* **115** (2015) 081101 [arXiv:1503.02320] [INSPIRE].

[41] DES, FERMI-LAT collaborations, A. Drlica-Wagner et al., *Search for Gamma-Ray Emission from DES Dwarf Spheroidal Galaxy Candidates with Fermi-LAT Data*, *Astrophys. J.* **809** (2015) L4 [arXiv:1503.02632] [INSPIRE].

[42] D. Hooper and T. Linden, *On The Gamma-Ray Emission From Reticulum II and Other Dwarf Galaxies*, *JCAP* **09** (2015) 016 [arXiv:1503.06209] [INSPIRE].

[43] S. Li, Y.-F. Liang, K.-K. Duan, Z.-Q. Shen, X. Huang, X. Li et al., *Search for gamma-ray emission from eight dwarf spheroidal galaxy candidates discovered in Year Two of Dark Energy Survey with Fermi-LAT data*, *Phys. Rev.* **D 93** (2016) 043518 [arXiv:1511.09252] [INSPIRE].

[44] DES, FERMI-LAT collaborations, A. Albert et al., *Searching for Dark Matter Annihilation in Recently Discovered Milky Way Satellites with Fermi-LAT*, *Astrophys. J.* **834** (2017) 110 [arXiv:1611.03184] [INSPIRE].

[45] B. Bertoni, D. Hooper and T. Linden, *Is The Gamma-Ray Source 3FGL J2212.5+0703 A Dark Matter Subhalo?*, *JCAP* **05** (2016) 049 [arXiv:1602.07303] [INSPIRE].

[46] B. Bertoni, D. Hooper and T. Linden, *Examining The Fermi-LAT Third Source Catalog In Search Of Dark Matter Subhalos*, *JCAP* **12** (2015) 035 [arXiv:1504.02087] [INSPIRE].

[47] Z.-Q. Xia et al., *A Spatially-Extended Stable Unidentified GeV Source: 3FGL J1924.8-1034*, arXiv:1611.05565 [INSPIRE].

[48] Y.-P. Wang et al., *Testing the dark matter subhalo hypothesis of the gamma-ray source 3FGL J2212.5+0703*, *Phys. Rev.* **D 94** (2016) 123002 [arXiv:1611.05135] [INSPIRE].

[49] A. Berlin, D. Hooper and S.D. McDermott, *Simplified Dark Matter Models for the Galactic Center Gamma-Ray Excess*, *Phys. Rev.* **D 89** (2014) 115022 [arXiv:1404.0022] [INSPIRE].

[50] S. Ipek, D. McKeen and A.E. Nelson, *A Renormalizable Model for the Galactic Center Gamma Ray Excess from Dark Matter Annihilation*, *Phys. Rev.* **D 90** (2014) 055021 [arXiv:1404.3716] [INSPIRE].

[51] C. Boehm, M.J. Dolan, C. McCabe, M. Spannowsky and C.J. Wallace, *Extended gamma-ray emission from Coy Dark Matter*, *JCAP* **05** (2014) 009 [arXiv:1401.6458] [INSPIRE].

[52] D. Hooper, *Z' mediated dark matter models for the Galactic Center gamma-ray excess*, *Phys. Rev.* **D 91** (2015) 035025 [arXiv:1411.4079] [INSPIRE].

[53] A. Berlin, P. Gratia, D. Hooper and S.D. McDermott, *Hidden Sector Dark Matter Models for the Galactic Center Gamma-Ray Excess*, *Phys. Rev.* **D 90** (2014) 015032 [arXiv:1405.5204] [INSPIRE].

[54] P. Agrawal, B. Batell, D. Hooper and T. Lin, *Flavored Dark Matter and the Galactic Center Gamma-Ray Excess*, *Phys. Rev.* **D 90** (2014) 063512 [arXiv:1404.1373] [INSPIRE].

[55] E. Izaguirre, G. Krnjaic and B. Shuve, *The Galactic Center Excess from the Bottom Up*, *Phys. Rev.* **D 90** (2014) 055002 [arXiv:1404.2018] [INSPIRE].

[56] C. Cheung, M. Papucci, D. Sanford, N.R. Shah and K.M. Zurek, *NMSSM Interpretation of the Galactic Center Excess*, *Phys. Rev.* **D 90** (2014) 075011 [arXiv:1406.6372] [INSPIRE].

[57] D.G. Cerdeño, M. Peiró and S. Robles, *Low-mass right-handed sneutrino dark matter: SuperCDMS and LUX constraints and the Galactic Centre gamma-ray excess*, *JCAP* **08** (2014) 005 [arXiv:1404.2572] [INSPIRE].

[58] A. Alves, S. Profumo, F.S. Queiroz and W. Shepherd, *Effective field theory approach to the Galactic Center gamma-ray excess*, *Phys. Rev.* **D 90** (2014) 115003 [arXiv:1403.5027] [INSPIRE].

JCAP02(2017)038

[59] D. Hooper, N. Weiner and W. Xue, *Dark Forces and Light Dark Matter*, *Phys. Rev.* **D 86** (2012) 056009 [arXiv:1206.2929] [INSPIRE].

[60] P. Ko, W.-I. Park and Y. Tang, *Higgs portal vector dark matter for* GeV *scale* γ*-ray excess from galactic center*, *JCAP* **09** (2014) 013 [arXiv:1404.5257] [INSPIRE].

[61] C. Boehm, M.J. Dolan and C. McCabe, *A weighty interpretation of the Galactic Centre excess*, *Phys. Rev.* **D 90** (2014) 023531 [arXiv:1404.4977] [INSPIRE].

[62] M. Abdullah, A. DiFranzo, A. Rajaraman, T.M.P. Tait, P. Tanedo and A.M. Wijangco, *Hidden on-shell mediators for the Galactic Center* γ*-ray excess*, *Phys. Rev.* **D 90** (2014) 035004 [arXiv:1404.6528] [INSPIRE].

[63] A. Martin, J. Shelton and J. Unwin, *Fitting the Galactic Center Gamma-Ray Excess with Cascade Annihilations*, *Phys. Rev.* **D 90** (2014) 103513 [arXiv:1405.0272] [INSPIRE].

[64] J.M. Cline, G. Dupuis, Z. Liu and W. Xue, *The windows for kinetically mixed Z'-mediated dark matter and the galactic center gamma ray excess*, *JHEP* **08** (2014) 131 [arXiv:1405.7691] [INSPIRE].

[65] Y.G. Kim, K.Y. Lee, C.B. Park and S. Shin, *Secluded singlet fermionic dark matter driven by the Fermi gamma-ray excess*, *Phys. Rev.* **D 93** (2016) 075023 [arXiv:1601.05089] [INSPIRE].

[66] C. Karwin, S. Murgia, T.M.P. Tait, T.A. Porter and P. Tanedo, *Dark Matter Interpretation of the Fermi-LAT Observation Toward the Galactic Center*, arXiv:1612.05687 [INSPIRE].

[67] K. Ghorbani, *Fermionic dark matter with pseudo-scalar Yukawa interaction*, *JCAP* **01** (2015) 015 [arXiv:1408.4929] [INSPIRE].

[68] LUX collaboration, D.S. Akerib et al., *Results from a search for dark matter in the complete LUX exposure*, *Phys. Rev. Lett.* **118** (2017) 021303 [arXiv:1608.07648] [INSPIRE].

[69] PandaX-II collaboration, A. Tan et al., *Dark Matter Results from First 98.7 Days of Data from the PandaX-II Experiment*, *Phys. Rev. Lett.* **117** (2016) 121303 [arXiv:1607.07400] [INSPIRE].

[70] CMS collaboration, *Search for narrow resonances in dilepton mass spectra in proton-proton collisions at* $\sqrt{s}$ *= 13 TeV and combination with 8 TeV data*, submitted to Phys. Lett. B (2016) [arXiv:1609.05391] [INSPIRE].

[71] CMS collaboration, *Search for narrow resonances decaying to dijets in proton-proton collisions at* $\sqrt{s} = 13$ *TeV*, *Phys. Rev. Lett.* **116** (2016) 071801 [arXiv:1512.01224] [INSPIRE].

[72] CMS Collaboration, *Search for dark matter in final states with an energetic jet, or a hadronically decaying W or Z boson using* 12.9 fb^{-1} *of data at* $\sqrt{s} = 13$ TeV, CMS-PAS-EXO-16-037 (2016).

[73] CMS collaboration, *An inclusive search for new phenomena in final states with one or more jets and missing transverse momentum at* 13 *TeV with the AlphaT variable*, CMS-PAS-SUS-16-016 (2016).

[74] ATLAS collaboration, *Search for new high-mass resonances in the dilepton final state using proton-proton collisions at* $\sqrt{s} = 13$ *TeV with the ATLAS detector*, ATLAS-CONF-2016-045 (2016).

[75] ATLAS collaboration, *Search for new phenomena in final states with an energetic jet and large missing transverse momentum in pp collisions at* $\sqrt{s} = 13$ *TeV using the ATLAS detector*, *Phys. Rev.* **D 94** (2016) 032005 [arXiv:1604.07773] [INSPIRE].

[76] ATLAS collaboration, *Search for new phenomena in events with a photon and missing transverse momentum in pp collisions at* $\sqrt{s} = 13$ *TeV with the ATLAS detector*, *JHEP* **06** (2016) 059 [arXiv:1604.01306] [INSPIRE].

JCAP02(2017)038

[77] CMS collaboration, *Search for a neutral MSSM Higgs boson decaying into tautau at 13 TeV*, CMS-PAS-HIG-16-006 (2016).

[78] CMS collaboration, *Search for a narrow heavy decaying to bottom quark pairs in the 13 TeV data sample*, CMS-PAS-HIG-16-025 (2016).

[79] OPAL, DELPHI, LEP Working Group for Higgs boson searches, ALEPH, L3 collaborations, R. Barate et al., *Search for the standard model Higgs boson at LEP*, *Phys. Lett.* **B 565** (2003) 61 [hep-ex/0306033] [INSPIRE].

[80] M.J. Dolan, F. Kahlhoefer, C. McCabe and K. Schmidt-Hoberg, *A taste of dark matter: Flavour constraints on pseudoscalar mediators*, *JHEP* **03** (2015) 171 [*Erratum ibid.* **07** (2015) 103] [arXiv:1412.5174] [INSPIRE].

[81] A. Alloul, N.D. Christensen, C. Degrande, C. Duhr and B. Fuks, *FeynRules 2.0 - A complete toolbox for tree-level phenomenology*, *Comput. Phys. Commun.* **185** (2014) 2250 [arXiv:1310.1921] [INSPIRE].

[82] J. Alwall, R. Frederix, S. Frixione, V. Hirschi, F. Maltoni, O. Mattelaer et al., *The automated computation of tree-level and next-to-leading order differential cross sections and their matching to parton shower simulations*, *JHEP* **07** (2014) 079 [arXiv:1405.0301] [INSPIRE].

[83] V. Hirschi and O. Mattelaer, *Automated event generation for loop-induced processes*, *JHEP* **10** (2015) 146 [arXiv:1507.00020] [INSPIRE].

[84] T. Sjöstrand, S. Mrenna and P.Z. Skands, *A Brief Introduction to PYTHIA 8.1*, *Comput. Phys. Commun.* **178** (2008) 852 [arXiv:0710.3820] [INSPIRE].

[85] DELPHES 3 collaboration, J. de Favereau, C. Delaere, P. Demin, A. Giammanco, V. Lemaître, A. Mertens et al., *DELPHES 3, A modular framework for fast simulation of a generic collider experiment*, *JHEP* **02** (2014) 057 [arXiv:1307.6346] [INSPIRE].

[86] M. Duerr, F. Kahlhoefer, K. Schmidt-Hoberg, T. Schwetz and S. Vogl, *How to save the WIMP: global analysis of a dark matter model with two s-channel mediators*, *JHEP* **09** (2016) 042 [arXiv:1606.07609] [INSPIRE].

[87] C. Englert, M. McCullough and M. Spannowsky, *S-Channel Dark Matter Simplified Models and Unitarity*, *Phys. Dark Univ.* **14** (2016) 48 [arXiv:1604.07975] [INSPIRE].

[88] G. Busoni et al., *Recommendations on presenting LHC searches for missing transverse energy signals using simplified s-channel models of dark matter*, arXiv:1603.04156 [INSPIRE].

[89] F. Kahlhoefer, K. Schmidt-Hoberg, T. Schwetz and S. Vogl, *Implications of unitarity and gauge invariance for simplified dark matter models*, *JHEP* **02** (2016) 016 [arXiv:1510.02110] [INSPIRE].

[90] J. Abdallah et al., *Simplified Models for Dark Matter Searches at the LHC*, *Phys. Dark Univ.* **9-10** (2015) 8 [arXiv:1506.03116] [INSPIRE].

[91] BaBar collaboration, J.P. Lees et al., *Search for hadronic decays of a light Higgs boson in the radiative decay* $\Upsilon \to \gamma A^0$, *Phys. Rev. Lett.* **107** (2011) 221803 [arXiv:1108.3549] [INSPIRE].

[92] BaBar collaboration, J.P. Lees et al., *Search for a low-mass scalar Higgs boson decaying to a tau pair in single-photon decays of* $\Upsilon(1S)$, *Phys. Rev.* **D 88** (2013) 071102 [arXiv:1210.5669] [INSPIRE].

[93] BaBar collaboration, J.P. Lees et al., *Search for di-muon decays of a low-mass Higgs boson in radiative decays of the* $\Upsilon(1S)$, *Phys. Rev.* **D 87** (2013) 031102 [arXiv:1210.0287] [INSPIRE].

[94] BaBar collaboration, J.P. Lees et al., *Search for a light Higgs resonance in radiative decays of the Y(1S) with a charm tag*, *Phys. Rev.* **D 91** (2015) 071102 [arXiv:1502.06019] [INSPIRE].

JCAP02(2017)038

[95] J.D. Clarke, R. Foot and R.R. Volkas, *Phenomenology of a very light scalar (100 MeV $< m_h <$ 10 GeV) mixing with the SM Higgs*, *JHEP* **02** (2014) 123 [arXiv:1310.8042] [INSPIRE].

[96] U. Haisch and J.F. Kamenik, *Searching for new spin-0 resonances at LHCb*, *Phys. Rev.* **D 93** (2016) 055047 [arXiv:1601.05110] [INSPIRE].

[97] J. Kopp, V. Niro, T. Schwetz and J. Zupan, *DAMA/LIBRA and leptonically interacting Dark Matter*, *Phys. Rev.* **D 80** (2009) 083502 [arXiv:0907.3159] [INSPIRE].

[98] C. Savage, G. Gelmini, P. Gondolo and K. Freese, *Compatibility of DAMA/LIBRA dark matter detection with other searches*, *JCAP* **04** (2009) 010 [arXiv:0808.3607] [INSPIRE].

[99] H.-Y. Cheng and C.-W. Chiang, *Revisiting Scalar and Pseudoscalar Couplings with Nucleons*, *JHEP* **07** (2012) 009 [arXiv:1202.1292] [INSPIRE].

[100] A.L. Fitzpatrick, W. Haxton, E. Katz, N. Lubbers and Y. Xu, *The Effective Field Theory of Dark Matter Direct Detection*, *JCAP* **02** (2013) 004 [arXiv:1203.3542] [INSPIRE].

[101] F. Calore, I. Cholis, C. McCabe and C. Weniger, *A Tale of Tails: Dark Matter Interpretations of the Fermi GeV Excess in Light of Background Model Systematics*, *Phys. Rev.* **D 91** (2015) 063003 [arXiv:1411.4647] [INSPIRE].

[102] B. Batell, T. Lin and L.-T. Wang, *Flavored Dark Matter and R-Parity Violation*, *JHEP* **01** (2014) 075 [arXiv:1309.4462] [INSPIRE].

[103] P. Agrawal, S. Blanchet, Z. Chacko and C. Kilic, *Flavored Dark Matter and Its Implications for Direct Detection and Colliders*, *Phys. Rev.* **D 86** (2012) 055002 [arXiv:1109.3516] [INSPIRE].

[104] P. Agrawal, Z. Chacko, C. Kilic and R.K. Mishra, *A Classification of Dark Matter Candidates with Primarily Spin-Dependent Interactions with Matter*, arXiv:1003.1912 [INSPIRE].

JCAP02(2017)038

Journal of Cosmology and Astroparticle Physics
An IOP and SISSA journal

Hidden sector dark matter and the Galactic Center gamma-ray excess: a closer look

Miguel Escudero,[a] **Samuel J. Witte**[a,b] **and Dan Hooper**[c,d,e]

[a]Instituto de Física Corpuscular (IFIC), CSIC-Universitat de València, Apartado de Correos 22085, E-46071 Valencia, Spain
[b]University of California, Los Angeles, Department of Physics and Astronomy, Los Angeles, CA 90095, U.S.A.
[c]Fermi National Accelerator Laboratory, Center for Particle Astrophysics, Batavia, IL 60510, U.S.A.
[d]University of Chicago, Department of Astronomy and Astrophysics, Chicago, IL 60637, U.S.A.
[e]University of Chicago, Kavli Institute for Cosmological Physics, Chicago, IL 60637, U.S.A.

E-mail: miguel.escudero@ific.uv.es, switte@physics.ucla.edu, dhooper@fnal.gov

Received September 28, 2017
Revised November 10, 2017
Accepted November 13, 2017
Published November 24, 2017

Abstract. Stringent constraints from direct detection experiments and the Large Hadron Collider motivate us to consider models in which the dark matter does not directly couple to the Standard Model, but that instead annihilates into hidden sector particles which ultimately decay through small couplings to the Standard Model. We calculate the gamma-ray emission generated within the context of several such hidden sector models, including those in which the hidden sector couples to the Standard Model through the vector portal (kinetic mixing with Standard Model hypercharge), through the Higgs portal (mixing with the Standard Model Higgs boson), or both. In each case, we identify broad regions of parameter space in which the observed spectrum and intensity of the Galactic Center gamma-ray excess can easily be accommodated, while providing an acceptable thermal relic abundance and remaining consistent with all current constraints. We also point out that cosmic-ray antiproton measurements could potentially discriminate some hidden sector models from more conventional dark matter scenarios.

Keywords: dark matter experiments, dark matter theory

ArXiv ePrint: 1709.07002

https://doi.org/10.1088/1475-7516/2017/11/042

JCAP11(2017)042

Contents

1 Introduction

A number of groups have reported the presence of a significant excess of GeV-scale gamma rays from the region surrounding the Galactic Center [1–11], with spectral and morphological characteristics that are broadly consistent with that predicted from annihilating dark matter particles. Although this signal's possible connection with dark matter has received a great deal of attention (see, for example, refs. [12–38]), astrophysical origins of this emission have also been extensively discussed. In particular, scenarios have been proposed in which the GeV excess is generated by a large population of unresolved millisecond pulsars [39–45], or by a series of recent cosmic-ray outbursts [46–48]. Outburst scenarios, however, require a significant degree of tuning in their parameters [46], and pulsars can generate this signal only if the population of these objects in the Inner Galaxy is different from those observed in globular clusters or in the field of the Milky Way [39, 43, 45, 49].

Dark matter scenarios capable of accounting for the observed gamma-ray excess are also quite strongly constrained. In particular, the null results of direct detection experiments [50–52], as well as the LHC (Large Hadron Collider) and other collider experiments, exclude many models in which the dark matter is an electroweak-scale thermal relic. Although there exist models in which the dark matter could generate the gamma-ray excess without violating these stringent constraints (featuring pseudoscalar mediators, or near resonance spin-1 mediators, for example) [53], these results motivate us to consider models in which the dark matter does not couple directly to the particle content of the Standard Model, but instead produce other hidden sector particles in their annihilations, which decay through very small couplings to the Standard Model. Such hidden sector dark matter models have been previously explored, including within the context of the Galactic Center excess [34–37].

In this paper, we revisit the possibility that the Galactic Center gamma-ray excess may be generated by the annihilations of hidden sector dark matter particles. In the following section, we describe three such models, and calculate in each the dark matter's thermal relic abundance, low-velocity annihilation cross section, and elastic scattering cross section with nuclei. We then go on to calculate the gamma-ray spectrum that is generated through dark

JCAP11(2017)042

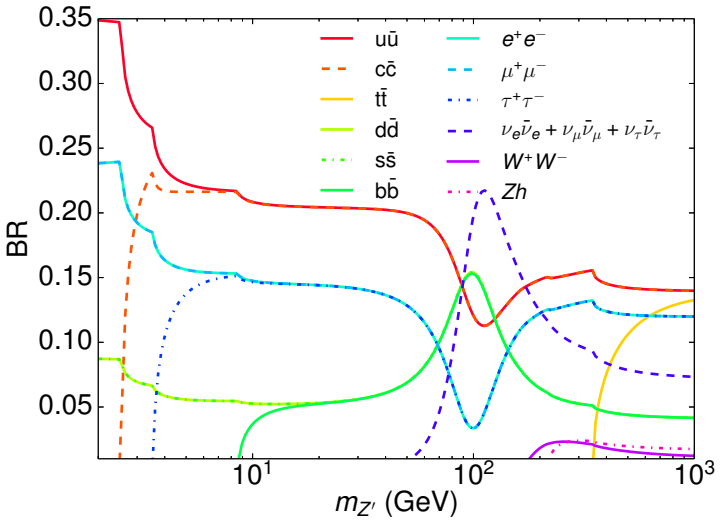

Figure 1. The branching ratios of a hidden sector Z' which couples to the Standard Model through kinetic mixing with Standard Model hypercharge.

matter annihilations in each model, and compare these results to the observed spectral shape and intensity of the Galactic Center excess. In each case we find broad regions of parameter space that can provide a good fit to the observed characteristics of the gamma-ray excess. We also discuss additional constraints on the vector and Higgs portal scenarios, and consider how hidden sector dark matter models can be further tested and probed in the future, including through cosmic-ray antiproton measurements.

2 Hidden sector dark matter

Hidden sector models fall into broad classifications, depending on the interactions which connect the hidden sector to the particle content of the Standard Model [54, 55]. Particularly attractive are the scenarios known as the vector portal [56], the Higgs portal [57–60], and the neutrino portal [61–64]. In this study, we focus on our attention on the first two of these possibilities, which are described in the following two subsections (for recent studies of dark matter phenomenology in neutrino portal models, see refs. [65–72]). We then describe three dark matter models which incorporate these portals between the hidden sector and the Standard Model.

2.1 The vector portal

We begin by considering a hidden sector which contains a broken $U_D(1)$ symmetry, resulting in a massive gauge boson, Z'. We also assume that no scalar fields are charged simultaneously under both the Standard Model and hidden sector gauge groups. The kinetic terms in the hidden sector Lagrangian are given by:

$$\mathcal{L}_{\rm kinetic} \supset -\frac{1}{4}\hat{B}_{\mu\nu}\hat{B}^{\mu\nu} - \frac{1}{4}\hat{F}'_{\mu\nu}\hat{F}'^{\mu\nu} - \frac{\epsilon}{2}\hat{B}_{\mu\nu}\hat{F}'^{\mu\nu}\,, \tag{2.1}$$

where $\hat{B}_{\mu\nu}$ and $\hat{F}'_{\mu\nu}$ are the stress-energy tensors of $U_Y(1)$ and $U_D(1)$, respectively. After the diagonalization of the kinetic terms, and subsequently the mass terms, the relevant

JCAP11(2017)042

interactions between the hidden sector Z' and the Standard Model fermions are described by the following (assuming $\epsilon \ll 1$) [73–75]:

$$\mathcal{L}_{Z',\,\text{fermions}} = Z'^{\mu} \sum_f \bar{f} \gamma_\mu (g_v^f + g_a^f \gamma_5) f \,, \tag{2.2}$$

where the vector and axial couplings are given as follows:

$$\begin{aligned} g_v^f &= \frac{\epsilon}{(m_Z^2 - m_{Z'}^2)} \left[m_{Z'}^2 \, g_Y \, \frac{(Y_{f_R} + Y_{f_L})}{2} - m_Z^2 \, g \, \sin\theta_W \cos\theta_W \, Q_f \right], \\ g_a^f &= \frac{\epsilon}{(m_Z^2 - m_{Z'}^2)} \left[m_{Z'}^2 \, g_Y \, \frac{(Y_{f_R} - Y_{f_L})}{2} \right]. \end{aligned} \tag{2.3}$$

Here, Q_f and $Y_{f_{R,L}}$ denote electric charge and hypercharge, respectively, θ_W the weak mixing angle, and g_Y and g are the Standard Model U(1) and SU(2) gauge couplings, respectively.

The branching ratios for the Z' are shown in figure 1. For values of $m_{Z'}$ which are either much greater than or much less than m_Z, these decays are dominated by final states consisting of charged leptons and up-type quarks, due to the large values of these fermions' hypercharge. For $m_{Z'} \sim m_Z$, however, a cancellation occurs, leading to a large branching fraction to neutrinos and down-type quarks.

If ϵ is not too small, interactions of the Z' can maintain kinetic equilibrium between the hidden sector and the Standard Model in the early universe. In particular, processes of the type $Z' f \leftrightarrow \gamma f$ will exceed the rate of Hubble expansion at a temperature T if the following condition is satisfied: $\epsilon \gtrsim 3 \times 10^{-8} \times (T/\text{GeV})^{1/2} \, (g_\star/75)^{1/4}$, where $g_\star$ is the effective number of degrees-of-freedom at temperature T (see, for example, appendix 7 of ref. [76]).

2.2 The Higgs portal

We next consider interactions between the hidden sector and the Standard Model which are generated through mixing with the Higgs boson. We introduce a complex scalar, ϕ, which transforms as a singlet under the Standard Model gauge symmetries and that is charged under a new local $U_D(1)$ symmetry. Including all renormalizable interactions, this symmetry leads to the following scalar potential:

$$V = -\mu_H^2 (H^\dagger H) + \lambda_H (H^\dagger H)^2 - \mu_\phi^2 \phi^\dagger \phi + \lambda_\phi (\phi^\dagger \phi)^2 + \lambda_{H\phi} (H^\dagger H) \, (\phi^\dagger \phi) \,, \tag{2.4}$$

where H is the Standard Model Higgs doublet. After both electroweak and dark symmetry breaking, both scalars develop vacuum expectation values, so that in the unitary gauge

$$H = \begin{pmatrix} 0 \\ \frac{v_H + \tilde{h}}{\sqrt{2}} \end{pmatrix} , \qquad \phi = \frac{v_\phi + \tilde{\rho}}{\sqrt{2}} \,. \tag{2.5}$$

The scalar sector then contains two CP even massive real scalars, $\tilde{h}$ and $\tilde{\rho}$, which mix. Upon diagonalization of the mass matrix, this leads to the mass eigenstates h and ρ. The state h is identified as the Standard Model Higgs boson with a mass of $m_h \approx 125\,\text{GeV}$. The mixing angle between these two states is given by:

$$\tan 2\theta = \frac{\lambda_{H\phi} \, v_H \, v_\phi}{\lambda_\phi \, v_\phi^2 - \lambda_H \, v_H^2} \,. \tag{2.6}$$

JCAP11(2017)042

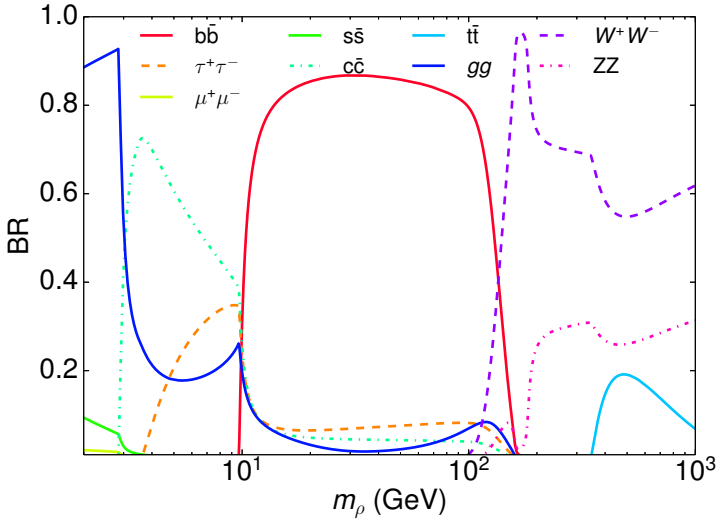

Figure 2. The branching ratios of a hidden sector scalar, ρ, which couples to the Standard Model through mixing with the Higgs boson.

The remaining couplings can be written in terms of the physical masses and this mixing angle:

$$\lambda_H = \frac{m_h^2 \cos^2\theta + m_\rho^2 \sin^2\theta}{2v_H^2}\,, \quad \lambda_\phi = \frac{m_h^2 \sin^2\theta + m_\rho^2 \cos^2\theta}{2v_\phi^2}\,, \quad \lambda_{H\phi} = \frac{(m_\rho^2 - m_h^2)\sin 2\theta}{2v_H v_\phi}\,,$$
$$\mu_H^2 = \lambda_H v_H^2 + \frac{1}{2}\lambda_{H\phi} v_\phi^2\,, \qquad \mu_\phi^2 = \lambda_\phi v_\phi^2 + \frac{1}{2}\lambda_{H\phi} v_H^2\,. \tag{2.7}$$

We have implicitly assumed that the CP-odd state contained in ϕ corresponds to the longitudinal mode of the hidden sector Z', so that it gets its mass through the Higgs mechanism, namely $m_{Z'} = 2g_D v_\phi$, where g_D is the coupling strength of the $U_D(1)$ symmetry and we have assumed that the ϕ field carries two units of $U_D(1)$ charge. Due to this mixing, the couplings of the Higgs boson to Standard Model particles are rescaled by a factor of $\cos\theta$, such that the total width is given by $\Gamma(h \to \mathrm{SM}) = \cos^2\theta\,\Gamma_{\mathrm{SM}}$, where $\Gamma_{\mathrm{SM}} = 4.07\,\mathrm{MeV}$. In addition, if $m_\rho < m_h/2$, the Higgs boson will be able to decay to $\rho\rho$, with a width that is given as follows:

$$\Gamma(h \to \rho\rho) = \frac{(m_h^2 + 2m_\rho^2)^2}{128\pi m_h^2 v_H^2 v_\phi^2}(m_h^2 - 4m_\rho^2)^{1/2}\,(v_H\cos\theta - v_\phi \sin\theta)^2 \sin^2 2\theta\,. \tag{2.8}$$

The branching ratios of this hidden sector scalar are shown in figure 2, as computed using HDECAY [77]. As expected, these decays are dominated by final states which include Standard Model gauge bosons and heavy fermions.

If $\lambda_{H\phi}$ is not too small, kinetic equilibrium will be maintained between the hidden sector and the Standard Model in the early universe. By comparing the rate for $\phi\phi \leftrightarrow HH$ to that of Hubble expansion, we find that kinetic equilibrium is maintained between these sectors at $T \sim$ GeV temperatures as long as $\lambda_{H\phi} \gtrsim 10^{-7}$, corresponding to $\sin^2\theta \gtrsim 10^{-13}\,(v_\phi/300\,\mathrm{GeV})^2$.

2.3 Dirac dark matter and the vector portal

First, we will consider dark matter in the form of a Dirac Fermion, Ψ, which is charged under a broken $\mathrm{U(1)_D}$ and thus couples to a hidden sector Z'. In particular, we will consider

JCAP11(2017)042

the case in which the Z' gets its mass via the Stueckelberg mechanism [78] and mixes with Standard Model hypercharge as described in section 2.1. A Dirac mass term for Ψ is allowed in the Lagrangian, and the dark matter's stability is ensured by a residual Z_2 symmetry. Among other studies, this model has been considered previously in ref. [74] within a similar context.

The relevant Lagrangian of this model is given by:

$$\mathcal{L} \supset \bar{\Psi}(i\partial\!\!\!/ - m_\Psi)\Psi + g_D Z'^\mu \bar{\Psi}\gamma_\mu \Psi \,. \tag{2.9}$$

The early universe phenomenology of the hidden sector is dominated by the process $\bar{\Psi}\Psi \to Z'Z'$, with a cross section that is given by:

$$\begin{aligned}\sigma_{\Psi\Psi\to Z'Z'} = & \frac{g_D^4}{8\pi s\left(s-4m_\Psi^2\right)\left(2m_{Z'}^2-s\right)} \\ & \times\left[\frac{\left(s-2m_{Z'}^2\right)\sqrt{\left(s-4m_\Psi^2\right)\left(s-4m_{Z'}^2\right)}\left(4m_\Psi^4+m_\Psi^2 s+2m_{Z'}^4\right)}{m_\Psi^2\left(s-4m_{Z'}^2\right)+m_{Z'}^4}\right. \\ & \quad +\left(8m_\Psi^4+m_\Psi^2\left(8m_{Z'}^2-4s\right)-4m_{Z'}^4-s^2\right) \\ & \quad \left.\times\ln\left(\frac{-\sqrt{\left(s-4m_\Psi^2\right)\left(s-4m_{Z'}^2\right)}+2m_{Z'}^2-s}{\sqrt{\left(s-4m_\Psi^2\right)\left(s-4m_{Z'}^2\right)}+2m_{Z'}^2-s}\right)\right] .\end{aligned} \tag{2.10}$$

In the low-velocity limit (relevant for indirect detection), this reduces to:

$$\sigma_{\Psi\bar{\Psi}\to Z'Z'}v = \frac{g_D^4}{4\pi m_\Psi\left(m_{Z'}^2-2m_\Psi^2\right)^2}\left[m_\Psi^2-m_{Z'}^2\right]^{3/2}+\mathcal{O}(v^2)\,. \tag{2.11}$$

For the purposes of direct detection, the dominant process is spin-independent scattering, with the following cross section per nucleon:

$$\sigma_{\text{nucleon}}^{\text{Dirac}} = \frac{\mu_{\Psi N}^2 g_D^2}{\pi m_{Z'}^4}\left[g_v^u(1+Z/A)+g_v^d(2-Z/A)\right]^2 , \tag{2.12}$$

where $g_v^{u,d}$ are as defined in eq. (2.3), $\mu_{\Psi N}$ is the reduced mass of the dark matter-nucleon system, and A and Z are the atomic mass and number of the target nucleus, respectively.

In figure 3, we summarize some aspects of the dark matter phenomenology in this model. Throughout each frame, we have chosen the value of the coupling g_D in order to obtain a thermal relic abundance equal to the measured cosmological dark matter density. Throughout this study, we calculate the relic abundance following the method described in refs. [74, 81] (see also refs. [82–84]). In doing so, we assume that ϵ is large enough to maintain kinetic equilibrium between the hidden sector and the Standard Model at the time of dark matter freeze-out (see section 2.1). If this condition is not satisfied, the elastic scattering cross section with nuclei and the low-velocity annihilation cross section could be either larger or smaller than those shown here [76, 85].

In the left frame of figure 3, we plot the maximum value of ϵ, as derived from direct detection constraints [50, 79, 80]. In the right frame, we plot the annihilation cross section evaluated at a velocity of $v = 10^{-3}c$, as appropriate for indirect searches. Note that for $m_\Psi \sim m_{Z'}$, the low-velocity cross section is reduced, due to differing velocity distributions in the early and contemporary universe.

JCAP11(2017)042

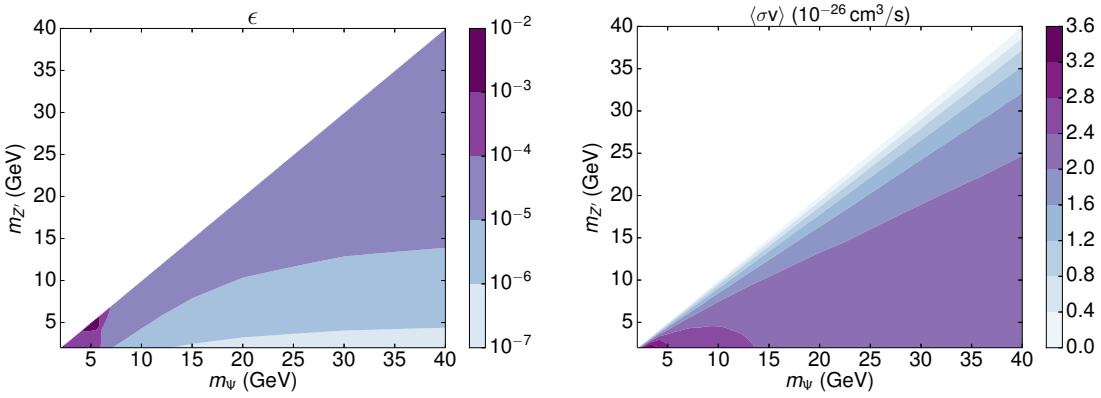

Figure 3. A summary of the phenomenology in a model with a Dirac fermion dark matter candidate, Ψ, which annihilates to a Z' pair, which then decay through kinetic mixing with Standard Model hypercharge. Throughout each frame, we have chosen the value of the hidden sector gauge coupling in order to obtain a thermal relic abundance equal to the measured cosmological dark matter density. In the left frame, we plot the maximum value of the kinetic mixing parameter, ϵ, as derived from direct detection constraints [50, 79, 80]. In the right frame, we plot the annihilation cross section (in units of 10^{-26} cm^3/s) evaluated at a velocity of $v = 10^{-3}c$, as appropriate for indirect searches.

2.4 Vector dark matter and the Higgs portal

Fermionic dark matter can annihilate to a pair of spin-0 particles efficiently in the low-velocity limit only through a product of both scalar and pseudoscalar couplings. Alternatively, we can also consider either scalar or vector dark matter, either of which can annihilate efficiently to a pair of scalars at low velocities. Here we focus on the case of a model that includes a vector dark matter candidate, X, and a scalar, ϕ, with charge assignment 2 [86, 87]. We further impose a Z_2 symmetry to stabilize the dark matter, and which also prohibits the possibility of any kinetic mixing. The relevant Lagrangian contains the following terms (in addition to those corresponding to the scalar potential of eq. (2.4)):

$$\begin{aligned}\mathcal{L} \supset & -\frac{1}{4}X_{\mu\nu}X^{\mu\nu} + (D^\mu\phi)^\dagger (D_\mu\phi) \\ & \equiv -\frac{1}{4}X_{\mu\nu}X^{\mu\nu} + \frac{1}{2}\partial_\mu\tilde{\rho}\partial^\mu\tilde{\rho} + \frac{1}{2}m_X^2 X_\mu X^\mu \left(1 + 2\frac{\tilde{\rho}}{v_\phi} + \frac{\tilde{\rho}^2}{v_\phi^2}\right) , \end{aligned} \quad (2.13)$$

where $m_X = 2g_D v_\phi$. Note that in this model the dark matter candidate X corresponds to the U(1)$_D$ gauge boson, although due to the Z_2 symmetry $\epsilon = 0$.

In this model, the dark matter annihilation cross section in the limit $\sin^2\theta \to 0$ is given as follows:

$$\begin{aligned}\sigma_{XX\to\rho\rho} = & \frac{1}{288\pi s v_\phi^4 \left(s - 4m_X^2\right)} \\ & \times \left[\frac{2\ln\left(\frac{2m_\rho^2 + s\left(\sqrt{\beta_X\beta_\rho}-1\right)}{2m_\rho^2 - s\left(\sqrt{\beta_X\beta_\rho}+1\right)}\right)^2}{2m_\rho^4 - 3m_\rho^2 s + s^2} \left\{48m_X^8\left(m_\rho^2 - s\right) - 8m_X^6\left(16m_\rho^4 - 4m_\rho^2 s - 3s^2\right)\right.\right. \\ & \left. + 4m_X^4\left(10m_\rho^6 + 2m_\rho^4 s - 3m_\rho^2 s^2\right) + 2m_X^2 m_\rho^2 s\left(4m_\rho^4 - 5m_\rho^2 s + s^2\right)\right. \\ & \left.\left. + m_\rho^6\left(-3m_\rho^4 - m_\rho^2 s + s^2\right)\right\}\right] \end{aligned} \quad (2.14)$$

JCAP11(2017)042

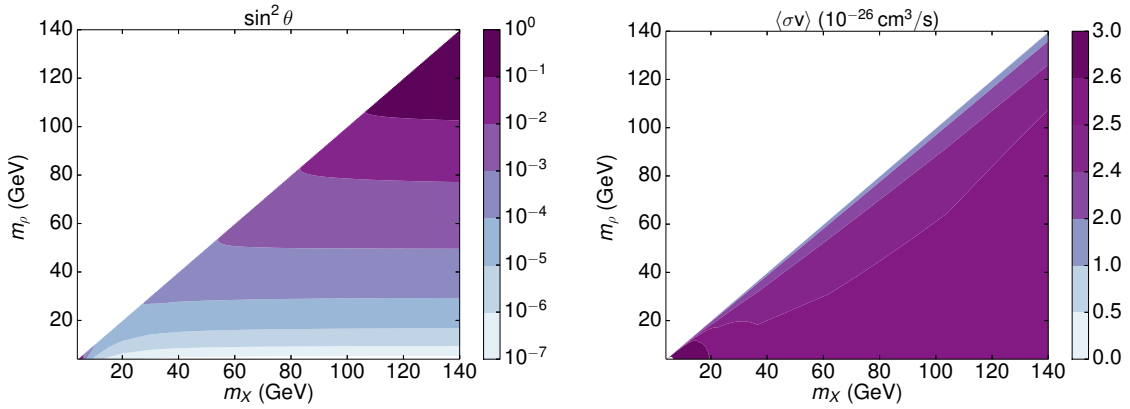

Figure 4. A summary of the phenomenology in a model with a vector dark matter candidate, X, which annihilates to a pair of scalars, ρ, which decay through mixing with the Standard Model Higgs boson. Throughout each frame, we have chosen the value of the hidden sector vacuum expectation value in order to obtain a thermal relic abundance equal to the measured cosmological dark matter density. In the left frame, we plot the maximum value of the Higgs mixing parameter, $\sin^2\theta$, as derived from direct detection constraints [50, 79, 80]. In the right frame, we plot the annihilation cross section (in units of 10^{-26} cm^3/s) evaluated at a velocity of $v = 10^{-3}c$, as appropriate for indirect searches.

$$+\frac{\sqrt{\beta_X\beta_\rho}s}{6\left(m_\rho^2-s\right)^2}\left\{72m_X^4\left(2m_\rho^2+s\right)^2+4m_X^2\left(20m_\rho^6-75m_\rho^4s+s^3\right)\right.$$
$$\left.+24m_\rho^8+28m_\rho^6s-3m_\rho^4s^2+6m_\rho^2s^3-s^4\right\}+\frac{1}{6}\beta_X\beta_\rho^{3/2}s^3$$
$$\left.+\frac{2\sqrt{\beta_X\beta_\rho}s\left(48m_X^8-32m_X^6m_\rho^2+4m_X^4\left(6m_\rho^4-4m_\rho^2s+s^2\right)+4m_X^2m_\rho^4\left(s-2m_\rho^2\right)+m_\rho^8\right)}{m_X^2\left(s-4m_\rho^2\right)+m_\rho^4}\right],$$

where $\beta_{\rho,X}=\sqrt{1-4m_{\rho,X}^2/s}$. In the low-velocity limit, this reduces to:

$$\sigma_{XX\to\rho\rho}v=\frac{m_X^2\sqrt{1-m_\rho^2/m_X^2}}{36\pi v_\phi^4}\frac{\left(176m_X^8-320m_X^6m_\rho^2+240m_X^4m_\rho^4-80m_X^2m_\rho^6+11m_\rho^8\right)}{\left(8m_X^4-6m_X^2m_\rho^2+m_\rho^4\right)^2}. \tag{2.15}$$

Interactions thorough the Higgs portal (see section 2.2) lead to the following spin-independent scattering cross section with nuclei:

$$\sigma_{\text{nucleon}}^{\text{Vector}}=\frac{f_N^2}{4\pi}\frac{\mu_{XN}^2m_N^2}{m_X^2}\left[\frac{m_X^2}{v_\phi v_H}\frac{\sin 2\theta}{2}\left(\frac{1}{m_\rho^2}-\frac{1}{m_h^2}\right)\right]^2, \tag{2.16}$$

where $f_N\simeq 0.3$ and m_N is the nucleon mass.

After fixing the value of v_ϕ to obtain the desired relic abundance, we calculate both the elastic scattering cross section with nuclei and the low-velocity annihilation cross section. These results are shown in figure 4.

We note that there exists significant parameter space within this model in which the mixing between the ρ and the Standard Model Higgs boson is quite significant, especially

JCAP11(2017)042

$m_{Z'}$	m_ρ	ρ Decay	Main Annihilation Channels
$2m_\chi > m_{Z'} > m_\chi$	$m_\rho < m_\chi, 2m_{Z'}$	$\rho \to SM$	$\chi\chi \to Z'\rho$
$m_{Z'} < m_\chi$	$2m_{Z'} > m_\rho > m_\chi$	$\rho \to SM$	$\chi\chi \to Z'\rho$ and $\chi\chi \to Z'Z'$
$m_{Z'} < m_\chi$	$m_\rho > m_\chi, 2m_{Z'}$	$\rho \to Z'Z' \to SM$	$\chi\chi \to Z'\rho$ and $\chi\chi \to Z'Z'$

Table 1. A summary of the distinctive regions of parameter space in a model with a hidden sector which contains dark matter in the form of a Majorana fermion, χ, along with an additional vector, Z', and scalar, ρ.

around $m_\rho \sim 125\,\text{GeV}$, where there is a cancellation in the dark matter's elastic scattering cross section with nuclei (see eq. (2.16)). In this region of parameter space, the process $XX \to h\rho$ can account for up to $\sim 20\%$ of dark matter annihilations, and $XX \to hh$ can account for at most $\sim 4\%$, after applying constraints from colliders, i.e. $\sin^2\theta \lesssim 0.1$ for all values of m_ρ (see section 4). We note that the gamma-ray spectrum that results from these channels are fairly similar to that from $XX \to \rho\rho$ in this mass range. Furthermore, the dark matter could also annihilate directly into Standard Model fermions thorough the Higgs resonance, although this channel is relevant only in a very narrow region of parameter space near $m_X \simeq m_h/2$ [88], and we do not consider this possibility further.

In these calculations, we have assumed that $\sin^2\theta$ is large enough to maintain kinetic equilibrium between the hidden sector and the Standard Model at the time of dark matter freeze-out (see section 2.2). If this is not the case, the elastic scattering cross section with nuclei and the low-velocity annihilation cross section could be either larger or smaller than those shown in figure 4 [76, 85].

2.5 Majorana dark matter and combined vector and Higgs portals

Lastly, we consider Majorana dark matter in the presence of two additional hidden sector states, namely a Z' and a scalar, ρ. Under a $U_D(1)$ symmetry, we assign charges of 2 for the ρ, and ± 1 for the two Majorana states, a combination which is free of anomalies. In order to prohibit mixing between the two fermions, we impose a discrete symmetry: $\chi_1 \to \chi_1$, $\chi_2 \to -\chi_2$. After spontaneous symmetry breaking the relevant terms of the Lagrangian are given by:

$$\mathcal{L} \supset \frac{1}{2}\sum_{i=1}^{2}\left[i\bar{\chi}_i\left(\partial\!\!\!/ - m_{\chi_i}\right)\chi_i \pm g_D Z'^\mu \bar{\chi}_i\gamma_\mu\gamma_5\chi_i - \frac{m_{\chi_i}}{v_\phi}\rho\bar{\chi}_i\chi_i\right], \tag{2.17}$$

where $m_{Z'} = 2g_D v_\phi$.

In order to limit the number of free parameters, we assume a hierarchy in mass such that $m_{\chi_2} \gg m_{\chi_1}$, so that the abundance of χ_2 is negligible compared to that of χ_1. For simplicity we will rename $\chi = \chi_1$, which we identify as our dark matter candidate.

There are several distinctive regions of parameter space within this model, which we summarize in table 1. We note that this model has been previously studied within the context of the Galactic Center Excess in ref. [74], although they restricted themselves to the case of $\chi\chi \to Z'Z'$. Also, the authors of refs. [89] and [90] have recently considered this two-portal scenario, although not within the context of the Galactic Center Excess.

JCAP11(2017)042

If the Z' is light enough that the process $\rho \to Z'Z'$ is kinematically allowed, it will be the dominant decay channel for the dark scalar, with a width given by:

$$\Gamma(\rho \to Z'Z') = \frac{m_\rho^3}{32\pi v_\phi^2}\left(1 - 4\frac{m_{Z'}^2}{m_\rho^2} + 12\frac{m_{Z'}^4}{m_\rho^4}\right)\sqrt{1 - \frac{4m_{Z'}^2}{m_\rho^2}}. \tag{2.18}$$

Although we utilize the full thermally-averaged cross section in our calculations, we present only the low-velocity annihilation cross section here due to the length of these expressions in this particular model:

$$\sigma v_{\chi\chi\to Z'Z'} = \frac{g_D^4}{4\pi m_\chi \left(m_{Z'}^2 - 2m_\chi^2\right)^2}\left[m_\chi^2 - m_{Z'}^2\right]^{3/2} + \mathcal{O}(v^2)\,, \tag{2.19}$$

$$\sigma v_{\chi\chi\to Z'\rho} = \frac{g_D^4}{64\pi m_\chi^4 m_{Z'}^4}\left[m_{Z'}^4 + \left(m_\rho^2 - 4m_\chi^2\right)^2 - 2m_{Z'}^2\left(4m_\chi^2 + m_\rho^2\right)\right]^{3/2} + \mathcal{O}(v^2) \tag{2.20}$$

and

$$\begin{aligned}\sigma v_{\chi\chi\to\rho\rho} = {} & \frac{g_D^4 m_\chi \sqrt{m_\chi^2 - m_\rho^2}\left(8m_\chi^4 - 8m_\chi^2 m_\rho^2 + 3m_\rho^4\right)\, v^2}{24\pi m_{Z'}^4\left(m_\rho^2 - 4m_\chi^2\right)^2\left(m_\rho^2 - 2m_\chi^2\right)^4} \\ & \times\left[288m_\chi^8 - 352m_\chi^6 m_\rho^2 + 200m_\chi^4 m_\rho^4 - 64m_\chi^2 m_\rho^6 + 9m_\rho^8\right].\end{aligned} \tag{2.21}$$

The Z' induces a spin-dependent scattering cross section between our Majorana dark matter candidate and nuclei:

$$\sigma^{\text{Majorana}}_{\text{nucleon, SD}} = \frac{3g_D^2 g_a^{u\,2}\mu_{\chi N}^2}{4\pi m_{Z'}^4}\,, \tag{2.22}$$

where g_a^u is the axial coupling of the up quark to the Z', as defined in Eq 2.3. Due to the comparatively weak constraints on spin-dependent scattering and the smallness of the axial coupling in the low $m_{Z'}$ regime, the value of ϵ is not significantly restricted in this mode.

Additionally, the dark matter will also experience a spin-independent interaction with nuclei as a result of Higgs exchange, with a cross section that is given by:

$$\sigma^{\text{Majorana, SI}}_{\text{nucleon}} = \sin^2 2\theta\,\frac{f_N^2}{4\pi}\,\frac{\mu_{\chi N}^2 m_\chi^2 m_N^2}{v_H^2 v_\phi^2}\left(\frac{1}{m_\rho^2} - \frac{1}{m_h^2}\right)^2\,, \tag{2.23}$$

leading to similar constraints on $\sin\theta$ as those shown in figure 4.

In figure 5 we plot the dark matter annihilation cross section in this model, as evaluated at a velocity of $v = 10^{-3}c$, as appropriate for indirect searches, for several values of the hidden sector ρ and Z' masses. Throughout each frame, we have chosen the value of the coupling, g_D, in order to obtain a thermal relic abundance equal to the measured cosmological dark matter density. In the upper frames, we note that thermal effects which depend on the mass of the hidden sector scalar can lead the low-velocity annihilation cross section to be significantly smaller than that naively expected of a thermal relic. Once again we have assumed that either ϵ or $\sin^2\theta$ is large enough to maintain kinetic equilibrium between the hidden sector and the Standard Model at the time of freeze-out. If this is not the case, the low-velocity annihilation cross section could be either larger or smaller than those shown in figure 5 [76, 85].

JCAP11(2017)042

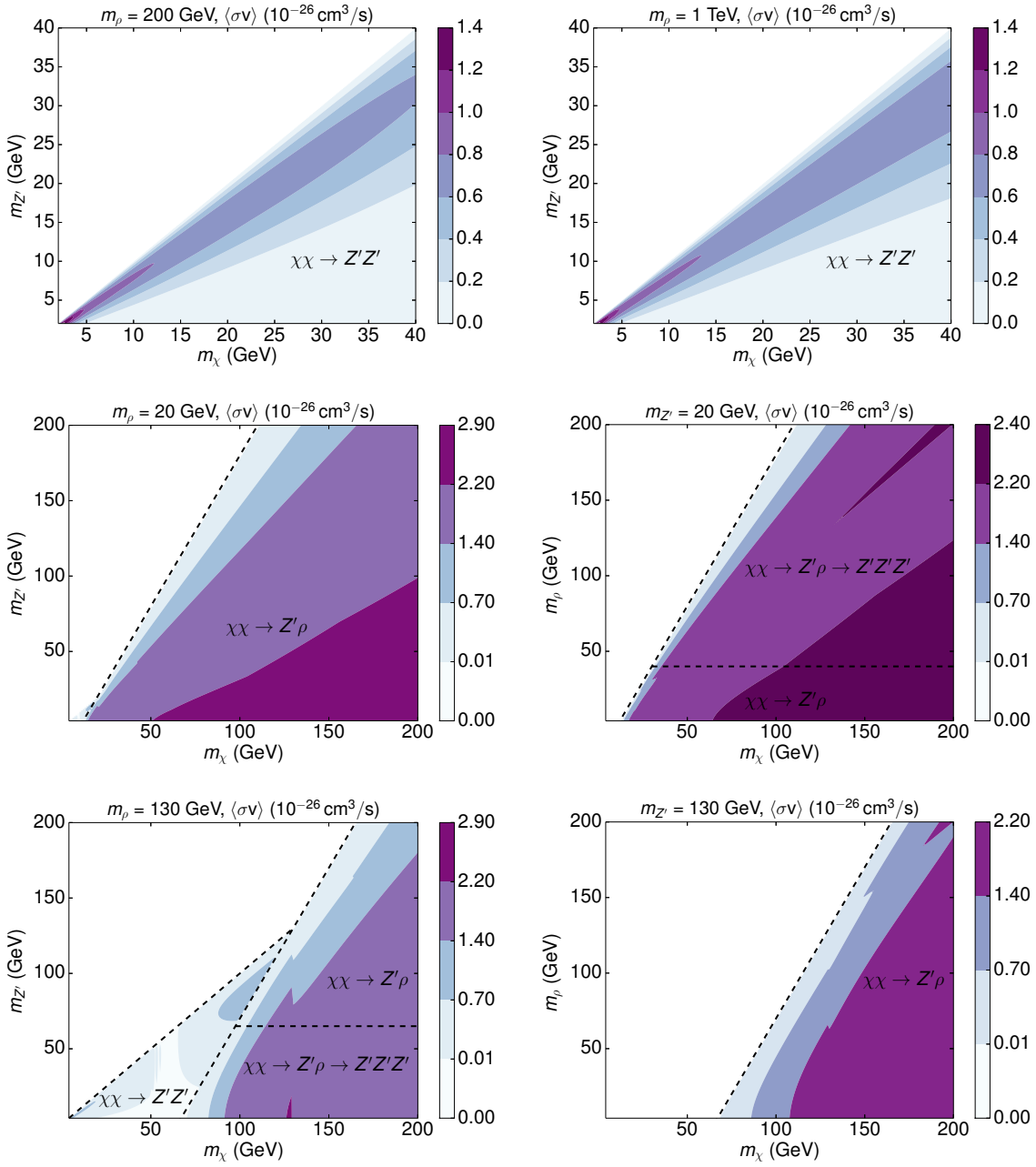

Figure 5. The annihilation cross section evaluated at a velocity of $v = 10^{-3}c$ for dark matter in the form of a Majorana fermion that resides within a hidden sector which contains a vector, Z', and a scalar ρ. In the upper frames, we show results for two cases in which $XX \to Z'Z'$ is the only kinematically allowed annihilation channel. In the middle and lower frames, a combination of the processes $XX \to Z'Z'$ and $XX \to Z'\rho$ are allowed. Whenever the $Z'\rho$ channel is open, it dominates the annihilation final state. The dashed lines demark the regions of parameter space in which different channel are kinematically allowed. Throughout each frame, the value of the hidden sector gauge coupling, g_D, was chosen in order to obtain a thermal relic abundance equal to the measured cosmological dark matter density.

JCAP11(2017)042

3 Fitting the spectrum of the Galactic Center excess

In this section, we calculate the gamma-ray spectrum from dark matter annihilations in the above described hidden sector models and determine the parameter space within these models that is capable of generating the observed features of the Galactic Center gamma-ray excess.

The gamma-ray flux from dark matter annihilations is described by the following:

$$\Phi(E_\gamma, b, \ell) = \frac{\langle \sigma v \rangle}{8\pi m_\chi^2} \frac{d\bar{N}_\gamma}{dE_\gamma}(E_\gamma) \frac{1}{\Delta\Omega} \int_{\rm los} \int_{\Delta\Omega} d\Omega \, ds \, \rho^2(r(s, b, \ell)) \,, \tag{3.1}$$

where $\langle \sigma v \rangle$ is the thermally averaged annihilation cross section, m_χ is the mass of the dark matter particle, $d\bar{N}_\gamma/dE_\gamma$ is the gamma-ray spectrum produced per annihilation and $\rho(r)$ is the dark matter density profile. The integrals are carried out over the observed line-of-sight (los), s, and over a segment of the sky of solid angle $\Delta\Omega$, denoted in terms of Galactic coordinates b and ℓ.

Throughout this study, we will adopt a dark matter density distribution that is described by a generalized Navarro-Frenk-White (NFW) profile:

$$\rho(r) = \rho_s \frac{(r/r_s)^{-\gamma}}{(1 + r/r_s)^{3-\gamma}} \,, \tag{3.2}$$

where r is the distance to the Galactic Center. Unless otherwise stated, we adopt $\gamma = 1.2$, $r_s = 20$ kpc, and we fix ρ_s by requiring that the dark matter density at a distance of 8.5 kpc from the Galactic Center is equal to $\rho_\oplus = 0.4\,{\rm GeV/cm^3}$.

The function $d\bar{N}_\gamma/dE_\gamma$ depends on the mass of the dark matter particle and its dominant annihilation channels. For each model, the gamma-ray spectrum is given by a sum over the decay channels of the intermediate state hidden sector particle(s). We emphasize that the gamma-ray spectrum from dark matter annihilations in hidden sector models depends not only on the dark matter mass and annihilation channels, but also on the mass of the intermediate state particles.

Following ref. [91], one can write the spectrum of gamma rays in the dark matter rest frame in terms of the gamma-ray spectrum in the rest frame of the intermediate state particle, ϕ:

$$\frac{d\bar{N}_\gamma}{dE_\gamma} = \frac{2}{m_\chi} \int_{-1}^{1} d\cos\theta \int_0^1 dx' \left(\frac{dN}{dx'}\right)_\phi \delta(2x - x' - \cos\theta x' \sqrt{1-\kappa^2}) \,, \tag{3.3}$$

where $x \equiv E_\gamma/m_\chi$, E_γ is the photon energy in the frame of the dark matter, $x' \equiv 2E'_\gamma/m_\phi$, E'_γ is the photon energy in the frame of ϕ, and $\kappa \equiv m_\phi/m_\chi$. The angular integration can be performed analytically, leading to

$$\frac{d\bar{N}_\gamma}{dE_\gamma} = \frac{2}{m_\chi} \int_{t_{\rm min}}^{t_{\rm max}} \frac{dx'}{x'\sqrt{1-\kappa^2}} \left(\frac{dN}{dx'}\right)_\phi \,, \tag{3.4}$$

where the integration limits are defined as

$$t_{\rm max} = \min\left[1 \,, \frac{2x}{\kappa^2}\left(1 + \sqrt{1-\kappa^2}\right)\right] \,, \;\; t_{\rm min} = \frac{2x}{\kappa^2}\left(1 - \sqrt{1-\kappa^2}\right) \,. \tag{3.5}$$

JCAP11(2017)042

In the limit of small κ, eq. (3.4) reduces to

$$\frac{d\bar{N}_\gamma}{dE_\gamma} = \frac{2}{m_\chi} \int_x^1 \frac{dx'}{x'} \left(\frac{dN}{dx'}\right)_\phi . \tag{3.6}$$

A publicly available code for the calculation of cascade spectra, using the direct annihilation spectrum tabulated in ref. [92], has been presented and described in refs. [91, 93]. The spectrum used for the analysis of $\chi\chi \to Z'Z'$ (with $m_{Z'} > 2$ GeV) and $\chi\chi \to \rho\rho$ were produced using this code. This code does not, however, include annihilations to mesons, as is required in the case of a light Z', nor does it allow for the immediate computation of the spectrum that arises from annihilations featuring asymmetric boosts, such as in the case of $\chi\chi \to Z'\rho$. In the case of $m_{Z'} \lesssim 2\,\text{GeV}$, the calculation of the branching fractions is non-trivial due to the appearance of hadronic resonances which invalidate the QCD description in terms of final state quarks. At masses $m_{Z'} \lesssim 1.5\,\text{GeV}$, the Z' decays predominately to electrons, muons, and a small number of hadronic resonances. In this low-mass regime, we adopt the branching fractions as presented in ref. [94] and utilized PYTHIA 8 [95] to obtain the gamma-ray spectra from the decays of the Z' to mesons. The cascade spectra for these decay channels was then computed using eq. (3.6). The code of refs. [91, 93] was used to compute the e^+e^- and $\mu^+\mu^-$ spectrum for this decay. For the case of annihilations to multiple intermediate state particle species (i.e. $\chi\chi \to Z'\rho$) we generalized eq. (3.3) to asymmetric annihilations using the results of ref. [36] and utilized this result.

We note that although the above expressions were derived in ref. [91] for the case of scalars, it has been shown that the spectrum arising from the decay of vectors with reasonable angular dependencies leads to similar modifications to the spectrum. Thus we treat the vector portal models using the same formalism as those of the Higgs portal.

To assess whether a given dark matter model is capable of generating the observed features of the Galactic Center gamma-ray excess, we utilize the results of the Fermi data analysis carried out by Calore, Cholis and Weniger [8]. More specifically, we extract the data points, statistical errors, and the first three principal components of the decomposition of the covariance matrix of residuals, as shown in figures 14 and 12 of ref. [8], respectively. We then calculate the value of the χ^2, which is given as follows:

$$\chi^2 = \sum_{i,j} \left(\frac{d\bar{N}_\gamma}{dE_{\gamma,i}}(\boldsymbol{\Theta}) - \frac{dN_\gamma}{dE_{\gamma,i}}\right) \Sigma_{ij}^{-1} \left(\frac{d\bar{N}_\gamma}{dE_{\gamma,j}}(\boldsymbol{\Theta}) - \frac{dN_\gamma}{dE_{\gamma,j}}\right) , \tag{3.7}$$

where Σ_{ij} is full covariance matrix, given by

$$\Sigma_{ij} = (\sigma_i^2)\delta_{i,j} + \Sigma_{ij,\text{mod}}^{\text{trunc}} + \Sigma_{ij,\text{res}} . \tag{3.8}$$

Here, $dN_\gamma/dE_{\gamma,i}$ and $d\bar{N}_\gamma/dE_{\gamma,i}(\boldsymbol{\Theta})$ are the measured and predicted flux in bin i, and $\boldsymbol{\Theta}$ denotes the parameters of the dark matter model under consideration. $\Sigma_{ij,\text{mod}}^{\text{trunc}}$ is the truncated covariance matrix which accounts for empirical model systemics, approximated here (and in ref. [8]) using the first three principal components, and $\Sigma_{ij,\text{res}}$ accounts for the residual systematics below 1 GeV, modeled as:

$$\Sigma_{ij,\text{res}} = \frac{dN}{dE_i^{\text{res}}} \frac{dN}{dE_j^{\text{res}}} + \delta_{i,j} \frac{dN}{dE_i^{\text{res}}} \frac{dN}{dE_j^{\text{res}}} . \tag{3.9}$$

In figure 6 we compare the observed spectrum of the Galactic Center gamma-ray excess with that predicted for a selection of annihilating dark matter models. The vertical black

JCAP11(2017)042

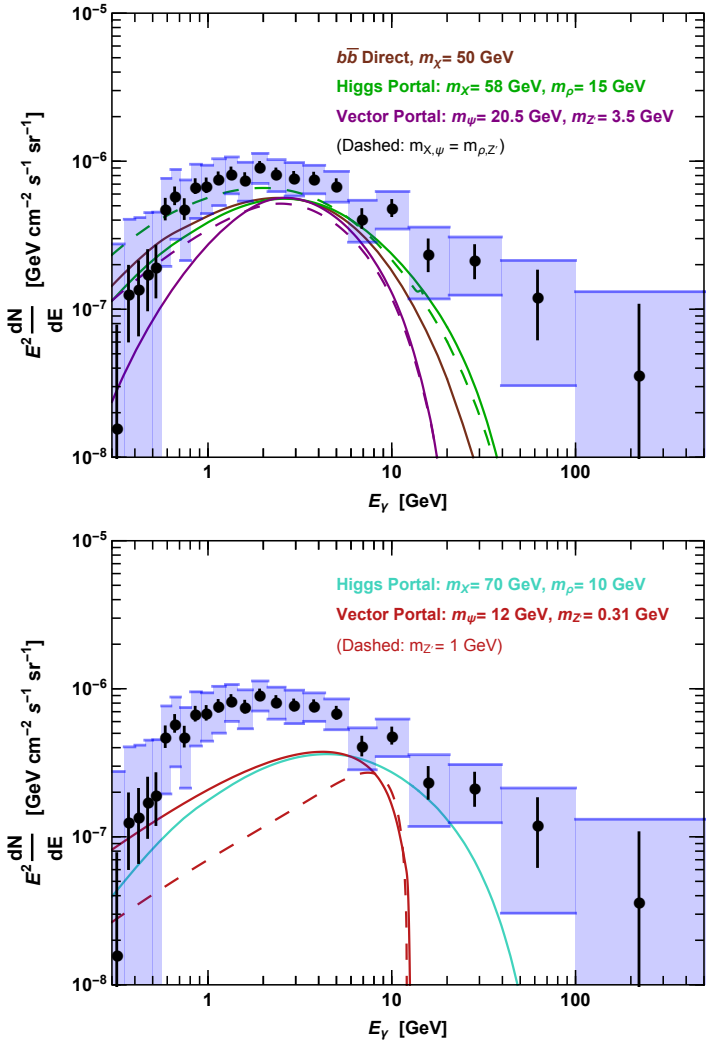

Figure 6. The spectrum of the Galactic Center gamma-ray excess as presented in ref. [8] compared with that predicted in selected dark matter models. The black error bars represent the statistical uncertainty while blue bands represent the diagonal contributions to the covariance matrix from the statistical errors and modeling systematics. Each of the models shown in the upper frame provides a good fit to the data (featuring p-values in the range of 0.37 to 0.46), while those in the lower frame do not (featuring p-values of 0.02 or less).

error bars correspond to the statistical error in each bin, while the blue bars represent the diagonal contributions of the statistical errors and modeling systematics to the covariance matrix.[1] The upper frame of this figure illustrates that dark matter can provide a good fit to the observed spectrum if it annihilates directly to Standard Model particles (such as in the case of a 50 GeV dark matter particle annihilating directly to $b\bar{b}$, featuring a p-value of 0.43) and also if it instead annihilates to intermediate unstable states (such as a 58 GeV dark matter particle which annihilates to a pair of 15 or 58 GeV particles that decay through the Higgs portal, or a 20.5 GeV dark matter particle which annihilates to a pair of 3.5 or

[1] We exclude here the residual systemics below 1 GeV so that a direct comparison can be made with figure 14 of ref. [8].

JCAP11(2017)042

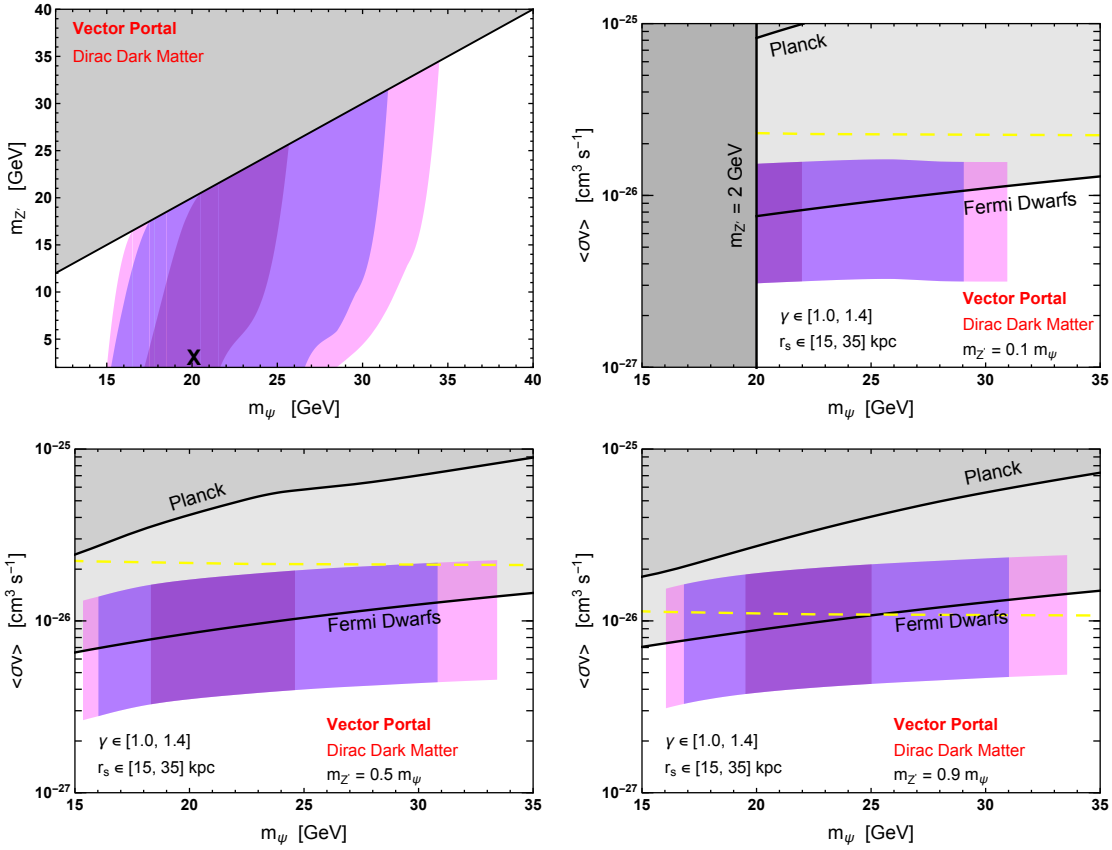

Figure 7. Parameter space in a model with dark matter in the form of a Dirac fermion, Ψ, that annihilates to pairs of hidden sector vectors, Z', which decay to the Standard Model through the vector portal (see section 2.3). In the upper left frame, the bands denote the regions in which the model provides a fit to the measured Galactic Center gamma-ray excess which yields a $p-$value of ≥ 0.32 (dark purple), ≥ 0.10 (violet), and ≥ 0.05 (magenta). The best-fit point is shown with an 'X'. In the other three frames, we plot the best-fit range for the dark matter annihilation cross section in this model, for the case of $m_{Z'} = 0.1\, m_\Psi$, $0.5\, m_\Psi$ or $0.9\, m_\Psi$. The vertical width of the band corresponds to varying the parameters of the halo profile as indicated. Also shown are bounds from Fermi's observations of dwarf galaxies [96] and from Planck [97, 98]. The yellow dashed lines are the contours over which the thermal relic abundance is equal to the measured cosmological dark matter density. This model can account for the entirety of the dark matter and generate the observed characteristics of the Galactic Center gamma-ray excess for $m_\Psi \sim 15 - 35\,\text{GeV}$ and $m_{Z'} \sim (0.8 - 1)\, m_\Psi$.

20.5 GeV particles that decay through the vector portal, which each provide p-values in the range of 0.37 to 0.46).[2] In the lower frame, we show some examples of dark matter models which do not provide a good fit to the observed gamma-ray spectrum. In particular, we find no parameter space with $m_{Z'} < 2\,\text{GeV}$ which provides a good fit to the data. For each dark matter model shown in figure 6, the value of the annihilation cross section was selected to provide the best-fit to the measured spectrum of the Galactic Center excess (adopting $\gamma = 1.2$, $R_\oplus = 8.5$ kpc, and $\rho_\oplus = 0.4\,\text{GeV/cm}^3$).

In figure 7, we show results for a model with a Dirac fermion dark matter candidate, X, that annihilates to pairs of hidden sector vectors, Z', which then decay to the Standard Model

[2]Due to correlations between error bars, the models shown in figure 6 generally provide a better fit to the data than may appear.

JCAP11(2017)042

through the vector portal (see section 2.3). We show both the parameter space that yields a good fit to the measured spectrum of the excess and the range of low-velocity annihilation cross sections that are favored by this fit. More specifically, we calculate the χ^2 for the best-fit value of the annihilation cross section for each point of the parameter space. In the upper left panel, we highlight the regions which yield $p-$values ≥ 0.32 (dark purple), ≥ 0.10 (violet), and ≥ 0.05 (magenta), and mark the best-fit point with an 'X'. In the remaining three panels, we show the best-fit annihilation cross section, $\langle \sigma v \rangle$, as a function of the dark matter mass, for three values of $m_{Z'}/m_{\Psi}$. The vertical width of this band denotes the impact of varying γ between 1 and 1.4 and r_s between 15 and 35 kpc. Note that by varying the local dark matter density between 0.2 and 0.6 GeV/cm^3 this band would be further extended by a factor of 2.25 (4) downward (upward). The colors of these band have the same meaning as in the upper left panel.[3]

Also shown in figure 7 are constraints on the dark matter annihilation cross section as derived from Fermi's observations of dwarf spheroidal galaxies [96] and from Planck. Regarding the constraint from Planck, we follow the approach of refs. [97, 98] (adopting the '3 keV' prescription) to calculate the impact of dark matter annihilation on the history of recombination. The bounds from dwarf spheroidal galaxies are calculated following the statistical procedure outlined in [99] using the 19 dwarf galaxies with measured J-factors listed in table 1 of [96]. Specifically, for each model and for each choice of dark matter and mediator mass, the spectrum is calculated from 500 MeV to 500 GeV and compared with the precomputed bin-by-bin likelihood analyses for each dwarf provided in [100]. Uncertainties in the J-factor are treated with a Gaussian likelihood term as shown in eq. 3 of [99]. In the case of constraints from dwarf galaxies, one should bear in mind that these constraints are subject to non-negligible uncertainties, such as those associated with departures from spherical symmetry [101–103] and with issues associated with stellar membership [104].

The dashed yellow lines shown in figure 7 represent the parameter space which yields a thermal relic abundance equal to the measured cosmological dark matter density. In this model, we can account for the entirety of the dark matter and generate the observed characteristics of the Galactic Center gamma-ray excess for $m_{\Psi} \sim 15-35$ GeV and $m_{Z'} \sim (0.8-1)\, m_{\Psi}$, agreeing well with previous studies [38].

We note that it is possible to construct hidden sector dark matter models which feature a Z' with very different decay modes than those considered here. For example, motivated by recent anomalies associated with semi-leptonic b-decays, models have been discussed in which a Z' obtains flavor non-universal couples via mixing with an additional vector-like family, leading to large couplings to third generation fermions. Although we do not explicitly study models of this variety here, we note that they can also provide a good fit to the observed characteristics of the Galactic Center gamma-ray excess [105].

In figure 8, we repeat this exercise for the case of a vector dark matter candidate that annihilates to hidden sector scalars which then decay through the Higgs portal (see section 2.4). In this model, we find an even larger region of parameter space that can account for the entirety of the dark matter and generate the observed characteristics of the Galactic Center gamma-ray excess, corresponding to for $m_X \sim 70 - 110$ GeV and $m_{\rho} \gtrsim 10$ GeV.

[3]The $p-$values corresponding to the bands in the right panel of figure 8 only correspond to spectral fit (i.e. they do not include morphological information), and thus changes in the density profile can be absorbed into the cross section without altering the χ^2 value. We have chosen here to simply scan over a reasonable range of astrophysical parameters that are approximately consistent with the morphology of the observed gamma-ray excess.

JCAP11(2017)042

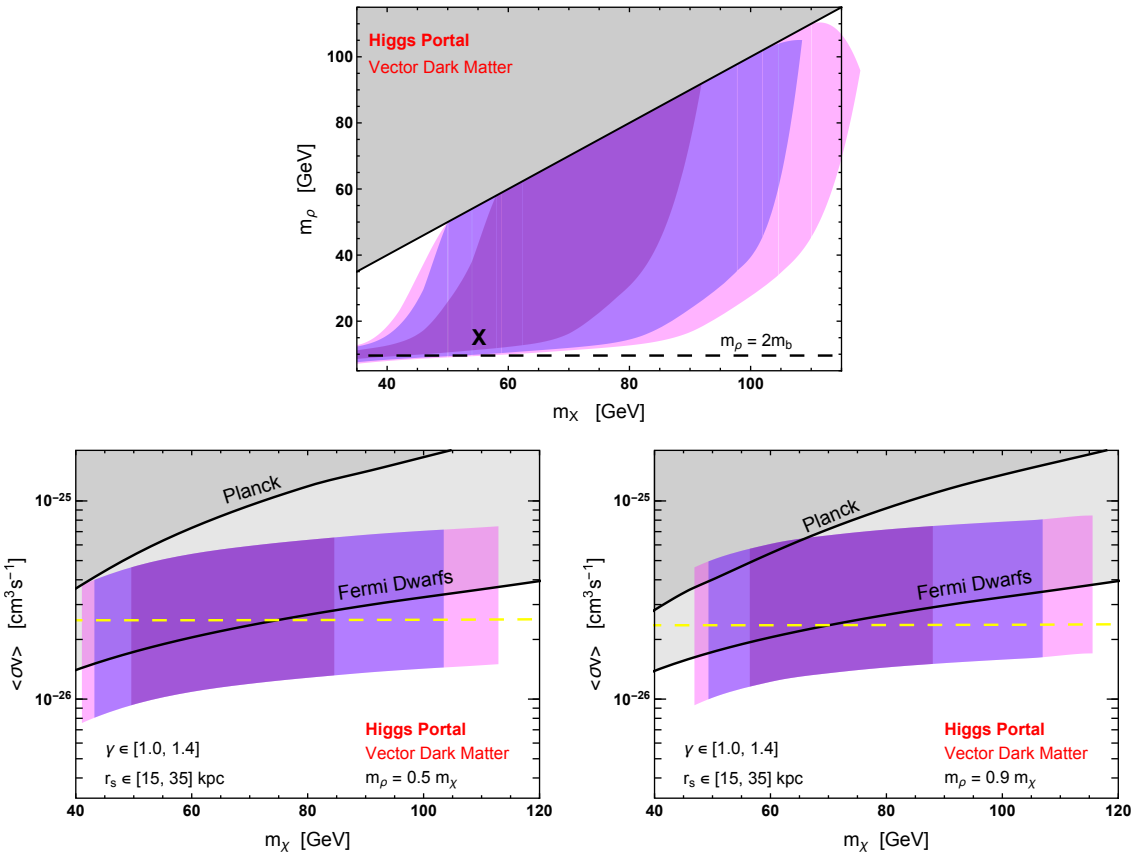

Figure 8. As in figure 7, but for dark matter in the form of a vector that annihilates to pairs of scalars which decay to the Standard Model through the Higgs portal (see section 2.4). This model can account for the entirety of the dark matter and generate the observed characteristics of the Galactic Center gamma-ray excess for $m_X \sim 70 - 110\,\text{GeV}$ and for a wide range of m_ρ.

Lastly, in figure 9, we show results for the case of Majorana dark matter which annihilates to combinations of scalars and vectors which decay to the Standard Model through the Higgs and vector portals, respectively. We show results for several selected values of m_ρ and $m_{Z'}$. We find that this model can accommodate the observed features of gamma-ray excess with either $m_{Z'} \lesssim 40\,\text{GeV}$ or $m_\rho \lesssim 70\,\text{GeV}$.

4 Additional constraints

In addition to constraints derived from direct detection experiments, one can also consider collider signals of the vector and Higgs portal scenarios. Current and projected sensitivities to the vector portal model have been in calculated in ref. [106], and we present these in the left frame of figure 10. More specifically, we plot the current constraints from electroweak precision observables at the LHC (orange), the projected sensitivity for the high luminosity LHC assuming $\sqrt{s}$ =14 TeV and 3ab^{-1}, and the projected sensitivity for a future collider such as the ILIC or Giga$Z$. Since the Z' in this model couples directly to quarks, it can be produced at the LHC via Drell-Yan production, and we plot the projected sensitivity to this signal for the high luminosity LHC, assuming $\sqrt{s}$ =14 TeV and 3 ab^{-1}. Across the parameter space shown, however, we find that the constraints from direct dark matter searches can be

JCAP11(2017)042

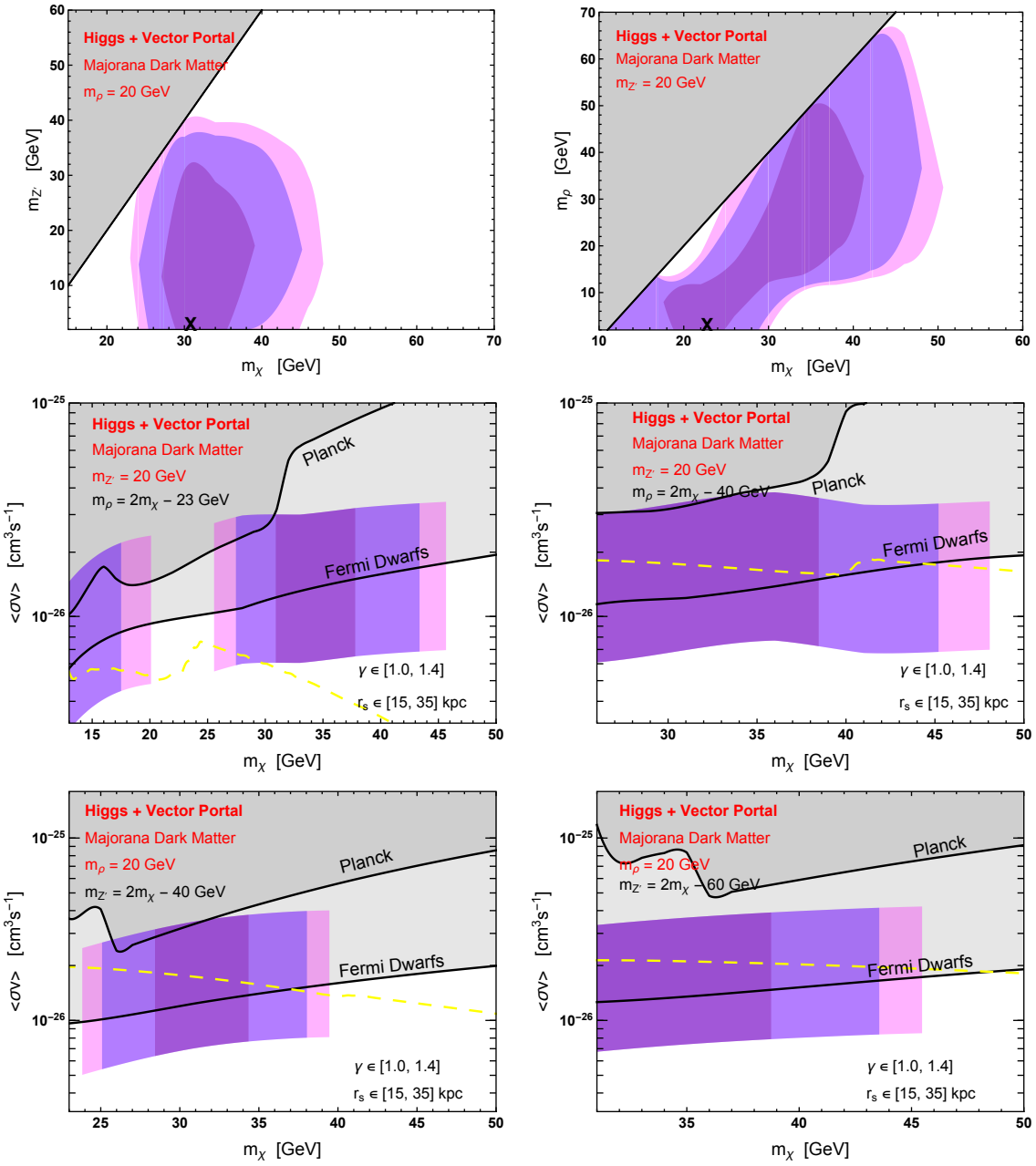

Figure 9. As in figures 7 and 8, but for dark matter in the form of a Majorana fermion that annihilates to combinations of scalars and vectors which decay to the Standard Model through the Higgs and vector portals, respectively (see section 2.5). This model can account for the entirety of the dark matter and generate the observed characteristics of the Galactic Center gamma-ray excess over substantial regions of parameter space.

considerably more restrictive, in particular in the case of Dirac dark matter. In addition to current constraints, we also present projected constraints from LUX-ZEPLIN (LZ) and DARWIN, as calculated and presented in ref. [107].

Light scalar particles which mix with the Standard Model Higgs boson have been probed extensively by LEP. LEP probes the Higgs-scalar mixing angle thorough the indirect inter-

JCAP11(2017)042

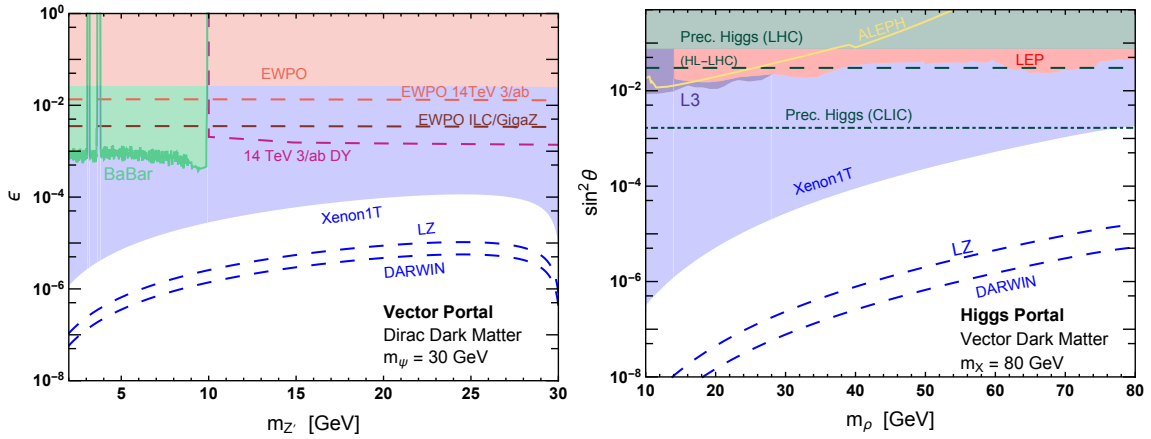

Figure 10. Collider and direct detection constraints on the Dirac dark matter vector portal model (left) and the vector dark matter Higgs portal model (right). Constraints denoted by dashed or dot-dashed lines represent projected sensitivities. Note that in the case of Majorana vector portal dark matter, constraints from electroweak precision observables are more restrictive than those derived from direct detection experiments.

action of the hidden sector scalar and the Standard Model Z. This constraint is shown in the right frame of figure 10 for a combination of data from LEP [108], ALPEH [109] and L3 [110].

Precision measurements of the Higgs couplings at the LHC can also be used to constrain the Higgs portal mixing angle. Here, we consider a number of searches performed by both ATLAS and CMS [111–121] for various Higgs production channels and decay modes, performing a global fit of these measurements and presenting the resulting exclusion contours in the right frame of figure 10. We then repeated this exercise for the projected sensitivity of the high luminosity LHC [122, 123] and the Compact Linear Collider (CLIC) [124]. As shown in the right frame of figure 10, even these projected constraints are unlikely to be competitive with those derived from direct detection experiments. Again, these constraints are clearly much less restrictive than those derived from the results of direct detection experiments, with the exception of the case in which $m_\rho \sim m_h$.

5 Summary and outlook

In light of recent results from both direct dark matter searches and the LHC, dark matter models that are capable of generating the Galactic Center gamma-ray excess have become increasingly tightly constrained [53]. It is straightforward to evade these constraints, however, within the context of models in which the dark matter does not directly couple to the Standard Model, but instead annihilates into unstable particles that reside within a hidden sector. In this paper, we have revisited this class of models and demonstrated that they generically contain a broad range of parameter space that is capable of self-consistently generating the spectral shape and intensity of the observed gamma-ray excess.

Our main results are summarized in figure 11. Throughout each frame, we have chosen the hidden sector coupling in order to obtain a thermal relic abundance equal to the measured cosmological dark matter density. The bands denote the regions in which the model provides a good fit to the measured Galactic Center gamma-ray excess (yielding a $p-$value greater than 0.32, 0.10, or 0.05), and we also show the regions that are disfavored by Fermi's observations

JCAP11(2017)042

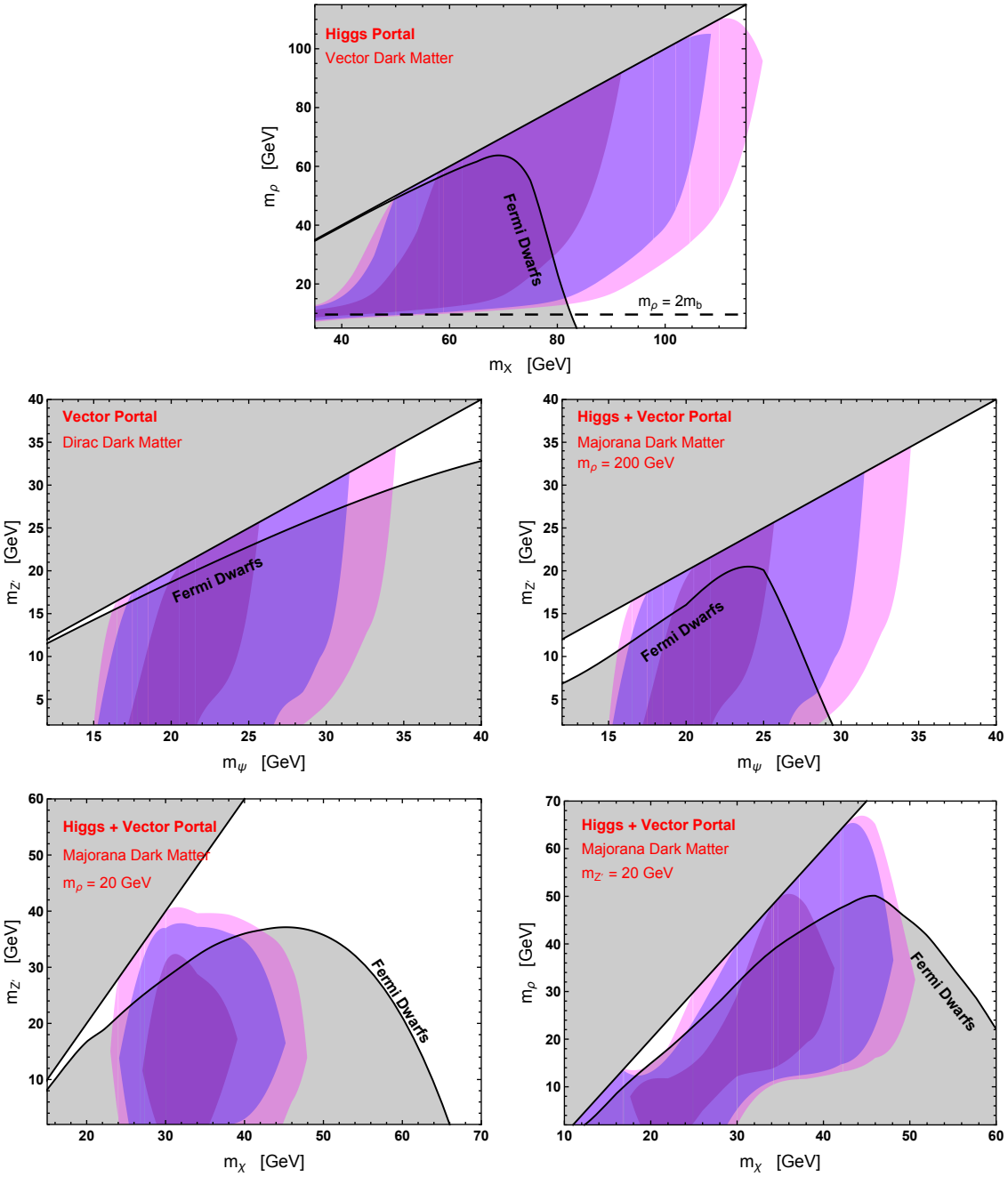

Figure 11. A summary of the parameter space in the hidden dark matter models considered in this study. Throughout each frame, we have chosen the hidden sector coupling in order to obtain a thermal dark matter relic abundance equal to the measured cosmological dark matter density. The bands denote the regions in which the model provides a fit to the measured Galactic Center gamma-ray excess which yields a $p-$value of ≥ 0.32 (dark purple), ≥ 0.10 (violet), and ≥ 0.05 (magenta), and we also show the regions that are disfavored by Fermi's observations of dwarf spheroidal galaxies [96]. In each of these models, there exists substantial parameter space that can accommodate the observed characteristics of the Galactic Center gamma-ray excess, while remaining consistent with other constraints.

JCAP11(2017)042

of dwarf spheroidal galaxies [96]. From the four frames of this figure, it is clear that there exists substantial regions of parameter space in each of the models considered that can accommodate the observed characteristics of the Galactic Center gamma-ray excess, while remaining consistent with other constraints.

In the case of Dirac vector portal dark matter (middle left), the constraints from dwarf galaxies lead us to favor the regions of parameter space in which the dark matter is not much heavier than $m_{Z'}$. In contrast, Majorana dark matter is less restricted by dwarf constraints (middle right). We also find that the vector dark matter Higgs portal scenario (upper frame) is viable for $m_X \sim 70-110\,\text{GeV}$ and for a wide range of scalar masses. We find that Majorana dark matter with a combination of Higgs and Vector portals (lower frames) favors parameter space in which $m_\chi \sim 10-50\,\text{GeV}$, $m_\rho \lesssim 70\,\text{GeV}$ and $m_{Z'} \lesssim 40\,\text{GeV}$.

In many respects, the class of hidden sector models considered in this study is very difficult to test. Although future direct detection experiments will gradually become sensitive to hidden sectors that are even more decoupled from the Standard Model (i.e. with even smaller values of ϵ or $\sin^2\theta$ within the context of the vector portal and Higgs portal, respectively), viable parameter space will continue to exist well below the projected reach of such experiments. Similarly, the LHC will only be able to probe a relatively small fraction of the parameter space within this class of models.

Unlike direct detection and collider experiments, however, dark matter annihilation signals are not generally suppressed in hidden sector models. In each of the models considered in this study, one predicts a gamma-ray flux from the Milky Way's population of dwarf spheroidal galaxies that likely to fall within the ultimate reach of the Fermi Gamma-Ray Space Telescope [96, 125–128], after including the anticipated discoveries of new dwarf galaxies by DES and LSST [129].

Measurements of the cosmic-ray antiproton spectrum by AMS-02 are also expected to be sensitive to much of the hidden sector dark matter parameter space that has been considered in this study. Intriguingly, a $\sim$4.5 σ excess has been reported in this channel, peaking at energies of approximately $\sim$10-20 GeV [130, 131] (see also ref. [132]). Furthermore, the characteristics of the antiproton and gamma-ray excesses suggest that they could potentially be generated by annihilations of the same dark matter candidate.

In figure 12, we show the spectrum of antiprotons that is predicted to be generated per dark matter annihilation, prior to any transport through the Galaxy, for several choices for the dark matter's mass and annihilation channel. For the simple case of a dark matter candidate that annihilates directly to $b\bar{b}$, masses in the range of $\sim$50-90 GeV have been shown to be able to accommodate the spectral shape of the antiproton excess [130, 131]. In this figure, we compare this to the case of a Higgs portal model with $m_X = 80\,\text{GeV}$ and $m_\rho = 30\,\text{GeV}$ or 70 GeV, and for a vector portal model with $m_\psi = 25\,\text{GeV}$ and $m_{Z'} = 20\,\text{GeV}$ (each of which provide a good fit to the gamma-ray excess). The Higgs portal models shown predict an antiproton signal that would be very difficult to distinguish from that of a more conventional WIMP. In contrast, the suppression of the antiproton flux (especially at $E_{\bar{p}} \gtrsim 10\,\text{GeV}$) in the vector portal model is rather distinctive, and could provide a way to discriminate this model from other dark matter scenarios that are capable of generating the observed gamma-ray excess.

JCAP11(2017)042

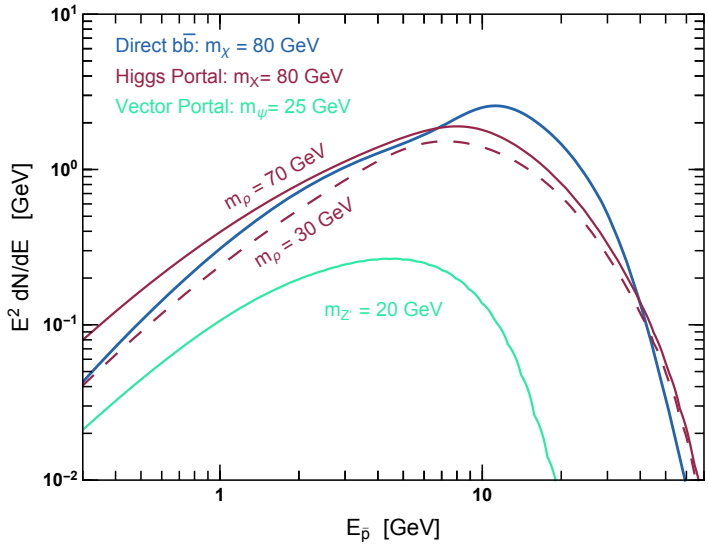

Figure 12. The spectrum of antiprotons generated per dark matter annihilation, prior to any transport through the Galaxy, for several choices for the mass and annihilation channel. For the simple case of a dark matter candidate that annihilates directly to $b\bar{b}$, masses in the range of ∼50-90 GeV have been shown to be able to accommodate the spectral shape of the antiproton excess [130, 131]. The Higgs portal models shown predict an antiproton signal that would be very difficult to distinguish from that of a more conventional WIMP. In contrast, the antiproton flux is significantly suppressed in the vector portal model shown, especially at $E_{\bar{p}} \gtrsim 10\,\mathrm{GeV}$.

Acknowledgments

ME would like to thank the Fermilab Theoretical Physics Department for hospitality. ME is supported by Spanish Grant FPU13/0311 of MECD. ME also is supported by the European Union's Horizon 2020 research and innovation programme under the Marie Skłodowska-Curie grant agreement No 690575. SJW is supported by the European Union's Horizon 2020 research and innovation program under the Marie Skłodowska-Curie grant agreement No. 674896. This work was performed in part at Aspen Center for Physics, which is supported by National Science Foundation grant PHY-1607611. This manuscript has been authored in part by the Fermi Research Alliance, LLC under Contract No. DE-AC02-07CH11359 with the U.S. Department of Energy, Office of Science, Office of High Energy Physics. The United States Government retains and the publisher, by accepting the article for publication, acknowledges that the United States Government retains a non-exclusive, paid-up, irrevocable, world-wide license to publish or reproduce the published form of this manuscript, or allow others to do so, for United States Government purposes.

References

[1] L. Goodenough and D. Hooper, *Possible evidence for dark matter annihilation in the inner Milky Way from the Fermi Gamma Ray Space Telescope*, arXiv:0910.2998 [INSPIRE].

[2] D. Hooper and L. Goodenough, *Dark matter annihilation in the Galactic Center as seen by the Fermi Gamma Ray Space Telescope*, *Phys. Lett.* **B 697** (2011) 412 [arXiv:1010.2752] [INSPIRE].

JCAP11(2017)042

[3] D. Hooper and T. Linden, *On The Origin Of The Gamma Rays From The Galactic Center*, *Phys. Rev.* **D 84** (2011) 123005 [arXiv:1110.0006] [INSPIRE].

[4] K.N. Abazajian and M. Kaplinghat, *Detection of a gamma-ray source in the Galactic Center consistent with extended emission from dark matter annihilation and concentrated astrophysical emission*, *Phys. Rev.* **D 86** (2012) 083511 [*Erratum ibid.* **D 87** (2013) 129902] [arXiv:1207.6047] [INSPIRE].

[5] C. Gordon and O. Macias, *Dark matter and pulsar model constraints from galactic center Fermi-LAT gamma ray observations*, *Phys. Rev.* **D 88** (2013) 083521 [arXiv:1306.5725] [INSPIRE].

[6] D. Hooper and T.R. Slatyer, *Two emission mechanisms in the Fermi bubbles: a possible signal of annihilating dark matter*, *Phys. Dark Univ.* **2** (2013) 118 [arXiv:1302.6589] [INSPIRE].

[7] T. Daylan et al., *The characterization of the gamma-ray signal from the central Milky Way: a case for annihilating dark matter*, *Phys. Dark Univ.* **12** (2016) 1 [arXiv:1402.6703] [INSPIRE].

[8] F. Calore, I. Cholis and C. Weniger, *Background model systematics for the Fermi GeV excess*, *JCAP* **03** (2015) 038 [arXiv:1409.0042] [INSPIRE].

[9] FERMI-LAT collaboration, M. Ajello et al., *Fermi-LAT observations of high-energy γ-ray emission toward the Galactic Center*, *Astrophys. J.* **819** (2016) 44 [arXiv:1511.02938] [INSPIRE].

[10] C. Karwin, S. Murgia, T.M.P. Tait, T.A. Porter and P. Tanedo, *Dark matter interpretation of the Fermi-LAT observation toward the Galactic Center*, *Phys. Rev.* **D 95** (2017) 103005 [arXiv:1612.05687] [INSPIRE].

[11] FERMI-LAT collaboration, M. Ackermann et al., *The Fermi Galactic Center GeV excess and implications for dark matter*, *Astrophys. J.* **840** (2017) 43 [arXiv:1704.03910] [INSPIRE].

[12] S. Ipek, D. McKeen and A.E. Nelson, *A renormalizable model for the Galactic Center gamma ray excess from dark matter annihilation*, *Phys. Rev.* **D 90** (2014) 055021 [arXiv:1404.3716] [INSPIRE].

[13] E. Izaguirre, G. Krnjaic and B. Shuve, *The Galactic Center excess from the bottom up*, *Phys. Rev.* **D 90** (2014) 055002 [arXiv:1404.2018] [INSPIRE].

[14] P. Agrawal, B. Batell, D. Hooper and T. Lin, *Flavored dark matter and the Galactic Center gamma-ray excess*, *Phys. Rev.* **D 90** (2014) 063512 [arXiv:1404.1373] [INSPIRE].

[15] A. Berlin, D. Hooper and S.D. McDermott, *Simplified dark matter models for the Galactic Center gamma-ray excess*, *Phys. Rev.* **D 89** (2014) 115022 [arXiv:1404.0022] [INSPIRE].

[16] A. Alves, S. Profumo, F.S. Queiroz and W. Shepherd, *Effective field theory approach to the Galactic Center gamma-ray excess*, *Phys. Rev.* **D 90** (2014) 115003 [arXiv:1403.5027] [INSPIRE].

[17] C. Boehm, M.J. Dolan, C. McCabe, M. Spannowsky and C.J. Wallace, *Extended gamma-ray emission from Coy dark matter*, *JCAP* **05** (2014) 009 [arXiv:1401.6458] [INSPIRE].

[18] J. Huang, T. Liu, L.-T. Wang and F. Yu, *Supersymmetric subelectroweak scale dark matter, the Galactic Center gamma-ray excess and exotic decays of the* 125 *GeV Higgs boson*, *Phys. Rev.* **D 90** (2014) 115006 [arXiv:1407.0038] [INSPIRE].

[19] D.G. Cerdeño, M. Peiró and S. Robles, *Low-mass right-handed sneutrino dark matter: SuperCDMS and LUX constraints and the Galactic Centre gamma-ray excess*, *JCAP* **08** (2014) 005 [arXiv:1404.2572] [INSPIRE].

[20] N. Okada and O. Seto, *Gamma ray emission in Fermi bubbles and Higgs portal dark matter*, *Phys. Rev.* **D 89** (2014) 043525 [arXiv:1310.5991] [INSPIRE].

JCAP11(2017)042

[21] K. Freese, A. Lopez, N.R. Shah and B. Shakya, *MSSM A-funnel and the Galactic Center excess: prospects for the LHC and direct detection experiments*, *JHEP* **04** (2016) 059 [arXiv:1509.05076] [INSPIRE].

[22] N. Fonseca, L. Necib and J. Thaler, *Dark matter, shared asymmetries and Galactic Gamma ray signals*, *JCAP* **02** (2016) 052 [arXiv:1507.08295] [INSPIRE].

[23] G. Bertone et al., *Global analysis of the pMSSM in light of the Fermi GeV excess: prospects for the LHC Run-II and astroparticle experiments*, *JCAP* **04** (2016) 037 [arXiv:1507.07008] [INSPIRE].

[24] J.M. Cline, G. Dupuis, Z. Liu and W. Xue, *Multimediator models for the Galactic Center gamma ray excess*, *Phys. Rev.* **D 91** (2015) 115010 [arXiv:1503.08213] [INSPIRE].

[25] A. Berlin, S. Gori, T. Lin and L.-T. Wang, *Pseudoscalar portal dark matter*, *Phys. Rev.* **D 92** (2015) 015005 [arXiv:1502.06000] [INSPIRE].

[26] A. Achterberg et al., *A description of the Galactic Center excess in the Minimal Supersymmetric Standard Model*, *JCAP* **08** (2015) 006 [arXiv:1502.05703] [INSPIRE].

[27] D.G. Cerdeno, M. Peiro and S. Robles, *Fits to the Fermi-LAT GeV excess with RH sneutrino dark matter: implications for direct and indirect dark matter searches and the LHC*, *Phys. Rev.* **D 91** (2015) 123530 [arXiv:1501.01296] [INSPIRE].

[28] J. Liu, N. Weiner and W. Xue, *Signals of a light dark force in the Galactic Center*, *JHEP* **08** (2015) 050 [arXiv:1412.1485] [INSPIRE].

[29] D. Hooper, *Z' mediated dark matter models for the Galactic Center gamma-ray excess*, *Phys. Rev.* **D 91** (2015) 035025 [arXiv:1411.4079] [INSPIRE].

[30] G. Arcadi, Y. Mambrini and F. Richard, *Z-portal dark matter*, *JCAP* **03** (2015) 018 [arXiv:1411.2985] [INSPIRE].

[31] M. Cahill-Rowley, J. Gainer, J. Hewett and T. Rizzo, *Towards a supersymmetric description of the Fermi Galactic Center excess*, *JHEP* **02** (2015) 057 [arXiv:1409.1573] [INSPIRE].

[32] P. Ko and Y. Tang, *Galactic center γ-ray excess in hidden sector DM models with dark gauge symmetries: local Z_3 symmetry as an example*, *JCAP* **01** (2015) 023 [arXiv:1407.5492] [INSPIRE].

[33] S.D. McDermott, *Lining up the Galactic Center gamma-ray excess*, *Phys. Dark Univ.* **7-8** (2015) 12 [arXiv:1406.6408] [INSPIRE].

[34] M. Abdullah et al., *Hidden on-shell mediators for the Galactic Center γ-ray excess*, *Phys. Rev.* **D 90** (2014) 035004 [arXiv:1404.6528] [INSPIRE].

[35] A. Martin, J. Shelton and J. Unwin, *Fitting the Galactic Center gamma-ray excess with cascade annihilations*, *Phys. Rev.* **D 90** (2014) 103513 [arXiv:1405.0272] [INSPIRE].

[36] A. Berlin, P. Gratia, D. Hooper and S.D. McDermott, *Hidden sector dark matter models for the Galactic Center gamma-ray excess*, *Phys. Rev.* **D 90** (2014) 015032 [arXiv:1405.5204] [INSPIRE].

[37] D. Hooper, N. Weiner and W. Xue, *Dark forces and light dark matter*, *Phys. Rev.* **D 86** (2012) 056009 [arXiv:1206.2929] [INSPIRE].

[38] M. Cirelli, P. Panci, K. Petraki, F. Sala and M. Taoso, *Dark matter's secret liaisons: phenomenology of a dark* U(1) *sector with bound states*, *JCAP* **05** (2017) 036 [arXiv:1612.07295] [INSPIRE].

[39] I. Cholis, D. Hooper and T. Linden, *Challenges in explaining the Galactic Center gamma-ray excess with millisecond pulsars*, *JCAP* **06** (2015) 043 [arXiv:1407.5625] [INSPIRE].

JCAP11(2017)042

[40] J. Petrović, P.D. Serpico and G. Zaharijas, *Millisecond pulsars and the Galactic Center gamma-ray excess: the importance of luminosity function and secondary emission*, *JCAP* **02** (2015) 023 [arXiv:1411.2980] [INSPIRE].

[41] T.D. Brandt and B. Kocsis, *Disrupted globular clusters can explain the Galactic Center gamma ray excess*, *Astrophys. J.* **812** (2015) 15 [arXiv:1507.05616] [INSPIRE].

[42] S.K. Lee, M. Lisanti, B.R. Safdi, T.R. Slatyer and W. Xue, *Evidence for unresolved γ-ray point sources in the inner galaxy*, *Phys. Rev. Lett.* **116** (2016) 051103 [arXiv:1506.05124] [INSPIRE].

[43] D. Hooper and G. Mohlabeng, *The gamma-ray luminosity function of millisecond pulsars and implications for the GeV excess*, *JCAP* **03** (2016) 049 [arXiv:1512.04966] [INSPIRE].

[44] R. Bartels, S. Krishnamurthy and C. Weniger, *Strong support for the millisecond pulsar origin of the Galactic center GeV excess*, *Phys. Rev. Lett.* **116** (2016) 051102 [arXiv:1506.05104] [INSPIRE].

[45] D. Hooper and T. Linden, *The gamma-ray pulsar population of globular clusters: implications for the GeV excess*, *JCAP* **08** (2016) 018 [arXiv:1606.09250] [INSPIRE].

[46] I. Cholis et al., *The Galactic Center GeV excess from a series of leptonic cosmic-ray outbursts*, *JCAP* **12** (2015) 005 [arXiv:1506.05119] [INSPIRE].

[47] J. Petrović, P.D. Serpico and G. Zaharijaš, *Galactic Center gamma-ray "excess" from an active past of the Galactic Centre?*, *JCAP* **10** (2014) 052 [arXiv:1405.7928] [INSPIRE].

[48] E. Carlson and S. Profumo, *Cosmic ray protons in the inner galaxy and the Galactic Center gamma-ray excess*, *Phys. Rev.* **D 90** (2014) 023015 [arXiv:1405.7685] [INSPIRE].

[49] D. Haggard, C. Heinke, D. Hooper and T. Linden, *Low mass X-ray binaries in the inner galaxy: implications for millisecond pulsars and the GeV excess*, *JCAP* **05** (2017) 056 [arXiv:1701.02726] [INSPIRE].

[50] XENON collaboration, E. Aprile et al., *First dark matter search results from the XENON1T experiment*, *Phys. Rev. Lett.* **119** (2017) 181301 [arXiv:1705.06655] [INSPIRE].

[51] PandaX-II collaboration, X. Cui et al., *Dark matter results from 54-ton-day exposure of PandaX-II experiment*, *Phys. Rev. Lett.* **119** (2017) 181302 [arXiv:1708.06917] [INSPIRE].

[52] LUX collaboration, D.S. Akerib et al., *Results from a search for dark matter in the complete LUX exposure*, *Phys. Rev. Lett.* **118** (2017) 021303 [arXiv:1608.07648] [INSPIRE].

[53] M. Escudero, D. Hooper and S.J. Witte, *Updated collider and direct detection constraints on dark matter models for the Galactic Center gamma-ray excess*, *JCAP* **02** (2017) 038 [arXiv:1612.06462] [INSPIRE].

[54] M. Pospelov, A. Ritz and M.B. Voloshin, *Secluded WIMP dark matter*, *Phys. Lett.* **B 662** (2008) 53 [arXiv:0711.4866] [INSPIRE].

[55] N. Arkani-Hamed, D.P. Finkbeiner, T.R. Slatyer and N. Weiner, *A theory of dark matter*, *Phys. Rev.* **D 79** (2009) 015014 [arXiv:0810.0713] [INSPIRE].

[56] B. Holdom, *Two* U(1)*'s and epsilon charge shifts*, *Phys. Lett.* **B 166** (1986) 196.

[57] V. Silveira and A. Zee, *Scalar phantoms*, *Phys. Lett.* **B 161** (1985) 136.

[58] B. Patt and F. Wilczek, *Higgs-field portal into hidden sectors*, hep-ph/0605188 [INSPIRE].

[59] J. McDonald, *Gauge singlet scalars as cold dark matter*, *Phys. Rev.* **D 50** (1994) 3637 [hep-ph/0702143] [INSPIRE].

[60] C.P. Burgess, M. Pospelov and T. ter Veldhuis, *The minimal model of nonbaryonic dark matter: a singlet scalar*, *Nucl. Phys.* **B 619** (2001) 709 [hep-ph/0011335] [INSPIRE].

[61] P. Minkowski, $\mu \to e\gamma$ *at a rate of one out of* 10^9 *muon decays?*, *Phys. Lett.* **B 67** (1977) 421.

JCAP11(2017)042

[62] M. Gell-Mann, P. Ramond and R. Slansky, *Complex spinors and unified theories*, *Conf. Proc.* **C 790927** (1979) 315 [arXiv:1306.4669] [INSPIRE].

[63] T. Yanagida, *Horizontal symmetry and masses of neutrinos*, *Conf. Proc.* **C 7902131** (1979) 95 [INSPIRE].

[64] R.N. Mohapatra and G. Senjanović, *Neutrino mass and spontaneous parity violation*, *Phys. Rev. Lett.* **44** (1980) 912 [INSPIRE].

[65] A. Falkowski, J.T. Ruderman and T. Volansky, *Asymmetric dark matter from leptogenesis*, *JHEP* **05** (2011) 106 [arXiv:1101.4936] [INSPIRE].

[66] Y.-L. Tang and S.-h. Zhu, *Dark matter annihilation into right-handed neutrinos and the Galactic Center gamma-ray excess*, arXiv:1512.02899 [INSPIRE].

[67] V. Gonzalez Macias and J. Wudka, *Effective theories for dark matter interactions and the neutrino portal paradigm*, *JHEP* **07** (2015) 161 [arXiv:1506.03825] [INSPIRE].

[68] V. González-Macías, J.I. Illana and J. Wudka, *A realistic model for dark matter interactions in the neutrino portal paradigm*, *JHEP* **05** (2016) 171 [arXiv:1601.05051] [INSPIRE].

[69] M. Escudero, N. Rius and V. Sanz, *Sterile neutrino portal to dark matter I: the* $\mathrm{U}(1)_{B-L}$ *case*, *JHEP* **02** (2017) 045 [arXiv:1606.01258] [INSPIRE].

[70] M. Escudero, N. Rius and V. Sanz, *Sterile neutrino portal to dark matter II: exact dark symmetry*, *Eur. Phys. J.* **C 77** (2017) 397 [arXiv:1607.02373] [INSPIRE].

[71] B. Batell, T. Han and B. Shams Es Haghi, *Indirect detection of neutrino portal dark matter*, arXiv:1704.08708 [INSPIRE].

[72] M.D. Campos, F.S. Queiroz, C.E. Yaguna and C. Weniger, *Search for right-handed neutrinos from dark matter annihilation with gamma-rays*, *JCAP* **07** (2017) 016 [arXiv:1702.06145] [INSPIRE].

[73] K.S. Babu, C.F. Kolda and J. March-Russell, *Implications of generalized* Z*-*Z' *mixing*, *Phys. Rev.* **D 57** (1998) 6788 [hep-ph/9710441] [INSPIRE].

[74] J.M. Cline, G. Dupuis, Z. Liu and W. Xue, *The windows for kinetically mixed* Z'*-mediated dark matter and the Galactic Center gamma ray excess*, *JHEP* **08** (2014) 131 [arXiv:1405.7691] [INSPIRE].

[75] S. Gopalakrishna, S. Jung and J.D. Wells, *Higgs boson decays to four fermions through an abelian hidden sector*, *Phys. Rev.* **D 78** (2008) 055002 [arXiv:0801.3456] [INSPIRE].

[76] A. Berlin, D. Hooper and G. Krnjaic, *PeV-scale dark matter as a thermal relic of a decoupled sector*, *Phys. Lett.* **B 760** (2016) 106 [arXiv:1602.08490] [INSPIRE].

[77] A. Djouadi, J. Kalinowski and M. Spira, *HDECAY: a program for Higgs boson decays in the standard model and its supersymmetric extension*, *Comput. Phys. Commun.* **108** (1998) 56 [hep-ph/9704448] [INSPIRE].

[78] B. Körs and P. Nath, *A Stueckelberg extension of the standard model*, *Phys. Lett.* **B 586** (2004) 366 [hep-ph/0402047] [INSPIRE].

[79] CRESST collaboration, G. Angloher et al., *Results on light dark matter particles with a low-threshold CRESST-II detector*, *Eur. Phys. J.* **C 76** (2016) 25 [arXiv:1509.01515] [INSPIRE].

[80] EDELWEISS collaboration, E. Armengaud et al., *A search for low-mass WIMPs with EDELWEISS-II heat-and-ionization detectors*, *Phys. Rev.* **D 86** (2012) 051701 [arXiv:1207.1815] [INSPIRE].

[81] J.M. Cline, K. Kainulainen, P. Scott and C. Weniger, *Update on scalar singlet dark matter*, *Phys. Rev.* **D 88** (2013) 055025 [arXiv:1306.4710] [INSPIRE].

JCAP11(2017)042

[82] G. Steigman, B. Dasgupta and J.F. Beacom, *Precise relic WIMP abundance and its impact on searches for dark matter annihilation*, *Phys. Rev.* **D 86** (2012) 023506 [arXiv:1204.3622] [INSPIRE].

[83] P. Gondolo and G. Gelmini, *Cosmic abundances of stable particles: improved analysis*, *Nucl. Phys.* **B 360** (1991) 145 [INSPIRE].

[84] K. Griest and D. Seckel, *Three exceptions in the calculation of relic abundances*, *Phys. Rev.* **D 43** (1991) 3191 [INSPIRE].

[85] A. Berlin, D. Hooper and G. Krnjaic, *Thermal dark matter from a highly decoupled sector*, *Phys. Rev.* **D 94** (2016) 095019 [arXiv:1609.02555] [INSPIRE].

[86] P. Ko, W.-I. Park and Y. Tang, *Higgs portal vector dark matter for GeV scale γ-ray excess from galactic center*, *JCAP* **09** (2014) 013 [arXiv:1404.5257] [INSPIRE].

[87] P. Ko and Y. Tang, *Dark Higgs channel for FERMI GeV γ-ray excess*, *JCAP* **02** (2016) 011 [arXiv:1504.03908] [INSPIRE].

[88] M. Escudero, A. Berlin, D. Hooper and M.-X. Lin, *Toward (finally!) ruling out Z and Higgs mediated dark matter models*, *JCAP* **12** (2016) 029 [arXiv:1609.09079] [INSPIRE].

[89] N.F. Bell, Y. Cai and R.K. Leane, *Dark forces in the Sky: signals from Z′ and the dark Higgs*, *JCAP* **08** (2016) 001 [arXiv:1605.09382] [INSPIRE].

[90] M. Duerr, F. Kahlhoefer, K. Schmidt-Hoberg, T. Schwetz and S. Vogl, *How to save the WIMP: global analysis of a dark matter model with two s-channel mediators*, *JHEP* **09** (2016) 042 [arXiv:1606.07609] [INSPIRE].

[91] G. Elor, N.L. Rodd and T.R. Slatyer, *Multistep cascade annihilations of dark matter and the Galactic Center excess*, *Phys. Rev.* **D 91** (2015) 103531 [arXiv:1503.01773] [INSPIRE].

[92] M. Cirelli et al., *PPPC 4 DM ID: A Poor Particle Physicist Cookbook for Dark Matter Indirect Detection*, *JCAP* **03** (2011) 051 [*Erratum ibid.* **10** (2012) E01] [arXiv:1012.4515] [INSPIRE].

[93] G. Elor, N.L. Rodd, T.R. Slatyer and W. Xue, *Model-independent indirect detection constraints on hidden sector dark matter*, *JCAP* **06** (2016) 024 [arXiv:1511.08787] [INSPIRE].

[94] M. Buschmann, J. Kopp, J. Liu and P.A.N. Machado, *Lepton jets from radiating dark matter*, *JHEP* **07** (2015) 045 [arXiv:1505.07459] [INSPIRE].

[95] T. Sjöstrand, S. Mrenna and P.Z. Skands, *A brief introduction to PYTHIA 8.1*, *Comput. Phys. Commun.* **178** (2008) 852 [arXiv:0710.3820] [INSPIRE].

[96] DES, Fermi-LAT collaboration, A. Albert et al., *Searching for dark matter annihilation in recently discovered Milky Way satellites with Fermi-LAT*, *Astrophys. J.* **834** (2017) 110 [arXiv:1611.03184] [INSPIRE].

[97] T.R. Slatyer, *Indirect dark matter signatures in the cosmic dark ages. I. Generalizing the bound on s-wave dark matter annihilation from Planck results*, *Phys. Rev.* **D 93** (2016) 023527 [arXiv:1506.03811] [INSPIRE].

[98] T.R. Slatyer, *Indirect dark matter signatures in the cosmic dark ages II. Ionization, heating and photon production from arbitrary energy injections*, *Phys. Rev.* **D 93** (2016) 023521 [arXiv:1506.03812] [INSPIRE].

[99] Fermi-LAT collaboration, M. Ackermann et al., *Searching for dark matter annihilation from Milky Way dwarf spheroidal galaxies with six years of Fermi Large Area Telescope data*, *Phys. Rev. Lett.* **115** (2015) 231301 [arXiv:1503.02641] [INSPIRE].

[100] M. Wood, *Figures and data files associated with the Fermi LAT paper "Searching for dark matter annihilation from milky way dwarf spheroidal galaxies with six years of fermi-lat data"*, http://www-glast.standford.edu/pub_data/1048/.

JCAP11(2017)042

[101] N. Klop, F. Zandanel, K. Hayashi and S. Ando, *Impact of axisymmetric mass models for dwarf spheroidal galaxies on indirect dark matter searches*, *Phys. Rev.* **D 95** (2017) 123012 [arXiv:1609.03509] [INSPIRE].

[102] K. Ichikawa et al., *Foreground effect on the J-factor estimation of classical dwarf spheroidal galaxies*, *Mon. Not. Roy. Astron. Soc.* **468** (2017) 2884 [arXiv:1608.01749] [INSPIRE].

[103] J.L. Sanders, N.W. Evans, A. Geringer-Sameth and W. Dehnen, *Indirect dark matter detection for flattened dwarf galaxies*, *Phys. Rev.* **D 94** (2016) 063521 [arXiv:1604.05493] [INSPIRE].

[104] N.W. Evans, J.L. Sanders and A. Geringer-Sameth, *Simple J-factors and D-factors for indirect dark matter detection*, *Phys. Rev.* **D 93** (2016) 103512 [arXiv:1604.05599] [INSPIRE].

[105] J.M. Cline, J.M. Cornell, D. London and R. Watanabe, *Hidden sector explanation of B-decay and cosmic ray anomalies*, *Phys. Rev.* **D 95** (2017) 095015 [arXiv:1702.00395] [INSPIRE].

[106] D. Curtin, R. Essig, S. Gori and J. Shelton, *Illuminating dark photons with high-energy colliders*, *JHEP* **02** (2015) 157 [arXiv:1412.0018] [INSPIRE].

[107] S.J. Witte and G.B. Gelmini, *Updated constraints on the dark matter interpretation of CDMS-II-Si data*, *JCAP* **05** (2017) 026 [arXiv:1703.06892] [INSPIRE].

[108] OPAL, DELPHI, LEP Working Group for Higgs boson searches, ALEPH, L3 collaboration, R. Barate et al., *Search for the standard model Higgs boson at LEP*, *Phys. Lett.* **B 565** (2003) 61 [hep-ex/0306033] [INSPIRE].

[109] ALEPH collaboration, D. Buskulic et al., *Search for a nonminimal Higgs boson produced in the reaction $e^+e^- \to hZ^*$*, *Phys. Lett.* **B 313** (1993) 312 [INSPIRE].

[110] L3 collaboration, M. Acciarri et al., *Search for neutral Higgs boson production through the process $e^+e^- \to Z^*H^0$*, *Phys. Lett.* **B 385** (1996) 454 [INSPIRE].

[111] ATLAS and CMS collaborations, *Measurements of the Higgs boson production and decay rates and constraints on its couplings from a combined ATLAS and CMS analysis of the LHC pp collision data at $\sqrt{s} = 7$ and 8 TeV*, *JHEP* **08** (2016) 045 [arXiv:1606.02266] [INSPIRE].

[112] CMS collaboration, *Search for narrow resonances in dilepton mass spectra in proton-proton collisions at $\sqrt{s} = 13$ TeV and combination with 8 TeV data*, *Phys. Lett.* **B 768** (2017) 57 [arXiv:1609.05391] [INSPIRE].

[113] CMS collaboration, *Higgs to WW measurements with* 15.2 fb^{-1} *of* 13 *TeV proton-proton collisions*, CMS-PAS-HIG-16-021 (2016).

[114] CMS collaboration, *Measurements of properties of the Higgs boson decaying into the four-lepton final state in pp collisions at $\sqrt{s} = 13$ TeV*, arXiv:1706.09936 [INSPIRE].

[115] CMS collaboration, *Measurements of properties of the Higgs boson in the diphoton decay channel with the full 2016 data set*, CMS-PAS-HIG-16-040 (2017).

[116] CMS collaboration, *Inclusive search for the standard model Higgs boson produced in pp collisions at $\sqrt{s} = 13$ TeV using $H \to b\bar{b}$ decays*, CMS-PAS-HIG-17-010 (2017).

[117] ATLAS collaboration, *Measurements of Higgs boson properties in the diphoton decay channel with* 36.1 fb^{-1} *pp collision data at the center-of-mass energy of* 13 *TeV with the ATLAS detector*, ATLAS-CONF-2017-045 (2017).

[118] ATLAS collaboration, *Measurements of the Higgs boson production cross section via Vector Boson Fusion and associated WH production in the $WW^* \to \ell\nu\ell\nu$ decay mode with the ATLAS detector at $\sqrt{s} = 13$ TeV*, ATLAS-CONF-2016-112 (2016).

[119] ATLAS collaboration,, *Measurement of the Higgs boson coupling properties in the $H \to ZZ^* \to 4\ell$ decay channel at $\sqrt{s} = 13$ TeV with the ATLAS detector*, ATLAS-CONF-2017-043 (2017).

JCAP11(2017)042

[120] ATLAS collaboration,, *Search for the Standard Model Higgs boson produced in association with top quarks and decaying into $b\bar{b}$ in pp collisions at $\sqrt{s}$ = 13 TeV with the ATLAS detector*, ATLAS-CONF-2016-080 (2016).

[121] ATLAS collaboration, *Evidence for the $H \to b\bar{b}$ decay with the ATLAS detector*, ATLAS-CONF-2017-041 (2017).

[122] M. Slawinska, *High-luminosity LHC prospects with the upgraded ATLAS detector*, PoS(DIS2016)266 [arXiv:1609.08434] [INSPIRE].

[123] CMS collaboration, *Projected performance of Higgs analyses at the HL-LHC for ECFA 2016*, CMS-PAS-FTR-16-002 (2017).

[124] H. Abramowicz et al., *Higgs physics at the CLIC electron–positron linear collider*, *Eur. Phys. J.* **C 77** (2017) 475 [arXiv:1608.07538] [INSPIRE].

[125] D. Hooper and T. Linden, *On the gamma-ray emission from Reticulum II and other dwarf galaxies*, *JCAP* **09** (2015) 016 [arXiv:1503.06209] [INSPIRE].

[126] A. Geringer-Sameth, S.M. Koushiappas and M.G. Walker, *Comprehensive search for dark matter annihilation in dwarf galaxies*, *Phys. Rev.* **D 91** (2015) 083535 [arXiv:1410.2242] [INSPIRE].

[127] A. Geringer-Sameth et al., *Indication of Gamma-ray Emission from the Newly Discovered Dwarf Galaxy Reticulum II*, *Phys. Rev. Lett.* **115** (2015) 081101 [arXiv:1503.02320] [INSPIRE].

[128] S. Li et al., *Search for gamma-ray emission from eight dwarf spheroidal galaxy candidates discovered in year two of dark energy survey with Fermi-LAT data*, *Phys. Rev.* **D 93** (2016) 043518 [arXiv:1511.09252] [INSPIRE].

[129] FERMI-LAT collaboration, E. Charles et al., *Sensitivity projections for dark matter searches with the Fermi Large Area Telescope*, *Phys. Rept.* **636** (2016) 1 [arXiv:1605.02016] [INSPIRE].

[130] A. Cuoco, M. Krämer and M. Korsmeier, *Novel dark matter constraints from antiprotons in light of AMS-02*, *Phys. Rev. Lett.* **118** (2017) 191102 [arXiv:1610.03071] [INSPIRE].

[131] M.-Y. Cui, Q. Yuan, Y.-L.S. Tsai and Y.-Z. Fan, *Possible dark matter annihilation signal in the AMS-02 antiproton data*, *Phys. Rev. Lett.* **118** (2017) 191101 [arXiv:1610.03840] [INSPIRE].

[132] D. Hooper, T. Linden and P. Mertsch, *What does the PAMELA antiproton spectrum tell us about dark matter?*, *JCAP* **03** (2015) 021 [arXiv:1410.1527] [INSPIRE].

JCAP11(2017)042

Parte III

Resumen de la tesis

Capítulo 6

Resumen de la tesis

6.1 Objetivos

El objetivo de esta tesis es el estudio de las implicaciones cosmológicas y fenomenológicas de la materia oscura. La evidencia gravitatoria de la materia oscura es incuestionable, sin embargo, su naturaleza representa uno de los mayores misterios de la física moderna. De esta sabemos que representa el $\sim 26\%$ del contenido energético del Universo y que además forma el $\sim 86\%$ de toda la materia [13]. Sin embargo, la notable evidencia gravitatoria de la materia oscura contrasta llamativamente con la falta de señales en la multitud de experimentos diseñados para estudiar sus propiedades no gravitatorias. En esta tesis, desde una perspectiva fenomenológica, hemos estudiado las implicaciones cosmológicas de varias partículas que podrían ser la materia oscura en el universo, hemos desarrollado modelos teóricos de partículas elementales con candidatos que están relacionados con los neutrinos estériles (que a través del mecanismo del *seesaw* – balancín – dotan de masa a los neutrinos ligeros) y hemos estudiado las consecuencias en experimentos terrestres – susceptibles a alguna propiedad no gravitatoria – de candidatos tipo WIMP[1], particularmente de aquellos que interactúan con los bosones Z y Higgs del Modelo Estándar y de los que son capaces de generar el exceso de rayos gamma observado provenientes del centro galáctico.

A fin de proporcionar un resumen detallado de esta tesis, en la sección 6.2 exponemos brevemente la evidencia gravitatoria de la materia oscura motivando así la importancia de su estudio. En la sección 6.3 describimos las características esenciales que un aspirante a ser la materia oscura ha de cumplir, y enumeramos cuales son los candidatos más populares y estudia-

[1] Weakly-Interacting-Massive-Particle, es decir, partícula masiva débilmente interactiva.

dos. En la sección 6.4 describimos las técnicas de búsqueda de partículas de materia oscura tipo WIMP tanto en experimentos terrestres como a través de observaciones cosmológicas. En la sección 6.5 detallamos la metodología utilizada en esta tesis, para finalmente exponer los resultados y conclusiones del trabajo desarrollado en este estudio en la sección 6.6.

6.2 La existencia de la materia oscura

6.2.1 Materia oscura en galaxias y cúmulos de galaxias

La evidencia astrofísica y cosmológica de la existencia de la materia oscura es indiscutible. La materia oscura domina la dinámica de las galaxias y los cúmulos de galaxias. De hecho, la materia oscura representa aproximadamente el 95% de la masa en una galaxia típica [17]. Esto lo sabemos a raíz de multitud de estudios, de estos los más representativos son:

- Curvas de rotación de las galaxias espirales

  Los astrónomos miden las velocidades de rotación en las galaxias espirales y encuentran que estas, en vez de decrecer con la distancia al centro galáctico, se mantienen constantes [14]. Esta medida supone un hecho inexplicable si sólo consideramos la materia visible presente (estrellas y gas). La velocidad de rotación de los objetos en una galaxia, nos permite saber la masa contenida M dentro de un radio R. Utilizando la tercera ley de Kepler relacionamos estas tres variables $v = \sqrt{\frac{MG}{R}}$ dónde G es la constante de Newton. Por lo tanto, el hecho de que la velocidad se mantenga constante a distancias muy grandes comparadas con el radio visible de la galaxia implica que hay materia que no vemos. Y además en unas cantidades muy superiores a la visible, tal que $M(R) \propto R$ para que $v = \text{cte}$.

- Lentes gravitacionales

  La teoría de la relatividad general de Einstein implica que los rayos de luz se curvan debido a la presencia de distribuciones de materia en su camino. En concreto, los cúmulos de galaxias suponen una distorsión y amplificación de las imágenes de galaxias distantes. Por medio del efecto lente gravitatorio, estas distorsiones y amplificaciones permiten inferir la presencia de la materia oscura en cúmulos de galaxias, de nuevo, en cantidades muy superiores a la materia ordinaria [15].

6.2.2 Materia oscura en el Cosmos

Las consecuencias astrofísicas de la materia oscura son categóricas. Pero quizás aún más lo sean sus implicaciones cosmológicas. A día de hoy, la materia oscura es un ingrediente indispensable para nuestro entendimiento de la evolución del universo, en el que esta representa el $\sim 84\%$ de toda la materia y contribuye a un $\sim 26\%$ de la energía en el universo [13].

En 1930 Hubble descubrió que el universo se expande. La expansión del universo se entendió como una consecuencia directa de la teoría del *Big Bang* (gran estallido). La teoría del Big Bang está basada en una única premisa: el universo es homogéneo e isótropo, es decir, que es igual en todas las direcciones y en todos los puntos. Claramente esto no es cierto si pensamos localmente en términos del sistema solar $\sim 10^{13}$ m, tampoco lo es a escala galáctica $\sim 10^{21}$ m pero sí a muy grandes escalas $\gtrsim 10^{27}$ m (ver Escala del Universo). La expansión del universo es consecuencia directa de la aplicación de la teoría de la relatividad general sobre un universo homogéneo e isótropo. La teoría de Einstein nos permite entender cómo se expande el universo y las ecuaciones que lo gobiernan implican claramente que el universo en el pasado era más pequeño y más caliente. Cabe reseñar que actualmente no sólo sabemos que el universo se expande, sino que además lo hace aceleradamente [40, 41]. El descubrimiento de la expansión acelerada del universo les valió a Perlmutter, Schmidt y Reiss el premio Nobel de Física en 2011. La responsable de esta expansión acelerada es la llamada energía oscura, de la cual sabemos que representa un $\sim 69\%$ de la energía del universo y que se comporta de forma muy similar a una constante cosmológica (Λ) en las ecuaciones de Einstein [13]. El Modelo Cosmológico Estándar se denomina ΛCDM (*cold dark matter*, materia oscura fría) debido a sus dos componentes principales: una constante cosmológica y la materia oscura fría.

La teoría del *Big Bang*, además de implicar la expansión del universo, predice con mucha precisión la abundancia de los diferentes núcleos en el mismo. Actualmente el universo tiene 13,8 mil millones de años, sin embargo, cuando tenía tan sólo 1 segundo su temperatura era de diez mil millones de grados centígrados (mil veces mayor que el interior del Sol). A esas temperaturas, el universo era tan denso y caliente que los núcleos todavía no se habían formado; conforme el universo se expandió y enfrió, los núcleos más ligeros se formaron, dando lugar a un universo en el que la materia visible está formada por un $\sim 75\%$ de Hidrógeno, un $\sim 25\%$ de Helio y muy pequeñas cantidades de Deuterio $\sim 10^{-5}$ y de Litio $\sim 10^{-10}$. Aunque pequeñas, estas cantidades han sido medidas en estrellas y el acuerdo entre la predicción de la teoría del *Big Bang* y las observaciones tanto de Deuterio como de Helio es excelente. Esta concordancia tiene profundas implicaciones

dado que la extrapolación de la que resulta es extrema, el universo se ha expandido mil millones de veces desde que los elementos se formaron pero aún así las predicciones casan perfectamente con las observaciones. Debido al éxito de esta extrapolación (entre otras), a día de hoy el modelo cosmológico se basa en la teoría del *Big Bang*. Consúltese Ref. [305] para una exposición brillante, pedagógica y divulgativa del universo primitivo.

El papel de la materia oscura en la evolución del universo es fundamental. Su rol cósmico consiste en ser la semilla de las grandes estructuras que observamos a día de hoy en el universo. Pese a que este era originalmente muy homogéneo e isótropo había presentes unas pequeñas inhomogeneidades primordiales consecuencia de las fluctuaciones cuánticas de un campo escalar que expandió de manera acelerada el universo primordial, cuando este tenía tan solo 10^{-34} segundos (este período es llamado *inflación*). Las ecuaciones de Einstein nos permiten describir cómo evolucionan estas perturbaciones primitivas y sabemos que hasta que el universo no es lo suficientemente frío no crecen. Debido a que *i)* en términos cosmológicos hay unas 5 veces más materia oscura que materia ordinaria (núcleos y electrones) y que *ii)* la materia oscura no interactúa con el campo electromagnético (de ahí que sea oscura), las perturbaciones de materia oscura pueden empezar a crecer mucho antes que las perturbaciones de materia ordinaria. Esto implica que las inhomogeneidades que observamos a día de hoy en el universo local (como las galaxias, en concreto la Vía Láctea) nacieron gracias a la presencia de la materia oscura. Además, estudios de formación de estructuras han demostrado que la materia oscura no puede poseer una considerable velocidad primordial, de ahí que el paradigma actual se denomine de materia oscura fría.

6.3 Candidatos a materia oscura

A día de hoy sólo tenemos evidencia de que la materia oscura interactúa gravitatoriamente, pero sabemos que hay varios requisitos que un candidato a ser materia oscura ha cumplir: tiene que interactuar débilmente consigo mismo, no debe interactuar con las partículas conocidas[2] o debe hacerlo débilmente (donde débilmente no significa necesariamente a través de la fuerza electrodébil del Modelo Estándar) y finalmente no puede ser nucleónico (no está formado por protones y neutrones). Los candidatos a ser la materia oscura del universo suelen estar relacionados con alguna de las cuestiones que el Modelo Estándar de física de partículas no es capaz de responder: la generación de la masa de los neutrinos activos, el problema de la

[2]Enmarcadas dentro del llamado Modelo Estándar de partículas, ver [306] para una breve exposición en Español.

carga-paridad en las interacciones fuertes, el problema de las jerarquías o la generación de la asimetría bariónica en el universo primitivo. A día de hoy, el candidato por excelencia a ser la materia oscura del universo es el WIMP. Esta partícula se puede generar en el universo primitivo de una forma muy sencilla y en la cantidad adecuada para representar el $\sim 26\%$ del contenido energético del universo. En esta tesis hemos estudiado la fenomenología de los WIMPs en detalle. Por completitud, cabe mencionar que el siguiente candidato a materia oscura en orden de popularidad es el axion en el rango de masas $1 - 100\,\mu$eV. Además, el neutrino estéril en el rango del keV, la materia oscura asimétrica y los agujeros negros primordiales son también candidatos considerablemente populares y estudiados.

6.4 Búsquedas de materia oscura tipo WIMP

Los WIMPs se producen en el universo primitivo por medio de un desequilibrio entre sus aniquilaciones con partículas ligeras y su producción a través de estas. Sabiendo que los WIMPs se aniquilan a partículas del modelo estándar en el universo primitivo, se han desarrollado tres técnicas básicas para detectarlos: *i)* a través de sus choques con núcleos en detectores terrestres (detección directa), *ii)* por medio de sus aniquilaciones en varios escenarios astrofísicos y cosmológicos (detección indirecta), y *iii)* a través de su producción en colisionadores de partículas.

1. **Detección Directa**

   En la Vía Láctea, como en cualquier otra galaxia, la materia oscura está presente en cantidades sustanciales. En concreto, a través de medidas cinemáticas, sabemos que en las vecindades del sistema solar la materia oscura se encuentra con una densidad energética de $\rho_\odot \simeq 0.3\,\mathrm{GeV/cm^3}$. Asumiendo que la materia oscura está compuesta de partículas, y si suponemos por ejemplo que estas tienen la misma masa que el Hidrógeno, deberíamos tener unas 300 partículas de materia oscura por cada litro. La búsqueda de materia oscura de forma directa es quizás la técnica más precisa desarrollada hasta el momento para encontrar WIMPs. El concepto detrás de la búsqueda es simple: como hay partículas de materia oscura en nuestras vecindades y estas viajan con velocidades de $v \sim 300\,\mathrm{km/s}$ se espera que los WIMPs crucen la tierra y de vez en cuando choquen con los núcleos terrestres depositando pequeñas cantidades de energía tras cada choque. Dadas las masas típicas de los WIMPs (MeV-TeV) y sus pequeñas velocidades (comparadas con la luz), las energías depositadas suelen ser muy pequeñas $E = 0.1 - 50\,\mathrm{keV}$. Estas energías suelen dar lugar a excitaciones

térmicas, a fotones resultantes de las excitaciones de los núcleos y a la ionización de los propios núcleos. Para encontrar estos WIMPs diferentes laboratorios subterráneos han sido construidos (soterrados para tener menos ruido de fondo), dónde los materiales típicamente usados como blanco son elementos como el Xenón o el Argón, cristales centelleadores o detectores de Germanio. A día de hoy los experimentos de Xenón tienen una masa fiducial de 1 tonelada y en el futuro se espera que puedan llegar a múltiples. Actualmente ninguno de los experimentos en la búsqueda directa de materia oscura, prominentemente XENON1T [135], PandaX [137] y LUX [136], ha encontrado ninguna señal atribuible a los WIMPs. Estos resultados suponen una fuerte cota a múltiples modelos de materia oscura, sobre todo para masas $> 10\,\mathrm{GeV} \simeq 10\,m_p$ (dónde m_p es masa del protón).

2. **Detección Indirecta**

   Dado que los WIMPs se aniquilan en el universo primitivo, se espera que también lo sigan haciendo a día de hoy, aunque con una cadencia mucho menor. La frecuencia de las aniquilaciones de materia oscura viene dada por $\Gamma = \langle \sigma v \rangle \, n_\chi^2/2$ (dónde $\langle \sigma v \rangle$ es su sección eficaz de aniquilación y n_χ es su densidad numérica) y por lo tanto, la probabilidad de aniquilación de partículas de materia oscura será mayor en las regiones más densas. Regiones típicas en las que se espera una gran densidad de materia oscura son el centro galáctico y las galaxias enanas satélite de la Vía Láctea. Cuando dos partículas de materia oscura se aniquilan generan una cascada de partículas que resultan en un espectro de fotones, electrones, positrones, neutrinos y diferentes núcleos. Entre ellos, las técnicas más fiables de búsqueda de materia oscura se realiza buscando fotones y neutrinos, dado estas partículas no se desvían. Sin embargo, debido a la débil interacción de los neutrinos, los rayos gamma suponen la fuente más sólida de cotas a la aniquilación de materia oscura. En particular, la colaboración Fermi-LAT [138], mediante la búsqueda de fotones en las galaxias satélite, ha excluido WIMPs aniquilándose a canales hadrónicos con $m \lesssim 50\,\mathrm{GeV}$. Además de las búsquedas de rayos cósmicos, las anisotropías del fondo cósmico de microondas resultan también ser muy sensibles a la aniquilación de materia oscura en la llamada época oscura, cuando el universo tenía entre 3.8×10^5 y 7×10^9 años. A través de las precisas observaciones que el satélite Planck [12] ha realizado del fondo cósmico de microondas se ha excluido la posibilidad de que la materia oscura con masas $\lesssim 10\,\mathrm{GeV}$ se aniquile, vía procesos con momento angular 0, independientemente del canal de aniquilación [13] (siempre que no sea a neutrinos).

3. **Producción en colisionadores de partículas**

   Si los WIMPs interactúan con las partículas del Modelo Estándar han de poderse producir en colisionadores de partículas (siempre que la energía del acelerador sea mayor que la masa de los WIMPs). Las partículas de materia oscura, dada sus débiles interacciones, si son producidas en choques de partículas simplemente escaparán el detector y sólo podrán ser inferidas por una aparente falta de energía al reconstruir la cinemática del evento. La búsqueda más genuina de materia oscura en el LHC[3] son las de jet + *missing energy*. Estas suponen una fuerte cota a diferentes partículas tipo WIMP [139, 140]. Los WIMPs también pueden ser producidos a través de las desintegraciones de los bosones Z y el Higgs. La coincidencia entre las predicciones del Modelo Estándar y los resultados experimentales suponen unas cotas muy fuertes a modelos dónde la materia oscura es suficientemente ligera $m_\chi \lesssim m_Z/2$, $m_H/2$ y se acopla de forma directa a estos bosones. Aparte de estos canales de producción, típicamente los modelos de WIMPs, a parte de la materia oscura, suelen incluir otras partículas que son más fáciles de detectar en las colisiones. A este respecto, las colaboraciones ATLAS y CMS han acotado considerablemente las posibles interacciones de las partículas mediadoras entre los WIMPs y el Modelo Estándar, ya sea a través de sus desintegraciones a leptones o a quarks.

La falta de señales en las búsquedas de materia oscura restringe considerablemente la naturaleza de la materia oscura tipo WIMP, en particular su masa e interacciones con las partículas del Modelo Estándar. La comunidad científica está centrada en la búsqueda de estas partículas, y como hemos descrito en los párrafos anteriores, por medio de técnicas y estudios muy eficaces y variados. En la próxima década la sensibilidad de los experimentos va a mejorar cuantitativamente, de no encontrarse ninguna señal convincente, la hipótesis de que los WIMPs son las materia oscura se depreciará notablemente.

[3] Large Hadron Collider, el gran colisionador de hadrones alojado en el CERN.

6.5 Metodología

Dada la perspectiva fenomenológica adoptada en esta tesis, el espectro de métodos utilizados ha sido amplio, tanto en términos de técnicas analíticas como numéricas.

Desde una perspectiva teórica, se han utilizado técnicas de teoría cuántica de campos para realizar cálculos perturbativos de secciones eficaces y procesos de desintegración. Se han considerado diferentes argumentos teóricos como unitariedad, perturbatividad, ausencia de anomalías e invarianza ante escala. En lo referente al universo primitivo, se ha hecho uso extensivo de la ecuación de Boltzmann para calcular la abundancia de diferentes partículas y para resolver la recombinación de los electrones en el proceso de desacoplamiento del fondo cósmico de microondas. Estos cálculos se han realizado de manera autónoma y también mediante el uso de códigos como *micrOMEGAs* o *Recfast* respectivamente.

Para realizar estudios cosmológicos, se han utilizado técnicas analíticas y numéricas para describir la expansión del Universo bajo diferentes hipótesis, calcular las perturbaciones de materia en el universo temprano, así como el colapso no lineal de estructuras en modelos distintos al de la materia oscura fría. En concreto, hemos estudiado los casos de materia oscura que interactúa con neutrinos o materia oscura compuesta de una componente fría y otra caliente. Para una gran variedad de cálculos cosmológicos se ha hecho uso del código *CLASS* y para contrastar varios modelos con datos cosmológicos el código *MontePython*.

Debido al enfoque fenomenológico adoptado en esta tesis, los datos experimentales han estado presentes en todos los estudios realizados. Las técnicas estadísticas utilizadas han sido bayesianas y frecuentistas para realizar los análisis de datos de experimentos cosmológicos y de física de partículas respectivamente. Se han utilizado distribuciones de probabilidad de Gauss, de Poisson y de χ^2 entre otras. Se han utilizado técnicas Monte Carlo (incluyendo cadenas de Markov) para la realización de diferentes análisis, así como la matriz de Fisher para estudiar el alcance de futuros experimentos.

Finalmente, a lo largo de la tesis hemos utilizado multitud de búsquedas en aceleradores de partículas, para este fin hemos simulado las colisiones de modelos más allá del estándar en *MadGraph* para contrastar lo esperado en las modelos considerados con los datos actuales obtenidos en los distintos experimentos del LHC.

6.6 Resultados y conclusiones

La naturaleza de la materia oscura representa uno de los mayores enigmas de la física actual. En aras de descifrar su esencia, en esta tesis: hemos acotado algunas propiedades de la materia oscura mediante análisis de datos cosmológicos, hemos desarrollado modelos de partículas fundamentales con candidatos bien motivados y también hemos contrastado estos y otros modelos con los datos más recientes de experimentos terrestres y espaciales que buscan la materia oscura a través de sus propiedades no gravitatorias.

Sabemos que, por lo general, la interacción de la materia oscura con las partículas del Modelo Estándar ha de ser débil. Sin embargo, debido a la naturaleza elusiva de los neutrinos, estos representan la excepción a esta regla. En [1], con el objetivo de acotar esta posibilidad, exploramos las implicaciones cosmológicas de materia oscura que interactúa con neutrinos. Para ello, aplicando la teoría de la relatividad general, hicimos un cálculo analítico del sistema de ecuaciones que describen las perturbaciones en un universo con interacciones entre neutrinos y materia oscura. Además, implementamos este sistema de ecuaciones en un código cosmológico para su rápida solución numérica (*CLASS*). La interacción entre la materia oscura y los neutrinos resulta en la supresión de perturbaciones cosmológicas. Para acotar la intensidad de esta interacción utilizamos las observaciones del fondo cósmico de microondas (CMB) realizadas por el satélite Planck así como la distribución de galaxias del catálogo WiggleZ. Analizamos estos datos con métodos Bayesianos (como es costumbre en cosmología debido a la cantidad y complejidad de los datos), y en concreto construimos nuestro propio *likelihood* – o función verosimilitud – para analizar los datos del catálogo WiggleZ mientras que utilizamos el propio *likelihood* de la colaboración Planck dónde se tienen en cuenta todos los factores instrumentales de la medida del CMB. Además del análisis con datos actuales, exploramos el alcance de medidas futuras del fondo cósmico de microondas y de futuros catálogos de galaxias, como es el caso de DESI. Para ello utilizamos el formalismo estadístico de la matriz de Fisher. Gracias a este estudio pudimos obtener las cotas más fuertes hasta la fecha sobre la sección eficaz entre la materia oscura y los neutrinos utilizando teoría lineal de perturbaciones cosmológicas, es decir, sin recurrir a simulaciones numéricas de la formación de estructuras a gran escala. Además, encontramos que los futuros catálogos de galaxias (como DESI) serán de mucha utilidad para acotar este tipo de interacciones.

La complejidad y riqueza del Modelo Estándar de partículas (en el que hay varias partículas estables: protones, electrones, fotones y neutrinos, así como sus respectivas antipartículas), indica que la materia oscura no tiene por qué estar compuesta de una única partícula. En [2] consider-

amos un escenario en el que la materia oscura está formada por partículas frías y calientes, y utilizamos las medidas del fondo cósmico de microondas obtenidas por el satélite Planck, las medidas tomográficas de la estructura a gran escala del catálogo KiDS y el número de galaxias satélite en la Vía Láctea para acotar la fracción de materia oscura caliente que está permitida dadas las observaciones cosmológicas actuales. Para realizar el estudio, de nuevo, utilizamos técnicas Bayesianas para analizar las distintas observaciones y además utilizamos técnicas semianalíticas para describir el número de galaxias satélite en la Vía Láctea partiendo de la teoría de colapso gravitatorio esférico. Como resultado de este estudio, encontramos que la materia oscura ha de ser mayoritariamente fría y obtuvimos una cota sobre la fracción de materia oscura que puede ser caliente en función de su masa (o temperatura). Encontramos que estas cotas son complementarias a las obtenidas en los estudios del bosque de Lyman-α.

El origen de la masa de los neutrinos y la naturaleza de la materia oscura representan dos de las incógnitas más importantes del Modelo Estándar de física de partículas. Puesto que los neutrinos oscilan han de tener masa. La masa de las partículas masivas del Modelo Estándar viene dada a través del mecanismo de Higgs. Sin embargo, la masa de los neutrinos es mucho más pequeña que la del resto de los fermiones del Modelo Estándar (el electrón, los quarks, ...) y esto hace pensar que el mecanismo que dota de masa a los neutrinos es distinto al de Higgs. El mecanismo del seesaw (balancín en inglés) resuelve de forma elegante la presencia de una pequeña masa de los neutrinos a través de la mezcla de los neutrinos activos del Modelo Estándar con unos neutrinos estériles mucho más pesados. Tanto la masa como la magnitud de las interacciones de estos neutrinos estériles son desconocidas. Desde un punto de vista teórico es muy interesante relacionar el mecanismo de generación de masa de los neutrinos con la naturaleza de la materia oscura en el universo. En [3] construimos un modelo teórico, enmarcado dentro de una simetría global $U(1)_{B-L}$ espontáneamente rota, en el que la materia oscura y los neutrinos estériles van de la mano. Una de las mayores implicaciones fenomenológicas del modelo es la existencia de un bosón de Goldstone, el llamado *majoron*. La fenomenología del modelo estudiado en [3] es muy rica: consideramos la generación de la materia oscura en el universo primitivo, las posibles señales en colisionadores de partículas, en experimentos de detección directa de materia oscura y también en búsquedas indirectas de materia oscura. Para realizar dicho estudio utilizamos técnicas básicas de teoría cuántica de campos y de termodinámica en el universo en expansión. En este estudio encontramos que si el campo escalar con simetría carga-paridad positiva es suficientemente masivo, la materia oscura se aniquila predominantemente a neutrinos estériles. Sin embargo, debido a la presencia del majoron, esta aniquilación sólo da lu-

gar a señales en experimentos que buscan rayos cósmicos para masas de la materia oscura superiores a 100 GeV. Con el mismo objetivo de relacionar la materia oscura con los neutrinos estériles, en [4] consideramos a los neutrinos estériles como los interlocutores entre un sector oscuro y el Modelo Estándar. En este modelo, la materia oscura es la partícula más ligera del sector oscuro y además es estable de forma natural. Este modelo tiene implicaciones directas en experimentos susceptibles a las aniquilaciones de materia oscura, como es el caso de Fermi-LAT o Planck.

A día de hoy, los WIMPs representan el candidato más popular a ser la materia oscura del universo. Los WIMPs son generados en el universo primigenio a través de un desequilibrio entre su aniquilación y su producción. El mediador que da lugar a estos procesos con partículas ligeras puede ser (o no) del Modelo Estándar, en cualquier caso, los mediadores más icónicos son los bosones del Modelo Estándar Z y Higgs. En [5] estudiamos desde una perspectiva general los modelos de materia oscura en los cuales los WIMPs se aniquilan por mediación de los bosones Z o Higgs. Consideramos fermiones, escalares y vectores acoplados a estos bosones y estudiamos su producción en el universo primitivo así como las cotas existentes sobre estos modelos provenientes de experimentos de detección directa y de colisionadores de partículas. Encontramos que la gran mayoría del espacio de parámetros en estos modelos estaba excluido y que experimentos futuros acotarán el resto salvo por el caso de WIMPs con interacciones pseudoescalares con el boson de Higgs.

El exceso de rayos gamma provenientes del centro galáctico supone la señal más plausible de materia oscura hasta la fecha. La señal ha sido intensamente estudiada por diferentes grupos desde hace nueve años y muestra, con un alto grado de confianza estadística, un espectro morfológico y energético compatible con el esperado por las aniquilaciones de materia oscura tipo WIMP. El espectro observado favorece masas de entre 30-70 GeV con una distribución igual a la encontrada en simulaciones numéricas de materia oscura fría. Además de la interpretación en términos de materia oscura, esta señal también podría ser explicada por pulsares. Los púlsares tienen un espectro energético muy similar, sin embargo estos deberían encontrarse en el centro galáctico en cantidades muy superiores a las observadas en cúmulos globulares. A día de hoy, la interpretación del exceso no está clara. Desde el punto de vista de física de partículas, es fundamental identificar las propiedades de los WIMPs que podrían ser responsables de este exceso. En consecuencia, en [6] consideramos modelos simplificados de materia oscura para determinar cuales de estos eran compatibles tanto con el exceso de rayos gamma provenientes del centro galáctico como con las intensas búsquedas de materia oscura en aceleradores de partículas y en experimentos de detección directa. Con objeto de este estudio, simu-

lamos el experimento de detección directa LUX para obtener cotas a otras interacciones no proporcionadas por la colaboración. Además, simulamos colisiones en el LHC con los modelos considerados y las contrastamos con los datos obtenidos por las colaboraciones ATLAS y CMS. Por último, también realizamos un estudio sobre las cotas existentes a partículas escalares y pseuodoescalares proporcionados por las factorías de mesones B. Como resultado de este estudio, encontramos que los modelos simplificados con mediadores vectoriales y con mediadores con color estaban excluidos. Encontramos que los modelos con mediadores pseudoescalares, en general, sobrevivían a las distintas búsquedas. Este estudio demostró que los modelos que pueden explicar el exceso, en el caso de que la materia oscura se aniquile directamente a partículas del Modelo Estándar, están fuertemente acotados debido a las infructuosas búsquedas de WIMPs en diferentes experimentos terrestres. Este hecho nos motivó a realizar un estudio dónde consideramos que la materia oscura forma parte de un sector oscuro que se comunica muy débilmente con el Modelo Estándar. En [7] estudiamos la compatibilidad de varios sectores oscuros con la señal del centro galáctico así como con las cotas sobre la aniquilación a la materia oscura extraídas de las búsquedas de fotones provenientes de las galaxias satélite de la Vía Láctea. Para ello, estudiamos en mucho detalle la producción de la materia oscura en el universo primitivo, pues para los modelos considerados era crucial considerar las regiones resonantes en las que varias partículas tienen masas similares. Y además, realizamos un estudio estadístico de la compatibilidad espectral de la señal para cada modelo así como de su compatibilidad con las cotas del experimento Fermi-LAT y de las medidas del fondo cósmico de microondas realizadas por el satélite Planck.

En resumen, en esta tesis hemos investigado las implicaciones cosmológicas y fenomenológicas de la materia oscura. Desde la perspectiva cosmológica nos hemos centrado en la complementariedad de observables en el universo primitivo y reciente en modelos que van más allá del paradigma actual, ΛCDM. En concreto hemos estudiado modelos con materia oscura que interactúa con neutrinos y materia oscura formada por partículas frías y calientes. Estos estudios nos han servido para entender algunas propiedades de la materia oscura que pueden afectar al universo observable. Desde una perspectiva fenomenológica, hemos estudiado la posible conexión de la materia oscura con los neutrinos estériles, así como modelos WIMP genéricos. Estos estudios nos han permitido entender, por ejemplo, las propiedades que la materia oscura puede tener si está relacionada con la generación de masa de los neutrinos activos. Respecto al estudio de candidatos WIMP convencionales, hemos explorado exhaustivamente la compatibilidad de modelos en los que los WIMP se aniquilan por mediación de los bosones Z y Higgs con las búsquedas fallidas en colisionadores de partículas y en experimentos

de detección directa. Y por último, en este estudio, hemos resaltado la naturaleza de la materia oscura en los modelos capaces de explicar el exceso de rayos gamma del centro galáctico.

La perspectiva complementaria adoptada en esta tesis ha resultado muy útil para acotar la naturaleza de la materia oscura. Sin embargo, a día de hoy, aún no sabemos qué es. Aún así, esta tesis ha servido para estudiar varias posibilidades y explorar la fenomenología de candidatos muy bien motivados. En los años venideros, nuevos datos del fondo cósmico de microondas, de la distribución de galaxias en el universo, de la búsqueda en aceleradores y de experimentos de detección directa e indirecta nos proporcionarán una gran cantidad de información que resultará muy relevante para mejorar nuestro conocimiento sobre la naturaleza de la materia oscura. La precisión que van a tener estos futuros experimentos es tal, que la hipótesis de que la materia oscura está formada por partículas tipo WIMP será o corroborada o considerablemente devaluada en favor de otras posibilidades. Esto hace de la próxima década un período clave para determinar si la materia oscura es de tipo WIMP.